Universiteit Gent

Faculteit Ingenieurswetenschappen

Vakgroep Chemische Proceskunde en Technische Chemie

Single Event Microkinetic Model for Steam Cracking of Hydrocarbons

'Single Event' Microkinetisch Model voor Stoomkraken van Koolwaterstoffen

Kevin Van Geem

Promotor: Prof. Dr. ir. G. B. Marin

Proefschrift tot het verkrijgen van de graad van

Doctor in de toegepaste wetenschappen: Scheikunde

Academiejaar 2005-2006

Promotor:

      Prof. dr. Ir. G.B. Marin

'Single event' microkinetisch model
voor het stoomkraken van koolwaterstoffen

Single Event Microkinetic Model
for Steam Cracking of Hydrocarbons

Kevin Van Geem

UNIVERSITEIT
GENT

Promotor:

      Prof. G.B. MARIN   Universiteit Gent

Examencommissie:

      Prof. L. TAERWE   Universiteit Gent

      Prof. M.-F. REYNIERS   Universiteit Gent

      Dr. F. BATTIN-LECLERC   ENSIC

      Prof. W. GREEN   Massachusetts Institute of Technology

      Prof. G. HEYNDERICKX   Universiteit Gent

      Prof. J. THYBAUT   Universiteit Gent

      Prof. R. VAN KEER   Universiteit Gent

Universiteit Gent, Vakgroep Chemische Proceskunde & Technische Chemie

Laboratorium voor Petrochemische Techniek

Krijgslaan 281 – S5

B-9000 Gent

Dankwoord

Deze thesis is niet het werk van één persoon, maar het resultaat van een intensieve samenwerking met vele personen. Mijn dank gaat dan ook uit naar alle mensen die me bijgestaan hebben gedurende de laatste 4 jaar. Uiteraard verdienen velen een bijzonder woordje van dank:

Prof. dr. ir. Guy B. Marin wens ik te bedanken voor de kans en het vertrouwen die hij mij gegeven heeft om een nieuw vakgebied te verkenen. Stap voor stap hebt u mij wegwijs gemaakt in de wetenschappelijk wereld. Een doctoraat is ook een beetje vallen en opstaan, remember mijn eerste presentatie in San Francisco. Toch kijk ik met veel plezier terug op onze samenwerking. Een betere promotor kon ik mijzelf niet wensen.

Een speciaal woordje gaat zeker ook naar Prof. Marie-Francoise Reyniers die me steeds heeft bijgestaan met raad en daad over de meest uiteenlopende zaken. Veel heb ik aan jou te danken en dat zal ik nooit vergeten. Soise, bedankt!

A special thanks to Prof. William H. Green for your help, advices, and encouragements, which drove me to explore and learn new things. I should not forget to thank all the people at MIT, who helped to make my stay in Boston one of the best times in my life. Susan, Jing, Joanna, His Wu, John, Paul, Sandeep, Sally, Robert, Luwi … Thanks.

It is nice working if you have fantastic colleagues. Maarten, Bart, Ionel, Tanguy, Georgios, Mark, Geraldine, Jidong, Arno, Joris Thybaut, Isabelle, Juray, Gorik, Joris Wieme, Roberto, Rhona, Rado, Edward, Veerle … Thank you!

Verder dank ik het LPT-personeel, in het bijzonder ing. R. De Coster, M. Lottin, A. Snoeck, H. Heene, G. Verenghen en E. Van Damme omdat zij steeds klaar stonden voor het oplossen van mijn kleine en grote problemen en de goede sfeer die zij in het labo brachten. Zonder jullie zou dit werk er nooit gekomen zijn.

Al mijn vrienden wil ik bedanken voor de mooie momenten. Uiteraard mag ook mijn studentjes niet vergeten. Helge, Ineke, Jan, Juan, Raquel, Klaar bedank ik voor de leuke tijd die we samen hebben beleefd, niet alleen op wetenschappelijk gebied.

Last but not least zou ik mijn mama, papa, zusje en mijn schat willen bedanken. Jullie hebben er alles aan gedaan om mijn leven zo gemakkelijk mogelijk te laten verlopen de afgelopen jaren, zonder jullie had ik dit nooit gekund, bedankt!

Notation

Roman symbols

A	pre-exponential factor	s^{-1} or mol m^{-3} s^{-1}
B	inter-fin distance	m
C_B	carbon atom in a benzene ring	-
C_d	double bounded carbon atom	-
C_j	concentration of component j	kmol m^{-3}
CIP	Coil Inlet Pressure	MPa
CIT	Coil Inlet Temperature	K
C_n	carbon number	-
COP	Coil Outlet Pressure	MPa
COT	Coil Outlet Temperature	K
c_p	heat capacity	kJ mol^{-1} K^{-1}
C_t	triple bounded carbon atom	-
$C\bullet$	radical carbon atom	-
Δc_i^g	group error from the QSSA	kmol m^{-3}
Δc_i^S	instantaneous error from the QSSA	kmol m^{-3}
D	diffusion coefficient	m^2 s^{-1}
d	specific density	kg m^{-3}
Da	Damköhler number	k^0_{ref} τ
d_{eq}	equivalent tube diameter	m
D_m	molecular diffusion coefficient	m^2 s^{-1}
d_t	internal tube diameter	m
d_w	thickness of the wall	m
E_a	activation energy	kJ mol^{-1}
Eu	Euler number	d_t p_t f^{-1} v_a^{-2} L^{-1}
f	Fanning friction factor	-
F	flow rate	kg s^{-1}
f_A	contribution to the pre-exponential factor	s^{-1} or mol m^{-3} s^{-1}

$f_{i,j}$	stoichiometric coefficient of molecule i for constraint j	variable
f_j	value of constraint j	variable
F_j	molar flow Rate	$kg\ s^{-1}$
$\boldsymbol{f_{min}}$	error tolerance	-
Fo	Fourier number	$\tau_{\lambda r}^{-1}\ \tau$
F_t	total molar flow rate	$mol\ s^{-1}$
$\%F_k$	weight percent of PIONA class k	-
G	mass flux	$kg\ m^{-2}\ s^{-1}$
$\%G_k$	volume percent of the boiling point k	-
ΔG_{rxn}	reaction free energy	$kJ\ mol^{-1}$
h	convection coefficient	$kJ\ m^{-2}\ s^{-1}\ K^{-1}$
$\Delta_r H^0$	standard reaction enthalpy	$kJ\ mol^{-1}$
J_{ik}	element of the Jocobian matrix	s^{-1}
J_j	molar flux vector for species j	$mol\ m^{-2}\ s^{-1}$
k	reaction rate coefficient	s^{-1} or $mol\ m^{-3}\ s^{-1}$
k^0_{ref}	reference reaction rate coefficient	s^{-1}
KDU	vector containing the double bonded carbon atoms	-
KRADP	radical position	-
L	reactor length	m
N	number of molecules in the library	-
M	molar mass	$kg\ mol^{-1}$
$\underline{M}$	Boolean relation matrix	-
n	scale factor	-
Δn	mole change in a reaction	-
P	pitch of the fin	m
p_A	partial pressure of component A	MPa
p_c	critical pressure	MPa
p_t	total pressure	MPa
Pe	Peclet number	$\tau^{-1}\ \tau_{Dr}$
PRC	Pseudo Rate Coefficient	variable
q	heat flux	$kJ\ m^{-2}\ s^{-1}$

Q	volumetric flow rate	$m^3 \, s^{-1}$
Q_p	partition function	
r	radial position	m
R	universal gas constant	$kJ \, mol^{-1} \, K^{-1}$
r_b	radius of the bend	m
$r_{c \, j}$	coking rate of reaction in which j participates	$kg \, m^{-2}_{reactor} \, s^{-1}$
R_{char}	characteristic flux of the system	s^{-1}
Re	Reynolds number	$v \, d_t \, \rho \, \mu^{-1}$
r_f	rate of formation	$mol \, m^{-3} \, s^{-1}$
R_j	total rate of change of the amount of component j	$mol \, m^{-2} \, s^{-1}$
R_{leak}	leakage flux	s^{-1}
R_{min}	minimal flux	s^{-1}
RPRC	Relative Pseudo Rate Coefficient	variable
$R_{reacted(j)}$	net rate of change for species j	s^{-1}
$R_{species(j)}$	flux to species j	s^{-1}
r_V	reaction rate	$mol \, m^{-3} \, s^{-1}$
R_V	netto production rate	$mol \, m^{-3} \, s^{-1}$
S	entropy	$kJ \, mol^{-1} \, K^{-1}$
S(x)	Shannon's entropy	-
$\Delta S^{o, \neq}$	standard entropy of activation	$kJ \, mol^{-1} \, K^{-1}$
t	time	s
T	process gas temperature	K
T_b	boiling point	K
T_c	critical temperature	K
v	velocity	$m \, s^{-1}$
V	volume	m^3
V_E	equivalent reactor volume	m^3
V_m	molar volume	$m^3 \, mol^{-1}$
Δv	group contribution to the molar volume	$m^3 \, mol^{-1}$
w_i	weighing factor of component I	-
X	contribution to the activation energy	$kJ \, mol^{-1}$

x	axial position	m
x_i	mole fraction of component i	-
Y_A	yield of product A	wt %
z	axial coordinate	m
Z_c	the critical compressibility factor	-

Greek symbols

α	conversion factor depending on the units of p_t	-
δ	dilution	-
ε	distance to the wall	m
ε_D	turbulent diffusivity	$m^2\,s^{-1}$
ε_H	turbulent conductivity	$kJ\,m^{-1}\,s^{-1}$
ε_k	variable concerning constraint k	-
θ	dimensionless temperature	-
θ_t	residence time	s
λ	thermal conduction coefficient	$kJ\,m^{-1}\,s^{-1}$
λ_j	Lagrange multiplier	-
λ_m	molecular conduction coefficient	$kJ\,m^{-1}\,s^{-1}$
λ_w	conduction coefficient of the wall	$kJ\,m^{-1}\,s^{-1}$
ζ	Nekrasov factor for bends	-
ρ	density of the process gas mixture	$kg\,m^{-3}$
τ_w	shear stress	$kg\,s^{-2}\,m^{-1}$
τ	residence time	s
τ_{Dr}	time scale for radial diffusion	s
$\tau_{\lambda r}$	time scale for radial conduction	s
ξ	normalized radial position	-
η	wetted perimeter of the tube	m
κ	the angle of the tube bend	-
$\nu_{k,j}$	stoechiometric coefficient of the component j	-
μ	dynamic viscosity	Pa s
μ_j	Lagrange multiplier	-

ν	kinematic viscosity	$m^2\ s^{-1}$
ν_j	Lagrange multiplier	-
$\xi(x_i)$	objective function	-
π	probability	-
σ_k	error linked to constraint k	variable
σ'_m	standard deviation linked to constraint m	variable
σ_{ext}	external symmetry number	-
σ_{int}	internal symmetry number	-
ω	circumference	m
Ω	cross sectional surface area	m^2

Subscripts

0	initial
a	axial
ab	abstraction
ad	addition
b	backward
calc	calculated
coke	coke
c-c	c-c scission
eq	equilibrium
exp	experimental
ext	external
f	forward
glob	global
int	internal
j	component
ol	olefin
r	radial or reference or reactant
rec	recombination
ref	reference

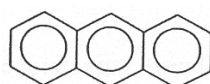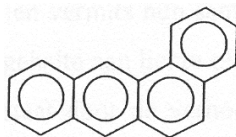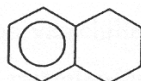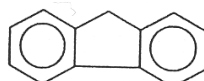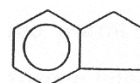|	
rot	rotation
trans	translation
vib	vibration
β	β-scission
'	dimensionless
≠	transition state

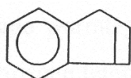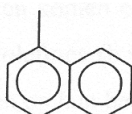## List of components
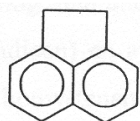
acenaphthene
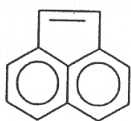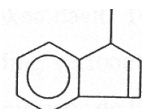
acenaphthylene

anthracene

benzene

chrysene

decaline

fluorene

indane

indene

1-methylnaphthalene

1-methylindene
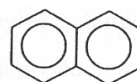
naphthalene
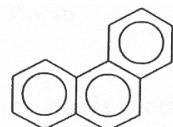
phenanthrene
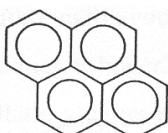
pyrene
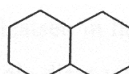
tetraline

toluene

Contents

(+) Van Geem K.M., Reyniers M.F., Marin G.B., Song J., Mattheu D.M., Green W.H. Automatic Network generation using RMG for Steam Cracking of n-Hexane, AIChE Journal, 52, 2, 718-730, 2006.

(*) Van Geem K.M., Heynderickx G.J., Marin G.B. A Comparison of One and Two-dimensional Reactor Models for Steam Cracking: Effect on Yields and Coking Rate, AIChE Journal, 50, 173–183, 2004.

(°) Van Geem K.M., Reyniers M.F., Marin G.B. Two severity indices for scale-up of steam cracking coils, Ind. Eng. Chem. Res., 44, 3402-3411, 2005.

Samenvatting

Stoomkraken van koolwaterstoffen is één van de basisprocessen in de petrochemische industrie. De koolwaterstoffen worden bij hoge temperaturen (1000 à 1150K) onder toevoeging van stoom omgezet tot commercieel interessante producten. Zo worden lichte olefines gevormd zoals ethyleen, propyleen en butadieen. Tevens ontstaan aromaten en zwaardere bijproducten. De gebruikte koolwaterstofvoedingen gaan van lichte alkanen zoals ethaan en propaan tot complexe koolwaterstofmengsels zoals nafta en gasolie. De krakingseenheden bestaan uit 2 grote delen: een warme sectie, waar de koolwaterstoffen gekraakt worden in ovens, en een koude sectie, waar de gevormde producten gescheiden worden. In dit werk ligt de nadruk op de warme sectie en meerbepaald op de reactoren.

Olefines en aromaten zijn de onmisbare componenten voor de chemische industrie. Ze zijn de bouwstenen voor allerhande producten die we gebruiken in het dagelijkse leven en dienen dan ook net zoals koelwater en elektriciteit zo goedkoop mogelijk geproduceerd te worden. Stoomkraken van koolwaterstoffen is het belangrijkste productieproces voor deze producten en is bijgevolg één van de belangrijkste processen uit de petrochemische industrie. Een nauwkeurige voorspelling van de productopbrengsten is voor verschillende redenen cruciaal. Enerzijds zijn gedurende de laatste decennia de winstmarges significant gedaald. Stoomkrakers zijn de meest energie verslindende installaties van de chemische industrie en de hoge energieprijzen wegen op de marges. Optimalisatie van het oven, de reactoren en de scheidingstrein is noodzakelijk omdat het energieverbruik van deze eenheden meer dan 70 % van de kosten vertegenwoordigd. Ook de keuze van de voeding is niet onbelangrijk. Immers deze heeft een grote invloed op de productendistributie en bijgevolg ook op de winst. Uiteraard hebben goede voedingen ook hun prijs. Klassiek wordt gebruik gemaakt van ethaan of nafta als voeding. Daarnaast is er een trend om ook steeds meer zware voedingen te kraken (zware nafta, lichte gasolie of vacuüm gasolie) die echter aanleiding geven tot een lagere opbrengst aan lichte olefines. De reden voor het gebruik van deze zwaardere voedingen is hun overschot op de markt omdat ze steeds minder gebruikt worden als brandstof. Naast het winstaspect wordt ook steeds meer gelet op de invloed van het proces op het milieu. Moderne krakingsinstallaties zijn nog steeds verantwoordelijk voor de emissie van grote hoeveelheden broeikasgassen, in het bijzonder CO_2. Het Kyoto protocol eist

dat de emissies van deze gassen drastisch dienen gereduceerd worden. Tot slot is er de opkomst van vele alternatieve processen voor de productie van olefines. Deze zijn potentieel goedkoper en hebben bovendien een lager impact op het milieu.

In dit werk zijn verschillende methoden ontwikkeld voor het accuraat voorspellen van de productopbrengsten bij het kraken van een welbepaalde koolwaterstofvoeding. Single event microkinetische modellering is hiervoor de meest aangewezen methode. Daarom is een nieuw fundamenteel simulatie model ontwikkeld dat toelaat de kraking van zowel lichte koolwaterstoffen (ethaan, propaan en butaan fracties) als zware koolwaterstoffracties (nafta, gasolie en VGO) te simuleren. Het ontwikkelde simulatiemodel bestaat uit twee elementen: het reactormodel en het single event microkinetisch model. De nadruk in dit werk ligt op de ontwikkeling van het microkinetisch model. Het reactienetwerk wordt opgedeeld in 2 delen: een β-netwerk en een μ-netwerk. In het μ-netwerk wordt het krakingsgedrag van moleculen beschreven met 6 of meer koolstofatomen. Na homolytische splitsing, waterstofabstractie- of additiereacties vormen deze moleculen nieuwe radicalen. Dit zijn over het algemeen radicalen met een zuiver μ karakter. Het feit dat deze laatste enkel monomoleculaire reacties ondergaan wordt met groot voordeel toegepast. Het monomoleculair karakter maakt het mogelijk de concentraties van de μ radicalen uit de continuïteitsvergelijkingen te elimineren indien de pseudo stationaire toestand voor de reactieve μ-radicalen verondersteld wordt. Bijgevolg worden het aantal continuïteitsvergelijkingen gevoelig beperkt. De ontbinding van de μ-radicalen moet eindigen wanneer bimoleculaire reactiemogelijkheden ontstaan of met andere woorden van zodra een radicaal gevormd wordt dat ook een uitgesproken β-karakter bezit. De reacties van deze componenten zijn ondergebracht in het β-netwerk. Het aantal reacties in het microkinetisch model zijn drastisch uitgebreid. Dit is enerzijds door het beschouwen van enkel nieuwe reactiemogelijkheden zoals 1,4-isomerisatiereacties en competitie tussen 1,5- en 1,6-cyclisatiereacties. Anderzijds is dit gebeurd door het beschouwen van een groot aantal nieuwe componenten en reacties. Bijzondere aandacht is gegaan naar de vorming van zware producten tijdens het stoomkrakingsproces, meer bepaald componenten uit de gevormde kraakbenzine fractie en de fuel-olie fractie.

De bovenstaande modelhypothesen zijn geverifieerd aan de hand van een netwerk opgesteld met het automatisch netwerkgenereringsprogramma RMG. Uit een studie voor het kraken van n-hexaan blijkt dat inderdaad het vooropstellen van radicalen met een zuiver μ-karakter

gerechtvaardigd is. Bovendien blijkt het ook gerechtvaardigd om pseudo stationaire toestandshypothese toe te passen voor de concentraties van de μ-radicalen. Ook blijkt dat de zogenaamde disproportioneringsreacties kunnen verwaarloosd worden en dat de druk tijdens het stoomkraken voldoende hoog is om de kinetische parameters in de hoge druk limiet te beschouwen.

Het mag duidelijk zijn uit voorgaande paragrafen dat het manueel opstellen van een dergelijk uitgebreid en ingewikkeld reactienetwerk een nagenoeg onmogelijke taak is. Daarom is er voor gekozen om het volledige reactienetwerk automatisch te laten genereren via een computerprogramma. In dit programma worden chemische structuren voorgesteld door binaire relatiematrices. De elementaire reactiestappen worden dan gesimuleerd door wiskundige bewerkingen op deze relatiematrices uit te voeren. De voorstelling aan de hand van binaire relatiematrices heeft als belangrijk nadeel dat ze niet uniek is. Het gebruik van een compact en eenduidig labelsysteem is hiervoor de meest aangewezen oplossing. De modellering vereist ook de kennis van een groot aantal onbekende kinetische parameters. Om dit euvel te omzeilen wordt gebruik gemaakt van een groep-additieve methode. Dit zorgt er voor dat het aantal parameters in het model drastisch wordt gereduceerd. Voor iedere reactie uit een welbepaalde familie worden structurele contributies in rekening gebracht ten opzichte van een referentiereactie om de activeringsenergie en de pre-exponentiële factor te bepalen.

In Hoofdstuk 4 wordt het fundamentele simulatiemodel besproken. Een nieuwe routine DASSL is gebruikt voor het oplossen van het stijf stelsel van differentiaal vergelijkingen. In vergelijking met de oude oplosser worden kleine verschillen voor de berekende productopbrengsten waargenomen. Het simultaan oplossen van de differentiaalvergelijkingen heeft ook tot gevolg dat de simulatietijd met een factor 3 toeneemt. Het fundamentele simulatiemodel is gevalideerd aan de hand van 150 experimenten afkomstig uit het experimentele gegevensbestand van pilootexperimenten. Een goede overeenkomst tussen gesimuleerde en experimenteel waargenomen productopbrengsten wordt vastgesteld. Belangrijk is ook dat het huidig simulatiemodel wel instaat is om goede simulatieresultaten te produceren voor moeilijke koolwaterstofvoedingen zoals nafteenrijke naftas, ethaan/tolueen mengsels en VGO fracties. Om de gebruiksvriendelijkheid van het fundamentele simulatiemodel te verbeteren is een grafische interface ontwikkeld die het mogelijk maakt op iedere computer draaiend op een Windows besturingssysteem simulaties uit te voeren. Ook voor het

experimentele gegevensbestand is een grafische interface ontwikkeld die toelaat op eenvoudige wijze experimenten toe te voegen.

In Hoofdstuk 5 zijn drie industriële stoomkrakingsovens gesimuleerd aan de hand van een gekoppelde oven/reactor simulatie. In eerste instantie is een ethaankrakingsoven gesimuleerd en is het effect van de keuze van het reactormodel nagegaan op de simulatieresultaten. Voor de industriële reactor met een diameter van 0.1 m treden belangrijke radiale gradiënten op, zowel voor de temperatuur als voor de concentratie van de componenten. Hierdoor ontstaan kleine maar significante verschillen tussen de gesimuleerde opbrengsten met een 1-dimensionaal en 2-dimensionaal reactor model. Voor de reactoren met een kleinere zijn de radiale gradiënten beperkt omdat zij een sterker 1-dimensionaal karakter vertonen. Het gebruik van meer dimensionale modellen is belangrijker voor het accuraat simuleren van cokesvorming. Hierbij is de kennis van de temperatuur, de concentraties van de verschillende componenten nabij de wand onontbeerlijk voor een goede voorspelling van de cokesvormingsnelheid aan de hand van een rigoureus kinetisch model. Als tweede industriële simulatie is een Kellogg Millisecond oven gevoed met een industriële propaanvoeding beschouwd. Finaal is ook een Lummus oven gesimuleerd die gevoed wordt met gasolie. Steeds wordt een goed overeenkomst waargenomen tussen gesimuleerde en de industrieel waargenomen productopbrengsten.

In Hoofdstuk 6 zijn twee alternatieven uitgewerkt voor het rechtstreekse experimenteel opschalen van stoomkrakingsreactoren. Enerzijds is er een methode ontwikkeld op basis van de kraakscherpte. Anderzijds is ook met behulp van de gelijkvormigheidtheorie nagegaan hoe resultaten van een kleine pilootreactor kunnen opgeschaald worden naar een grote installatie en omgekeerd. Kraakscherpte-indices worden door de industrie gebruikt om op een eenvoudige wijze inzicht te krijgen in de productendistributie. Echter 1 kraakscherpte-index is onvoldoende om de opbrengsten op eenduidige wijze vast te leggen, er zijn ten minste 2 kraakscherpte-indices noodzakelijk. Immers de productendistributie bij het kraken van een welbepaalde voeding wordt volledig bepaald door zowel de temperatuur als de partieel drukken van de verschillende componenten. De effecten van procescondities op de productopbrengsten kunnen dan terug gebracht worden tot wijzigingen van hetzij de temperatuur, hetzij de druk of een combinatie van beide. Een uitgebreide analyse van het reactienetwerk voor het stoomkraken toont aan dat de verhouding van de ethyleen- op ethaanopbrengsten een goede maat is voor de druk, terwijl de methaanopbrengst een goede maatstaf is voor de temperatuur. Experimenten en simulaties tonen

aan dat de combinatie van deze 2 kraakscherpte-indices toelaat om de productendistributie op eenduidige wijze te bepalen.

De tweede methode is gebaseerd op de gelijkvormigheidtheorie en meerbepaald op een analyse van de dimensieloze criteria volgend uit de volledige mathematische beschrijving van het proces. Hieruit blijkt dat het onmogelijk is om aan alle dimensieloze criteria te voldoen in 2 verschillende buisreactoren. Het enige alternatief is werken onder partiële gelijkvormigheid en vanzelfsprekend leidt dit tot verschillen. Echter, de verschillen blijven beperkt indien welbepaalde gelijkvormigheidcriteria behouden blijven. Simulatieresultaten voor zowel ethaan als n-butaan tonen aan dat het effect van het verwaarlozen van radiale uniformiteiten belangrijker is dan het effect van niet werken onder hetzelfde drukprofiel indien de gemiddelde druk in de reactor maar nagenoeg dezelfde is. Bovendien blijkt uit de kengetallen dat enkel dezelfde radiale uniformiteiten kunnen gerealiseerd worden in 2 reactoren met dezelfde reactordiameter. Dit inzicht is gebruikt voor het ontwerp van de ideale pilootreactor heeft belangrijke gevolgen voor het ontwerp van de ideale pilootreactor, i.e. een pilootreactor die voor dezelfde procescondities aanleiding geeft tot nagenoeg dezelfde productendistributie als de beschouwde industriële reactor.

In Hoofdstuk 7 is een methode ontwikkeld die toelaat op een snelle en nauwkeurige wijze de gedetailleerde voedingsamenstelling van nafta fracties te bepalen aan de hand van standaard-ASTM-methodieken (e.g. specifieke dichtheid, kooktraject, PIONA gewichtsfracties, gemiddelde molaire massa e.d.), de zogenaamde commerciële karakteriseringindices. De molfracties worden bepaald door het maximaliseren van de Shannon entropie. Dit criterium garandeert dat een specifieke molecule niet over een andere molecule kan geprefereerd worden bij afwezigheid van informatie. Een goede overeenkomst tussen gesimuleerde en analytisch bepaalde moleculaire samenstellingen van naftafracties wordt waargenomen indien voldoende commerciële indices gekend zijn. De snelle reconstructie van naftafracties maakt deze methode bovendien bijzonder geschikt voor de koppeling met het fundamentele simulatiemodel ontwikkeld voor stoomkraken. Vergelijking tussen simulatieresultaten en experimentele resultaten verkregen op de pilootinstallatie toont aan dat een beperkte bibliotheek bestaande uit enkel de kerncomponenten aanleiding geeft tot goede simulatieresultaten in combinatie met het fundamenteel simulatiemodel voor stoomkraken.

Summary

Steam cracking of hydrocarbons is one of the most important processes of the petrochemical industry. In this process hydrocarbons are cracked into commercially more important products such as light olefins and aromatics. Feedstocks ranging from light alkanes such as ethane and propane up to complex mixtures such as naphthas and heavy gas oils are converted at temperatures ranging from 1000-1150 K in tubular reactors suspended in large gas-fired furnaces. A steam cracking plant can be separated into two sections: a hot section where the hydrocarbons are cracked and a cold section for the separation of the products. In this work the focus is on the hot section and in particular on the reactors.

Olefins and aromatics are considered key components of the chemical industry. They form the building blocks for a wide range of derivates used in our daily lives. Olefins and aromatics are now considered commodities. Similar to electricity or cooling water, they must be produced at the lowest cost, continuously, and reliably to feed integrated downstream units. The steam cracking process is the main production process for these light olefins and can thus be considered one of the most important processes of the petrochemical industry. An accurate prediction of the product yields is crucial for several reasons. First of all the profit margins of steam crackers have decreased significantly. Steam crackers are the most energy consuming installations of the chemical industry and the increasing energy prices weigh on the margins. Optimization of the design of the furnace, the reactors and the separation section is necessary because the energy consumption determines over 70% of the costs. Another crucial factor affecting the economics is an appropriate feedstock selection because the latter has an important influence on the product distribution. However, good feedstocks come at a price. The decreasing demand for heavy fractions as fuel results in large remains of these low cost fuels and makes these feedstocks more and more interesting from an economic point of view. Next to economics also environmental issues gain importance. Modern olefin plants are still responsible for emissions of large amounts of greenhouse gasses, especially CO_2. The Kyoto protocol states that the emissions of CO_2 should be drastically reduced. Finally, there is an increased competition from alternative processes for the production of light olefins. These are potentially cheaper and have a lower impact on the environment.

In this work different methods are discussed to accurately predict the product yields obtained from a specific feedstock. Single event microkinetic modeling is the most appropriate solution because once the fundamental simulation model is developed results can be easily gathered and computer simulations take only a limited time. Therefore a new simulation model for steam cracking is developed. In a first phase the single event microkinetic reaction network is developed. The new reaction network is just as previously developed reaction networks divided in two sub networks; the monomolecular μ network and the β network. This is because monomolecular reactions generally dominate for species with more than 5 carbon atoms (μ radicals) apart from some exceptions. The kinetics for the μ network are described by analytical expressions based on the pseudo steady state assumption for the radical reaction intermediates. For β radicals bimolecular reactions cannot be neglected, making it necessary to construct a separate sub-network: the β network. The number of reactions considered in the single event microkinetic model is extended, while also the number of species considered is drastically increased. This makes the new reaction network the most extensive reaction network ever generated for steam cracking. The assumptions made for constructing the reaction network are also verified using a new rate based network generator called RMG. Under the specified conditions the μ radical hypothesis is indeed valid. Also the error for applying the quasi steady assumption state for the group of μ radicals is negligible. An indication of the effect of pressure dependence of the rate coefficients can also be obtained using RMG. In our case the effect of pressure dependence on the predicted conversion and the yields of the major products for n-hexane steam cracking under the specified conditions is limited. In Chapter 3 more details are given of how the reaction network is practically constructed. Topics such as how the species are represented, which group contribution method is implemented for calculating the activation energies and pre-exponential factors, and the considered species are discussed.

In Chapter 4 the reactor model COILSIM1D is discussed. A new stiff solver DASSL is implemented in COILSIM1D. The implementation of this solver shows that the simulated methane, ethylene, butadiene and propylene yield differ slightly from the values obtained with the old solver. However, solving the balances simultaneously with a stiff solver comes at a price, the simulation time increases significantly. The developed fundamental simulation model is validated using 150 pilot plant experiments from the experimental database of pilot plant experiments. Excellent agreement is obtained between the simulated and experimental product

yields. In contrast to older simulation models now even for difficult feedstocks such as VGO, heavy naphthas and ethane/toluene mixtures a good agreement between the simulated and experimentally determined product distribution is obtained. An important improvement is also the development of a graphical user interface. This interface improves the user friendliness and makes it possible to carry out simulations on any recent PC running on a Windows operating system. Also for the experimental database a GUI is developed that allows searching and expanding the database.

In Chapter 5 three industrial steam cracking furnaces are simulated via a coupled reactor/furnace simulation. First an industrial ethane cracking furnace is simulated. Comparison of the simulation results obtained with a 1-dimensional and 2-dimensional reactor model shows that important radial gradients exist, not only for the temperature but also for the molecular and in particular the radical species. These profiles are the origin for small but significant differences between the simulated product yields. The effects on the product yields for heavier feedstocks become smaller because the necessary heat fluxes for heavier feedstocks are lower. For the same reasons the differences between the simulated product yields with the 2-dimensional and 1-dimensional reactor model are almost non-existing for pilot plant reactors. Using the 2-dimensional reactor model is more important for describing coke formation because the 2-dimensional reactor model allows to account for the coke precursor concentrations adequately and, hence, to properly simulate the coking rates with a fundamental coking model. Next a propane cracking furnace and a gas oil cracking furnace are simulated. Comparison between the industrial and simulated product yields shows that accurate simulation results are obtained in both cases.

Chapter 6 discusses two methods for scaling up steam cracking coils. The first one is based on the severity concept. Reaction path analysis shows that two carefully chosen severity indices are sufficient to unambiguously characterize the product yields for a given feedstock: one severity index being a measure for the temperature and the other index being a measure for the reactants partial pressure. The methane yield is an appropriate measure for the temperature, while the ethylene over ethane yield ratio can be considered a reliable measure for the reactants partial pressures. Simulations and experiments show that for a given feedstock the methane yield and the ethylene over ethane yield ratio are independent indices and that they unambiguously characterize the observed product yields: i.e. the use of a third severity index is not necessary.

The second scale-up method discussed in Chapter 6 is scale-up based on dimensional analysis of the model equations. These dimensionless model equations show that complete similarity can never be reached for 2 different tubular reactors. Scale-up is thus only possible under partial similarity and inevitably this leads to differences. However, if the criteria of similarity are relaxed with care only small differences between units of different scale can be obtained. Two different relaxation strategies are distinguished; the first one aims at realizing the same axial pressure profile neglecting radial non-uniformities, the second focuses on realizing the same radial temperature profile. Neglecting the similarity of the radial temperature profile leads to larger differences as compared to the differences resulting from neglecting the similarity of the axial pressure profile. In the case of ethane cracking differences between units of different scale resulting from neglecting the similarity of the radial temperature profile can be up to 4.0% (rel.) for the conversion and up to 1.2 % (rel.) for the ethylene yield. This insight was used to design a pilot plant reactor ideal to scale down a Lummus SRT-I reactor and a pilot plant reactor for studying intrinsic kinetics.

In Chapter 7 a method for feedstock reconstruction for naphtha fractions is discussed using the analytically determined commercial indices as input. This method is based on Shannon's entropy criterion and creates a molecular composition that meets all the boundary conditions set by the available commercial indices. A reasonable correspondence is observed between predicted and experimentally determined naphtha compositions if sufficient commercial indices of the mixture are available. The fast reconstruction of a molecular composition makes the feedstock module SimCO very attractive for implementation in the simulation package for steam cracking. The combination of these two simulation tools makes it possible to obtain simulation results even faster than before because no time is wasted for determining a detailed molecular composition. Simulation results show that the quality of the simulations improves if a library containing only key components of naphtha fractions is used instead of an extensive library.

Chapter 1:

General Introduction

1.1   Introduction

Steam cracking of hydrocarbons is one of the most important processes of the petrochemical industry. In this process hydrocarbons are cracked into commercially more important products such as light olefins and aromatics. Feedstocks ranging from light alkanes such as ethane and propane up to complex mixtures such as naphthas and heavy gas oils are converted at temperatures ranging from 900-1200 K in tubular reactors suspended in large gas-fired furnaces. The olefin plants often form the centerpiece of an entire petrochemical complex, see Figure 1.1. Refineries provide the cracking feed, while the effluent streams from the cracker are used in downstream units, e.g. polyethylene and polypropylene units.
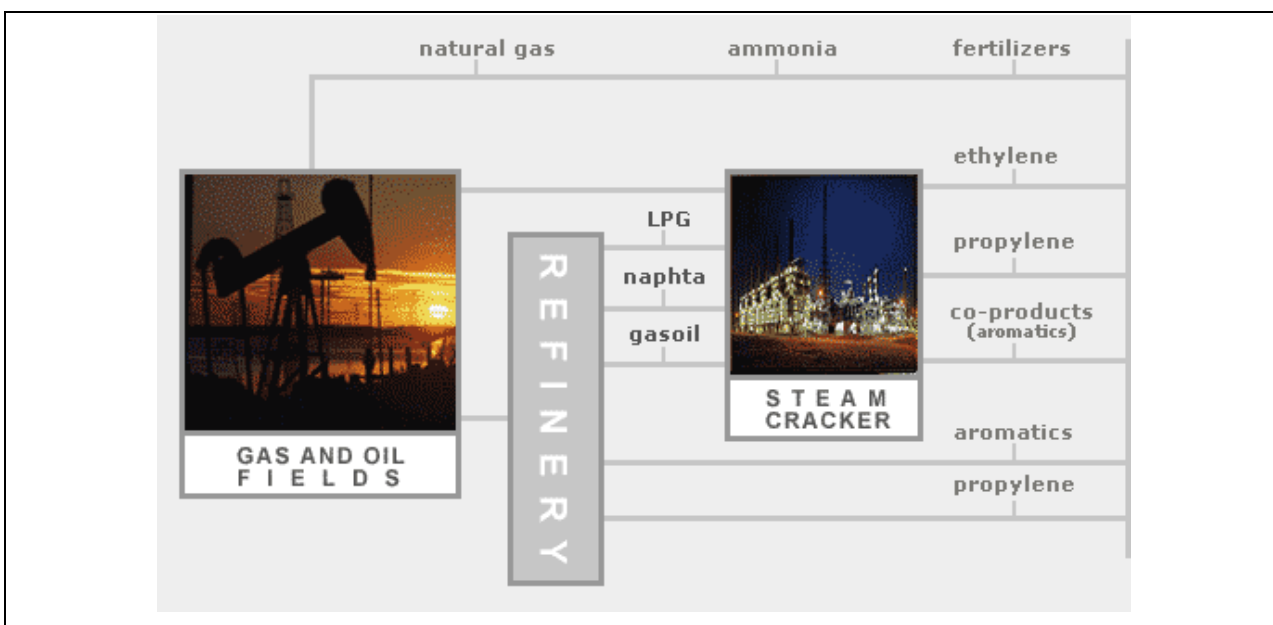
Figure 1.1: Situation of the steam cracking process in the petrochemical industry

A steam cracking plant can be separated into two sections: a *hot section* where the hydrocarbons are cracked and a *cold section* for the separation of the products. Figure 1.2 shows a schematic overview of a typical steam cracking plant.
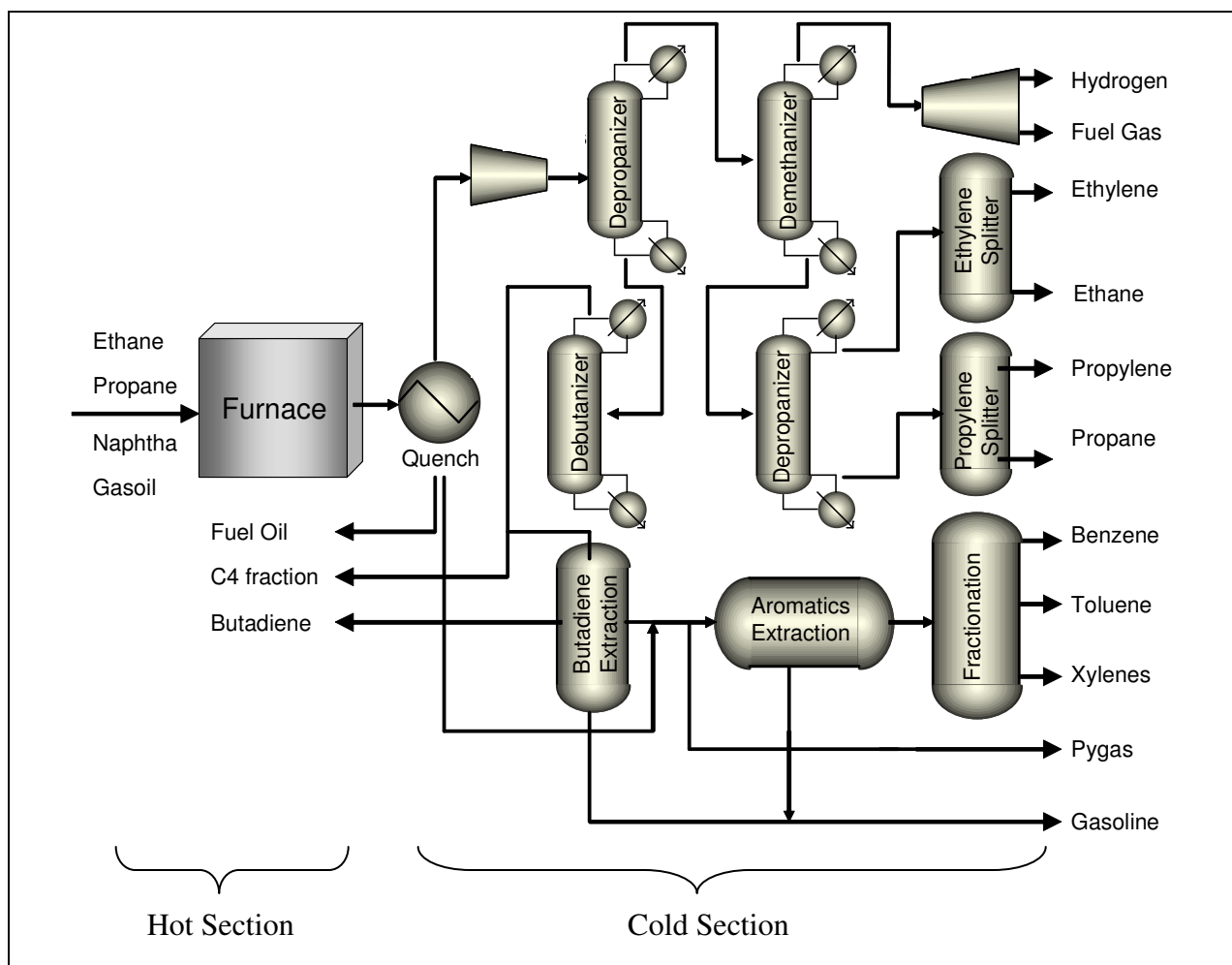
Figure 1.2: Schematic overview of the hot and cold section of a typical steam cracking plant (Marin, 2006)

The hot section can be further divided into a radiation section, a transition section and a convection section, see Figure 1.3. In the radiation section the feed is cracked in tubular reactors suspended in gas fired furnaces. The heat required for the endothermic reactions is provided by radiation burners in the side walls or long flame burners in the bottom of the furnace. The coil outlet temperature in industrial furnaces varies between 750 °C and 850 °C according the

processed feedstock. Obtained conversions for ethane furnaces are commonly in the range between 55 % and 65 %. For naphtha feedstocks the propylene to ethylene ratio varies between 0.65 and 0.75 kg/kg. Steam is added to the feed to reduce the partial pressure of the hydrocarbons and to limit the secondary reactions destroying the olefins.

Convection Section

Transition Section
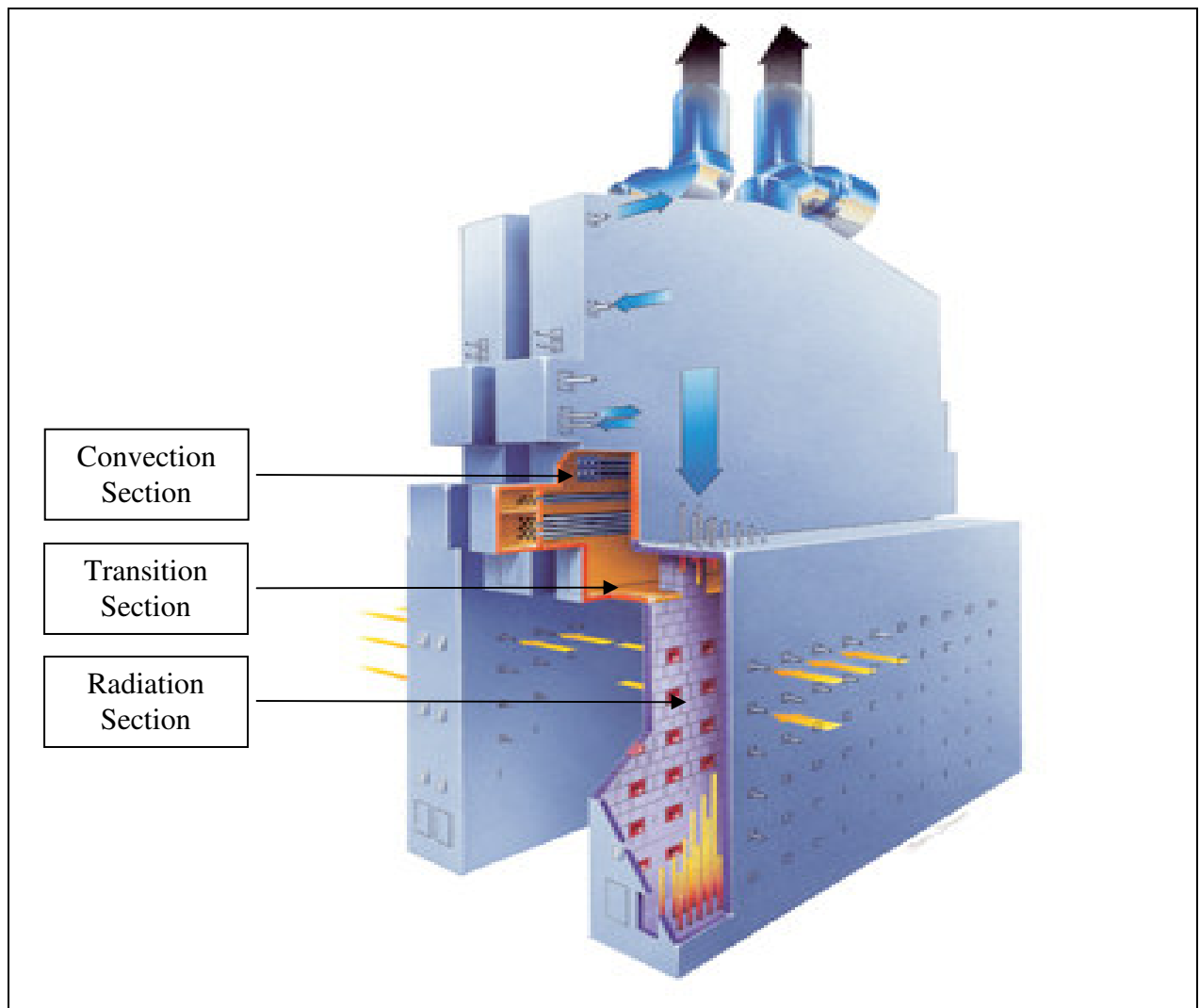
Radiation Section

Figure 1.3: Schematic overview of the convection section and the radiation section of a steam cracking furnace (http://www.abb.com/lummus)

The heat generated by the flue gas is recuperated in the convection section for the preheating of the feed and dilution steam and for the generation of high-pressure steam, which can be used for instance for the operation of turbines.

Upon leaving the furnace reaction section, the obtained product mixture enters the quench section, where heavy oil and water is used to cool the gases and to quench or terminate the chemical reactions. As the water or oil cools the gases, heat is recovered as steam that is utilized in other parts of the process. At this point, the hydrocarbon gases need to be liquefied for purification, and this is done by compressing the gases to high pressures (3.8 MPa) and cooling them to very low temperatures (-150 °C). Once the gases are liquefied, they are moved to the fractionation system and are separated by distillation columns as ethylene, propylene, a crude C_4-fraction, pyrolysis gasoline and fuel gas. Auxiliary units are often present to further purify some of the co-products including a propylene splitter to purify propylene, a butadiene extraction unit to separate 1,3 butadiene and butenes, and an aromatics extraction unit to recover benzene, toluene and xylenes.
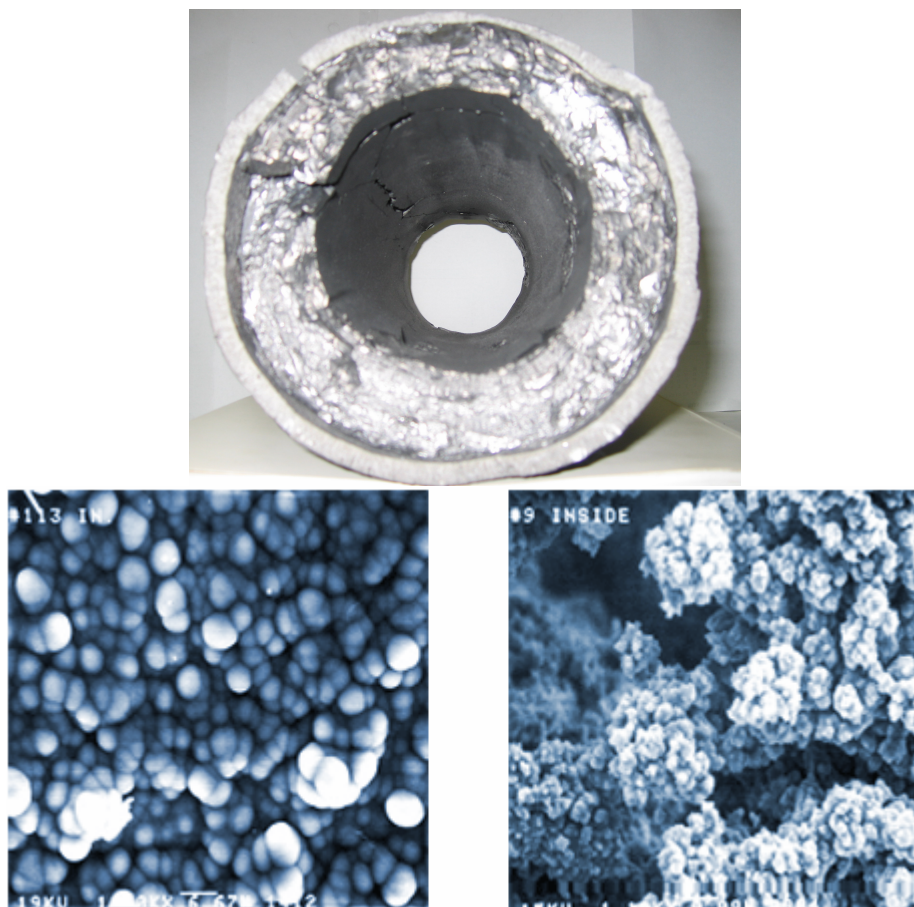
Figure 1.4: Visualization of pyrolytic coke on the metal surface of a cracking tube

During the steam cracking process a carbonaceous residue is formed on the inner wall of the reactor tubes, see Figure 1.4. The growth rate of this coke layer increases with increasing wall temperature, but depends also strongly on the feedstock composition. The coke layer on the wall increases the pressure drop over the reactor. To retain a constant conversion level and selectivity an increase of the heat input is necessary. Applying a higher reactor inlet pressure allows to keep the coil outlet pressure (COP), imposed by the separation train, at a constant level. If the external tube skin temperature reaches its maximum allowable temperature or if the pressure drop becomes too high, the unit is taken out of operation for a decoking cycle. In this decoking phase the coke is burnt off with a controlled air/steam mixture.

1.2   The Olefins Market

Olefins and aromatics are considered key components of the chemical industry. They form the building blocks for a wide range of derivates used in our daily lives. Olefins and aromatics are now considered commodities. Similar to electricity or cooling water, they must be produced at the lowest cost, continuously and reliably to feed integrated downstream units, which are the real profit centers (Buffenoir et al., 2004). The applications of olefins and aromatics are numerous and their derivatives are traded around the world. The main derivatives for ethylene are polyethylene (PE), ethylene oxide (EO), ethylene dichloride (EDC) and styrene (STY), see Figure 1.5.
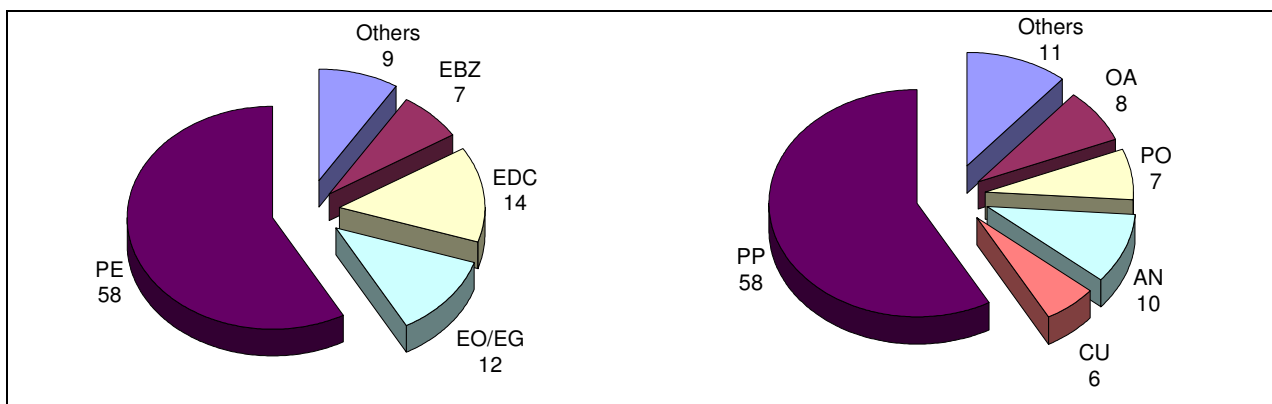
Figure 1.5: Derivatives from ethylene and propylene (CMAI – World olefins analysis, 2001)

Polyethylenes of various density and melt flow account for more than 50% of world ethylene demand. The primary use of polyethylene is in film applications for packaging, carrier bags and trash liners. Ethylene oxide is a key raw material in the production of surfactants and detergents. It is also used to manufacture ethylene glycols, which are in turn used in soft drinks and food packaging and textiles. Styrene monomer is used principally in polystyrene for packaging and insulation, as well as in styrene butadiene rubber for tires and footwear. Styrene is, next to cyclohexane for the production of caprolactam (nylon), also the major derivative of benzene. In case of propylene the main applications are polypropylene (PP), acrylonitrile (AN), propylene oxide (PO), oxo-alcohols (OA) and cumene (CU). Acrylonitrile is used to make acrylic fibers; rugged plastics for computer housings; and nitrile rubber for oil-resistant hoses.

Globally the demand for these derivatives is continuously rising, reflecting in a growing demand for ethylene, propylene and benzene. This is illustrated in Figure 1.6 where the evolution of the ethylene production capacity in the World is shown in the past decade. In 2004 the ethylene production capacity increased with 2.1 million tons produced per year (tpy) to 112.9 million tpy, see Table 1.1.

	Ethylene Capacity (tpy)		Change	
	Jan. 1, 2005	Jan. 1, 2004	(tpy)	(%)
Asia Pacific	30˙095˙000	29˙346˙000	749˙000	2.55
Eastern Europe, FSU	8˙137˙000	7˙582˙000	555˙000	7.32
Middle East, Africa	11˙217˙000	11˙012˙000	205˙000	1.86
North America	35˙114˙000	34˙412˙000	702˙000	2.04
South America	4˙385˙500	4˙363˙000	22˙500	0.52
Western Europe	23˙957˙000	24˙063˙000	-106˙000	-0.44
Total Capacity	**112˙905˙500**	**110˙778˙000**	**2˙127˙500**	**1.92**

Table 1.1: Evolution of ethylene production capacity from 2004 to 2005 (Nakamura, 2005)

The main part of this additional capacity resulted from net expansions in existing sites (Nakamura, 2005). In North America, operating conditions increased because the demand for ethylene outgained capacity additions. It is expected that the global ethylene production capacity

will grow at an average of 5.0 % each year in the upcoming decennium. Most future growth in ethylene production capacity will occur in the Middle East and Asia, while North America and Western Europe will experience relatively flat capacity growth, see Figure 1.6. The Middle East and Asia will become the second and third largest producing regions in the world, each leveraging 'low-cost' incentives in the ethylene end-use chain.
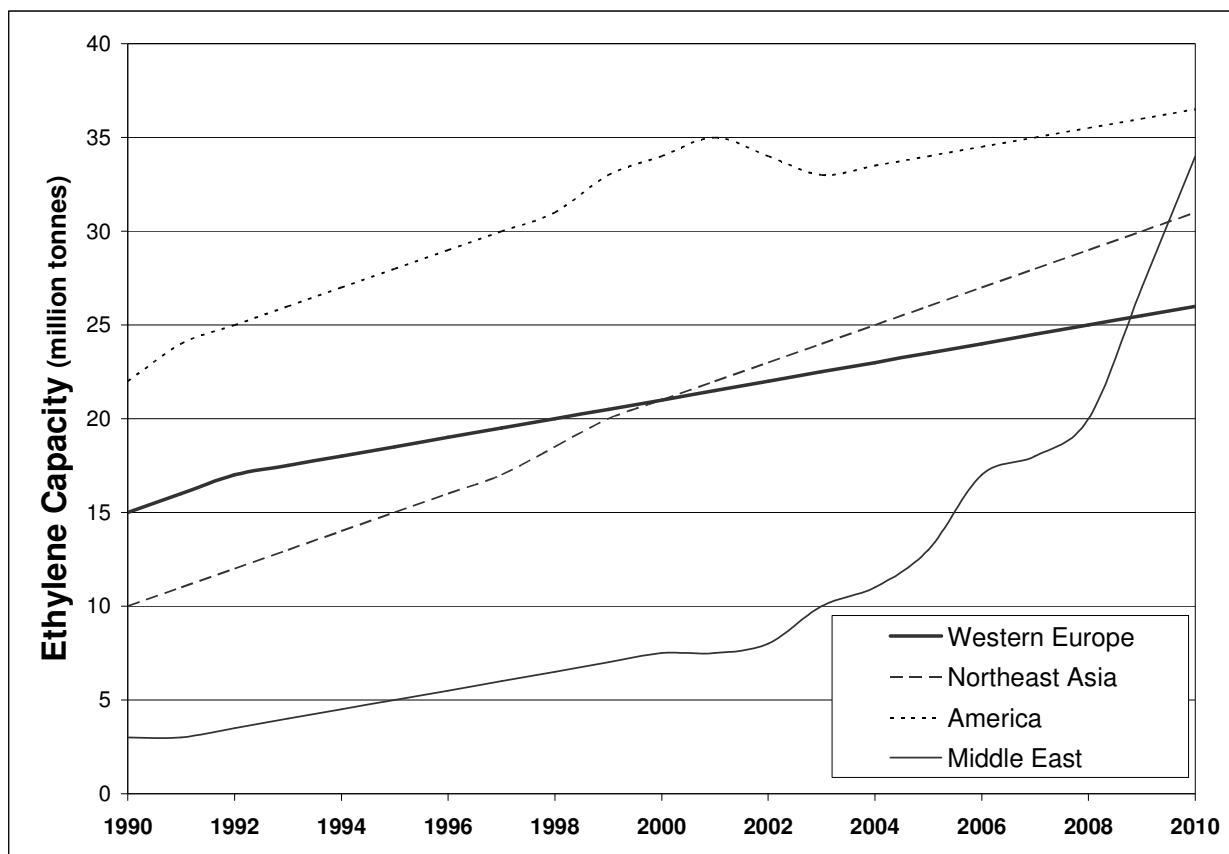
Figure 1.6: Estimated evolution of ethylene production capacity until 2010 (Nakamura, 2005)

In Table 1.2 the ethylene production capacities in 2004 are shown of the five most important ethylene producers. Several major companies have huge production facilities but none of them is a predominant player in this branch of the petrochemical industry. Dow Chemical had the largest ethylene production capacity in 2004, closely followed by Exxon Mobil. Total petrochemicals, the company with the largest production capacity in Belgium, is considered to be the seventh most important producer of ethylene (Nakamura, 2005).

Company	Sites	Capacity, tpy	
		Entire Company	**Partial Interests**
Dow Chemical	14	12˙900˙000	9˙938˙550
Exxon Mobil	15	11˙432˙000	8˙313˙000
Shell Chemicals	10	8˙981˙000	6˙862˙000
SABIC	5	7˙111˙000	5˙312˙000
BP	8	6˙229˙000	4˙782˙000

Table 1.2: Ethylene production capacity of the most important petrochemical companies [Entire Company: 100 % owned by company, Partial Interests: Olefin production site partially owned] (Nakamura, 2005)
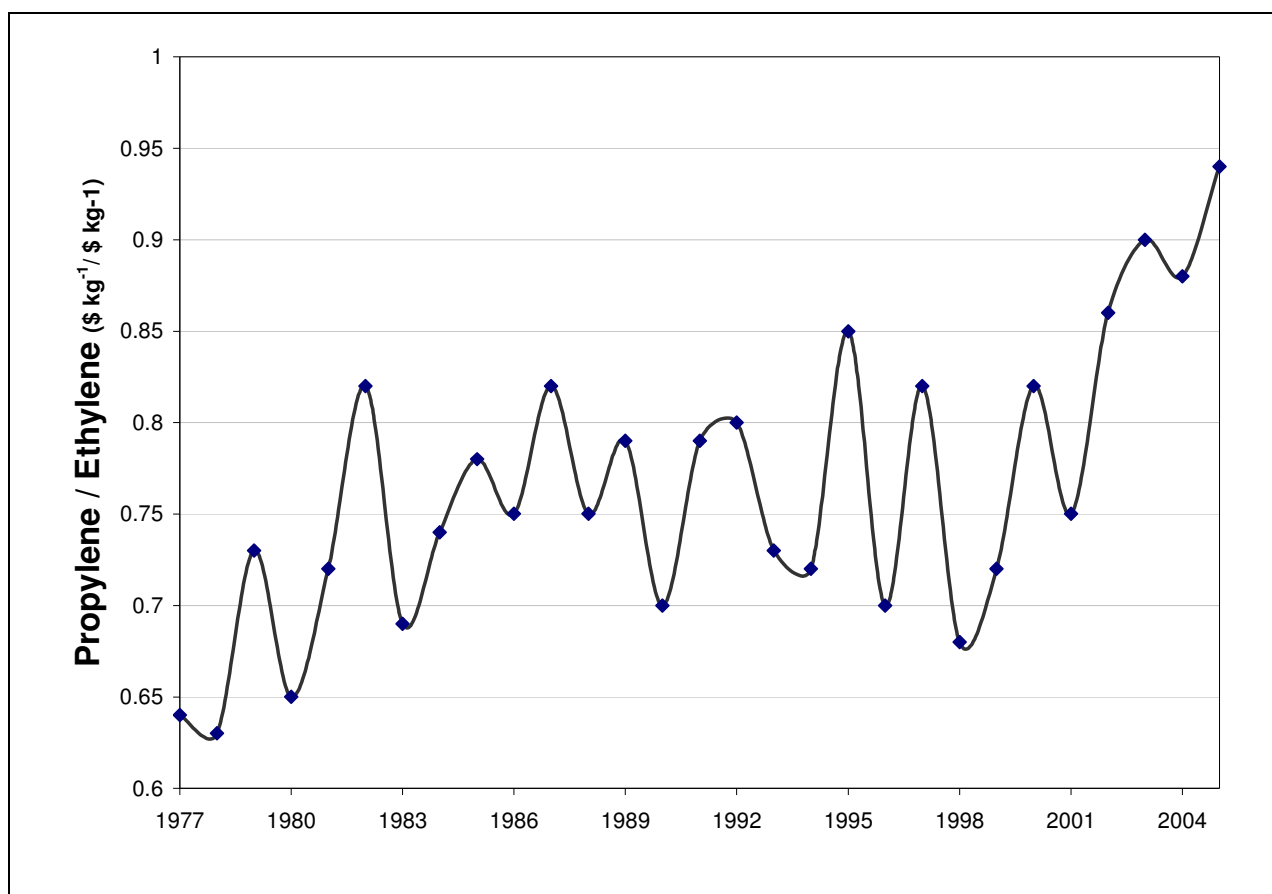
Figure 1.7: Evolution of the propylene to ethylene price over the past decades. (Van Camp, 2005)

During the seventies, eighties and nineties the main focus of a steam cracking plant was to maximize the production of ethylene. This has recently changed, more and more in Europe and Asia propylene becomes the desired product. This is because the demand for propylene is increasing drastically, certainly compared to ethylene. In Figure 1.7 the evolution of the propylene to ethylene price is shown. The price of propylene compared to ethylene is almost continually rising, increasing more rapidly the past five years. In 2005 for the first time the price of propylene equaled the price of ethylene, and it is expected that this trend will continue.

	Ethane	**Propane**	**Butane**	**Naphtha**	**Gas oil**	**Others**
Ethylene Capacity (million tpy)	28.5	7.6	3.0	50.3	3.7	1.8
Relative Capacity (%)	30.0	8.0	3.2	53.0	3.9	1.9

Table 1.3: Ethylene capacity produced with different types of feedstocks in 2004 (Nakamura, 2004)

In steam cracking plants several feedstocks can be used ranging from light gases such as ethane or propane or complex mixtures such as naphtha, gas oil and VGO, see Table 1.3. Which type of feedstock is used is mainly determined by the local availability. In the United States light paraffins have been, and continue to be the predominant feedstocks (Nakamura, 2005). The reason is the large availability of natural gas liquids from the American energy industry (McConnell and Head, 1980). Ethane is the most efficient feedstock for the production of ethylene, while the production of other products such as methane, propylene, C_4^+ hydrocarbons is minimized. This implies that it requires the simplest processing unit with the lowest capital investment. Heavier feedstocks require higher investment costs due to the more complex design of the cold separation section. A disadvantage of using ethane is its strong refractory character, and consequently ethane requires high coil outlet temperatures to crack. Globally, naphtha is the most commonly applied feedstock in crackers. In Europe, the feedstock is for more than 90 % naphtha because of the unavailability of liquefied petroleum gases (LPG) and the demand of gas oils as heating oil. Heavier feedstocks such as gas oils and VGO's crack easier than the lighter

hydrocarbons but they have a higher coking tendency. This can drastically decrease the run length of the installation. Also fouling in the TLE can become a problem when the feedstocks become heavier. The final decision concerning the feedstock used for olefin production is based on maximizing the return on investment. Availability of feedstock, capital costs and the ability to market co-products and maximize their relative values are all considerations that have to be taken into account when determining the size and the location of a new configuration.

1.3   The Future of Steam Cracking

In the next decennia steam cracking of hydrocarbons faces some major challenges. One of them comes from the competition of alternative processes for the production of light olefins. Alternative routes include the catalytic dehydrogenation (Chauvel et al., 1989; Buonomo et al., 1997; Moulijn et al., 2001; Bhasin et al., 2001) or oxidative dehydrogenation of ethane and propane (Mamedov and Cortes Corberan, 1995; Bhasin et al., 2001), the catalytic cracking of C_4/C_5 alkenes (Bolt and Glanz, 2002), the olefins conversion process (Grootjans et al., 2005), the oxidative pyrolysis of ethane (Chen et al., 1998), the conversion of methanol to ethylene/propylene mixtures (Moulijn et al., 2001; Kvisle et al., 2002; Morgan, 2003) – also called MTO for methanol-to-olefins – or the oxidative coupling of methane (Quang, 1991; Raimbault, 1991; Edwards et al., 1991; Chen et al., 1994; Lunsford, 1997). All these alternatives require complex processes with large investments, which stem from the need to minimize fast catalyst deactivation and provide the necessary heat of reaction – for instance in alkane dehydrogenation or methanol-based routes – or to minimize the combustion to CO_2/H_2O and manage the resulting heat release – for instance in the oxidative dehydrogenation and methane coupling routes. Autothermal oxidative dehydrogenation of alkanes over noble metal catalysts offers one of the most promising alternatives for steam cracking. An economic analysis (Lange et al., 2005) revealed that ethane oxycracking might at best be marginally more attractive than ethane steam cracking of comparable ethylene yields. This is however a very optimistic assumption because of the very optimistic assumptions on yields (Lange et al., 2005). The advantage of the cheaper oxycracking reactor is almost completely lost by the cost of making (or purchasing) O_2 to feed the oxycracker. Schmidt et al. (2000) found the same conclusion based on their economic analysis.

Another important challenge is how to keep increasing the sizes of olefin plants. Since the end of World War II, plant sizes have increased from 10000 tonnes per year to more than a million tonnes per year while the required energy decreased by a factor 3 (Cole, 1996). The main reason to increase the size of these crackers is that the cost per ton ethylene produced decreases when the plant is operated at full capacity. Not only the investment cost per ton ethylene produced decreases, but also several fixed costs decrease drastically with increasing size of the olefin plant (Buffenoir et al., 2004). The current bottleneck for these single train mega crackers is situated in some mechanical aspects, in particular in the dimension and the construction of compressors (Buffenoir et al., 2004). Practically this implies that it is difficult to construct single train crackers with an ethylene production capacity larger than 1.5 million tpy.

From environmental point of view the steam cracking remains an important concern. Steam cracking is the most energy-consuming process in the chemical industry (Ren et al., 2006). Modern olefin plants operate highly energy efficient; nevertheless they are still responsible for the emissions of large amounts of greenhouse gases, especially CO_2. Carbon dioxide is formed in the furnace where methane (byproduct of the steam cracking process) is burned to produce the necessary heat for the endothermic steam cracking process. The steam cracking process currently accounts for approximately 180-200 million tons of CO_2 emissions worldwide (Ren et al., 2006). The Kyoto protocol states that the emissions of CO_2 should be drastically reduced. Also, the furnace inevitably produces pollutants such as NO_x, generating future concern.

Finally, there is a tendency to use exotic feedstocks, e.g. heavy hydrocarbon feedstocks such as VGO or polyethylene. The demand for heavy gas oils and VGO's as fuel is becoming less and less important, resulting in large remains of these low cost fuels. Therefore they become more and more interesting as alternative for naphtha. The problem is that the cracking behavior differs significantly of that of lighter fractions and that these fractions have a very strong coking tendency. Also fouling problems in the TLE and the tubing make that companies show a certain resistance for using these fractions. If these problems could be resolved or drastically reduced heavy fractions will become an interesting alternative.

1.4 Objectives

The main objective of this work is the extension of the single event microkinetic model (SEMK) used in the steam cracking simulation software. This extension is carried out in two directions; one, extending the number of components included in the reaction network, two, extending the number of reactions considered in the reaction network. Extending the number of components in the reaction network is necessary to improve the description of the cracking behavior of heavy hydrocarbon feedstocks. Therefore the maximum carbon number of components considered in the reaction network should be extended and some new classes of components (e.g. naphtheno aromatic compounds) have to be considered. Also new compounds formed from these heavy compounds should be admitted in the reaction network. Special attention is paid to components part of the formed fuel oil fraction, e.g. the formation of poly-aromatic compounds. However renewing the software for steam cracking does not only concern the size of the reaction network. Another important aspect in the present work is the creation of user-friendly software. Therefore a user friendly environment is created, e.g. via a graphical user interface.

In Chapter 2 the construction of the reaction network is discussed. The model assumptions are explained and verified using a test problem. In Chapter 3 the main principles of how the reaction network is generated are specified. This part clarifies how the reaction rules are translated to mathematical operations, how the kinetic parameters are determined and which group contribution method is used, how species are identified, etc. In Chapter 4 the reactor model equations are specified and the simulation model is validated using pilot plant experiments. Also the most recent changes made to the pilot plant are discussed and the graphical user interface for the simulation model is shown. Chapter 5 shows the results of several simulations of industrial steam cracking plants. In Chapter 6 two methods for scale-up of steam cracking coils are discussed. The first is based on the "severity" concept but uses two severity indices instead of one to unambiguously characterize the product yields for a given feedstock. The second method discussed in this chapter is scale-up based on dimensionless analysis. This method consists of building a unit similar to an industrial one and operating it under conditions of complete or partial similarity. In Chapter 7 a method for fast feedstock reconstruction based on the average properties of a mixture is evaluated. In this case a method based on maximization

of Shannon's entropy criterion is applied to predict the detailed feedstock composition based on the commercial indices of the mixture. Finally in chapter 8 the general conclusions are drawn and an outlook for the future is presented.

1.5   References

Bhasin M.M., McCain J.H., Volta B.V., Imai T., Pujado P.R. Dehydrogenation and Oxydehydrogenation of Paraffins to Olefins, Appl. Catal. A, 221, 397, 2001.

Bolt H.V., Glanz S. Increase propylene yields cost-effectively, Hydrocarbon Process, 12, 77, 2002.

Buffenoir M.H., Aubry J.M., Hurstel X. Large Ethylene Plants present Unique Design, Construction Challenges, Oil & Gas Journal, 102, 60-65, 2004.

Buonomo F., Sanfilippo D., Trifido F. in: G. Ertl, H. Knozinger, J. Weitkamp (Eds.), Handbook of Heterogeneous Catalysis, vol. 5,Wiley–VCH, 2140, 1997.

Cole D. Olefin Economics Impacts of the Technology Supplier, Proc. 8 th Ethylene Producers Conference, New York, USA, 1996.

Chauvel A., Lefebvre G. Petrochemical Processes – Technical and Economic Characteristics. 1. Synthesis-gas Derivatives and Major Hydrocarbons, Technip, 1989.

Chen Q., Schweitzer E.J.A., Van den Oosterkamp P.F., Berger R.J., De Smet C.R.H., Marin G.B. Oxidative Pyrolysis of Ethane, Ind. & Eng. Chem. Res., 3248-3251, 1997.

Chen Q., Couwenberg P.M., Marin G.B. The Oxidative Coupling of Methane with Cofeeding of Ethane, Ctalysis Today, 21, 309-319, 1994.

Edwards J.H., Do K.T., Tyler R.J. The OXCO Process – a new Concept for the Production of Olefins from Natural Gas, Stud. Surf. Sci. Catal., 61, 489, 1991.

Kvisle S., Nilsen H.R., Fuglerud T., Grønvold A., Vora B.V., Pujado P.R., Barger P.T., Andersen J.M. Methanol to olefins (MTO), Erdol Erdgas Kohle, 118, 361, 2002.

Lange J.P., Schoonebeek R.J., Mercera P.D.L., Van Breukelen F.W. Oxycracking of Hydrocarbons: Chemistry, Technology and Economic Potential, Applied Catalysis A, 283, 243-253, 2005.

Lunsford J.H. in: Ertl G., Knozinger H., Weitkamp J. (Eds.), Handbook of Heterogeneous catalysis, vol. 4, Wiley–VCH, 1843, 1997.

Mamedov E.A., Corberan V.C. Oxidative Dehydrogenation of Lower Alkanes on Vanadium-oxide-based Catalysts- the Present State-of-the-art and Outlooks, Appl. Catal. A 127, 1, 1995.

Marin G.B. Syllabus Petrochemical Processes, Ghent University, 2006.

Moulijn J.A., Makkee M., Van Diepen A. Chemical Process Technology, Wiley, 2001.

Nakamura D.N. Global Ethylene Capacity Growth Slows to Lowest Level since mid-1980s, Oil & Gas Journal, 102, 48, 2004.

Nakamura D.N. Global Ethylene Producers add 2 million tpy of Capacity in 2004, Oil & Gas Journal, 103, 47, 2005.

Raimbault C., Cameron C.J. Synergy between Stable Carbonates and Yttria in Selective Catalytic-Oxidation and Alternative Processes, Energy, 31, 325-351, 2006.

Ren T., Patel M., Block K. Olefins from Conventional and Heavy Feedstocks: Energy use in Steam Cracking and Alternative Processes, Energy, 31, 425-351, 2006.

Schmidt L.D., Siddall J., Baerden M. New Ways to make Old Chemicals, AIChE Journal, 46, 1492-1495, 2000.

Van Camp C. Toekomst chemische industrie in Vlaanderen – Het standpunt van de industrie, KVIV Chemie voor meer Toekomst, Brussel, 2005.

Chapter 2:

Single Event Microkinetic Model

2.1   Introduction

The importance of the steam cracking process to the petrochemical industry has justified the continuous interest for developing new and better mathematical simulation models during the last four decades. Mathematical modeling has the important advantage that once the model is developed, results can be easily gathered and computer simulations take only a limited time (Dente and Ranzi, 1979). Since the pioneers work of Rice (1931, 1934, 1943) there is a general consensus about the free radical mechanism. Still several different types of mathematical models have been developed to simulate the steam cracking process. This was mainly caused by the difficulties encountered with solving the stiff set of differential equations resulting from the free radical mechanism in the early seventies. In literature a distinction is made between three different types of models: empirical models, global kinetic models and detailed kinetic models. Empirical models use a large database of experimental results to fit a number of empirical correlations for the yields of the main products as function of some easily measurable process variable, e.g. Davis and Farell (1973) and Shu and Ross (1982). Global kinetic models are still frequently used and developed, e.g. Kumar and Kunzru (1987), Pant and Kunzru (1997), Belohlav et al. (2003). The most sophisticated global models, e.g. Sundaram and Froment (1977), take the free radical mechanism in consideration but the models themselves are composed of the corresponding global reactions. However, also these models are out of date because the mathematical difficulties encountered for solving the detailed kinetic models are overcome by the development of stiff solvers. For an accurate description of chemical kinetics applicable over a wide range of process conditions and feedstocks, a detailed kinetic model is required (Froment, 1992). One of the main challenges of this type of models is the construction

of a kinetic model that captures the essential chemistry of the system while a manageable size is retained.

Nowadays computers are used not only to solve the simulation numerically, but also to generate the network, construct the model and calculate the kinetic parameters. Large-scale detailed kinetic models find increasing use in the modeling of combustion processes, atmospheric chemistry, soot formation, and other areas of industrial or environmental interest. Because such microkinetic models may contain up to thousands of reactions and species, constructing them by hand can be tedious and error-prone. Therefore many research groups have developed computer tools to automatically generate these mechanisms (Clymans and Froment, 1984; Chinnick et al., 1988; Hillewaert et al., 1988; Chevalier et al. 1990; Froment, 1991; DiMaio and Lignola, 1992; Quann and Jaffe, 1992; Blurock, 1995; Ranzi et al., 1995; Broadbelt et al., 1994; Prickett and Mavrovouniotis, 1997; Susnow et al., 1997; Warth et al., 2000; Battin-Leclerc et al., 2000; Battin-Leclerc, 2002). A key difficulty of these mechanism generation programs is that they produce large numbers of kinetically unimportant reactions and species. Therefore sometimes expert user involvement is employed to limit the size of the reaction network. Also several assumptions help to retain the mechanism within manageable sizes. The most important assumption is surely the μ radical hypothesis. This hypothesis assumes that bimolecular reactions can be neglected for radicals with more than 5 carbon atoms (Ranzi et al. 1983). The latter are also called μ radicals. Radicals that are only involved in bimolecular reactions such as the hydrogen radical, the methyl radical or the benzyl radical are called β radicals [βμ rules of Goldfinger-Letort-Niclause (Laidler, 1987)]. An intermediate category are βμ radicals such as the ethyl radical, which have a β character at low temperatures and a μ character at high temperatures. However the μ character of heavy radicals is not the only assumption made in the microkinetic model. In the next paragraphs the considered reaction families, the construction of the microkinetic model, the used assumptions and the proposed innovations are further discussed and evaluated.

2.2   Important Reaction Families

Generally a detailed reaction network is generated by allowing the feedstock components to react according to different reaction families. Examples are hydrogen abstraction reactions either

intra- and intermolecular, addition reactions (intra- and intermolecular) etc. Rice and coworkers (1931, 1934, 1943) showed that steam cracking of hydrocarbons proceeds through a free radical mechanism and that three important reaction families can be distinguished:

- Carbon-carbon and carbon-hydrogen bond scissions of molecules and the reverse radical-radical recombinations:

$$R_1 - R_2 \rightleftharpoons R_1^{\bullet} + R_2^{\bullet}$$
[2. 1]

- Hydrogen abstraction reactions, both intra- and intermolecular:

$$R_1 - H + R_2^{\bullet} \rightleftharpoons R_1^{\bullet} + R_2 - H$$
[2. 2]

- Radical addition to olefins and the reverse β scission of radicals, both intra- and intermolecular:

$$R_1^{\bullet} + R_2 = R_3 \rightleftharpoons R_1 - R_2 - R_3^{\bullet}$$
[2. 3]
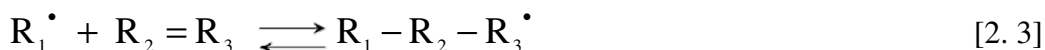
In the next paragraphs the importance of these three reaction families is discussed. Also several innovations such as removing all global reactions or adding new reaction families are discussed.

2.2.1   C-C and C-H bond scissions of molecules and radical recombinations

Steam cracking of hydrocarbons is initiated by breaking the molecule into radicals. n-Paraffins and olefins lead to the formation of 2 radicals, naphthenic compounds can lead to a biradical through ring opening. Substituted aromatics generally split off a small group in the side chain leading to a paraffinic radical and an aromatic radical. Evidently the scission of the bond occurs first on the weakest bond in the molecule. In other words, the scission of a molecule in which a more stable radical is formed is more favored. For example, in cracking of 2,2-dimethylbutane, the step yielding an ethyl and a t-butyl radical is the most favorable reaction. Also, in olefin and aromatic cracking, the C-C bonds in β position in respect to the double bond or phenyl ring always break predominantly because the presence of the double bond or phenyl ring weakens the bonds in β position.

Reaction	A (s^{-1})	n	E$_a$ (kJ mol^{-1})	k$_{(1073K)}$
n-hexaan $\rightarrow$ C$_5$H$_{11}^{\bullet}$ + CH$_3^{\bullet}$ (*)	2.6 10^{21}	-1.4	374	0.09
n-hexaan $\rightarrow$ C$_4$H$_9^{\bullet}$ + C$_2$H$_5^{\bullet}$ (*)	3.0 10^{23}	-2.0	369	0.24
n-hexaan $\rightarrow$ C$_3$H$_7^{\bullet}$ + C$_3$H$_7^{\bullet}$ (*)	1.7 10^{23}	-1.9	369	0.25
n-hexaan $\rightarrow$ C$_6$H$_{13}^{\bullet (p)}$ + H$^{\bullet}$ (*)	9.5 10^{17}	-0.7	412	6.9 10^{-5}
n-hexaan $\rightarrow$ C$_6$H$_{13}^{\bullet (s)}$ + H$^{\bullet}$ (*)	9.4 10^{15}	0.1	421	7.3 10^{-5}
1-butene $\rightarrow$ C$_3$H$_5^{\bullet}$ + CH$_3^{\bullet}$ (o)	1.7 10^{15}	0	306	2.1
1-butene $\rightarrow$ C$_2$H$_5^{\bullet}$ + C$_2$H$_3^{\bullet}$ (o)	1.3 10^{16}	0	383	1.6 10^{-2}
toluene$\rightarrow$ C$_6$H$_5^{\bullet}$ + CH$_3^{\bullet}$ (+)	1.0 10^{16}	0	427	1.6 10^{-5}
toluene$\rightarrow$ C$_7$H$_7^{\bullet}$ + H$^{\bullet}$ (+)	3.1 10^{15}	0	373	2.3 10^{-3}

Table 2.1: Kinetic parameters and corresponding reaction rate coefficients at 1073 K for the C-C and C-H scission reaction of n-hexane, 1-butene and toluene. [the modified Arrhenius equation is used for the reaction rate coefficient: k = A T^n exp(-E$_a$ /RT)] (*) Van Geem et al., 2006, (o) Plehiers (1991), (+) Bounaceur et al. (2000)

The C-C scission reactions and C-H scission reactions of molecules and the reverse recombination reactions are very important reactions for steam cracking because they determine the total radical concentration in the reaction mixture. Hence, these reactions determine to a large extent the rate of disappearance of the molecules. However, not all bond scission reactions of molecules should be considered. In Table 2.1 the rate coefficients at 1073 K of the C-C and C-H scission reactions of n-hexane are given. The reaction rates of the C-H scission reactions can be neglected compared to those of the C-C scission reactions. Apart from some exceptions, such as methane, C-H scission reactions of molecules should not be considered as a reaction possibility. Furthermore, not every C-C scission of a molecule should be incorporated in the microkinetic model. Indeed, the reaction rates of C-C scission reactions of molecules that lead to the formation of vinylic radicals are significantly slower than those that lead to alkyl radicals (Vercauteren, 1991). For example Table 2.1 shows that the reaction rate of the C-C scission reaction of 1-butene that leads to a vinyl and an ethyl radical is negligible compared to the reaction rate of the C-C scission reaction of 1-butene giving an allyl radical and a methyl radical.

Similarly, C-C scission reactions that lead to the formation of an arylic radical can also be neglected. For naphthenic compounds only C-C scissions of bonds of the paraffin side chain are considered. This assumption is a point of discussion because C-C scissions inside the ring lead to a biradical that forms relatively easily an α-olefin. The latter can react further and form other products. Especially for fractions with a significant amount of naphthenic compounds these reactions can become important (Plehiers, 1991).

In principle for every scission reaction of a molecule the reverse recombination has to be incorporated in the microkinetic model because the balance between scission and recombination reactions determines the total radical concentration in the reaction mixture. However, it is immediately clear that for μ radicals this is not necessary. These large radicals decompose much faster into olefins and β radicals than they recombine. The recombination reactions of the formed β radicals determine then the kinetic chain length. Hence, the recombination reactions of the μ radicals can be neglected without losing any accuracy.

2.2.2   Hydrogen abstraction reactions

In a hydrogen abstraction reaction a hydrogen atom is transferred from a molecule to a radical. This produces a new radical and a new molecule. The reaction rate coefficient of a hydrogen abstraction is determined by two factors, the nature of the abstracting radical (methyl, ethyl, etc) and the nature of the cracked C-H bond. It is well known that vinyl type and phenyl type radicals are the most active radicals, while allylic type of radicals are the most inactive, with benzyl in the same category. The activity sequence of the hydrocarbon radicals are in decreasing order (Chen, 1988):

vinyl > phenyl > hydrogen > methyl > primary > secondary > tertiary > allyl > benzyl
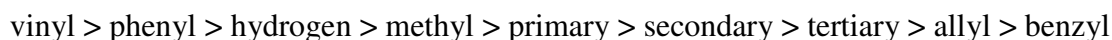
The strength of the C-H bond is characterized by its bond dissociation energy. In paraffins a distinction is made between primary, secondary and tertiary carbon atoms. The C-H bond strength decreases from primary to tertiary. Hence, the energy necessary to abstract a hydrogen atom from a molecule decreases from primary to tertiary. In olefins and aromatics the C-H bond in β position with respect to a double bond or a phenyl ring are weaker than any of the C-H bonds in the paraffinic molecules, while the bonds in α position are stronger.

Hydrogen abstractions are mainly important for β and βμ radicals. For μ radicals all bimolecular reactions and thus all hydrogen abstractions by these radicals can be neglected (Plehiers, 1989). In the original free radical mechanism of Rice and coworkers only hydrogen, methyl and ethyl radicals could abstract hydrogen atoms. However, abstraction reactions of other radicals such as the allyl radical or the benzyl radical are also important.

A special hydrogen abstraction reaction is an isomerization reaction. Here the radical abstracts a hydrogen atom from itself either via a five-membered ring transition state, i.e. 1,4 isomerization, or via a six-membered ring transition state, i.e. 1,5 isomerization. Taking into account 1,4 isomerization reactions is a first innovation to the microkinetic model because these reactions were not considered in the microkinetic model for heavy hydrocarbons generated by Vercauteren (1991). Considering only 1,4 and 1,5 isomerization reactions implies that isomerization reactions should only be considered for radicals with 5 or more carbon atoms. However the shift of i-propyl to n-propyl and the isomerizations between butyl radicals are repeatedly proposed in literature (Benson, 1976; Dente et al., 1979; Plehiers, 1989; Froment 1992). Benson proposed a triangular transition state but a number of intermolecular reactions could also explain the shift of i-propyl to n-propyl.

Isomerization reactions are very fast reactions, a lot faster than the following β scissions. Hence the isomers can be considered in equilibrium. For example, when octane is cracked several C8 radicals are formed and these interconvert into each other up to equilibrium (Chen, 1988). If an olefinic or a side chain of a substituted aromatic is long enough, intramolecular isomerization reactions are also possible for these species. However, since the double bond or phenyl ring stiffens the chain, the reaction rates of these reactions will be lower than that of the reaction rate of isomerization reactions of paraffinic radicals. In contrast with previous (Plehiers, 1989; Vercauteren, 1991) work these reactions are now considered to occur at finite rates in the microkinetic model.

Previously hydrogen abstraction reactions involving both a molecule and a radical or a single radical have been discussed. Another hydrogen abstraction reaction is a disproportionation reaction: a hydrogen abstraction reaction between either two molecules or two radicals. For example the disproportionations of two ethyl radicals is considered by Dente et al. (1979) in SPYRO:

$$C_2H_5{}^{\bullet} + C_2H_5{}^{\bullet} \underset{\longleftarrow}{\longrightarrow} C_2H_4 + C_2H_6$$
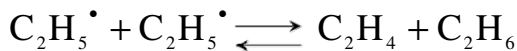
Allara and Shaw (1980) claim that the reaction rates of the disproportionation reactions between two radicals are generally an order of magnitude smaller than the rate of the recombination reactions of the same two radicals. The results of Kerr (1973) further indicate that disproportionation reactions are not important under the typical conditions used in steam cracking furnaces. Therefore, similar to Plehiers (1989) and Vercauteren (1991), all disproportionations are omitted in the microkinetic model. In Section 2.4.3 it is shown that indeed disproportionation reactions are not important for steam cracking.

2.2.3   β scission and addition reactions

In β scission reactions a large radical decomposes by scission of either the C-C bond or the C-H bond in β position, forming an olefin and a new radical. Just like the double bond and the phenyl-ring the uncoupled free electron strengthens the bonds in alpha position with respect to it and weakens the bond in β position. Baas (1963) showed that the bond in β position weakens 25 kJ mol^{-1}, while the bond in α position strengthens by the same amount. For the decomposition of a paraffinic radical the C-C bond in β position breaks dominantly although the scission of the C-H bond also occurs. In the case of olefinic radicals the scission does not necessarily occur in the C-C bond in β position of the free electron because the C-H in β position can be weaker (Chen, 1988). Substituted aromatic radicals split off a group in the side chain and preferably form an aromatic molecule with an olefinic side chain, e.g. styrene. The nature of the decomposing radical alone does not completely determine the reaction rate of the β scission. The rate depends also on the nature of the formed radical and the formed olefin. Indeed, comparing two β scissions of the same radical, the path leading to a conjugated diolefin is favored over the path forming an unconjugated diolefin. For the following sequence of the product radicals, the β scission rate decreases from left to right (Chen, 1988):

   vinyl and phenyl < hydrogen < methyl < primary < secondary < tertiary < allyl and benzyl

Similarly the rate for β scission increases from left to right in the following sequence of the formed olefin:

acetylene < ethylene < propylene < 2-butene < 2-methyl-2-butene < conjugated dienes

The reverse reaction of a β scission reaction of a radical is a radical addition reaction to an olefin. Radical addition reactions are important reactions because they are responsible for the production of heavier species that can ultimately lead to the formation of heavy products. If the radical adds to an asymmetric olefin the question arises where the addition will occur, and thus, which radical is favorably formed. It has been well established (Tedder and Walton, 1980) that for addition reactions the atoms and radicals preferentially add to the least substituted carbon atom of the double bond because of steric effects. For the additions on mono-substituted ethylene, the influence of the substituents on the orientation of the addition decreases progressively from left to right for the following substituents:

phenyl > vinyl > tertiary > secondary > primary > methyl > allyl > benzyl

If the olefin has two different substituents at two ends of the double bond, the addition on the end with the group on the right of the sequence is preferred.

Next to intermolecular addition reactions also intramolecular addition reactions are possible. Similar effects as those discussed for the intermolecular addition reactions are important for determining which radical is formed. For cyclizations always two reaction paths are possible:
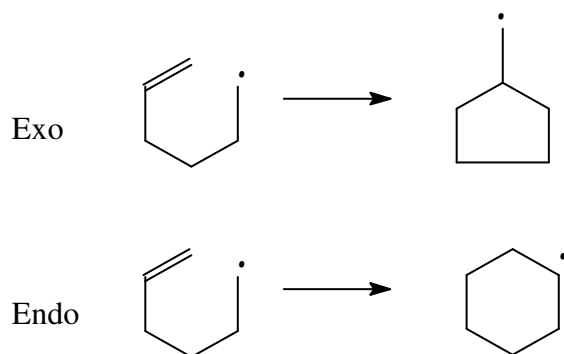
In the reaction product the radical is either outside of the ring (exo) or part of the ring (endo). The endo form is the enthalpically favored radical, while the exo form is entropically favored (Plehiers, 1991). Van Speybroeck et al. (2001) showed that the activation energy of the 1,6 cyclization is 30 kJ mol^{-1} lower than the activation energy of the corresponding 1,5 cyclization.

Therefore it is necessary to introduce separate kinetic parameters for 1,5- and 1,6- cyclizations. The latter is in contrast with previous work of Vercauteren (1991), who considered the exo and endo cyclization reactions always equally important.
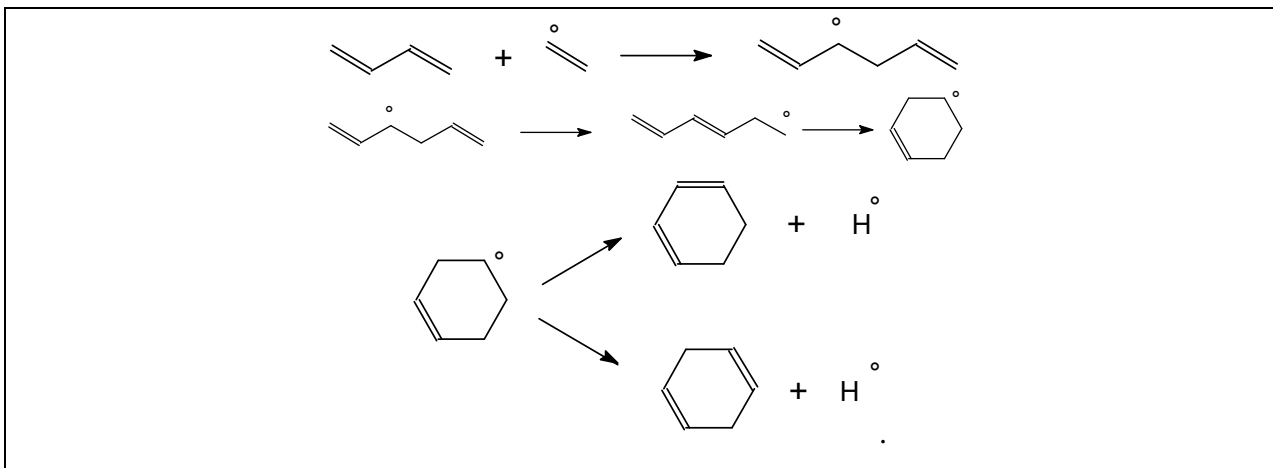
Figure 2.1: Formation of precursors of aromatic compounds starting from small olefins

Another group of addition reactions are the cycloaddition reactions. Here two molecules combine to form a ring. In these reactions two π-bonds are converted to two σ-bonds. The best known cycloaddition reactions are the Diels-Alder reactions. An important innovation to the microkinetic model is that no Diels-Alder reactions have been included in the microkinetic model, not even to describe the formation of aromatic compounds. Kopinke et al. (1983) found that under the standard conditions of steam cracking (T = 600 –900°C, p_t = 0.1 –0.3 MPa, res. time 0.1 – 1 s) Diels-Alder reactions and other molecular reactions are not the main route for the formation of aromatic compounds. In contrast to previous work aromatic compounds are formed via additions of radicals to olefins and di-olefins. In Figure 2.1 a set of addition reactions is shown which lead to precursors for benzene.

2.2.4   Other reaction families

Although the previous three reaction families are the dominant reaction families for steam cracking other reaction families can also become important. One of these reactions are electrocyclizations. An electrocyclic reaction is the concerted interconversion of a conjugated

polyene and a cycloalkene. Consider for example the following electrocyclic reaction of 1,3,5-hexatriene with the formation of 1,3 cyclohexadiene:
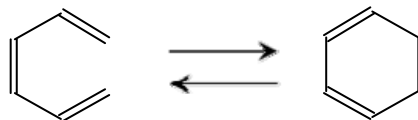
[2. 4]

Electrocyclizations are very fast reactions (Shiess and Dinkel, 1981) and are important routes towards the formation of aromatic compounds (Jutz, 1978; Kopinke et al., 1987). Therefore electrocyclic reactions are considered as a reaction possibility in this network.

Another reaction family that can be important under steam cracking conditions is a sigmatropic rearrangement. A sigmatropic rearrangement is a concerted intramolecular shift of an atom or a group of atoms. The best known sigmatropic rearrangement is the Cope rearrangement. Consider for example the rearrangement of 1,5-heptatriene in 3-methyl-1,5-hexadiene:
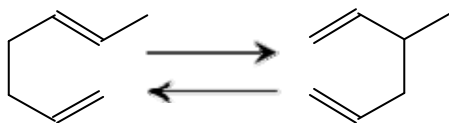
[2. 5]

Sigmatropic shifts can be clearly responsible for certain rearrangements in the product spectrum, however in this work they are not considered as a reaction possibility.

Although there is a general consensus about the free radical mechanism of Rice (1931, 1934, 1943) for cracking paraffins, this is not so when olefins are cracked (Plehiers, 1991). Olefins disappear via a combination of radical reactions and concerted molecular reaction pathways (Benson, 1970; Plehiers, 1991). The latter are mostly retro-ene reactions. The joining of a double or triple bond to an alkene reactant having a transferable allylic hydrogen is called an ene reaction. The reverse reaction is called a retro-ene reaction. Consider for example the retro-ene reaction of 1-hexene giving two propylene molecules:
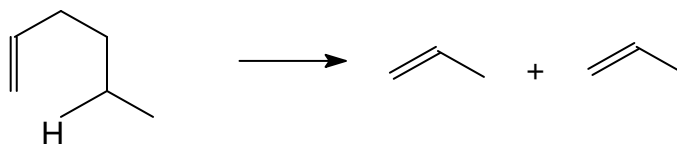
[2. 6]

Ranzi et al., (2001) and Warth et al. (1998) both consider this reaction family. Kopinke et al. (1983) found no indication that this reaction was important. However other authors such as Richard et al. (1978) found that retro-ene reactions were responsible for 10% of the formed long olefins. In the present work no retro-ene reactions are considered in the microkinetic model.

2.3   Reaction Network

2.3.1   Alternatives for reaction network construction

Several research institutions have generated detailed reaction networks for the steam cracking process. Most of that work was devoted to the study of the cracking behavior of single components, but these studies are generally of limited use. The petrochemical industry is more interested in fundamental simulation models for complex mixtures such as SPYRO (Van Goethem et al., 2001; Dente et al., 1979), CRACKER (Joo et al., 2000) and CRACKSIM (Clymans and Froment, 1984; Van Geem et al., 2004). The reaction network used in CRACKER is not as detailed as those used in either CRACKSIM or SPYRO. A lot of components and reactions are lumped in CRACKER, while the values of the kinetic parameters of many reactions are not physically possible. The construction of the CRACKSIM reaction network and the reaction network used in SPYRO is very similar. The CRACKSIM and SPYRO reaction networks are separated into two different sub networks: the C_4^- network and the C_5^+ network. This division is based on the assumption that monomolecular reactions dominate for large μ radicals (Ranzi et al., 1983). The C_4^- network consists of all the reactions of species with 4 or less carbon atoms. The C_5^+ network, also called the primary network or short PRIM (Wauters, 1997), decomposes a formed μ radical into olefinic products and C_4^- species and eliminates the concentrations of the intermediate μ radicals by assuming that they are in pseudo steady state. This method makes it possible to accurately describe the cracking behavior for feedstocks up to light naphtha, but for heavier feedstocks the description is incomplete. Many reactions of heavy

components are not considered by Plehiers (1989) nor Vercauteren (1991). This can be easily overcome by increasing the maximal carbon number of components included in the reaction network and introducing some new families of components like poly-aromatic and naphtheno-aromatic compounds. Another issue relates to the formation of heavier products formed from both light feedstocks as well as from heavy fractions. This is not that easily solved and requires fundamental changes to the construction of the microkinetic model and therefore different alternatives have to be evaluated.

One possibility has been implemented by De Buck (1999). De Buck extended the reaction network with a number of important reactions that lead to the build up of some heavy components, e.g. naphthalene. Some serious questions about this approach immediately arise, indeed it is surely not evident to define a priori all the reactions from feedstock molecules and intermediates to heavy products. As the cracking conditions vary some reactions gain importance while others become less important, and these differ as the feedstock composition changes. Furthermore, when a single reaction is added to the reaction network basically all the kinetic parameters should be re-estimated. This was not done by De Buck (1999). Moreover the values obtained for the kinetic parameters of some reactions are not physically reasonable.

A second alternative is the construction of the reaction network using a reaction order criterion (Broadbelt et al., 1994), so called rank based construction of a reaction network. Starting from the feedstock components a reaction network is generated. The feedstock molecules react according to the different reaction families and form a group of "new" species from 0-th order. The radicals and molecules react further and form first order species, and so on. The order of the products is the highest order of the reactants plus 1 for molecules and the highest order of the reactants for radicals, because radicals need an extra step to form molecules (Broadbelt et al., 1994). A problem of this type of approach is that in principle the reaction network can become infinite, because addition reactions continuously lead to the formation of new species not yet included in the reaction network. Broadbelt et al. (1994) eliminated this problem by using a carbon count stop criterion for the formed species to limit the network growth. The algorithm discussed here applied to ethane pyrolysis leads to a network of first order containing 29 species if the maximum carbon number of the species equals 3. It grows to 691 species if the reaction order grows to 5.
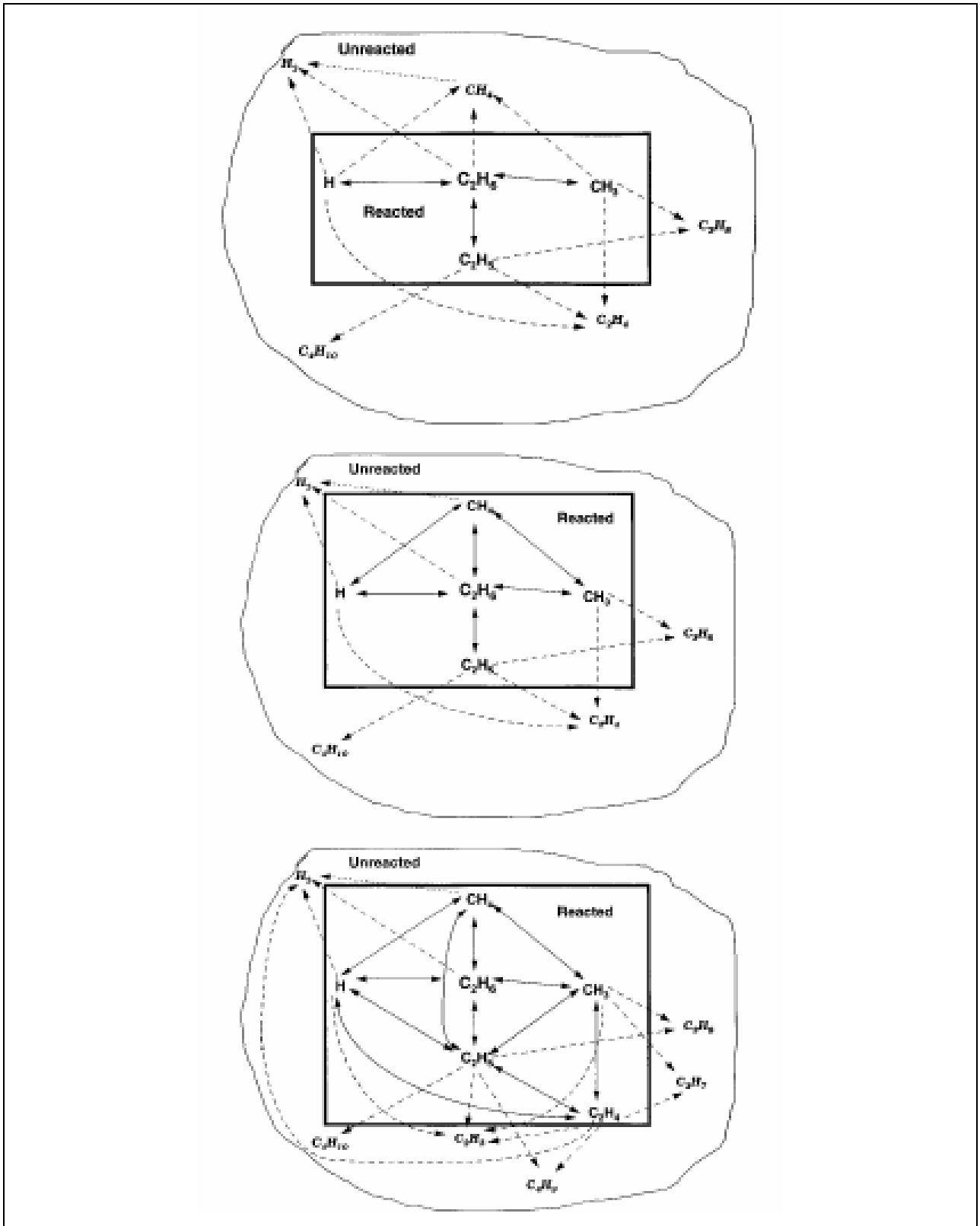
Figure 2.2: Rate-based network construction for ethane steam cracking (Susnow et al., 1997)

A third possibility is rate-based construction of kinetic models (Susnow et al., 1997; Song 2004; Van Geem et al., 2006). Here the reaction network is generated iteratively with a characteristic rate as yard stick. The principle of this method is illustrated in Figure 2.2. For a number of components the differential equations are solved, giving the concentration profiles of the different species. Next, a new reaction network of higher order is generated and based on the values of the kinetic parameters and the calculated concentration profiles of the reacting components, the rates of formation of the new components are calculated. If the maximum value of the rate of formation of the new species is higher than the characteristic rate of the system, the new species is added to the list of reacting components. With this new set of species a new reaction network is generated. In this way only species that react fast enough are included in the reaction network. A model for ethane cracking generated via the rate-based algorithm with as characteristic rate 0.01% of the rate of disappearance of ethane consists of 169 species.

A fourth alternative is developed by Klinke et al. (1997) for describing the cracking behavior of pentadecyl benzene based on the work of Turanyi (1990). Turanyi made a distinction between important, necessary and unnecessary species. The construction of the reaction network is similar as discussed in the previous paragraphs for the rate-based construction (Susnow et al., 1997) or the rank based construction of reaction networks (Broadbelt et al., 1994). However, the criterion to incorporate a new species in the reaction network is no longer based on a characteristic rate or the carbon number of a species but on the following value:

$$B_i = \sum_{n=1}^{N} \frac{\partial \ln R_{V,n}(t)}{\partial \ln c_i(t)} \qquad\qquad [2.7]$$

with $c_i(t)$ the concentration of a possible new component i and $R_{V,n}(t)$ the net rate of production of a species n already included in the reaction network, i.e. a species considered important or necessary in the reaction network.

The group in Nancy (Warth et al., 1998; Battin-Leclerc et al., 2000; Warth et al., 2000; Battin-Leclerc, 2002) used another approach to automatically generate detailed mechanisms for combustion problems. In EXGAS (Warth et al., 1998; Battin-Leclerc et al., 2000) a reaction network is made of three parts: a C_0-C_1-C_2 reaction base, a computer generated primary mechanism (only the species in the initial mixture are considered as reactants), and a computer

generated secondary mechanism comprising reactions whose reactants are the molecular products of the primary mechanism, see Figure 2.3.
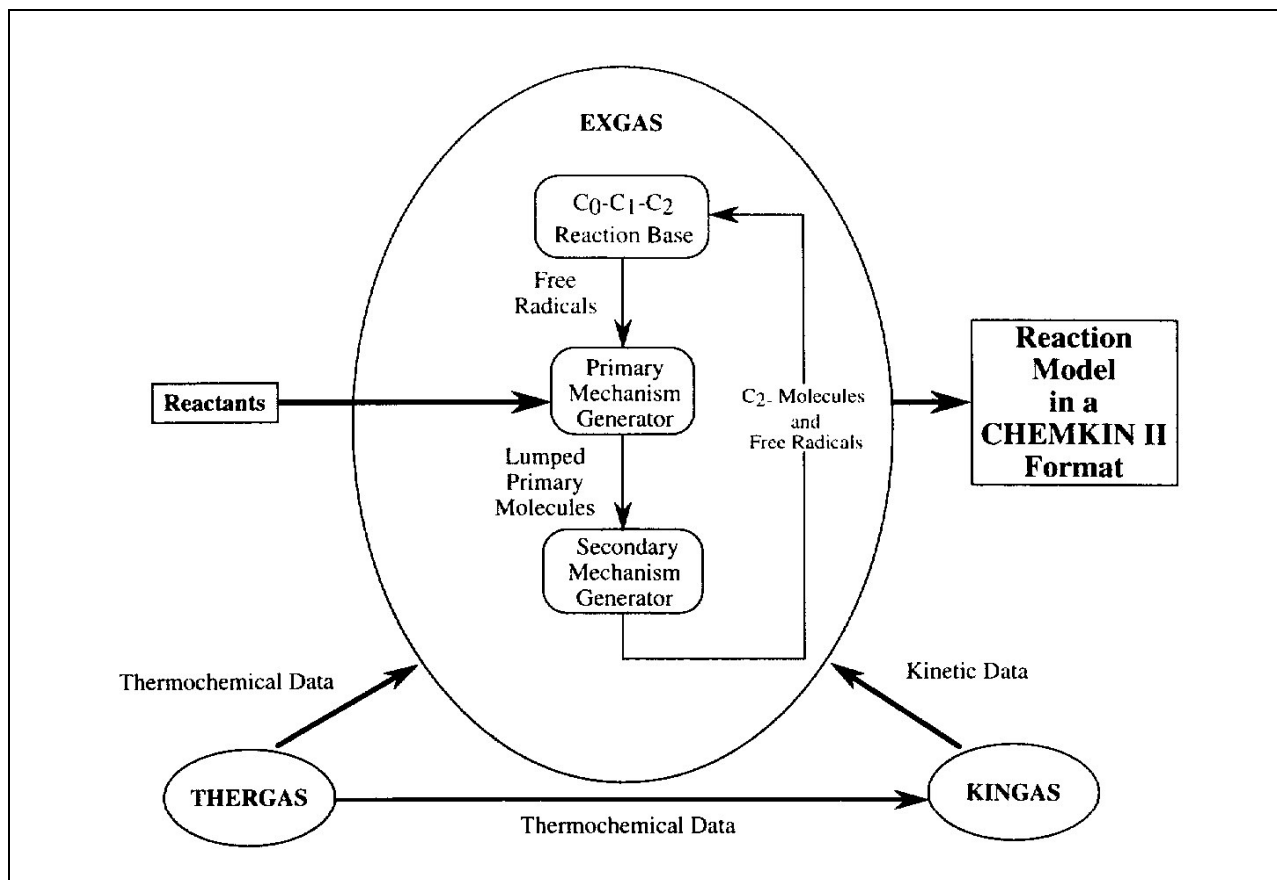
Figure 2.3: Global scheme of the reaction network generation software EXGAS (Warth et al., 1998)

It is obvious that the presence of oxygen in the reaction mixture makes reaction network generation more complex: more reaction families and species need to be considered, finding an unique representation of species becomes more difficult, etc. Nevertheless this kind of network construction (separating the reaction network in different parts) shows similarities with the previously discussed methods for generating reaction networks for steam cracking (Van Goethem et al., 2001; Dente et al., 1979; Clymans and Froment, 1984). Moreover, in EXGAS also the βμ rules of Goldfinger-Letort-Niclause (Laidler, 1987) are applied.

The last method (Warth et al., 1998; Battin-Leclerc et al., 2000) shows that a separation of the reaction network in different parts and using the βμ rules of Goldfinger-Letort-Niclause (Laidler, 1987) is still an attractive option. The other alternatives (Broadbelt et al., 1994; Susnow et al., 1997; Song 2004; Klinke et al., 1997) are also interesting options but they have two common disadvantages making them unattractive; these methods are time-consuming and a generated network for a particular system has a limited application range. By the latter is meant that a network is only valid for a particular set of conditions and a particular feedstock, and hence, new networks need to be generated almost continuously. For light feedstocks such as ethane this is not such a dramatic problem, but as the feedstocks get heavier the time to generate the reaction network grows, and thus a lot of time is wasted. Moreover, although for example rate-based construction of reaction networks leads to significantly smaller networks, still a lot of unimportant reactions are included (Van Geem et al., 2006). The latter is discussed in Section 2.4. That is why for the generation of the new network none of the previously discussed approaches is implemented. Instead an approach similar to the one implemented by Plehiers (1989) and Vercauteren (1991) seems more appropriate. In the next paragraph the construction of the new reaction network is discussed in detail.

2.3.2   Network Construction

Developing a detailed reaction network is a major challenge. On the one hand the size of the reaction network can become huge as the number of reactions and species increases exponentially with the average carbon number of the feedstock (Broadbelt et al., 1994). On the other hand, developing these reaction networks implies that both the thermo-chemistry and kinetic parameters are known. Fortunately it can be safely accepted for steam cracking that monomolecular reactions dominate for species with more than 5 carbon atoms (Ranzi et al., 1983). This allows distinguishing between two networks: the monomolecular μ network and the β network, which contains both uni- and bimolecular reactions. The kinetics for the former can be described by analytical expressions based on the pseudo steady state assumption (PSSA) for the radical reaction intermediates (Hillewaert et al., 1988). In Table 2.2 the rate estimates for the reactions of the 2-methylhept-1-yl radical are shown. The reaction rates at 1073 K show that unimolecular β scissions are significantly faster than the other bimolecular reaction possibilities.
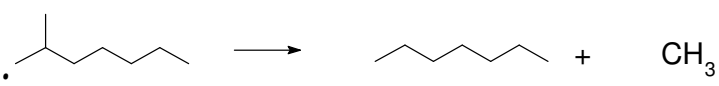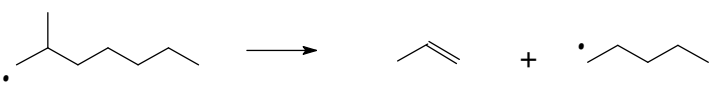
1073 K	O(k)	*	O(C)	=	O(k')
[β scission reaction: 2-methylheptyl radical → heptene + CH$_3$]	10^7				
[β scission reaction: 2-methylheptyl radical → alkene + pentyl radical]	10^6	*	1	=	10^7
Hydrogen Abstraction	10^6	*	10^{-2}	=	10^4
Addition	10^5	*	10^{-3}	=	10^2
Recombination	10^8	*	10^{-7}	=	10^1

Table 2.2: Estimates for the values of the reaction rates of the 2-methylhept-1-yl radical [O(k): the order of the reaction rate coefficient k. O(k) and O(k') are calculated based on the following expressions: β scission $r_{V,\beta} = k_\beta\, C_R$; abstraction $r_{V,ab} = (k_{ab}\, C_F)\, C_R = k_{ab}'\, C_R$; addition $r_{V,ad} = (k_{ad}\, C_{ol})\, C_R = k_{ad}'\, C_R$; recombination $r_{V,rec} = (k_{rec}\, C_{R\beta})\, C_R = k_{rec}'\, C_R$]
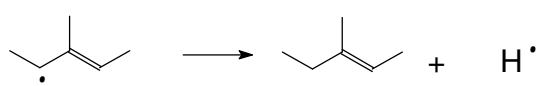
1073 K	O(k)	*	O(C)	=	O(k')
[β scission reaction: 3-methyl-3-pentene-2-yl radical → diene + H$\cdot$]	10^2	*	1	=	10^2
Hydrogen Abstraction	10^3	*	10^{-2}	=	10^1
Addition	10^6	*	10^{-3}	=	10^3
Recombination	10^8	*	10^{-7}	=	10^1

Table 2.3: Estimates for the values of the reaction rates of the 3-methyl-3-pentene-2-yl radical [O(k): the order of the reaction rate coefficient k. O(k) and O(k') are calculated based on the following expressions: β scission $r_{V,\beta} = k_\beta\, C_R$; abstraction $r_{V,ab} = (k_{ab}\, C_F)\, C_R = k_{ab}'\, C_R$; addition $r_{V,ad} = (k_{ad}\, C_{ol})\, C_R = k_{ad}'\, C_R$; recombination $r_{V,rec} = (k_{rec}\, C_{R\beta})\, C_R = k_{rec}'\, C_R$]

For species with 5 or less carbon atoms the µ radical hypothesis does not hold, making it no longer possible to use the analytical expressions based on the PSSA. Therefore it is necessary to stock their reactions in a separate sub network; the β network. It is immediately clear that the separation of radicals into µ, β and βµ radicals based on the number of carbon atoms is very

rough. Several exceptions on this rule of thumb exist, e.g. the benzyl radical, but according to the previously defined rule they are not considered in the β network. Also several other radicals can have both a β and μ character, such as radicals with no possibility of C-C scissions and no possibility of isomerization followed by a C-C scission. Consider the 3-methyl-3-pentene-2-yl radical. The radical can only decompose via a slow C-H scission, but this reaction path is not the dominant disappearance route. In Table 2.3 the estimates of the rate of disappearance of this radical show that addition reactions can be much more important under steam cracking conditions than scission reactions. A similar reasoning also holds for the 1-phenyl-2-pentene-4-yl radical. Hence, some radicals with more than 5 carbon atoms cannot be considered as pure μ radicals without introducing errors.
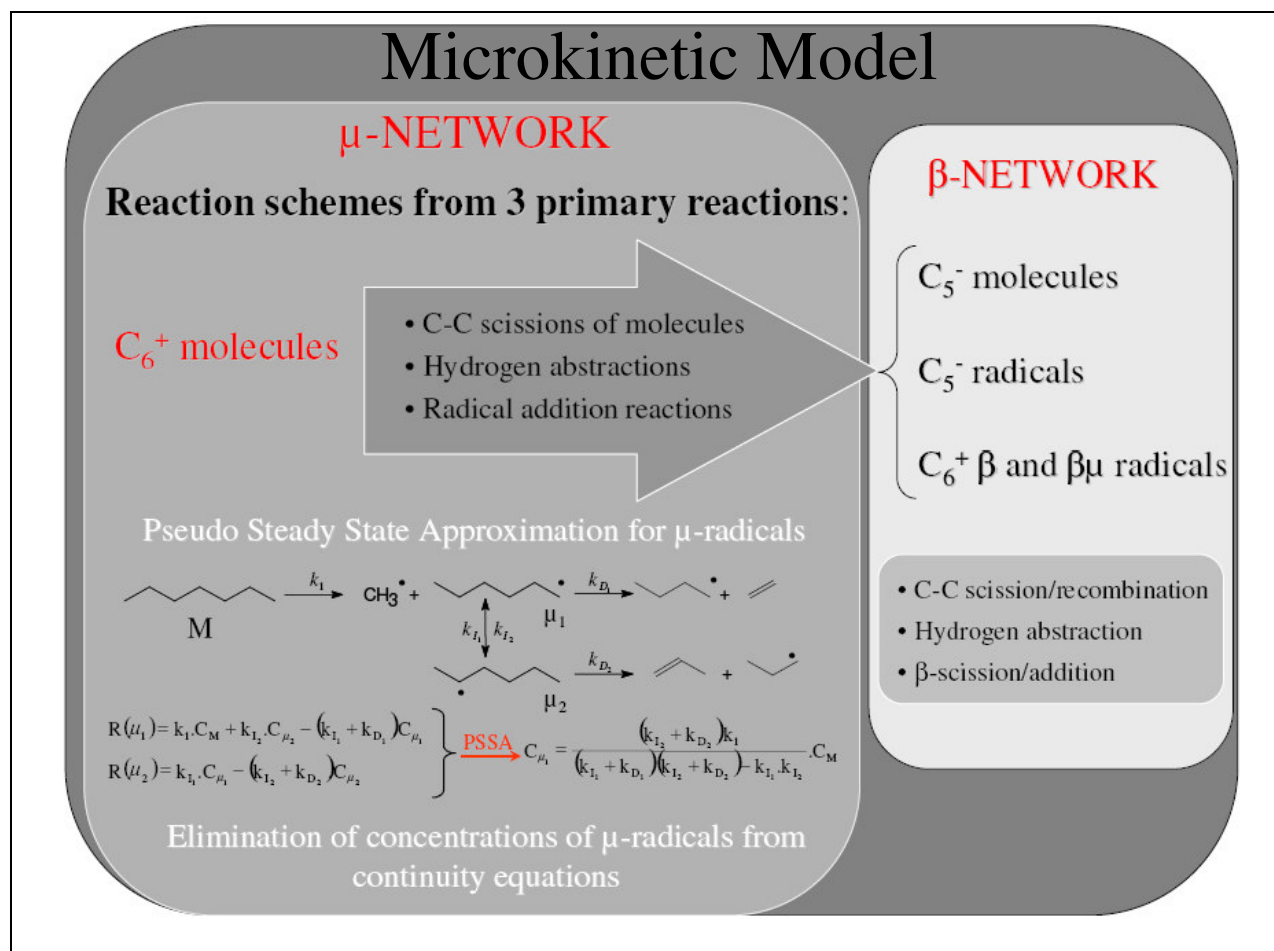
Figure 2.4: Overview of the construction of the single event microkinetic model. Interaction of the μ network with the β network

The previous results show that the separation of radicals into μ, β and βμ radicals based on the number of carbon atoms is too rough. Therefore it is necessary to introduce another category of radicals; the so called C_6^+ β and βμ radicals. For the latter the bimolecular reactions such as addition reactions and hydrogen abstraction reactions are not negligible, and consequently these reactions should be included in the β network. The β network further includes the reactions of the smaller radicals. In Figure 2.4 an overview is given of the construction of the complete microkinetic model. In the μ network reaction schemes are generated for all molecules with 6 or more carbon atoms. There are 3 primary reactions considered in the μ network: C-C scission reactions of molecules, hydrogen abstractions by β and βμ radicals and C_6^+ β and βμ radicals, and radical addition reactions by β and βμ radicals and C_6^+ β and βμ radicals. The concentrations of the intermediate μ radicals are eliminated by assuming the PSSA for these radicals. The β scission of the formed μ radicals is stopped when only olefins and radicals from the β network remain.

2.3.3   Generation of the β network

The β network considers all reactions from the three reaction families for species with 5 or less carbon atoms. This results in a large number of radical intermediates and elementary reactions. Therefore a computer program is developed that generates the β network automatically based on the binary relation matrix concept. In this concept the cracking rules are translated into matrix operations performed on the Boolean relation matrix, representing the species structure (Hillewaert et al., 1988). The construction of the reaction network is shown in Figure 2.5. Starting from an initial pool of molecules, possibilities for scission reactions, hydrogen abstraction reactions and addition reactions are identified. Cyclization reactions are considered as intramolecular additions, while isomerization reactions are considered as intramolecular hydrogen abstractions. For every forward reaction introduced in the network the corresponding reverse reaction is also incorporated in the network. These reactions result in a number of formed radicals and molecules. The new radicals are added to the radical pool and the molecules are added to the molecule pool. In the next iteration the new species react with each other and with other species of the radical and molecule pool and the network is constructed gradually. To limit the number of reactions a carbon count stop criterion is applied (Broadbelt at al., 1994), i.e.

species are only added when they have less than n_m carbon atoms for a molecule, and n_r carbon atoms for a radical. Here, both n_m and n_r are set equal to 5. The resulting β network comprises more than 2000 reactions and over 500 species. This is a drastic expansion compared to the work of Plehiers (1989) or Vercauteren (1991). Their β network contained only 500 reactions and considered almost no reactions involving species with 5 carbon atoms.
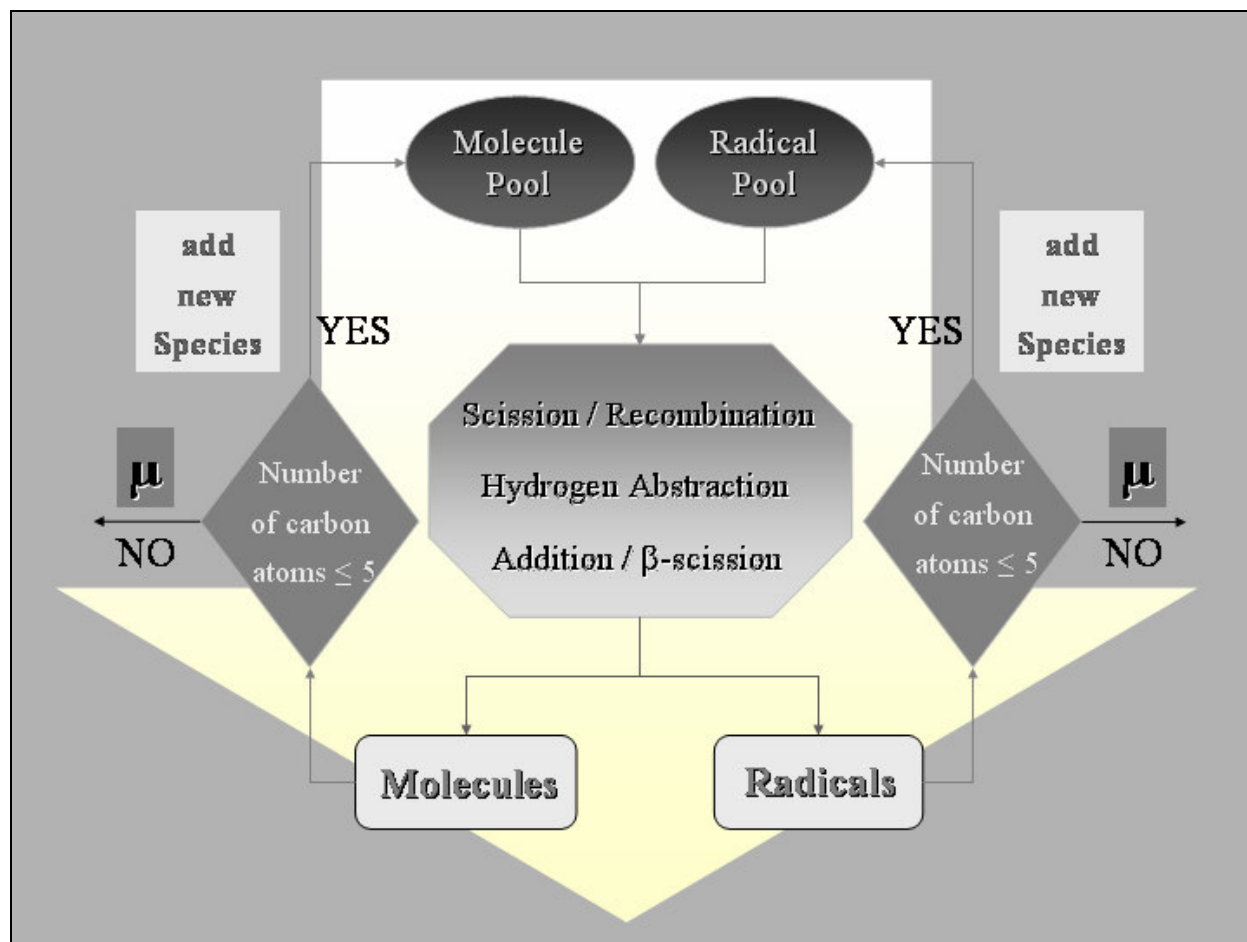
Figure 2.5: Generation of the β network

2.3.4   Generation of the μ network

The existence of radicals with a pure μ character is essential for separating the reaction network into two parts: a β and a μ network. As stated earlier for radicals with a μ character the monomolecular β scission and isomerization reactions are much faster than the bimolecular

hydrogen abstraction and addition reactions. Clymans and Froment (1984) and Hillewaert et al. (1988) concluded based on experimental results that this assumption surely holds for heavy paraffinic and iso-paraffinic radicals. Under typical steam cracking conditions these authors observed no saturated products with a chain length of more than 5 carbon atoms, except for non-converted feedstock molecules. For example during the cracking of n-decane neither n-nonane, n-octane, n-heptane nor n-hexane are found in the product spectrum. Moreover, no 1-decene is experimentally observed. This product could be formed after addition of a primary decyl radical to ethylene followed by a β scission of the resulting dodecyl radical.

The existence of radicals with a pure µ character enable the generation of reaction schemes for these radicals describing their disappearance via a set of monomolecular reaction steps. Because they are only involved in monomolecular reactions, the resulting set of differential equations for the µ radicals is linear in their concentrations. These concentrations can then be easily eliminated of the set of model equations if the pseudo steady state is assumed for the concentrations of the µ radicals. This hypothesis assumes that the net rate of formation of highly reactive reaction intermediates in a reaction sequence equals zero (Bodenstein and Lutkemeyer, 1924). The unknown concentrations of the reactive reaction intermediates can then be found as the solution of the set of linear model equations. In the next few paragraphs both the generation of the reaction schemes starting from different primary reactions as well as the elimination of the concentrations of the intermediate µ radicals are illustrated by some examples. Also important aspects such as the additivity of the reaction schemes and calculation of the pseudo rate coefficients are briefly discussed. The reader is referred to Vercauteren (1991) for more details.

2.3.4.1 *Reaction schemes from C-C scission reactions, hydrogen abstractions and addition reactions*

Three primary reactions are considered in the µ network: C-C scission reactions of molecules, hydrogen abstraction reactions by β and βµ radicals and addition reactions to olefins by β and βµ radicals. Based on these three primary reactions a reaction network is generated for each molecule with 6 or more carbon atoms. These three primary reactions all lead ultimately to the formation of a number of µ radicals which decompose via β scissions and isomerization reactions to olefins and β and βµ radicals. The set of linear algebraic equations is solved via the simple Gauss-Jordan elimination. The reaction scheme for the disappearance of a component is

in fact reduced to a simple format in which only the component and the products, formed via the monomolecular reactions, are considered. In Figure 2.6 an example of a reaction scheme generated for n-nonane is shown starting from the C-C scission reactions of this molecule.
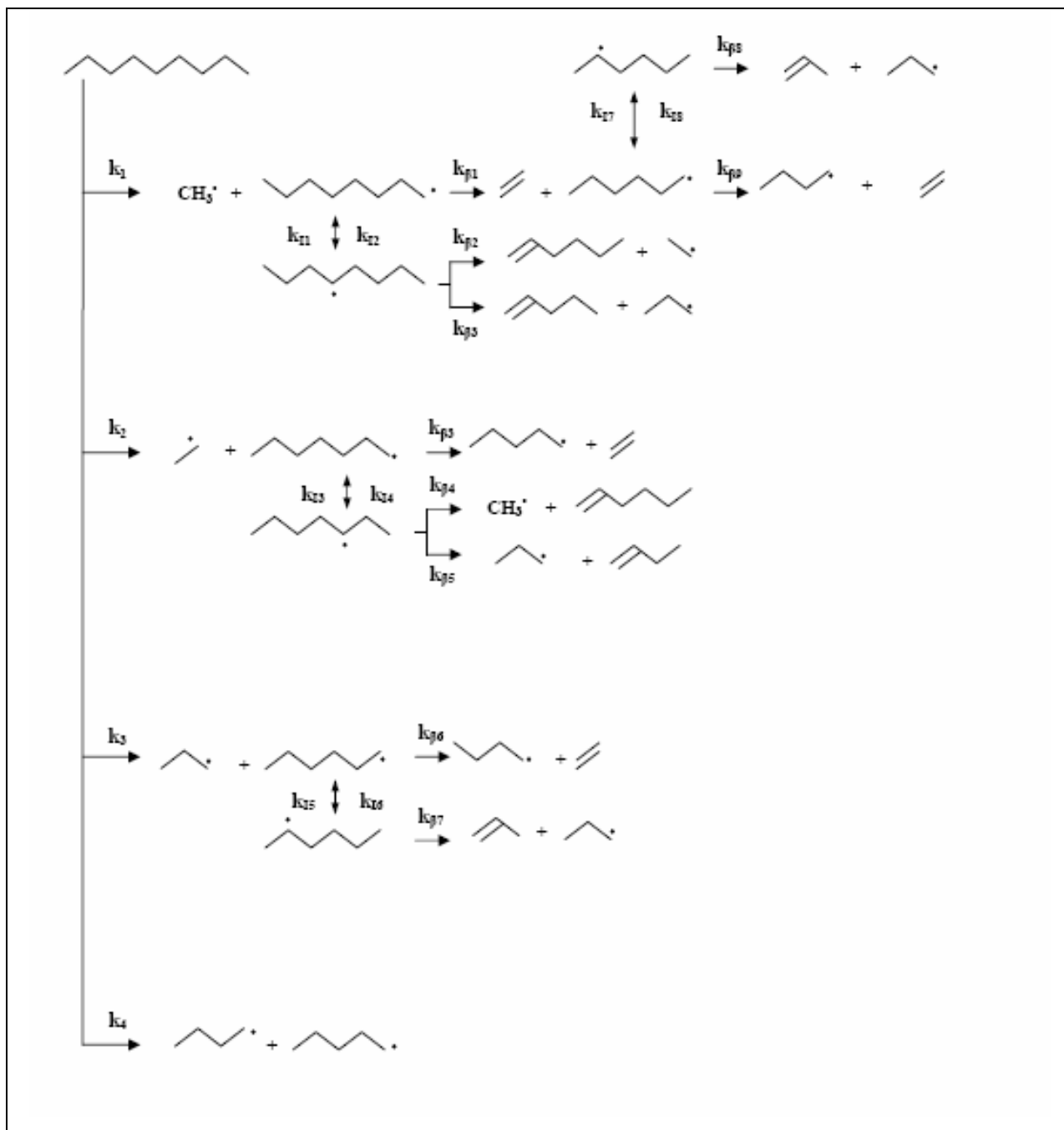
Figure 2.6: Reaction scheme for n-nonane starting from a C-C scission reaction

The initiation occurs through the cleavage of a C-C bond, resulting in two radicals. These radicals react further in the propagation reactions. C-H scission is not considered, since the reaction rate coefficients for C-H scission reactions of paraffins are much smaller than the reaction rate coefficients of C-C scission reactions of molecules, see Table 2.2 in Section 2.3.2. The disappearance rate of n-nonane (M) by C-C scission is according to the reaction scheme in Figure 2.6:

$$R_V(M) = \left(\sum_{i=1}^{4} k_i \right).C_M \qquad [2.8]$$

The net formation rate of the 1-octylradical (μ_1) from n-nonane by initiation and the formation rate of the 3-octylradical (μ_2) by isomerization from μ_1 can be written as:

$$R_V(\mu_1) = k_{I_1}.C_M + k_{I_2}.C_{\mu_2} - \left(k_{I_1} + k_{D_1} \right)C_{\mu_1} \qquad [2.9]$$

$$R_V(\mu_2) = k_{I_1}.C_{\mu_1} - \left(k_{I_2} + k_{D_2} \right)C_{\mu_2} \qquad [2.10]$$

Taking into account the hypothesis of the pseudo steady state approximation, the net formation rates of the μ radicals can be set equal to zero:

$$R_V(\mu_1) = R_V(\mu_2) = 0 \qquad [2.11]$$

The set of equations [2.9] – [2.10] can be solved for the concentrations of μ_1 and μ_2:

$$C_{\mu_1} = \frac{\left(k_{I_2} + k_{D_2} \right).k_1}{\left(k_{I_1} + k_{D_1} \right).\left(k_{I_2} + k_{D_2} \right) - k_{I_1}.k_{I_2}}.C_M \qquad [2.12]$$

$$C_{\mu_2} = \frac{k_1.k_{I_1}}{\left(k_{I_1} + k_{D_1} \right).\left(k_{I_2} + k_{D_2} \right) - k_{I_1}.k_{I_2}}.C_M \qquad [2.13]$$

The concentrations of the other μ radicals can be derived according to a similar procedure. In general, the following form is obtained:

$$C_{\mu_i} = F_i.C_M \qquad [2.14]$$

The factor F_i is the ratio of sums and products of reaction rate coefficients and is temperature dependent. The 1-octylradical decomposes to an ethylene molecule and a 1-hexylradical (μ_1'). The formation rates for the descendants by β scission of the 1-octylradical are:

$$R_v(C_2H_4) = R_v(\mu_1') = \frac{k_{D_1}.(k_{I_2} + k_{D_2}).k_1}{(k_{I_1} + k_{D_1}).(k_{I_2} + k_{D_2}) - k_{I_1}.k_{I_2}} C_M \qquad [2.15]$$

k_{D1} F_1 is defined as the pseudo rate coefficient (PRC) of formation of ethylene from n-nonane. Figure 2.6 shows that ethylene can also be formed along other reaction paths in the reaction scheme. The total PRC for formation of ethylene starting from initiation of n-nonane is a sum of terms. These terms originate from the formation rates of ethylene by cleavage of radicals formed out of n-nonane or by cleavage of other intermediate radicals. The μ radicals among the descendants, such as n-heptyl and n-hexylradicals, are treated in a similar way. For each group of isomer μ radicals, the set of continuity equations has to be solved. The rates of formation of the formed olefins and β radicals can then finally be written as:

$$R_v(O_j) = k^{pseudo}(O_j).C_M \qquad [2.16]$$

$$R_v(\beta) = k^{pseudo}(\beta).C_M \qquad [2.17]$$

in which M is the molecule that is initiated, while $k^{pseudo}(O_j)$ and $k^{pseudo}(R_l)$ are pseudo rate coefficients for the formation of an olefin and a β or $\beta\mu$ radical. The scheme in Figure 2.6 can formally be written as a single global reaction:

$$n\,C_9H_{20} \rightarrow \sum_{j=1}^{n_{ol}} \frac{k^{pseudo}(O_j)}{\left(\sum_{i=1}^{4}k_i\right)} O_j + \sum_{l=1}^{n_{rad}} \frac{k^{pseudo}(\beta)}{\left(\sum_{i=1}^{4}k_i\right)} \beta \qquad [2.18]$$
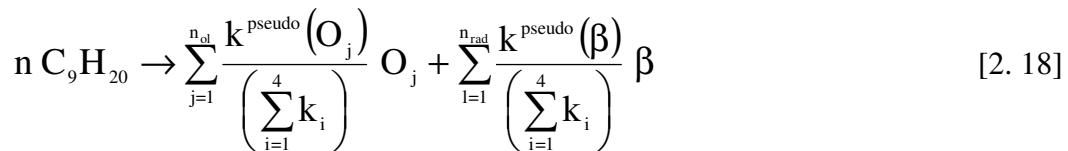
Similar to the reaction scheme generated for n-nonane in Figure 2.6 other reaction schemes can be generated starting from a different primary reaction such as a hydrogen abstraction reaction by a β radical or an addition reaction to an olefin. In Figure 2.7 an example is given of a reaction scheme generated for 1-heptene starting from an addition reaction. The addition of β or βμ radicals to a double bond almost always gives two different radicals, depending on the double bonded carbon atom with whom the radical is connected. When a radical adds to an olefin, the radical itself is incorporated in the final structure. This implies that the nature of the radical is of great importance. Next to the addition of hydrogen and methyl radicals, also the addition of other β and βμ radicals is taken into account.

If the double bond is in β position of the free electron, a resonance stabilized radical is formed. In previous work mesomerization reactions were considered as a separate reaction family with a set of corresponding kinetic rate coefficients (Plehiers, 1989; Vercauteren, 1991). This is clearly incorrect and mesomerization reactions are no longer considered as a separate reaction possibility. In Chapter 3 more detail is given how the species are represented and how reaction possibilities are identified to account for resonance. The β scission of the resonance stabilized radical is possible if a C-C bond is in β position.

A supplementary reaction possibility in Figure 2.7 is the formation of cyclic radicals. The competition of cyclization reactions with β scission reactions is of great importance for the formation of cyclic products in the cracking scheme. These cyclic products are important precursors for the coke formation (Kopinke et al., 1988). Ring closure of olefinic radicals can occur if the free electron is five or six carbon atoms from the double bonded carbon atom. These internal radical additions are thermodynamically favored for a six ring, since the ring tension in a six ring is much smaller than in a five ring. If however the free radical is outside the ring after cyclization, the 1,5 cyclization is kinetically favored with regard to the 1,6 cyclization (Walsh, 1970; Van Speybroeck et al., 2004). For example consider the cyclization of the 7-heptenylradical leading to the formation of a methylcyclohexylradical. This cyclic radical can decompose into the original olefinic radical by cleavage of the ring in the C-C bond that is in β position of the free electron. Since this is a quasi equilibrated reaction, the cleavage of the C-H bond in β position of the free electron is no longer negligible and should be considered.
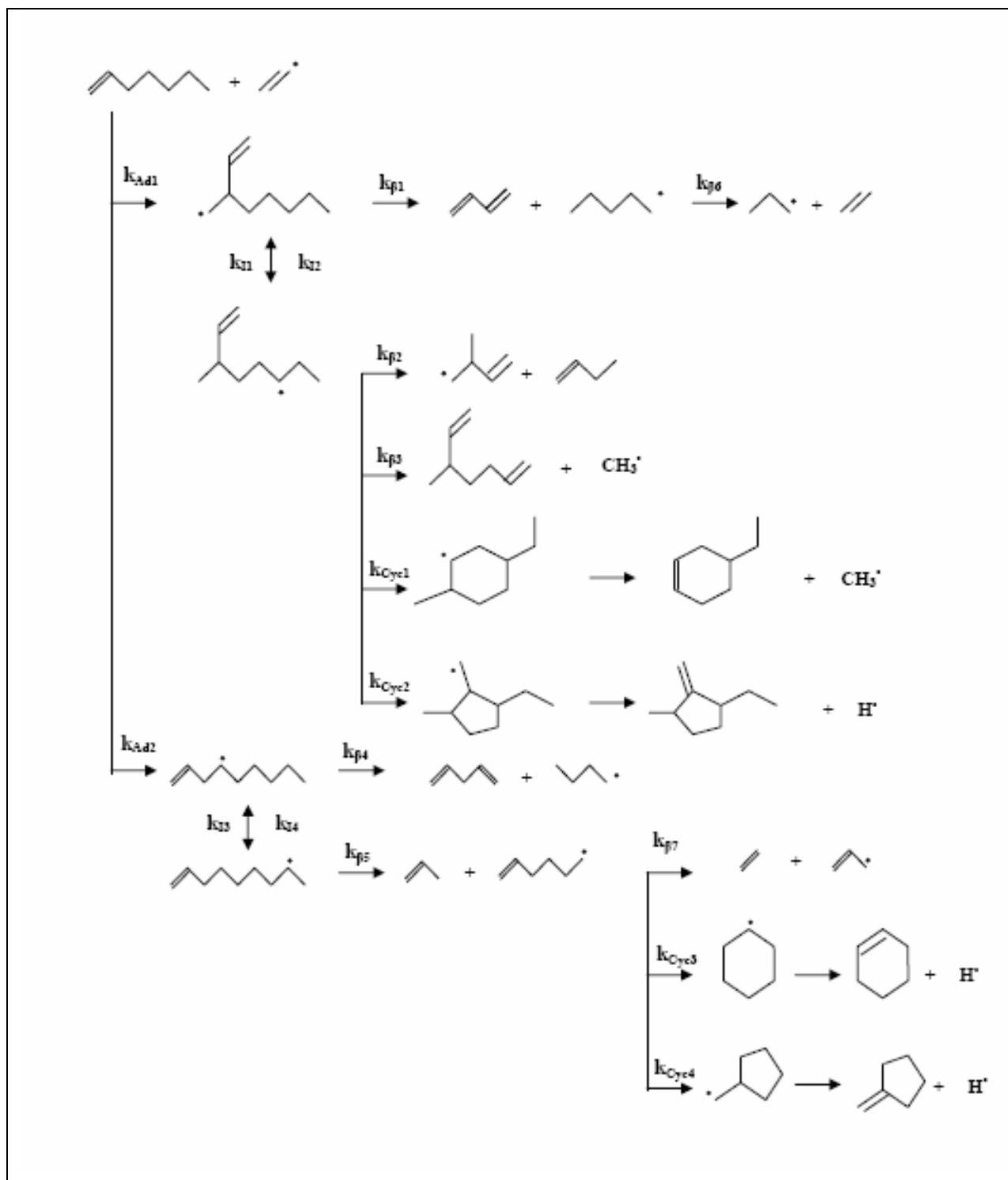
Figure 2.7: Reaction scheme for 1-heptene starting from vinyl addition

In the reaction scheme of Figure 2.7 the β scissions of the cyclic radicals that do not give two products are neglected. The cleavage of a C-C bond in the ring requires more energy than that of an aliphatic C-C bond (Stein and Rabinovitch, 1975). The above hypothesis also implies that the rate of the reversible reaction:

$$\text{ring closure} \; \rightleftharpoons \; \text{ring opening} \qquad\qquad [2.\,19]$$

is smaller than the rate of cleavage of a C-H bond in the ring. For the consecutive reactions

$$\text{olefinic radical} \rightleftharpoons \text{cyclic radical} \; \rightarrow \; \text{cyclic olefin} + H^\bullet \qquad [2.\,20]$$
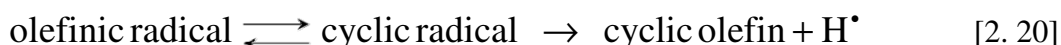
the concept of the rate-determining step can be applied. The above reaction sequence can be reduced to the simple reaction:

$$\text{olefinic radical} \; \rightarrow \; \text{cyclic olefin} + H^\bullet \qquad\qquad [2.\,21]$$
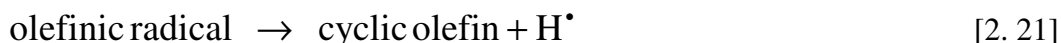
in which the kinetics are determined by the slowest step in the sequence, i.e. the cyclization reaction. Vercauteren (1991) eliminated all cyclic olefins from the reaction schemes by applying the PSSA for their concentrations and assuming that hydrogen abstraction reactions are the only mode of disappearance. Indeed, when not a lot of naphthenes, are present in the feedstock the concentration of the cyclic olefins is much lower than the concentration of the aliphatic olefins and the concentrations of the cyclic olefins can be eliminated without losing accuracy. However, for a feedstock containing a significant amount of naphthenes this is no longer true. Therefore the formed cyclic olefins are now considered as products in the reaction schemes. One of the difficulties of introducing cyclic olefins is that they have in comparison to aliphatic olefins much more isomers. These isomers originate in the cracking by hydrogen shifts and sigmatropic shifts. Hence, the number of components considered in the reaction network is drastically increased.

2.3.4.2 *Additivity of reaction schemes*

It is clear from the previous paragraphs that for a mixture of heavy hydrocarbons it is very unlikely that one particular μ radical, e.g. the primary hexyl radical, is considered in only a single reaction scheme. For example the primary hexyl radical can be formed via a hydrogen abstraction reaction by a β radical from n-hexane or via the β scission of a primary octyl radical.

Elimination of these intermediate μ radicals is then only possible when their concentrations are known for the complete reaction network. This implies that for almost every new feedstock a new reaction network would have to be generated, making the simulation program unattractive for industrial practice. The question arises if it is not possible to separate the complete reaction scheme into smaller sub-schemes where the PSSA is applied for the μ radicals. Consider the simplified reaction scheme in equation [2.22], where a μ radical is formed via three reactions:

$$\begin{matrix} \mathbf{A} \\ \mathbf{B} \\ \mathbf{C} \end{matrix} \quad \longrightarrow \mathbf{\mu} \quad \xrightarrow{\mathbf{k_\beta}} \quad \mathbf{O} + \mathbf{\beta} \qquad [2.22]$$
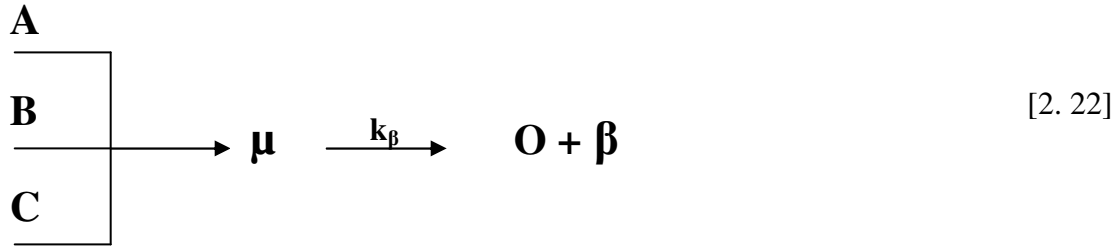
The continuity equation for the μ radical can be written as follows if the PSSA is assumed:

$$R_{VA} + R_{VA} + R_{VA} = k_\beta C_\mu \qquad [2.23]$$

Separating the scheme of equation [2.22] in three sub-schemes leads to:

$$\begin{matrix} \mathbf{A} \longrightarrow \mathbf{\mu} \xrightarrow{\mathbf{k_\beta}} \mathbf{O} + \mathbf{\beta} \\ \mathbf{B} \longrightarrow \mathbf{\mu} \xrightarrow{\mathbf{k_\beta}} \mathbf{O} + \mathbf{\beta} \\ \mathbf{C} \longrightarrow \mathbf{\mu} \xrightarrow{\mathbf{k_\beta}} \mathbf{O} + \mathbf{\beta} \end{matrix} \qquad [2.24]$$
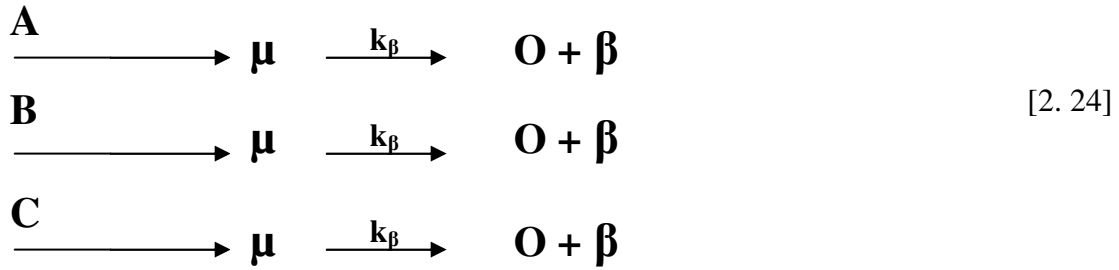
Applying the PSSA to each of the smaller reaction schemes leads to 3 continuity equations for the μ radical:

$$R_{VA} = k_\beta C_\mu^A$$

$$R_{VB} = k_\beta C_\mu^B \qquad [2.25]$$

$$R_{VC} = k_\beta C_\mu^C$$

Because the concentration of the μ radical in the global reaction scheme is equal to the sum of the concentrations of the μ radicals in the different subsystems, equation [2.26] holds:

$$C_\mu = C_\mu^A + C_\mu^B + C_\mu^C$$ [2. 26]

Combining equation [2.25] with equation [2.26] leads to equation [2.23]. Hence, the sum of the rates of formation in the sub-schemes equals the rate of formation of the global reaction scheme.

The previous principle can be extended to the reaction schemes discussed in the previous sections. Therefore, nevertheless that the reaction schemes are interconnected via the intermediate μ radicals and olefins, still the reaction network describing the cracking of a hydrocarbon mixture follows from the sum of the reaction schemes of the individual components. If the expression for the rate of disappearance of the μ radicals would no longer be linear in one of the concentrations of the μ radicals, then the additivity of the reaction schemes would no longer hold (Vercauteren, 1991).

2.3.4.3 *Calculation of the Pseudo Rate Coefficients*

The pseudo rate coefficients (PRC) k^{pseudo} for the formation of the products resulting from a reaction scheme are a complex function of multiple elementary reaction rate coefficients. Hence, they are just as the PRC of a feedstock component temperature dependent. This implies that in principle the PRC's have to be calculated for every temperature that could be observed in the reactor. By a simple re-scaling operation the temperature dependence can be drastically reduced. First a reference reaction for the considered primary reaction is chosen. For example for C-C scission reactions the formation of 2 methyl radicals from ethane is chosen as reference reaction. The PRC's in the reaction scheme of a disappearance of a component M is then equal to the product of the relative pseudo rate coefficient (RPRC) $k^{pseu,rel}$ and a reference factor k_{ref}:

$$k^{pseudo}(M) = k^{pseu,rel}(M) \ k_{ref}$$ [2. 27]

The largest temperature dependence is captured by the reference reaction rate coefficient, while the RPRC is only slightly dependent on the temperature, see Figure 2.8. Hence, it is sufficient to know the RPRC's for only a small number of temperatures. Vercauteren (1991) showed that the RPRC's have to be determined in intervals of 20 K between 800 K and 1300 K. During a reactor

simulation the RPRC is only calculated if the temperature of the previous calculation of the RPRC's differs more than 10 K of the temperature at the current axial position. The rate of formation of the products and the rate of disappearance of the reactants is then calculated by multiplying the RPRC with the corresponding reference factor. Vercauteren (1991) showed that the differences for the reaction rates are maximally 1%. Hence, it can be concluded that the introduction of the RPRC's substantially decreases the number of temperature points where the reaction schemes have to be generated.
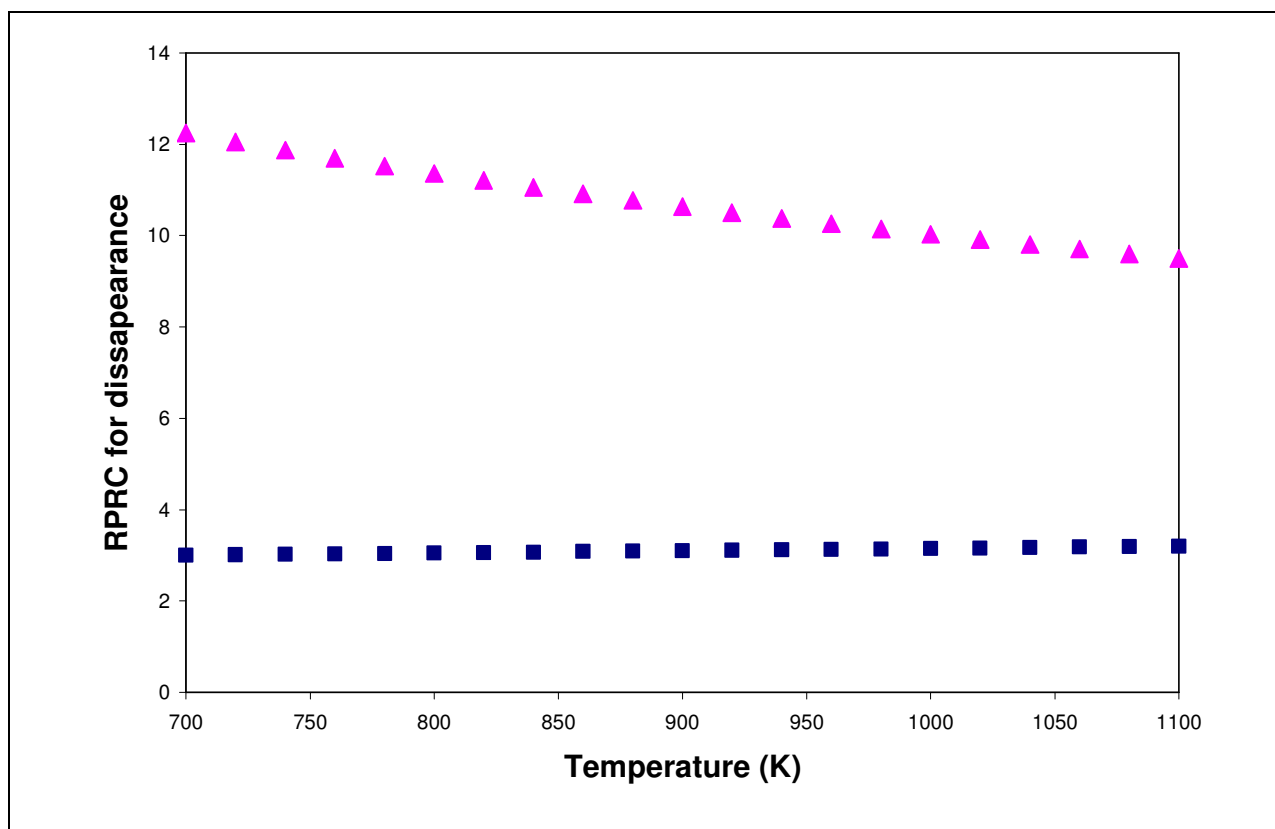
Figure 2.8: Temperature dependence of the relative pseudo rate coefficient (RPRC) for disappearance of n-hexane via a C-C scission reaction [■] and hydrogen abstraction reaction [▲].

2.4   Verification of the model assumptions [(+)]

2.4.1   Introduction

In the previous paragraphs of this chapter the construction of the new reaction network was discussed. Several assumptions are commonly made in models for steam cracking and pyrolysis to limit the network growth and network generation time. Although some of them can be supported by experimental evidence, e.g. the μ radical hypothesis, still some doubts remain about others. Therefore a test problem has been studied with a rate-based network generation program to verify if the made assumptions really hold (Van Geem et al., 2006). A pressure dependent reaction network is generated for n-hexane steam cracking. n-Hexane is selected as feedstock because it is an excellent model compound for the cracking behavior of light naphtha fractions. Naphtha feedstock molecules typically have a carbon number in the range from 5 to 10 and are mostly paraffinic or iso-paraffinic in nature.

Rate-based termination of computer-generated reaction mechanisms provides a physicochemical criterion for including reactions and species (Broadbelt et al., 1994; Broadbelt et al., 1995; Broadbelt et al., 1996); only those pathways whose flux exceeds some minimum flux criterion R_{min} are included in the network. XMG (Exxon-Mobil Mechanism Generator) was the first network generation software applying the rate-based termination criteria (Susnow et al, 1997) and is based on the NETGEN code developed by Klein and coworkers (Broadbelt et al., 1994). XMG has been further elaborated, adding several new features. Matheu et al. (2003 [a], 2003 [c]) created XMG-Pdep, the first mechanism generator to systematically include pressure dependent reactions. Recently a new mechanism generator, RMG, belonging to the same family has been developed by Green and co-workers (Song et al, 2003). RMG includes XMG-PDep's capabilities but also features the implementation of advanced technologies, such as graph representation of reaction families and a hierarchical tree-structured database for retrieving thermal and kinetic parameters, and the use of object-oriented technology. These changes strongly facilitate to continuously improve the level of detail in the description of the chemistry as compared with prior network generation software (Song, 2004).

The first model assumption tested is which reactions should and should not be included in the reaction network. The network includes 3 basic reaction families: C-C scissions of molecules

and the reverse radical recombinations, hydrogen abstractions, addition reactions and the reverse β scissions. Within these reaction families further distinction is possible; e.g. intra-molecular radical additions or so-called cyclization reactions are a member of the addition/β scission reaction family. Maybe one of those reactions, e.g. cyclization reactions forming a four ring is very important and should be included in the reaction network, while now these reactions are omitted. Another important aspect is how important the different reaction families are. Answers on questions like: "Are hydrogen abstractions more important than recombination reactions for example?" or "How sensitive are the product yields to the kinetics of the recombination reaction family?" can help the modeler significantly.

Another assumption tested is the μ radical hypothesis (Ranzi et al., 1983; Clymans and Froment, 1984; Warth et al., 1998). As stated earlier also this assumption states that for large radicals bimolecular reactions can be neglected. These large radicals are called μ radicals or radicals having a μ character since, in the model, their reaction possibilities are restricted to monomolecular reactions only. In steam cracking, radicals containing more than 5 carbon atoms are traditionally considered μ radicals (Ranzi et al., 1983; Clymans and Froment, 1984). RMG does not take into account the assumption of the existence of μ radicals a priori, hence, the generated reaction mechanism for n-hexane can be used to test the μ radical hypothesis.

Other commonly made assumptions are the long-chain hypothesis, allowing a partial separation of the fast propagation reactions from the slower initiation/termination reaction (Gavalas, 1966; La Marca et al., 1990), and the pseudo steady state approximation (PSSA) for the concentration of some reactive intermediates (Hillewaert et al., 1988). Careful use of both these assumptions can simplify the solution of the kinetic equations considerably. None of these assumptions is made a priori in RMG − the complete set of kinetic equations is integrated using a stiff solver. RMG thus provides the possibility to validate these frequently used approximations.

Finally, all previous models for naphtha steam cracking have assumed that the rates of most of the scission and addition reactions are in the high pressure-limit. Most models account, at least implicitly, for the fall-off behavior of a handful of reactions of atoms and very small molecules; here the issue is whether or not it is necessary to consider pressure dependence for the many reactions of large polyatomics. Recent work has indicated that some reactions of even large molecules and radicals proceed via pressure dependent pathways (Wong et al., 2003), with steam cracking lying in the pressure - temperature region where a transition from the high pressure-

limit to pressure dependent behavior can be expected. Dean (1990) showed that the use of pressure dependent kinetic parameters is important for the pyrolysis of methane, as it introduces fast pathways to form C5 ring species thereby significantly altering the overall kinetics. The importance of including pressure dependent pathways for polyatomics was further illustrated for high-conversion ethane pyrolysis (Matheu et al., 2003 [b]; Matheu et al., 2003 [d]), methane autocatalysis and high-conversion ethane pyrolysis (Matheu et al., 2003 [c]). The new mechanism generator RMG allows evaluating the overall effect of pressure dependence on the simulated yields.

2.4.2   RMG: Reaction Mechanism Generation algorithm

RMG uses a set of "reaction families" to generate all possible reactions that a given chemical species can undergo as such and in the presence of the other species in the mechanism. Each reaction family represents a particular type of an elementary chemical reaction, such as C-C scission of molecules, or radical addition to a double bond. RMG represents the individual chemical species as a 2-dimensional connectivity graph and defines the possible reactions by considering the possible mutations of the graph. The newly formed species are then considered as candidates for further reactions and their reactions can be added to RMG's chemical kinetic model.

As most mechanism generation tools, RMG obtains the necessary thermochemical data from an electronic database of literature values, whenever possible. In most instances, however, it must resort to group contribution methods to estimate enthalpies of formation, heat capacities, entropies, and certain other data required for modeling pressure dependent reactions. In this example for n-hexane steam cracking, literature thermochemistry data were taken from the database assembled by Wijaya et al. (2005). The group contribution package of Song and coworkers (Song, 2004), embedded in RMG, was used to obtain estimates whenever literature values were not available. The used group contribution values were taken from Benson (1976), from Lay et al. (1995) and from Sumathi et al. (2002 [a], 2002 [b], 2003). The values for the thermodynamic properties obtained at different temperatures are used to fit the coefficients of the NASA polynomials used in CHEMKIN (Kee et al., 2004).

Similarly, RMG draws rate coefficient information from a library of literature-based kinetic rate coefficients whenever these are available, as in Matheu et al. (2003 [c]). For the vast majority of RMG-determined reaction possibilities, no values are available and the algorithm thus uses a large set of so called "rate rules", stored in a kinetics database to estimate the rate coefficients for each reaction. The rate rule database contains mainly high-level quantum chemistry calculation results from Sumathi et al. (2001 [a], 2001 [b], 2002 [a], 2003), from Wijaya et al. (2003) and from Saeys et al. (2004), and experimental rate coefficients from the Livermore group (Curran et al., 2002). If the reaction is pressure dependent, the rate rule is a "high pressure-limit" rate rule and serves as an input to a CHEMDIS (Chang et al., 1997) calculation of k(T,P) (Matheu et al., 2001). Based on Matheu's work (2003 [b]) a set of net pressure dependent reactions were added which reflect the propargyl + propargyl network and its associated isomerizations, from the results of Miller and Klippenstein (2003).

RMG considers every reaction of the form A + B → C, B → C, or B → C + D to initiate a partial pressure dependent reaction network, such as those described in Matheu et al. (2001). During mechanism generation, RMG builds a set of these partial pressure dependent networks, and from these, it constructs net pressure dependent reactions and estimates their rate coefficients $k(T,P)$. Each partial pressure dependent network is explored by only one activated isomer at a time. RMG continually evaluates a "leakage" flux $R_{\text{leak}(i)}$ for each partial network i. This value represents the flux to all parts of the network not yet explored; $R_{\text{leak}(i)}$ decreases as activated isomers are explored and added to the network.

RMG periodically constructs a set of ordinary differential equations (ODEs) representing the evolution of the system described by its current mechanism. At each time step, it calculates the flux $R_{\text{species}(j)}$ to each candidate species that is not yet included in the mechanism; j runs over all possible candidates for inclusion. It also evaluates each leakage flux $R_{\text{leak}(i)}$, where i runs over all partial pressure dependent networks. RMG selects that species or pressure dependent network having the largest flux and explores its reactions, adding the species and/or reactions to the kinetic model. The process is "complete" when RMG can solve the ordinary differential equations to a user-specified conversion, with all fluxes to non-included parts of the mechanism less than the scaled flux criterion R_{min}, over the entire integration time t. The flux criterion R_{min} is given by:

$$R_{min}(t) = f_{min} R_{char}(t) \qquad \text{[2. 28]}$$

$R_{char}(t)$ is the characteristic rate for the whole mechanism at time t, as given by Song et al. (2002):

$$R_{char}(t) = \sqrt{R^2_{reacted(j)}(t)} \qquad \text{[2. 29]}$$

and f_{min} is a user-specified tolerance, typically 0.1-1%. $R_{reacted(j)}(t)$ represents the net rate of change of each species present in the mechanism at time t.

To build the ordinary differential equations required during mechanism generation, RMG must implicitly assume a reactor model. RMG uses a very simple, perfectly-mixed batch reactor model, at constant temperature and pressure. Hence RMG as such cannot simulate an experiment performed in for example the LPT pilot plant as the reactor used in the pilot plant is a tubular reactor exhibiting an axial temperature and pressure profile. This shortcoming is circumvented by combining the RMG generated mechanism at constant temperature and pressure with CHEMKIN (Kee et al., 2004). CHEMKIN'S PLUG tool solves the set of differential equations describing an arbitrary-geometry plug-flow reactor using the implicit numerical software DASSL (Li and Petzold, 1999). The temperature and pressure profile used in PLUG are taken from the corresponding pilot plant experiment. Matheu et al. (2003 [b]) used a similar strategy for modeling a set of ethane pyrolysis experiments. However, combining CHEMKIN with the RMG generated mechanism is not straightforward; altering the input values used to generate the reaction network with RMG influences the size, the number of included species and the kinetics of the reaction network. Special care has to be taken as to which values are used to generate the reaction network, in particular the choice of the temperature and pressure can noticeably affect the details of the model predictions. As the actual pressure drop in the pilot plant set-up is quite small (0.04 MPa, < 20% CIP), it is not surprising that the use of a fixed pressure in RMG to generate the reaction network does not affect the number of included species and the kinetics of the reaction network. The isothermal approximation in the reactor clearly could be a much more important source of error. However, it is observed that if the highest temperature of the corresponding pilot plant experiment (in this case ± 1075 K) is chosen, a model is generated which includes all the species and reactions that are important over the whole temperature range

(Van Geem et al., 2006). The problem of estimating the range of conditions over which an automatically-generated reaction mechanism is valid has been discussed previously by Song et al. (2002).

Another technical but important issue concerns the transformation of pressure dependent reactions into the appropriate CHEMKIN format (Kee et al., 2004). Here, a modified Arrhenius format, as presented by Dean et al. (1990), has been used. The QRRK code CHEMDIS (Chang et al., 1997) is used in this work to fit modified Arrhenius forms to $k(T,P)$ values at constant pressure over a limited temperature range, as demonstrated previously by Dean (1990). CHEMDIS and THERFIT (Bozzelli et al., 2000) provide estimates of the rate coefficients $k(T,P)$ for pressure dependent reactions, using the kinetics as input. The fitted Arrhenius parameters for $k(T,P)$ have no physical meaning and are specific for a given pressure, but as a fitting form they allow accurate reproduction of calculated $k(T,P)$ values in the temperature and pressure range considered in this work. This representation allows RMG to represent its mechanism in a suitable CHEMKIN input file, using 'pressure dependent' rate coefficients that are valid for one particular pressure but spanning a temperature range. In this work, a model generated at P = 0.21 MPa was used and compared with a model generated using the high pressure limit values for the rate coefficient (P→∞).

	Considered Species	Considered Reactions	Included Species	Included Reactions
Error Tolerance: 0.01 **Conversion: 50 %**	147	513	19	194
Error Tolerance: 0.005 **Conversion: 20 %**	541	1660	33	616
Error Tolerance: 0.005 **Conversion: 50 %**	2121	6219	60	1178

Table 2.4: Effect of the input values (Error Tolerance f_{min} and Conversion) on the size of the reaction network and on the number of species in the reaction network [both considered and included reactions and species]. Reaction networks generated at a pressure of 0.22 MPa, a temperature of 1025 K, and initial n-hexane and H_2O concentrations of 10^{-6} mol m^{-3}.

The size and the number of species considered and included in the reaction network depend mainly on the conversion level and the user-defined tolerance f_{min}. In Table 2.4 the number of species and reactions considered and ultimately included in the reaction network are given for different conversion levels and user-defined tolerances. Obviously, lower tolerances and higher conversion levels lead to larger reaction networks. At 0.22 MPa, 1025 K, an initial n-hexane concentration of 10^{-6} mol m^{-3}, a user-defined tolerance $f_{min} = 0.005$ and a conversion set at 50 %, the generated reaction network consists of 60 species and 1178 reactions, while RMG considered 2121 species and 6219 reactions. The generated reaction mechanism consists of 20 C-C and C-H scission reactions of molecules and their reverse reactions, 432 hydrogen abstractions, 32 isomerization reactions, 512 disproportionations (and their reverse reactions), 81 additions and the corresponding 81 β scissions.

CIP (MPa)	0.24 - 0.28
COP (MPa)	0.20 - 0.24
CIT (K)	873
COT (K)	953 – 1075
Dilution (kg $_{steam}$/kg $_{Hydrocarbon}$)	0.4
Hydrocarbon Flow Rate (kg/h)	3.0 - 4.0
Conversion (%)	25 - 75

Table 2.5: Experimental conditions used for the cracking of n-hexane in the LPT pilot plant installation.

The results obtained with the generated reaction network have been compared with experimental results obtained from the LPT pilot plant to verify the models ability to represent the n-hexane steam cracking behavior. A description of this experimental setup is given in Chapter 4. The reaction network generated at 0.22 MPa, 1025 K, an initial n-hexane concentration of 10^{-6} mol m^{-3}, a user-defined tolerance $f_{min} = 0.005$ and a conversion set at 50 %reaction network is used for the simulations. This network includes all the major and minor products observed in the pilot plant experiments: n-hexane, hydrogen, methane, acetylene, ethylene, ethane, methyl acetylene, propadiene, propylene, butadiene, 1-butene, 2-butene and 1-

pentene. As the tube diameter in the pilot plant reactor is very small (i.e. d = 10 mm), the radial temperature gradients are far less pronounced (< 15 K) thereby allowing a reasonable accurate simulation using a 1-dimensional reactor model. Hence, there are no problems to use CHEMKIN's PLUG utility (Kee et al., 2004) for the simulations.

	Full Mechanism (wt %)	**Reduced Mechanism** (wt %)	**Experimental Results** (wt %)
H_2 yield	0.4	0.6	0.4
CH_4 yield	6.0	5.5	5.6
C_2H_2 yield	0.2	0.2	0.3
C_2H_4 yield	19.0	21.2	19.3
C_2H_6 yield	2.7	2.1	3.3
C_3H_4 yield	0.2	0.5	0.2
C_3H_6 yield	10.4	11.6	10.8
C_4H_6 yield	4.4	5.0	2.7
$1-C_4H_8$ yield	4.4	3.6	5.8
$2-C_4H_8$ yield	1.8	1.6	0.4
$1-C_5H_{10}$ yield	1.1	1.9	2.2
C_6H_6 yield	0.0	0.0	0.1
C_6H_{14}-conversion	50.9	53.8	51.5

Table 2.6: Simulated conversion and product yields for n-hexane steam cracking. Full Mechanism of 60 species and 1178 reactions: reaction network generated with RMG at a pressure of 0.22 MPa, a temperature of 1025 K, an initial n-hexane concentration of 10^{-6} mol m^{-3}, a user-defined tolerance of 0.005 and a conversion set at 50 %. Reduced Mechanism of 24 species and 58 reactions: from Full Mechanism using combination of sensitivity analysis and rate of production analysis [Simulation Conditions: CIT = 873 K; COT = 997 K, CIP = 0.27 MPa, COP = 0.24 MPa, F: 4.0 kg h^{-1}; δ = 0.4 kg /kg]

Ten pilot plant experiments have been simulated. These are pure predictions, i.e. no parameters were adjusted to fit the experimental data. The experimental conditions used in this work are summarized in Table 2.5. The flow rate of the hydrocarbon feedstock is varied from 3 kg h^{-1} to 4kg h^{-1}, while the coil outlet temperature (COT) varies from 953 K to 1075 K. The dilution is kept at a fixed value of 0.4 kg$_{steam}$ / kg$_{hydrocarbons}$. The coil inlet pressure (CIP) varies from 0.24 MPa to 0.28 MPa. The coil outlet pressure (COP) varies from 0.20 MPa to 0.24 MPa. These conditions correspond with hexane conversions ranging from 25 to 75 %. The simulation results are compared with the experimental data in Table 2.6. A good agreement between simulation results and experimental data for the main reaction products was obtained. The yields for the minor products 2-butene, 1-pentene and butadiene deviate significantly from the experimentally observed yields. In Figure 2.9 a parity plot for the conversion is given, while in Figure 2.10 the parity plot for the major products (methane, ethylene and propylene) is shown.
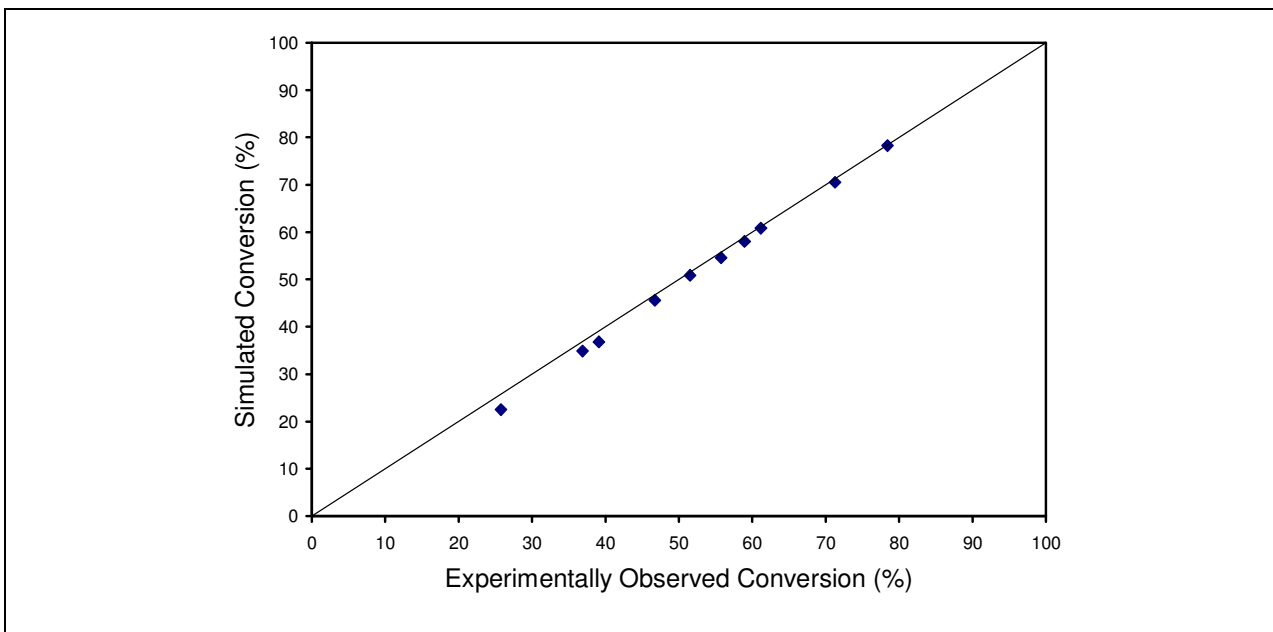
Figure 2.9: Parity plot for the conversion of n-hexane simulated with the Full Mechanism considering 60 species and 1178 reactions. [Simulation Conditions: CIT = 873 K; COT: 953 K – 1090 K; CIP: 0.26 – 0.28 MPa; COP: 0.22 MPa -0.24 MPa; F: 3.0 – 4.0 kg h^{-1}; δ = 0.4 kg /kg]
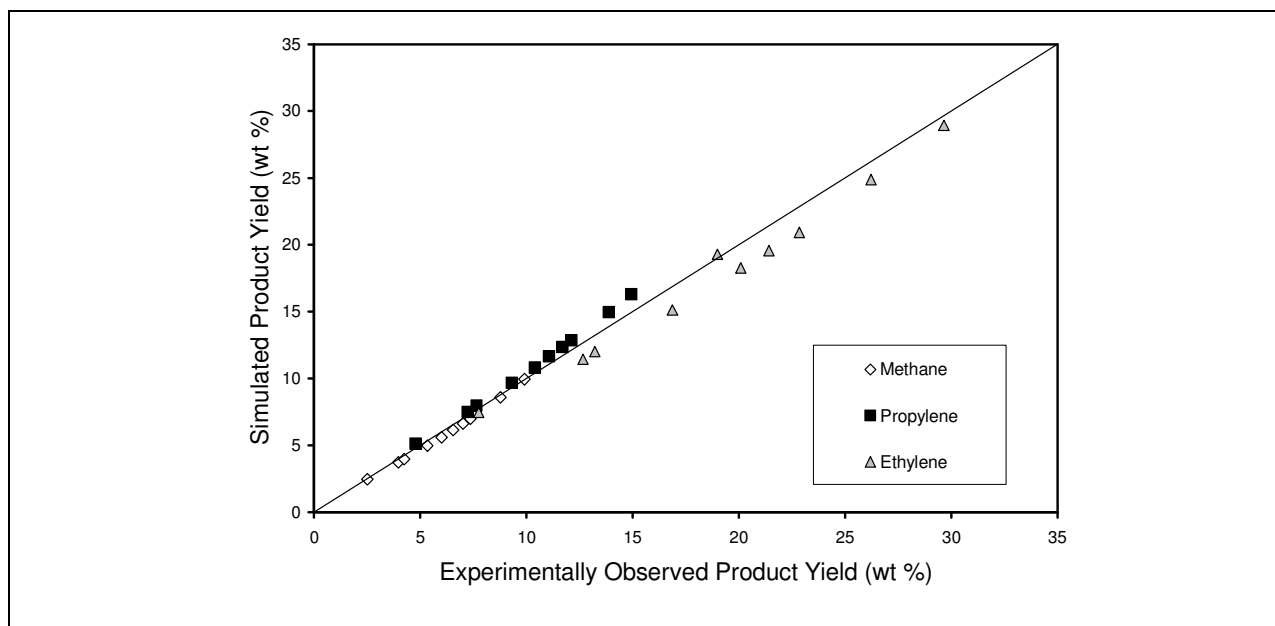
Figure 2.10: Parity plot for the yields of methane, ethylene and propylene simulated with the Full Mechanism considering 60 species and 1178 reactions. [Simulation Conditions: CIT = 873 K; COT: 953 K – 1090 K; CIP: 0.26 – 0.28 MPa; COP: 0.22 MPa -0.24 MPa; F: 3.0 – 4.0 kg h^{-1}; δ = 0.4 kg /kg]
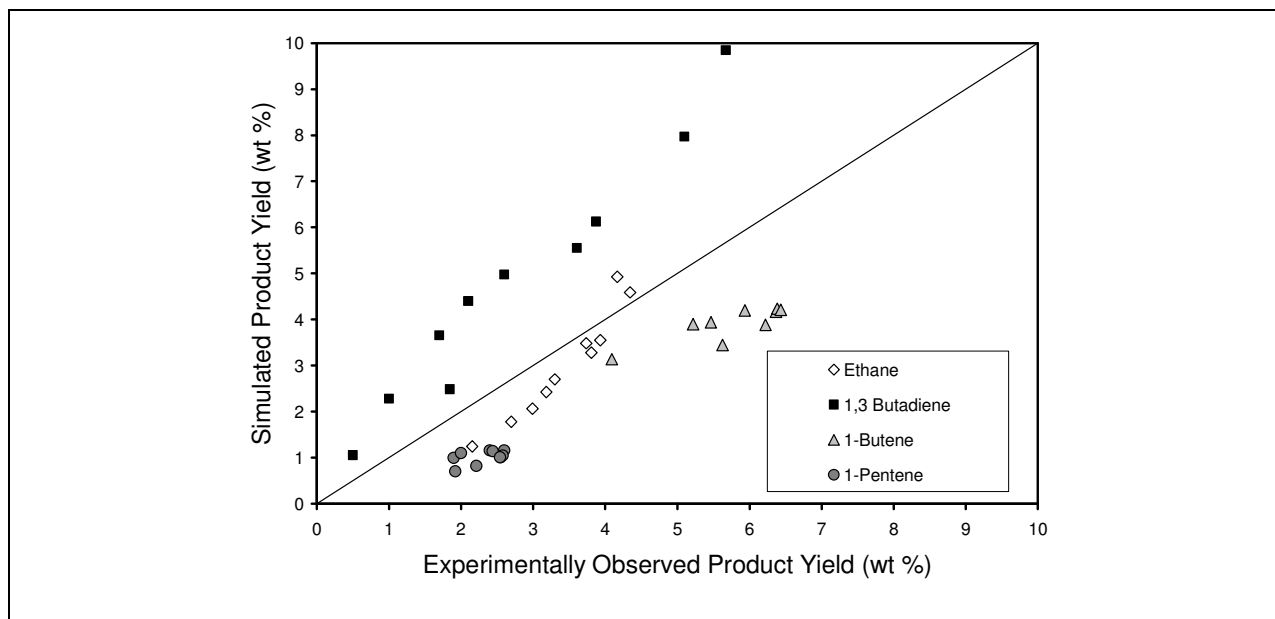
Figure 2.11: Parity plot for the yields of ethane, 1-butene, butadiene and 1-pentene simulated with the Full Mechanism considering 60 species and 1178 reactions. [Simulation Conditions: CIT = 873 K; COT: 953 K – 1090 K; CIP: 0.26 – 0.28 MPa; COP: 0.22 MPa -0.24 MPa; F: 3.0 – 4.0 kg h^{-1}; δ = 0.4 kg /kg]

Even under severe cracking conditions, the conversion and the yields of the main products are accurately simulated. In Figure 2.11 the parity plot for ethane, 1-butene, butadiene and 1-pentene is shown. These results illustrate that although for the minor products the simulation results are reasonable, significant deviations for the yields of 1-butene, butadiene and 1-pentene especially at higher conversions can be noticed.

2.4.3 Full versus reduced mechanisms

The reaction network generated with RMG is reduced to its most important reactions using the combination of sensitivity analysis (Caracotsios et al., 1985; Turanyi, 1990) and rate of production analysis (Turanyi 1989; Rota et al., 1994; Brock et al., 1998; Turanyi, 1997; Tomlin et al., 1995). CHEMKIN 4.0 (Kee et al., 2004) is used to calculate the sensitivity coefficients and the production rates of the species. In agreement with Brock et al. (1998) reactions are included in the skeletal mechanism if the sensitivity coefficients are higher than 0.1 or if the net rate is higher than 5% of the net rate of the fastest step in the considered time interval. The full reaction network consisting of 1178 reactions can then be reduced to 55 reactions. Internal hydrogen abstraction reactions are called isomerization reactions, while bimolecular radical radical hydrogen abstraction reactions are called disproportionation reactions.

The reduced mechanism presented in Table 2.7 is able to capture the main trends of the full mechanism. Indeed, the simulation results obtained using the reduced network (see Table 2.6) illustrate that the reduced mechanism is perfectly able to simulate the n-hexane experiments with only a minor loss of accuracy as compared to the full mechanism. This clearly shows that although the rate-based algorithm leads to more compact mechanisms than some other reaction mechanism generation strategies, a large number of kinetically unimportant reactions are still included in the full mechanism. Note that the kinetic parameters in Table 2.7 correspond to the high pressure limit values for the forward reactions and that all forward reactions are endothermic. Reporting the fitted Arrhenius parameters from fitting $k(T,P)$ at a fixed pressure would only cause confusion because those values have no physical meaning and are particular to a specific pressure and narrow temperature range. The kinetics for the reverse exothermic reactions are calculated based on the thermochemistry and the values of the forward endothermic reactions.

Reaction	log(A)	n	E_a	Reaction	log(A)	n	E_a
C-C Scission and Recombination				**Hydrogen Abstraction**			
C6H14 ↔ C3H7●(1) + C3H7●(1)	23.5	-2.0	369	H2 + C4H7●(1) → 1-C4H8 + H●	6.8	2.1	42
C6H14 ↔ C4H9●(1) + C2H5●	23.2	-1.9	369	H2 + C4H7●(v) → 1-C4H8 + H●	12.8	0.0	43
C6H14 ↔ C5H11●+ CH3●	21.4	-1.4	374	H2 + C4H7●(al) → 2-C4H8 + H●	6.5	2.1	79
C2H6 ↔ CH3●+ CH3●	23.9	-2.2	384	H2 + C4H7●(al) → 1-C4H8 + H●	5.9	2.4	84
Hydrogen Abstraction				H2 + C3H5● ↔ H● + C3H6	6.5	2.1	79
C6H14 + C4H7(al)● ↔ C6H13●(3) + 1-C4H8	12.3	0.5	99	H2 + CH3● → H● + CH4	7.2	1.7	41
C6H14 + C4H7(al)● ↔ C6H13●(2) + 1-C4H8	12	0.7	99	**Beta scission and Addition**			
C6H14 + C4H7(al)● ↔ C6H13●(1) + 1-C4H8	9.5	1.4	108	C6H13●(3) ↔ CH3● + C5H10	17.3	-0.6	142
C6H14 + C4H7(al)● ↔ C6H13●(3) + 2-C4H8	17.8	-1.4	98	C6H13●(3) ↔ C2H5● + 1-C4H8	19.5	-1.2	142
C6H14 + C4H7(al)● ↔ C6H13●(2) + 2-C4H8	17.3	-1.2	98	C6H13●(2) ↔ C3H7●(1) + C3H6	20.3	-1.5	142
C6H14 + C4H7(al)● ↔ C6H13●(1) + 2-C4H8	15.3	-0.6	108	C6H13●(1) ↔ C4H9●(1) + C2H4	21.7	-1.9	144
C6H14 + C3H5● ↔ C6H13●(3) + C3H6	17.9	-1.4	98	C5H11● ↔ C3H7●(1) + C2H4	21.7	-1.9	144
C6H14 + C3H5● ↔ C6H13●(2) + C3H6	17.4	-1.2	98	C5H11● ↔ C2H5●(1) + C3H6	20.1	-1.4	142
C6H14 + C3H5● ↔ C6H13●(1) + C3H6	15.5	-0.6	108	C5H11● ↔ H● + C5H10	13	0.1	153
C3H4 + C4H7(al)● ↔ C3H3● + 1-C4H8	14.2	0	129	C5H9● ↔ CH3● + C4H6	19.2	-1.2	171
C2H6 + C6H13●(3) ↔ C2H6● + C6H14	8.6	0.9	61	C4H9●(1) ↔ C2H5● + C2H4	21.5	-1.8	144
C2H6 + C6H13●(2) ↔ C2H6● + C6H14	9.2	0.7	62	C4H9●(2) ↔ CH3● + C3H6	16.9	-0.9	142
C2H6 + C6H13●(1) ↔ C2H6● + C6H14	11.8	0	62	C4H9●(2) ↔ H● + 2-C4H8	11.3	0.4	147
C2H6 + C4H7●(al) ↔ 1-C4H8 + C6H14	9.3	1.4	108	C4H9●(2) ↔ H● + 1-C4H8	11.0	0.7	155
C2H4 + C6H13●(1) ↔ C2H3● + C6H14	12.5	0.2	80	C4H7●(v) ↔ CH3● + C3H4	17.8	-0.9	150
C2H4 + CH3● ↔ C2H3● + CH4	16.1	-0.3	84	C4H7●(1) ↔ C2H3● + C2H4	18.4	-1.5	173
C2H4 + C3H5● ↔ C3H6 + C2H3●	15.9	-0.4	129	C3H7●(1) ↔ CH3● + C2H4	18.6	-1.3	145
CH4 + C5H9● ↔ CH3● + C5H10	14.3	0.1	126	C3H7●(1) ↔ C3H6 + H●	12.1	0.5	155
CH4 + C6H13●(1) ↔ CH3● + C6H14	4.1	2.4	61	C2H5● ↔ H● + C2H4	13.3	0.2	160
CH4 + C6H13●(2) ↔ CH3● + C6H14	2.4	2.9	60	C2H3● ↔ H● + C2H2	12.1	0.6	157
CH4 + C6H13●(3) ↔ CH3● + C6H14	2.0	3.1	60	**Isomerization**			
CH4 + C4H7●(al) ↔ 1-C4H8 + CH3●	14.4	0.2	126	C6H13●(2) ↔ C6H13●(1)	8.3	0	69
CH4 + C4H7●(al) ↔ 2-C4H8 + CH3●	15.2	-0.5	108	**Disproportion (reverse & forward)**			
H2 + C6H13●(3) ↔ H● + C6H14	3.4	2.6	41	C4H6+1-C4H8↔C4H7●(al)+ C4H7●(al)	14.1	-0.7	166
H2 + C6H13●(2) ↔ H● + C6H14	5.5	2.1	43	C2H6 + C2H4 ↔ C2H5● + C2H5●	15.4	-0.3	273
H2 + C6H13●(1) ↔ H● + C6H14	3.1	2.8	40	C2H4 + CH4 ↔ C2H5● + CH3●	11.3	1.1	287

Table 2.7: Skeletal mechanism: reduction via the combination of sensitivity analysis and rate of production analysis. [A: s^{-1} for monomolecular reactions and mol m^{-3} s^{-1} for bimolecular reactions, E_a: in kJ mol^{-1}]. Note: the kinetic parameters correspond to the high pressure limit values for the forward endothermic reactions and the modified Arrhenius equation is used for the reaction rate coefficient: k = A T^n exp(-E_a /RT).

The reduced mechanism in Table 2.7 suggests that isomerization reactions and disproportionation reactions are of limited importance. Only 1 isomerization reaction is included

in the skeletal mechanism, while only 4 disproportionation reactions out of the 512 disproportionation reactions originally present in the full mechanism remain present in the compact mechanism. Many pyrolysis/steam cracking models completely neglect unimolecular isomerization reactions and bimolecular radical radical disproportionation reactions while others lump isomeric radicals together, implicitly assuming that unimolecular isomerization reactions are equilibrated. Here the hypothesis is tested whether these reaction families are indeed negligible under steam cracking conditions.

	Mechanism 1 (wt %)	**Mechanism 2** (wt %)	**Full Mechanism** (wt %)
H_2 yield	0.4	0.4	0.4
CH_4 yield	6.2	5.9	6.0
C_2H_2 yield	0.2	0.2	0.2
C_2H_4 yield	19.3	20.3	19.0
C_2H_6 yield	2.8	2.7	2.7
C_3H_4 yield	0.2	0.2	0.2
C_3H_6 yield	10.7	9.6	10.4
C_4H_6 yield	4.7	4.2	4.4
$1\text{-}C_4H_8$ yield	4.3	5.2	4.4
$2\text{-}C_4H_8$ yield	1.7	1.0	1.8
$1\text{-}C_5H_{10}$ yield	1.1	1.0	1.1
C_6H_{14} conversion	51.5	50.8	50.9

Table 2.8: Simulated conversion and product yields for n-hexane steam cracking with 3 different mechanisms. Mechanism 1: Disproportionation reaction family not considered. Mechanism 2: Isomerization reaction family not considered. Full Mechanism of 1178 reactions: all reaction families considered [Simulation Conditions: CIT = 873 K; COT = 997 K; CIP = 0.27 MPa; COP = 0.24 MPa, F: 4.0 kg h^{-1}; δ = 0.4 kg /kg]

The results in Table 2.8 show that these two reaction families do not play an important role under the specified conditions. Especially the disproportionation reactions are of no importance. The yields of the major and minor products remain practically unchanged when disproportionations are not considered in the reaction network. This is in sharp contrast to what is observed in autocatalytic methane pyrolysis (Matheu et al. 2003 [c]) where the reverse of the disproportionation reactions is a significant source of radicals. Unimolecular isomerization reactions are not entirely negligible in naphtha steam cracking. Removing this reaction family completely from the network results in a small shift from propylene to ethylene along with a significant shift from 2-butene to 1-butene.
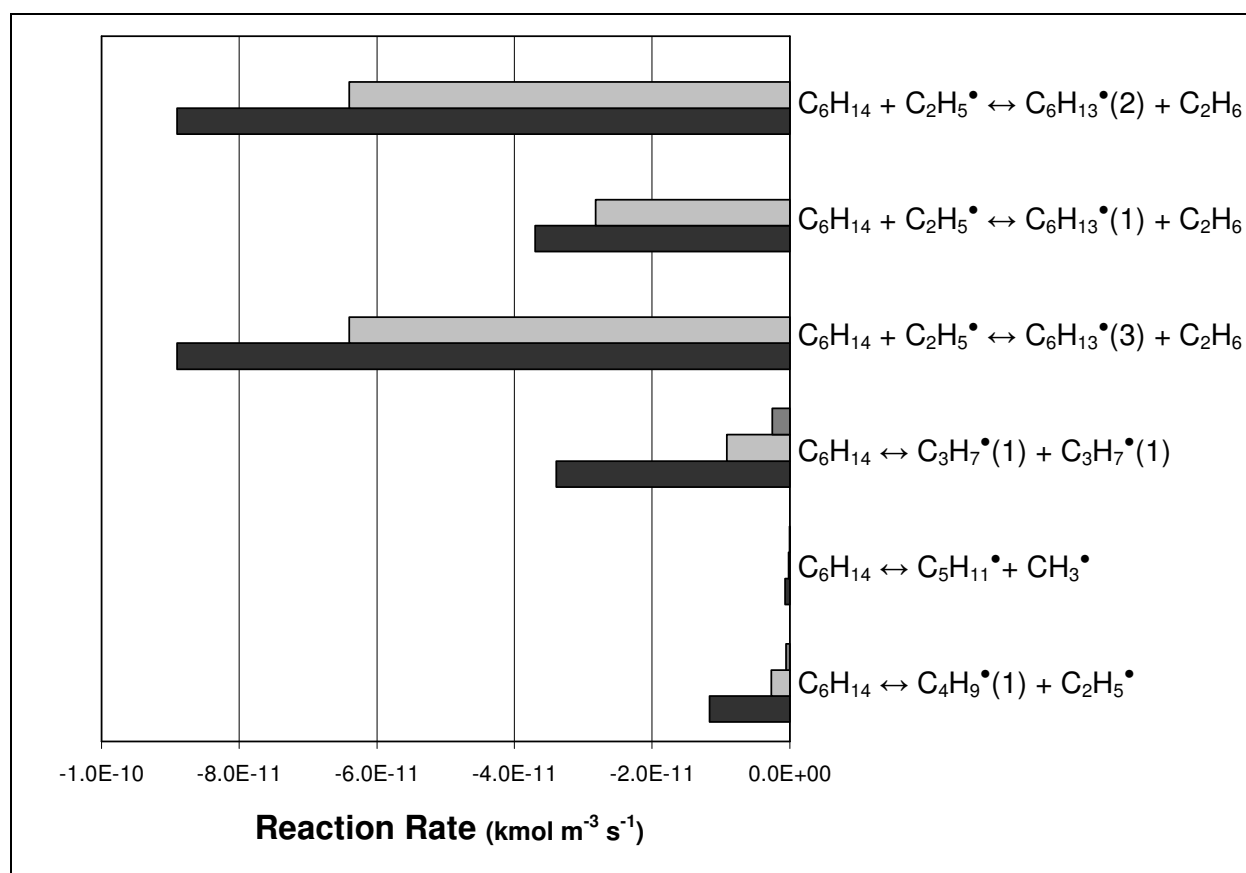
Figure 2.12: Comparison between reaction rates (kmol m^{-3} s^{-1}) of hydrogen abstraction reactions from n-hexane and C-C scissions of n-hexane. ▊ inlet: 0.0 m, ▊ middle: 6.2 m, ▊ outlet: 12.3 m

The results of the rate of production analysis can give an indication of the local importance of a reaction. Some reactions, such as the C-C scissions of n-hexane, are very important at short axial distances in the tubular reactor, see Figure 2.12. Other reactions, such as the hydrogen abstraction reactions from n-hexane, are less important in the early stages of the reactor but gain in importance towards the reactor outlet. A sensitivity analysis was manually performed by simultaneous variation of the forward and the reverse rate coefficients for the elementary steps in order to ensure thermodynamic consistency. The rate rules for the scission reactions were found to be most critical for the agreement with experimental data. Multiplying all of the rate rules in the kinetic database for scission reactions with a factor 10 prior to generation strongly affects the simulated product distribution. The built-in thermodynamic consistency incorporated in RMG makes that the recombination rate rules, combined with the assumed thermochemistry, determine the kinetic parameters of the corresponding reverse reactions, i.e. the C-C scissions of the n-hexane molecules; narrowing the uncertainties in both the recombination rate estimates and in the thermochemistry estimates could further improve the accuracy of the predictions. The model predictions are less sensitive to the rate coefficients of the bimolecular H-abstraction reactions, the key propagation step in the process.

Two reaction families are equally important in determining the conversion of n-hexane: the hydrogen abstraction reactions and the C-C scission reactions of n-hexane. The hydrogen abstraction reactions convert n-hexane, while the C-C scission reactions and the recombination reactions determine the global radical concentration, and thus the concentration of β radicals that can abstract hydrogen atoms from the feed molecules. The bar plot in Figure 2.12 shows that the reaction rates of the hydrogen abstractions from n-hexane are, apart from the inlet section, significantly faster than the rate of the C-C scission of n-hexane. This is further illustrated in Table 2.9, where the sum of the rates of all hydrogen abstraction reactions from n-hexane and the sum of the rates of all C-C scission reactions from n-hexane are given as a function of the axial distance in the reactor. From the data presented in Table 2.9 the kinetic chain length at different axial positions can be calculated. The kinetic chain length is defined as the ratio of the rate of propagation to the rate of termination. In the steady state, the rate of initiation and the rate of termination are equal; hence the kinetic chain length is equal to the ratio of the rate of propagation to the rate of initiation. The results in Table 2.9 show that initially the kinetic chain length is over 100, dropping to 80 in the middle of the reactor, while near the reactor outlet the

kinetic chain length is slightly higher than 40. On average a kinetic chain length of about 50 is found for an n-hexane conversion of 50%. For higher n-hexane conversions the average kinetic chain length drops to lower values.

	Reaction rate (mol m^{-3} s^{-1})		
	5 % reactor length	50% reactor length	95% reactor length
$\sum_i r_{V,i,C-C \text{ scission reactions}}$	$3.42\ 10^{-1}$	$1.71\ 10^{-1}$	$5.45\ 10^{-2}$
$\sum_i r_{V,i,\text{Hydrgen abstractions}}$	65.05	14.83	2.39
Kinetic Chain length	190	86	44

Table 2.9: Values of the reaction rates for all C-C scission reactions and all hydrogen abstraction reactions during the cracking of pure n-hexane.

$\sum_i r_{V,i,C-C \text{ scission react}}$ sum of the reaction rates of the hydrogen abstraction reactions from n-hexane

$\sum_i r_{V,i,\text{Hydrgen abstractions}}$ sum of the reaction rates of all C-C scission reactions of hexane

The results of the rate of production analysis also allow an easy identification of the important reaction pathways. For example, the bar plot for the production rates of ethylene in Figure 2.13 shows that most of the ethylene is produced via the β scission of the ethyl radical:

$$C_2H_5{}^{\bullet} \rightleftharpoons C_2H_4 + H^{\bullet} \qquad\qquad [2.\ 30]$$

Other reactions contributing significantly to the ethylene production are the β scissions of the primary hexyl radicals and the primary propyl radicals. The β scissions of the primary butyl radicals contribute to the ethylene production to a lesser extent.
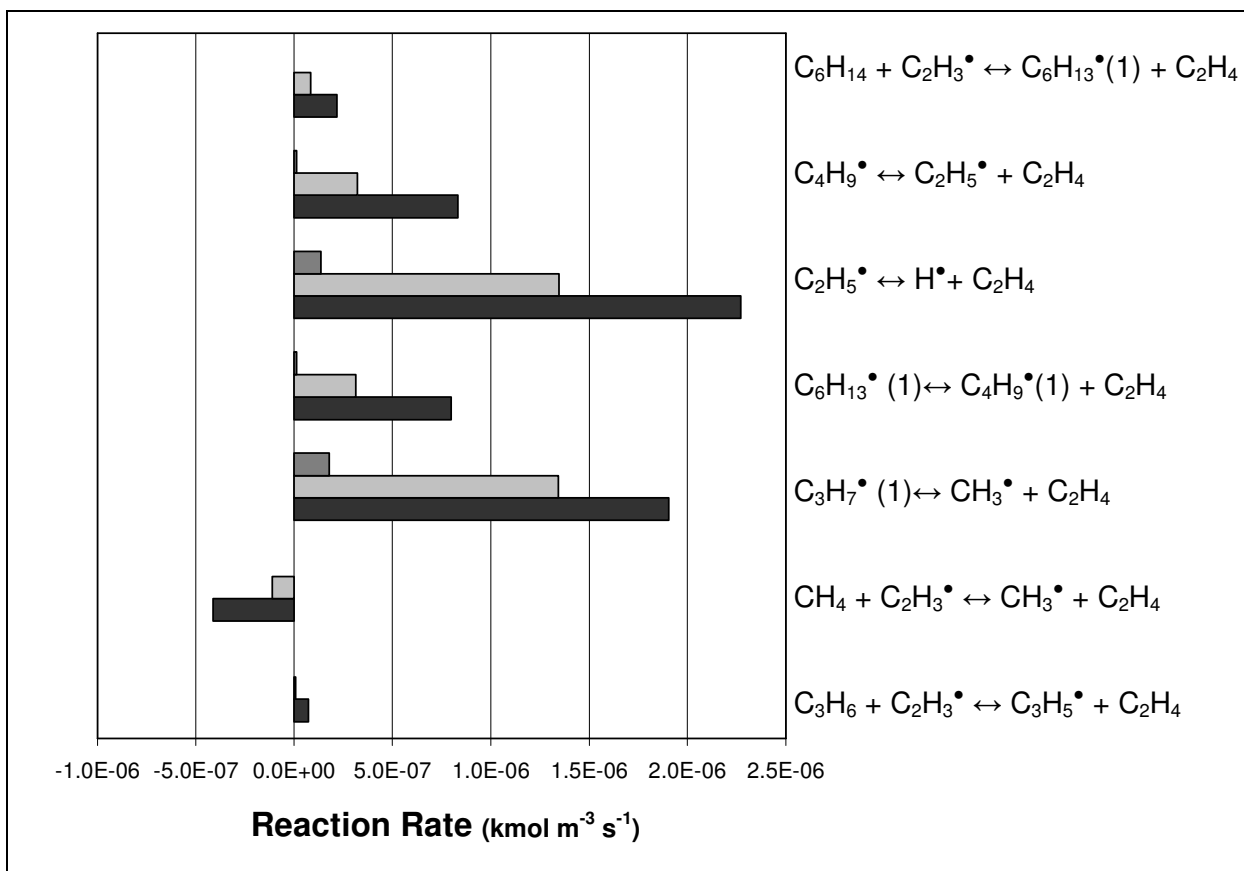
Figure 2.13: Bar plot showing the reaction rates for the important reactions involved in the formation and disappearance of ethylene. ▨ inlet: 0.0 m, ▨ middle: 6.2 m, ▉ outlet: 12.3 m

Identifying the important pathways to propylene is not as straightforward as for ethylene. Only the balanced system of addition reactions, β scission reactions and hydrogen abstractions can explain the propylene behavior (Van Damme et al., 1984). The rate of production analysis shows that the β scission of the 2-hexyl radicals is the most important reaction for propylene formation:

$$C_6H_{13}{}^{\bullet}(2) \;\rightleftharpoons\; C_3H_6 + C_3H_7{}^{\bullet} \qquad\qquad [2.\,31]$$

Other minor paths that contribute significantly to the formation of propylene are the C-H β scission of the secondary propyl radical and the β scission of the secondary butyl radical. The rate of production analysis shows that a set of hydrogen abstractions involving allylic radicals are

also important for an accurate prediction of the propylene yield, e.g. the hydrogen abstractions from ethylene:

$$C_2H_4 + C_3H_5{}^\bullet(al) \; \rightleftharpoons \; C_3H_6 + C_2H_3{}^\bullet \qquad [2.32]$$
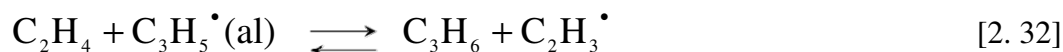
As stated earlier, the simulation results for the components of the C4-fraction could be improved. This fraction is valuable and thus important for steam cracking, because it can be used to produce gasoline (from butenes) and rubbers (from butadiene). The parity plot in Figure 2.11 shows that both 1-butene and 1-pentene are systematically underpredicted while butadiene is systematically overpredicted. The results from the rate of production analysis show that both 1-butene and 1-pentene are almost entirely formed via the β scission of the 3-hexyl radical:

$$C_6H_{13}{}^\bullet(3) \; \rightleftharpoons \; 1\text{-} C_4H_8 + C_2H_5{}^\bullet \qquad [2.33]$$

$$C_6H_{13}{}^\bullet(3) \; \rightleftharpoons \; 1\text{-}C_5H_{10} + CH_3{}^\bullet \qquad [2.34]$$
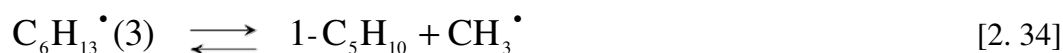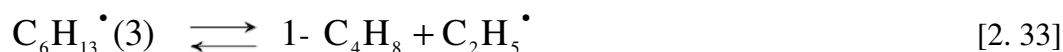
Both 1-butene and 1-pentene are partly converted to butadiene. Hydrogen abstraction from 1-butene leads to the formation of the allylic 1-buten-3-yl radical, while the C-H β scission of the 1-buten-3-yl radical yields butadiene:

$$C_4H_7{}^\bullet \; \rightleftharpoons \; C_4H_6 + H^\bullet \qquad [2.35]$$

Hydrogen abstraction from 1-pentene leads to the formation of the allylic 1-penten-3-yl $C_5H_9{}^\bullet$ radical, and the following β scission of this radical forms butadiene:

$$C_5H_9{}^\bullet \; \rightleftharpoons \; C_4H_6 + CH_3{}^\bullet \qquad [2.36]$$

The rate coefficients for one or both of the reactions [2.35] or [2.36] may be too high in the model, but also the estimation of the thermochemistry of the 1-buten-3-yl radical or the 1-penten-3-yl radical (since endothermic reactions [2.35] and [2.36] will be very sensitive to the thermochemistry as a consequence of the built-in thermodynamic consistency in RMG) can be responsible for the poor simulation results for butadiene. Indeed, model-predicted concentrations of many of the minor species, including butadienes, butanes, and pentenes, may depend strongly

on the uncertain thermochemistry of resonance-stabilized radicals, as noted in Matheu et al. (2005). Only a few of these radicals have well-established heats of formation and heat capacities [e.g. allyl (Wenthold et al., 1996), propargyl (Afeefy et al., 2001; Sabbe et al., 2005), and cyclopentadienyl (Roy et al., 2001; Kiefer et al., 2001)]. For the rest, including species like 1-buten-3-yl, even detailed, quantum-chemistry-based thermochemical estimates are fraught with uncertainty (Henry et al., 2002; Sumathi and Green, 2002 [b]).

The set of net pressure dependent reactions reflecting the propargyl + propargyl network and its associated isomerizations, based on the results of Miller and Klippenstein (2003), does not lead to the formation of a significant amount of benzene under the conditions used in this study. Addition reactions to olefinic products followed by cyclization reactions are probably more important for the formation of benzene, toluene and xylene under steam cracking conditions at the lower conversions studied here (20 –75% hexane conversion). However, both model and experiment agree that less than 1.0 of the hexane is converted into C6+ products at a total hexane conversion of 75 %.

At the temperatures and pressures applied in steam cracking the thermodynamically favored products from those considered in the reaction network are clearly hydrogen and benzene. Even at low temperatures of 600 K n-hexane will be completely converted at equilibrium. This is also shown from the estimated equilibrium concentrations calculated with the EQUIL tool from the CHEMKIN package (Kee et al., 2004). The equilibrium concentrations for the main products at 1000 K staring from pure n-hexane are: C_6H_6 20 mol %, H_2 80 mol %, CH_4 10^{-9} mol % and C_2H_4 10^{-8} mol %. Benzene cannot be considered as the final product because benzene will ultimately form polycyclic aromatic hydrocarbons (PAH) and cokes via reactions omitted in the present model.

2.4.4   μ Hypothesis and PSSA for μ radicals

In industrial practice it is very important to determine modeling results as quickly as possible. This implies the implementation of fast solvers, and encourages the use of models containing only a few species and reactions. But as the average carbon number of the feedstock increases, the number of reactions and the number of species increases exponentially (Broadbelt et al., 1996). Therefore modelers are always trying to reduce mechanisms, making them as

compact as possible, and also to reduce the stiffness so the models can be solved more rapidly. A commonly applied assumption in modeling steam cracking and pyrolysis is the μ hypothesis for large aliphatic radicals (Ranzi et al., 1983; Clymans and Froment, 1984; Warth et al., 1998), i.e. bimolecular reactions are neglected for these radicals. These large radicals are called μ radicals because they are involved in monomolecular reactions only. As stated earlier, in steam cracking radicals with more than 5 carbon atoms are considered μ radicals (Ranzi et al., 1983; Clymans et al., 1984). Small radicals, such as the ethyl or propyl radical, are usually allowed to react by both unimolecular and bimolecular pathways. Benzyl and methyl radicals on the other hand are usually assumed to react only bimolecularly, i.e. their unimolecular reactions are neglected [βμ rules of Goldfinger-Letort-Niclause (Laidler, 1987)]. RMG does not make any of these assumptions, hence, the generated reaction mechanism and the reduced mechanism for n-hexane can be used to check the validity of the μ hypothesis. The results presented here indicate that the μ hypothesis can indeed be used for large aliphatic radicals as no bimolecular reactions of radicals with six or more carbon atoms are incorporated in the generated and reduced mechanisms by the RMG software, see Table 2.7, because these reactions are not fast enough during any time step to be included by the rate-based criterion with the error tolerance applied in this work.

To overcome the stiffness problem of the continuity equations the radical concentrations are often computed using the PSSA (Bodenstein and Lutkemeyer, 1924). There is some concern about the accuracy of this approximation, so in some steam cracking models the PSSA is only assumed to hold for the μ radicals (Clymans and Froment, 1984; Ranzi et al., 2000). In the present model the concentration of all species is calculated exactly using a stiff integrator, and KINALC (Turanyi, 1997) is used to estimate the errors introduced by applying the PSSA for each species in the reaction network. In Table 2.10 the lifetime and the instantaneous error from the pseudo steady state approximation are given for some typical species in the reaction network. The latter is an indication of which species can be considered in the pseudo steady state (Turanyi et al., 1993). If the continuity equations are written as:

$$\frac{dc_i}{dt} = f_i(c_i, k_j^{'}) = -\sum_j \nu_{ij} r_{v,j} \qquad [2.37]$$

the instantaneous error from the PSSA on the concentration of a single species Δc_i^s can be estimated by:

$$\Delta c_i^s = \frac{1}{J_{ii}} \frac{dc_i}{dt}$$

[2. 38]

where $J_{ik} = \left[\dfrac{\partial f_i(\overline{c}, \overline{k})}{\partial c_k} \right]$.

	$z_1 = 0.2$ m		$z_2 = 10$ m	
	$\left\| \Delta c_i^s / c_i \right\|$	**Lifetime (s)**	$\left\| \Delta c_i^s / c_i \right\|$	**Lifetime (s)**
H_2	$6.68 \ 10^1$	1.17	$1.02 \ 10^1$	11.9
CH_4	$1.479 \ 10^2$	2.53	$2.58 \ 10^1$	19.1
C_2H_4	2.23	$3.80 \ 10^{-2}$	0.14	0.12
C_3H_6	3.16	$5.58 \ 10^{-2}$	0.18	0.15
C_4H_6	1.74	$1.12 \ 10^{-2}$	0.12	$6.73 \ 10^{-2}$
C_4H_8	1.46	$3.38 \ 10^{-2}$	0.11	0.13
C_6H_{14}	0.99	$2.37 \ 10^{-1}$	1.00	3.1
$H^\bullet$	$1.31 \ 10^{-4}$	$7.86 \ 10^{-9}$	$3.67 \ 10^{-8}$	$6.90 \ 10^{-9}$
$CH_3^\bullet$	$3.44 \ 10^{-4}$	$2.27 \ 10^{-6}$	$9.07 \ 10^{-6}$	$2.25 \ 10^{-6}$
$C_2H_3^\bullet$	$2.74 \ 10^{-4}$	$2.66 \ 10^{-7}$	$1.27 \ 10^{-6}$	$3.76 \ 10^{-7}$
$C_2H_5^\bullet$	$3.82 \ 10^{-5}$	$2.31 \ 10^{-7}$	$7.13 \ 10^{-6}$	$3.32 \ 10^{-6}$
$C_3H_5^\bullet(al)$	$1.46 \ 10^{-3}$	$8.14 \ 10^{-5}$	$1.40 \ 10^{-4}$	$1.16 \ 10^{-4}$
$C_4H_9^\bullet(1)$	$3.83 \ 10^{-5}$	$2.60 \ 10^{-10}$	$5.11 \ 10^{-10}$	$7.45 \ 10^{-9}$
$C_6H_{13}^\bullet(1)$	$1.71 \ 10^{-5}$	$3.10 \ 10^{-7}$	$1.81 \ 10^{-6}$	$1.10 \ 10^{-7}$
$C_6H_{13}^\bullet(2)$	$5.51 \ 10^{-5}$	$3.34 \ 10^{-9}$	$1.61 \ 10^{-8}$	$7.75 \ 10^{-9}$
$C_6H_{13}^\bullet(3)$	$5.56 \ 10^{-5}$	$2.94 \ 10^{-9}$	$1.97 \ 10^{-8}$	$8.21 \ 10^{-9}$

Table 2.10: Lifetime and estimated Single Pseudo Steady State Species Error (Δc_i^s) in the beginning and the middle of the reactor. [Conditions z_1: T = 927 K; P = 0.21 MPa, Conditions z_2: T= 987 K, P = 0.19 MPa]

The life time in the reactor is typically in the order of 10^{-1} s for molecules and 10^{-6} s for radicals. For larger radicals the life-time is on average shorter, e.g. for radicals with six or more carbon atoms the lifetime is in the order of 10^{-9} s, see Table 2.10. The results in Table 2.10 further show that the instantaneous error from applying the pseudo steady state for all radicals is small, in particular for the radicals with 5 or more carbon atoms. Hence, these results give a first indication that the PSSA can be applied for the μ radicals. The error resulting from the application of the PSSA to the group of μ radicals can be calculated using the following equation (Turanyi, 1993):

$$\Delta c_i^g = \frac{1}{J_{ii}} \frac{dc_i}{dt} - \frac{1}{J_{ii}} \sum_{k \neq i} J_{ik} \Delta c_k^g \qquad [2.39]$$

where i and k run over all QSS species in the group. The calculation of the group errors therefore requires the solution of a coupled set of linear algebraic equations. If the group errors of all species remain small, then the chosen group of species can be considered as QSS species. In this case the group error for the group of radicals with 5 or more carbons atoms can be neglected. Hence, it can be concluded that in this case the PSSA for μ radicals is valid.

2.4.5 Importance of pressure dependence

The effect of the pressure on the reaction rate coefficient is usually neglected in steam cracking simulations. The available software programs [SPYRO (Van Goethem et al., 2001; Dente et al., 1979), CRACKER (Joo et al., 2000), CRACKSIM (Clymans and Froment, 1984; Van Geem et al., 2004) neglect the pressure dependence of the rate coefficients. Dean et al. (1990) and Grenda et al. (2003) showed that the inclusion of pressure dependence can be important for the pyrolysis of methane. Also for high-conversion ethane steam cracking (Matheu et al. 2003), oxidative coupling of methane (Chen et al., 1994) and methane autocatalysis (Matheu et al., 2003) including pressure dependent pathways proved to be important, especially for an accurate prediction of the yields of the minor products. For reactions of large molecules (more than 8-10 heavy atoms) the high pressure limit approximation is almost always used in literature (Larson et al., 1984; Curran et al., 1998). However, Wong et al. (2003) suggested that this approximation might not be correct, and demonstrated that under standard steam cracking

conditions some of the β scission reactions can be pressure dependent, e.g. the β scission of a primary butyl radical forming an ethyl radical and ethylene. Their analysis of the molecular size dependence of falloff and chemical activation indicates that many reaction families are pressure dependent even for very large molecules and even under relatively high pressure conditions. The question arises if the high pressure limit approximation used in most steam cracking models could affect the predictions under typical conditions.

The current version of RMG generates 2 reaction networks; one reaction network where pressure dependence is taken into account, and another reaction network with the reaction rate coefficients fixed at the high pressure limit. In all cases (including many commercial steam cracking models) pressure dependence is included for a handful of small-molecule reactions e.g. $H+H+M=H_2+M$, whose rates are very well established. The unresolved issue is how to handle the more complicated chemically-activated reactions of larger molecules, where the true pressure dependence is unknown and it is challenging to compute the rates accurately. Note that the required computational cost, and the required detailed transition-state information for every elementary step in each pressure dependent system, make the most accurate methods, such as an RRKM/master equation approach, impractical at present for on-line k(T,P) predictions. The CHEMDIS calculations used here to compute k(T,P) are typically within a factor of 3 of the most accurate methods for computing k(T,P), but are much faster and more easily automated (Matheu et al. 2003 [c]). The difference between the yields calculated based on the two reaction networks makes it possible to estimate the overall effect of pressure dependence on the simulation results. In Table 2.11 the simulation results obtained with the two different reaction networks are given. It is clear that for the major products the differences are relatively unimportant. However, a small but significant difference is seen for the simulated ethylene yield. There are several reasons why for n-hexane cracking pressure dependence remains relatively unimportant. First, the effect of pressure dependence on the conversion is limited because the reactions strongly affecting the conversion, i.e. C-C scission and hydrogen abstractions, are only slightly pressure dependent or are pressure independent. Wong et al. (2003) reported that C-C molecular scissions are pressure independent up to very high temperatures, while the hydrogen abstraction reactions are pressure independent. Secondly, many of the strongly pressure dependent small-molecule reactions are quasi equilibrated, hence, their exact rates in forward or reverse direction are not important. This is the case for the β scission reaction of the ethyl radical and the reverse addition reaction.

Although $k(T,P)/k_\infty(T)$ equals 0.68 at 1000 K for both the forward and reverse reaction and n-hexane conversion is quite sensitive to these reactions, the effect of pressure dependence on the conversion remains small. Also, the effect on the product yields is limited because the rate of most β scission reactions of larger radicals is high resulting in the absence of competitive reaction pathways. Even if the main pathway's rate is changed by a factor of 2, the product distribution would not be significantly affected. Moreover, the different β scission reactions of a larger radical all have similar pressure dependences, hence, weakening the effect of pressure on the product distribution even more.

	High pressure Limit Mechanism (wt %)	Pressure dependent Mechanism (wt %)
H_2 **yield**	0.4	0.4
CH_4 **yield**	5.9	6.0
C_2H_2 **yield**	0.3	0.2
C_2H_4 **yield**	19.5	19.0
C_2H_6 **yield**	2.7	2.7
C_3H_4 **yield**	0.2	0.2
C_3H_6 **yield**	10.7	10.4
C_4H_6 **yield**	4.1	4.4
1-C_4H_8 **yield**	4.4	4.4
2-C_4H_8 **yield**	1.8	1.8
1-C_5H_{10} **yield**	1.0	1.1
C_6H_{14} **conversion**	51.1	50.9

Table 2.11: Simulated conversion and product yields for n hexane steam cracking with the high pressure limit mechanism (kinetic parameters in the high pressure limit) and pressure dependent mechanism (pressure dependent kinetic parameters). [Simulation Conditions: CIT = 873 K, COT = 997 K, CIP = 2.7 MPa, COP = 2.4 MPa, F: 4.0 kg h^{-1}, δ = 0.4 kg /kg]

As stated earlier, n-hexane can be considered a model compound for naphtha steam cracking. Light and heavy naphthas are the most commonly applied hydrocarbon feedstocks in

industrial steam cracking installations, e.g. in Europe and Asia more than 90 % of the steam cracking feeds are naphtha feedstocks. The conclusions found in this work for n-hexane cracking will most probably also hold for naphtha steam cracking. While neglecting pressure dependence in naphtha steam cracking leads to small but noticeable errors on the product yields, it appears that the high pressure limit approximation commonly applied in simulation packages for steam cracking of complex mixtures is sufficiently accurate for most practical purposes.

2.4.6   Results obtained with RMG

The made assumptions for constructing the microkinetic model are verified using a new rate-based network generator, RMG developed by the Green group (Song et al., 2003). As test problem n-hexane steam cracking is chosen because n-hexane can be considered a model compound for naphtha steam cracking. The simulation results obtained with the RMG generated microkinetic model show that disproportionation reactions do not seem to be of any importance under typical steam cracking conditions. The sensitivity analysis performed on the kinetic rate rules shows that the accurate quantitative simulation results for n-hexane steam cracking depend strongly on the accuracy of the bond scission rate rules.

Generating a reaction mechanism for n-hexane using RMG verifies the µ radical hypothesis. RMG does not take into account any assumption to generate a detailed reaction mechanism, and is hence an excellent tool to test this and other assumptions employed in conventional modeling. Under these conditions these hypotheses as applied in steam cracking, i.e. bimolecular reactions involving radicals with more than 5 carbon atoms are not fast compared to unimolecular reaction possibilities and can hence be neglected, is indeed valid. Also the PSSA for the radicals has been tested, in particular the error resulting from assuming the pseudo steady state for the group of µ radicals. The results obtained with KINALC (Turanyi, 1997) show that the error for applying the pseudo steady state for the group of µ radicals is negligible.

An indication of the effect of pressure dependence of the rate coefficients can also be obtained using RMG. In this case the effect of pressure dependence on the predicted conversion and the yields of the major products is limited. This implies that the assumption used in many simulation programs for naphtha cracking – that all potentially pressure dependent reactions are in the high pressure limit – does not strongly perturb predicted yields and product distributions.

2.5   Conclusions

A new single event microkinetic model for steam cracking of hydrocarbons is developed based on the free radical mechanism. The microkinetic model is divided in two sub models; the monomolecular μ network and the β network. This is because monomolecular reactions generally dominate for species with more than 5 carbon atoms (μ radicals) apart from some exceptions (C_6^+ β and βμ radicals). The kinetics for the μ network can be described by analytical expressions based on the PSSA for the radical reaction intermediates. Innovations to the μ network are:

- New reaction possibilities: 1,4 isomerization reactions and electrocyclizations
- Competition between 1,5 cyclizations and 1,6 cyclizations and separate kinetic parameters
- New primary reactions: all addition reactions of β and βμ radicals
- New molecules in the reaction schemes: cyclic olefins, di-, tri- and tetra-aromatics, naphtheno-aromatics
- Extension of the maximum carbon number

Innovations to the β network are:

- Automated generation of the β network
- Considers bimolecular reactions of β and βμ radicals of all C_5 radicals
- Bimolecular reactions of C_6^+ β and βμ radicals
- Carbon Count stop criterion

These innovations make it possible to omit global reactions from the microkinetic model.

2.6   References

Afeefy H.Y., Liebman J.F., Stein S.E. Neutral Thermochemical Data, in NIST Chemistry Webbook, NIST Standard Reference Database Number 69, Linstrom PJ; Mallard W G eds, Gaithersburg, MD, 2001.

Allara D.L., Shaw R. A Compilation of the Kinetic Parameters for the Thermal Degradtion of n-Alkane Molecules, J. Phys. Chem. Ref. Data., 9(3), 523-559, 1980.

Baas C.J. PhD dissertation, Delft University, 1963.

Battin-Leclerc F., Glaude P.A., Warth V., Fournet R., Scacchi G., Come G.M. Computer Tools for Modelling the Chemical Phenomena Related to Combustion, Chem. Eng. Sci., 55, 2883, 2000.

Battin-Leclerc F., Development of kinetic models for the Formation and Degradation of unsaturated Hydrocarbons at high Temperature, Phys. Chem. Chem. Phys., 4, 2072-2078, 2002.

Belohlav Z., Zamostny P., Henrik T. The Kinetic Model for olefins Production, Chemical Engineering and Processing, 42, 461-473, 2003.

Benson S.W. Some Recent Developments in Gas-Phase Pyrolysis of Hydrocarbons, Advances in Chemistry Series, 97, 1-19, 1970.

Benson S.W. Thermochemical Kinetics, John Wiley & Sons, New York, 2nd edition, 1976.

Blurock E.S. Reaction – System for Modeling Chemical Reactions, J. Chem. Inf. Comp. Sci., 35, 607,1995.

Bodenstein M., Lutkemeyer H. Die Photochemische Bildung von Bromwasserstoff und die Bildungsgeschwindigkeit der Brommolekel aus den Atomen, Z. Phys. Chem., 114, 208, 1924.

Bounaceur R., Scacchi G., Marquaire P.M., Domine F. Mechanistic modeling of the thermal cracking of tetralin, Ind. Eng. Chem. Res., 39, 4152-4165, 2000.

Bozzelli J.W., Chang A.Y., Dean A.M. Molecular Density of States from Estimated Vapor Phase Heat Capacities, Int. J. Chem. Kin., 29, 161-170, 1997.

Broadbelt L.J., Stark S.M., Klein M.T. Computer-generated Pyrolysis Modeling – on-the-fly Generation of Species, Reactions, and Rates, Ind. Eng. Chem. Res., 33, 790-799, 1994.

Broadbelt L.J, Stark S.M, Klein M.T. Termination of Computer-Generated Reaction-Mechanisms – Species rank-Based Convergence Criterion, Ind. Eng. Chem. Res., 34, 2566-2573, 1995.

Broadbelt L.J., Stark S.M., Klein M.T. Computer Generated Reaction Modeling: Decomposition and Encoding Algorithms for Determining Species Uniqueness, Comp. Chem. Eng., 20, 113, 1996.

Brock E.E., Savage P.E., Barker J.R. A Reduced Mechanism for Methanol Oxidation in Supercritical Water, Chem. Eng. Sci., 53, 857-867, 1998.

Caracotsios M., Stewart W.E. Sensitivity Analysis of Initial-Value Problems with Mixed ODES and Algebraic Equations, Comp. Chem. Eng., 9, 359-365, 1985.

Chang, A.Y., Bozzelli J.W., Dean A.M. Kinetic Analysis of Complex Chemical Activation and Unimolecular Dissociation Reactions using QRRK Theory and the Modified strong Collision Approximation, Z. Phys. Chem., 214, 1533-1568, 2000.

Chen Q. The Thermal Cracking of Substituted Aromatics and 1,5-Hexadiene, PhD dissertation, UGent, 1988.

Chen Q., Couwenberg P.M., Marin G.B. Effect of Pressure on the Oxidative Coupling of Methane in the Absence of Catalyst, AIChE Journal, 40, 521-535, 1994.

Chevalier C., Warnatz J., Melenk H. Automatic Generation of Reaction-Mechanisms for the Description of the Oxidation of Higher Hydrocarbons, Ber. Buns. Phys. Chem., 94, 1362-1367, 1999.

Chinnick S.J., Baulch D.L., Ayscough P.B. An Expert System for Hydrocarbon Pyrolysis Reactions, Chemometrics and Intelligent Laboratory Systems, 5, 39, 1988.

Clymans P.J., Froment G.F. Computer Generation of Rate Equations in the Thermal Cracking of Normal and Branched Paraffins, Comp. Chem. Eng., 8, 137-142, 1984.

Curran H.J., Gaffuri P., Pitz W.J., Westbrook C.K. A Comprehensive Modeling Study of n-Heptane Oxidation, Combustion & Flame, 114, 149, 1998.

Davis, H.G., Farell, T.J. Relative and Absolute Rates of Decomposition of Light Paraffins under Practical Operation Conditions. Ind. Eng. Chem. Process Des. Dev., 12, 171-181, 1973.

Dean A.M. Detailed Kinetic Modeling of Autocatalysis in Methane Pyrolysis, J. Phys. Chem., 94, 1990.

De Buck J. Kinetsche Studie van de Cokesvorming bij het Thermisch Kraken van Koolwaterstoffen, Master thesis, UGent, 1999.

Dente M., Ranzi E., Goossens A.G. Detailed Prediction of Olefin Yields from Hydrocarbon Pyrolysis trough a Fundamental Simulation-Model (SPYRO), Comp. Chem. Eng., 3, 61-75, 1979.

DiMaio F.P., Lignola P.G. KING, a Kinetic Network Generator, Chem. Eng. Sci., 47, 2713, 1992.

Froment G.F. Chemical Reactions in Complex Systems: the Mobil Workshop, A.V. Sapre and F.J. Krambeck, New York, Van Nostrand Reinhold, 1991.

Froment G.F. Kinetics and Reactor Design in the Thermal Cracking for Olefin Production, Chem. Eng. Sci., 47, 2163, 1992.

Gavalas G.R. The Long Chain Approximation in Free Radical Reaction Systems, Chem. Eng. Sci., 21, 133-144, 1966.

Grenda J.M., Androulakis I.P., Dean A.M., Green W.H. Application of Computational Kinetic Mechanism Generation to Model the Autocatalytic Pyrolysis of Methane, Ind. Eng. Chem. Res., 42, 1000-1010, 2003.

Henry D.J., Parkinson C.J., Radom L. An assessment of the performance of high-level theoretical procedures in the computation of heats of formation of small open-shell molecules, J. Phys. Chem. A, 106, 7927-7936, 2002.

Hillewaert L.P, Dierickx J.L., Froment GF. Computer-Generation of Reaction Schemes and Rate-Equations for Thermal-Cracking, AIChE Journal, 34, 17, 1988.

Jutz C., Aromatic and Heteroaromatic Compounds by Electrocyclic Ring Closure with Elimination, Top. Curr. Chem., 73, 125-130, 1978.

Joo E., Lee K., Lee M., Park S. CRACKER – a PC Based Simulator for Industrial Cracking Furnaces, Comp. Chem. Eng., 24, 1523-1528, 2000.

Kee R.J., Rupley F.M., Miller J.A., Coltrin M.E., Grcar J.F., Meeks E., Moffat H.K., Lutz, G. Dixon-Lewis A.E., Smooke M.D., Warnatz J., Evans G.H., Larson R.S., Mitchell R.E., Petzold L.R., Reynolds W.C., Caracotsios M., Stewart W.E., Glarborg P., Wang C., Adigun O., Houf W.G., Chou C.P., Miller S.F., Ho P., Young D.J. CHEMKIN Release 401, Reaction Design, Inc, San Diego, CA, 2004.

Kerr J.A. Rate Processes in the Gas Phase, in Free Radicals, Volume I, edited by Kochi J., Wiley, New York, 1973.

Kiefer J.H., Tranter R.S., Wang H., Wagner A.F. Thermodynamic functions for the cyclopentadienyl radical: The effect of Jahn-Teller distortion, Int. J. Chem. Kin., 33, 834-845, 2001.

Klinke D.J., Broadbelt L.J. Mechanism Reduction during Computer Generation of Compact Reaction Models, AIChE Journal, 43, 1828-1837, 1997.

Kopinke, F.D., Ondruschka, B., Zimmerman, G. Indications of a puzzling mechanism in the pyrolysis of 1,3-butadiene, Tetrahedron Letters, 24, 869-872, 1983.

Kopinke F.D., Bach G., Ondruschka B., Zimmerman G. Tendencies of Aromatization in Steam Cracking of Hydrocarbons, Ind. Eng. Chem. Res., 26, 2393-2397, 1987.

Kopinke F.D., Zimmerman G., Nowak S. On the Mechanism of Coke Formation in Steam Cracking – Conclusions Obtained from Tracer Experiments, Carbon, 26, 117-124, 1988.

Kossiakoff A., Rice F.O. Thermal Cracking of Hydrocarbons. Resonance Stabilization and Isomerization of Free Radicals, J. Am. Chem. Soc., 65, 590, 1943.

Kumar P., Kunzru D. Modeling of naphtha pyrolysis. Ind. Eng. Chem. Process Des. Dev., 24, 774-782, 1985.

Laidler K.J. Chemical Kinetics, 3rd ed., Harper & Row, New York, 311, 1987.

LaMarca C., Linanati C., Klein M.T. Design of Kinetically Coupled Complex Reaction Systems, Chem. Eng. Sci., 45, 2059-2065, 1990.

Larson C.W., Patrick R., Golden D.M. Pressure and Temperature-Dependence of Unimolecular Bond Fission Reactions – an Approach for Combustions Modelers, Combustion & Flame, 58, 229, 1984.

Lay T.H., Bozzelli J.W., Dean A.M., Ritter E.R. Hydrogen Atom Bond Increments for Calculation of Thermodynamic Properties of Hydrocarbon Radical Species, J. Phys. Chem., 99, 14514–14527, 1995.

Li S., Petzold L.R. Design of New DASPK for Sensitivity Analysis, UCSB Technical report, 1999.

Matheu D.M., Lada T.A., Green W.H., Grenda J.M., Dean A.M. Rate-Based Screening of Pressure dependent Reaction Networks, Comp. Phys. Comm., 138, 237-249, 2001.

Matheu D.M., Green W.H., Grenda J.M. Capturing Pressure dependence in Automated Mechanism Generation: Reactions through Cycloalkyl Intermediates, Int. J. Chem. Kin., 35, 95-119, 2003 [a].

Matheu D.M., Saeys M., Grenda J.M., Marin G.B., Green W.H. New Models and Pathways for Methane and Ethane Pyrolysis from Automated, Pressure dependent Mechanism Generation, AIChE Annual meeting, San Francisco, CA, USA, 2003 [b].

Matheu D.M., Dean A.M., Grenda J.M., Green W.H. Mechanism Generation with Integrated Pressure dependence: A New Model for Methane Pyrolysis, J. Phys. Chem. A, 107: 8552-8565, 2003 [c].

Matheu D.M., Grenda J.M., Saeys M., Green W.H. New, computer-discovered pathways for methane and ethane pyrolysis, Preprints of the ACS Division of Fuel Chemistry, 2003 [d].

Matheu D.M., Grenda J.M. A Systematically-Generated, Pressure dependent Mechanism for High-Conversion Ethane Pyrolysis Part I: Pathways to the Minor Products, J. Phys. Chem. A, 109, 5332-5342, 2005.

Miller J.A., Klippenstein S.J. The Recombination of Propargyl Radicals and other Reactions on a C6H6 Potential, J. Phys. Chem. A, 107, 783-7799, 2003.

Pant K.K., Kunzru D. Pyrolysis of Methylcyclohexane: Kinetics and Modeling, Chem. Eng. Journal, 67, 123-129, 1997.

Plehiers P.M. Rigoureuze Modellen voor de Simulatie van Fornuizen voor de Thermische Kraking van Lichte Koolwaterstoffen, PhD dissertation, UGent, 1989.

Prickett S.E., Mavrovouniotis M.L. Construction of Complex Reaction Systems, Comp. Chem. Eng., 21, 1219-1325, 1997.

Quann R.J., Jaffe S.B. Structure-Oriented Lumping – Describing the Chemistry of Complex Hydrocarbon Mixtures, Ind. Eng. Chem. Res., 31 , 2483-2497, 1992.

Ranzi E., Dente M., Plerucci S., Biardi G. Initial Product Distribution from Pyrolysis of Normal and Branched Paraffins, Ind. & Eng. Chem. Fund., 22, 132-139, 1983.

Ranzi E., Faravelli T., Gaffuri P., Sogaro A. Low Temperature Combustion – Automatic-Generation of Oxidation Reactions and Lumping procedures, Combustion & Flame., 102, 179-192, 1995.

Ranzi E., Dente M., Goldaniga A., Bozzano G., Faravelli T. Lumping procedures in Detailed Kinetic Modeling of gasification, pyrolysis, partial oxidation and combustion of hydrocarbon mixtures, Progress in Energy and Combustion Science, 27, 99-139, 2001.

Richard C., Scacchi G., Back M.H. Ene Reactions of Olefins. II. The addition of ethylene to 2-butene and the Decomposition of 3-methylpent-ene, Int. J. Chem. Kin, 10, 307-324, 1978.

Rice F.O. The Thermal Decomposition of Organic Compounds from the Standpoint of Free Radicals, J. Am. Chem. Soc., 53, 1959, 1931.

Rice F.O., Herzfeld K.F. The Thermal Decomposition of Organic Compounds from the Standpoint of Free Radica1s. VI. The Mechanism of Some Chain Reactions, J. Am. Chem. Soc., 56, 284, 1934.

Rota R., Bonini F., Servida A., Morbidelli M., Carra S. Validation and Updating of Detailed Kinetic Mechanisms: The Case of Ethane Oxidation, Ind. Eng. Chem. Res., 33, 2540-2553, 1994.

Roy K., Braun-Unkhoff M., Frank P., Just T. Kinetics of the Cyclopentadiene decay and the recombination of Cyclopentadienyl Radicals with H-atoms: Enthalpy of formation of the Cyclopentadienyl Radical, Int. J. Chem. Kin., 33, 821-833, 2001.

Sabbe M.K., Saeys M., Reyniers M.F., Marin G.B. Group Additive Values for the Gas Phase Standard Enthalpy of Formation of Hydrocarbons and Hydrocarbon Radicals, J. Phys. Chem. A, 109, 7466-7480, 2005.

Saeys M., Reyniers M.F., Marin G.B., Van Speybroeck V., Waroquier M. Ab Initio Group Contribution Method for Activation Energies for Radical Additions, AIChE Journal, 50, 426-444, 2004.

Shiess P., Dinkel R. Uber den Anteil sigmatroper 1,5-Wanderung von Kohlenwasserstoffgruppen bei der Thermolytischen Skelettisomerisierung 5,5,-disubstituierter 1,3 cyclohexadiene, Helv. Chim. Acta, 64, 801-812, 1981.

Shu W.R., Ross L.L. Cracking severity index in pyrolysis of petroleum fractions. Ind. Eng. Chem. Process Des. Dev. 21, 371-377, 1982.

Song J., Stephanopoulos G., Green W.H. Valid Parameter Range Analyses for Chemical Reaction Kinetic Models, Chem. Eng. Sci., 57, 4475-4491, 2002.

Song J., Raman S., Yu J., Wijaya C.D., Stephanopoulos G., Green W.H. RMG: the Next Generation of Automatic Chemical Reaction Mechanism Generator, proceedings AIChE Annual meeting, San Francisco, CA, USA, 2003.

Song J. RMG: a tool for Automatic Network generation, PhD Dissertation, Massachusetts Institute of Technology, 2004.

Stein S.E., Rabinovitch B.S. Ring Opening and Isomerization of a Series of Chemically Activated Cycloalkyl radicals, J. Phys. Chem., 79, 191-198, 1975.

Sumathi R., Carstensen H.H., Green W.H. Reaction Rate Prediction via Group Additivity, Part 1: H Abstraction from Alkanes by H and CH3, J. Phys. Chem A, 105, 6910-6925, 2001 [a].

Sumathi R., Carstensen H.H., Green W.H. Reaction Rate Prediction via Group Additivity, Part 2: H Abstraction from Alkenes, Alkynes, Alcohols and Acids by H atoms, J. Phys. Chem. A., 105, 8969-8984, 2001 [b].

Sumathi R., Green W.H. A priori Rate Constants for Kinetic Modeling, Theoretical Chemistry Accounts., 108, 187-213, 2002 [a].

Sumathi R., Green W.H. Missing thermochemical groups for large unsaturated hydrocarbons: Contrasting predictions of G2 and CBS-Q, J. Phys. Chem. A, 106 (46), 11141-11149, 2002 [b].

Sumathi R., Green W.H. Oxygenate, Oxyalkyl, and Alkoxycarbonyl Thermochemistry and Rates for Hydrogen Abstraction from Oxygenates, Phys. Chem. Chem. Phys., 5, 3402-3417, 2003.

Sundaram K.M., Froment G.F. Modeling of thermal-Cracking Kinetics. 1. Thermal Cracking of Ethane, Propane and their Mixtures, Chem. Eng. Sci., 32, 601-608, 1977.

Susnow R.G., Dean A.M., Green W.H., Peczak P., Broadbelt L.J. Rate-Based Construction of Kinetic Models for Complex Systems, J. Phys. Chem. A, 101, 3731, 1997.

Tedder J.M., Walton J.C. The Importance of Polarity and Steric Effects in Determining the Rate and Orientation of Free radical Addition to Olefins – Rules for Detremining the Rate and the Preferred Orientation, Tetrahedron, 36, 701-707, 1980.

Tomlin A.S., Pilling M.J., Merkin J.H., Frindley J., Burgess N., Gough A. Reduced Mechanism for Propane Pyrolysis, Ind. Eng. Chem. Res., 34, 3749-3760, 1995.

Turanyi T., Berces T., Vajda S. Reaction-Rate Analysis of Complex Kinetic Systems, Int. J. Chem. Kin., 21, 83-99, 1989.

Turanyi T. Sensitivity Analysis of Complex kinetic Systems. Tools and Applications. J. Math. Chem., 5, 203-204, 1990.

Turanyi T., Tomlin A.S., Pilling M.J. On the Error of the Quasi-Steady-State Approximation J. Phys. Chem., 97, 163-172, 1993.

Turanyi T. Applications of Sensitivity Analysis to Combustion Chemistry, Reliability Engineering & System Safety, 57, 41-48, 1997.

Van Damme P.S., Willems P.A., Froment G.F. Temperature, not Time, Controls Steam Cracking Yields, Oil & Gas Journal, 68-73, 1984.

Van Geem K.M., Reyniers M.F., Marin G.B. First Principles based Reaction Network for Steam Cracking, AIChE Annual Meeting, Austin, TX, USA, 2004.

Van Geem K.M., Reyniers M.F., Marin G.B., Song J., Mattheu D.M., Green W.H. Automatic Network generation using RMG for Steam Cracking of n-Hexane, AIChE Journal, 52, 2, 718-730, 2006.

Van Goethem M.W.M., Kleinendorst F.I., Van Leeuwen C., Van Velzen N. Equation-Based SPYRO® Model and Solver for the Simulation of the Steam Cracking Process, Comp. Chem. Eng., 25, 905-911, 2001.

Van Speybroeck V., Borremans Y., Van Neck D., Waroquier M., Wauters S., Saeys M., Marin G.B. Ab Initio Study of Radical Reactions: Cyclization Pathways for the Butylbenzene radical (II), J. Phys. Chem. A, 105, 7713-7723, 2001

Walsh R. Cyclic Alkyl Radical Isomerization: a Correction to the Literature, Int. J. Chem. Kin., 2, 71-74, 1970.

Vercauteren C. Rigoureuze Kinetische Schema's voor de Thermische Kraking van Koolwaterstoffen, PhD dissertation, UGent, 1991.

Warth V., Battin-Leclerc F., Fournet P.A., Glaude P.A., Côme G.M., Scacchi G. Computer Based Generation of Reaction Mechanisms for Gas-Phase Oxidation, Comp. Chem., 24, 541, 2000.

Warth V., Stef N., Glaude P.A., Battin-Leclerc F., Scacchi G., Côme G.M. Computer-Aided Derivation of Gas-Phase Oxidation Mechanisms: Application to the Modeling of the Oxidation of n-Butane, Combustion & Flame., 114, 81-102,1998.

Wauters S. PRIM manual, UGent, 1997.

Wenthold P.G., Polak M.L., Lineberger W.C. Photoelectron Spectroscopy of the Allyl and 2-Methylallyl Anions, J. Phys. Chem., 100 , 6920-6926, 1996.

Wijaya C.D., Sumathi R., Green W.H. Cyclic Ether Formation from Hydroperoxyalkyl Radicals (QOOH), J. Phys. Chem. A, 107, 4908-4920, 2003.

Wijaya C.D. PhD Dissertation, Massachusetts Institute of Technology, 2005.

Wong B.M., Matheu D.M., Green W.H. Temperature and Molecular Size Dependence of the High pressure Limit, J. Phys. Chem. A, 107, 6206-6211, 2003.

Chapter 3:

Network Generation

3.1   Introduction

The reaction network, i.e., the relationships among reactants, intermediates, and products, forms the basis for understanding complex reaction systems and for developing detailed models quantifying their kinetics. An accurate reaction network allows a better understanding and allows the optimization of product yields. Many experimental and theoretical techniques exist to obtain reaction networks. For microkinetic modeling automated network generation is the most appropriate method (Froment, 1991; Broadbelt et al., 1994; Green et al., 2001; Matheu et al., 2003; Wong et al., 2004). Automated network generation is based on the idea that some prior, often minimal, knowledge of the chemistry may be used to generate a complex reaction network, as complex networks are simply the manifestation of a small number of reaction families being applied to a large number of species. Knowledge of the appropriate reaction families is gained through experimental studies or complementary theoretical investigations of the reactions of interest and then translated into algorithms that the computer can utilize to generate networks automatically. Ideally, this method is well suited for any class of reactions considered in a specific process. While the crucial element of this technique is the initial knowledge of typical reactions that occur, it also provides a framework for testing ideas about likely chemical transformations that can occur. Furthermore, it can also result into specific reactions that the user may not have conceived or included in a reaction network developed manually, simply because of the vast number of possibilities.

To implement automated network generation for a particular reaction, the user must input the structure of the reactants, the set of reaction rules that are believed to capture the essential chemical transformations, the rules for their implementation and declare how the reaction rate coefficients are assigned to the considered reactions (Braodbelt et al., 1994; Green et al., 2001). For example, if the user desires to build a reaction network for ethane steam cracking, reaction

rules need to be defined for C-C bond scissions, hydrogen abstractions, β scissions, radical recombinations, radical addition and electrocyclizations. The core algorithms transform this information into reactant/product relationships, i.e. the reaction network. Finally reaction rate coefficients are assigned to the different reactions. Note that automated network generation is faithful to the reaction rules that are provided by the user, i.e. new transformations are not suggested by the software. However, application of the reaction rules to the reactants and their progeny facilitates network construction while providing capabilities for estimating rate constants as the reactions are revealed, and thus model generation and solution can be easily carried out in an iterative mode.

In the next paragraphs more details are given about how the reaction network is generated. The first step consists of identifying the species that should and should not be considered in the reaction network. Then a proper representation of the species is chosen that allows finding the different reactions. Finally a method is selected to assign systematically the appropriate pre-exponential factor and activation energy to a new reaction.

3.2 Species Selection

3.2.1 Molecules

The main part of the molecular species considered in the reaction network are molecules which are traditionally present in cracking feedstocks. These are for example n-paraffinic and iso-paraffinic compounds with less than 34 carbon atoms. Nonetheless, even for single event microkinetic models, it is not only convenient but also necessary to adopt several simplifications and lumping procedures in order to avoid an excessive number of chemical species and reactions (Ranzi et al., 2001). In principle, complete single event modeling of virgin naphthas or gasoils would require a detailed knowledge of the composition of the feedstock. However, this would be impossible because, in general, the real detailed composition of these fractions is not experimentally available and, moreover, the dimensions of the kinetic scheme and its computing times would be unacceptable. That is one of the main reasons that lumping is introduced in the reaction scheme. In Table 3.1 an overview is given of the components considered in the reaction network.

Hydrocarbon Type	Lowest Carbon number	Highest Carbon number	Number
hydrogen	-	-	1
n-paraffins	1	33	33
iso-paraffins			
2-methyl	4	10	7
3-methyl	6	10	5
4-methyl	8	10	3
2,2-dimethyl	5	10	6
2,3-dimethyl	6	10	5
2,4-dimethyl	7	10	4
2,5-dimethyl	8	10	3
2,6-dimethyl	9	10	2
3,3-dimethyl	7	10	4
3,4-dimethyl	8	10	3
3-ethyl	7	10	4
2,2,3-trimethyl	7	10	4
2,3,4-trimethyl	8	10	3
2-methyl,3-ethyl	8	10	3
lump	11	33	23
naphthenes			
5-ring: unbranched side chain	5	20	16
5-ring: branched side chain	8	20	13
5-ring: methyl branched side chains	7	9	3
6-ring: unbranched side chain	6	20	15
6-ring: branched side chain	9	20	12
6-ring: methyl branched side chains	8	9	2
Poly naphthenes: unbranched side chain	10	20	11
Poly naphthenes: branched side chain	13	20	8
olefins			
1-olefins and 2-olefins	2	32	60
di-olefins: unbranched side chain	3	31	29
di-olefins: branched side chain	5	32	28
acetylenes	2	3	3
cyclic mono-olefins	5	20	18
cyclic di-olefins	5	20	17
iso-olefins	4	32	29
naphthenic and aromatic olefins	8	20	15
aromatics			
mono-aromatics: unbranched side chain	6	20	15
mono-aromatics: branched side chain	8	20	15
di-aromatics: unbranched side chain	10	20	11
di-aromatics: branched side chain	13	20	8
tri-aromatics: unbranched side chain	14	20	7
tri-aromatics: branched side chain	17	20	4
poly-aromatics: unbranched side chain	18	24	7
poly-aromatics: branched side chain	21	24	4
indenes	9	12	4
naphtheno aromatics	10	20	11
Total	**1**	**33**	**478**

Table 3.1: List of molecules and lumps considered in the reaction network

Several components in Table 3.1 are lumped components. In Table 3.2 an overview of the different lumped components is given. The latter shows that all iso-paraffinic compounds with more than 11 carbon atoms are lumped into one single pseudo-component per carbon number. Consider a mixture of m iso-paraffinic compounds I_k with the same molecular weight. When these components are lumped into one single pseudo-component S, the pseudo rate coefficient k^{pseudo} for disappearance of the lumped component S is calculated as a weighed sum of the pseudo rate coefficients of the individual components:

$$k^{pseudo}(S) = \sum_{k=1}^{m} w_k k^{pseudo}(I_k)$$

[3. 1]

with w_k the weighing factor for component I_k. Only for the lumped component a continuity equation needs to be considered. Note that the differences in the pseudo rate coefficients of the different components should remain as small as possible because only then it is allowed to replace the different components by a single lumped component (Wei and Kuo, 1969; Kuo and Wei, 1969). That is why one lumped component is defined per carbon number and per class of components. The composition of each lumped component consists then solely from isomers.

Hydrocarbon Type	Lowest Carbon number	Highest Carbon number	Number
iso-paraffins			
lump	11	33	23
naphthenes			
5-ring: branched side chain	8	20	13
6-ring: branched side chain	9	20	12
Poly naphthenes: branched side chain	14	20	8
olefins			
2-olefins	2	32	60
di-olefins: branched and unbranched side chain	3	31	29
cyclic mono-olefins and di-olefins	5	20	18
iso-olefins	4	32	29
naphthenic and aromatic olefins	8	20	15
aromatics			
mono-aromatics: branched side chain	9	20	12
di-aromatics: unbranched side chain	14	20	7
tri-aromatics: unbranched side chain	18	20	3
poly-aromatics: branched side chain	22	24	3

Table 3.2: Lumped components considered in the reaction network

Principally, the weighing factors w_k should be determined from the detailed analytical composition of the feedstock (Ranzi et al., 2001). This implies that for each feedstock new lumped components need to be defined. Vercauteren (1991) used fixed weighing factors for the iso-paraffinic compounds. Based on the analysis of a large amount of naphtha and kerosene fractions he found that the distribution of the different isomers is more or less independent of the feedstock. This conclusion was confirmed by Ranzi et al. (2001). Of course, it is true that the lumping procedure restricts the range of validity of the model. For instance, it is no longer possible to use the existing model to analyze the decomposition of a specific pure component that has been lumped. However, if there is interest in the behavior of a specific isomer, it is always both possible and easy to remove one or other hypothesis and to enlarge the kinetic scheme explicitly to include that component. This lumping flexibility is one of the relevant advantages of mechanistic kinetic schemes. In Table 3.3 the values for the weighing factors for iso-paraffinic compounds are given. The latter are identical to those used by Vercauteren (1991).

Isomer	Weighing Factor
2-methyl	0.207
3-methyl	0.231
4-methyl	0.128
5-methyl	0.157
3-ethyl	0.191
2,3-dimethyl	0.060
2,4-dimethyl	0.026
others	0.000

Table 3.3: Weighing factors for the iso-paraffinic lumped components

Note that the weighing factors can significantly influence the simulation results. Especially for the simulated ethylene and propylene yield the differences can become significant (Vercauteren, 1991). In particular when large amounts of di- and tri-methyl substituted iso-paraffins with more than 10 carbon atoms are present in the mixture it can be necessary to re-determine the lumped components. Otherwise this can lead to significant errors.

Other important compounds are naphthenic compounds. In some cases, e.g. for some "exotic" naphthas, their fractions can be over 50 wt% of the total feedstock mixture. A distinction is made between naphthenic compounds with a five or six ring and with multiple rings. Again components with more than 10 carbon atoms are lumped into one single component per carbon number. Note that still a distinction is made between the type of naphthenic molecule (5 or 6 ring or multiple rings; branched and unbranched side chain) as shown in Table 3.1. For the lumping of the naphthenic compounds equal weighing factors are used for each constituent. Vercauteren (1991) lumped the naphthenic compounds in a similar way.

It is also necessary to lump the intermediate components properly. Ranzi et al. (2001) distinguished between linear and branched olefins for each carbon number. In the present work the description for the intermediate olefins is a lot more detailed. A distinction is made between branched and unbrached olefins, between di and mono olefins and between cyclic, aromatic and paraffinic olefins. The choice of which lumped component should be selected depends on which isomers are mostly formed in the reaction schemes. For molecules with a long chain it is certainly so that most of the C-C scissions and hydrogen abstraction reactions take place in the long chain. This justifies the choice for the olefins with double bounds on the other side of the chain as lumped components. Figure 3.1 shows that when a hydrogen is abstracted from 4-methyloctane mainly 1-olefins are formed in the primary reaction scheme. The amount of unbranched mono olefins with the double bond not in α position is small. Therefore only a distinction is made between olefins with the double bond 1- and 2-olefins. The 2-olefins represent all unbranched olefins for which the double bond is not situated in α position. Similarly all unbranched di-olefins are represented by lumped components for which the double bonds are located at both ends of the chain. These assumptions are introduced because, compared to the 2-olefins and α,ω di-olefins, the concentrations of the other olefins belonging to these categories of molecules are almost negligible. Moreover, comparison of the reaction schemes for these isomers shows that most of the formed radicals in the respective reaction schemes are identical. Lumping of these components not only results in a reduction of the number of species but also reduces the number reaction schemes that should be generated. A new group of molecules introduced in the reaction scheme are cyclic mono-olefins. Vercauteren (1991) eliminated these molecules from the reaction scheme by assuming the pseudo steady state for these molecules and assuming that hydrogen abstractions were the only reaction possibility for these species.
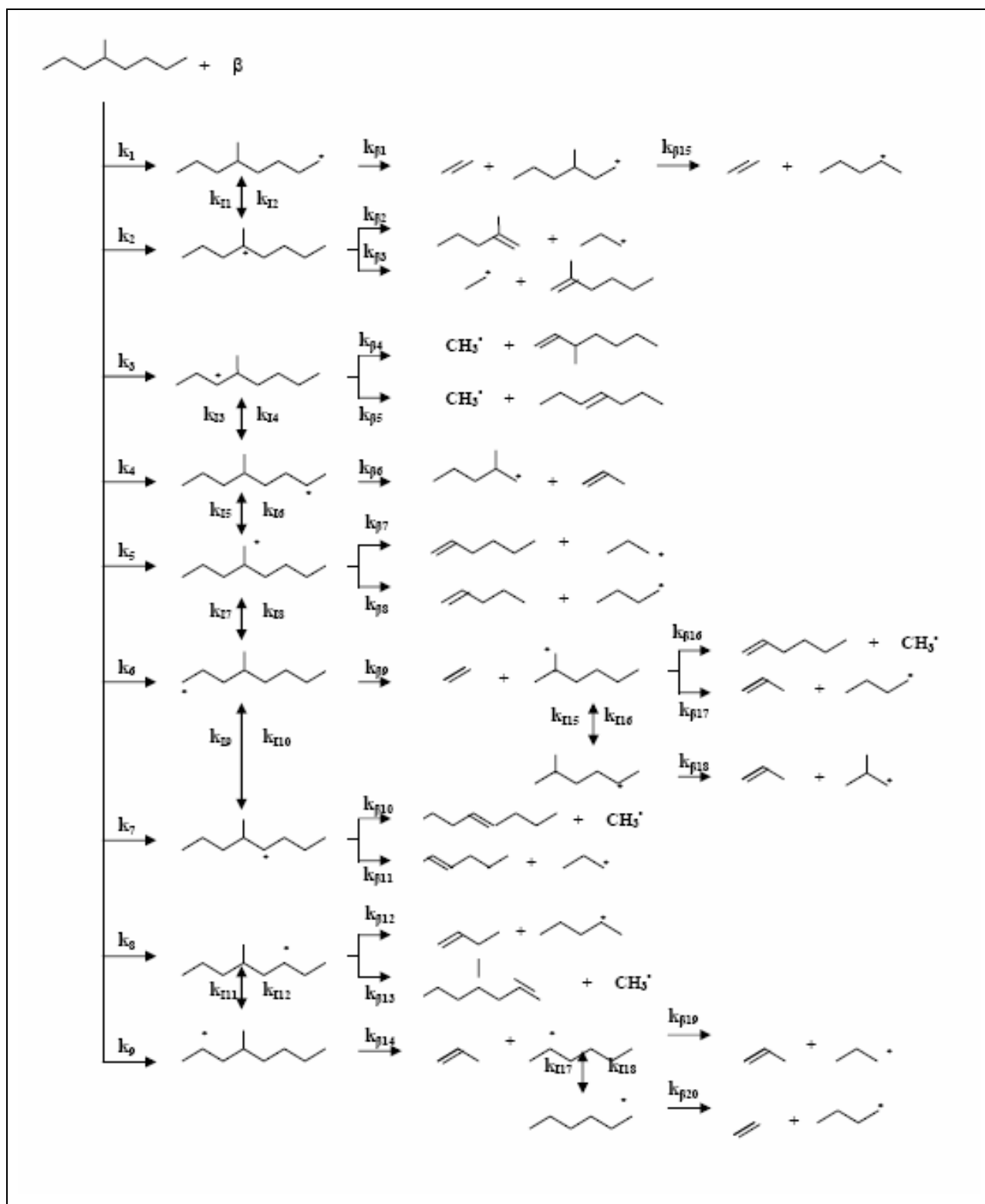
Figure 3.1: Primary reaction scheme of a hydrogen abstractions from 4-methyloctane

The iso-olefinic compounds with more than 6 carbon atoms are lumped in one single component per carbon number. Similar to Vercauteren (1991) equal weighing factors are used for iso-olefinic compounds because the exact composition of these branched olefins in the reaction mixture cannot be easily determined experimentally. Indeed, each branched olefin is formed in the reaction schemes of several iso-paraffinic compounds, which differ both in size and character. The choice of the olefins with the double bond in α position of the methyl branches can be explained by the preferential abstraction of tertiary hydrogen atoms on 3-, 4- and 5-methyl paraffins. The latter can also be seen in the reaction scheme of 4-methyloctane in Figure 3.1. Abstraction of the tertiary hydrogen leads to iso-olefinic compounds with the double bond in α position. Moreover, in the scheme for 4-methyloctane only iso-olefinic compounds with the double bond in α position are formed.

Note that in Table 3.1 no olefins with 3 double bonds are present. This is because the concentrations of the molecules are eliminated by assuming the pseudo steady state for their concentrations and assuming that electrocyclizations are the only reaction for the disappearance of these molecules. Electrocyclizations are very fast reactions (Shiess and Dinkel, 1981) and are important routes towards the formation of aromatic compounds (Jutz, 1978; Kopinke et al., 1987).

Also for the aromatic compounds several lump components are introduced as can be seen in Table 3.2. The mono, di, tri and poly aromatics with a branched side chain are lumped per carbon number. Vercauteren did not consider most of these compounds. In fact compared to Vercauteren (1991) the number of components is more than 40 % higher, and compared to the network of Plehiers (1989) the number of components has more than doubled. The main reasons are the introduction of more aromatic compounds and increasing the maximum carbon number of the molecules. The introduction of more di-, tri-, poly- and naphtheno-aromatic compounds is on the one hand necessary to be able to simulate VGO fractions. On the other hand these molecules form also an important part of the pyrolysis fuel oil (PFO) fraction. The PFO fraction is the heavy fraction [boiling point higher than 473 K] formed during steam cracking of liquid feedstocks. The most important components of the PFO fraction are: naphthalene, methyl naphthalene, fluorene, acenaphthalene, anthracene, phenantrene, methyl anthracene, methyl phenantrene, pyrene and chrysene (Lauer, 1988; Plehiers, 1991; Nomura et al., 1995; Bolado, 2003).

	Pyrolysis Fuel Oil Composition (wt%)		
	Naphtha 1*	Naphtha 2*	Naphtha 3 °
methyl indene	0.5	1.0	8.9
naphthalene	4.2	7.0	7.0
dimethyl indene	0.9	1.7	6.7
2-methyl naphthalene	6.2	8.2	5.0
1-methyl naphthalene	5.4	6.6	4.3
biphenyl	5.5	5.9	1.9
ethyl naphthalene	2.2	2.2	4.5
methyl biphenyl	3.1	2.4	2.9
dimethyl naphthalene	4.5	3.2	7.0
vinyl naphthalene	1.3	1.4	3.1
acenaphthalene	1.9	1.6	1.9
methyl vinyl naphthalene	1.7	1.0	3.3
ethyl methyl naphthalene	0.6	0.5	2.3
methyl acenaphthalene	0.9	0.5	5.7
trimethyl naphthalene	0.5	0.4	1.1
fluorene	3.6	3.2	1.5
methyl fluorene	1.9	2.3	1.7
phenantrene	6.3	4.5	2.3
anthracene	0.8	0.6	0.9
methyl phenantrene	3.4	3.6	2.5
methyl anthracene	0.9	0.5	0.5
fluoranthene	1.1	1.0	0.4
pyrene	1.3	1.0	0.4
chrysene	0.4	0.3	0.3

Table 3.4: Weight fractions of the main components of the pyrolysis fuel oil fraction (PFO) formed during the cracking of 3 different naphtha fractions (total fuel oil fraction = 100 wt %) [* Lauer, 1988; ° Bolado, 2003]

In Table 3.4 an overview is given of the main components of the fuel oil fraction formed during the cracking of three naphtha feedstocks. No unconverted feedstock molecules are specified in Table 3.4 because in industry almost all the naphtha feedstock molecules with a boiling point higher than 474 K are typically converted. Knowing more details about the heavy fraction formed during cracking is in particular important to understand the coke formation phenomenon. As stated previously, these heavy components are important precursors of coke formation in both the reactor and the TLE. However, also for environmental reasons it is important to know the composition of the PFO fraction. As this fraction contains mainly aromatics this stream is highly carcinogenic and direct contact with this stream can cause serious health problems (American Chemical Council, 2003). Another problem encountered with PFO is gum formation by thermal polymerization, causing combustion problems if the fraction is used as fuel. These considerations show that it is important to extend the reaction network of Vercauteren (1991) with reactions involving the aromatic compounds part of the PFO fraction.

In Table 3.1 no distinction is made between molecules belonging to the µ network and molecules belonging to the β network. This is because making such a distinction for molecules does not really make sense. In fact almost all the molecules considered in the microkinetic model are considered in the µ network either as product or as reactant. For example, ethylene can be formed via decomposition of a heavy µ radical in the µ network, or via a small β radical such as the ethyl radical in the β network. Additions by C_5 radicals to ethylene are than again primary reactions considered in the µ network. Only some molecules with more than 5 carbon atoms are considered in the µ network.

3.2.2 Radicals

All possible radicals with five or less carbon atoms are considered in the reaction network. Important is that in contrast to Dente et al. (1986) no lumping of radicals is allowed. This model assumption causes strong distortions of the product distribution because some chemical transformations are considered that are chemically impossible. Introducing the µ radical concept already drastically reduces the number of radicals for which a continuity equation should be solved. In contrast to Vercauteren (1991) also bimolecular reactions involving radicals with 5 carbon atoms are considered. These used to be eliminated by assuming a µ-character and

applying the pseudo steady state assumption. This means that the number of radicals for which a continuity equation must be solved doubles. In Table 3.4 an overview of the considered radicals is given.

hydrogen radical	methyl radical
vinyl radical	ethyl radical
allyl radical	prop-1-en-1-yl radical
prop-1-en-2-yl radical	1-propy radical
2-propyl radical	1-butyl radical
2-butyl radical	tert-butyl radical
isobutyl radical	2-methylallyl radical
pent-3-en-1-yl radical	1-penten-3-yl radical
but-3-en-1-yl radical	1,4-pentadien-3-yl radical
neopentyl radical	3-methyl-1-buten-3-yl radical
3-butenyl,2 methylene radical	2-methylbut-2-yl radical
butyl,2-methylene- radical	1-pentyl radical
2-pentyl radical	3-pentyl radical
3-cyclopentenyl radical	1-buten-3-yl radical
cyclopentadienyl radical	3-butenyl, 2-methyl radical
cyclopentyl radical	2-penten-4-yl radical
cyclohexyl radical	2-cyclopentenyl radical
benzyl radical	1-phenyleth-1-yl radical
2-phenyleth-1-yl radical	1-naphtyl methyl radical
1-phenantryl methyl radical	1-anthracyl methyl radical
1-peryl methyl radical	

Table 3.5: List of radicals considered in the single event microkinetic model for steam cracking

Another important extension is the consideration of several aromatic radicals. The following aromatic radicals are explicitly accounted for in reaction network: the benzyl radical, the 2-phenyleth-1-yl radical, the 1-phenyleth-1-yl radical and the 1-naphtyl methyl radical.

Vercauteren (1991) eliminated the benzyl radical by assuming that the only reaction possibility of this radical was a hydrogen abstraction and that the pseudo steady state assumption (PSSA) could be applied for its concentration. Other aromatic radicals were either not considered in the reaction network or their concentrations were eliminated by assuming that they were μ radicals and the PSSA (Vercauteren, 1991). If the aromatic fraction is important then reactions of these radicals will be partly responsible for components of the pyrolysis fuel oil (PFO) fraction. This is important because components of the PFO fraction are believed to be important precursors for coke formation in both the reactor and in the TLE. Also the introduction of aromatic radicals is important for accurately simulating experiments with large amounts of toluene in the feedstock.

3.3   Computer generation of the reaction network

Techniques that have been developed for automated network generation all operate according to the same basic principles. First information is provided about the reactants and the reaction families, and then the computer transforms this information into the reaction network, i.e., a list of reactant/product pairs. Computer generation of reaction species, properties and networks relies heavily on three capabilities concerning the atomic connectivity of species:

- the representation of constituent atoms and their chemical environment in a molecule
- the implementation of chemical reactions and determination of reaction products
- the determination of the uniqueness of chemical species

In the next paragraphs these 3 different aspects are discussed in more detail.

3.3.1 Species representation

The same approach as Clymans and Froment (1984) has been used for representation of the species and for the investigation of the reaction possibilities. Clymans and Froment (1984) used the binary relation matrix concept for their computer generation of the reaction paths for the pyrolysis of normal and branched paraffins. The basic principle is that every chemical structure can be represented by a graph. This graph can be translated into a binary relation matrix. The columns and rows represent the carbon atoms in the graph, while the elements of the matrix, m_{ij},

are 1 or zero whether there is a C-C bond between the carbon atoms i and j or not. As in the Boolean algebra 1 is 'true' and 0 is 'false'. The representation can be illustrated for the 1-hexylradical. The matrix M represents the structure of the radical, while the variable n^{RAD} represents the radical position. The cracking rules can then be translated to matrix operations performed on the Boolean relation matrix (Hillewaert et al. 1988).

$$\underline{M} = \begin{bmatrix} 0 & 1 & 0 & 0 & 0 & 0 \\ 1 & 0 & 1 & 0 & 0 & 0 \\ 0 & 1 & 0 & 1 & 0 & 0 \\ 0 & 0 & 1 & 0 & 1 & 0 \\ 0 & 0 & 0 & 1 & 0 & 1 \\ 0 & 0 & 0 & 0 & 1 & 0 \end{bmatrix}$$

$$n^{RAD} = 1$$
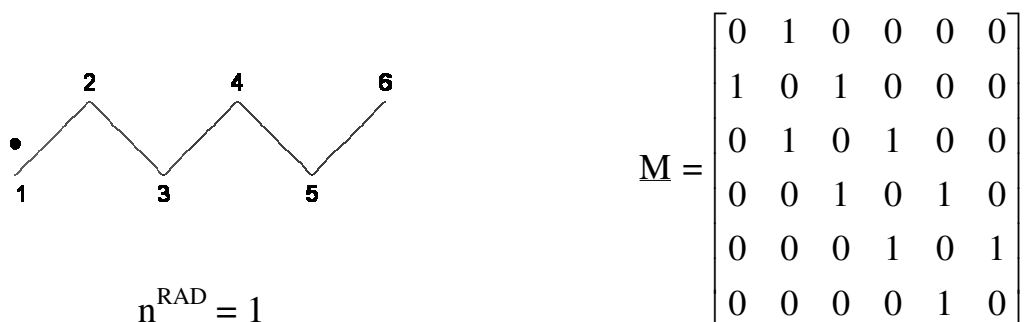
3.3.2 Reaction identification

3.3.2.1 *C-C scission of molecules and recombination*

All C-C scission possibilities are given by the non-zero elements of the binary relation matrix $\underline{M}$. Only the upper part above the diagonal of the matrix is considered, otherwise the scissions are double counted. Consider for example the C-C scission of n-hexane into the 1-butyl radical and the ethyl radical:

$$\underline{M} = \begin{bmatrix} 0 & 1 & 0 & 0 & 0 & 0 \\ 1 & 0 & 1 & 0 & 0 & 0 \\ 0 & 1 & 0 & 1 & 0 & 0 \\ 0 & 0 & 1 & 0 & 1 & 0 \\ 0 & 0 & 0 & 1 & 0 & 1 \\ 0 & 0 & 0 & 0 & 1 & 0 \end{bmatrix} \longrightarrow \underline{M}' = \begin{bmatrix} 0 & 1 & 0 & 0 & 0 & 0 \\ 1 & 0 & 1 & 0 & 0 & 0 \\ 0 & 1 & 0 & 1 & 0 & 0 \\ 0 & 0 & 1 & 0 & 0 & 0 \\ 0 & 0 & 0 & 0 & 0 & 1 \\ 0 & 0 & 0 & 0 & 1 & 0 \end{bmatrix}$$
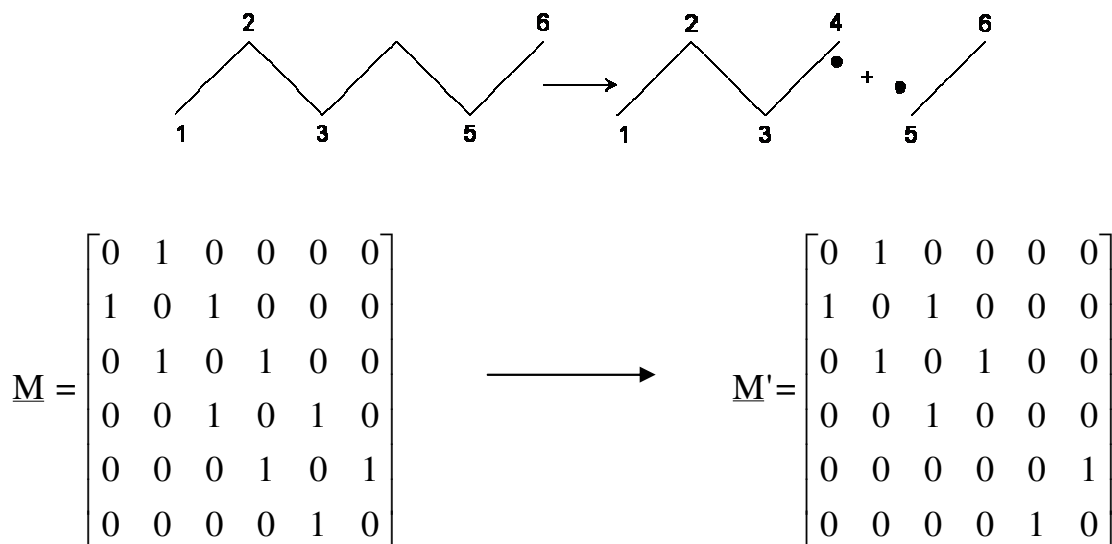
This new matrix is split into two matrices $\underline{R}_1$ and $\underline{R}_2$. A renumbering of the species is also carried out in the program.

$$\underline{R}_1 = \begin{bmatrix} 0 & 1 \\ 1 & 0 \end{bmatrix}$$

$$n^{RAD} = 1$$

$$\underline{R}_2 = \begin{bmatrix} 0 & 1 & 0 & 0 \\ 1 & 0 & 1 & 0 \\ 0 & 1 & 0 & 1 \\ 0 & 0 & 1 & 0 \end{bmatrix}$$
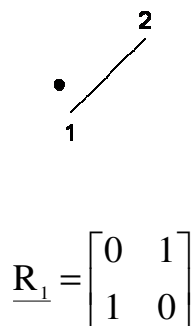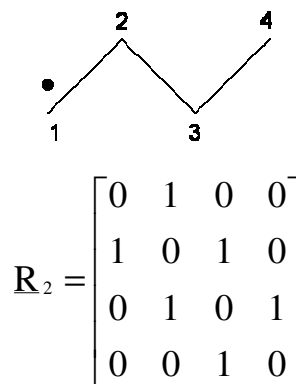
$$n^{RAD} = 1$$

Special care has to be taken in case of olefins, aromatics or naphthenes. For olefinic and aromatic compounds, the C-C scissions in which double bonded or aromatic carbon atoms participate, are not taken into account. This also implies that breaking of the C-C bond in α-position to the double bond or aromatic ring is excluded. Such bonds are stronger due to the presence of the π-bond (Baas, 1963), hence scission can be neglected compared to the other C-C scission possibilities. Scission reactions of naphthenes by scission of the C-C bond inside a ring are slower than those of paraffins (Tsang, 1978) and are thus not considered in the reaction network. The reason is the fast inverse reaction, the recombination of the formed diradical. In mixtures with paraffinic feed components, or in presence of side chains, the C-C scissions inside the ring are negligible (Vanneste, 1985). When cracking naphthenes without side chains, these reactions become important, since they are the only source for the formation of β radicals.

The reverse recombination reactions are obtained in a similar way. Instead of removing a bond, a new bond is introduced between the 2 carbon atoms carrying the free electrons of the two radicals. The number of carbon atoms is set equal to the sum of the individual carbon numbers of the radicals.

3.3.2.2 *Hydrogen abstraction reactions*

All abstraction possibilities are determined by means of the relation matrix $\underline{M}$ and the vectors $\underline{D}$ and $\underline{A}$, which contain the positions of the double bonded and aromatic carbon atoms. In mathematical formulas a hydrogen abstraction corresponds to the filling of the variable n^{RAD}, which contains the position of the free electron. The formed radical has the same binary relation matrix as the original molecule, since no C-C bonds are broken. The vectors D and A prevent abstraction of hydrogen atoms from sp^2-hybridisized carbon atoms. Since the rate of abstraction of these hydrogen atoms is much smaller than that of the other abstraction possibilities, it is justified to omit these reactions apart form some exceptions. Consider for example the hydrogen abstraction by a β radical from hexane:
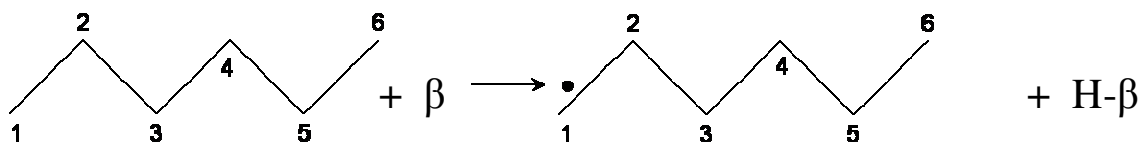
The 1-hexyl radical is characterized by:

$$\underline{M} = \begin{bmatrix} 0 & 1 & 0 & 0 & 0 & 0 \\ 1 & 0 & 1 & 0 & 0 & 0 \\ 0 & 1 & 0 & 1 & 0 & 0 \\ 0 & 0 & 1 & 0 & 1 & 0 \\ 0 & 0 & 0 & 1 & 0 & 1 \\ 0 & 0 & 0 & 0 & 1 & 0 \end{bmatrix} \qquad n^{RAD} = 1$$

Another hydrogen abstraction reaction is an internal hydrogen abstraction, i.e. a 1,5- and 1,4-isomerization reactions. These reaction possibilities are given by respectively the fourth and the third power of the binary relation matrix $\underline{M}$. Tracing isomerization possibilities is indeed equivalent to tracing fourth order and third order relations. To find the 1,5-isomerizations first the square of the matrix $\underline{M}^2 - \underline{I}$ needs to be calculated. The diagonal elements have no meaning because they do not represent new isomerization reactions, and therefore are removed. Some bonds in this isomerization step appear twice. Finally all isomerization possibilities follow from the binary relation matrix $\underline{M}'^4$:

$$\underline{M}'^4 = \left(\underline{M}^2 - \underline{I}\right)^2 - \underline{I} - \left(\underline{M}^2 - \underline{I}\right)$$

[3. 2]

Hence, the 1,5-isomerisation possibilities of the 1-hexyl radical are traced by means of:

$$\underline{M}'^4 = \begin{bmatrix} 0 & 0 & 0 & 0 & 1 & 0 \\ 0 & 0 & 0 & 0 & 0 & 1 \\ 0 & 0 & 0 & 0 & 0 & 0 \\ 0 & 0 & 0 & 0 & 0 & 0 \\ 1 & 0 & 0 & 0 & 0 & 0 \\ 0 & 1 & 0 & 0 & 0 & 0 \end{bmatrix}$$

Since the free electron is located on carbon atom 1, the 1-hexyl radical isomerizes to the hexyl radical with radical position on carbon atom 5. For an isomerization reaction only the variable n^{RAD} changes. Both radicals have the same binary relation matrix $\underline{M}$.
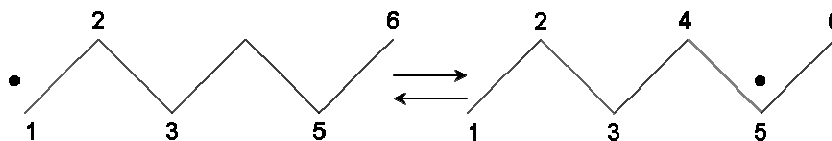
The transition state of the intra molecular 1,5- and 1,4-isomerization reactions is a ring structure, and thus requires a sufficient flexibility of the chain. Olefinic radicals are hampered when the double bond participates in the intermediate hexagonal ring structure and therefore are not likely to isomerize. Before performing the isomerization, first it has to be determined whether or not double bonded carbon atoms are involved in the ring formation. Only in the case no evident decomposition is possible the isomerization is considered. For example for the 3-en-1-hexyl radical the 1,5-isomerization is important (Kopinke et al., 1983):
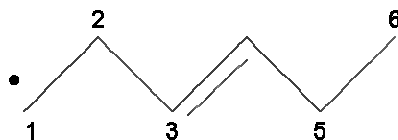
Isomerization of cyclic radicals occurs when the free electron is located in a long side chain. Another possibility is that the second side chain is in ortho position of the side chain on which the free electron is situated. Isomerization over a set of coupled C-C bonds that belong to a ring system are excluded because these reactions are slow (Kopinke et al. , 1983). Isomerization is avoided by setting the second order relations between two ring carbon atoms in the matrix $\underline{M}^2 - \underline{I}$ equal to zero.

3.3.2.3 *Addition and β scission*

The vector $\underline{D}$ with the positions of the double bonded carbon atoms determines the possible addition locations. The binary relation matrix of the formed μ radical in the addition of other β radicals is not the same as for the olefin, because the adding radical changes the structure of the olefin. The binary relation matrix of the olefin is expanded with as many rows and columns as there are carbon atoms in the β radical. Consider for example the addition of a methyl radical to 1-hexene:
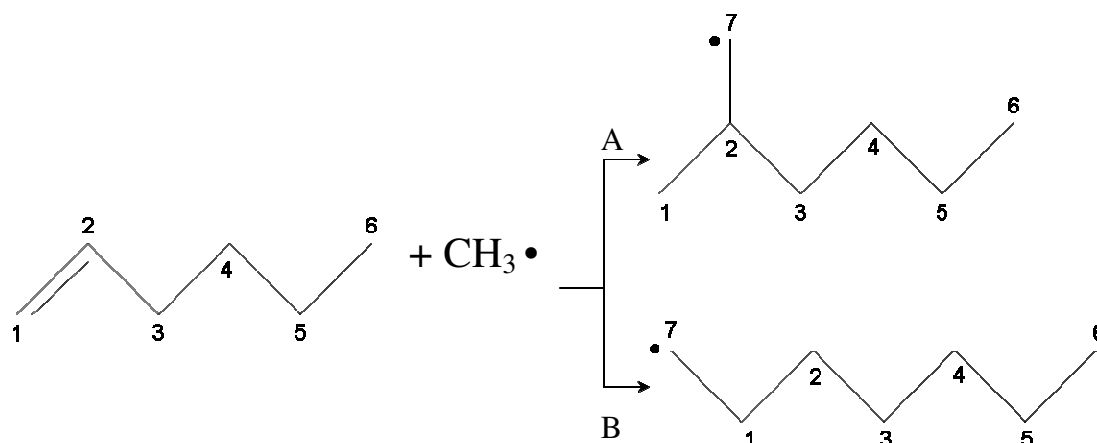
1-Hexene is represented by the following relation matrix $\underline{M}$ and vector $\underline{D}$:

$$\underline{M} = \begin{bmatrix} 0 & 1 & 0 & 0 & 0 & 0 \\ 1 & 0 & 1 & 0 & 0 & 0 \\ 0 & 1 & 0 & 1 & 0 & 0 \\ 0 & 0 & 1 & 0 & 1 & 0 \\ 0 & 0 & 0 & 1 & 0 & 1 \\ 0 & 0 & 0 & 0 & 1 & 0 \end{bmatrix} \qquad \underline{D} = \begin{bmatrix} 1 \\ 2 \end{bmatrix}$$

The matrix $\underline{M}'$, that represents the μ radical, is derived from $\underline{M}$ by adding a row and a column, that represent the carbon atom from the added methyl radical. The relations, that represent the new C-C bonds, are set equal to one. For reaction possibility A these are m'_{27} and m'_{72}. For reaction possibility B these are m'_{17} and m'_{71}. The binary relation matrices, that represent the respective radicals, are:

$$
\underline{M}'_1 = \begin{bmatrix} 0 & 1 & 0 & 0 & 0 & 0 & 0 \\ 1 & 0 & 1 & 0 & 0 & 0 & 1 \\ 0 & 1 & 0 & 1 & 0 & 0 & 0 \\ 0 & 0 & 1 & 0 & 1 & 0 & 0 \\ 0 & 0 & 0 & 1 & 0 & 1 & 0 \\ 0 & 0 & 0 & 0 & 1 & 0 & 0 \\ 0 & 1 & 0 & 0 & 0 & 0 & 0 \end{bmatrix}
\qquad
\underline{M}'_2 = \begin{bmatrix} 0 & 1 & 0 & 0 & 0 & 0 & 1 \\ 1 & 0 & 1 & 0 & 0 & 0 & 0 \\ 0 & 1 & 0 & 1 & 0 & 0 & 0 \\ 0 & 0 & 1 & 0 & 1 & 0 & 0 \\ 0 & 0 & 0 & 1 & 0 & 1 & 0 \\ 0 & 0 & 0 & 0 & 1 & 0 & 0 \\ 1 & 0 & 0 & 0 & 0 & 0 & 0 \end{bmatrix}
$$

$$
n^{RAD} = 7 \qquad\qquad\qquad n^{RAD} = 1
$$

In the special case that the adding β radical is a hydrogen radical, the formed μ radicals are presented by the same binary relation matrices as the olefin from which they are generated.

Next to external addition reactions also internal addition reactions are considered. Ring formation of olefinic radicals takes place when the radical position is at a distance of four (1,5-cyclization) or five (1,6-cyclization) carbon atoms from the double bonded carbon atom. The possibilities for 1,6-cyclization are found by the fifth power of the binary relation matrix. The third order relations, deduced from the third power of $\underline{M}$, have to be removed. These represent cyclizations, in which a bond appears twice in the ring structure. The following expression allows to trace the 1,6-cyclisation possibilities :

$$
\underline{M}'^5 = \underline{M} \cdot \left(\left(\underline{M}^2 - \underline{I} \right)^2 - \underline{I} - \left(\underline{M}^2 - \underline{I} \right) \right) - \left(\underline{M} \cdot \left(\underline{M}^2 - \underline{I} \right) - \underline{M} \right) \qquad [3. 3]
$$

Consider for example the cyclization of the hex-1-en-6-yl radical:
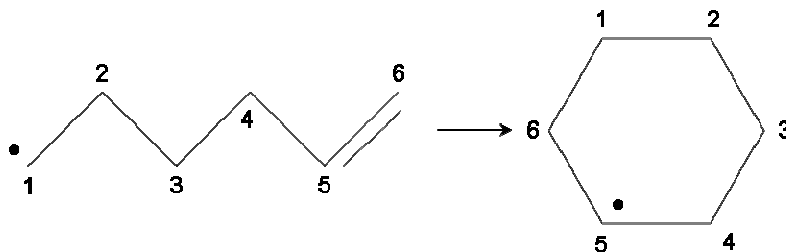
In matrix representation the hex-1-en-6-yl radical is given by:

$$\underline{M} = \begin{bmatrix} 0 & 1 & 0 & 0 & 0 & 0 \\ 1 & 0 & 1 & 0 & 0 & 0 \\ 0 & 1 & 0 & 1 & 0 & 0 \\ 0 & 0 & 1 & 0 & 1 & 0 \\ 0 & 0 & 0 & 1 & 0 & 1 \\ 0 & 0 & 0 & 0 & 1 & 0 \end{bmatrix} \qquad n^{RAD} = 1 \qquad \underline{D} = \begin{bmatrix} 5 \\ 6 \end{bmatrix}$$

A fifth order relation exists between C_1 and C_6, as can be deduced from:

$$\underline{M}'^5 = \begin{bmatrix} 0 & 0 & 0 & 0 & 0 & 1 \\ 0 & 0 & 0 & 0 & 0 & 0 \\ 0 & 0 & 0 & 0 & 0 & 0 \\ 0 & 0 & 0 & 0 & 0 & 0 \\ 0 & 0 & 0 & 0 & 0 & 0 \\ 1 & 0 & 0 & 0 & 0 & 0 \end{bmatrix}$$

Since the free electron is located on the sixth carbon atom, that is double bonded, a 1,6-cyclization possibility is found. The free electron moves then to second carbon atom. The cyclic radical is represented by a new binary relation matrix $\underline{M}'$, that results from the original matrix $\underline{M}$ by adding the relations m'_{16} and m'_{61}.

$$\underline{M} = \begin{bmatrix} 0 & 1 & 0 & 0 & 0 & 1 \\ 1 & 0 & 1 & 0 & 0 & 0 \\ 0 & 1 & 0 & 1 & 0 & 0 \\ 0 & 0 & 1 & 0 & 1 & 0 \\ 0 & 0 & 0 & 1 & 0 & 1 \\ 1 & 0 & 0 & 0 & 1 & 0 \end{bmatrix} \qquad n^{RAD} = 5$$

The 1,5-cyclization possibilities are obtained from the fourth power of the binary relation matrix:

$$\underline{M}'^4 = \left(\underline{M}^2 - \underline{I}\right)^2 - \underline{I} - \left(\underline{M}^2 - \underline{I}\right) \qquad\qquad [3.4]$$

A radical decomposes by scission of the C-C bond in β position of the free electron. Two carbon atoms i and j are in β position of each other if there exists at least one carbon atom that fulfills

$$m_{ik} \cdot m_{kj} = 1 \text{ and } k \neq i,j \qquad\qquad [3.5]$$

Tracing these 1,3 relations between carbon atoms is equivalent to calculating the square of the binary relation matrix $\underline{M}$. Since each carbon atom is connected to itself by two bonds with his neighboring carbon atom, the elements on the diagonal of the matrix $\underline{M}^2$ represent no real β position, hence they can be set equal to zero. The scission possibilities are then given by the non-zero elements in the matrix $\underline{M}^2 - \underline{I}$, with $\underline{I}$ the unit matrix. Consider for example the β scission of the 1-hexyl radical:
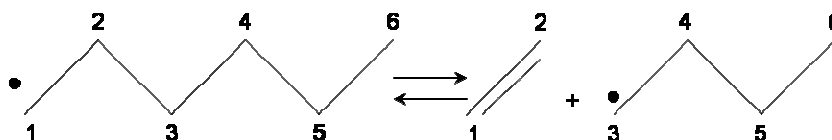
The matrix $\underline{M}^2 - \underline{I}$ is given by:

$$\underline{M}^2 - \underline{I} = \begin{bmatrix} 0 & 0 & 1 & 0 & 0 & 0 \\ 0 & 0 & 0 & 1 & 0 & 0 \\ 1 & 0 & 0 & 0 & 1 & 0 \\ 0 & 1 & 0 & 0 & 0 & 1 \\ 0 & 0 & 1 & 0 & 0 & 0 \\ 0 & 0 & 0 & 1 & 0 & 0 \end{bmatrix}$$

The relation $(\underline{M}^2 - \underline{I})_{13}$ equals 1 indicates that there is a β scission possibility where the free electron moves from first carbon atom to the third carbon atom. In this case k equals 2 and the double bond of the resulting olefin is located between the first and the second carbon atom. Ethylene has the binary relation matrix $\underline{O}$, whereas $\underline{R}$ and the variable n^{RAD} specify the 1-butylradical.

$$\underline{O} = \begin{matrix} 1 \\ 2 \end{matrix} \begin{bmatrix} 0 & 1 \\ 1 & 0 \end{bmatrix} \qquad \overline{D} = \begin{bmatrix} 1 \\ 2 \end{bmatrix} \qquad \underline{R} = \begin{matrix} 3 \\ 4 \\ 5 \\ 6 \end{matrix} \begin{bmatrix} 0 & 1 & 0 & 0 \\ 1 & 0 & 1 & 0 \\ 0 & 1 & 0 & 1 \\ 0 & 0 & 1 & 0 \end{bmatrix}$$

$$n^{RAD} = 3$$

Note that the second order relations, in which double bonded carbon atoms participate, have to be omitted. The C-C bond in α position is stronger by the presence of the double bond, hence this scission is significantly slower than the other possibilities. Furthermore, scission of the double bond is also impossible. When a double bond is located in γ position of the free electron and the only available C-C bond is situated in α position with regard to the double bond, then the C-H bond in β position to the free electron is broken. The radical reacts through the scission of the bond that has the lowest activation energy. The activation energy for breaking the C-H bond in the 2-hexen-5-yl radical is only 285 kJ mol^{-1}, while that of a C-C bond is 350 kJ mol^{-1} (Moens, 1982). Tracing the C-H scission comes down to tracing the carbon atom that is in α position to the free electron as well to the double bond. This carbon atom forms a new double bond together

with the carbon atom, on which the free electron was located. The original position of the free radical is eliminated.

3.3.3 Species uniqueness

One of the problems of the Boolean relation matrix representation is species uniqueness. Also if a self-learning system is implemented, storage of the matrices demands large memory capacities. Therefore a compact and unique label formulation should be introduced to characterize a species unambiguously. Several methods have and continue to be developed to represent species in a unique way (Clymans and Froment, 1984; Vynckier and Froment, 1991; Broadbelt et al., 1994; Warth et al., 1998; Wauters and Marin, 2001; Rovner, 2005). Clymans and Froment (1984) used the binary relation matrix concept for their computer-generation of the reaction paths and the corresponding rate equations in case of pyrolysis of normal and branched paraffins. The basic principle is that every chemical structure can be represented by a graph (Balaban, 1976; Trinajstic, 1983; King and Rouvray, 1987). This graph can be translated into a binary relation matrix. Also Vynckier and Froment (1991) used this approach for the generation of a network for hydrocracking. Besides the binary relation matrix a standardized name is assigned to each species consisting of a scalar indicating the charge and two arrays of integers, one specifying whether the carbon atoms are primary, secondary, tertiary or quaternary and the other characterizing each carbon atom using the codes mentioned in Table 3.6. Wauters and Marin (2001) used a similar method for generating a model based on elementary reactions for coke formation during steam cracking.

1	aromatic carbon atom
2	naphthenic carbon atom that is part of a double bond
3	other naphthenic carbon atom
4	acyclic carbon atom that is part of a double bond
5	other acyclic carbon atom

Table 3.6: Codes used for identifying the carbon atoms (Vynckier and Froment, 1991)

Broadbelt et al. (1994) developed a variant of the graph theory-based generation in which as well reactants and products as the reactions themselves are represented by matrices. The implementation of these graph theory concepts and algorithms requires efficient representation and encoding of the graphs. The adjacency matrix (Tarjan, 1977) for a graph, G, is the n-by-n matrix $M = (m_{ij})$ with elements 0 and 1, such that $m_{ij} = 1$ if (v_i, v_j) is an edge of G or a connection between vertices (or atoms) of G and $m_{ij} = 0$ otherwise. The bond and electron (BE) matrix (Ugi, 1979) augments the adjacency matrix and provides a description of not only the connectivity of a molecule but also its formal electronic state. The diagonal element, ii, of the BE matrix gives the number of non-bonded valence electrons of atom i, and off-diagonal entries, ij, provide the connectivity and bond order of atoms i and j. An example BE matrix for ethyl radical is shown in Figure 3.2. The rows of the BE matrix correspond to the atoms in the order in which they are numbered in the picture on the left. Chemical reaction may then be carried out via simple manipulations of the BE matrices of reactant molecules. The BE matrix is well suited for description of chemical reactions because the number of atoms actually affected in a chemical reaction is small. The BE sub-matrix comprising only those atoms is small and dense. To carry out a particular reaction type, the reaction matrix that quantifies the change in the electronic configurations and the connectivity among the atoms affected by reaction is determined. The reaction matrices can then be identified by simple matrix subtraction operations of the reactant and product matrices.
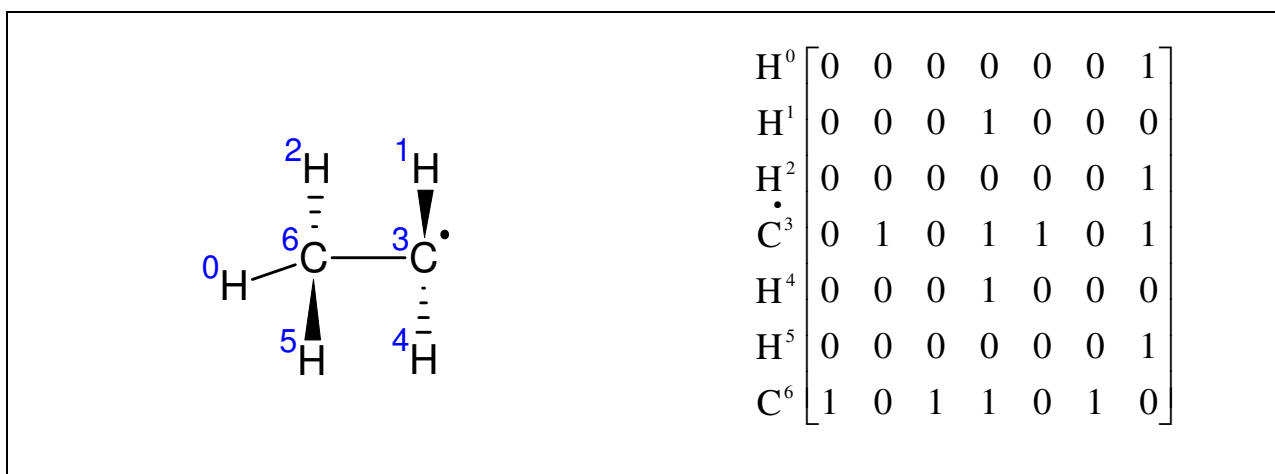
Figure 3.2: Molecular structure of ethyl radical and its bond-electron matrix representation that specifies atomic connectivity.

Warth et al. (1998) used a 1-dimensional notation for generating the reaction network with EXGAS. This 1-dimensional representation needs to be linked by the computer to an internal representation, which permits one to store species (reactants and products) in a unique format by using a canonicity algorithm. Roughly speaking, this 1-dimensional representation is very close to the semideveloped notation in the case of non-cyclic compounds, in particular with the same use of parentheses for substituents. The difference lies mainly in the position of indices for the chemical elements (these are put on the same line as the elements) and in the description of chemical bonds. Thus, / is used for a single bond and // for a double one. Normal valences are assumed for elements, making use of implicit chemical bonds. For example, /(ch2/ch3)2 represents n-butane, while • ch2/ch3 represents an ethyl radical.

Recently a free IUPAC software code InChi (International Chemical Identifiers) was developed that converts structures to computer-readable representations (Rover, 2005). The InChI algorithm converts a chemical structure drawn with software into an alphanumeric string of characters, and vice versa. The different types of structural information (atomic connectivity, stereochemistry, electronic charge, etc) are represented separately within the InChI string and are divided by slash marks. The string for naphthalene for instance is: 1/C10H8/c1-2-6-10-8-4-3-7-9(10)5-1/h1-8H. The first "1" refers to the version of the software. The next segment of the string provides the molecular information. The third segment is the connection table, which indicates how the atoms are connected. The last segment provides information about the hydrogen atoms.

Code	Nature of carbon atom
0	Cyclic mesomeric carbon atom
1	Bridge head aromatic carbon atom
2	Bridge head satured naphthenic carbon atom
3	Bridge head unsatured naphthenic carbon atom
4	Aromatic carbon atom
5	Unsatured naphthenic carbon atom
6	Satured naphthenic carbon atom
7	Acyclic mesomeric carbon atom
8	Acyclic double bonded carbon atom
9	Paraffinic carbon atom

Table 3.7: Codes for carbon atoms used in the label formulation

In the present work a label formulation similar to Vynckier and Froment (1991) and Wauters and Marin (2001) is used to represent the species in a unique way. This label consists of the characteristic elements of the hydrocarbons. A first characteristic element used in the label formulation is the degree of substitution by non-hydrogen atoms of the carbon atoms in the structure. A second characteristic element are structural aspects such as: double bonded carbon atoms, radical position, presence of a ring, see Table 3.7. Thus the label consists of two vectors. The first vector contains the degrees of substitution by non-hydrogen atoms belonging to the structure, the second vector contains the codes of the carbon atoms in the structure (Vynckier and Froment, 1991, Wauters and Marin, 2001). A scalar is needed to represent the location of the free electron for radicals. The dimension of the vectors of the label defines the size of the species.

The above labeling code does not yet guarantee the uniqueness of the label, since the carbon atoms can be numbered differently, as shown in Figure 3.3.

Figure 3.3: Non-unique numbering of a species (l) main chain $l \rightarrow r$; (r) main chain $r \rightarrow l$

This problem is circumvented by introducing a number of priority rules (Vynckier and Froment, 1991). For **Acyclic** compounds the following rules have been introduced in order of importance:

- The first carbon atom is always a primary carbon
- The first carbon atom has to be chosen so that a main chain of maximal length is obtained
- For branched species, the numbering of the main chain starts at the primary carbon atom which gives the lowest rank for the branches
- If the species is unsatured, the unsatured carbons must have the lowest rank number
- For radicals the numbering should yield the lowest number for the carbon atom carrying the free-electron

For **Cyclic** compounds the following rules have been introduced in order of importance:

- The numbering starts at a ring carbon atom
- If a ring carbon atom is charged, it obtains rank number 1
- The carbon atom which carries the most side chains obtains rank 1
- For ring carbon atoms with an equal number of side chains the priority of the carbon atoms follows the numbering of the types of carbon atoms: a mesomeric carbon atom has the highest priority, starting at the atom of highest priority
- If further discrimination is necessary the carbon atom that yields the lowest rank for the free-electron obtains rank 1

A new feature in the code is the localization of mesomeric carbon atoms. The delocalization of the electron over several bonds has always been a problem for modelers. It is not possible to represent a delocalized electron by a two-dimensional representation. Only the mesomeric extremes can be represented, e.g. the pent-2-en-1-yl and the pent-1-en-3-yl radical [2]:
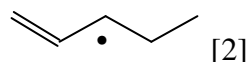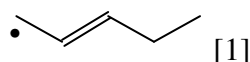
Several solutions have been proposed. One of the most popular methods is the introduction of a fast reaction of the outer forms. This reaction has a reaction rate coefficient orders higher than the reaction rate coefficient of other reactions of these species. Off course the applied solution has no chemical meaning because the reactant and the product are the same. The new code and priority rules provide that the vectors of the label of the different mesomeric extremes are equal, but the position of the free-electron remains different. Hence, both extremes still do not have totally the same label. Therefore only one label is kept, in particular the one with the lowest value for the scalar. This method is illustrated in Figure 3.4. In practice this means that all reaction possibilities still can be found, but that different mesomeric forms of the same species are not considered as different species.

Working with the Boolean relation matrix representation as proposed by Clymans and Froment (1984) does not make it possible to represent a mesomeric species in a unique way.

Therefore the new solution method is a significant improvement. In the program, the binary relation matrices are transformed into the label formulation for storage, and vice versa. Due to the unique label no double counting of the species is encountered.
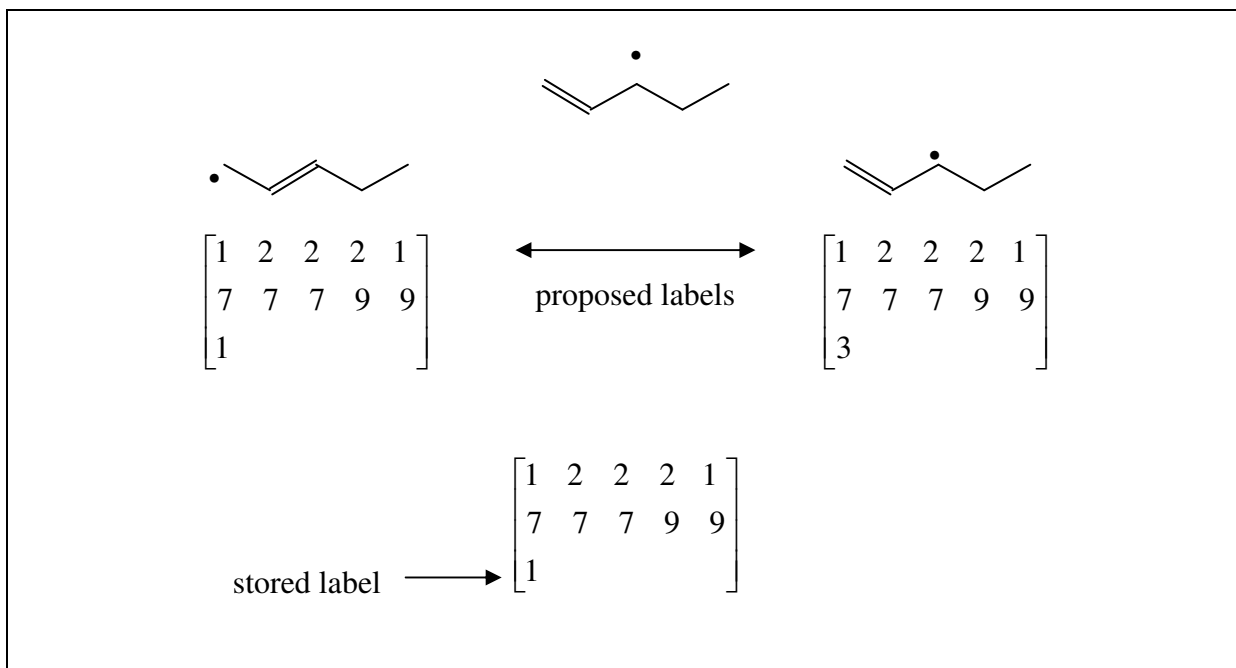
Figure 3.4: Label formulation for the pent-2-en-1-yl and the pent-1-en-3-yl radical radical, proposed and stored label

3.4   Calculation of the reaction rate coefficients

3.4.1 Introduction

The above mentioned reaction network contains only reactions that can be considered elementary. According to IUPAC (McNaught and Wilkinson, 1997), an elementary reaction is defined as "a reaction for which no reaction intermediates have been detected or need to be postulated in order to describe the chemical reaction on a molecule scale. An elementary reaction is assumed to occur in a single step and to pass through a single transition state." Hence, in the rate equation, the order of the reaction coincides with the molecularity of the considered reaction. The reaction rate coefficient is a temperature-dependent parameter described by the Arrhenius expression:

$$k(T) = A \ exp\left(-\frac{E_a}{R \ T} \right)$$

[3. 6]

with A the pre-exponential factor, E_a the activation energy, R is the molar gas constant, and T the temperature. For the calculation of the activation energies of the radical reactions generally either a group contribution method (Willems and Froment, 1988 [a,b]; Saeys, 2003; Song, 2004; Sabbe et al., 2005) or an Evans-Polanyi relationship (Broadbelt et al., 1994; Susnow et al., 1997; De Witt et al., 2000; Green et al., 2001) is used. In the present work a group contribution method developed by Saeys is used to calculate the activation energies and the pre-exponential factors (Saeys, 2003; Saeys et al., 2004; Saeys et al., 2006). The basic principles of structural contribution methods were first discussed by Kossiakoff and Rice (1943) in their seminal article on the steam cracking of hydrocarbons. An alternative approach is followed by Sumathi et al. (2001 [a,b]; 2002). In their work, the transition state is the central concept of the method, and group additive values were introduced for transition-state-specific moieties, so-called supergroups. Properties of the transition state, such as $\Delta_f H^0$, S_0, and $c_p(T)$, were calculated with accurate ab initio methods. Indeed, no experimental data for transition states can be obtained directly. This approach was followed for hydrogen abstraction reactions involving hydrocarbons, alcohols, aldehydes, and acids. Saeys' method belongs to a second category which focuses on the activation energy, that is, the difference between the standard enthalpy of formation of the transition state and the standard enthalpy of formation of the reactants. As in the method by Sumathi et al. (2001 [a,b]; 2002), the transition state is the central concept of the method, but the results are cast in a format similar to the structural contribution method of Willems and Froment (1988) [a,b]. This method is related to Benson's group additive method for thermodynamic data (Benson, 1976). In Benson's method a group is defined as "a polyvalent atom (ligancy $\geq$ 2) in a molecule together with all its ligands" (Benson, 1976). A group is characterized as X-$(A)_i(B)_j(C)_k(D)_l$, where X is the polyvalent central atom, attached to i A atoms, j B atoms, etc. For hydrocarbons the central atom X is a carbon atom. Different types of carbon atoms are distinguished: C_d stands for a double bounded carbon atom, C_t for a triple bounded carbon atom, C• stands for a radical carbon atom and C_B for a carbon atom in a benzene ring.

The use of structural contributions to calculate the activation energy and the pre-exponential factor of radical reactions results from the strong analogy that exists between the different

reactions, considering their mechanism (Rice, 1943). Moens (1982) and Clymans (1982) and later on Willems and Froment (1988) [a,b] worked out the following procedure. For each reaction family a reference reaction is defined. The pre-exponential factor and the activation energy of the reference reaction serve as a basis for the calculations. For any reaction in the considered family, the pre-exponential factor and the activation energy are obtained by adding contributions to the reference values, which account for the structural differences between the mechanism of the considered reaction and the reference reaction. The pre-exponential factor obtained from the structural contribution method is finally multiplied by the number of single events, i.e. the number of energetic equivalent reaction paths from reactant(s) to product(s). The reference value of the pre-exponential factor is thus defined for the 'single event'. Considering single events and tracing structural analogies between the reaction gives a substantial reduction of the number of parameters in the model.

3.4.2 Thermodynamic consistency
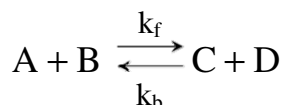
For any reversible elementary chemical reaction,

$$A + B \underset{k_b}{\overset{k_f}{\rightleftharpoons}} C + D$$

there holds a relations between forward reaction kinetics and backward reaction kinetics:

$$K_{c,eq} = \frac{k_f}{k_b} \qquad\qquad [3.\ 7]$$

$K_{c,eq}$ is called the equilibrium coefficient, and it is related to the free energy change of the above reaction by the equation:

$$\frac{k_f}{k_b} = K_{c,eq} = (R\ T)^{-\Delta n} \exp\left(\frac{-\Delta G^0_{rxn}}{R\ T}\right) \qquad\qquad [3.\ 8]$$

where T is the reaction temperature, R is the molar gas constant, ΔG°_{rxn} is the reaction free energy, and Δn is the mole change in the reaction. Thermodynamic consistency thus requires that

the activation energy for the forward and the reverse reaction are related to the standard reaction enthalpy as in equation [3.9]:

$$\Delta_r H° = E_{a,add} - E_{a,\beta-scis} - R\ T$$ [3. 9]

Because of this relation only two of the three parameters can be determined independently. The computationally most efficient approach is to calculate the contributions only for the forward addition reactions (i.e. involving the smallest molecules) and to obtain the contributions for the activation energies for e.g. the β scission reactions via equation [3.9], using values for the standard reaction enthalpy. These could be calculated from tabulated, experimentally determined group additive values (GAV's) for the reactants and the products. Saeys et al. (2004) choose not to use this approach because in their ab initio group contribution method this would lead to a mix of theoretical and experimental data, losing the full ab initio character and the internal consistency of the method. Therefore Saeys et al. (2004) used separate contributions for the reverse reactions, to develop a fully ab initio group contribution method. This does not imply that the developed method is not thermodynamically consistent. If there exists a good agreement between the reaction enthalpies obtained from the differences of the group contribution activation energies and values obtained from Benson's group additivity method, which was the case for Saeys et al. (2004), thermodynamic consistency is retained.

3.4.3 Number of single events

The number of single events is the number of energetic equivalent reaction paths from reactant(s) to product(s). Other terms used to address the number of single events are reaction path degeneracy, symmetry factor or statistical factor. The single event concept follows directly from the transition state theory (Eyring, 1935). The rate coefficient for an elementary reaction is given by:

$$k(T) = \frac{k_B T}{h} e^{\frac{\Delta S^{o,\neq}}{R}} e^{-\frac{\Delta H^{o,\neq}}{RT}}$$

[3. 10]

with k_B the Boltzmann constant ($1.83 \ 10^{-23}$ J K^{-1}), h the Planck constant ($6.62 \ 10^{-34}$ J s) and $\Delta H^{o,\neq}$ en $\Delta S^{o,\neq}$ the standard enthalpy and the standard entropy of activation. Values for the latter are calculated as the difference between the state functions of the transition state and those of the reactant(s). The standard entropy of a molecule consists of several contributions, one due to the translation of a molecule, a second for the rotation of the molecule as a whole, a third associated with the internal rotation of parts of the molecule around specific bonds and a last one attributed to the various vibration modes of the bonds within the molecule:

$$S = S_{trans} + S_{rot,ext} + S_{rot,int} + S_{vib}$$ [3. 11]

Both rotational contributions include a contribution related to the symmetry of the molecule:

$$S_{rot,ext} = \underline{S}_{rot,ext} - R \ln \sigma_{ext}$$ [3. 12]

$$S_{rot,int} = \underline{S}_{rot,int} - R \ln \sigma_{int}$$ [3. 13]

with $\underline{S}_{rot,ext}$ and $\underline{S}_{rot,int}$ the intrinsic external and internal rotational entropy and σ_{ext} and σ_{int} the external and internal symmetry number of the molecule. If the reactant contains n chiral centers, 2^n enantiomers can be distinguished. When the formation of these different optical isomers cannot be observed separately the reactant is considered as a racemic mixture of its distinctive enantiomers which leads to an extra mixing contribution to the entropy

$$S_{mix} = R \ln 2^n$$ [3. 14]

in the expression for the entropy. Introducing the global symmetry number as

$$\sigma_{glob} = \frac{\sigma_{int} \sigma_{ext}}{2^n}$$ [3. 15]

the expression of the rate coefficient k' for an elementary step can be written as a multiple of a single event coefficient k:

$$k' = \frac{\sigma_{glob,r}}{\sigma_{glob,\neq}} \frac{k_B T}{h} e^{\frac{\Delta S^{0,\neq}}{R}} e^{-\frac{\Delta H^{0,\neq}}{RT}}$$ [3. 16]

with

$$n_e = \frac{\sigma_{glob,r}}{\sigma_{glob,\neq}}$$

[3. 17]

the number of single events defined as the ratio of the global symmetry number of the reactant(s) and that of the activated complex. Note that in most cases n_e equals the number of distinct ways in which the elementary step can occur, and that the preceeding equation is consistent with the formula for incorporating reaction path degeneracy into the transition state theory (Pollak and Pechukas, 1978; Karas et al., 1992):

$$k' = \frac{m^{\neq}\sigma^r}{m^r\sigma^{\neq}} \frac{k_B T}{h} \frac{Q_p^{\neq}}{Q_p^r} e^{-\frac{\Delta H^{0,\neq}}{RT}}$$

[3. 18]

m^r and $m^{\neq}$ being the number of optical isomers of reactant and transition state and with Q_p^r and $Q_p^{\neq}$ the partition function of reactant and transition state. The factor $m^r/m^{\neq}$ is introduced because some energetic equivalent reaction paths cannot interconvert into each other via rotation, e.g. when a new chiral center is created in the transition state. The latter is the case for the secondary addition of a methyl radical to propylene. In Figure 3.5 the transition states for this reaction is shown.
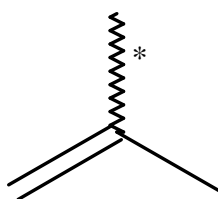
Figure 3.5: Transition State for the secondary addition of a methyl radical to propylene

Several methods have been developed to calculate the number of single events. Bischop and Laidler (1965, 1969) defined their statistical factor as the number of different sets of chemically plausible products that can be formed if all identical atoms in the reactant molecules are labeled. A similar method has been applied by Vercauteren (1991) and Song (2004). The redundancy of a

reaction is equal to the number of equivalent reaction structures from the same reactants. For example, consider the following hydrogen abstraction reaction:

$$CH_4 + H^{\bullet} \underset{\longleftarrow}{\longrightarrow} CH_3 + H_2$$
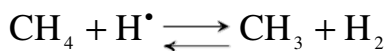
This reaction has a redundancy of 4 because there are four equivalent hydrogen atoms in methane to be abstracted by the hydrogen radical. Pollak and Pechoukas (1978) found some shortcomings to Bischop and Laidler's method (1965, 1969) because in certain special cases the number of single events can be overrated. However, also in the present work the number of single events is set equal to the redundancy of a reaction because in most cases the number of single events is correctly accounted for.

3.4.4 Addition reactions and β scission

3.4.4.1 *General concept of Saeys' group contribution method*

The standard enthalpy of formation of hydrocarbons can be determined accurately with Benson's group additivity method (Benson, 1976; Cohen and Benson, 1992; 1993). The standard enthalpy of formation of a molecule is then written as a sum of contributions for the different groups. In Benson's group additivity method, all of the above contributions are called group additivity values (GAVs).
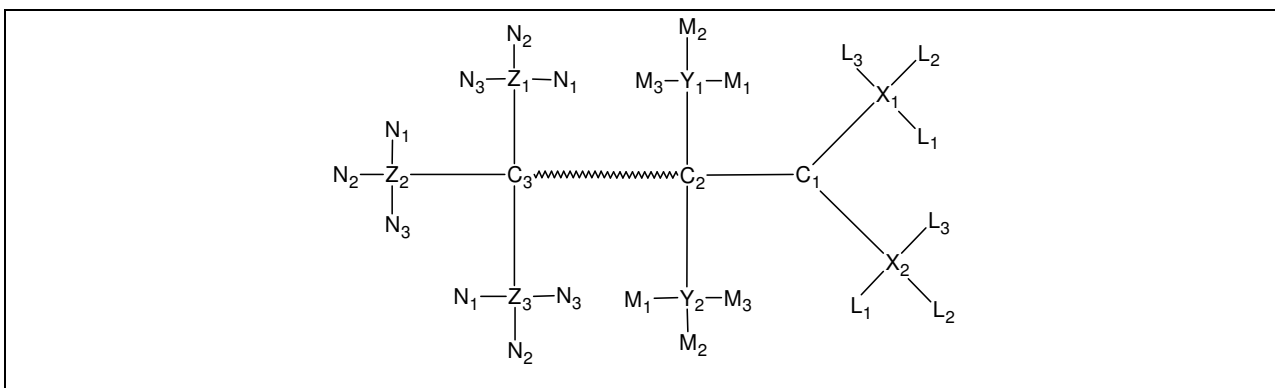
Figure 3.6: The transition state for an addition/β scission reaction

In a completely analogous way, the standard enthalpy of formation of a transition state can be written. This requires the introduction of a number of new groups and new types of carbon atoms, next to C, C•, C_d, C_t and C_B. In Figure 3.6, the transition state of a radical addition reaction is shown. The transition-state-specific groups are those which involve the carbon atoms C_1, C_2, or C_3. These three atoms change in carbon type during the reaction; C_1 changes from C_d to C•, C_2 changes from C_d to C, and C_3 changes from C• to C. In the transition state, these three atoms are of a carbon type which does not occur in molecules. As a result, group additivity values need to be calculated for the corresponding new groups. The standard enthalpy of formation of the transition state can be written as a sum of group additivity values of the primary groups (Saeys et al., 2004):

$$\Delta_f H°(TS) = \sum_{i=1}^{3} GAV(C_i^{TS}) \qquad [3.19]$$

The central parameters in a kinetic model are however the activation energies. Activation energies are obtained by taking the difference between the standard enthalpy of formation of the transition state and the standard enthalpy of formation of the reactant(s):

$$E_a = \Delta_f H°_{Transition State} - \Delta_f H°_{Reactants} + \left(1 - \Delta n^{\neq}\right) R\ T \qquad [3.20]$$

Substitution of equation [3.19] for the standard enthalpy of formation of the transition state, as well as for the standard enthalpy of formation of the reactants into equation [3.20] leads to:

$$E_a = \sum_{i=1}^{3} \Delta GAV(C_i) + \left(1 - \Delta n^{\neq}\right) RT \qquad [3.21]$$

where:

$$\Delta GAV(C_i) = GAV_{Transition State} - GAV_{Reactants} \qquad [3.22]$$

Indeed, the non-transition-state-specific GAVs cancel out. Equation [3.22] defines the group contribution method. The activation energies can thus be expressed as a sum of so-called activation group additivity values, ΔGAVs.

The group contribution method, equation [3.22] can be reformulated by introducing a reference reaction for each reaction family. Instead of using the activation group additivity values ΔGAV directly, the activation energy can be written as the activation energy of a well-chosen reference or standard reaction plus perturbation terms which depend on the primary, secondary and tertiary contributions,

$$E_a = E_{a,Ref} + X_{reaction}[C_1] + X_{reaction}[C_2] + X_{reaction}[C_3]$$
[3. 23]

The perturbation terms take into account the structural difference between the reference reaction and the studied reaction. This perturbation term is composed of standard activation group additivity values, $X_{reaction}[C_i]$, i.e. relative to the activation energy of the reference reaction. This reformulation of the group contribution method sets two of the primary activation group additivity values, $\Delta GAV(C_i)$, from equation [3.22] equal to zero for the reference reaction.

This formulation resembles that of Willems and Froment (1988) [a,b], and situates the latter within the framework of Benson's group additive method. The main difference is that the method of Willems and Froment (1988) [a,b] considers only explicitly the structure of the reactant and product radical and not that of the transition state to determine the activation energy.

3.4.4.2 *Hydrocarbon radical additions and reverse β scission*

Saeys et al. (2004) showed that to calculate the activation energy for a general addition/β scission reaction, see Figure 3.7, a distinction should be made between three important contributions: a contribution involving the attacked carbon atom, a contribution involving the formed radical and a contribution involving the attacking radical.

Figure 3.7: General format of an addition/β scission reaction

ADDITION		β SCISSION	
Reference Reaction			
$CH_3^{\bullet} + C_2 = C_1 \longleftarrow H - C_3 - C_2 - C_1^{\bullet}$			
$E_{a,\,ref\,add\,C}$	$\log(A_{ref\,add\,C})$	$E_{a,\,ref\,\beta\,C}$	$\log(A_{ref\,\beta\,C})$
Contributions C_1			
$X_{add\,C}\,[C_1\text{-}(C)(H)]$	$f_{A,add\,C}\,[C_1\text{-}(C)(H)]$	$X_{\beta\,C}\,[C_1\text{-}(C)(H)]$	$f_{A,\beta\,C}\,[C_1\text{-}(C)(H)]$
$X_{add\,C}\,[C_1\text{-}(C)_2]$	$f_{A,add\,C}\,[C_1\text{-}(C)_2]$	$X_{\beta\,C}\,[C_1\text{-}(C)_2]$	$f_{A,\beta\,C}\,[C_1\text{-}(C)_2]$
$X_{add\,C}\,[C_1\text{-}(C_d)(H)]$	$f_{A,add\,C}\,[C_1\text{-}(C_d)(H)]$	$X_{\beta\,C}\,[C_1\text{-}(C_d)(H)]$	$f_{A,\beta\,C}\,[C_1\text{-}(C_d)(H)]$
$X_{add\,C}\,[C_1\text{-}(C_d)(C)]$	$f_{A,add\,C}\,[C_1\text{-}(C_d)(C)]$	$X_{\beta\,C}\,[C_1\text{-}(C_d)(C)]$	$f_{A,\beta\,C}\,[C_1\text{-}(C_d)(C)]$
$X_{add\,C}\,[C_1\text{-}(C_d)_2]$	$f_{A,add\,C}\,[C_1\text{-}(C_d)_2]$	$X_{\beta\,C}\,[C_1\text{-}(C_d)_2]$	$f_{A,\beta\,C}\,[C_1\text{-}(C_d)_2]$
$X_{add\,C}\,[C_1\text{-}(C_t)(H)]$	$f_{A,add\,C}\,[C_1\text{-}(C_t)(H)]$	$X_{\beta\,C}\,[C_1\text{-}(C_t)(H)]$	$f_{A,\beta\,C}\,[C_1\text{-}(C_t)(H)]$
$X_{add\,C}\,[C_1\text{-}(C_t)(C)]$	$f_{A,add\,C}\,[C_1\text{-}(C_t)(C)]$	$X_{\beta\,C}\,[C_1\text{-}(C_t)(C)]$	$f_{A,\beta\,C}\,[C_1\text{-}(C_t)(C)]$
$X_{add\,C}\,[C_1\text{-}(C_B)(H)]$	$f_{A,add\,C}\,[C_1\text{-}(C_B)(H)]$	$X_{\beta\,C}\,[C_1\text{-}(C_B)(H)]$	$f_{A,\beta\,C}\,[C_1\text{-}(C_B)(H)]$
$X_{add\,C}\,[C_1\text{-}(C_B)(C)]$	$f_{A,add\,C}\,[C_1\text{-}(C_B)(C)]$	$X_{\beta\,C}\,[C_1\text{-}(C_B)(C)]$	$f_{A,\beta\,C}\,[C_1\text{-}(C_B)(C)]$
$X_{add\,C}\,[C_{1,allene}\text{-}(C_d)]$	$f_{A,add\,C}\,[C_{1,allene}\text{-}(C_d)]$	$X_{\beta\,C}\,[C_{1,allene}\text{-}(C_d)]$	$f_{A,\beta\,C}\,[C_{1,allene}\text{-}(C_d)]$
Contributions C_2			
$X_{add\,C}\,[C_2\text{-}(C)(H)]$	$f_{A,add\,C}\,[C_2\text{-}(C)(H)]$	$X_{\beta\,C}\,[C_2\text{-}(C)(H)]$	$f_{A,\beta\,C}\,[C_2\text{-}(C)(H)]$
$X_{add\,C}\,[C_2\text{-}(C)_2]$	$f_{A,add\,C}\,[C_2\text{-}(C)_2]$	$X_{\beta\,C}\,[C_2\text{-}(C)_2]$	$f_{A,\beta\,C}\,[C_2\text{-}(C)_2]$
$X_{add\,C}\,[C_2\text{-}(C_d)(H)]$	$f_{A,add\,C}\,[C_2\text{-}(C_d)(H)]$	$X_{\beta\,C}\,[C_2\text{-}(C_d)(H)]$	$f_{A,\beta\,C}\,[C_2\text{-}(C_d)(H)]$
$X_{add\,C}\,[C_2\text{-}(C_d)(C)]$	$f_{A,add\,C}\,[C_2\text{-}(C_d)(C)]$	$X_{\beta\,C}\,[C_2\text{-}(C_d)(C)]$	$f_{A,\beta\,C}\,[C_2\text{-}(C_d)(C)]$
$X_{add\,C}\,[C_2\text{-}(C_t)(H)]$	$f_{A,add\,C}\,[C_2\text{-}(C_t)(H)]$	$X_{\beta\,C}\,[C_2\text{-}(C_t)(H)]$	$f_{A,\beta\,C}\,[C_2\text{-}(C_t)(H)]$
$X_{add\,C}\,[C_2\text{-}(C_t)(C)]$	$f_{A,add\,C}\,[C_2\text{-}(C_t)(C)]$	$X_{\beta\,C}\,[C_2\text{-}(C_t)(C)]$	$f_{A,\beta\,C}\,[C_2\text{-}(C_t)(C)]$
$X_{add\,C}\,[C_2\text{-}(C_B)(H)]$	$f_{A,add\,C}\,[C_2\text{-}(C_B)(H)]$	$X_{\beta\,C}\,[C_2\text{-}(C_B)(H)]$	$f_{A,\beta\,C}\,[C_2\text{-}(C_B)(H)]$
$X_{add\,C}\,[C_2\text{-}(C_B)(C)]$	$f_{A,add\,C}\,[C_2\text{-}(C_B)(C)]$	$X_{\beta\,C}\,[C_2\text{-}(C_B)(C)]$	$f_{A,\beta\,C}\,[C_2\text{-}(C_B)(C)]$
$X_{add\,C}\,[C_{2,t}\text{-}(H)]$	$f_{A,add\,C}\,[C_{2,t}\text{-}(H)]$	$X_{\beta\,C}\,[C_{2,t}\text{-}(H)]$	$f_{A,\beta\,C}\,[C_{2,t}\text{-}(H)]$
$X_{add\,C}\,[C_{2,t}\text{-}(C)]$	$f_{A,add\,C}\,[C_{2,t}\text{-}(C)]$	$X_{\beta\,C}\,[C_{2,t}\text{-}(C)]$	$f_{A,\beta\,C}\,[C_{2,t}\text{-}(C)]$
$X_{add\,C}\,[C_{2,t}\text{-}(C_d)]$	$f_{A,add\,C}\,[C_{2,t}\text{-}(C_d)]$	$X_{\beta\,C}\,[C_{2,t}\text{-}(C_d)]$	$f_{A,\beta\,C}\,[C_{2,t}\text{-}(C_d)]$
$X_{add\,C}\,[C_{2,allene}]$	$f_{A,add\,C}\,[C_{2,allene}]$	$X_{\beta\,C}\,[C_{2,allene}]$	$f_{A,\beta\,C}\,[C_{2,allene}]$
Contributions C_3			
$X_{add\,C}\,[C_3\text{-}(C)(H)_2]$	$f_{A,add\,C}\,[C_3\text{-}(C)(H)_2]$	$X_{\beta\,C}\,[C_3\text{-}(C)(H)_2]$	$f_{A,\beta\,C}\,[C_3\text{-}(C)(H)_2]$
$X_{add\,C}\,[C_3\text{-}(C)_2(H)]$	$f_{A,add\,C}\,[C_3\text{-}(C)_2(H)]$	$X_{\beta\,C}\,[C_3\text{-}(C)_2(H)]$	$f_{A,\beta\,C}\,[C_3\text{-}(C)_2(H)]$
$X_{add\,C}\,[C_3\text{-}(C)_3]$	$f_{A,add\,C}\,[C_3\text{-}(C)_3]$	$X_{\beta\,C}\,[C_3\text{-}(C)_3]$	$f_{A,\beta\,C}\,[C_3\text{-}(C)_3]$
$X_{add\,C}\,[C_3\text{-}(C_d)(H)_2]$	$f_{A,add\,C}\,[C_3\text{-}(C_d)(H)_2]$	$X_{\beta\,C}\,[C_3\text{-}(C_d)(H)_2]$	$f_{A,\beta\,C}\,[C_3\text{-}(C_d)(H)_2]$
$X_{add\,C}\,[C_3\text{-}(C_d)(C)(H)]$	$f_{A,add\,C}\,[C_3\text{-}(C_d)(C)(H)]$	$X_{\beta\,C}\,[C_3\text{-}(C_d)(C)(H)]$	$f_{A,\beta\,C}\,[C_3\text{-}(C_d)(C)(H)]$
$X_{add\,C}\,[C_3\text{-}(C_d)(C)_2]$	$f_{A,add\,C}\,[C_3\text{-}(C_d)(C)_2]$	$X_{\beta\,C}\,[C_3\text{-}(C_d)(C)_2]$	$f_{A,\beta\,C}\,[C_3\text{-}(C_d)(C)_2]$
$X_{add\,C}\,[C_3\text{-}(C_d)_2(H)]$	$f_{A,add\,C}\,[C_3\text{-}(C_d)_2(H)]$	$X_{\beta\,C}\,[C_3\text{-}(C_d)_2(H)]$	$f_{A,\beta\,C}\,[C_3\text{-}(C_d)_2(H)]$
$X_{add\,C}\,[C_3\text{-}(C_d)_2(C)]$	$f_{A,add\,C}\,[C_3\text{-}(C_d)_2(C)]$	$X_{\beta\,C}\,[C_3\text{-}(C_d)_2(C)]$	$f_{A,\beta\,C}\,[C_3\text{-}(C_d)_2(C)]$
$X_{add\,C}\,[C_3\text{-}(C_t)(H)_2]$	$f_{A,add\,C}\,[C_3\text{-}(C_t)(H)_2]$	$X_{\beta\,C}\,[C_3\text{-}(C_t)(H)_2]$	$f_{A,\beta\,C}\,[C_3\text{-}(C_t)(H)_2]$
$X_{add\,C}\,[C_3\text{-}(C_t)(C)(H)]$	$f_{A,add\,C}\,[C_3\text{-}(C_t)(C)(H)]$	$X_{\beta\,C}\,[C_3\text{-}(C_t)(C)(H)]$	$f_{A,\beta\,C}\,[C_3\text{-}(C_t)(C)(H)]$
$X_{add\,C}\,[C_3\text{-}(C_t)(C)_2]$	$f_{A,add\,C}\,[C_3\text{-}(C_t)(C)_2]$	$X_{\beta\,C}\,[C_3\text{-}(C_t)(C)_2]$	$f_{A,\beta\,C}\,[C_3\text{-}(C_t)(C)_2]$
$X_{add\,C}\,[C_3\text{-}(C_B)(H)_2]$	$f_{A,add\,C}\,[C_3\text{-}(C_B)(H)_2]$	$X_{\beta\,C}\,[C_3\text{-}(C_B)(H)_2]$	$f_{A,\beta\,C}\,[C_3\text{-}(C_B)(H)_2]$
$X_{add\,C}\,[C_3\text{-}(C_B)(C)(H)]$	$f_{A,add\,C}\,[C_3\text{-}(C_B)(C)(H)]$	$X_{\beta\,C}\,[C_3\text{-}(C_B)(C)(H)]$	$f_{A,\beta\,C}\,[C_3\text{-}(C_B)(C)(H)]$
$X_{add\,C}\,[C_{3,d}\text{-}(H)]$	$f_{A,add\,C}\,[C_{3,d}\text{-}(H)]$	$X_{\beta\,C}\,[C_{3,d}\text{-}(H)]$	$f_{A,\beta\,C}\,[C_{3,d}\text{-}(H)]$

Table 3.8: Hydrogen radical addition and β scission reactions: Contributions for the radical addition and β scission reaction

Hence, the activation energy of this reaction can be calculated with the following equation:

$$E_a = E_{a,ref_{add}} + X_{add} [C_1] + X_{add} [C_2] + X_{add} [C_3]$$

[3. 24]

The pre-exponential factor is calculated by a similar formula:

$$\log(A) = \log(A_{a,ref_{add}}) + f_{A,add}[C_1] + f_{A,add}[C_2] + f_{A,add}[C_3] + \log(n_e)$$ [3. 25]

In equation [3.25] $A_{a,ref\ ad}$ corresponds with the single event pre-exponential factor of the reference reaction.

The decomposition of 1-propyl is taken as the reference reaction for the β scission reactions and the methyl addition to ethylene. The reverse reaction is taken as the reference reaction for the radical addition reactions, see Table 3.7. These are the smallest molecules in the homologous sets and it would be possible to do highly accurate quantum chemical calculations for these reactions or to use accurate experimental data. Table 3.7 further shows the different contributions used to calculate the activation energies and the pre-exponential factors. Separate contributions for the formation of 5- and 6-membered carbon rings are introduced. This implies that next to 1,6-cyclization reactions always the 1,5-cyclization reaction possibilities are considered in competition. Van Speybroeck et al. (2001) and Jursic (1999) found that the activation energy for the formation of 6-membered rings is approximately 30 kJ/mol lower than that for 5-ring formation.

3.4.4.3 *Hydrogen radical additions and reverse β scission*

For the hydrogen addition to alkenes and alkynes and the reverse β scission reactions separate contributions were introduced for three reasons. First, the strength of the C-H bond is significantly higher than that of the C-C bond, leading to a higher enthalpy of reaction and a lower addition barrier. The second reason is the different structure of the transition state. The transition state for the hydrogen addition is earlier (at longer relative C-H bond) than the transition state for the addition of carbon-centered radicals. The different structure of the reactive moiety at the transition state is expected to lead to distinct contributions. Third, not only the carbon-centered radical is relatively closer to the alkene at the transition state, it is also more

bulky. This leads to stronger interactions which might influence the relative barriers for addition to the crowded carbon atoms.

ADDITION		β SCISSION	
Reference Reaction			
H• + C₂ ... C₁ ... H C₂ C₁• (reaction diagram)			
$E_{a,\ ref\ add\ H}$	$A_{ref\ add\ H}$	$E_{a,\ ref\ \beta\ H}$	$A_{ref\ \beta\ H}$
Contributions C₁			
$X_{add\ H}\ [C_1\text{-}(C)(H)]$	$f_{A,add\ H}\ [C_1\text{-}(C)(H)]$	$X_{\beta\ H}\ [C_1\text{-}(C)(H)]$	$f_{A,\beta\ H}\ [C_1\text{-}(C)(H)]$
$X_{add\ H}\ [C_1\text{-}(C)_2]$	$f_{A,add\ H}\ [C_1\text{-}(C)_2]$	$X_{\beta\ H}\ [C_1\text{-}(C)_2]$	$f_{A,\beta\ H}\ [C_1\text{-}(C)_2]$
$X_{add\ H}\ [C_1\text{-}(C_d)(H)]$	$f_{A,add\ H}\ [C_1\text{-}(C_d)(H)]$	$X_{\beta\ H}\ [C_1\text{-}(C_d)(H)]$	$f_{A,\beta\ H}\ [C_1\text{-}(C_d)(H)]$
$X_{add\ H}\ [C_1\text{-}(C_d)(C)]$	$f_{A,add\ H}\ [C_1\text{-}(C_d)(C)]$	$X_{\beta\ H}\ [C_1\text{-}(C_d)(C)]$	$f_{A,\beta\ H}\ [C_1\text{-}(C_d)(C)]$
$X_{add\ H}\ [C_1\text{-}(C_d)_2]$	$f_{A,add\ H}\ [C_1\text{-}(C_d)_2]$	$X_{\beta\ H}\ [C_1\text{-}(C_d)_2]$	$f_{A,\beta\ H}\ [C_1\text{-}(C_d)_2]$
$X_{add\ H}\ [C_1\text{-}(C_t)(H)]$	$f_{A,add\ H}\ [C_1\text{-}(C_t)(H)]$	$X_{\beta\ H}\ [C_1\text{-}(C_t)(H)]$	$f_{A,\beta\ H}\ [C_1\text{-}(C_t)(H)]$
$X_{add\ H}\ [C_1\text{-}(C_t)(C)]$	$f_{A,add\ H}\ [C_1\text{-}(C_t)(C)]$	$X_{\beta\ H}\ [C_1\text{-}(C_t)(C)]$	$f_{A,\beta\ H}\ [C_1\text{-}(C_t)(C)]$
$X_{add\ H}\ [C_1\text{-}(C_B)(H)]$	$f_{A,add\ H}\ [C_1\text{-}(C_B)(H)]$	$X_{\beta\ H}\ [C_1\text{-}(C_B)(H)]$	$f_{A,\beta\ H}\ [C_1\text{-}(C_B)(H)]$
$X_{add\ H}\ [C_1\text{-}(C_B)(C)]$	$f_{A,add\ H}\ [C_1\text{-}(C_B)(C)]$	$X_{\beta\ H}\ [C_1\text{-}(C_B)(C)]$	$f_{A,\beta\ H}\ [C_1\text{-}(C_B)(C)]$
$X_{add\ H}\ [C_{1,allene}\text{-}(C_d)]$	$f_{A,add\ H}\ [C_{1,allene}\text{-}(C_d)]$	$X_{\beta\ H}\ [C_{1,allene}\text{-}(C_d)]$	$f_{A,\beta\ H}\ [C_{1,allene}\text{-}(C_d)]$
Contributions C₂			
$X_{add\ H}\ [C_2\text{-}(C)(H)]$	$f_{A,add\ H}\ [C_2\text{-}(C)(H)]$	$X_{\beta\ H}\ [C_2\text{-}(C)(H)]$	$f_{A,\beta\ H}\ [C_2\text{-}(C)(H)]$
$X_{add\ H}\ [C_2\text{-}(C)_2]$	$f_{A,add\ H}\ [C_2\text{-}(C)_2]$	$X_{\beta\ H}\ [C_2\text{-}(C)_2]$	$f_{A,\beta\ H}\ [C_2\text{-}(C)_2]$
$X_{add\ H}\ [C_2\text{-}(C_d)(H)]$	$f_{A,add\ H}\ [C_2\text{-}(C_d)(H)]$	$X_{\beta\ H}\ [C_2\text{-}(C_d)(H)]$	$f_{A,\beta\ H}\ [C_2\text{-}(C_d)(H)]$
$X_{add\ H}\ [C_2\text{-}(C_d)(C)]$	$f_{A,add\ H}\ [C_2\text{-}(C_d)(C)]$	$X_{\beta\ H}\ [C_2\text{-}(C_d)(C)]$	$f_{A,\beta\ H}\ [C_2\text{-}(C_d)(C)]$
$X_{add\ H}\ [C_2\text{-}(C_t)(H)]$	$f_{A,add\ H}\ [C_2\text{-}(C_t)(H)]$	$X_{\beta\ H}\ [C_2\text{-}(C_t)(H)]$	$f_{A,\beta\ H}\ [C_2\text{-}(C_t)(H)]$
$X_{add\ H}\ [C_2\text{-}(C_t)(C)]$	$f_{A,add\ H}\ [C_2\text{-}(C_t)(C)]$	$X_{\beta\ H}\ [C_2\text{-}(C_t)(C)]$	$f_{A,\beta\ H}\ [C_2\text{-}(C_t)(C)]$
$X_{add\ H}\ [C_2\text{-}(C_B)(H)]$	$f_{A,add\ H}\ [C_2\text{-}(C_B)(H)]$	$X_{\beta\ H}\ [C_2\text{-}(C_B)(H)]$	$f_{A,\beta\ H}\ [C_2\text{-}(C_B)(H)]$
$X_{add\ H}\ [C_2\text{-}(C_B)(C)]$	$f_{A,add\ H}\ [C_2\text{-}(C_B)(C)]$	$X_{\beta\ H}\ [C_2\text{-}(C_B)(C)]$	$f_{A,\beta\ H}\ [C_2\text{-}(C_B)(C)]$
$X_{add\ H}\ [C_{2,t}\text{-}(H)]$	$f_{A,add\ H}\ [C_{2,t}\text{-}(H)]$	$X_{\beta\ H}\ [C_{2,t}\text{-}(H)]$	$f_{A,\beta\ H}\ [C_{2,t}\text{-}(H)]$
$X_{add\ H}\ [C_{2,t}\text{-}(C)]$	$f_{A,add\ H}\ [C_{2,t}\text{-}(C)]$	$X_{\beta\ H}\ [C_{2,t}\text{-}(C)]$	$f_{A,\beta\ H}\ [C_{2,t}\text{-}(C)]$
$X_{add\ H}\ [C_{2,t}\text{-}(C_d)]$	$f_{A,add\ H}\ [C_{2,t}\text{-}(C_d)]$	$X_{\beta\ H}\ [C_{2,t}\text{-}(C_d)]$	$f_{A,\beta\ H}\ [C_{2,t}\text{-}(C_d)]$
$X_{add\ H}\ [C_{2,t}\text{-}(C_t)]$	$f_{A,add\ H}\ [C_{2,t}\text{-}(C_t)]$	$X_{\beta\ H}\ [C_{2,t}\text{-}(C_t)]$	$f_{A,\beta\ H}\ [C_{2,t}\text{-}(C_t)]$
$X_{add\ H}\ [C_{2,allene}]$	$f_{A,add\ H}\ [C_{2,allene}]$	$X_{\beta\ H}\ [C_{2,allene}]$	$f_{A,\beta\ H}\ [C_{2,allene}]$

Table 3.9: Hydrogen radical addition and β scission reactions: Contributions for the radical addition and β scission reaction

Saeys (2003) showed that although the hydrogen and carbon-centered radical addition reactions and the reverse β scission reactions are governed by similar factors, the use of separate contributions is required. The activation energies for reactions involving hydrogen radicals are not simply shifted by 30 kJ mol⁻¹ from the activation energies for the reactions involving carbon-

centered radicals. The larger separation of the fragments in the transition state of reactions involving hydrogen radicals makes certain contributions more important and others less important. This implies also that a new reference should be chosen. Saeys (2003) proposed to use the addition of a hydrogen radical to ethylene and the reverse β scission as reference reactions. The different contributions are specified in Table 3.9.

3.4.5 Hydrogen abstraction reactions

Saeys et al. (2006) consider in their group contribution method for hydrogen abstraction reactions two important contributions: one being a contribution for the abstracting radical, the other a contribution for the formed radical.
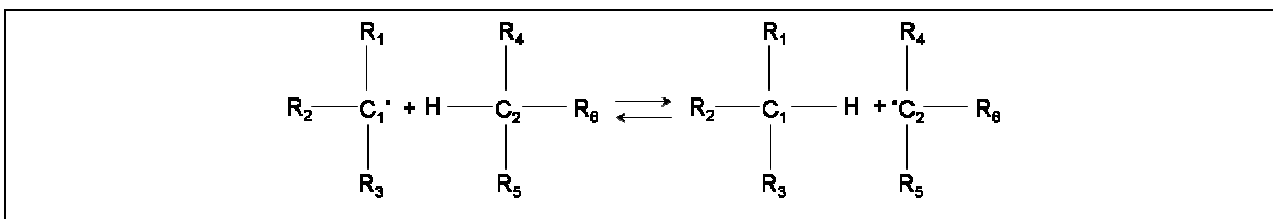
Figure 3.8: General format of a hydrogen abstraction reaction

This implies that the activation energy for a general hydrogen abstraction, see Figure 3.8, is calculated with the following formula:

$$E_a = E_{a,ref_{ab}} + X_{ab}[C_1] + X_{ab}[C_2]$$

[3. 26]

Similarly, for the pre-exponential factor the following formula is used:

$$\log(A) = \log(A_{a,ref_{ab}}) + f_{A,ab}[C_1] + f_{A,ab}[C_2] + \log(n_e)$$

[3. 27]

In equation [3.27] $A_{a,ref\ ab}$ corresponds with the single event pre-exponential factor of the reference reaction. This formulation agrees completely with the one used by Willems and Froment (1988) [a,b], and situates the latter within the framework of Benson's group additive method. The abstraction of a hydrogen atom from ethane by a hydrogen radical is chosen as the

reference reaction. In Table 3.10 the contributions for the abstracting and the formed radical are given.

HYDROGEN ABSTRACTION			
Reference Reaction			
$H^{\bullet} + H-C_2-C-H \rightleftharpoons H-H + {}^{\bullet}C_2-C-H$ (with H substituents)			
$E_{a,\ ref\ ab}$		$A_{ref\ ab}$	
Contributions C_1		**Contributions C_2**	
$X_{ab}\ [C_1\text{-}(H)_3]$	$f_{A,ab}\ [C_1\text{-}(H)_3]$	$X_{ab}\ [C_2\text{-}(H)_3]$	$f_{A,ab}\ [C_2\text{-}(H)_3]$
$X_{ab}\ [C_1\text{-}(C)(H)_2]$	$f_{A,ab}\ [C_1\text{-}(C)(H)_2]$	$X_{ab}\ [C_2\text{-}(C)(H)_2]$	$f_{A,ab}\ [C_2\text{-}(C)(H)_2]$
$X_{ab}\ [C_1\text{-}(C)_2(H)]$	$f_{A,ab}\ [C_1\text{-}(C)_2(H)]$	$X_{ab}\ [C_2\text{-}(C)_2(H)]$	$f_{A,ab}\ [C_2\text{-}(C)_2(H)]$
$X_{ab}\ [C_1\text{-}(C)_3]$	$f_{A,ab}\ [C_1\text{-}(C)_3]$	$X_{ab}\ [C_2\text{-}(C)_3]$	$f_{A,ab}\ [C_2\text{-}(C)_3]$
$X_{ab}\ [C_1\text{-}(C_d)(H)_2]$	$f_{A,ab}\ [C_1\text{-}(C_d)(H)_2]$	$X_{ab}\ [C_2\text{-}(C_d)(H)_2]$	$f_{A,ab}\ [C_2\text{-}(C_d)(H)_2]$
$X_{ab}\ [C_1\text{-}(C_d)(C)(H)]$	$f_{A,ab}\ [C_1\text{-}(C_d)(C)(H)]$	$X_{ab}\ [C_2\text{-}(C_d)(C)(H)]$	$f_{A,ab}\ [C_2\text{-}(C_d)(C)(H)]$
$X_{ab}\ [C_1\text{-}(C_d)(C)_2]$	$f_{A,ab}\ [C_1\text{-}(C_d)(C)_2]$	$X_{ab}\ [C_2\text{-}(C_d)(C)_2]$	$f_{A,ab}\ [C_2\text{-}(C_d)(C)_2]$
$X_{ab}\ [C_1\text{-}(C_d)_2(H)]$	$f_{A,ab}\ [C_1\text{-}(C_d)_2(H)]$	$X_{ab}\ [C_2\text{-}(C_d)_2(H)]$	$f_{A,ab}\ [C_2\text{-}(C_d)_2(H)]$
$X_{ab}\ [C_1\text{-}(C_d)_2(C)]$	$f_{A,ab}\ [C_1\text{-}(C_d)_2(C)]$	$X_{ab}\ [C_2\text{-}(C_d)_2(C)]$	$f_{A,ab}\ [C_2\text{-}(C_d)_2(C)]$
$X_{ab}\ [C_1\text{-}(C_t)(H)_2]$	$f_{A,ab}\ [C_1\text{-}(C_t)(H)_2]$	$X_{ab}\ [C_2\text{-}(C_t)(H)_2]$	$f_{A,ab}\ [C_2\text{-}(C_t)(H)_2]$
$X_{ab}\ [C_1\text{-}(C_t)(C)(H)]$	$f_{A,ab}\ [C_1\text{-}(C_t)(C)(H)]$	$X_{ab}\ [C_2\text{-}(C_t)(C)(H)]$	$f_{A,ab}\ [C_2\text{-}(C_t)(C)(H)]$
$X_{ab}\ [C_1\text{-}(C_t)(C)_2]$	$f_{A,ab}\ [C_1\text{-}(C_t)(C)_2]$	$X_{ab}\ [C_2\text{-}(C_t)(C)_2]$	$f_{A,ab}\ [C_2\text{-}(C_t)(C)_2]$
$X_{ab}\ [C_1\text{-}(C_t)_2(H)]$	$f_{A,ab}\ [C_1\text{-}(C_t)_2(H)]$	$X_{ab}\ [C_2\text{-}(C_t)_2(H)]$	$f_{A,ab}\ [C_2\text{-}(C_t)_2(H)]$
$X_{ab}\ [C_1\text{-}(C_t)_2(C)]$	$f_{A,ab}\ [C_1\text{-}(C_t)_2(C)]$	$X_{ab}\ [C_2\text{-}(C_t)_2(C)]$	$f_{A,ab}\ [C_2\text{-}(C_t)_2(C)]$
$X_{ab}\ [C_1\text{-}(C_B)(H)_2]$	$f_{A,ab}\ [C_1\text{-}(C_B)(H)_2]$	$X_{ab}\ [C_2\text{-}(C_B)(H)_2]$	$f_{A,ab}\ [C_2\text{-}(C_B)(H)_2]$
$X_{ab}\ [C_1\text{-}(C_B)(C)(H)]$	$f_{A,ab}\ [C_1\text{-}(C_B)(C)(H)]$	$X_{ab}\ [C_2\text{-}(C_B)(C)(H)]$	$f_{A,ab}\ [C_2\text{-}(C_B)(C)(H)]$
$X_{ab}\ [C_1\text{-}(C_B)(C)_2]$	$f_{A,ab}\ [C_1\text{-}(C_B)(C)_2]$	$X_{ab}\ [C_2\text{-}(C_B)(C)_2]$	$f_{A,ab}\ [C_2\text{-}(C_B)(C)_2]$
$X_{ab}\ [C_{1,d}\text{-}(H)]$	$f_{A,ab}\ [C_{1,d}\text{-}(H)]$	$X_{ab}\ [C_{2,d}\text{-}(H)]$	$f_{A,ab}\ [C_{2,d}\text{-}(H)]$
$X_{ab}\ [C_{1,d}\text{-}(C)]$	$f_{A,ab}\ [C_{1,d}\text{-}(C)]$	$X_{ab}\ [C_{2,d}\text{-}(C)]$	$f_{A,ab}\ [C_{2,d}\text{-}(C)]$
$X_{ab}\ [C_{1,cyclo}\text{-}(H)]$	$f_{A,ab}\ [C_{1,cyclo}\text{-}(H)]$	$X_{ab}\ [C_{2,cyclo}\text{-}(H)]$	$f_{A,ab}\ [C_{2,cyclo}\text{-}(H)]$
$X_{ab}\ [C_{1,cyclo}\text{-}(C)]$	$f_{A,ab}\ [C_{1,cyclo}\text{-}(C)]$	$X_{ab}\ [C_{2,cyclo}\text{-}(C)]$	$f_{A,ab}\ [C_{2,cyclo}\text{-}(C)]$
$X_{ab}\ [C_{1,cycloallylic}\text{-}(H)]$	$f_{A,ab}\ [C_{1,cycloallylic}\text{-}(H)]$	$X_{ab}\ [C_{2,cycloallylic}\text{-}(H)]$	$f_{A,ab}\ [C_{2,cycloallylic}\text{-}(H)]$
$X_{ab}\ [C_{1,cycloallylic}\text{-}(C)]$	$f_{A,ab}\ [C_{1,cycloallylic}\text{-}(C)]$	$X_{ab}\ [C_{2,cycloallylic}\text{-}(C)]$	$f_{A,ab}\ [C_{2,cycloallylic}\text{-}(C)]$
$X_{ab}\ [C_{1,cyclobenzyl}\text{-}(H)]$	$f_{A,ab}\ [C_{1,cyclobenzyl}\text{-}(H)]$	$X_{ab}\ [C_{2,\ cyclobenzyl}\text{-}(H)]$	$f_{A,ab}\ [C_{2,\ cyclobenzyl}\text{-}(H)]$
$X_{ab}\ [C_{1,\ cyclobenzyl}\text{-}(C)]$	$f_{A,ab}\ [C_{1,\ cyclobenzyl}\text{-}(C)]$	$X_{ab}\ [C_{2,\ cyclobenzyl}\text{-}(C)]$	$f_{A,ab}\ [C_{2,\ cyclobenzyl}\text{-}(C)]$

Table 3.10: Hydrogen abstraction reactions: Contributions for the formed and attacking radical

Intramolecular hydrogen abstraction reactions are isomerization reactions. Both 1,4- and 1,5-isomerizations are considered in the reaction network. The contribution method for isomerization reactions is completely similar as discussed for the external hydrogen abstraction reactions. The values for the pre-exponential factor and the activation energy are calculated by adding the contributions for the attacking and the formed radical to the value of the reference reaction. For 1,5-isomerizations the reference reaction is the isomerization reaction of the

primary radical forming a secondary radical. For 1,4-isomerizations the reference reaction is the isomerization reaction of the primary radical forming a secondary radical. In Table 3.6 the different contributions for the abstracting and the formed radical are specified for 1,5-isomerization reactions. For 1,4-isomerization reactions a completely similar table can be created as for the 1,5-isomerization reactions.

1,5-ISOMERIZATION			
Reference Reaction			
2 6 (radical at 1) →/← 2 4 6 (radical at 5)			
$E_{a,\,ref\ 1,5}$		$A_{ref\ 1,5}$	
Contributions C_1		**Contributions C_2**	
$X_{1,5}\,[C_1\text{-}(C)_2(H)]$	$f_{A,1,5}\,[C_1\text{-}(C)_2(H)]$	$X_{1,5}\,[C_5\text{-}(C)(H)_2]$	$f_{A,1,5}\,[C_5\text{-}(C)(H)_2]$
$X_{1,5}\,[C_1\text{-}(C)_3]$	$f_{A,1,5}\,[C_1\text{-}(C)_3]$	$X_{1,5}\,[C_5\text{-}(C)_3]$	$f_{A,1,5}\,[C_5\text{-}(C)_3]$
$X_{1,5}\,[C_1\text{-}(C_d)(H)_2]$	$f_{A,1,5}\,[C_1\text{-}(C_d)(H)_2]$	$X_{1,5}\,[C_5\text{-}(C_d)(H)_2]$	$f_{A,1,5}\,[C_5\text{-}(C_d)(H)_2]$
$X_{1,5}\,[C_1\text{-}(C_d)(C)(H)]$	$f_{A,1,5}\,[C_1\text{-}(C_d)(C)(H)]$	$X_{1,5}\,[C_5\text{-}(C_d)(C)(H)]$	$f_{A,1,5}\,[C_5\text{-}(C_d)(C)(H)]$
$X_{1,5}\,[C_1\text{-}(C_d)(C)_2]$	$f_{A,1,5}\,[C_1\text{-}(C_d)(C)_2]$	$X_{1,5}\,[C_5\text{-}(C_d)(C)_2]$	$f_{A,1,5}\,[C_5\text{-}(C_d)(C)_2]$
$X_{1,5}\,[C_1\text{-}(C_d)_2(H)]$	$f_{A,1,5}\,[C_1\text{-}(C_d)_2(H)]$	$X_{1,5}\,[C_5\text{-}(C_d)_2(H)]$	$f_{A,1,5}\,[C_5\text{-}(C_d)_2(H)]$
$X_{1,5}\,[C_1\text{-}(C_d)_2(C)]$	$f_{A,1,5}\,[C_1\text{-}(C_d)_2(C)]$	$X_{1,5}\,[C_5\text{-}(C_d)_2(C)]$	$f_{A,1,5}\,[C_5\text{-}(C_d)_2(C)]$
$X_{1,5}\,[C_1\text{-}(C_t)(H)_2]$	$f_{A,1,5}\,[C_1\text{-}(C_t)(H)_2]$	$X_{1,5}\,[C_5\text{-}(C_t)(H)_2]$	$f_{A,1,5}\,[C_5\text{-}(C_t)(H)_2]$
$X_{1,5}\,[C_1\text{-}(C_t)(C)(H)]$	$f_{A,1,5}\,[C_1\text{-}(C_t)(C)(H)]$	$X_{1,5}\,[C_5\text{-}(C_t)(C)(H)]$	$f_{A,1,5}\,[C_5\text{-}(C_t)(C)(H)]$
$X_{1,5}\,[C_1\text{-}(C_t)(C)_2]$	$f_{A,1,5}\,[C_1\text{-}(C_t)(C)_2]$	$X_{1,5}\,[C_5\text{-}(C_t)(C)_2]$	$f_{A,1,5}\,[C_5\text{-}(C_t)(C)_2]$
$X_{1,5}\,[C_1\text{-}(C_t)_2(H)]$	$f_{A,1,5}\,[C_1\text{-}(C_t)_2(H)]$	$X_{1,5}\,[C_5\text{-}(C_t)_2(H)]$	$f_{A,1,5}\,[C_5\text{-}(C_t)_2(H)]$
$X_{1,5}\,[C_1\text{-}(C_t)_2(C)]$	$f_{A,1,5}\,[C_1\text{-}(C_t)_2(C)]$	$X_{1,5}\,[C_5\text{-}(C_t)_2(C)]$	$f_{A,1,5}\,[C_5\text{-}(C_t)_2(C)]$
$X_{1,5}\,[C_1\text{-}(C_B)(H)_2]$	$f_{A,1,5}\,[C_1\text{-}(C_B)(H)_2]$	$X_{1,5}\,[C_5\text{-}(C_B)(H)_2]$	$f_{A,1,5}\,[C_5\text{-}(C_B)(H)_2]$
$X_{1,5}\,[C_1\text{-}(C_B)(C)(H)]$	$f_{A,1,5}\,[C_1\text{-}(C_B)(C)(H)]$	$X_{1,5}\,[C_5\text{-}(C_B)(C)(H)]$	$f_{A,1,5}\,[C_5\text{-}(C_B)(C)(H)]$
$X_{1,5}\,[C_1\text{-}(C_B)(C)_2]$	$f_{A,1,5}\,[C_1\text{-}(C_B)(C)_2]$	$X_{1,5}\,[C_5\text{-}(C_B)(C)_2]$	$f_{A,1,5}\,[C_5\text{-}(C_B)(C)_2]$
$X_{1,5}\,[C_{1,cyclo}\text{-}(H)]$	$f_{A,1,5}\,[C_{1,cyclo}\text{-}(H)]$	$X_{1,5}\,[C_{5,cyclo}\text{-}(H)]$	$f_{A,1,5}\,[C_{5,cyclo}\text{-}(H)]$
$X_{1,5}\,[C_{1,cyclo}\text{-}(C)]$	$f_{A,1,5}\,[C_{1,cyclo}\text{-}(C)]$	$X_{1,5}\,[C_{5,cyclo}\text{-}(C)]$	$f_{A,1,5}\,[C_{5,cyclo}\text{-}(C)]$
$X_{1,5}\,[C_{1,cycloallylic}\text{-}(H)]$	$f_{A,1,5}\,[C_{1,cycloallylic}\text{-}(H)]$	$X_{1,5}\,[C_{5,cycloallylic}\text{-}(H)]$	$f_{A,1,5}\,[C_{5,cycloallylic}\text{-}(H)]$
$X_{1,5}\,[C_{1,cycloallylic}\text{-}(C)]$	$f_{A,1,5}\,[C_{1,cycloallylic}\text{-}(C)]$	$X_{1,5}\,[C_{5,cycloallylic}\text{-}(C)]$	$f_{A,1,5}\,[C_{5,cycloallylic}\text{-}(C)]$
$X_{1,5}\,[C_{1,cycloallylic}\text{-}(H)]$	$f_{A,1,5}\,[C_{1,cycloallylic}\text{-}(H)]$	$X_{1,5}\,[C_{5,cycloallylic}\text{-}(H)]$	$f_{A,1,5}\,[C_{5,cycloallylic}\text{-}(H)]$
$X_{1,5}\,[C_{1,cycloallylic}\text{-}(C)]$	$f_{A,1,5}\,[C_{1,cycloallylic}\text{-}(C)]$	$X_{1,5}\,[C_{5,cycloallylic}\text{-}(C)]$	$f_{A,1,5}\,[C_{5,cycloallylic}\text{-}(C)]$

Table 3.11: 1,5-Isomerization reactions: Contributions for the formed and attacking radical

3.4.6 C-C and C-H scission of molecules and recombination of radicals

For C-C and C-H scission of molecules and the reverse recombination reactions the method of Willems and Froment (1988) [a,b] is used because no ab initio group additive method is developed yet. Willems and Froment (1988) [a,b] assumed that the activation energy for the

recombination reactions is zero. The activation energy for the corresponding C-C scission reaction is therefore almost equal to the reaction heat:

$$E_{a,scis} = \Delta_r H^0_{scis} + R\ T$$

[3. 28]

Just as for the other reaction families a reference reaction is chosen. In this case the C-C scission reaction of butane giving two ethyl radicals is selected as reference reaction.
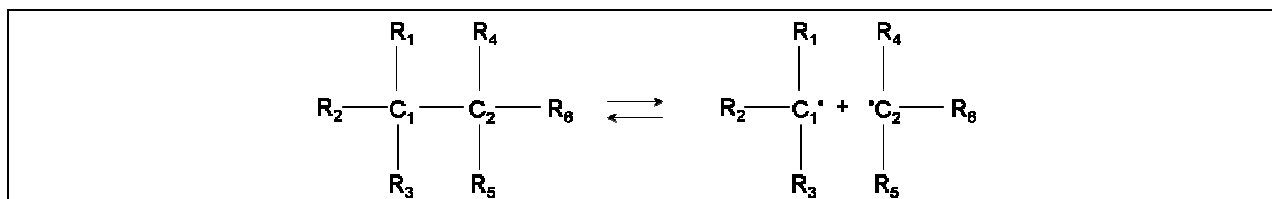
Figure 3.9: General format of a scission reaction

The activation energy of a general scission reaction in Figure 3.9 is calculated using:

$$E_a = E_{a,ref_{scis}} + X_{scis}\left[C_1\right] + X_{scis}\left[C_2\right]$$

[3. 29]

The pre-exponential factor for the scission reaction is given by:

$$\log(A) = \log(A_{a,ref_{scis}}) + f_{A,scis}\left[C_1\right] + f_{A,scis}\left[C_2\right] + \log(n_e)$$

[3. 30]

The activation energy is strongly related to the standard reaction enthalpy, and hence, the structural contributions can be determined from differences in the latter. To determine the standard reaction enthalpy the group contribution method of Benson is used (1976). The different contributions necessary to calculate the activation energy are specified in Table 3.12.

The calculation of the activation energy of the recombination reactions requires no parameters. The pre-exponential factor of the recombination reactions is calculated from thermodynamic consistency (Willems and Froment, 1988 [a,b]):

$$\ln\left(\frac{A_{rec}}{A_{scis}}\right) = \frac{\Delta S°}{R} - \Delta n\left(1 + R\ln\left(R'\ T\right)\right)$$

[3. 31]

with R' equal to $R*10^{-2}$. This equation is derived in Annex A.

C-C and C-H SCISSION			
Reference Reaction			
$H\!-\!C\!-\!C_1\!-\!C_2\!-\!C\!-\!H \rightleftharpoons H\!-\!C\!-\!C_1{}^{\bullet} + {}^{\bullet}C_2\!-\!C\!-\!H$ (each carbon bearing H substituents)			
$E_{a,\ ref\ scis}$		$A_{ref\ scis}$	
Contributions C_1		**Contributions C_2**	
$X_{scis}[H]$	$f_{A,scis}[H]$	$X_{scis}[H]$	$f_{A,scis}[H]$
$X_{scis}[C_1\text{-}(H)_3]$	$f_{A,scis}[C_1\text{-}(H)_3]$	$X_{scis}[C_1\text{-}(H)_3]$	$f_{A,scis}[C_1\text{-}(H)_3]$
$X_{scis}[C_1\text{-}(C)_2(H)]$	$f_{A,scis}[C_1\text{-}(C)_2(H)]$	$X_{scis}[C_2\text{-}(C)_2(H)]$	$f_{A,scis}[C_1\text{-}(C)_2(H)]$
$X_{scis}[C_1\text{-}(C)_3]$	$f_{A,scis}[C_1\text{-}(C)_3]$	$X_{scis}[C_2\text{-}(C)_3]$	$f_{A,scis}[C_1\text{-}(C)_3]$
$X_{scis}[C_1\text{-}(C_d)(H)_2]$	$f_{A,scis}[C_1\text{-}(C_d)(H)_2]$	$X_{scis}[C_2\text{-}(C_d)(H)_2]$	$f_{A,scis}[C_1\text{-}(C_d)(H)_2]$
$X_{scis}[C_1\text{-}(C_d)(C)(H)]$	$f_{A,scis}[C_1\text{-}(C_d)(C)(H)]$	$X_{scis}[C_2\text{-}(C_d)(C)(H)]$	$f_{A,scis}[C_1\text{-}(C_d)(C)(H)]$
$X_{scis}[C_1\text{-}(C_d)(C)_2]$	$f_{A,scis}[C_1\text{-}(C_d)(C)_2]$	$X_{scis}[C_2\text{-}(C_d)(C)_2]$	$f_{A,scis}[C_1\text{-}(C_d)(C)_2]$
$X_{scis}[C_1\text{-}(C_d)_2(H)]$	$f_{A,scis}[C_1\text{-}(C_d)_2(H)]$	$X_{scis}[C_2\text{-}(C_d)_2(H)]$	$f_{A,scis}[C_1\text{-}(C_d)_2(H)]$
$X_{scis}[C_1\text{-}(C_d)_2(C)]$	$f_{A,scis}[C_1\text{-}(C_d)_2(C)]$	$X_{scis}[C_2\text{-}(C_d)_2(C)]$	$f_{A,scis}[C_1\text{-}(C_d)_2(C)]$
$X_{scis}[C_1\text{-}(C_t)(H)_2]$	$f_{A,scis}[C_1\text{-}(C_t)(H)_2]$	$X_{scis}[C_2\text{-}(C_t)(H)_2]$	$f_{A,scis}[C_1\text{-}(C_t)(H)_2]$
$X_{scis}[C_1\text{-}(C_t)(C)(H)]$	$f_{A,scis}[C_1\text{-}(C_t)(C)(H)]$	$X_{scis}[C_2\text{-}(C_t)(C)(H)]$	$f_{A,scis}[C_1\text{-}(C_t)(C)(H)]$
$X_{scis}[C_1\text{-}(C_t)(C)_2]$	$f_{A,scis}[C_1\text{-}(C_t)(C)_2]$	$X_{scis}[C_2\text{-}(C_t)(C)_2]$	$f_{A,scis}[C_1\text{-}(C_t)(C)_2]$
$X_{scis}[C_1\text{-}(C_t)_2(H)]$	$f_{A,scis}[C_1\text{-}(C_t)_2(H)]$	$X_{scis}[C_2\text{-}(C_t)_2(H)]$	$f_{A,scis}[C_1\text{-}(C_t)_2(H)]$
$X_{scis}[C_1\text{-}(C_t)_2(C)]$	$f_{A,scis}[C_1\text{-}(C_t)_2(C)]$	$X_{scis}[C_2\text{-}(C_t)_2(C)]$	$f_{A,scis}[C_1\text{-}(C_t)_2(C)]$
$X_{scis}[C_1\text{-}(C_B)(H)_2]$	$f_{A,scis}[C_1\text{-}(C_B)(H)_2]$	$X_{scis}[C_2\text{-}(C_B)(H)_2]$	$f_{A,scis}[C_1\text{-}(C_B)(H)_2]$
$X_{scis}[C_1\text{-}(C_B)(C)(H)]$	$f_{A,scis}[C_1\text{-}(C_B)(C)(H)]$	$X_{scis}[C_2\text{-}(C_B)(C)(H)]$	$f_{A,scis}[C_1\text{-}(C_B)(C)(H)]$
$X_{scis}[C_1\text{-}(C_B)(C)_2]$	$f_{A,scis}[C_1\text{-}(C_B)(C)_2]$	$X_{scis}[C_2\text{-}(C_B)(C)_2]$	$f_{A,scis}[C_1\text{-}(C_B)(C)_2]$
$X_{scis}[C_{1,d}\text{-}(H)]$	$f_{A,scis}[C_{1,d}\text{-}(H)]$	$X_{scis}[C_{2,d}\text{-}(H)]$	$f_{A,scis}[C_{1,d}\text{-}(H)]$
$X_{scis}[C_{1,d}\text{-}(C)]$	$f_{A,scis}[C_{1,d}\text{-}(C)]$	$X_{scis}[C_{2,d}\text{-}(C)]$	$f_{A,scis}[C_{1,d}\text{-}(C)]$
$X_{scis}[C_{1,cyclo}\text{-}(H)]$	$f_{A,scis}[C_{1,cyclo}\text{-}(H)]$	$X_{scis}[C_{2,cyclo}\text{-}(H)]$	$f_{A,scis}[C_{1,cyclo}\text{-}(H)]$
$X_{scis}[C_{1,cyclo}\text{-}(C)]$	$f_{A,scis}[C_{1,cyclo}\text{-}(C)]$	$X_{scis}[C_{2,cyclo}\text{-}(C)]$	$f_{A,scis}[C_{1,cyclo}\text{-}(C)]$
$X_{scis}[C_{1,cycloallylic}\text{-}(H)]$	$f_{A,scis}[C_{1,cycloallylic}\text{-}(H)]$	$X_{scis}[C_{2,cycloallylic}\text{-}(H)]$	$f_{A,scis}[C_{1,cycloallylic}\text{-}(H)]$

Table 3.12: C-C and C-H scission reactions: Contributions for the formed and attacking radical

3.5   Conclusions

The single event microkinetic model is automatically generated. The reaction network is drastically expanded with new species:

- more di-, tri-, poly- and naphtheno-aromatic
- new heavy radicals, such as the benzyl radical

These innovations make it possible to better describe VGO cracking experiments and the formed pyrolysis fuel oil fraction compounds were introduced. Other innovations are:

- new label formulation to represent a mesomeric species in a unique way

- calculation of the activation energies and the pre-exponential factors by the new group additive method of Saeys et al. (2003; 2004; 2006)
- Systematically calculating the number of single events

3.6   References

American Chemical Council, Olefin panel, Fuel Oils Category, Report 201-14736A, http://www.epa.gov/chemrtk/fueloils/c13435rt.pdf, 2003.

Baas C.J. De Synthese van Isopreen uit Propeen. PhD dissertation, T.U. Delft, 1963.

Balaban A.T. Chemical applications of graph theory, Academic Press London, 1976

Benson S.W. Thermochemical Kinetics, 2nd Edition, J. Wiley and Sons, New York, 1976.

Bischop D.M., Laidler K.J. Symmetry Numbers and Statistical Factors in Rate Theory, J. Chem. Phys., 42, 1688, 1965.

Bischop D.M., Laidler K.J. Statistical Factors for Chemical Reactions, Trans. Faraday Soc., 66, 1685, 1969.

Broadbelt L.J., Stark S.M., Klein M.T. Computer-generated Pyrolysis Modeling – on-the-fly Generation of Species, Reactions, and Rates, Ind. Eng. Chem. Res., 33, 790-799, 1994.

Clymans P. De Produktie van Olefinen uit Gasolies en de Rigoureuze Simulatie van de Thermische Kraking, PhD dissertation, UGent, 1982.

Clymans P.J., Froment G.F. Computer Generation of Rate Equations in the Thermal Cracking of Normal and Branched Paraffins. Comp. Chem. Eng., 8, 137-142, 1984.

Dente M., Ranzi E., Barendregt S., Cronin P. Steam Cracking of Heavy Liquid Feedstocks. Cracking Yields Rigorously Predicted, AIChE Spring National Meeting, New Orleans, USA, 1986.

De Witt M.J., Dooling D.J., Broadbelt L.J. Computer generation of Reaction Mechanisms using Quantitative Rate Information: Application to Long-Chain Hydrocarbon Pyrolysis, Ind. Eng. Chem. Res., 39, 2228, 2000.

Eyring, H. The activated Complex in Chemical Reactions. J. Chem. Phys. 3:107-115, 1935.

Froment G.F. Chemical Reactions in Complex Systems: the Mobil Workshop, A.V. Sapre and F.J. Krambeck, New York, Van Nostrand Reinhold, 1991.

Green W.H., Barton P.I., Bhattacharjee B., Matheu D.M., Schwer D.A., Song J., Sumathi R., Carstensen H.H., Dean A.M., Grenda J.M. Computer Construction of Detailed Chemical Kinetic Models for Gas-Phase reactors, Ind. Eng. Chem. Res., 40, 5370, 2001.

Hillewaert L.P., Diericks J.L., Froment G.F. Computer-Generation of Reaction Schemes and Rate-Equations for Thermal-Cracking, AIChE Journal, 34, 17, 1988.

Jursic B.S. Preference in Formation of three-, five-, and six-membered rings in Cyclization of the primary unsaturated Radical studied with the Hybrid Density Functional Theory Method, Journal of Molecular Structure-Theochem, 492, 285-291, 1999.

Jutz C., Aromatic and Heteroaromatic Compounds by Electrocyclic Ring Closure with Elimination, Top. Curr. Chem., 73, 125-130, 1978.

Karas A.J., Gilbert R.G., Collins M.A. Rigorous Derivation of Reaction Path Degeneracy in Transition State Theory, Chem. Phys. Lett., 193:181-184, 1992.

King R.B., Rouvray D.H., Chemical Apllications of Topology and Group-Theory, Stud. phys. theor. chem., 51, 575, 1987.

Kopinke F.D., Bach G., Ondruschka B., Zimmerman G. Uber die Pyrolyse von Pent-1-en-4,4,5,5-5-d_5. J. Prakt. Chemie, 325, 699, 1983.

Kopinke F.D., Bach G., Ondruschka B., Zimmerman G. Tendencies of Aromatization in Steam Cracking of Hydrocarbons, Ind. Eng. Chem. Res., 26, 2393-2397, 1987.

Kuo J.C.W., Wei J. A Lumping Analysis in Monomolecular Reaction Systems – Analysis of Approximately Lumpable System, Ind. Eng. Chem. Fund., 8, 124, 1969.

Lauer J.C., Composition Détaillé de la Partie Volatile de l'Huile Lourde de Naphtha, Internal Report Centre de Recherches de Lorraine, Total, 1988.

Matheu D.M., Green W.H., Grenda J.M. Capturing Pressure dependence in Automated Mechanism Generation: Reactions through Cycloalkyl Intermediates, Int. J. Chem. Kin., 35, 95-119, 2003.

McNaught A.D., Wilkinson A. Compendium of Chemical Terminology. The Gold Book, 2nd Edition, Blackwell Science, 1997.

Moens J. Een Rigoureus Kinetisch Model voor de Simulation van de Thermische Kraking van Lichte Koolwaterstoffen en hun Mengsels, PhD dissertation, UGent, 1982.

Nomura A., Yamada J., Yarita T., Maeda T. Supercritical-fluid chromatograms of fuel oils on ODS-silica gel column using fluorescence, UV-absorption, and flame-ionization detectors Journal of supercritical fluids, 8, 329-333, 1995.

Pollak E., Pechukas P. Symmetry Numbers, not Statistical Factors, should be used in Absolute Rate Theory and in Bronsted Relations, Journal of American Chemical Society, 100, 2984-2991, 1978.

Plehiers P.M. Rigoureuze Modellen voor de Simulatie van Fornuizen voor de Thermische Kraking van Lichte Koolwaterstoffen, PhD dissertation, UGent, 1989.

Ranzi E., Dente M., Goldaniga A., Bozzano G., Faravelli T. Lumping procedures in detailed kinetic modeling of gasification, pyrolysis, partial oxidation and combustion of hydrocarbon mixtures, Progress in Energy and Combustion Science, 27, 99-139, 2001.

Rovner S.L. Chemical 'Namin' method unveiled, Chemical & Engineering News, 39, August 22, 2005.

Sabbe M.K., Saeys M., Reyniers M.F., Marin G.B., Van Speybroeck V., Waroquier M. Group additive values for the gas phase standard enthalpy of formation of hydrocarbons and hydrocarbon radicals, Journal of Physical Chemistry A, 109, 7466-7480, 2005.

Saeys M. Ab initio Modelling as a Tool for the Sustainable Development of Chemical processes, PhD dissertation, UGent, 2003.

Saeys M., Reyniers M.F., Marin G.B., Van Speybroeck V., Waroquier M. Ab initio group contribution method for activation energies for β scissions and radical additions. AIChE Journal, 50, 426-444, 2004.

Saeys M., Reyniers M.F., Van Speybroeck V., Waroquier M., Marin G.B. Ab initio group contribution method for activation energies of hydrogen abstraction reactions ChemPhysChem, 7, 188-199, 2006.

Shiess P., Dinkel R. Uber den Anteil sigmatroper 1,5-Wanderung von Kohlenwasserstoffgruppen bei der Thermolytischen Skelettisomerisierung 5,5,-disubstituierter 1,3-Cyclohexadiene, Helv. Chim. Acta, 64, 801-812, 1981.

Song J. RMG: a new reaction mechanism generator. PhD Dissertation, Massachusetts Institute of Technology, 2004.

Stein S.E., Rabinovitch B.S. Ring Opening and Isomerisation of a Series of Chemically Activated Cycloalkyl Radicals. J. Phys. Chem., 79, 191-198, 1975.

Susnow R.G., Dean A.M., Green W.H., Peczak P., Broadbelt L.J. Rate-Based Construction of Kinetic Models for Complex Systems, J. Phys. Chem. A, 101, 3731, 1997.

Tarjan, R. E. Graph Algorithms in Chemical Computation. Algorithms for Chemical Computations; Christoffersen, R. E., Ed. American Chemical Society: Washington, DC, 1977.

Trinajstic N., Chemical graph theory, CRC Press Boca Raton (Fla.), 1983.

Tsang W. Thermal Decomposition of Cyclopentane and Related Compounds. Int. J. Chem. Kin., 10, 599, 1978.

Ugi I., Bauer J., Brandt J., Freidrich J., Gasteiger J., Jochum C., Schubert W. New Applications of Computers in Chemistry, Angew. Chem., Int. Ed. Engl. 1979, 18, 111-123.

Vanneste P. De Thermische Kraking van Naftenische Typecomponenten. Master Thesis UGent, 1985.

Van Speybroeck V., Borremans Y., Van Neck D., Waroquier M., Wauters S., Saeys M., Marin G.B. Ab initio study of radical reactions: Cyclization pathways for the butylbenzene radical (II), Journal of Physical Chemistry A, 105, 7713-7723, 2001.

Vercauteren C. Rigoureuze Kinetische Schema's voor de Thermische Kraking van Koolwaterstoffen, PhD dissertation, UGent, 1991.

Vynckier E., Froment G.F. Kinetic and Thermodynamic Lumping of Multicomponent Mixtures. Eds. G. Astarita and S.I. Sandler, Elsevier Science Publishers B.V., Amsterdam, 131-161, 1991.

Warth V., Stef N., Glaude P.A., Battin-Leclerc F., Scacchi G., Côme G.M. Computer-Aided Derivation of Gas-Phase Oxidation Mechanisms: Application to the Modeling of the Oxidation of n-Butane, Combustion & Flame., 114, 81-102,1998.

Wei J., Kuo J.C.W. A Lumping Analysis in Monomolecular Reaction Systems – Analysis of the Exactly Lumpable System, Ind. Eng. Chem. Fund., 8, 114, 1969.

Willems P.A., Froment G.F. Kinetic modelling of the Thermal Cracking of Hydrocarbons. 1. Calculation of frequency factors, Ind. Eng. Chem. Res., 27, 1959, 1988 [a].

Willems P.A., Froment, G.F. Kinetic modelling of the Thermal Cracking of Hydrocarbons. 2. Calculation of Activation Energies, Ind. Eng. Chem. Res., 27, 1966, 1988 [b].

Wong H.W., Li X.G., Swihart M.T., Broadbelt L.J. Detailed Kinetic Modeling of Silicon Nanoparticle formation chemistry via Automated Mechanism Generation, Journal of Physical Chemistry A, 108, 10122-10132, 2004.

Chapter 4:

Validation of the Single Event Microkinetic Model

4.1   Introduction

In the search for higher performance and increased selectivity simulation models have become an indispensable tool for the chemical industry. Generally these simulation models consist of 2 parts; on the one hand a solver that solves the reactor model equations, on the other hand the reaction network and the physical properties of the considered species. The general build up of single event microkinetic simulation models for steam cracking of hydrocarbons is shown in Figure 4.1. These models account for both the chemical reactions and the physical transport phenomena.
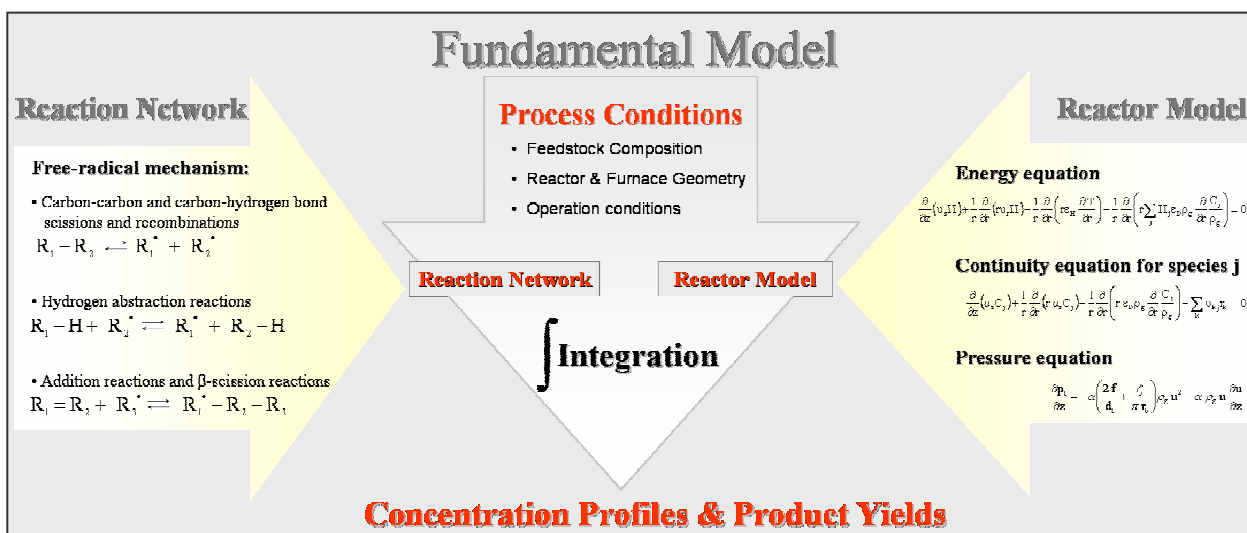
Figure 4.1: Illustration of the general construction of a single event microkinetic model for steam cracking of hydrocarbons

In the next paragraphs the structure of the simulation model, the solver and the calculation of the physical properties are discussed in more detail, before they are applied for the validation of the single event microkinetic model. The latter will be based on pilot plant data.

4.2   1-Dimensional Reactor Model Equations

Because the general equations for chemically reacting flow involve transport phenomena in addition to kinetics and thermodynamics, rigorous reactor models are by necessity multidimensional. However, there are often practical as well as mathematical reasons for considering idealized models of reduced dimensionality. For the simulation of smooth tubular reactor types the use of a 1-dimensional reactor plug-flow model is generally believed to provide a sufficient degree of accuracy, because all radial profiles are wiped out due to the high turbulence corresponding to Reynolds numbers of over 250 000 (Plehiers, 1989). The plug-flow reactor model implicitly assumes that there is no mixing in the axial (flow) direction but perfect mixing in the transverse direction(s). Smith (1981) showed that the absence of axial mixing allows maximizing the achievable reactant conversion. Likewise, the lack of transverse gradients implies that mass-transfer limitations are absent, again enhancing the reactor performance. Along with these practical advantages, the plug flow reactor is computationally efficient since it is modeled using first-order ordinary differential equations (ODE's), and no transport properties are needed. All resistance to heat transfer is located in a thin (laminar) film near the tube wall. De Saegher (1994) showed that for finned tubes it is better to use more dimensional reactor models.

Steam cracking is a non-isothermal, non-adiabatic and non-isobaric process. Hence, the 1 dimensional model equations consist of the transport equations for mass, momentum and energy. The steady state continuity equation for a component j in the process gas mixture over an infinitesimal volume element with cross sectional surface area Ω, circumference ω and length dz is:

$$\frac{dF_j}{dz} = \left(\sum_{k=1}^{n_r} \upsilon_{kj} \, r_{V,k} \right) \Omega \qquad [4.1]$$

with F_j the molar flow rate of component j, $r_{V,k}$ the reaction rate of reaction k, and υ_{kj} the stoechiometric coefficient of component j. The energy equation is given by:

$$\sum_{j} F_j\, c_{pj}\, \frac{dT}{dz} = \omega\, q + \Omega\, \sum_{k} R_{v,k}\left(-\Delta_f H_k^0\right)$$

[4. 2]

with q the heat flux to the process gas, c_{pj} the heat capacity of component j at temperature T, $\Delta_f H_k$ the standard enthalpy of species k, $R_{v,k}$ the net production rate for species k. The momentum equation accounting for friction and changes in momentum is given by:

$$\frac{dp_t}{dz} = -\alpha\left(\frac{2\,f}{d_t} + \frac{\zeta}{\pi\, r_b}\right)\rho\, v^2 - \alpha\, \rho\, v\, \frac{dv}{dz}$$

[4. 3]

with p_t the total pressure, α a conversion factor, f the Fanning friction factor, ρ the density of the gas mixture, r_b the radius of the bend, d_t the diameter and v the velocity. The momentum equation can be modified to yield a more convenient pressure drop equation by using the following equation for the process gas velocity using the ideal gas law:

$$v = \frac{4\,M\,F_t}{\pi\,\rho\,d_t^2} = \frac{G\,R\,T}{M\,p_t}$$

[4. 4]

with M the average molecular mass, F_t the total molar flow rate and G the mass flux. Applying the chain rule to equation [4.4] makes it possible to rewrite the derivative from v to z as follows:

$$\frac{dv}{dz} = \frac{G\,R}{p_t}\left(T\,\frac{d\left(\frac{1}{M}\right)}{dz} + \frac{1}{M}\frac{dT}{dz}\right) - \frac{G\,R\,T}{M\,p_t^2}\frac{dp_t}{dz}$$

[4. 5]

Substitution of equation [4.5] in equation [4.3] and rearranging results into:

$$\left(\frac{1}{M\,p_t} - \frac{p_t}{\alpha\,G\,R\,T}\right)\frac{dp_t}{dz} = \frac{d}{dz}\left(\frac{1}{M}\right) + \frac{1}{M}\left(\frac{1}{T}\frac{dT}{dz} + f\right)$$

[4. 6]

with

$$\frac{d}{dz}\left(\frac{1}{M}\right) = \frac{d}{dz}\left(\frac{\sum\limits_{j=1}^{n} F_j}{G\,\Omega}\right) = \left(\frac{\sum\limits_{j=1}^{n} \dfrac{dF_j}{dz}}{G\,\Omega}\right) \qquad\qquad [4.\,7]$$

The inlet conditions are $(z = 0)$:

$$C_j = C_{j0} \qquad\qquad T = T_0 \qquad\qquad p = p_0 \qquad\qquad [4.\,8]$$

The presence of the heat flux q in equation [4.2] requires imposing an axial heat flux profile, see Section 4.3.2.

4.3   Solving the 1-Dimensional Reactor Model Equations

4.3.1   Integration of balances

The reactor model equations to be solved are given by equations [4.1], [4.2] and [4.3]. The last two equations only have to be considered when, respectively, the temperature and/or pressure profile are not imposed. Based on the reactions, rate equations, and rate coefficients, the production rate of each component j by the reaction k, can be expressed as a function of the concentration of the involved species. The resulting set of continuity equations forms a system of stiff non-linear first order differential equations. The stiffness is caused by the large difference (several orders of magnitude) of the eigenvalues related to the molecular species on the one hand and the radical species on the other hand. To overcome the stiffness problem the numerical procedure presented by Dente et al. (1979) was applied in the past. In this procedure the net production rate of each component is split in a cumulative rate of formation term and a similar rate of disappearance term. Next, the rate of disappearance is assumed to be quasi-proportional to the concentration (actually the mass fraction) of the component, leading to the introduction of a pseudo rate coefficient. The resulting non-homogeneous first order differential equation is then integrated over a reactor length increment Δz small enough to consider the cumulative rate of formation and the pseudo rate coefficient to depend on z only. Based on the different magnitude and behavior of these variables for molecular and radical species the resulting integral equations

are then further evaluated. The increment Δz is chosen in such a way that (based on a number of criteria) the mean values for the cumulative rate of formation and the pseudo rate coefficient can be used for the molecular species, while a number of terms in the equation approach unity for the radical species, allowing an analytical integration. Because values of the cumulative rate of formation and the pseudo rate coefficient at the end of each interval Δz appear in the resulting algebraic equations, iteration for each interval is finally required. The calculations proceed until convergence is reached. More details, as well as the convergence criteria, can be found in Wauters (2002). Finally, it should be remarked that the method presented by Dente et al. (1979) for the radical species is a numerical equivalent of the well-known pseudo steady state (or also called the continuously varying steady-state) assumption (i.e. assuming steady state for certain species in each increment of the integration, leading to a set of algebraic equations to be solved simultaneously with the differential equations for the remaining species). De Saegher (1994) has studied the influence of several of such simplifying steady state approaches on the reactor calculation results and concluded that the pseudo steady state assumption actually doesn't hold for allyl-stabilized radicals. This can have a significant influence on, for example, the accuracy of the predicted butadiene yield (De Saegher, 1994). Today computational capabilities actually allow for solving all continuity equations without any steady state assumption to avoid such inaccuracies. Therefore a new solver DASSL (Li and Petzold, 1999) is implemented in COILSIM1D. DASSL uses backward differentiation formula (BDF) methods to solve a system of Differential Algebraic Equations (DAE) or Ordinary Differential Equations (ODE). The methods are variable step-size, variable order. The system of equations in DASSL is written in an implicit ODE form like:

$$F(t, y, y') = 0 \tag{4.9}$$

where y' denotes the time derivatives of y. The BDF methods used in DASSL require the solution of a large system of non linear equations

$$n$$

on each time step. Here, α_n and β_n are scalars which depend on the method and step size. In DASSL, this system is solved by a modified Newton iteration:

$$y_{n+1} = y_n - \left(\alpha_n \frac{\partial F}{\partial y'} + \frac{\partial F}{\partial y} \right)^{-1} F(t, y_n, \alpha_n y_n + \beta_n)$$ [4. 10]

The set of linear equations [4.11] is solved via a dense or banded solver in DASSL. The iteration matrix

$$\underline{A} = \alpha_n \frac{\partial F}{\partial y'} + \frac{\partial F}{\partial y}$$ [4. 11]

is computed and factored, and is then used for as many time steps as possible.

	Solver Dente et al. (1978) (wt %)	**DASSL (1999)** (wt %)
H$_2$-yield	0.9	0.9
CH$_4$-yield	20.6	20.3
C$_2$H$_2$-yield	0.9	0.9
C$_2$H$_4$-yield	35.2	34.9
C$_2$H$_6$-yield	3.4	3.4
C$_3$H$_4$-yield	0.9	0.9
C$_3$H$_6$-yield	17.7	17.9
C$_4$H$_6$-yield	2.3	2.5
1-C$_4$H$_8$-yield	1.5	1.6
2-C$_4$H$_8$-yield	0.4	0.5
C$_6$H$_6$-yield	2.4	2.5
C$_4$H$_{10}$-conversion	90.1	89.9

Table 4.1: Simulated conversion and product yields for n-butane steam cracking with 2 different solvers: the solver of Dente et al. (1979) and DASSL (Li and Petzold, 1999) [Simulation Conditions: CIT = 873 K; COT = 997 K; CIP = 0.27 MPa; COP = 0.24 MPa; F: 4.0 kg h^{-1}; δ = 0.4 kg /kg]

In Table 4.1 the yields and conversion for a n-butane cracking experiment (given temperature and pressure profile) are shown simulated with Dente et al.'s solver and DASSL.

Overall the yields agree quite well, but as found by De Saegher (1994) the simulated methane, ethylene, butadiene and propylene yield differ significantly. This is because of the steady state assumption for allylic radicals in Dente et al.'s solver. The main advantage of using the solver of Dente el al. is that the time to solve the differential equations is a factor 3 to 5 smaller. Dente et al. (1979) also proposed to solve the energy and pressure equations in an iterative manner, decoupled from the continuity equations, by means of a straightforward finite difference method. Decoupled solving of the energy and momentum equation does not lead to new errors. Nevertheless, in the new version of COILSIM1D this method is no longer applied; now the continuity equations, the energy equation and the momentum equation are solved simultaneously. Based on the process gas temperature and the (internal tube wall or coke) interface temperature, the coke formation rate is calculated in a separate step. The effect of coke formation on the continuity, energy and pressure equations is neglected because the actual amount of coke precursors being consumed in the coke formation process is very small (± 0.01 wt%). In case of a run-length simulation the local cumulating thickness of the deposited coke layer influences the energy and pressure equations through an additional resistance to heat transfer over the coke layer, and an increasing pressure drop as a result of the decreasing internal tube diameter. A coke layer thickness profile can be imposed as an initial boundary condition.

4.3.2   Calculation of the heat flux based on the wall temperature

The first term of the right hand side of the energy equation [4.2] corresponds to the heat flux over the reactor wall. The second term of the right hand side corresponds to the thermal power accompanying the endothermic steam cracking process. If the external wall temperature $T_{w,ext}$ profile is given the internal heat flux q should first be calculated. An energy balance over a cross section of the tube in Figure 4.2 gives:

$$q_{ext} L \ \pi \ (d_w + d_t) = \lambda \ L \ 2\pi \ r \ \frac{dT}{dr} \qquad [4.\ 12]$$

Integration of equation [4.13] leads to the internal wall temperature $T_{w,int}$:

$$T_{w,int} = T_{w,ext} - \frac{q_{ext}\,(d_w + d_t)}{2\,\lambda_w}\ln\left(\frac{d_w + d_t}{d_t}\right)$$
[4. 13]

with λ_w the conduction coefficient of the wall.
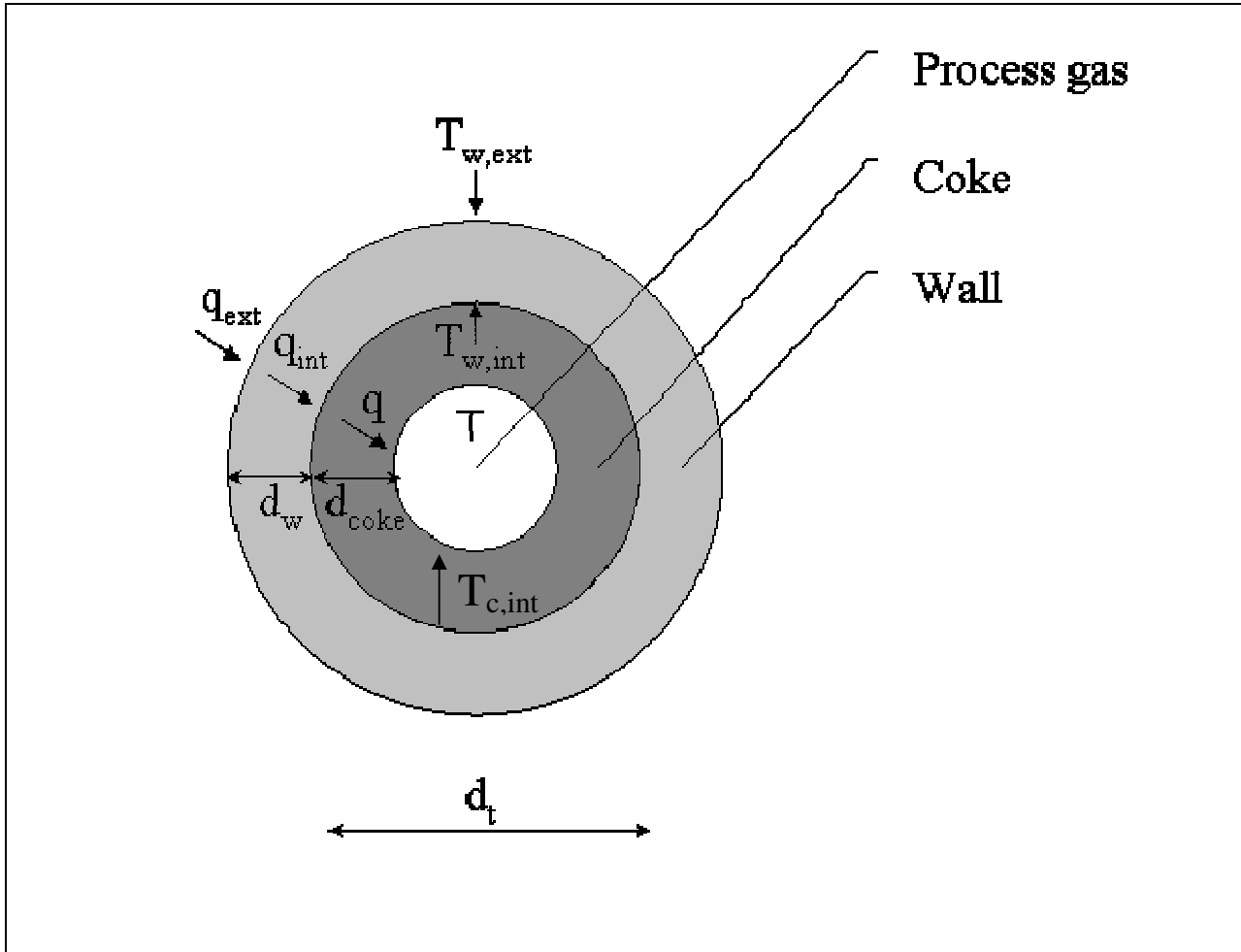
Figure 4.2: Heat balance over a cross section of a tube

Also for the temperature at the process gas/coke interface a similar equation as equation [4.14] can be obtained:

$$T_{c,int} = T_{w,int} - \frac{q_{int}\,(d_t)}{2\,\lambda_{coke}}\ln\left(\frac{d_t}{d_t - d_{coke}}\right)$$
[4. 14]

with λ_{coke} the conduction coefficient of the coke layer. Within the tube all temperature gradients are eliminated, and all resistance to heat transfer is located in a thin film near the wall. Hence, the temperature of the process gas is given by:

$$T = T_{c,int} - \frac{q}{h}$$

[4. 15]

with h the convection coefficient of the process gas. An energy balance over the cross section of the tube gives:

$$q_{int} d_t = q_{ext} (d_t + d_w) = q \ (d_t - d_{coke})$$

[4. 16]

Solving equation [4.14] for the external heat flux q_{ext} and [4.15] for the internal heat flux q gives after substitution in equation [4.17] the following expression for the internal heat flux q:

$$q = \frac{T_{w,ext} - T}{\dfrac{1}{h} + \dfrac{1}{\lambda_w} \ln\left(\dfrac{d_t + d_w}{d_t}\right) + \dfrac{1}{\lambda_{coke}} \ln\left(\dfrac{d_t}{d_t - d_{coke}}\right)}$$

[4. 17]

which can be substituted in equation [4.2].

4.4   Calculation of the physical and transport properties

4.4.1   The convection coefficient h_c

The convection coefficient for smooth tubes can be obtained from the Dittus-Boelter correlation:

$$Nu = 0.023 \, Re^{0.8} \ Pr^{0.4}$$

[4. 18]

The Reynolds, Nusselt and the Prandtl number are defined as follows:

$$Re = \frac{v \, d_t \, \rho}{\mu}$$

[4. 19]

$$Nu = \frac{h_c\, d_t}{\lambda} \qquad [4.\,20]$$

$$Pr = \frac{\mu\, c_p}{\lambda} \qquad [4.\,21]$$

with v the velocity, λ the thermal conductivity of the process gas, μ the viscosity of the process gas and c_p the heat capacity.

For finned tubes a distinction is made between spirally finned tubes, where the fins make a helix along the wall of the tube, or longitudinal fins, where the straight fins are placed on the inner side of the tube wall. The Reynolds number Re for finned tubes is also calculated according to equation [4.20] but the internal tube diameter is replaced by the equivalent diameter d_{eq}:

$$d_{eq} = \frac{\Omega}{4\,\eta} \qquad [4.\,22]$$

whit Ω the cross sectional area and η the wetted perimeter of the tube. The convection coefficient for finned tubes is calculated using the following equations (Reid et al., 1979):

  - Spirally finned tubes:

$$Nu = 0.242\, Re^{0.645}\, Pr^{0.4} \left(\frac{P}{d_{eq}}\right)^{a1} \left(\frac{B}{d_{eq}}\right)^{a2} \left(\frac{T}{T_w}\right)^{0.5} \qquad [4.\,23]$$

  - Longitudinal finned tubes:

$$Nu = 4.11\, Re_e^{0.326}\, Pr^{0.4} \left(\frac{P}{d_{eq}}\right)^{a3} \left(\frac{\pi\, d_i}{\eta}\right) \qquad [4.\,24]$$

with a1, a2 and a3 functions of the Reynolds number (Reid et al., 1979), d_i the internal diameter of the finless tube, P the pitch of the fin and B the inter-fin distance. The pitch P of a helix is the height over which this helix makes a full turn around its axis. B can be calculated as the length of

an arc connecting two consecutive fin center points. These equations are valid for turbulent flows, i.e. Re higher then 4000.

4.4.2   The friction factor f

Several correlations are available for the calculation of the Fanning friction factor. For rough straight tubes the friction factor f is obtained from the Colebrook equation (1939):

$$\frac{1}{\sqrt{f}} = -4 \log\left(\frac{\varepsilon}{3.7\, d_t} + \frac{1.256}{Re\sqrt{f}}\right) \qquad [4.\,25]$$

For smooth straight tubes this equation can be rewritten as follows (Reid et al., 1979):

$$\frac{1}{\sqrt{f}} = -4 \log\left(\frac{1.256}{Re\sqrt{f}}\right) \qquad [4.\,26]$$

Another possible equation for the calculation of the friction factor in smooth tubes is the Blasius equation (Reid et al., 1979):

$$f = 0.0791 (Re)^{-0.25} \qquad [4.\,27]:$$

For the tube bends the friction factor is calculated as following (Nekrasov, 1969):

$$f = \frac{0.092\, (Re)^{-0.2}}{d_t} + \frac{\chi}{\pi\, r_b} \qquad 4.\,28]$$

With r_b the radius of the bend and χ the Nekrasov factor given by:

$$\chi = 0.7\left(1 + \frac{\kappa}{\pi}\right)\left(0.051 + 0.19\frac{d_t}{r_b}\right) \qquad [4.\,29]$$

with κ the angle of the tube bend.

Again if the tubes are finned, a distinction is made between different types of finned tubes (Reid et al., 1979):

- **Spirally finned tube** (Lummus correlation)

$$f = 0.015\,\mathrm{Re_e^{0.089}}f_{cr}$$ [4. 30]

- **Straight finned tube** (Watkinson correlation)

$$f = 0.131\,\mathrm{Re_e^{-0.29}}\left(\frac{B}{d_{eq}}\right)^{0.17}f_{cr}$$ [4. 31]

- **Spirally finned tube** (Watkinson correlation)

$$f = 0.0546\,\mathrm{Re_e^{-0.15}}\left(\frac{P}{d_{eq}}\right)^{-0.24}f_{cr}$$ [4. 32]

The factor f_{cr} is the ratio of the wetted perimeter and the perimeter of the circle drawn to connect the valleys of consecutive fins. The influence of non-uniformity of the process gas over a cross section is obtained by multiplying the friction factor f with:

$$\left(\frac{\mu_w}{\mu}\right)^{0.5}$$ [4. 33]

whit μ_w the process gas viscosity calculated at the internal wall temperature.

4.4.3   The conduction coefficient λ_w

The conduction coefficient of the wall depends on the wall material. The materials are considered to be grey. For stainless steel the following equation is used (Reid et al., 1979):

$$\lambda_w = -2.014\ 10^{-3} + 7.216\ 10^{-6}\ T$$ [4. 34]

For aluminum the conduction coefficient is calculated from (Reid et al., 1979):

$$\lambda_w = 0.02967 + 33.92\ 10^{-6}\ T + 15.778\ 10^{-9}\ T^2 + 2.699\,10^{-12}\ T^3$$ [4. 35]

For silicon carbide the conduction coefficient is calculated from (Reid et al., 1979):

$$\lambda_w = 0.00717 + 12.11 \ 10^{-6} \ T + 7.119 \ 10^{-9} \ T^2 \qquad [4.\ 36]$$

4.4.4   The specific heat c_p

The specific heat of the reaction components can be calculated from:

$$c_p(T) = A + B.T + C.T^2 + D \ T^3 \qquad [4.\ 37]$$

with A, B, C and D mentioned in Reid et al. (1979). The proposed polynomials are valid in a temperature range between 300 and 1500 K.

4.4.5   The standard enthalpy of formation ΔH_f

The heat of formation for pure components is given by:

$$\Delta H°_f(T) = \Delta H°_f(T_0) + \int_{T_{ref}}^{T} c_p(T) dT \qquad [4.\ 38]$$

The reference temperature T_{ref} is 298.15 K. When the c_p is calculated from equation [4.38] the integral in [4.39] becomes:

$$\int_{Tref}^{T} c_p dT = A(T - T_{ref}) + \frac{B}{2}(T^2 - T_{ref}^2) + \frac{C}{3}(T^3 - T_{ref}^3) + \frac{D}{4}(T^4 - T_{ref}^4) \quad [4.\ 39]$$

4.4.6   The viscosity μ

The viscosity of the reacting mixture can be calculated from the Sutherland formula (Reid et al., 1979) derived from the kinetic gas theory:

$$\mu = \sum_{j=1}^{n_c} \frac{\mu_j}{1 + \sum_{i=1}^{n_c} \Phi_{ji} \frac{F_i}{F_j}}$$

[4. 40]

The Φ_{ji} are estimated by the Wilke formulas (Reid et al., 1977)

$$\Phi_{ji} = \frac{\left(1 + \left(\frac{\mu_j}{\mu_i}\right)^{\frac{1}{2}} \left(\frac{M_i}{M_j}\right)^{\frac{1}{4}}\right)^2}{\left(8\left(1 + \frac{M_j}{M_i}\right)\right)^{\frac{1}{2}}} \qquad i > j$$

[4. 41]

$$\Phi_{ij} = \frac{\mu_i}{\mu_j} \frac{M_j}{M_i} \Phi_{ji} \qquad i < j$$

[4. 42]

The theory of corresponding states leads to the following formulas for the viscosity:

- non-polar gases:

$$\mu_j \zeta_j = 1.10^{-7}\left(4.61\, T_{r_j}^{0.618} - 2.04\, \exp\left(-0.449\, T_{r_j}\right) + 0.1\right)$$
$$+ 1.9\, 10^{-7} \exp\left(-4.059\, T_{r_j}\right)$$

[4. 43]

- hydrogen:

$$\mu_j = 90.71\ 10^{-8}\left(0.1375\, T - 1.67\right)^{\frac{5}{8}}$$

[4. 44]

- polar gases:

$$\mu_j \zeta_j = Z_{c_j}^{-5/4}\ 10^{-8}\left(7.55\, T_{r_j} - 0.55\right)$$

[4. 45]

- steam:

$$\mu_j = 325.23 \ 10^{-8}(0.01162\,T - 0.55) \qquad\qquad [4.\,46]$$

whit T_c the critical temperature, p_c the critical pressure, Z_c the critical compressibility factor and ζ_j given by the following equation:

$$\zeta_j = \frac{(T_c)^{1/6}}{\left[(M_j)^{1/2}(p_{cj})^{1/3}\right]} \qquad\qquad [4.\,47]$$

The values of the critical temperature, pressure and the compressibility factor are tabulated in Reid et al. (1979).

4.4.7   The thermal conductivity λ

The thermal conductivity is calculated in the same way as the viscosity:

$$\lambda = \sum_{j=1}^{n_c} \frac{\lambda_j}{1 + \sum_{i=1}^{n_c}\Phi_{ji}\dfrac{F_i}{F_j}\times 1.065} \qquad\qquad [4.\,48]$$

Again different correlations were set up to calculate the thermal conductivity of a pure compound. Generally these correlations have the form

$$\lambda_i = (c_1 \times c_{pi} + c_2)\frac{\mu_i}{M_i} \qquad\qquad [4.\,49]$$

with λ_i the thermal conductivity, c_{pi} the molar heat capacity, M_i the molecular weight and c_1, c_2 constants for each component.

4.5   The LPT pilot plant

The Laboratorium voor Petrochemische Techniek has a pilot plant setup for studying the steam cracking process. This experimental setup allows measurement of the kinetics of the cracking reactions (Zajdlik et al. 2003) and of the coke deposition in both the radiant coil (Reyniers and Froment, 1995) and the transfer line exchanger [TLE] (Dhuyvetter et al., 2001).
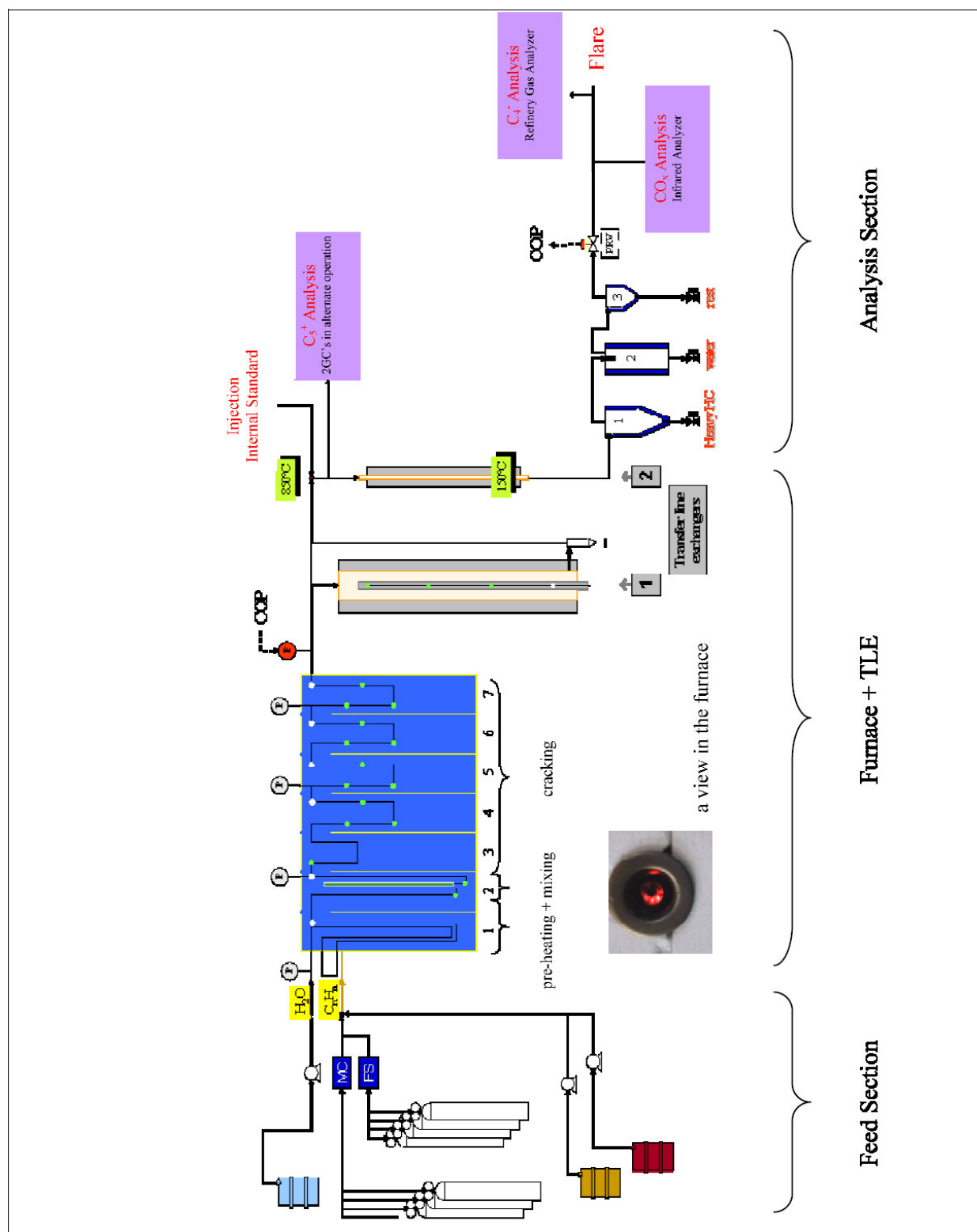
Figure 4.3: Overview of the LPT pilot plant setup

The pilot plant can be divided into three main parts: the feed section, the furnace with the coil and the analysis section, see Figure 4.3. The feed section allows measurement and regulation of different types of feedstocks. The mass flow instead of the volume flow of all feeds is measured to avoid inaccuracies of volume dependence on temperature and pressure. Also liquefied gases can be fed. If liquids are used the flow rate is measured as a mass difference per time interval. The flow is regulated by the pumping frequency. The same measurement method is used for heavier hydrocarbons such as vacuum gas oils or waxes. The heavier hydrocarbons are pumped preheated and melted by means of the heated pump. All types of feedstock can be fed simultaneously, which allows co-cracking of any feedstock. The furnace is divided into seven separate cells, see Figure 4.3, which can be fired independently to set any type of temperature profile in the reactor coil. Twenty thermocouples are located inside the reactor coil to measure the temperature of the reacting process gas. Five manometers measure the pressure profile along the coil. The exit pressure is controlled by means of a reduction valve.

The currently used reactor coil has a reaction section of 12.4 m long with an internal diameter of 9 mm. The maximal length of a reactor tube that can be used is ca. 22 m. These dimensions where chosen to achieve turbulent flow conditions in the coil with reasonable feed flow rates. Before entering the reaction zone, the hydrocarbons and the water are preheated separately in cells 1 and 2 and mixed in a mixer placed in cell 2. The reactor tube is suspended in the furnace, built of silica/alumina brick (Li23). External dimensions of the furnace are: 4 m long, 0.7 m wide and 2.6 m high. The wall thickness is 0.15 m. The furnace is heated by premixed natural gas and air distributed into ninety gas burners arranged on the sidewalls. Burners are placed in such a way that they provide a uniform heat distribution to the reactor coil. The cooling section consists of two TLE's, see Figure 4.4, which can be used simultaneously. Furthermore another cooler and two cyclones are used for additional cooling of the process gas and separation of condensed liquids. TLE1 is build especially to study coke deposition under TLE conditions. Its dimensions are designed to achieve turbulent flow conditions with effluent flow rates typical for the pilot unit. It consists of two concentric tubes: the reactor effluent flows through the inner tube while air, providing cooling of the effluent, flows co-currently through the outer tube. Both air and the process gas enter at the top of TLE1. Co-current flow of both streams was chosen since this provides a more uniform wall temperature profile along the TLE as compared to counter-current flow. By adjusting the air flow rate, the temperature profile of the

process gas in TLE1 can be regulated. TLE1 can also be heated to 900°C for decoking with air/steam. In TLE2, which is a concentric tube heat exchanger, the process gas is further cooled to 150°C by means of cooling oil. After TLE2 the heavy hydrocarbons part of the fuel oil fraction are condensed in a first condenser. In a second condenser the steam is condensed. Liquids remaining in the effluent are removed by a cyclone.
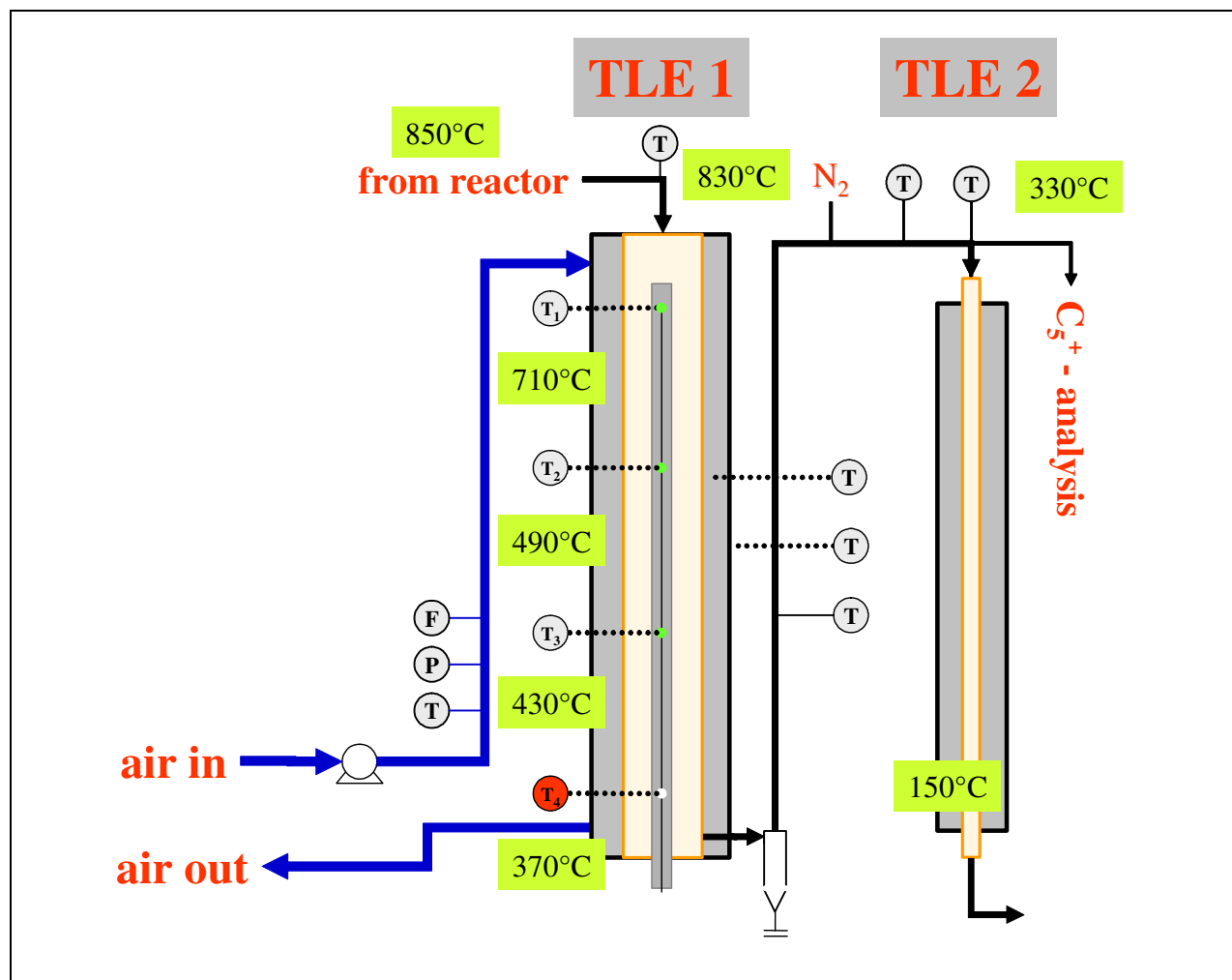
Figure 4.4: Overview of the cooling section in the LPT pilot plant setup

The pilot plant disposes of an extended on-line analysis section providing a product distribution ranging from C1 to C18 (boiling point ~ 400°C) and including H_2, CO, CO_2. At the reactor outlet, the injection of nitrogen provides an internal standard for the on-line analysis and contributes to a certain extent to the quenching of the process gas. Before the further cooling of the effluent in a TLE (Transfer Line Exchanger), a sample is taken for the on-line analytical

system. "The hot gas analysis" is provided by two automated gas chromatographs (GC) in alternate operation because the C_{5+} analysis lasts more than 70 minutes. These GC's are used especially for analysis of hydrocarbon fractions ranging from C_5 up to C_{18}. For a more detailed on-line analysis of the light hydrocarbons ranging from C1 up to C4, hydrogen and nitrogen, an automated refinery gas analyzer is used. The sample is taken from the quenched outlet gas stream, separated from higher hydrocarbons and water. An IR analyzer is used for continuous analysis of CO and CO_2. The IR analyzer can be used on-line during decoking and also during cracking experiments. The C_4- analysis takes about 30 minutes.

Calculations are based on the absolute flow rates of the effluent components. This is made possible by the injection of a precisely known nitrogen flow. From the peak surface areas of the TCD-channel of the automated refinery gas analyzer, the experimentally determined calibration factors on this instrument and the known amount of nitrogen, the flow rates of hydrogen, methane, CO_x and C_2 hydrocarbons are calculated. Using the methane flow rate as standard, the flow rates of the other components can be calculated for the other instruments. With these data, a product distribution in terms of weight percentages can be determined. Since the feed flow rate is known, yields and a material balance can also be calculated.
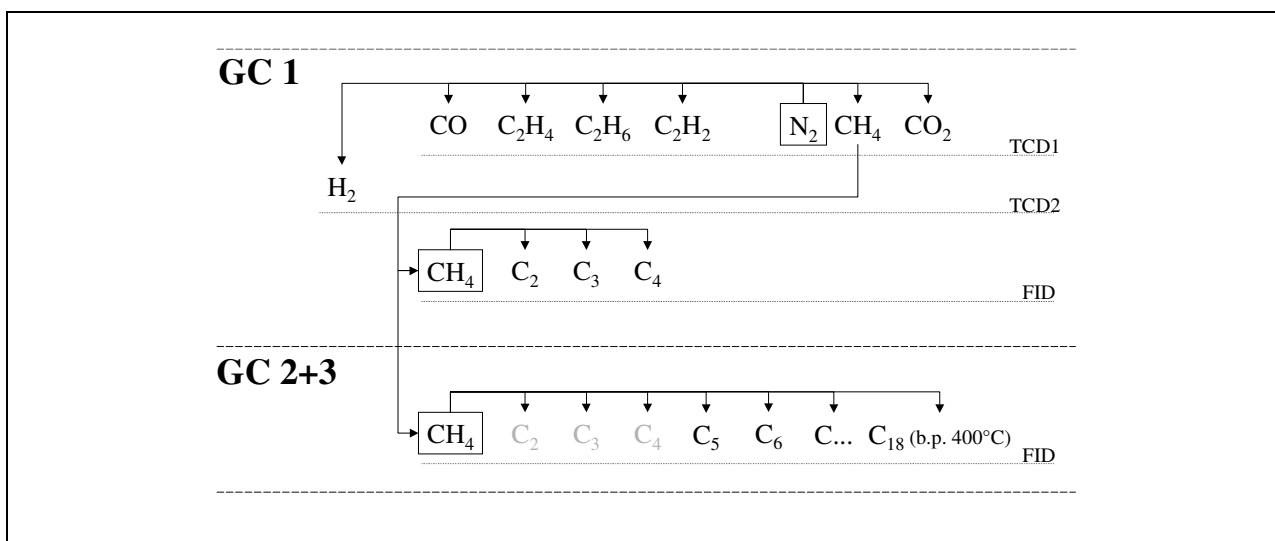
Figure 4.5: Overview of the cooling section in the LPT pilot plant setup

The pilot plant is partially automated. The inlet flow rates, the outlet temperature of each cell, outlet pressure and process gas sampling procedures are controlled electronically. As an interface between human supervisor and electronic control device a homemade software running in LabView is used. The pilot plant is equipped with the usual safety devices. The furnace is equipped with detectors on flame deflection, backfire, upper and lower limit of natural gas inlet pressure, proper functioning of venting and cooling of the flue gases. Also the reactor coil and all vessels under pressure are protected by safety valves.

4.6   Comparison between experimental and calculated data

The LPT pilot plant installation is a vital element for testing the simulation results obtained with the new single event microkinetic model. Indeed, to improve and extend the single event microkinetic simulation model for steam cracking experimental results on the pilot are indispensable. Over the years a lot of experiments have been carried out on the LPT pilot plant installation using feedstocks with widely varying characteristics, resulting in an extensive experimental database containing over 400 experiments obtained with over 50 different feedstocks. The feedstocks range from light gases, over naphthas to VGO's and even waxes. An compact overview of the experimental database is given in Table 4.2, while in Annex B more details are given about the different experiments. For these experiments both the operation conditions and the measured product yields of the main products are gathered and stored. To keep this database well organized a database program is developed that allows to neatly arrange the data, see Figure 4.6. This program makes it also possible to easily search the database.

Feed	HC flow (kg/hr)	Dilution (kg/kg)	COP (bar)	COT (°C)	Number of experiments
Light Feedstocks	2.1 - 5.2	0 -1.0	1.6 – 2.9	660 - 950	264
Naphthas	2.1 -6.5	0.2 – 1.5	1.6 – 2.5	700 - 930	158
Heavy Feedstocks	2.7 – 4.5	0.4 – 1.2	1.3 – 2.5	750 - 850	32

Table 4.2: Overview of the experimental database

    To validate the single event microkinetic simulation model the simulation results are compared with experimental data for a set of 150 experiments selected from the experimental database. This set of experiments covers a wide range of feedstocks ranging from ethane, over naphtha to VGO's. Special attention is paid to select also a large number of experiments that gave not so good simulation results with the older simulation models developed by Plehiers (1989) and Vercauteren (1991). De Roo (1998), De Buck (1999) and Bolado (2003) all found significant differences between the experimental and simulated product yields using the simulation models developed by either Plehiers (1989) or Vercauteren (1991). De Buck noticed that especially for the heavier products such as benzene, styrene and naphthalene significant differences are found. However, these problems are not restricted to heavier products. Problems are also found for ethane, propylene and butadiene (De Roo, 1998; Vercauteren, 1991; Bolado, 2003). The 1-dimensional reactor model is used for simulating the pilot plant reactor. Using more dimensional reactor models is not necessary as will be shown in Section 5.2.3.
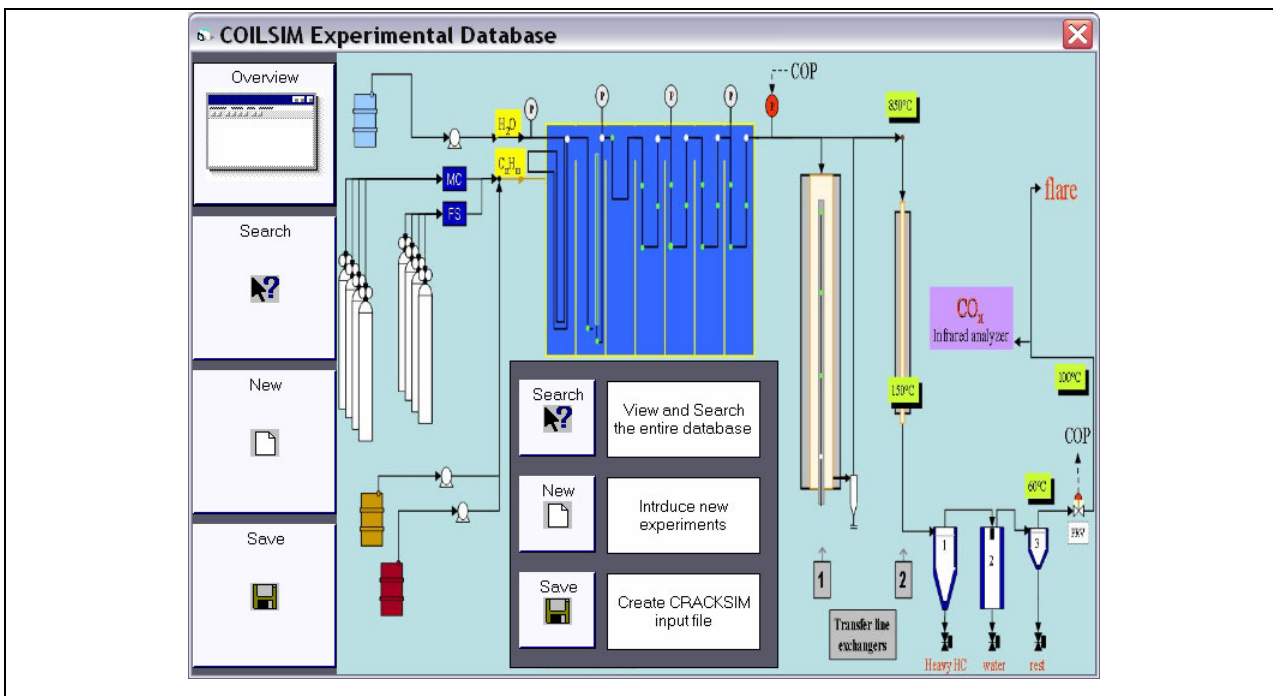
Figure 4.6: Graphical user interface for the experimental database

Figures 4.7-4.22 show the parity plots obtained for the main products [hydrogen, methane, acetylene, ethylene, ethane, propylene, propane, butadiene, 1-butene, iso-butene, 2-butene, iso-butane, n-butane, cyclopentadiene, benzene and toluene]. Figure 4.7 shows that the simulated hydrogen yield is well simulated. This is in contrast with the simulation results obtained by Vercauteren (1991) and De Roo (1998), who both noticed an underestimation of the hydrogen yield. In this case the hydrogen yield is slightly overestimated for naphtha experiments.

In Figure 4.8 the parity plot for the methane yield is shown. Methane is a cracking product from any component in the cracking mixture. Hence, differences found for the simulated methane yield will also reflect on the yields of the other products. However, Figure 4.8 shows that the simulation model is able to simulate the methane yield very accurately. The parity plot of acetylene is not as good as for methane but this is not unexpected, see Figure 4.9. Nevertheless, the parity plot is relatively good considering the low yields for this product and taking into account experimental inaccuracies.

The parity plot for ethylene is excellent, it is even better then the one found for methane. Even at severe cracking conditions the ethylene yield remains accurately simulated. This is no surprise because even the older models of Plehiers (1989) or Vercauteren (1991) were able to describe the ethylene yield quite accurately. These models had only trouble for some exotic feedstocks such as naphthas containing large amounts of naphthenes or ethane/toluene mixtures. Extending the kinetic model with some new reactions, i.e. reactions involving C_5 radicals and the benzyl radical, and re-estimating the kinetic parameters clearly lead to improved simulation results also for these fractions.

The parity plot for the ethane yield looks excellent, although this plot is slightly misleading. The high ethane yields correspond to ethane cracking experiments. Figure 4.11 shows that the conversion of ethane is accurately simulated both at low and high conversions. Some deviations are found for the ethane yield when naphtha is cracked. It seems difficult to obtain both very accurate ethane yields for these feedstocks and accurately simulate mixtures containing ethane.

For propylene the parity plot is also relatively good although some more deviations can be seen as for ethylene, see Figure 4.12. This is because the propylene yield results from a balance between addition reactions, β-scission reactions and hydrogen abstractions can explain the propylene behavior (Van Damme et al., 1984). A rate of production analysis shows that the β-scissions are generally the most important reactions for propylene (Van Geem et al., 2006).
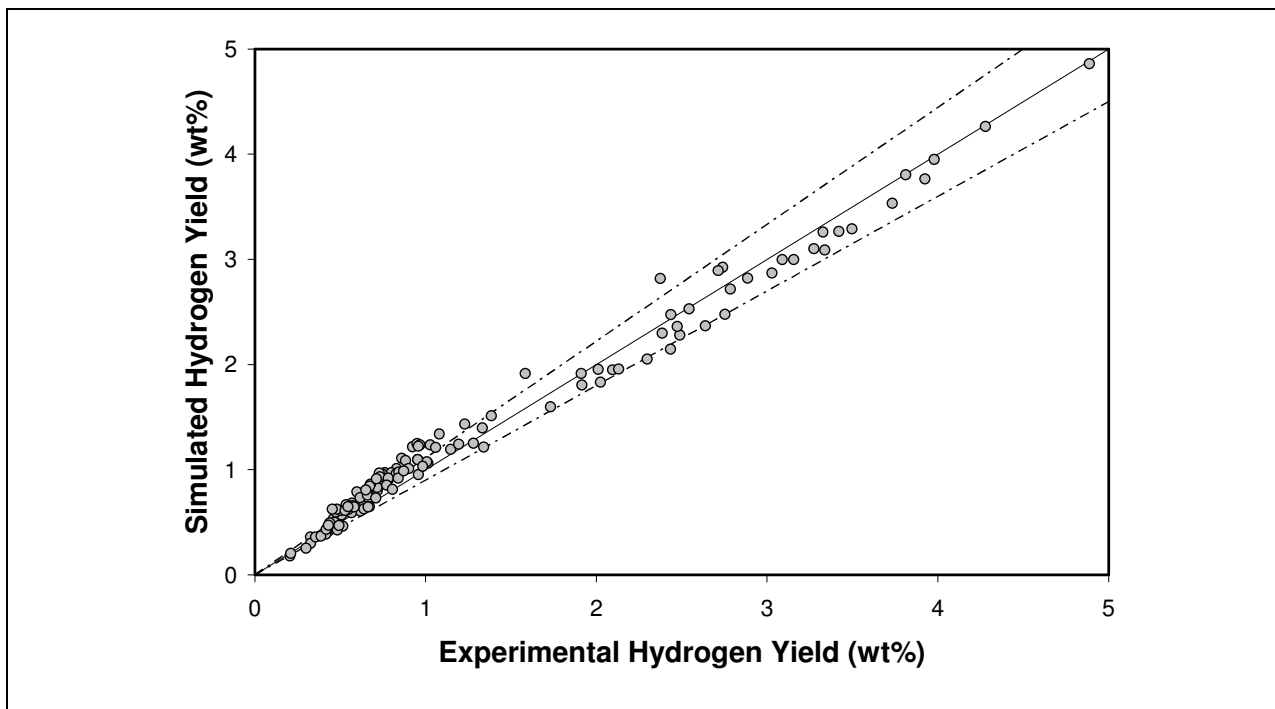
Figure 4.7: Parity plot for the hydrogen yield [- - - - 10 % (rel.) interval]
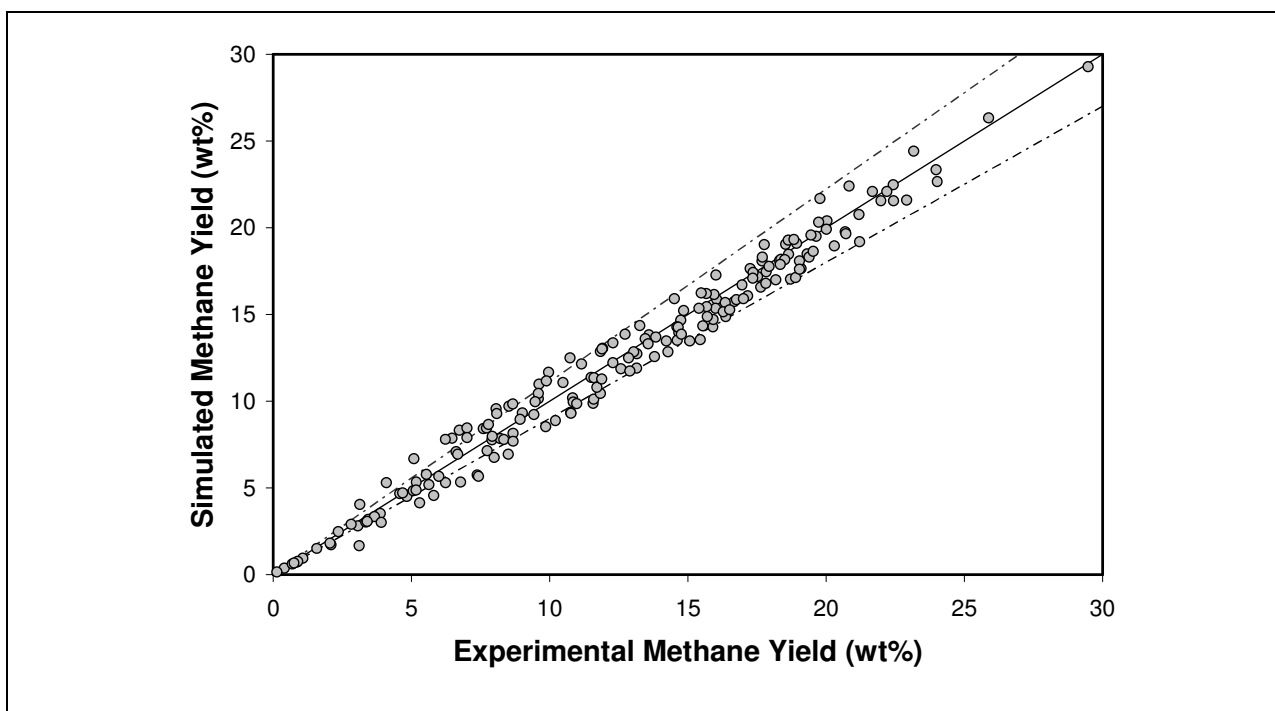
Figure 4.8: Parity plot for the methane yield [- - - - 10 % (rel.) interval]
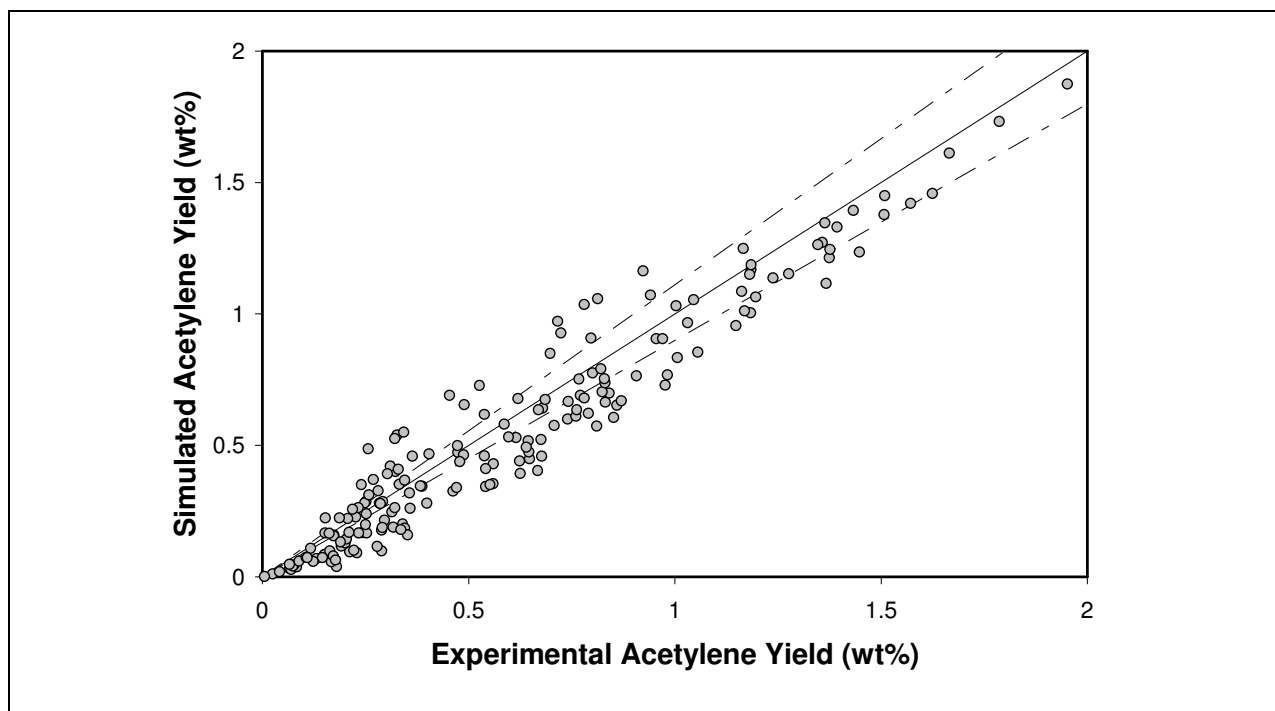
Figure 4.9: Parity plot for the acetylene yield [- - - - 10 % (rel.) interval]
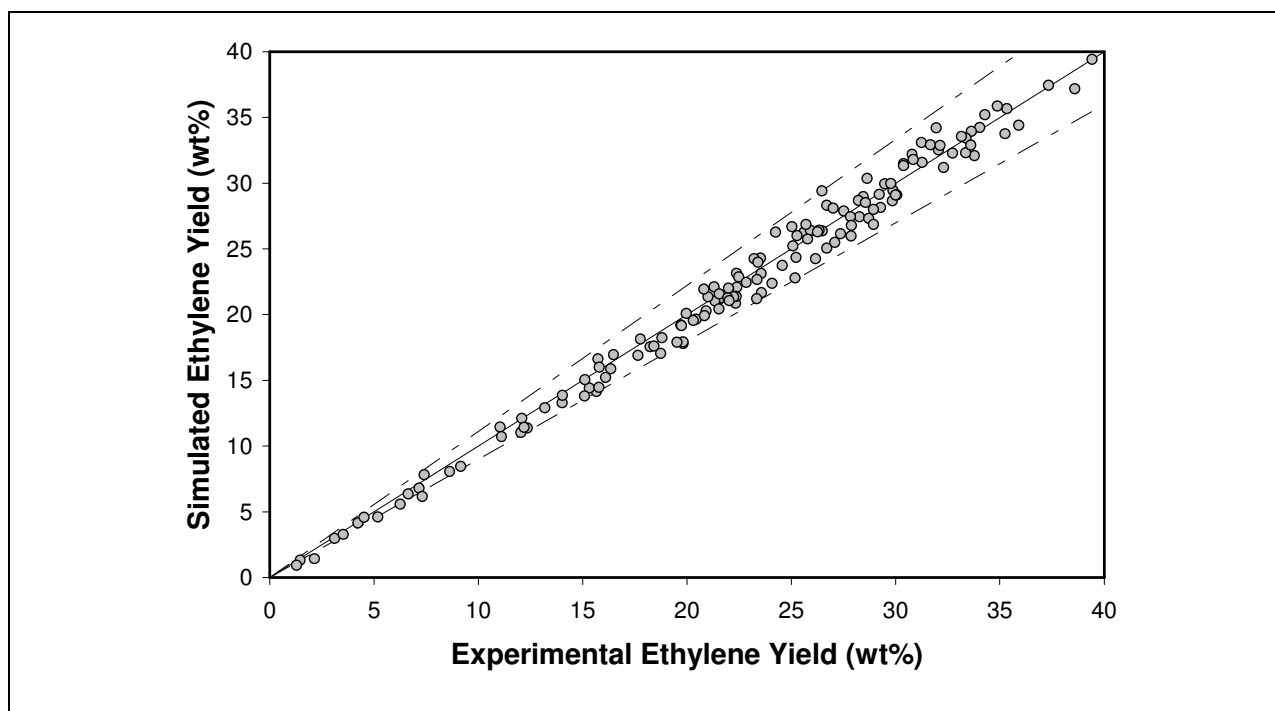
Figure 4.10: Parity plot for the ethylene yield [- - - - 10 % (rel.) interval]
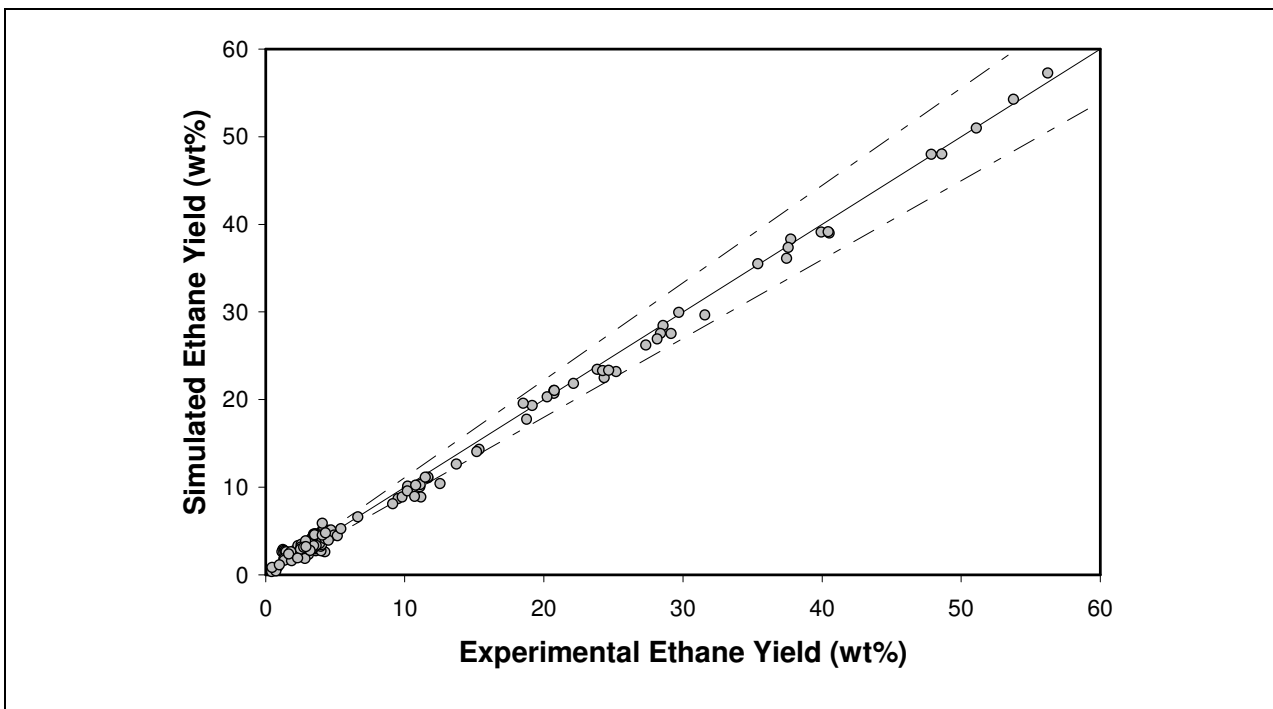
Figure 4.11: Parity plot for the ethane yield [- - - - 10 % (rel.) interval]
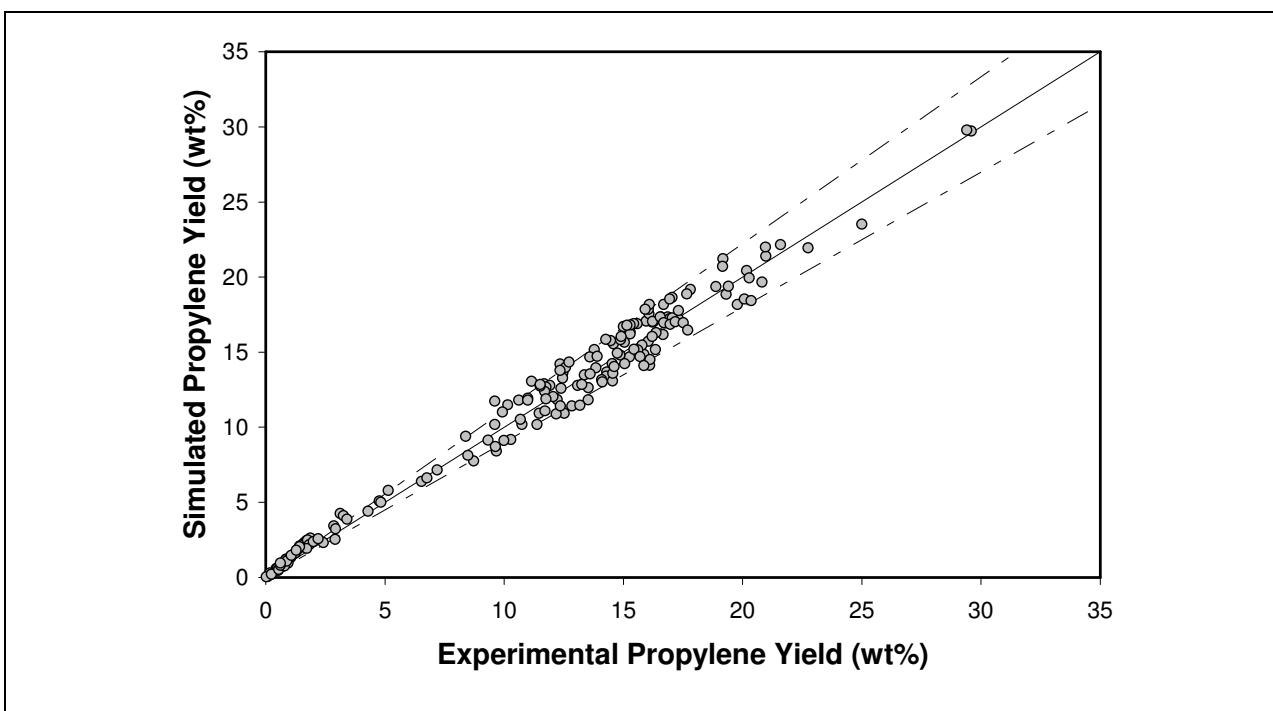
Figure 4.12: Parity plot for the propylene yield [- - - - 10 % (rel.) interval]

The parity plot for propane is excellent. The yield of propane during naphtha cracking experiments remains low, i.e. lower than 1 wt%. Hence, values for the propane yield higher than 1 wt% correspond to experiments with propane in the cracking mixture. Figure 4.13 shows that the conversion of propane is accurately simulated both at low and high conversions. Also the low yields corresponding to naphtha or gas oil cracking experiments are accurately simulated.

In Figure 4.14 the parity plot for butadiene is shown. This parity plot is certainly not perfect. Vercauteren (1991) also found significant deviations between the simulated and experimentally determined butadiene yields, although in the present work the deviations are drastically reduced. Similar as in the work of Vercauteren (1991) problems are mainly situated in the high severity range of the conditions. There the simulated butadiene yield is significantly higher than the experimentally observed butadiene yield. Vercauteren stated that at high severities part of the butadiene forms vinylacetylene. In the present work no species such as buta-1,3-dien-1-yl were considered either, and thus no vinylacetylene is formed from butadiene according to the present network.

The yields of the butenes 1-butene, iso-butene and 2-butene are all accurately simulated as can be seen in Figures 4.15, 4.16 and 4.17. Also for iso-butane and n-butane the parity plots are good. Note that the high yields of n-butane and iso-butane correspond to experiments with these components in the feedstock. Clearly the conversion of these two light hydrocarbons is well described by the single event microkinetic model simulation model. Also the yields of heavy products such as cyclopentadiene (CPD), benzene and toluene are simulated adequately, i.e. Figures 4.20-4.22. Benzene and toluene are the most important products of the pygas (pyrolysis gasoline) fraction. Hence, the previous results show also that the microkinetic model is able to accurately predict the pygas composition.

To illustrate that the single event microkinetic simulation model is also able to accurately simulate experiments with very difficult feedstocks that gave not so good simulation results in the past, some particular experiments of VGO's, toluene/ethane and naphthenic feedstocks are selected and simulated. In Table 4.3 the simulation results of an experiment using naphtha 1 are shown. This naphtha contains a high fraction of naphthenic compounds, see Table 4.4. The detailed composition of this naphtha feedstock is given in Annex C. In contrast to the results obtained with the simulation models developed by Plehiers (1989) and Vercauteren (1991) the simulated product yields agree quite well with the experimentally determined ones.
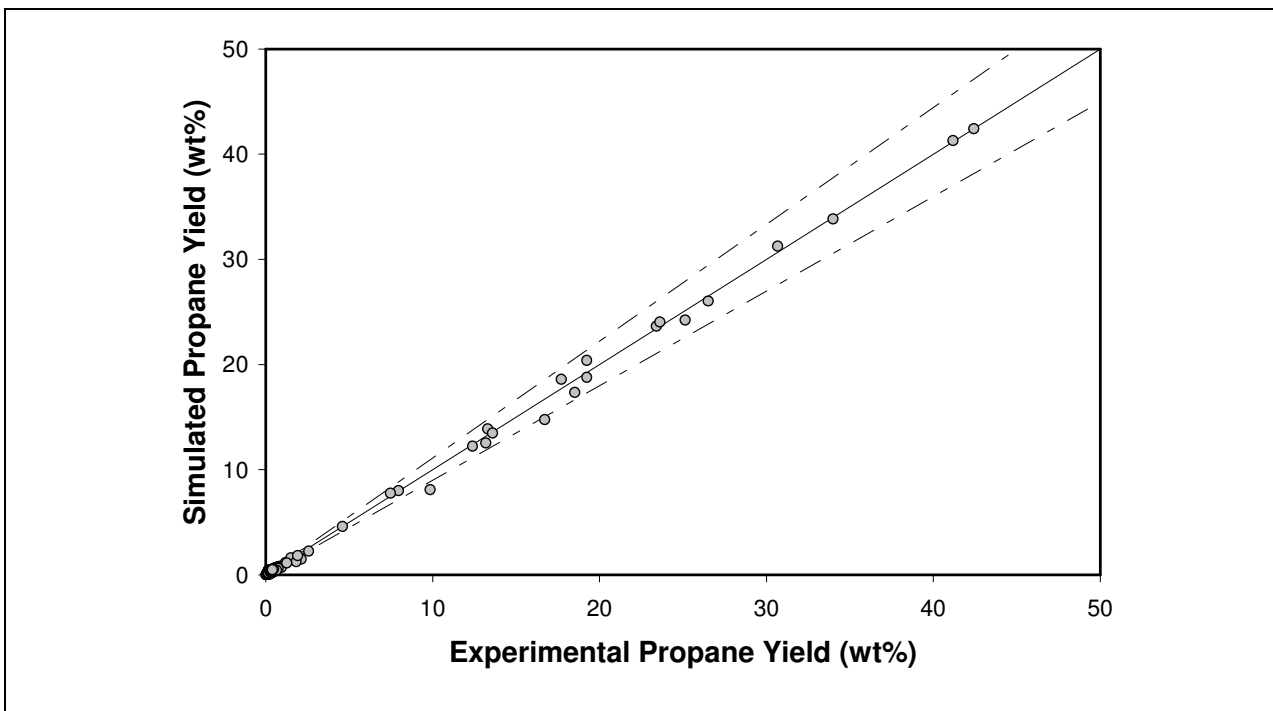
Figure 4.13: Parity plot for the propane yield [- - - - 10 % (rel.) interval]
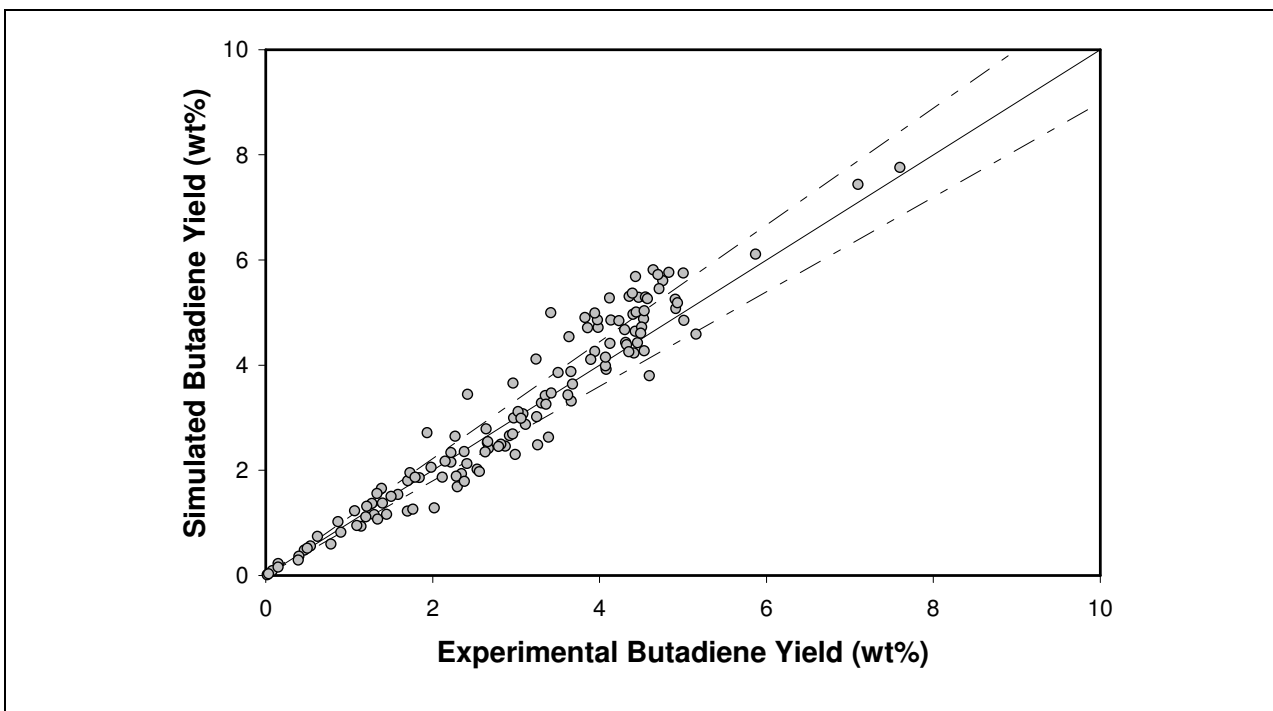
Figure 4.14: Parity plot for the butadiene yield [- - - - 10 % (rel.) interval]
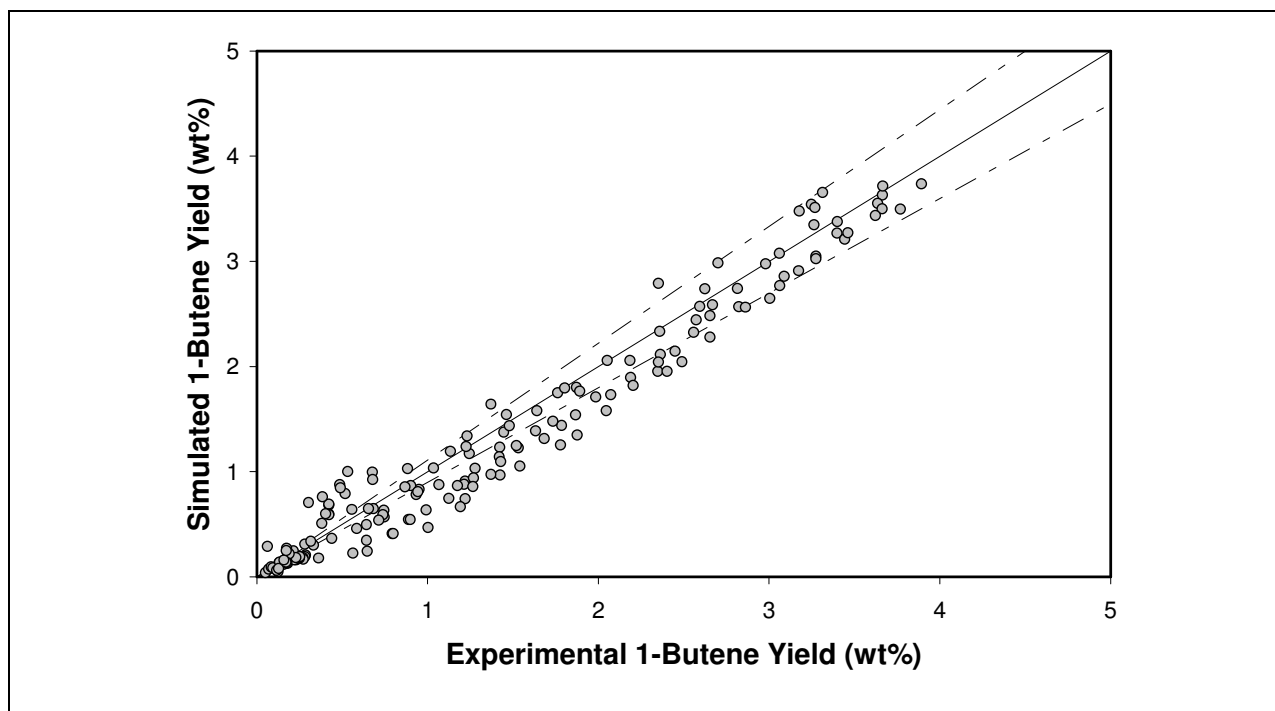
Figure 4.15: Parity plot for the 1-butene yield [- - - - 10 % (rel.) interval]
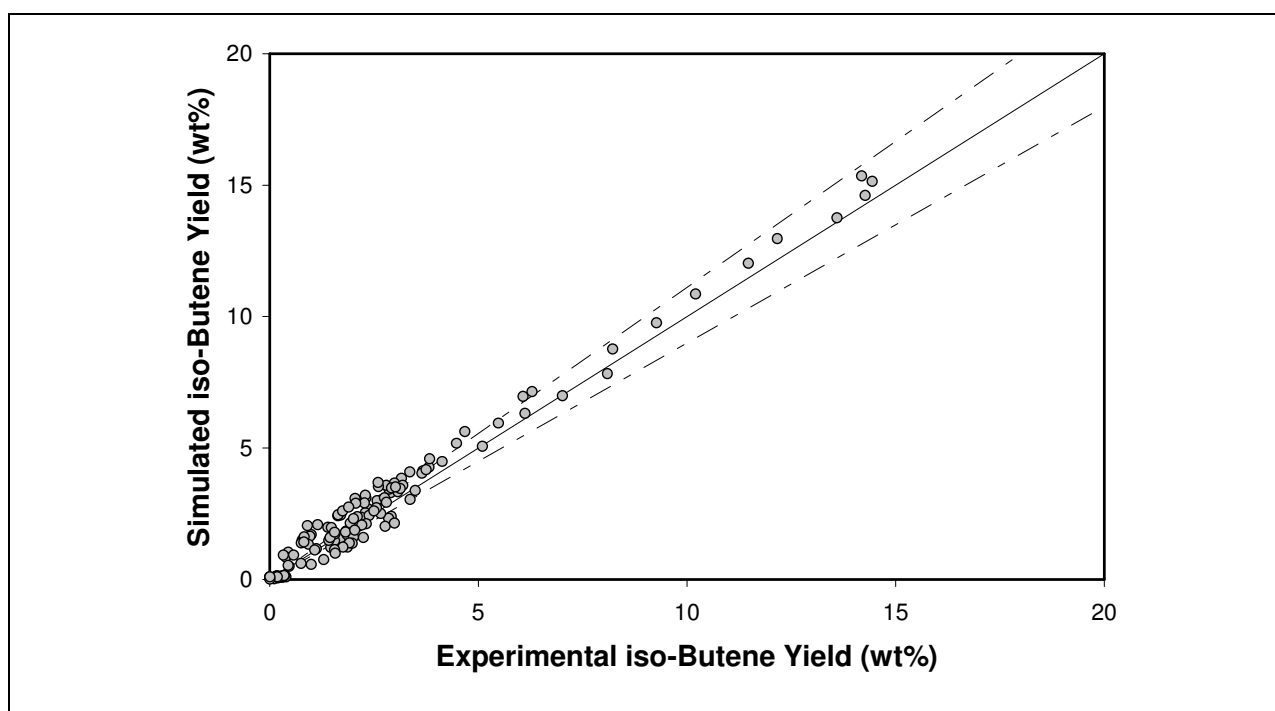
Figure 4.16: Parity plot for the iso-butene yield [- - - - 10 % (rel.) interval]
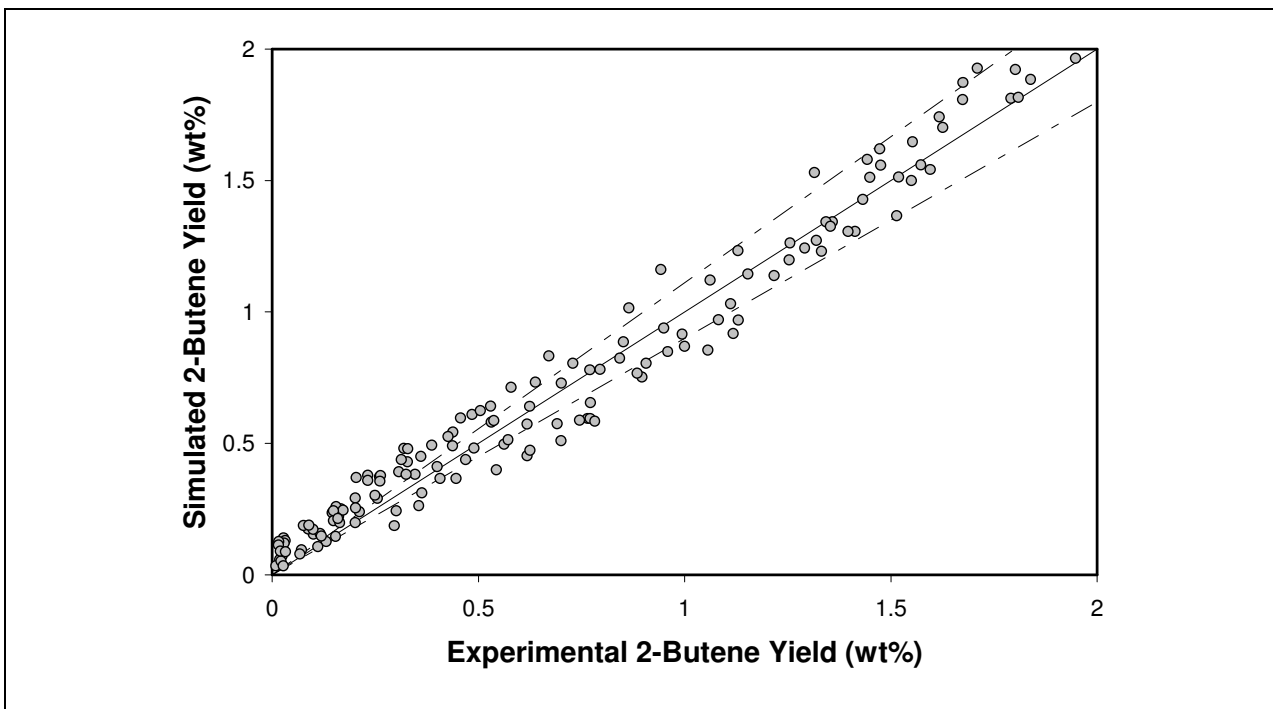
Figure 4.17: Parity plot for the 2-butene yield [- - - - 10 % (rel.) interval]
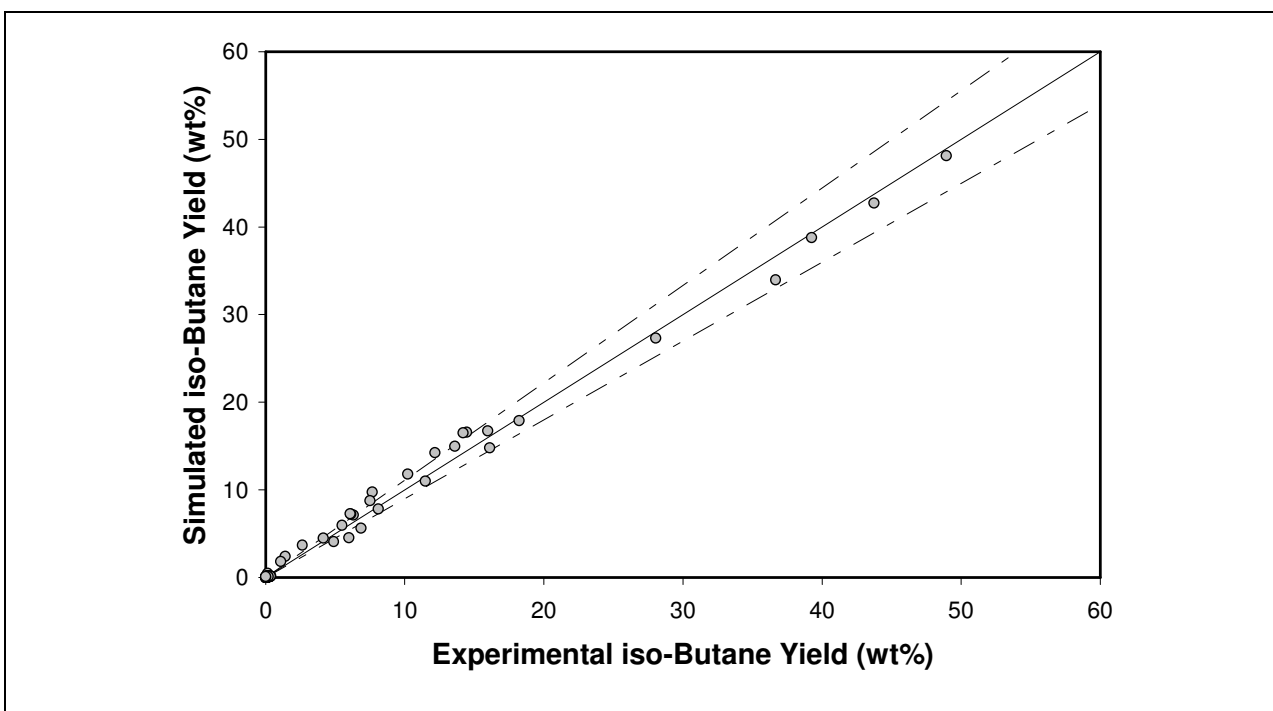
Figure 4.18: Parity plot for the iso-butane yield [- - - - 10 % (rel.) interval]
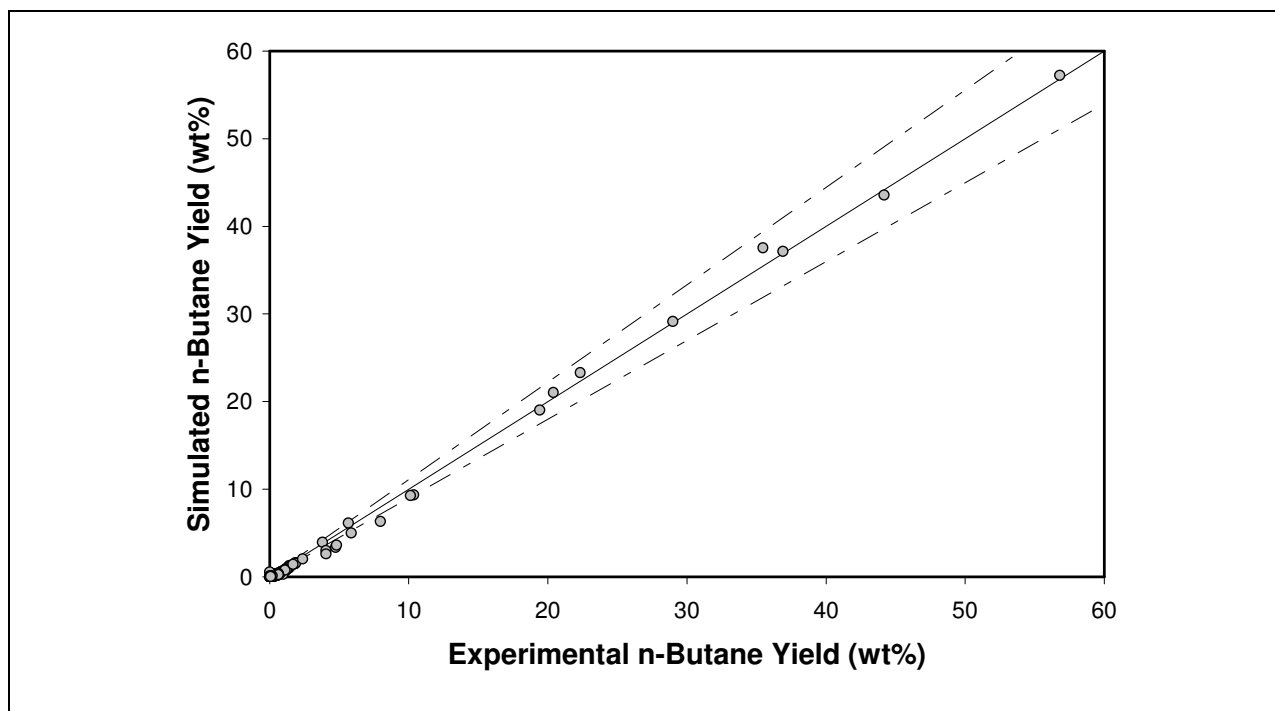
Figure 4.19: Parity plot for the n-butane yield [- - - - 10 % (rel.) interval]
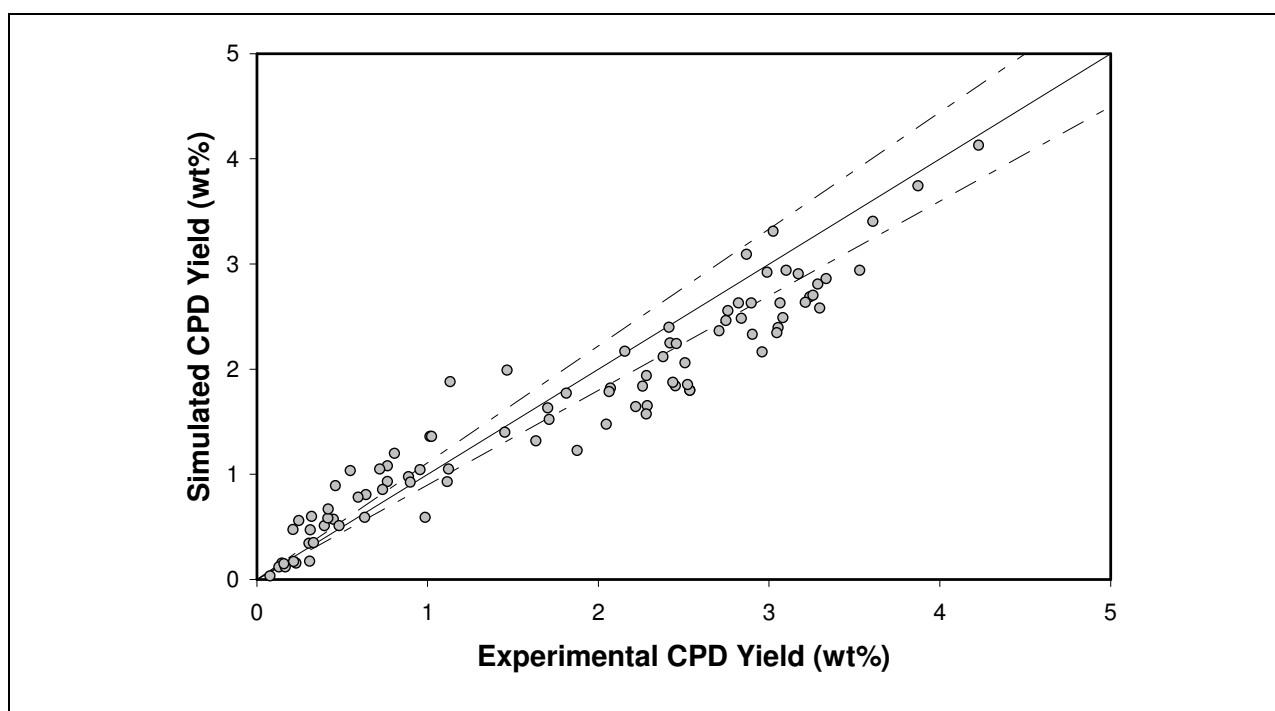
Figure 4.20: Parity plot for the cyclopentadiene (CPD) yield [- - - - 10 % (rel.) interval]
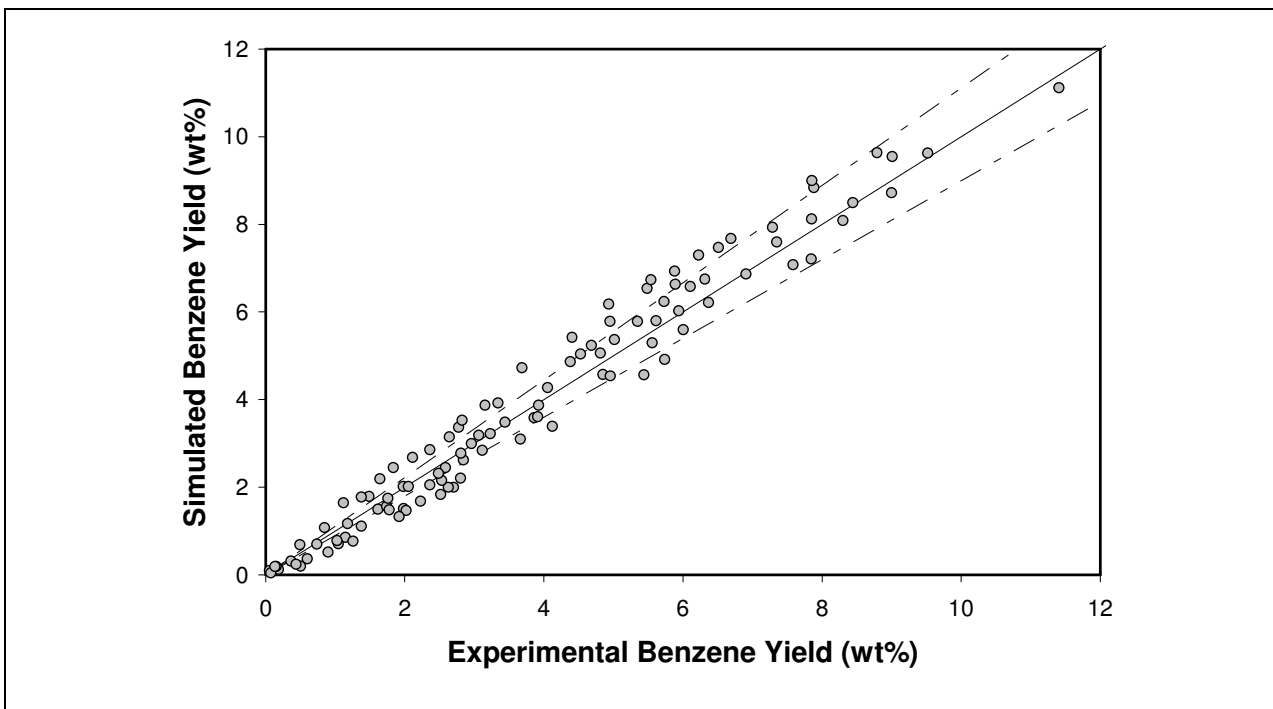
Figure 4.21: Parity plot for the benzene yield [- - - - 10 % (rel.) interval]
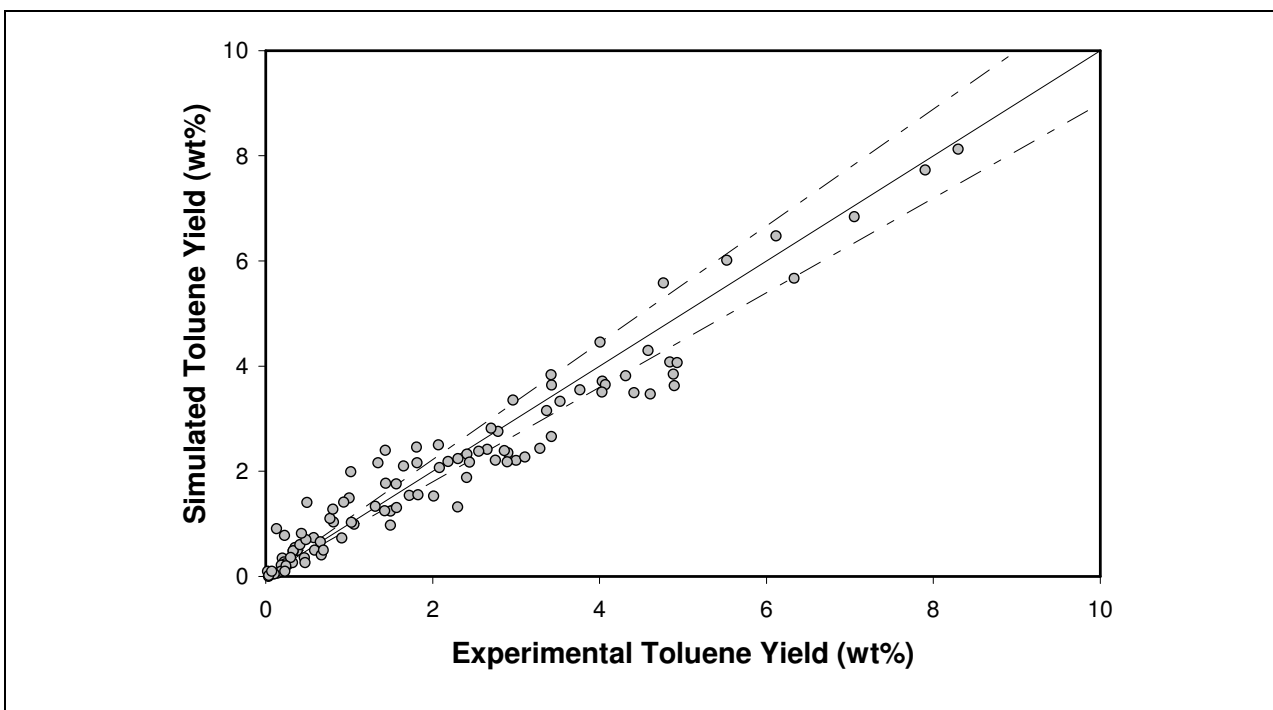
Figure 4.22: Parity plot for the toluene yield [- - - - 10 % (rel.) interval]

Product	Simulated Product Yields (wt %)	Experimental Product Yields (wt %)
Hydrogen	1.0	1.0
Methane	11.2	11.1
Acetylene	0.5	0.5
Ethylene	21.4	21.2
Ethane	3.1	3.3
Propylene	13.6	13.5
Butadiene	6.3	6.1
1-Butene	2.2	2.2
2-Butene	1.2	1.0
iso-Butene	2.0	2.2
Benzene	7.0	6.9
Toluene	5.8	5.7
Styrene	3.2	3.2
Naphthalene	1.0	1.0

Table 4.3: Simulated product yields for steam cracking of naphtha 1 [Simulation Conditions: CIT = 873 K; COT = 1118 K; CIP = 0.23 MPa; COP = 0.17 MPa; F: 1.3 10^{-3} kg s^{-1}; δ = 0.5 kg /kg; Commercial Indices see Table 4.4; detailed composition Annex C]

COMMERCIAL INDICES	
Specific density, 15/4°	0.76
PIONA-analysis (wt %)	
Paraffins	12.3
Iso-paraffins	21.6
Olefins	0.0
Naphthenes	50.8
Aromatics	15.8

Table 4.4: Commercial Indices of Naphtha 1. Detailed composition in Annex C.

Product	Simulated Product Yields (wt %)	Experimental Product Yields (wt %)
Hydrogen	3.0	2.9
Methane	4.3	4.2
Acetylene	0.4	0.4
Ethylene	36.5	36.3
Propylene	0.5	0.6
Butadiene	0.9	1.0
n-Butane	0.1	0.1
Benzene	8.7	8.6
Ethylbenzene	0.5	0.4
Styrene	1.7	1.5
Xylene	0.2	0.1
Propylbenzene	0.2	0.3
Indene	0.5	0.7
Naphthalene	0.2	0.4
Ethane conversion	66.4	65.8
Toluene conversion	42.0	41.3

Table 4.5: Simulated conversion and product yields for a toluene/ethane steam cracking experiment [Simulation Conditions: CIT = 873 K; COT = 1153 K; CIP = 0.27 MPa; COP = 0.20 MPa; 30 wt% Toluene; 70 wt% Ethane; F: 1.1 10^{-3} kg s^{-1}; δ = 0.4 kg /kg]

Table 4.5 shows that also for ethane/toluene mixtures a good agreement between simulated and experimentally determined product yields are now obtained. Introducing some new heavy radicals such as the benzyl radical clearly leads to an improved description of the cracking behavior of mixtures of toluene. In the models of Plehiers (1989) and Vercauteren (1991) the benzyl radical was not considered, and toluene decomposed via a single molecular reaction into benzene. This description was clearly not sufficient to describe the cracking behavior of fractions containing large amounts of toluene and therefore the reaction network was extended with several radical reactions of aromatic radicals. The results in Table 4.5 further show that also

several minor products such as ethylbenzene, n-propylbenzene and indenes are now accurately simulated.

COMMERCIAL INDICES	
Specific density, 15/4°	wax
PIONA-analysis (wt %)	
Paraffins	78.4
Iso-paraffins	0.1
Olefins	0.0
Naphthenes	0.0
Aromatics	21.5

Table 4.6: Commercial Indices of the VGO fraction. Detailed composition in Annex D.

Finally in Table 4.7 the simulation results for a VGO experiment are given. The commercial indices of this heavy hydrocarbon feedstock are specified in Table 4.6. These indices show that the feedstock consists mainly of heavy parraffinic and aromatic molecules. The detailed molecular composition is specified in Annex D. The latter is obtained by combining GC (quantitative) and GC-MS (qualitative) analysis results (Bolado, 2003). Also in this case a good agreement is observed between simulated and experimental data. As can be seen in Table 4.7 the simulation results are much better in comparison with the data obtained with the simulation model of Vercauteren (1991). One of the main reasons for the improved agreement is the drastic expansion of the reaction network. Indeed, on the one hand the maximum carbon number of possible feedstock molecules is increased from 25 to 33. On the other hand also some important new families of molecules are now considered such as naphtheno-aromatic and di-, tri- and poly-aromatic compounds. As the reaction networks generated by Plehiers (1989) or Vercauteren (1991) did not consider a lot of the components present in VGO fractions it is obvious that the simulation results were disappointing when VGO experiments were simulated (Bolado, 2003). This feedstock forms also a lot of heavy components part of the fuel oil fraction. Therefore in Table 4.7 the calculated amounts for the most important molecules of the fuel oil fraction are also specified. Unfortunately no detailed composition of the fuel oil fraction could be

experimentally determined because the analysis of the C_5^+ fraction was stopped after naphthalene (Bolado, 2003). This means that it is not possible to quantitatively compare the simulation results obtained for the pyrolysis fuel oil (PFO) fraction with experimental data.

Product	Simulated Product Yields (wt %)	Experimental Product Yields (wt %)
Hydrogen	0.6	0.6
Methane	10.1	9.1
Acetylene	0.2	0.2
Ethylene	22.8	22.0
Propylene	15.2	14.6
Propane	0.4	0.8
Butadiene	7.2	8.0
1-Butene + 2-Butene	4.0	4.3
iso-Butene	1.7	1.9
Benzene	6.8	6.2
Toluene	4.8	4.2
Styrene	1.2	0.9
Xylene	0.8	1.0
Ethylbenzene	0.2	0.3
Indene	0.9	0.6
Me-Indene	1.0	0.8
Naphthalene	1.4	0.9
Me-Naphthalene	3.5	-
Phenantrene	2.3	-
Me-Phenantrene	4.6	-
Anthracene	2.1	-
Me- Anthracene	3.4	

Table 4.7: Simulated product yields for a VGO steam cracking experiment [Simulation Conditions: CIT = 823 K; COT = 1068 K; CIP = 0.25 MPa; COP = 0.20 MPa; F: 1.1 10^{-3} kg s^{-1}; δ = 0.6 kg /kg]

Nevertheless, it is possible to compare the simulation results with data obtained from the collected fuel oil fraction in condenser 1 of the pilot plant installation shown in Figure 4.3. Bolado (2003) analyzed the PFO fraction formed during the experiments with the VGO fraction and found that the fuel oil consisted mostly of mono-, di-, tri- and tetra-aromatics. The main components were naphthalene, methylnaphthalene, phenantrene, methylphenantrene, anthracene and methylanthracene. This is in good agreement with the calculated fuel oil composition specified in Table 4.7. Hence, it can be concluded that the simulation model is able to calculate the PFO fraction formed during VGO cracking if the detailed molecular composition of the complex VGO feedstock is available. The latter is determining for obtaining accurate simulation results, especially for the composition of the PFO fraction and this is not straightforward for these fractions.

4.7   Graphical User Interface (GUI)

The current FORTRAN compilers such as Visual Fortran or Force 2.0 are able to generate Win32 applications. These DOS applications run just fine. They've got a perfectly logical interface, nice graphics, and run pretty fast. Why should it matter that they aren't native Windows programs? Technically, it probably doesn't. However, there are several incentives to improve the user-friendliness and visualization of these programs. One reason is that potential users seem to lose interest when you tell them your simulation program is a DOS program. Therefore a GUI has been created using Visual Basic.Net, see Figure 4.23. Visual Basic.Net has been chosen over other solutions because it is easy to use, has huge possibilities and the user friendliness is very high. The backbone of the program still remains a FORTRAN code, compiled with a Visual Fortran compiler creating an executable. The Graphical User Interface creates the input files and let the program run on the background. The GUI helps the user to move step by step through the simulation process. First the characteristics of the reactor are specified, then the process conditions are defined, and finally a feedstock composition needs to be specified. Once the input is complete the FORTRAN executable is called. Once the simulation is finished the results are visualized on the results screen of the GUI, see Figure 4.23. On this screen the yields of the most important products are shown, next to either the process gas temperature profile, the internal wall temperature profile or the pressure profile.
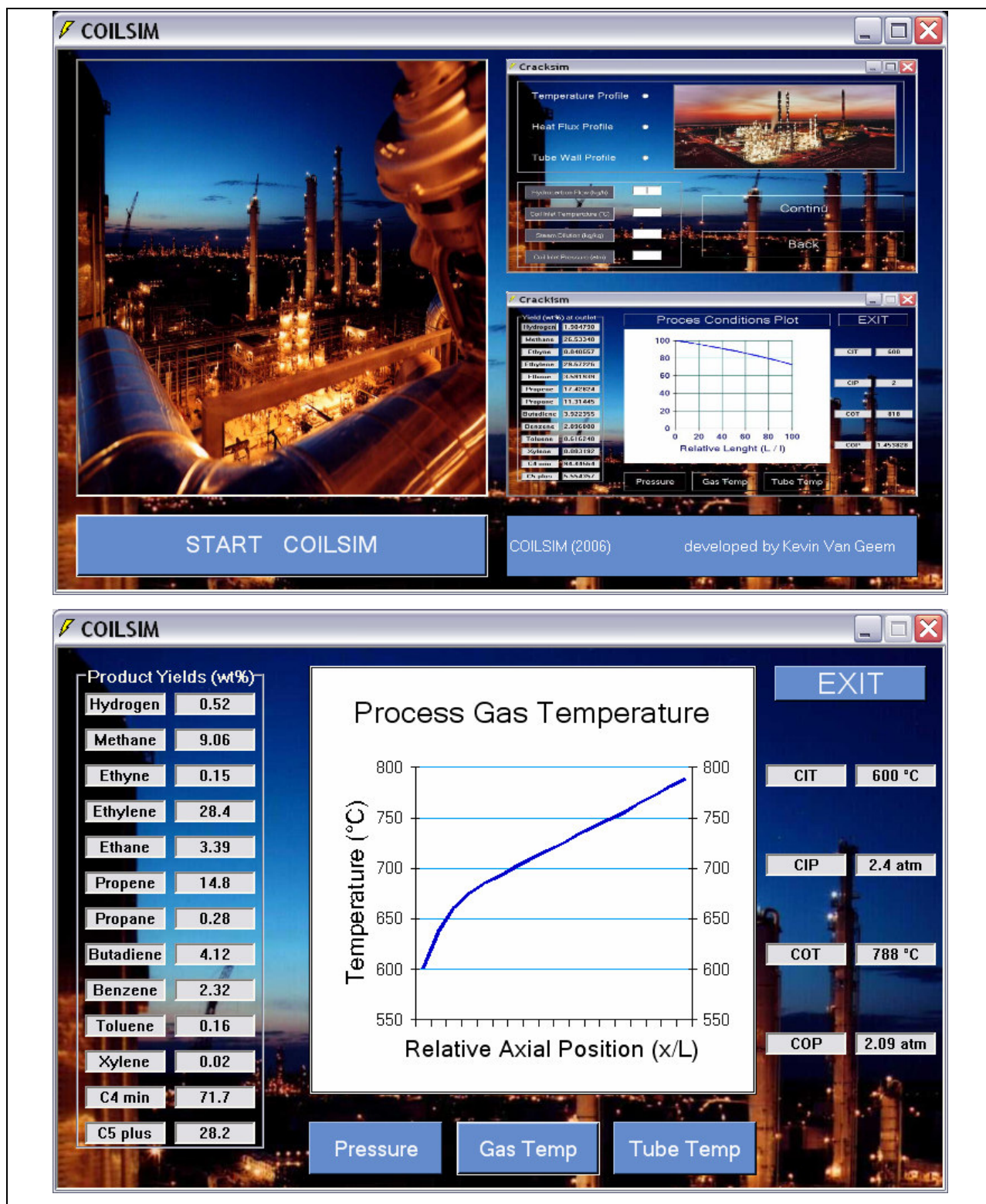
Figure 4.23: Start-up screen and results screen of the Graphical User Interface for the single event microkinetic simulation model for steam cracking

4.8   Conclusions

The implementation of a new stiff solver DASSL (Li and Petzold, 1999) allowed to verify the effect of the pseudo steady state assumption by comparison with the results obtained with the solver proposed by Dente et al. (1979). The simulated methane, ethylene, butadiene and propylene yield differ slightly. For the other products the simulation results remain almost unchanged. However, solving the balances simultaneously with a stiff solver comes at a price, the simulation time at least triples.

The developed single event microkinetic simulation model could be validated using pilot plant experiments obtained from the LPT pilot plant setup with a wide range of feedstocks. Excellent agreement is observed between the simulated and experimental data. Even for difficult feedstocks such as VGO, heavy naphthas and ethane/toluene mixtures a good agreement between the simulated and experimentally determined product distribution is obtained. This result is an enormous improvement because the simulation results obtained with the older simulation models developed by Plehiers (1989) and Vercauteren (1991) showed for these simulation problems significant shortcomings (De Roo, 1998; De Buck, 1999; Bolado, 2003).

A Graphical User Interface was also developed for the simulation program to make the program user friendlier. The GUI is developed in Visual Basic.Net and the application runs easily on any recent PC running on a Windows operating system. Also for the experimental database a GUI is developed that allows searching and expanding the database.

4.9   References

Bolado R.G. Kinetic Modeling of Thermal Cracking of Heavy Hydrocarbons, Master thesis, Ghent University, 2003.

De Buck J. Kinetische Studie van Cokesvorming bij het Thermisch Kraken van Koolwaterstoffen, Master thesis, Ghent University, 1999.

Dente M., Ranzi E. Detailed Prediction of Olefin Yields from Hydrocarbon Pyrolysis through a Fundamental Simulation Program SPYRO, Comp. Chem. Eng., 3, 61, 1979.

De Roo T. Modellering van Stroming, Modellering van Cokesvorming in de Warmtewisselaar stroomafwaarts van een Thermische Kraker, Master thesis, Ghent University, 1998.

De Saegher J.J. Modellering van Stroming, Warmtetransport en Reactie in Reactoren voor Thermisch Kraken van Koolwaterstoffen, Ph.D. thesis, Ghent University, 1994.

Li S., Petzold L.R. Design of New DASPK for Sensitivity Analysis, UCSB Technical report, 1999.

Plehiers P.M. Rigoureuze Modellen voor de Simulatie van Fornuizen voor de Thermische Kraking van Lichte Koolwaterstoffen, Ph.D. thesis, Ghent University, 1989.

Reid R.C., Prausnitz J.M., Poling B.R. Properties of gases and Liquids, McGraw-Hill, 1979.

Reyniers M.F., Froment G.F. Influence of Metal Surface and Sulfur Addition on Coke Deposition in the Thermal Cracking of Hydrocarbons, Ind. Eng. Chem. Res., 34, 773-785, 1995.

Smith J. M. Chemical Engineering Kinetics, McGraw-Hill Book Company, New York, 1981.

Van Damme P.S., Willems P.A., Froment G.F. Temperature, not Time, Controls Steam Cracking Yields, Oil & Gas Journal., 68-73, 1984.

Van Geem K.M., Reyniers M.F., Marin G.B., Song J., Mattheu D.M., Green W.H. Automatic Network generation using RMG for Steam Cracking of n-Hexane, AIChE Journal, 52, 718-730, 2006.

Vercauteren C. Rigoureuze Kinetische Schema's voor de Thermische Kraking van Koolwaterstoffen, PhD dissertation, UGent, 1991.

Wauters S, Marin G.B. Kinetic Modeling of Coke Formation during Steam Cracking, Ind. Eng. Chem. Res., 41, 2379, 2002.

Zajdlik R., Reyniers M.F., Marin G.B. Steam Cracking of Hydrocarbons in a Pilot Plant, AIChE Spring meeting. New Orleans, USA, 2003.

Chapter 5:

Simulation of Industrial Furnaces

5.1   Introduction

The reactors used for steam cracking of hydrocarbons are suspended in large gas fired furnaces, see Figure 5.1.
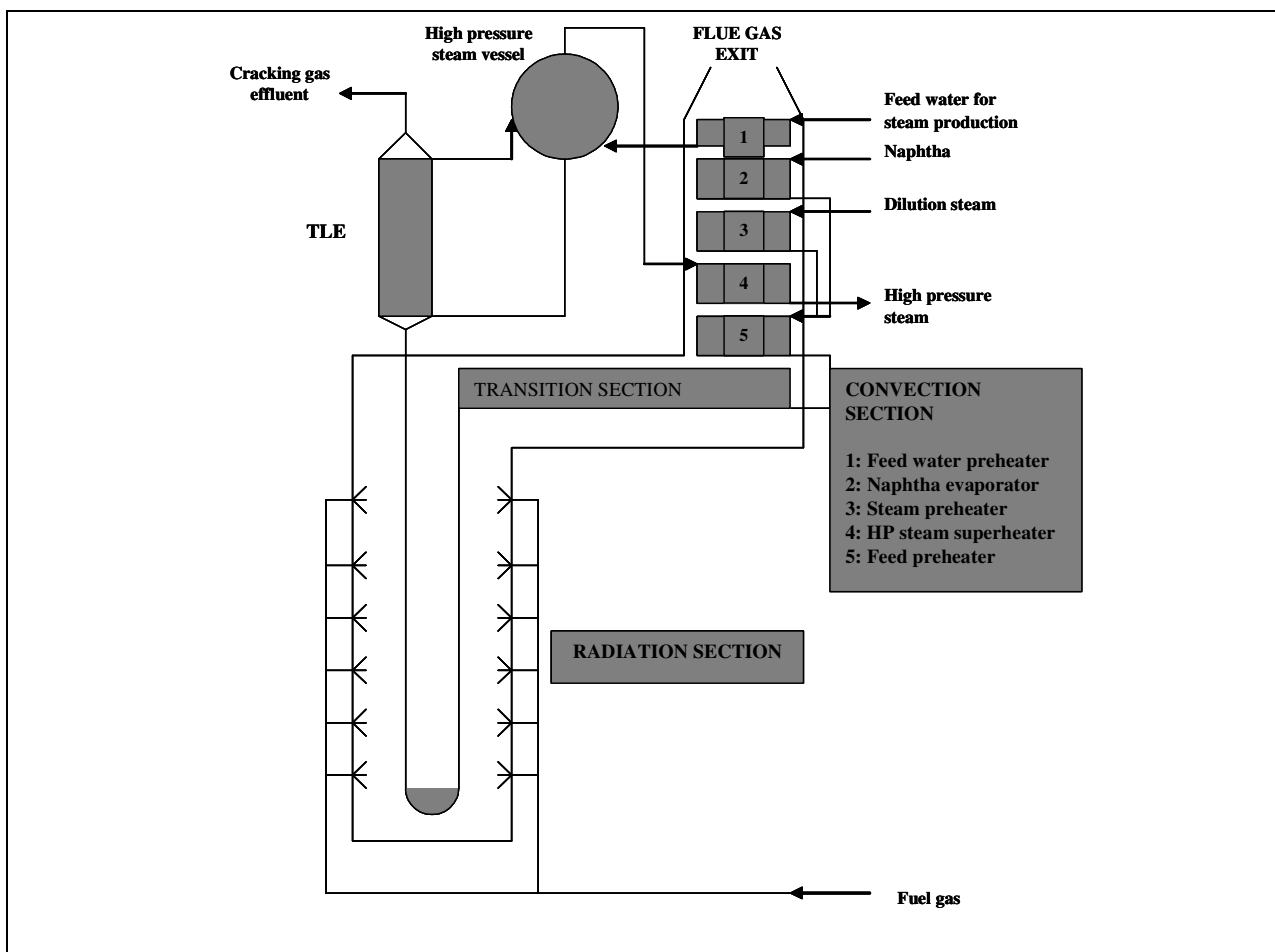
Figure 5.1: Schematic representation of the furnace section of an industrial cracking unit

The furnace section is composed of three large parts: the radiation section, the convection section and the adiabatic cross-over section. The coils are suspended in the radiation section. In the convection section the heat of the flue gases is utilized for preheating of the feed and for steam production. The cross-over section is the connection between the radiation and the convection section.

It seems obvious that when simulating an industrial cracker both the furnace and the reactor are taken into account. Otherwise the user of the reactor simulation program has a certain degree of freedom choosing the heat flux or tubeskin temperature profile, which is used as boundary condition for the reactor simulation. Indeed, it is absolutely not sure that the postulated heat flux or tubeskin temperature profile can be realized in the furnace. For example assuming a uniform temperature in the furnace (Lobo and Evans, 1939) leads to an unrealistic heat flux profile, and can as such lead to errors when simulating the reactor. Hence, furnace and reactor have to be considered as one single unit and have to be simulated as such. Indeed, a correct insight in the furnace performance can only be obtained by combining a flexible furnace simulation model that can generate a detailed temperature and heat flux distribution in the furnace, and a rigorous and reliable reactor simulation model that is based on a fundamental kinetic scheme (Plehiers and Froment, 1989).

At the Laboratorium voor Petrochemische Techniek several simulation models (FURNACE, COILSIM1D, COILSIM2D) have been developed that allow a rigorous simulation of the furnace and the reactor. The process gas temperatures are obtained via an iterative procedure, see Figure 5.2. This simulation method is developed by Vercammen and Froment (1980), Rao et al. (1988), Plehiers and Froment (1989) and Heynderickx and Nozawa (2005). For the calculation of the furnace the zone method of Hottel and Sarofim (1967) is used. First, the furnace is divided into a number of isothermal surface and volume zones. Then for each of these zones the energy balances, containing radiative, convective and conductive contributions are constructed. Process gas and tube skin temperature profiles in the furnace are then obtained by solving the energy balances. From these temperature profiles, a better estimate of the heat flux profile is obtained, based on which a new reactor simulation can be performed. With the resulting tube skin temperature profile, a new furnace simulation is carried out. This cycle is repeated until convergence is reached.
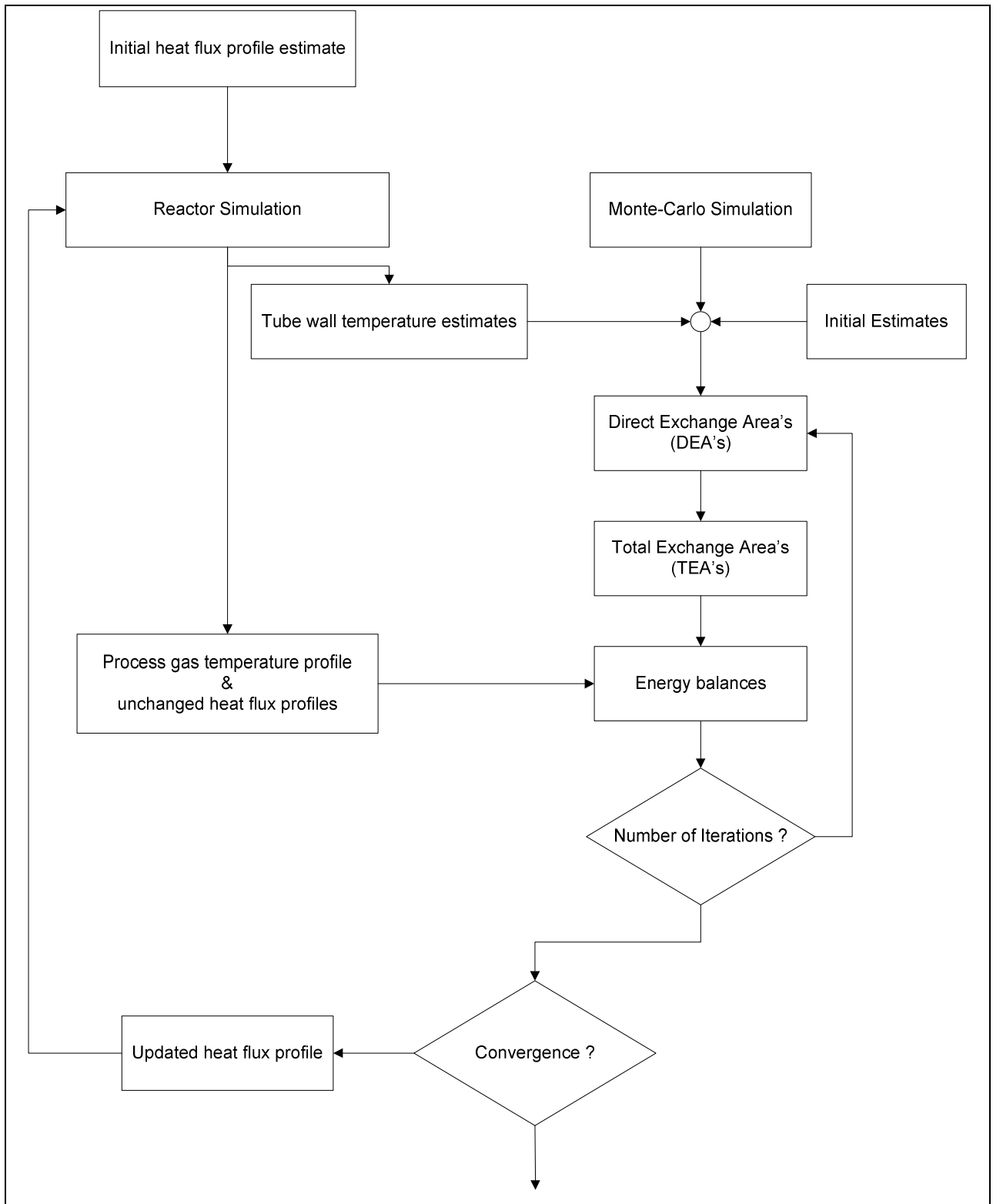
Figure 5.2: Flow chart of the procedure of a coupled reactor/furnace simulation

In the next paragraphs several industrial furnaces are simulated. First the necessity of using more dimensional reactor models is studied. Then two different industrial furnaces are simulated; a Kellog Millisecond furnace fed with propane and a Lummus furnace containing a 4-2-1 split coil fed with gas oil. The simulation results for these two furnaces are compared with industrial data.

5.2   2-Dimensional versus 1-Dimensional Reactor Model [(*)]

5.2.1   Introduction

Tubular reactors are used in industry for important processes such as steam cracking and polymerization. Their analysis and design is frequently based on 1-dimensional models, i.e. considering gradients only in the axial direction. Semi-empirical correlations can approximate the average radial concentration and temperature profiles from more dimensional models (Sundaram and Froment, 1979) but do not provide any information on the importance and consequences of the non-uniformities for the reactor performance. The latter is of particular importance for the endothermic steam cracking process. The trend towards high severity cracking (Plehiers and Froment, 1991) demands higher heat fluxes, higher process gas temperatures and shorter residence times. Higher heat fluxes amplify the radial temperature gradients and make the 1-dimensional plug-flow model insufficient (Froment, 1992). Furthermore, a radial temperature gradient implies that the conditions prevailing at the process gas/coke interface on the one hand, and the conditions in the center of the reactor coil on the other hand may differ appreciably (De Saegher, 1996). Coke formation at the interface conditions (Sundaram, 1981) or at averaged conditions as calculated with a 1-dimensional model will differ. It was shown before (Heynderickx et al., 1992) that circumferential non-uniformities in flux and temperature, due to the shadow effects in the furnace, also result in non-uniform coking rates and coke layer thicknesses. The radial temperature profile can have a significant effect on the calculated reactant concentrations and more in particular on those of the gas phase radicals at the internal wall of the reactor tubes (Reyniers, 1994). Hence, the implementation of more dimensional models for studying coke formation in tubular reactors seems to be inevitable. For reactor simulations the necessity of using more dimensional simulation models seems less

crucial. Sundaram and Froment (1979, 1980) coupled a global kinetic model for the cracking of ethane to a 2-dimensional reactor model. Their results confirm the existence of important radial temperature gradients. For molecular species on the contrary, they found that radial concentration gradients are less important. Valenyi et al. (1991) and Fagley (1992) proposed a 2-dimensional model for the cracking of ethane in a tubular reactor with laminar flow, using the simulation packet PHOENICS to solve the 2-dimensional mass, heat and momentum balances. The kinetic model consisted of 3 reactions between 5 molecular species. Radial temperature differences up to 200 K and also important radial molecular concentration gradients were found. No radical species were considered by any of these authors. Therefore in the next section a radical kinetic model is coupled to a 1-dimensional and a 2-dimensional reactor model. This makes it possible to estimate the effect of radial temperature and concentration profiles on the conversion and the product distribution. Also the effect of these radial gradients on the initial coking rate can be investigated. Therefore the results obtained with a coke formation model based on elementary reactions (Wauters and Marin, 2001), coupled to the 1-dimensional and 2-dimensional reactor model, are compared with reference data. This makes it further possible to study the effect on the calculated run length of the reactor.

5.2.2   2- Dimensional Reactor Model

The general form of the continuity for a chemical species j reacting in a flowing fluid varying density, temperature, and composition is (Bird et al., 1960):

$$\frac{\partial C_j}{\partial t} + \nabla(C_j\, v) + \nabla J_j = R_j \qquad\qquad [5.\,1]$$

with R_j the total rate of change of the amount of component j, v the linear velocity, J_j the molar flux vector for species j. If species j occurs in more than one phase, this continuity equation has to be written for each phase, but for steam cracking only one phase must be considered, the gas phase. Moreover, for steam cracking the steady state can be assumed, hence the first term of equation [5.1] can be dropped. The continuity equation can be easily transformed in its 2-dimensional form. A mass balance for a component j over an annulus with height dz, internal

radius r and external radius r+dr leads to the continuity equation for this component j in the process gas mixture (Bird et al., 2001, Froment and Bischoff, 1990):

$$\frac{\partial}{\partial z}\left(v_z \frac{C_j}{\rho}\right) + \frac{1}{r}\frac{\partial}{\partial r}\left(rv_r \frac{C_j}{\rho}\right) - \frac{1}{r}\frac{\partial}{\partial r}\left(r\varepsilon_D \rho \frac{\partial}{\partial r}\frac{C_j}{\rho}\right) - \sum_k \upsilon_{kj} r_k = 0 \qquad [5.\,2]$$

Bird et al. (1960) also derived rigorously the fundamental energy equation in various coordinate systems:

$$\sum_j M_j C_j c_{pj}\left(\frac{\partial T}{\partial t} + v\nabla T\right) = \sum_k \left(-\Delta_f H_k^0\right) R_{V,k}$$

$$+ \nabla(\lambda \nabla T) - \sum_j J_j \nabla H_j + q \qquad [5.\,3]$$

with M_j and c_{pj} the molar mass and the heat capacity of species j, λ is the thermal conductivity of the mixture, J_j the molar flux of species j, H_j are the partial molar enthalpies and q is the radiation heat flux. Again the first term can be dropped when the steady state is assumed. The corresponding 2-dimensional energy equation is then:

$$\frac{\partial}{\partial z}(v_z H) + \frac{1}{r}\frac{\partial}{\partial r}(r\,v_r H) - \frac{1}{r}\frac{\partial}{\partial r}\left(r\varepsilon_H \frac{\partial T}{\partial r}\right)$$

$$- \frac{1}{r}\frac{\partial}{\partial r}\left(r\sum_j H_j \varepsilon_D \rho \; \frac{\partial}{\partial r}\frac{C_j}{\rho}\right) = 0 \qquad [5.\,4]$$

The heat flux q moves to the boundary condition, see Equation [5.20]. Equation [5.4] considers heat transport and reaction simultaneously. The latter implies a good estimation of the simulated wall temperature. Bird et al. (2001) referred to the last term of equation [5.4] as the interdiffusional energy flux. The origin of this term is the diffusion of chemical species. Explicitly introducing the reaction enthalpy in equation [5.4] transforms the equation into:

$$v_z c_p \frac{\partial T}{\partial z} + \left[v_r c_p - \varepsilon_D \rho \sum_j (c_{pj}) \frac{\partial}{\partial r} \left(\frac{C_j}{\rho} \right) \right] \frac{\partial T}{\partial r} = \sum_k (-\Delta H_k) \ r_k \qquad [5.\ 5]$$

Radial pressure gradients are neglected and, hence, the momentum equation derived in the 1-dimensional case is retained.

$$\frac{dp_t}{dz} = -\alpha \left(\frac{2\,f}{d_t} + \frac{\zeta}{\pi\,r_b} \right) \rho \ v^2 - \alpha\,\rho \ v \frac{dv}{dz} \qquad [5.\ 6]$$

An extensive description of the 1-dimensional reactor model is given in Chapter 4.

In COILSIM2D, the 2-dimensional reactor model that has been developed at the LPT (De Saegher, 1994), the von Karman profile (Davies, 1972) is used for the axial velocity component v_a. Over the cross section three zones are considered; a laminar, a turbulent and a transition zone. In each zone the axial velocity is calculated using a different expression. In the laminar zone the axial velocity component is given by:

$$\frac{v_a}{v_*} = \frac{\varepsilon}{\varepsilon_*} \qquad [5.\ 7]$$

with ε the distance to the wall and

$$v_* = \sqrt{\frac{\tau_w}{\rho}} \qquad [5.\ 8]$$

and

$$\varepsilon_* = \frac{\nu}{v_*} \qquad [5.\ 9]$$

with ν the kinematic viscosity. In the transition zone the axial velocity component is:

$$\frac{v_a}{v_*} = -3.05 + 5 \ \ln\left(\frac{\varepsilon}{\varepsilon_*} \right) \qquad [5.\ 10]$$

In the turbulent zone the axial velocity component is:

$$\frac{v_a}{v_*} = 5.5 + 2.5 \ \ln\left(\frac{\varepsilon}{\varepsilon_*}\right)$$ [5. 11]

After calculating the axial velocity profile according to the previous equations the radial component of the velocity u_r can be deduced from the total mass balance:

$$\frac{\partial}{\partial z}(v_a \rho) + \frac{1}{r}\frac{\partial}{\partial r}(r \ v_r \ \rho) = 0$$ [5. 12]

The turbulent conductivity and diffusivity are calculated in COILSIM2D based on the correlation of Reichardt, corrected by Cebeci (Sundaram, 1977). The parameters have been further adjusted by Sundaram and Froment (1979). In equations [5.13] and [5.14] the expressions for the turbulent conductivity ε_H and the turbulent diffusivity ε_D are given.

$$\varepsilon_H = \lambda_m \left(1 + c_3 \ \mathrm{Re}^{c_1} \ \mathrm{Pr}^{c_2}\left(1 + 2\xi^2\right)\left(1 - \xi^2\right)\left(1 - e^a\right)\left(1 - e^{-a\sqrt{\mathrm{Pr}}/b}\right)\right)$$ [5. 13]

$$\varepsilon_D = D_m \left(1 + c_3 \ \mathrm{Re}^{c_1} \ \mathrm{Sc}^{c_2}\left(1 + 2\xi^2\right)\left(1 - \xi^2\right)\left(1 - e^a\right)\left(1 - e^{-a\sqrt{\mathrm{Pr}}/b}\right)\right)$$ [5. 14]

ξ represents the normalized radial position, c_1, c_2 and c_3 are given by 0.828664, 0.9440670 and 0.020530 respectively, while the following expressions hold for a and b:

$$a = (1 - \xi)\left(\frac{\mathrm{Re}}{2}\right)\sqrt{\frac{f}{2}}$$ [5. 15]

$$b = 34.96 + 28.79 \log(\mathrm{Pr}) + 33.95 \log^2(\mathrm{Pr})$$

$$+ 6.33 \log^3(\mathrm{Pr}) - 1.186 \log^4(\mathrm{Pr})$$ [5. 16]

In the laminar zone near the reactor wall, the conductivity equals the molecular conductivity λ_m, and the diffusivity equals the molecular diffusion coefficient D_m. COILSIM2D calculates the

Fanning friction factor from the Prandtl equation, see equation [4.27]. The boundary conditions for the 2-dimensional problem are:

- in the center of the tube (r = 0):

$$\frac{\partial T}{\partial r} = 0 \qquad\qquad v_r = 0 \qquad\qquad \frac{\partial}{\partial r}\left(\frac{C_j}{\rho}\right) = 0 \qquad\qquad [5.\ 17]$$

- at the inner reactor wall (r = R):

$$\varepsilon_D\ \rho\ \frac{\partial}{\partial r}\left(\frac{C_j}{\rho_g}\right) = \frac{r_{c,j}}{M_j} \qquad\qquad [5.\ 18]$$

- at the inlet (z = 0) :

$$T = T_0 \qquad\qquad C_j = C_{j0} \qquad\qquad p = p_0 \qquad\qquad [5.\ 19]$$

If the axial heat profile is imposed at the inner wall (r = R) the following boundary condition is added:

$$\frac{\partial T}{\partial r} = \frac{q}{\varepsilon_H} \qquad\qquad [5.\ 20]$$

The differential equations are solved via a finite difference method. The Cranck-Nicholson method is used to calculate the differential variations in the axial direction. The differential variations in the radial direction are approximated by the second order differential of the Lagrange polynomial. For the application of the integration procedure a number of grid points has to be defined. Due to the steep gradients near the wall a sufficiently small step size is required in that zone. The step size was varied according to a geometric progression: coarse in the core and fine near the wall. The set of differential equations for a specific variable in a radial section divided in n grid points i can then be rewritten in a tridiagonal format. For the concentration of component j equation [5.21] is obtained:

$$\begin{pmatrix} b_1 & d_1 & 0 & ...0 & 0 & 0 \\ a_2 & b_2 & d_2 & ...0 & 0 & 0 \\ ... & & & & & \\ 0 & 0 & 0 & ...0 & a_n & b_n \end{pmatrix} \begin{pmatrix} C_{j,1} \\ C_{j,2} \\ . \\ C_{j,n} \end{pmatrix} = \begin{pmatrix} e_1 \\ e_2 \\ . \\ e_n \end{pmatrix} \qquad [5.\,21]$$

This set of equations is solved simultaneously by the Thomas-algorithm.

As stated previously the implementation of a kinetic model based on a radical reaction mechanism results in a stiff set of differential equations. When the 2-dimensional reactor model is applied the Pseudo Steady State Approximation (PSSA) for the radicals cannot be used because it transforms the continuity equations for the radicals into algebraic equations. This makes it impossible to take into account the effect of diffusion of radicals from neighboring zones, which requires a differential equation. Therefore a special solution method is used for the 2-dimensional reactor model. An element e_i of the right hand side of equation [5.21] contains the reaction rates calculated with the applied kinetic model. It is convenient to separate this contribution into two parts, one describing the cumulative rate of formation of the j-th component by all reactions forming this component and the other describing the cumulative rate of disappearance of the same component.

$$\sum_k v_{kj} r_k = \sum_k v_{kj,f} \ r_{k,f} + \sum_k v_{kj,b} \ r_{k,b} \qquad [5.\,22]$$

The second term of the right hand side of equation [5.22] is a linear function of the concentration of component j in the i-th grid point of a section, neglecting the small contribution of possible recombination reactions. Equation [5.22] can then be rewritten:

$$\sum_k v_{kj} r_k = \sum_k v_{kj,f} \ r_{k,f} + K \, C_{j,i} \qquad [5.\,23]$$

Separation of the right hand side of equation [5.23] by moving the second term of the right hand side to the left side of equation [5.23] solves the stiffness problem. The diagonal elements of the tridiagonal matrix increase; hence, the stability of the solution is increased.

5.2.3   Importance of radial gradients on the simulated product yields

An extensive study is performed on an industrial ethane cracking furnace. Ethane has a strong refractory character and thus requires high coil outlet temperatures and high heat fluxes. The simulations have been performed for a furnace equipped with radiation burners. To have a good basis for the comparison of the results obtained with both reactor models, an identical heat flux profile is used as input. Hence, the same amount of energy is added to the process gas. The heat flux profile was obtained by performing a coupled simulation of the furnace and the reactor tubes, using the 1-dimensional reactor model.
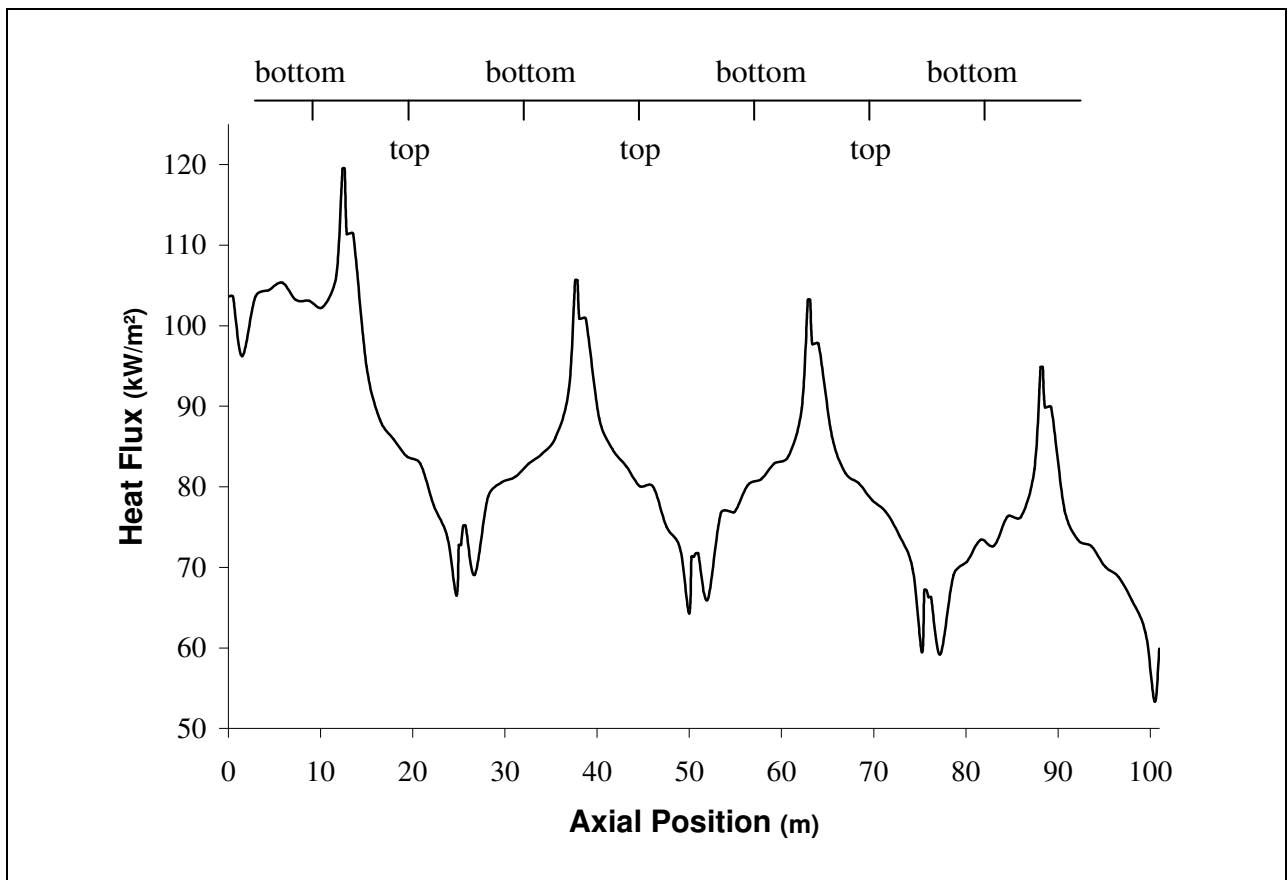
Figure 5.3: Heat flux from furnace to reactor as a function of the axial position in the reactor

For the simulated ethane cracking furnace the burners are located in the sidewalls on both sides of the coils. The heat flux profile can be determined by calculating the radiative heat transfer in the furnace (Heynderickx and Froment, 1998). The flue gas entering the furnace

through the burners delivers energy to the reactor wall and decreases therefore in temperature. In the bottom section of the furnace the flue gas temperature is higher due to the hampered flow. In the top section there are no burners so that the flue gas temperature profile is smoother. The non-uniformity of the flue gas temperature, results in a strongly varying heat flux to the process gas, as shown in Figure 5.3. Circumferential non-uniformities due to the shadow effect in the furnace are not taken into account. There was no coupled simulation of furnace and reactor coils performed using the 2-dimensional reactor model. For reasons of comparison, as explained above, the same heat flux profile was used.

FURNACE	
Furnace length	9.30 m
Furnace height	13.45 m
Furnace width	2.10 m
Thickness refractory material	0.23 m
Thickness insulation material	0.05 m
Number of burners	128
Heat input	14.43 MW
REACTOR COIL	
Number of reactors	4
Number of passes per reacor	8
Reactor length	100.96 m
Reactor diameter (int)	0.124 m
Wall thickness	0.008 m
Ethane flow rate per reactor coil	0.972 kg s^{-1}
Steam dilution	0.35 kg/kg
Coil Inlet Temperature (CIT)	873 K
Coil Inlet Pressure (CIP)	0.34 MPa

Table 5.1: Furnace and reactor geometry. Operating conditions for an ethane cracking furnace

The operating conditions and the furnace and reactor geometry are listed in Table 5.2. The total hydrocarbon flow rate through one reactor coil is 3.5 ton per hour. The inlet temperature of the process gas is 873 K. During the steam cracking of ethane a steam dilution of 0.35 kg steam per kg feed is applied. The steam reduces the partial pressure of the hydrocarbons in the gas phase and reduces the coke formation.
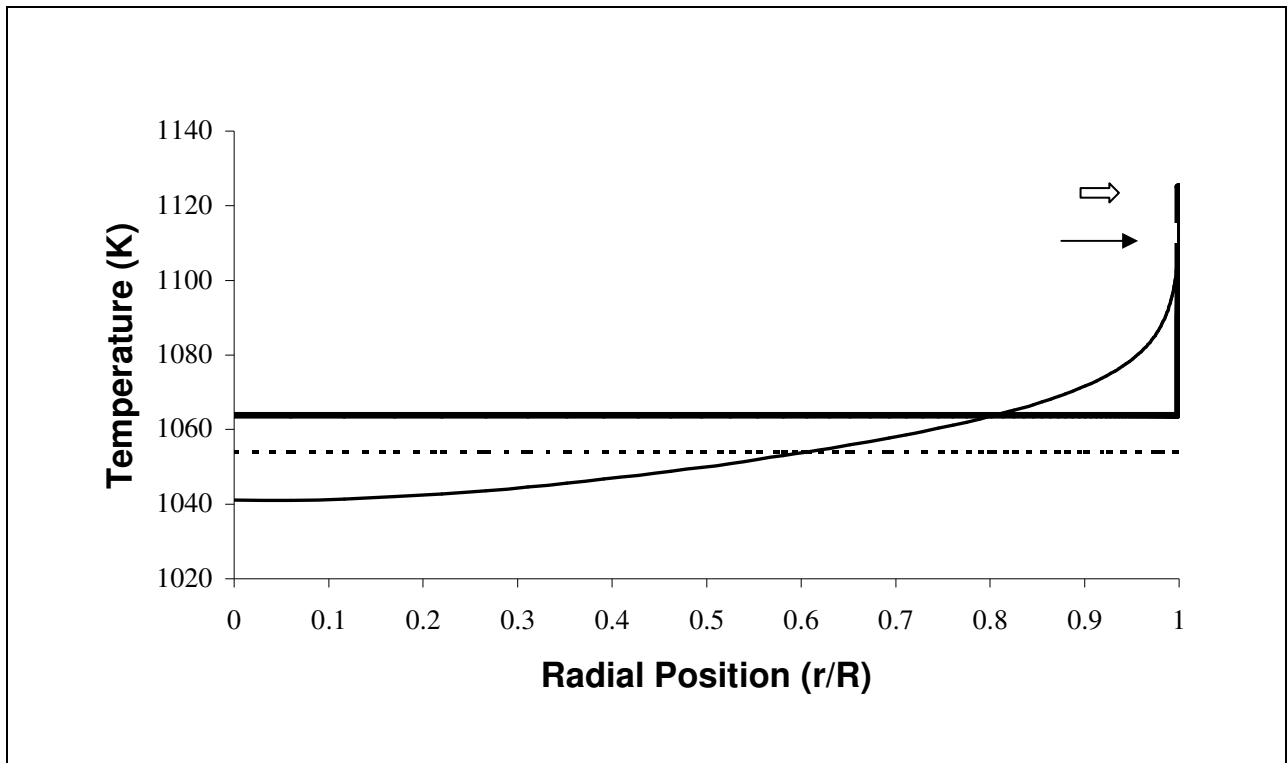
Figure 5.4: Process gas temperature in function of the radial position at an axial position of 50 m
──────── 1D reactor model ;──────── 2D reactor model ; - - - - average 2D temperature
◄── Int. wall temperature 2D reactor model; ⇐Int. wall temperature 1 dim. reactor model

The effect of using the 2-dimensional reactor model instead of the classically applied 1-dimensional reactor model can be evaluated based on the comparison of the simulation results obtained with the two reactor models. Figure 5.4 shows that for the process gas temperature important radial non uniformities exist in the reactor. The radial temperature profile simulated with the 2-dimensional model shows a strong gradient near the wall, but the gradients in the center of the tube cannot be neglected, in contrast to the 1-dimensional model. The total

temperature drop from the wall to the center is about 100 K for both models. In Figure 5.5 the average process gas temperature for the 2-dimensional simulation is also shown. For the calculation of the average process gas temperature for the 2-dimensional reactor model, the cup mixing temperature is applied (Bird et al., 2001):

$$T_{av} = \frac{\int_0^R T(r)\, u(r)\, r\, dr}{\int_0^R u(r)\, r\, dr} \qquad\qquad [5.24]$$

The results of Figure 5.4 are in agreement with the results simulated by Froment (1992) and Valenyi et al. (1991). Froment (1992) reported a similar radial temperature profile but with a stronger temperature drop near the wall for a pilot configuration with a reactor tube diameter of 0.037 m and, hence, a lower velocity.
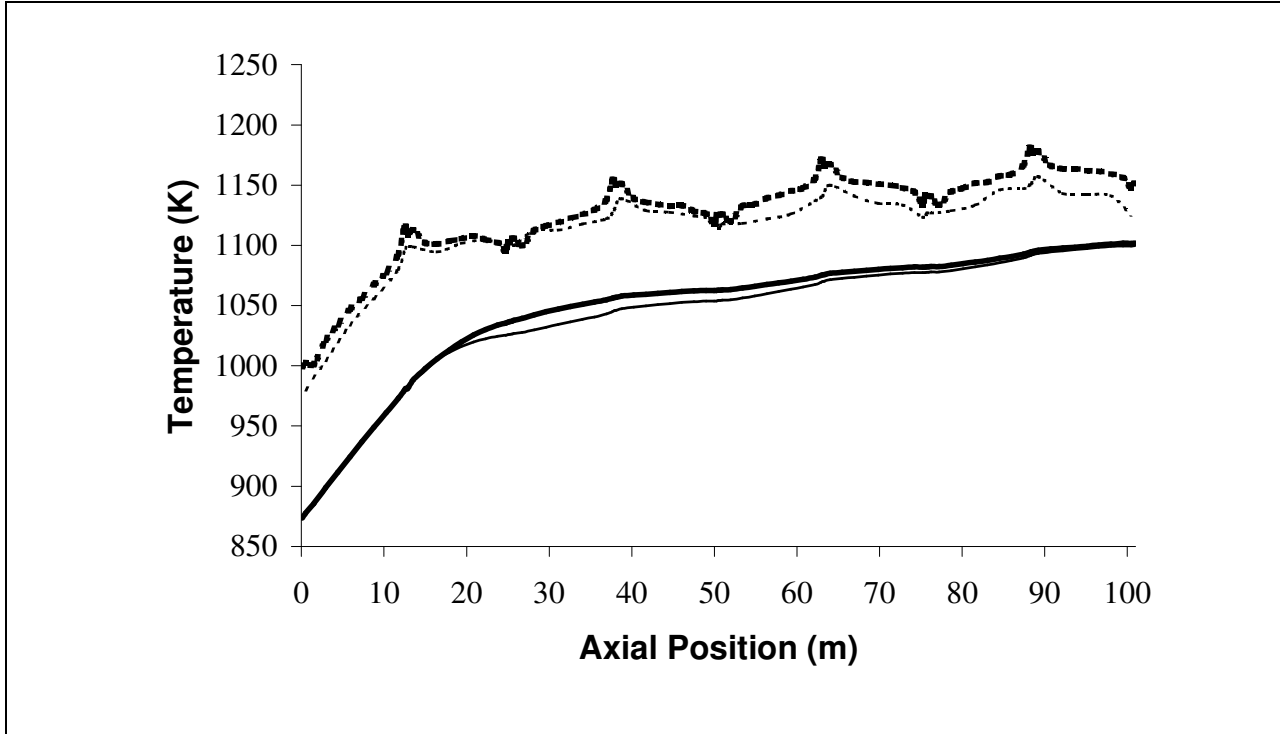
Figure 5.5: Average process gas temperature and internal tube skin temperature as a function of axial position in the reactor coil; ▬▬ process gas temperature 1D ; ─── average process gas temperature 2D ; ▬ ▬ tube skin temperature 1D ; – – – tube skin temperature 2D

In Figure 5.5 the axial profiles of the average process gas temperatures and the wall temperatures for the two simulation models in the reactor coil are given. Although important differences exist for the temperature in a radial section there is a good agreement between the average axial gas temperature calculated with the 2-dimensional reactor model and the axial gas temperature simulated with the 1-dimensional reactor model up to 25 m. From this position on, the cracking becomes significant and is more pronounced when the radial temperature profiles are accounted for. This leads to an average temperature which is lower for the 2-dimensional model. Near the outlet of the coil the difference diminishes.

The wall temperature for the 1-dimensional simulation is slightly higher than the one simulated with the 2-dimensional reactor model. This is due to the different calculation methods used for the wall temperatures. The Dittus-Boelter equation and the gas temperature are used in the 1-dimensional model, while in the 2-dimensional model heat transport and reaction are considered simultaneously. The latter implies a better simulation of the wall temperature. The higher wall temperature resulting from the 1-dimensional reactor model will have consequences for coke formation. Higher temperatures in the zone near the wall will increase the simulated coking rate. However, the slight change of external tube skin temperature profile will result in a small change of the heat flux profile when a complete simulation is carried out.

Product	1D	2D
	(wt %)	(wt %)
Hydrogen	3.1	3.0
Methane	2.9	3.7
Acetylene	0.4	0.4
Ethylene	41.4	41.2
Propylene	0.7	1.0
Butadiene	0.9	1.0
Ethane-conversion	51.0	51.8

Table 5.2: Comparison between simulated weight percentages (wt %) at the reactor outlet of the traditional single coil reactor simulated with the 1D and 2D reactor model

The results in Table 5.2 clearly show that the radial temperature profile indeed has an influence on the simulated product yields and the conversion. Especially for methane and propylene the yields calculated with the 2-dimensional model are significantly higher. On the other hand for ethylene the 2-dimensional model simulates a lower product yield. The existence of an important radial temperature profile is the main cause for the differences in product distribution obtained with both reactor models. The interpretation of radial and axial concentration profiles of the most important molecules and radicals, taking into account the radial and axial temperature profiles, allows explaining this. The main molecules in the kinetic model for the cracking of ethane are ethane, ethylene, propylene and hydrogen. The main radicals are the hydrogen, methyl, ethyl and allyl radical.
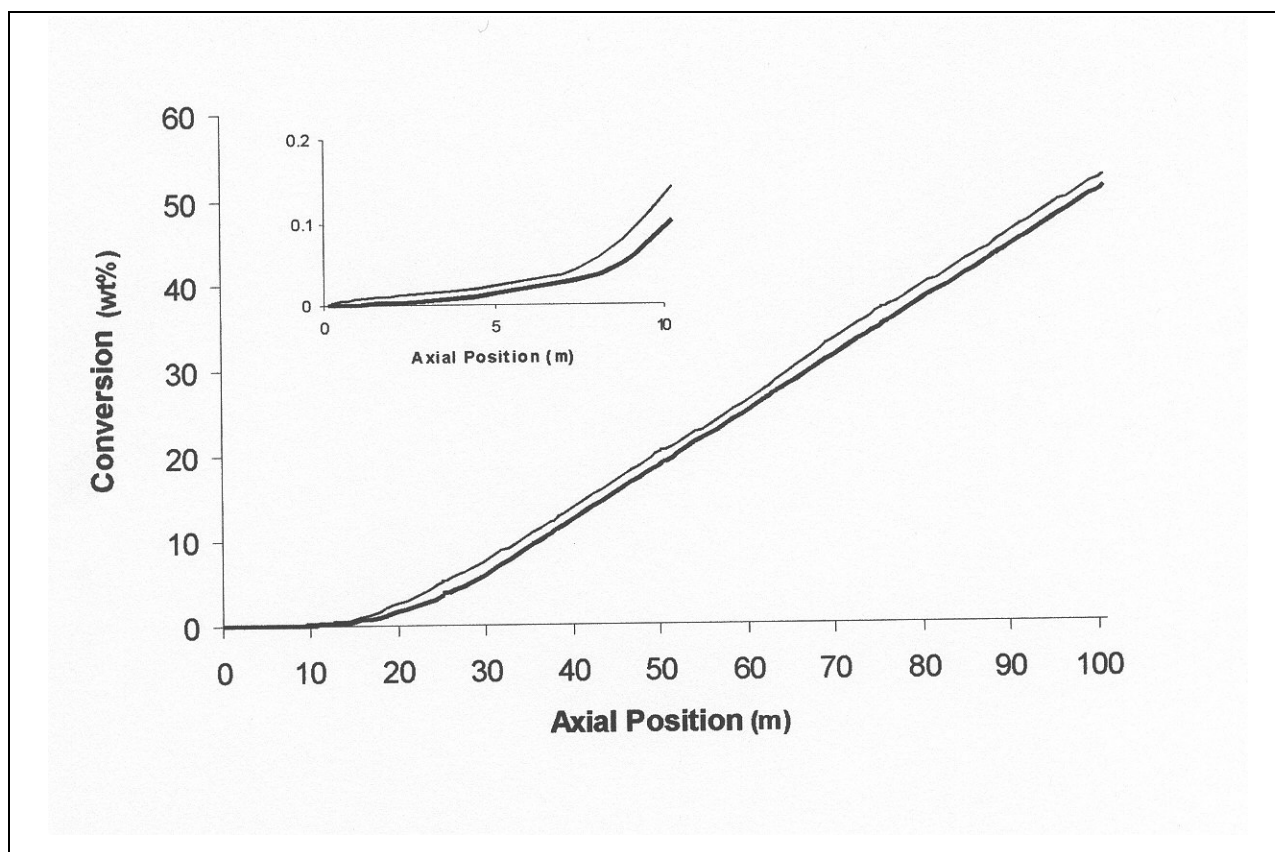
Figure 5.6: Ethane conversion as a function of the axial position in the reactor coil; ▬▬ 1D reactor model; ——— 2D reactor model

In Figure 5.6 the ethane conversion profile is shown. Such a profile shows an induction period corresponding with the heating of the process gases to the reaction temperature. This induction period is shorter for the 2-dimensional model because of the radial temperature profile. Figure 5.4 shows that in the zone near the wall the radial 2D process gas temperature is more than 60 K higher than the average 1D temperature and, hence, activation by C-C scission or C-H scission reactions will occur at an axial position closer to the inlet, as seen in Figure 5.6. This effect results in a higher ethane conversion obtained with the 2-dimensional reactor model. At temperatures below 1100 K the C-C scission of ethane with an activation energy of 368 kJ/mol is the main source of methyl radicals:

$$C_2H_6 \rightarrow CH_3^{\bullet} + CH_3^{\bullet} \tag{5.25}$$

The C-H scission reactions only become of some importance at much higher temperatures because of the higher activation energy of this reaction (411 kJ/mol). The influence of the small difference between the average process gas temperature simulated with the 2-dimensional model and the 1-dimensional temperature is of less importance. Once the cracking has started the conversion of ethane increases with an almost constant slope, as seen in Figure 5.6.
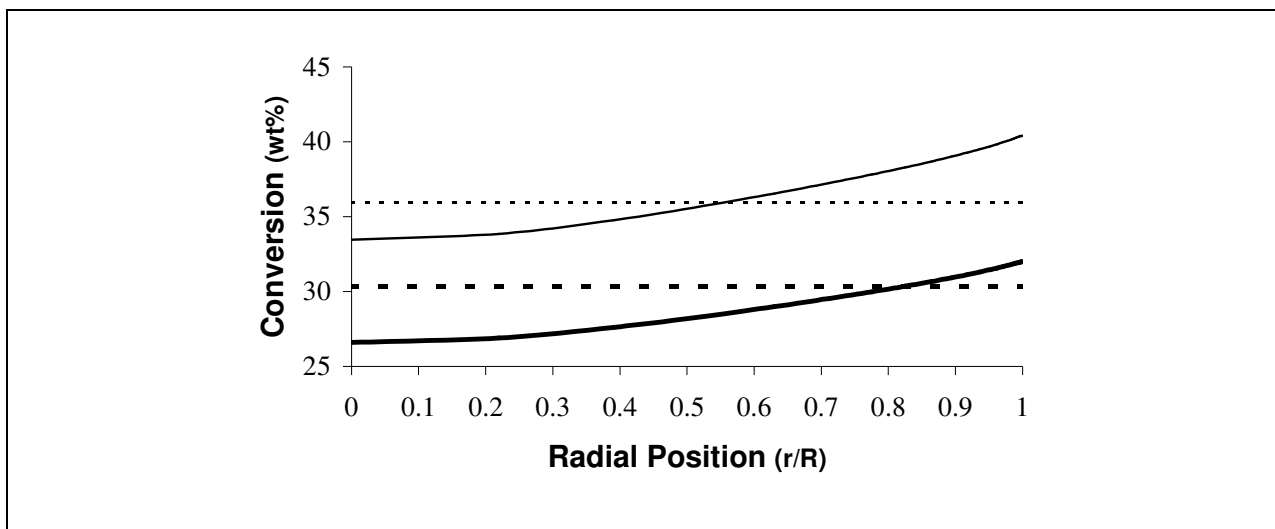
Figure 5.7: Conversion and ethylene yield as a function of the radial position at an axial position of 75 m; ▬▬ ethylene yield 2D; ▬ ▬ ethylene yield 1D; ——— ethane conversion 2D; - - - ethane conversion 1D

In Figure 5.7 the ethane conversion and the ethylene yield are shown over a cross section at an axial position of 75 m. The 2D radial process gas temperature profile is responsible for the radial differences in conversion. The higher conversion near the wall results in a higher ethylene yield in this zone and will also affect the yields of other products.

As shown in Table 5.2, the methane yield simulated with the 2-dimensional reactor model is considerably higher than simulated with the 1-dimensional reactor model. As a consequence of the radial process gas temperature profile and the resulting increase of C-C scission reactions of ethane, a higher methyl radical concentration is obtained. H-abstraction reactions by the methyl radical lead to the formation of methane. In this case the H-abstraction reaction of ethane is the main path to the formation of methane.

$$CH_3{}^\bullet + C_2H_6 \rightarrow CH_4 + C_2H_5{}^\bullet \qquad \text{[5. 26]}$$

The higher methane yield at the outlet is thus a direct consequence of the higher methyl radical concentration.

The lower ethylene yield simulated at the reactor outlet with the 2-dimensional reactor model is due to diffusion effects. Near the inlet of the reactor only the process gas temperature in the zone near the wall is high enough to activate the conversion of ethane. Decomposition of the ethyl radical is generally accepted to be the main reaction responsible for the production of ethylene from ethane:

$$C_2H_5{}^\bullet \rightarrow C_2H_4 + H^\bullet \qquad \text{[5. 27]}$$

The ethylene produced in the zone near the wall can diffuse to the center of the tube where the process gas temperatures are lower. These temperatures favor secondary reactions, among which addition reactions to methyl and ethyl radicals are very important:

$$CH_3{}^\bullet + C_2H_4 \rightarrow C_3H_7{}^\bullet \qquad \text{[5. 28]}$$

$$C_2H_5{}^\bullet + C_2H_4 \rightarrow C_4H_9{}^\bullet \qquad \text{[5. 29]}$$

This explains the higher yield of products such as propylene, 1-butene and butadiene, obtained with the 2-dimensional reactor model. For example, propylene is mainly formed by the β-scission of the $C_3H_7{}^{\bullet}$-radical:

$$C_3H_7{}^{\bullet} \rightarrow C_3H_6 + H^{\bullet} \qquad\qquad [5.\,30]$$

and in a minor amount from H-abstraction reactions by the allylic $C_3H_5{}^{\bullet}$ radical:

$$C_3H_5{}^{\bullet}\,(al) + C_2H_6 \rightarrow C_3H_6 + C_2H_5{}^{\bullet} \qquad\qquad [5.\,31]$$
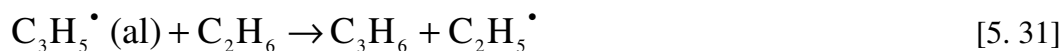
Diffusion of ethylene followed by addition of the methyl radical results in a higher propylene formation.
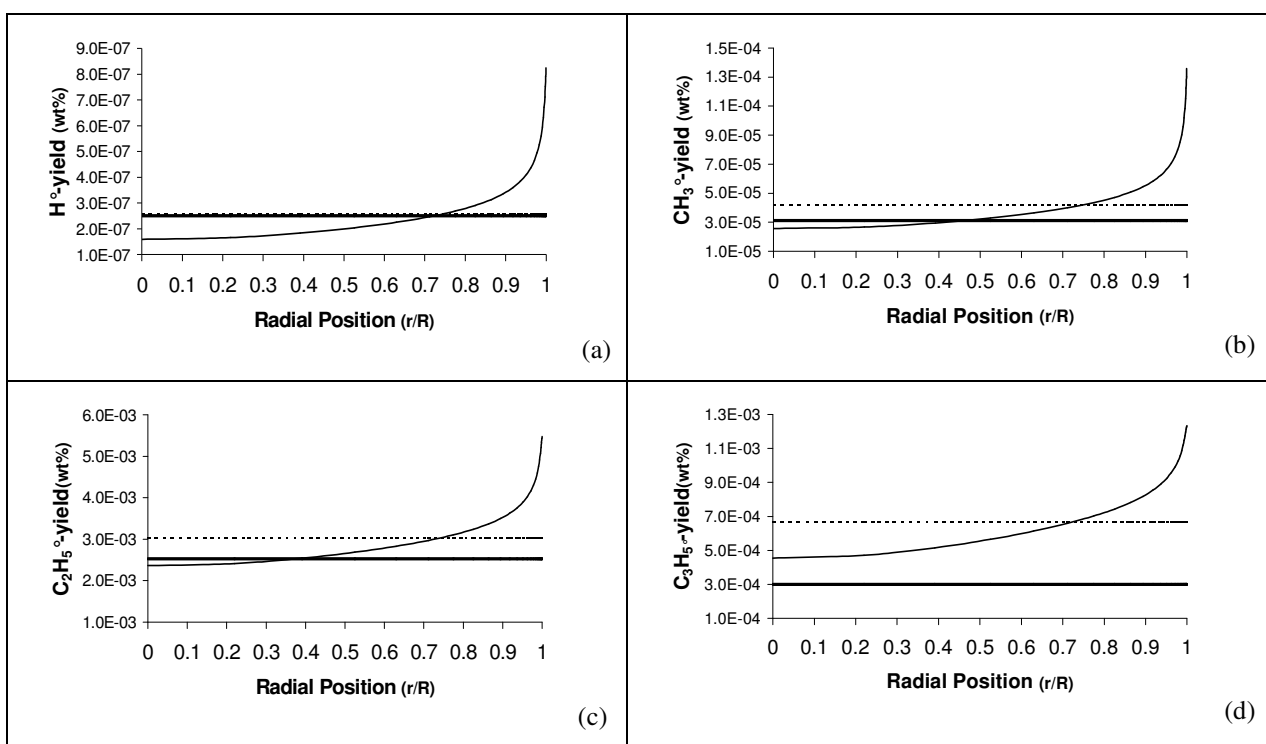
Figure 5.8: Simulated weight fraction profiles for 4 different radicals at an axial position of 75 m: —— 1D; —— 2D; - - - average 2D; (a) $H^{\bullet}$-radical, (b) $CH_3{}^{\bullet}$-radical, (c) $C_2H_5{}^{\bullet}$-radical, (d) allylic C_3H_5-radical.

The same reasoning that explains the lower ethylene yield also holds for the lower acetylene yield obtained with the 2-dimensional reactor model, see Table 5.2. Diffusion of acetylene to the center, followed by secondary reactions explains the lower acetylene yield. The effect is even more pronounced due to the faster secondary reactions of acetylene, which decrease the acetylene yield drastically in favor of heavier products.

In Figure 5.7 and Figure 5.8 respectively the radial yield profiles for ethylene and ethane, and for the main radicals are presented. Comparison of these profiles shows that the radial gradient for the radicals is much steeper than for the molecular species. The radial temperature profile results in strong radial gradients for the radicals, especially for the methyl radical and the hydrogen radical. These also strongly affect the radial non-uniformities for the heavier radicals and are responsible for the higher average radical concentration simulated with the 2-dimensional reactor model [Figure 5.8 (c) and (d)]. The radial average yield of the allylic radical is about 2 times higher when using the 2-dimensional reactor model, that of the methyl radical is almost 1.5 times higher. The latter is in contrast with the results for the hydrogen radical in Figure 5.8 (a). The average H-radical yield simulated with the 2-dimensional reactor model is almost identical to the one simulated with the 1-dimensional reactor model. This is because the yield of hydrogen depends strongly on the equilibrium with other products, and this is not significantly affected by using a 2D reactor model. On average the reacting mixture does not really change a lot if instead of a 1D reactor model a 2D reactor model is used. Hence the yield of hydrogen remains similar and the average concentration profiles of the radicals are almost identical.

The existence of the radial temperature profile in a tubular reactor clearly has an influence on the product yields. For a given average temperature, the presence of a radial temperature profile leads to a decrease of the yield of ethylene. This implies that tubes with a smaller diameter are beneficial because they possess a stronger 1-dimensional character. This is the case for reactor configurations such as the USC-Furnace (Ultra Selective Conversion) developed by Stone and Webster and the Kellogg Millisecond Furnace. Consider for example the Kellogg Millisecond Furnace. This type of furnace, consisting of a reactor with a large number of tubes (200) of small diameter ($3.5 \ 10^{-2}$ m) and short length (10 m) (Orriss and Yamaguchi, 1987), is known for its high ethylene yield. The total hydrocarbon flow rate of more than 20 ton hr^{-1} results in very high velocities in all of the 200 parallel tubes. The high ethylene yield of this type of reactor is generally explained by the short residence time. Indeed, short residence times reduce

the disappearance of light olefins because of secondary reactions such as addition reactions. Experimental work by Ennis et al. (1975) showed that residence times lower than 0.1 s are most favorable. Van Geem et al. (2004) showed that not only the short residence time but also a stronger 1-dimensional behavior is the cause for the high ethylene yield. The same reasoning as applied on a Millisecond reactor also holds for a pilot plant reactor. Moreover, the differences between the product yields and conversion simulated with the 1-dimensional reactor model and the 2-dimensional reactor model become negligible because of the very small radial temperature drop. Figure 5.9 shows the simulated radial temperature profile in the middle of the coil for an ethane cracking experiment in a pilot plant reactor using similar conditions as those used for the industrial case. The radial process gas temperature drop remains significantly smaller than the one observed in the industrial reactor. The simulation results indicate that under normal operation conditions the typical radial temperature drops in a pilot plant reactor fluctuate between 10 and 20 K.
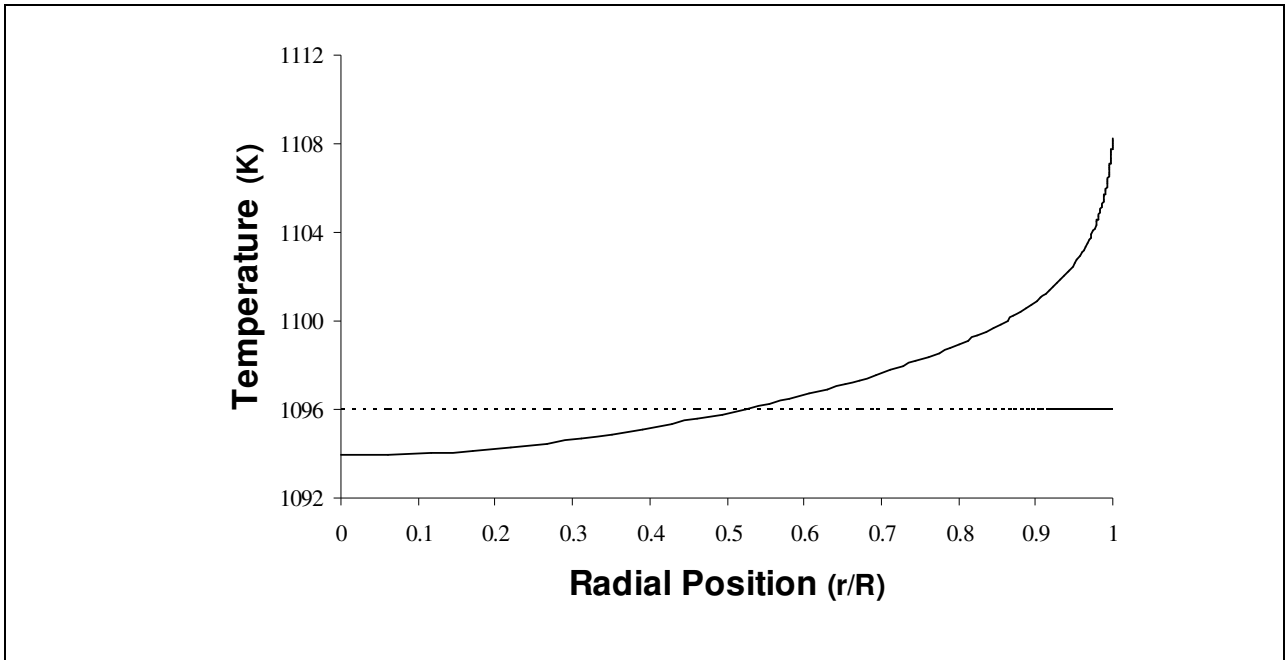
Figure 5.9: Process gas temperature in function of the radial position at an axial position of 6.7 m for a pilot plant reactor of 12.4 m; —— 2D reactor model; - - - average 2D temperature. [Simulation Conditions for ethane cracking experiment. CIT = 873 K; COT =1125 K; CIP = 0.21 MPa; COP = 0.16 MPa; F: 4.0 kg h^{-1}; δ = 0.4 kg /kg]

The previous study carried out for ethane steam cracking can also be repeated for other feedstocks. It can be expected that the effect of using a 2-dimensional instead of a 1-dimensional reactor model will be less pronounced for heavier feedstocks because these do not possess such a refractory character as ethane. Indeed, to obtain the same conversion the COT of the reactor, and thus the needed heat fluxes, are significantly reduced. Hence, as shown in Table 5.3 the differences between the simulation results obtained with a 2-dimensional and 1-dimensional reactor are less pronounced.

Product	1D	2D
	(wt %)	(wt %)
Hydrogen	0.6	0.6
Methane	14.0	14.7
Ethylene	22.4	22.0
Ethane	2.8	3.0
Propylene	20.0	19.7
Butadiene	1.2	1.5
1-Butene	2.3	2.2
2-Butene	0.6	0.6
Benzene	0.9	1.2
n-Butane conversion	68.1	68.9

Table 5.3: Comparison between simulated weight percentages (wt %) for n-butane steam cracking in a traditional single coil reactor simulated with the 1-D and 2-D reactor model [Simulation Conditions: CIT = 873 K; COT = 1065 K; CIP = 0.25 MPa; COP = 0.20 MPa; F: 0.972 kg s^{-1}; δ = 1.0 kg /kg]

5.2.4   Importance of radial gradients on the simulated coking rate

The coke formation at the internal skin of the reactor coil depends on the conditions prevailing at the process gas – coke interface. It is clear from the preceding results obtained with the 2-dimensional reactor model that these conditions differ appreciably from the process

conditions at the center of the reactor coil. In typical industrial units the temperature at the interface can be up to 100 K higher than the average process gas temperature. This has a significant effect on the gas phase concentrations and more in particular on those of the gas phase radicals. According to Reyniers et al. (1994) gas phase radicals generate radical sites on the cokes layer. Olefins can add to these radical sites and after dehydrogenation coke is formed. Therefore the effect of the radial temperature profile and the resulting gas phase radical concentration profile on the coking rate has been investigated for a traditional single coil reactor.

The simulation results using a fundamental kinetic coking model based on elementary reactions are studied. These results are compared with reference data calculated with the model of Plehiers (1989). The coking model of Plehiers (1989) coupled to a 1-dimensional reactor model, has been validated for experimental as well as industrial units and was found to be very useful for the prediction of coke formation in the steam cracking of light hydrocarbon feedstocks. The run length of several industrial cracking units has been simulated, showing a good agreement between industrial and simulated results. An agreement of results obtained with the coking model based on elementary reactions on the one hand, and those obtained with the coking model of Plehiers on the other hand, is therefore a good indication for the quality of the simulation results. The semi-empirical coking model of Plehiers considers ethylene and propylene as the only coke precursors. These components can add to the radical sites at the coke surface and form cokes. The coking rate is a function of the wall temperature and the concentration of ethylene and propylene. The coking model developed by Wauters and Marin (2001) on the other hand is a fundamental kinetic model for coke formation based on elementary reactions. The creation of radical sites on the coke layer is explicitly accounted for by considering the abstraction of hydrogen from surface species by gas phase radicals. The resulting radical surface species can add to unsaturated components in the gas phase, such as olefins and aromatics.

Figure 5.10: Reaction path for coke formation starting from propylene, hydrogen radicals and alkyl radicals. The coke layer is considered to be a polyaromatic surface (Wauters, 2001).
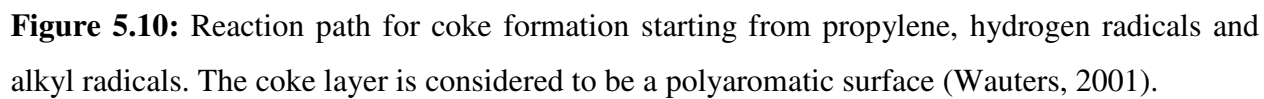
The possible coke formation reactions can be divided into five classes:

- hydrogen abstraction by gas phase radicals
- substitution by gas phase radicals at the coke surface
- addition of a radical surface species to a gas phase olefin and the reverse decomposition of a radical surface species in a smaller radical surface species and an olefin
- addition of a gas phase radical to a double bond in a surface species and the reverse decomposition of a radical surface species to an olefinic surface species and a radical
- cyclization of a radical surface species and decyclization

Figure 5.10 shows one of the reaction paths for coke layer growth starting from propylene, hydrogen radicals and alkyl radicals as coke precursors. The coke layer is considered to be a polyaromatic surface.

Considering each component in such a coke formation model leads to an enormous expansion of the reaction network. To obtain a rigorous but practical model, it is therefore necessary to select those gas phase components that are the most important coke precursors. The contribution of a gas phase component to coke formation is determined by the concentration of the component and the rate coefficients of the coking reactions in which the component is involved. In steam cracking of light feedstocks the concentration of the gas phase radicals varies between 10^{-6} mol m^{-3} and 10^{-1} mol m^{-3} (McConnell et al.; 1981). The latter was confirmed by the simulation results. For light feedstocks the hydrogen, methyl, ethyl, and allyl radicals were found to be the most important coke precursor radicals. Acetylene, ethylene, methylacethylene and propylene are unsaturated molecular components that favor coke formation.

The kinetics of the coke formation reactions are determined from those of corresponding gas phase reactions provided the presence of a solid phase is accounted for via a correction factor based on the collision theory (Wauters and Marin, 2002). It was found that the coking rate depends not only on the concentration of molecules and on the wall temperature, but in particular on the radical concentrations. A good estimation of the concentrations of the radicals in the zone near the wall is of the utmost importance for the fundamental coking model because their effect on the coking rate is as important as the effect of the wall temperature (Wauters and Marin, 2002).
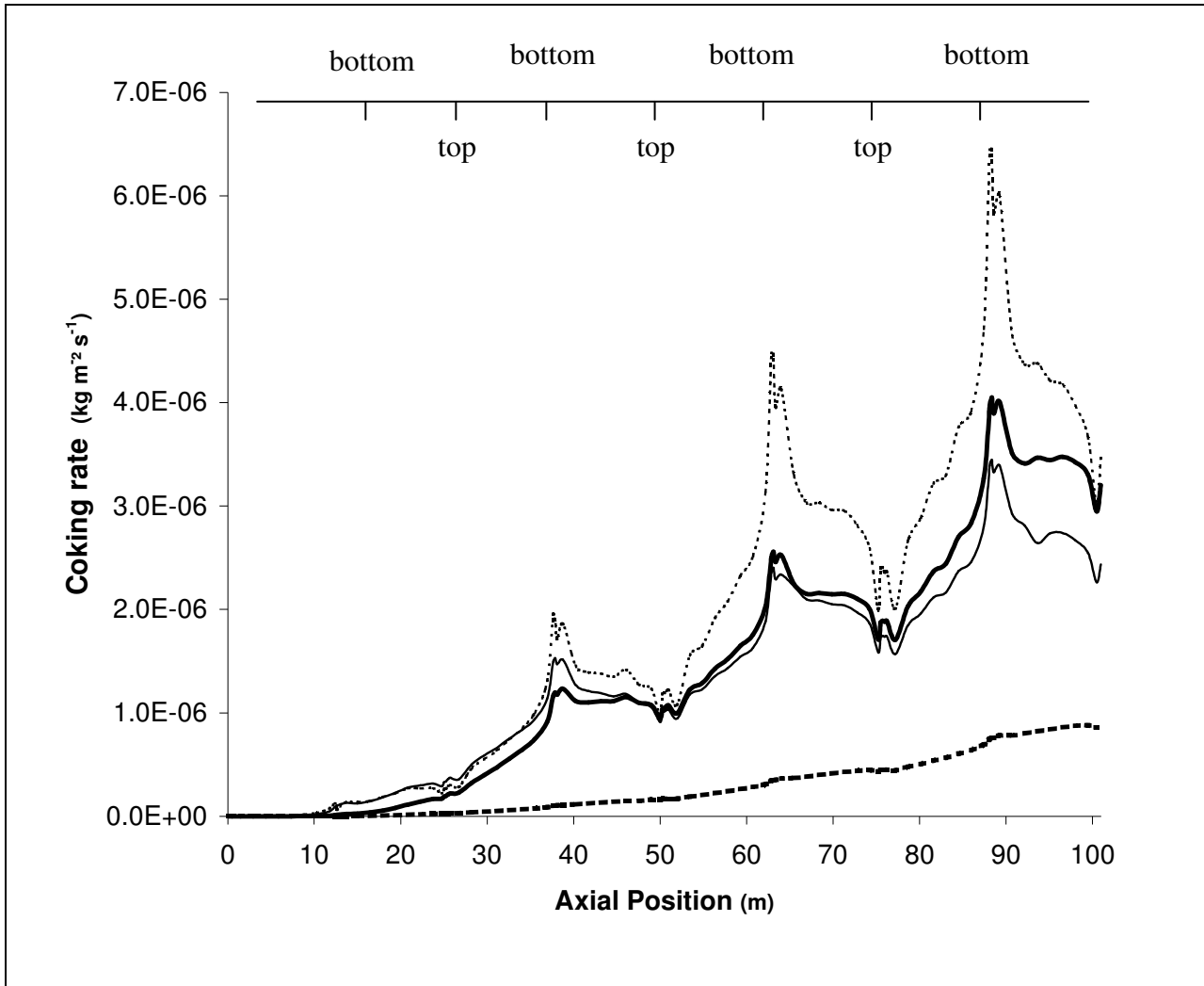
Figure 5.11: Coking rate as a function of the axial position in the reactor tube; ▬▬ reference profile; ▬ ▬ 1D reactor model, precursor concentrations calculated at process gas temperature ; − − − 1D reactor model, precursor concentrations calculated at interface temperature; ⎯⎯ 2D reactor model, precursor concentrations at interface

In Figure 5.11 the differences between the coking rate profiles calculated with the 1-dimensional and 2-dimensional reactor model, are presented and compared with the reference profile obtained from the semi-empirical model of Plehiers (1989).. Using a 1-dimensional reactor model and calculating the precursor concentrations at the process gas temperature clearly underestimates the coking rate. The wall temperature used in this simulation is the wall temperature calculated with the 1-dimensional reactor model. The reason for the large difference

between the calculated profile and the reference profile is twofold. On the one hand, the effect of the temperature for the calculation of the coking rate with the fundamental model is not as strongly affected by the temperature as the calculation of the coking rate calculated with the semi-empirical model (Wauters and Marin, 2002), i.e. the reference profile, due to differences in kinetics. On the other hand the precursor concentrations are those calculated in the process gas by the 1-dimensional reactor simulation. Table 5.4 shows the values of the concentrations of the main coke precursors and the temperature at z = 50 m. The concentrations calculated in the process gas with the 1-dimensional reactor simulation are lower than those prevailing at the interface as calculated with the 2-dimensional reactor model. The underestimation of the concentrations of the species results in a drastic underestimation of the coking rate. For example the underestimation of the methyl radical by a factor 5 results in a reduction of the coking rate by almost 50 % (Wauters and Marin, 2002).

	1D Process gas	1D Interface	2D
Temperature	1125	1125	1120
Concentrations			
C_2H_2	$6.3 \ 10^{-6}$	$6.7 \ 10^{-6}$	$6.3 10^{-6}$
C_2H_4	$3.7 \ 10^{-3}$	$3.5 \ 10^{-3}$	$3.7 \ 10^{-3}$
C_3H_4	$1.2 \ 10^{-7}$	$1.3 \ 10^{-7}$	$1.6 \ 10^{-7}$
C_3H_6	$1.7 \ 10^{-5}$	$3.6 \ 10^{-5}$	$4.3 \ 10^{-5}$
$H\cdot$	$9.8 \ 10^{-10}$	$7.6 \ 10^{-9}$	$3.6 \ 10^{-9}$
$CH_3\cdot$	$6.4 10^{-9}$	$4.8 \ 10^{-8}$	$4.0 \ 10^{-8}$
$C_2H_5\cdot$	$4.4 \ 10^{-7}$	$1.2 \ 10^{-6}$	$1.2 \ 10^{-6}$
$C_3H_5\cdot$	$1.3 \ 10^{-8}$	$7.2 \ 10^{-7}$	$8.8 \ 10^{-8}$

Table 5.4: Temperature (K) and concentrations (kmol m^{-3}) of the main coke precursors at the gas-coke interface (z = 50 m) with: 1 D reactor model, precursor concentrations calculated at process gas temperature; 1 D reactor model, precursor concentrations calculated at interface temperature; 2 D reactor model, precursor concentrations at interface

As an approximation, the concentrations of the coke precursors at the interface temperature have been calculated by solving the corresponding mass balances for the 1-dimensional reactor model but now at the interface temperature. The agreement between the 1-dimensional simulated profile and the reference profile is improved, but the coking rate is now overestimated. A higher temperature increases the precursor concentrations as compared to those calculated with the 2-dimensional model, see Table 5.4, and causes the overestimation of the coking rate.

As shown in Figure 5.11 the coking rate profile calculated with the coking model based on elementary reactions and using the 2-dimensional reactor model shows a good agreement with the reference profile obtained from the semi-empirical model of Plehiers (1989). The coke formation profile calculated with the model based on elementary reactions coupled to the 1-dimensional reactor model shows only small peaks, if any, at the higher tube wall temperatures. On the other hand, when coupled to the 2-dimensional reactor model the sharp peaks obtained for the coking rate profile calculated with the model of Plehiers are almost perfectly predicted. The peaks simulated with the latter are a direct consequence of the peaks in the tube wall temperature profile (Figure 5.5). This reasoning does not hold for the coking rate profile simulated with the fundamental coking model and the 2-dimensional reactor model. Here the effect of the interface temperature on the coke precursor concentrations is incorporated via the kinetics and the concentrations of the involved reactants, in particular of the radicals. Hence the coke precursor concentrations need to be calculated at the interface temperature. The latter can only be calculated accurately with a 2-dimensional reactor model. The simulation results clearly show the potential of this fundamental model coupled to a 2-dimensional reactor model and shows the importance of applying a more dimensional reactor model.

5.3   Propane Cracking Furnace

In this section a Kellogg Millisecond furnace shown in Figure 5.13 is simulated. A mixture containing more than 90 wt% propane is used as feedstock, see Table 5.5. A Kellogg Millisecond furnace consists of a large number of parallel reactors(160) of small diameter ($3.0 \ 10^{-2}$ m) and short length (10 m) (Orriss and Yamaguchi, 1987). The total hydrocarbon flow rate of more than 15 ton per hour results in very high velocities and short residence times (0.1 s) in the parallel tubes. The operating conditions and the main characteristics of the furnace and the reactor are

specified in Table 5.5. In the Millisecond furnace 40 long flame burners are used, that are situated in the bottom of the furnace, as can be seen in Figure 5.12. The heat is supplied by burning 0.8 kg s^{-1} methane, which is uniformly distributed over the 40 long flame burners.
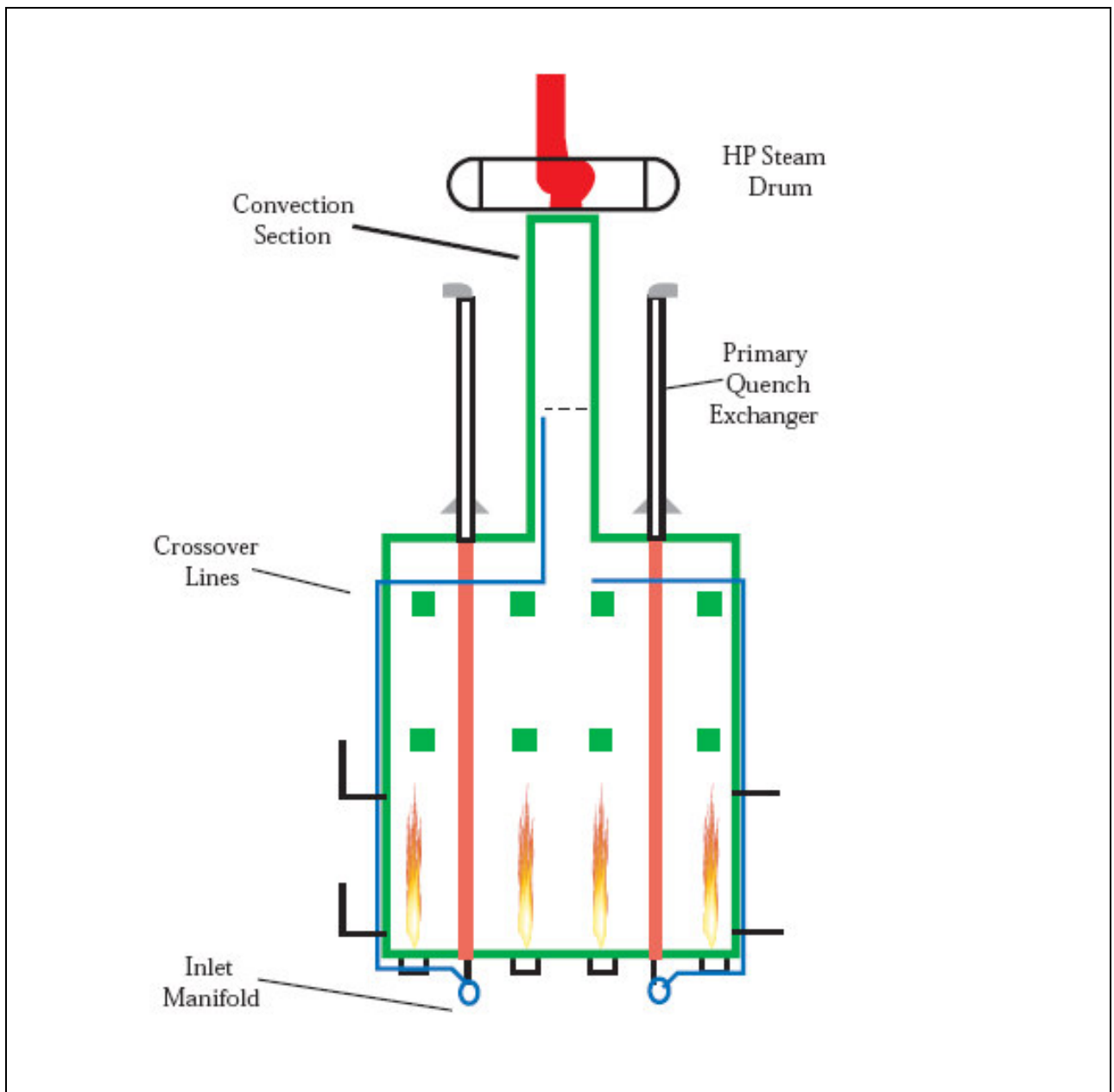
Figure 5.12: Schematic representation of a Kellogg Millisecond Furnace

FURNACE	
Furnace length	10.52 m
Furnace height	16.94 m
Furnace width	2.2 m
Thickness refractory material	0.23 m
Thickness insulation material	0.10 m
Number of burners	40
Heat input	39.15 MW
REACTOR COIL	
Number of reactors	160
Reactor length	10.30 m
Reactor diameter (int)	0.030 m
Wall thickness	0.012 m
PROCESS CONDITIONS	
Flow rate per reactor coil	$3.3 \ 10^{-2}$ kg s^{-1}
Steam dilution	0.63 kg/kg
Coil Inlet Temperature (CIT)	903 K
Coil Inlet Pressure (CIP)	0.23 MPa
Coil Outlet Temperature (COT)	1153 K
Coil Outlet Pressure (COP)	0.18 MPa
FEEDSTOCK COMPOSITION	
Ethane	1 wt%
Propylene	3 wt%
Propane	92 wt%
iso-Butane	2 wt%
n-Butane	1 wt%
n-Hexane	1 wt%

Table 5.5: Furnace, reactor geometry and process conditions used in the Kellogg Millisecond furnace
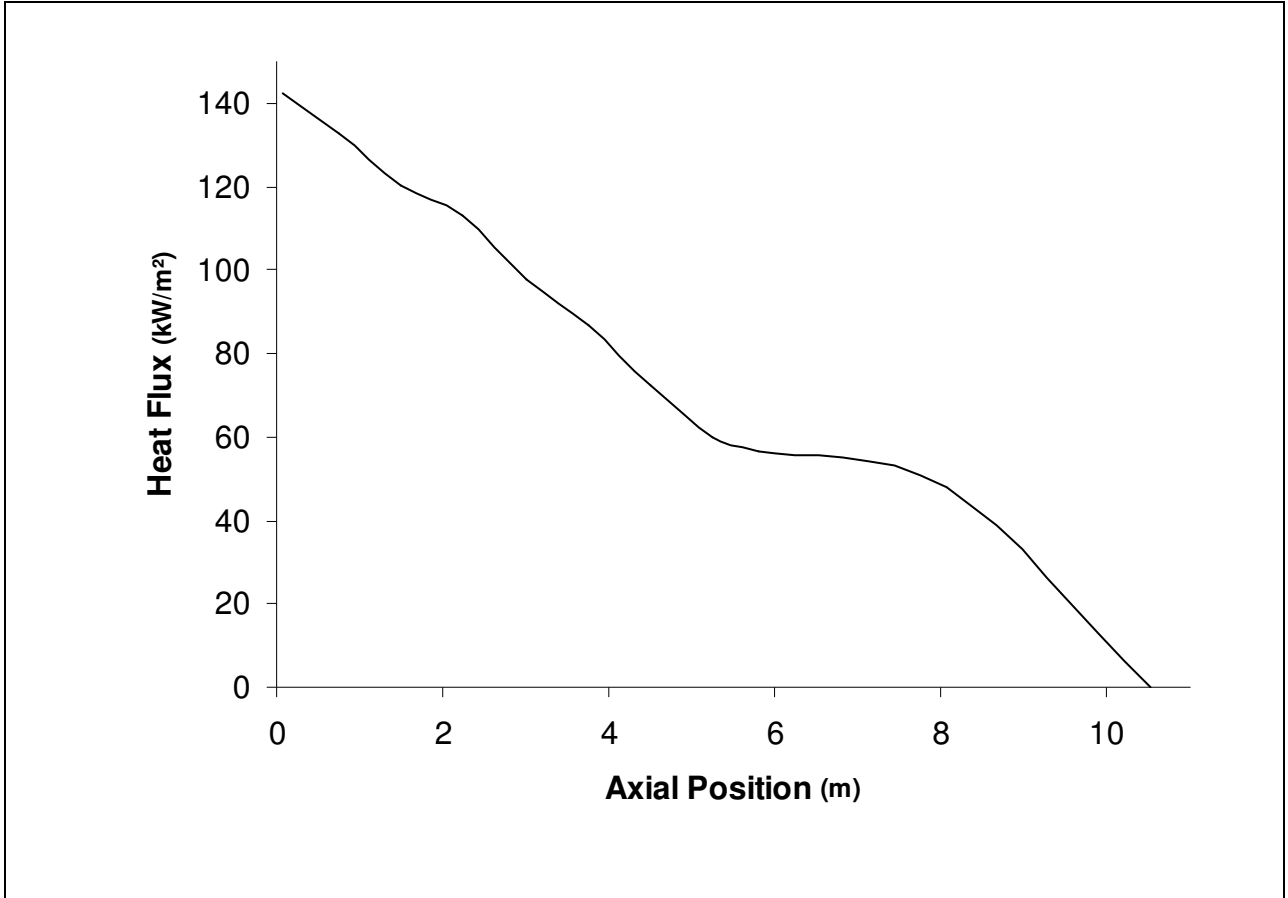
Figure 5.13: Heat flux from the Kellogg Millisecond furnace to a single Millisecond reactor as a function of the axial position in the reactor coil obtained by a coupled reactor/furnace simulation

A coupled reactor/furnace simulation is carried out to determine the product yields obtained in the cracking furnace. For the simulation of the Millisecond reactor a 1-dimensional simulation model is used although radial gradients can effect the product distribution as shown in section 5.2. However, the strong 1-dimensional character found in Millisecond reactors, results in only small differences between the product yields obtained with either a 1-dimensional or 2-dimensional reactor model (Van Geem et al., 2004). These differences are a lot smaller than the uncertainties on the results obtained from an industrial furnace. The industrial product yields are determined via overall mass balances and these are error prone. Moreover, the uncertainties on the specified conditions will inevitably also lead to errors. The simulated heat flux profile obtained via a coupled reactor/furnace simulation is shown in Figure 5.13.
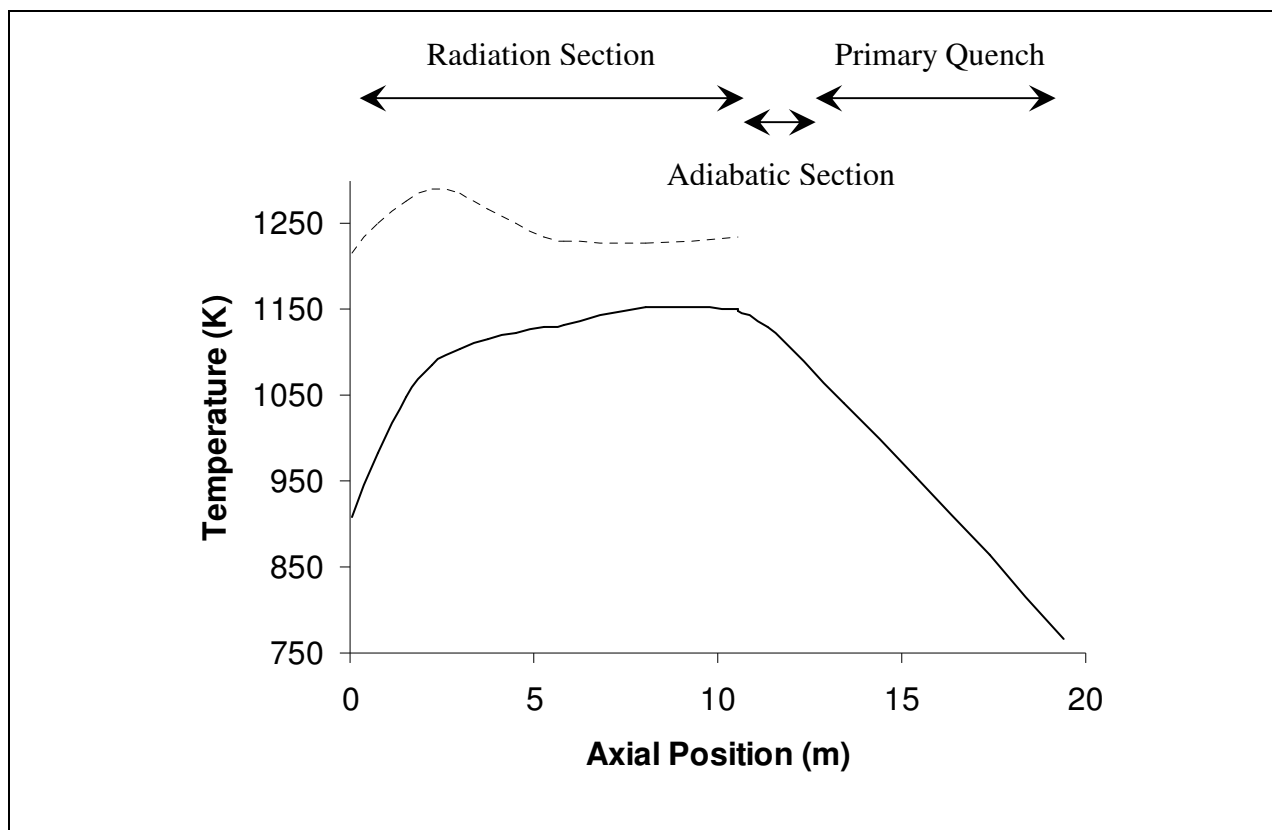
Figure 5.14: Process gas temperature and internal tube skin temperature as a function of the axial position in the reactor coil; —— process gas temperature; - - - tube skin temperature

In Figure 5.15 the resulting process gas temperature profile is shown. The temperature increases rapidly until the adiabatic section is reached. In the primary quench exchanger the temperature further decreases to about 760 K. It is very important to take the adiabatic section and the primary quench zone into account because the conversion still increases significantly in this part of the cracker. The simulation results and the industrial data are specified in Table 5.6. The most important differences are found for methane and ethylene. However, considering the accuracy of these industrial data it can be concluded that there exists in general a good agreement between the industrial and simulated product yields.

Product	Simulated Product Yields (wt %)	Industrial Product Yields (wt %)
Hydrogen	1.4	1.6
Methane	20.3	19.3
Acetylene	1.0	0.8
Ethylene	34.9	35.2
Ethane	3.3	2.9
Propylene	16.4	17.0
Propane	15.2	15.7
Butadiene	1.1	1.9
1-Butene	0.5	1.2
iso-Butene	0.4	0.2
2-Butene	0.2	-
iso-Butane	0.2	0.1
n-Butane	0.1	0.2
Benzene	1.4	-

Table 5.6: Comparison between simulated and industrially measured product yields (wt %) for an industrial Kellogg Millisecond furnace [Simulation Conditions: CIT = 903 K; COT = 1160 K; CIP = 0.23 MPa; COP = 0.18 MPa; F: 3.3 10^{-2} kg s^{-1}; δ = 0.33 kg /kg]

5.4   Gas oil Cracking Furnace

In this section a Lummus furnace fed with gas oil is simulated. The main dimensions and operating conditions of the simulated furnace are summarized in Table 5.7. Four reactors of the 4/2/1 split type (i.e., four inlets and one outlet for each coil) are suspended in the furnace. The process gas makes six passes through the furnace. A front and top view of the furnace are shown in Figure 5.15. The different passes of the reactor coil through the furnace have different diameters due to the split coil concept. The furnace is heated by means of 20 long flame burners in the furnace floor. The position of the burners is indicated in Figure 5.15. A detailed PIONA weight fraction distribution of the gas oil cracked in these coils is summarized in Table 5.8.

FURNACE	
Furnace length	8.00 m
Furnace height	12.33 m
Furnace width	3.00 m
Thickness refractory material	0.16 m
Thickness insulation material	0.08 m
Number of burners	20
Heat input	22.5 MW
REACTOR COIL	
4/2/1 split coil	
Number of reactors	4
Reactor length	45.60 m
Reactor diameter (int)	0.08 m / 0.12 m / 0.16 m
Wall thickness	0.01 m / 0.01 m / 0.01 m
PROCESS CONDITIONS	
Total Flow rate	3.28 kg s^{-1}
Steam dilution	0.40 kg/kg
Coil Inlet Temperature (CIT)	866 K
Coil Inlet Pressure (CIP)	0.22 MPa
Coil Outlet Temperature (COT)	1135 K
Coil Outlet Pressure (COP)	0.17 MPa

Table 5.7: Furnace and reactor geometry. Operating conditions used in the Lummus furnace
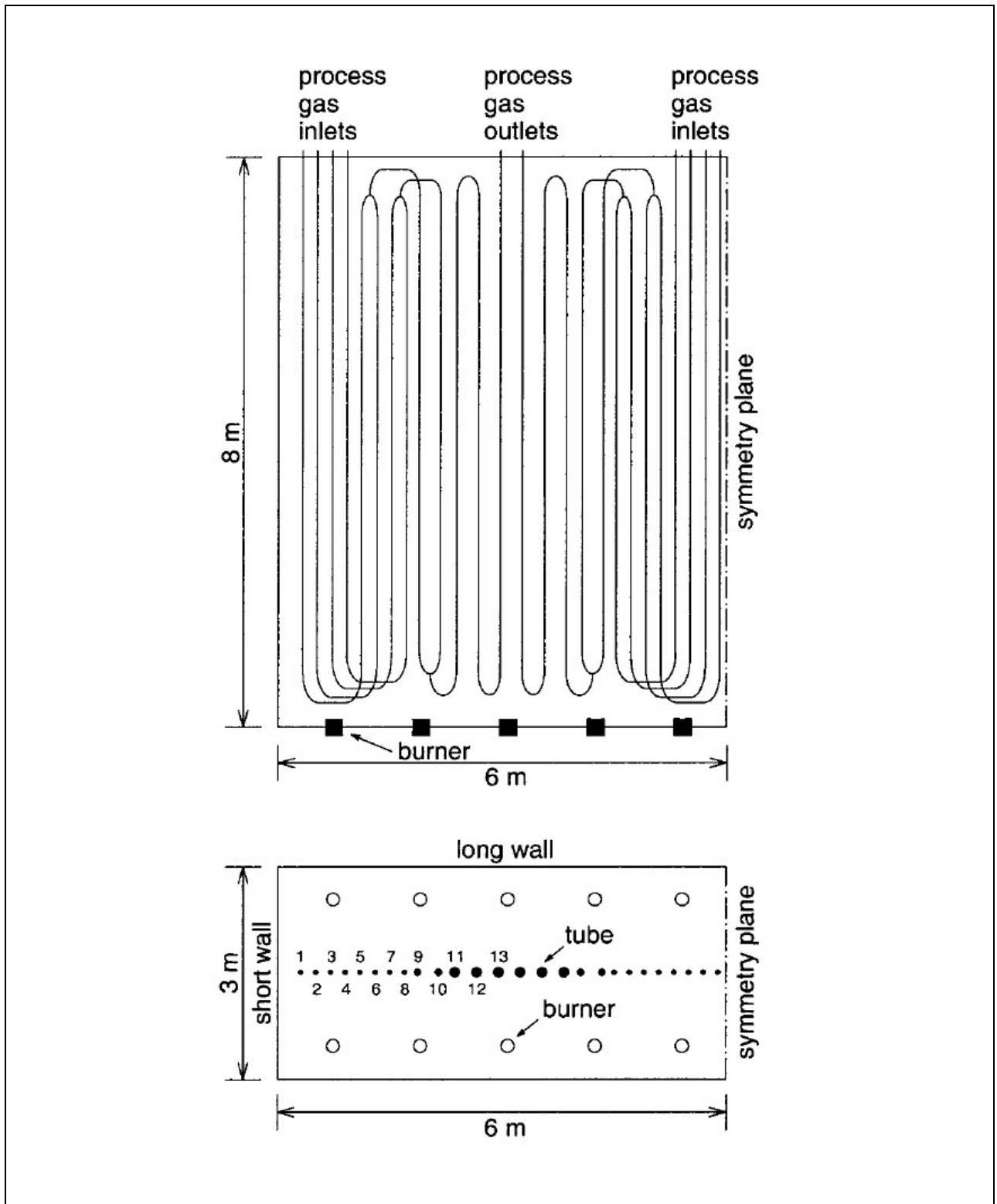
Figure 5.15: Gas oil cracking furnace: front and top views of the Lummus furnace

(wt%)	P	I	O	N	A
C_3	0.07	-	-	-	-
C_4	4.42	0.64	0.07	-	-
C_5	8.11	5.52	-	0.27	-
C_6	6.75	6.40	-	1.99	2.31
C_7	5.92	5.45	-	3.65	1.06
C_8	4.40	6.65	-	2.18	0.40
C_9	3.50	6.25	-	1.04	0.37
C_{10}	2.64	4.97	-	0.11	0.64
C_{11}	1.92	2.49	-	0.23	0.69
C_{12}	1.49	1.24	-	0.03	0.03
C_{13}	1.07	1.12	-	-	-
C_{14}	1.51	-	-	-	-
C_{15}	0.56	0.46	-	-	-
C_{16}	0.41	0.08	-	-	-
C_{17}	0.34	0.16	-	-	-
C_{18}	0.20	-	-	-	-
C_{19}	-	0.09	-	-	-
Sum	43.31	41.62	0.07	9.50	5.50

Table 5.8: Detailed PIONA weight fractions (wt%) of the gas oil fraction

Similar to the Millisecond Furnace in section 5.3 a 1-dimensional reactor model is used for the simulation of the reactor. As seen in section 5.2 the necessity of using more dimensional models for heavier feedstocks decreases. Moreover, the data provided by industry are error-prone and do not only relate to the gas oil furnace because the formed ethane and propane are cracked further in a separate ethane cracker. The calculated heat flux profile for the industrial gas oil cracker is shown in Figure 5.16, while the tubeskin and the process gas temperature are shown in Figure 5.17. The results in Table 5.9 show that there exists a good agreement between the industrial and simulated product yields considering the accuracy of the measured product spectrum.
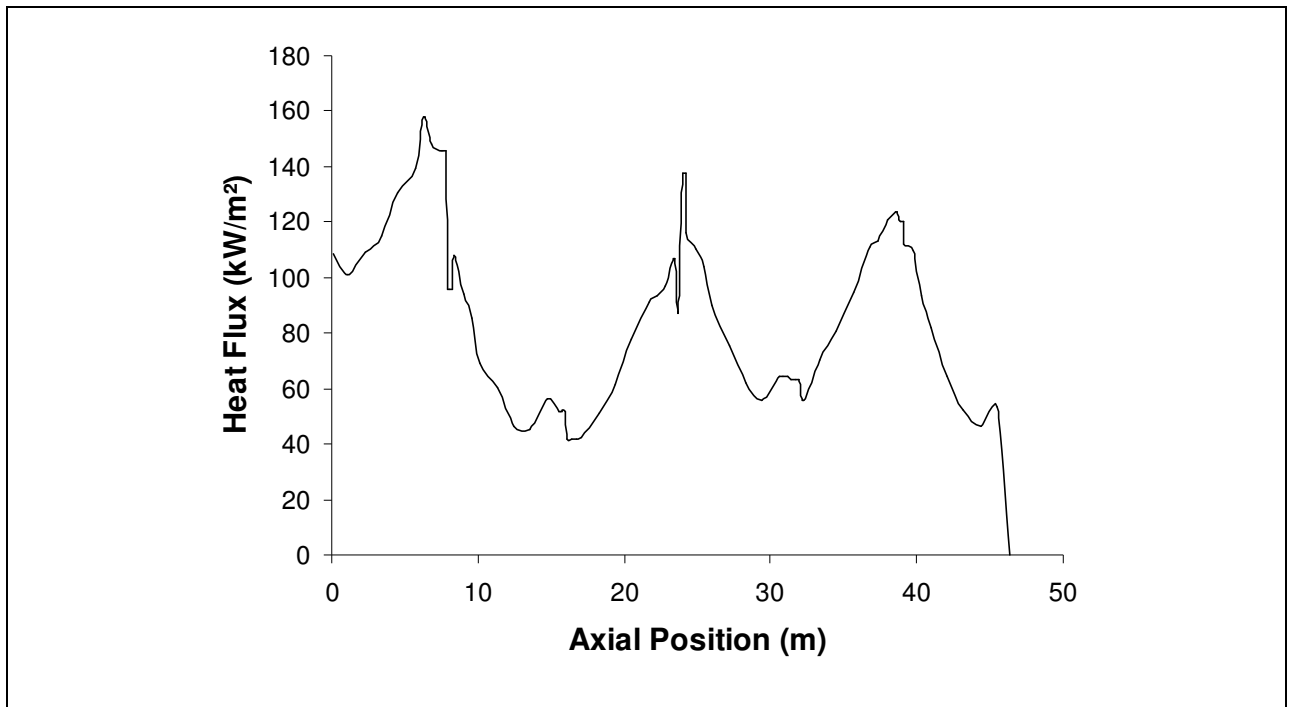
Figure 5.16: Heat flux from the furnace to the reactor as function of the axial position in the coil
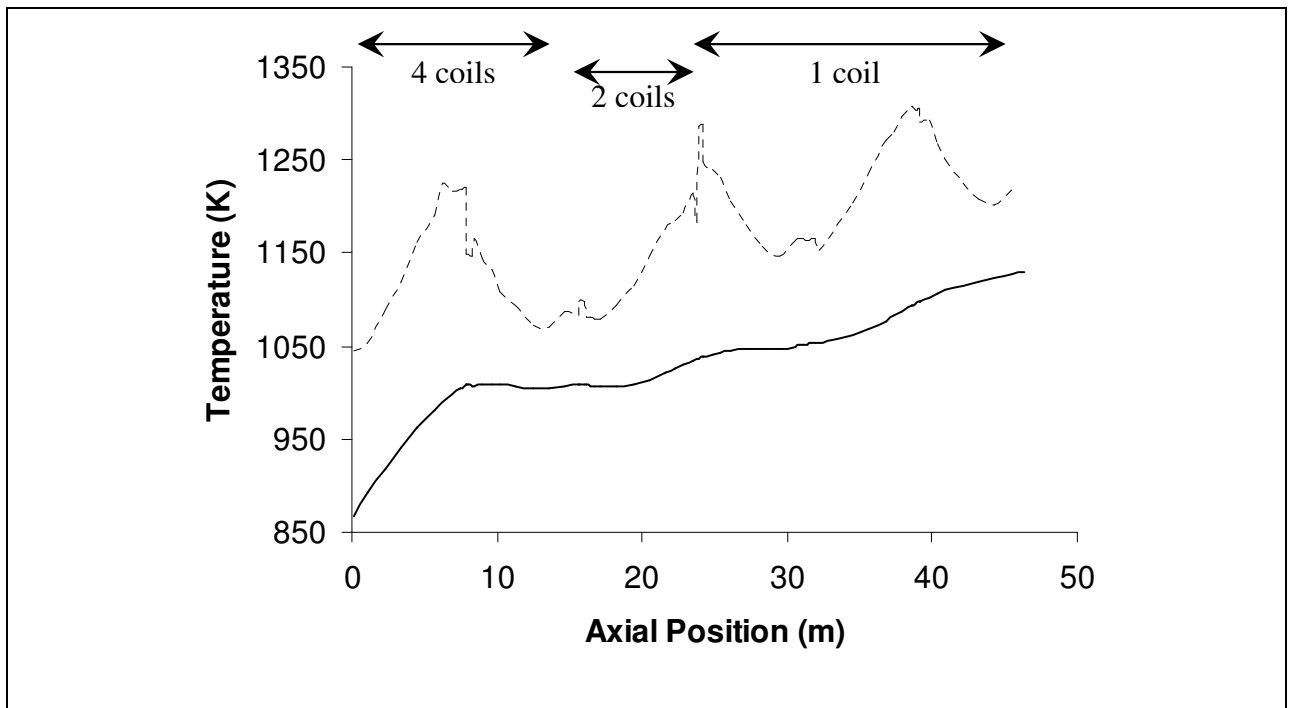
Figure 5.17: Process gas temperature and internal tube skin temperature as a function of the axial position in the reactor coil; —— process gas temperature; - - - tube skin temperature

Product	Simulated Product Yields (wt %)	Industrial Product Yields (wt %)
Hydrogen	1.0	1.4
Methane	16.3	16.3
Acetylene	0.5	0.4
Ethylene	31.5	32.7
Propylene	15.3	15.8
Sum C4-olefines	9.6	7.9
Butadiene	5.7	
1-Butene	1.4	-
iso-Butene	0.6	-
2-Butene	1.9	-
C5+	23.8	23.3

Table 5.9: Comparison between simulated and industrially measured product yields (wt %) for an industrial gas oil cracking furnace [Simulation Conditions: CIT = 866 K; COT = 1135 K; CIP = 0.23 MPa; COP = 0.18 MPa; F: 3.28 kg s^{-1}; δ = 0.4 kg /kg]

5.5   Conclusions

The simulation of industrial steam cracking furnaces demands a coupled simulation of the reactor and the furnace. First an industrial ethane cracking furnace is simulated. Comparison of the simulation results obtained with a 1-dimensional and 2-dimensional reactor model makes it possible to estimate the importance of radial temperature gradients on the simulation results. This comparison shows that for ethane steam cracking important radial gradients exist, not only for the temperature but also for the molecular and in particular the radical species. These profiles are the origin for small but significant differences between the simulated product yields. The effects on the product yields for heavier feedstocks become smaller because the necessary heat fluxes for heavier feedstocks are lower and the radial process gas diminishes. The same reason explains also why for pilot plant reactors the differences between the simulated product yields with the 2-dimensional and 1-dimensional reactor model are almost non-existing. Using the 2-dimensional

reactor model is more important for describing coke formation because the 2-dimensional reactor model allows to account for the coke precursor concentrations adequately and, hence, to properly simulate the coking rates in an industrial ethane steam cracker with a fundamental coking model.

Next to an industrial ethane cracking furnace also an industrial propane cracking furnace and an industrial gas oil cracking furnace are simulated. Comparison between the industrial and simulated product yields shows that accurate simulation results are obtained with a 1-dimensional reactor model in both cases. A 1-dimensional reactor model is used for the Kellogg Millisecond furnace because the radial temperature and concentration gradients become smaller (Van Geem et al., 2004). Also for the Lummus furnace fed with gas oil a 1-dimensional reactor model can be applied because for heavier feedstocks the necessity of using more dimensional simulation models is less crucial. From this it cannot be concluded, however, that run lengths can be calculated accurately with 1-dimensional reactor models.

5.6   References

Bird, R.B., Lightfood E.N., Stewart W.E. Transport Phenomena, J. Wiley, New York 1961.

Bird, R.B., Lightfood E.N., Stewart W.E. Transport Phenomena, J. Wiley, New York 2001.

Davies J.T. Turbulence Phenomena, Academic Press, London, 1972.

De Saegher J.J. Modellering van Stroming, Warmtetransport en Reactie in Reactoren voor de Thermische Kraking van Koolwaterstoffen, Ph.D. thesis, Ghent University, 1994.

De Saegher J.J., Detemmerman T., Froment G.F. Three Dimensional Simulation of High Severity Internally Finned Cracking Coils for Olefins Production, Revue de l'Institut Français du Petrole, 51, 246, 1996.

Ennis B.P., Boyd H.B., Orriss R. Olefin manufacture via millisecond pyrolysis, Chemtech, 693, 1975.

Fagley J.C. Simulation of Transport in Laminar, Tubular Reactors and Application to Ethane Pyrolysis, Ind. Eng. Chem. Res., 31, 58, 1992.

Froment G.F., Bishoff K.B. Chemical Reactor Design and Analysis, J. Wiley, New York 1990.

Froment G.F. Kinetics and Reactor Design in the Thermal Cracking for Olefin Production, Chem. Eng. Sci., 47, 2163, 1992.

Heynderickx G.J., Cornelis C.C., Froment G.F. Circumferential Tube Skin Temperature Profiles in Thermal Cracking Coils, AIChE Journal, 38, 1905, 1992.

Heynderickx, G.J., Froment G.F. Simulation and Comparison of the Run Length of an Ethane Cracking Furnace with Reactor Tubes of Circular and Elliptical Cross Sections, Ind. Eng. Chem. Res., 37, 914, 1998.

Heynderickx G.J., Nozawa M. Banded Gas and Nongray Surface Radiation Models for high-Emissivity Coatings, AICHE Journal, 51, 2721-2736.

Hottel H.C., Sarofim A.F. Radiative Transfer, McGraw-Hill, New York, 1967.

Lobo W.E., Evans J.E. Heat Transfer in the Radiant Section of Petroleum Heaters, Transactions of the American Institute of Chemical Engineers, 35, 743–778, 1939.

McConnell C.F. Head B.D. Pyrolysis of Ethane and Propane, 1981.

Orriss R., Yamaguchi H. Idemitsu's Chiba ethylene plant proves modern technology, Oil & Gas J., 9, 27, 1987.

Plehiers P.M. Rigoureuze Modellen voor de Simulatie van Fornuizen voor de Thermische Kraking van Lichte Koolwaterstoffen, Ph.D. thesis, Ghent University, 1989.

Plehiers P.M., Froment G.F. The Uno-Quattro Coil: High Severities for Increased Ethylene Selectivity, Ind. Eng. Chem. Res., 30, 1081, 1991.

Plehiers P.M., Froment G.F. Firebox Simulation of Olefin Units, Chem. Eng. Com., 80, 81, 1989.

Rao M.V.R., Plehiers P.M., Froment G.F. The Coupled Simulation of Heat Transfer and Reaction in a Pyrolysis Furnace, Chem. Eng. Sci., 43, 1222, 1988.

Reyniers G.C., Froment G.F., Kopinke F.D., Zimmerman G. Coke Formation in the Thermal Cracking of Hydrocarbons. 4. Modeling of Coke Formation in Naphtha Cracking, Ind. Eng. Chem. Res., 33, 2584, 1994.

Sundaram K.M. Kinetic Modeling of Thermal Cracking as a Basis for Reactor Simulation, PhD Thesis, Ghent University, 1977.

Sundaram K.M., Froment G.F. Comparison of Simulation Models for Empty Tubular Reactors, Chem. Eng. Sci., 34, 117, 1979.

Sundaram K.M., Froment G.F. 2 Dimensional Model for the Simulation of Tubular Reactors for Thermal Cracking, Chem. Eng. Sci., 35, 364, 1980.

Sundaram K.M., Van Damme P.S., Froment G.F. Coke Deposition in the Thermal Cracking of Ethane, AIChE J., 27, 946, 1981.

Valenyi L.J., Song Y., Fagley J.C. Carbon Deposition in Ethane Pyrolysis Reactors, Ind. Eng. Chem. Res., 30, 1078, 1991.

Van Geem K.M., Heynderickx G.J., Marin G.B. A Comparison of One and Two-dimensional Reactor Models for Steam Cracking: Effect on Yields and Coking Rate, AIChE Journal, 50, 173–183, 2004.

Vercammen H.A.J., Froment G.F. An Improved Zone Method for the Simulation of Radiation in Industrial Furnaces, Int. J. Heat Transfer, 649, 1980.

Wauters S., Marin G.B. Computer Generation of a Network of Elementary Steps for Coke Formation during the Thermal Cracking of Hydrocarbons, Chem. Eng. J., 82, 267, 2001.

Wauters S., Marin G.B. Kinetic Modeling of Coke Formation during Steam Cracking, Ind. Eng. Chem. Res., 41, 2379, 2002.

Wauters S., Marin G.B. De Kinetiek van Cokesvorming tidens het Thermisch Krake van Koolwaterstoffen op basis van Elementaire Reacties, Ph.D. thesis, Ghent University, 2001.

Chapter 6:

Scale-Up and Scale-down of Steam Cracking Coils

6.1   Introduction

Scaling up steam cracking coils is a difficult task. Two possible methods are commonly applied: mathematical modeling and direct experimental scale-up (Zlokarnik, 2002). Mathematical modeling is probably the most attractive solution because it has the advantage that once the model is developed, results can be easily gathered and computer simulations take only a limited time (Dente and Ranzi, 1979). Although there is a general consensus about the free radical mechanism several different types of kinetic models are used and developed to simulate the steam cracking process. A distinction can be made between three different types of models: empirical, global, and detailed kinetic models. For industrial practice only the last category is able to provide enough flexibility and accuracy, but developing such a detailed reaction network is a major challenge. On the one hand the size of the reaction network can become huge as the number of reactions and species increases exponentially with the average carbon number of the feedstock (Broadbelt et al., 1994). On the other hand, developing these reaction networks implies that both the thermo-chemistry and kinetic parameters are known. Moreover fundamental kinetic models work with a detailed feedstock composition and obtaining this information for naphthas, gas oils and VGO's is not straightforward. Therefore, direct experimental scale-up is still an interesting option.

In the next paragraphs two direct experimental scale-up approaches for steam cracking coils are discussed. The first one is based on the "severity" concept and scale-up is then performed based on experimental data obtained at the same severity. Applying reaction path analysis on a detailed reaction network shows that two appropriate severity indices uniquely determine the product spectrum. In the second approach the theory of similarity is applied to investigate whether it is possible to construct a small scale unit similar to an industrial one and realize the

same product spectrum under similar conditions. The restriction of working under similar conditions makes scale-up an even more challenging task.

6.2   Two Severity Indices for Scale-Up of Steam Cracking Coils [*]

A commonly applied direct scale-up method is based on the "severity" concept. Scale-up is then performed based on experimental data obtained at the same severity (Shu and Ross, 1982; Szepesy, 1980). This approach is not only used for scale-up, but also for control of process conditions. Ideally, in industry one would like to have a single controllable measure of the severity of the cracking that is independent of the scale of the reactor and that can function as a variable that can be set in order to obtain the desired product spectrum. For this reason the propylene over ethylene yield ratio (P/E-ratio) is still used in industrial practice. However, a single severity index does not unambiguously characterize the products yields (Van Damme et al. 1981, Van Geem et al., 2005). Therefore reaction path analysis is applied to find a set of independent severity indices that is able to uniquely determine the product spectrum and that directly relates to an independent variable, i.e. process condition, such as the dilution, the coil inlet pressure (CIP), the coil outlet temperature (COT).

6.2.1   Selection of severity indices

Product yields depend on process conditions such as temperature, feedstock, dilution, total pressure and residence time. The temperature profile and the partial pressure profile of the reactants in the reactor determine directly the reaction rates and hence characterize the product yields. Other process conditions such as residence time or dilution influence the product yields via the temperature profile and/or the partial pressure. The total pressure and the dilution influence the partial pressures in an obvious way. Van Damme et al. (1984) and Plehiers and Froment (1987) showed that there exists a strong correlation between the residence time and the established temperature profile. These showed that cracking at lower residence times requires higher temperatures to achieve a desired conversion, implying that at a lower residence time reactions with a high activation energy are favored, i.e. C-C and C-H β scission reactions, resulting in a higher selectivity to light olefins. In addition, the selectivity to heavier products such as aromatics will be lower as they are formed by addition reactions with relatively low

[*] Van Geem K.M., Reyniers M.F., Marin G.B. Two severity indices for scale-up of steam cracking coils, Ind. Eng. Chem. Res., 44, 3402-3411, 2005.

activation energies. Also, the definition of the residence time θ in equation [6.1] suggests that the residence time is not an independent variable but that it is a function of the temperature and the pressure profile in the reactor.

$$\theta = \int d\theta = \int \frac{1}{Q} dV = \int \frac{p_t}{F_t \, R \, T} dV \qquad [6.1]$$

As there is only a weak correlation between the temperature profile and the partial pressure profile, at least 2 severity indices are required to characterize the product yields: one providing a measure for the temperature and the other providing a measure for the reactants partial pressure in the reactor coil. For a given feedstock a judicious selection of the latter could possibly allow to account for the partial pressures of all the mixture components and, hence, in combination with a severity index characterizing the temperature profile completely determine the product yields.

6.2.1.1 *Severity Index accounting for the temperature*

In view of the endothermic character of the steam cracking process it is obvious that higher conversions are coupled to higher temperatures. Hence, the most concise measure for the temperature is the feedstock conversion or a severity index that correlates well with the conversion. One of the main problems of using the feedstock conversion is that its definition is straightforward for single components only and even then its use is not trivial; e.g. the conversion cannot exceed 100% while the product distribution still changes. These drawbacks have led to the definition of several other severity indices, e.g. the methane yield, the propylene over ethylene yield ratio, the equivalent reactor volume, etc.

According to Froment and coworkers the best measure for the conversion is the equivalent reactor volume (Van Damme et al., 1975; Froment, 1981; Van Camp et al., 1985; Froment, 1992). The equivalent reactor volume V_E is the volume of an isothermal and isobaric reactor that operates at a reference temperature T_R and a reference pressure p_R, yielding the same conversion as the actual reactor with its temperature and pressure profile.

$$V_E = \int_0^V \frac{p_t T_R}{p_R T} \exp\left[-\frac{E_a}{R}\left(\frac{1}{T} - \frac{1}{T_R} \right) \right] dV \qquad [6.2]$$

The equivalent reactor volume meets all the requirements for an appropriate severity index as its relation with conversion is independent of the operating conditions, the reactor geometry and the feed composition (Van Camp et al., 1985). In addition, unlike the conversion the equivalent reactor volume does not have an upper limit. However, it requires knowledge of the temperature and pressure profile, which is seldom the case in industry. Hence, other severity indices seem more appropriate. Reaction path analysis is applied to select a severity index that correlates well with the temperature in the reactor.

$$S \xrightarrow{k_{C-C}} 2\beta$$
$$\beta + S \xrightarrow{k_{ab}} \mu + H - \beta$$
$$\mu \xrightarrow{k_{\beta}} P_1 + \beta$$
$$2\beta \longrightarrow \left.\right\} \text{Recombination}$$
$$\beta + \mu \qquad \qquad \text{products}$$
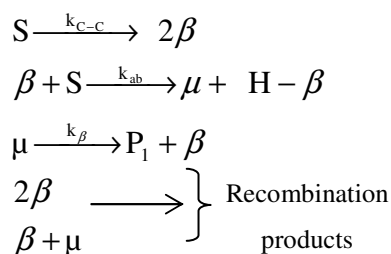
Figure 6.1: Elementary steps in the reaction of a component S via Rice-Herzfeld pyrolysis (Nigam et al., 1992). Simplified reaction network used for the selection of a severity index that is an appropriate measure for the temperature. [k_{C-C} is the reaction rate coefficient of a C-C scission reaction, k_{ab} is the reaction rate coefficient of a hydrogen abstraction reaction, k_{β} is the reaction rate coefficient of a β scission reaction.]

A detailed description of the steam cracking process is only possible using a fundamental reaction network involving hundreds of species and thousands of elementary reactions. However the qualitative features can be presented by a simplified network. The reaction scheme proposed by Nigam et al. (1992) in Figure 6.1 for the Rice-Herzfeld pyrolysis of a single component S is used to find an appropriate measure for the conversion. From the previous paragraphs it is obvious that this index will then also be a good measure for the temperature in the reactor. According to Rice and Herzfeld steam cracking of hydrocarbons proceeds through a free radical mechanism where three important reaction families can be distinguished:

- Carbon-carbon and carbon-hydrogen bond scissions in molecules without radicalar character and the reverse radical radical recombinations.

- Hydrogen abstraction reactions, both intra- and intermolecular. Isomerization reactions are intramolecular hydrogen abstractions.

- Radical addition to olefins and the reverse β scission of radicals, both intra- and intermolecular. Cyclization reactions are intramolecular additions.

In Table 6.1 characteristic values for the activation energies are given for the different types of reactions of these families. Hydrogen abstraction reactions and addition reactions are bimolecular reactions that have low activation energies. β scission reactions are monomolecular reactions with high activation energies. Hence, high temperatures and low pressures favor β scission reactions, while low temperatures and high pressures favor addition reactions and hydrogen abstractions.

Reaction Type	Activation Energy (kJ mol^{-1})
Hydrogen abstraction (formation of primary radical)	50
Hydrogen abstraction (formation of secondary radical)	40
Hydrogen abstraction (formation of tertiary radical)	30
β scission of radical (C-C bond breaking)	120
β scission of radical (C-H bond breaking)	170
Addition	20
Isomerization	50

Table 6.1: Characteristic values for the activation energy of the different types of reactions involved in steam cracking (Plehiers, 1989)

Three different types of products are formed via the intermediate μ and β radicals in the simplified reaction network of Figure 6.1: primary products (P_1), products formed via hydrogen abstraction reactions (H-β) and products formed via recombination reactions. The yields of the latter are generally negligible under standard cracking conditions. In the scheme a distinction is

made between two different types of radicals: β radicals with a β character and μ radicals with a μ character (Ranzi et al., 1983). μ Radicals react in unimolecular β scission reactions only. Large radicals formed directly from the feed molecules mainly have a μ character. This does not imply that μ radicals do not take part in reactions such as hydrogen abstractions or addition reactions, but their reaction rate via these types of reactions is much lower than the reaction rate via β scission. Isomerization reactions are also possible for μ radicals, but after isomerization again a β scission takes place. The reaction rate of these isomerization reactions is generally more than one order of magnitude higher than the reaction rate of the subsequent β scission. β and βμ radicals are mainly short radicals with 5 or less carbon atoms that undergo bimolecular reactions such as hydrogen abstractions and addition reactions. These radicals are not only species such as the hydrogen ($H^{\bullet}$) and the methyl radical ($CH_3^{\bullet}$), that do not have any other reaction possibility, but also ethyl ($C_2H_5^{\bullet}$), propyl ($C_3H_7^{\bullet}$), vinylic ($C_2H_3^{\bullet}$ and $C_3H_5^{\bullet}$) and allylic ($C_3H_5^{\bullet}$ and $C_4H_7^{\bullet}$) radicals. All the above mentioned small radicals except hydrogen and the methyl radical also have a μ character. However, compared to the β character, the μ character is less pronounced and becomes only important at higher temperatures. The reason is that radicals such as the ethyl radical and the but-1-en-3-yl radical have no C-C bond in β position, but only a C-H bond. Scission of this C-H bond has a very high activation energy, i.e. 170 kJ mol^{-1}, and hence becomes only important at high temperatures. Consequently these radicals have a β character at low temperatures, while at high temperatures they have both a β character and a μ character.

The elementary steps in the simplified reaction scheme suggest that two reactions are equally important in determining the conversion; the hydrogen abstraction reactions and the C-C scission reaction of the feed molecule. However, the reaction rate of the hydrogen abstraction reaction is significantly higher than the reaction rate of the C-C scission reaction of the feed molecules. The latter is illustrated in Table 6.2, where the sum of the reaction rates of all hydrogen abstraction reactions and the sum of the reaction rates of all C-C scission reactions are given at different positions in the reactor for the cracking of pure n-hexane. In the steady state the rate of initiation and the rate of termination are equal, and the kinetic chain length, defined by the ratio of the rate of propagation to the rate of termination, is equal to the ratio of the rate of propagation to the rate of initiation. For steam cracking of hydrocarbons under standard cracking conditions a kinetic chain length in the order of 100 can then be expected, see the results in Table 6.2. Hence, the reaction rate of the hydrogen abstraction reactions determines the conversion of

the feed component S. The reaction rate of the C-C scission reactions versus the recombination reaction determines the global radical concentration, and thus the concentration of β radicals that can abstract hydrogen from the feed molecule S. Although this conclusion might seem trivial it is not; it indicates that the yields of the products formed via hydrogen abstraction reactions of feed molecules, i.e. the products H-β in the reaction scheme, are directly related to the conversion. One of those products is methane; methane is almost entirely produced from hydrogen abstractions with methyl radicals. This suggests that the methane yield can be considered as an excellent measure for the conversion, and hence as stated in the previous section, for the temperature in the reactor. However the methane yield is not entirely independent of the reactants partial pressures. Van Camp et al. (1985) showed experimentally that the methane yield does indeed depend on the reactants partial pressures, but the dependence is not strongly pronounced. At low severities, i.e. methane yields lower than 12 wt % for cracking of a light naphtha, the methane yield can even be considered as independent of the total pressure (Van Camp et al., 1985). Hence, ideally a second index to characterize the product distribution would be an index that depends on the reactants partial pressure only. To identify this second severity index reaction path analysis is applied again, but this time on an extended version of the reaction scheme proposed by Nigam et al. (1992).

	Reaction rate (mol m^{-3} s^{-1})		
	5 % reactor length	50% reactor length	95% reactor length
$\sum_i r_{i,\text{C}-\text{C scission reactions}}$	$3.42\ 10^{-1}$	$1.71\ 10^{-1}$	$5.45\ 10^{-2}$
$\sum_i r_{i,\text{Hydrogen abstractions}}$	65.05	4.83	2.39

Table 6.2: Calculated values of the reaction rates for all C-C scission reactions and all hydrogen abstraction reactions during the cracking of pure n-hexane. [$\sum r_{i,\text{C-C scission reactions}}$: the sum of the reaction rates of all C-C scission reactions of hexane; $\sum r_{i,\text{Hydrogen abstractions}}$: the sum of the reaction rates of the hydrogen abstraction reactions by all radicals]

6.2.1.2 *Severity index accounting for the pressure*

In the reaction scheme of Nigam et al. (1992) in Figure 6.1 only a first distinction is made between the different formed products. Indeed, although sufficient for describing the reactions affecting the conversion of a single component S, to understand the formation of all the important products the reaction scheme of Nigam et al. (1992) in Figure 6.1 requires more detail. Therefore the reaction scheme in Figure 6.1 is extended with some new elementary steps, see Figure 6.2. Again the feedstock is represented by a single component S. μ, μ', μ'' represent radicals with a μ character, reacting only via monomolecular reactions, β represents radicals with a β character, reacting mainly via bimolecular reactions. P_1 represents the olefinic products from the β scission of μ radicals originating from the feed. P_2 represents products formed from addition reactions by β radicals and products P_1. P_3 represents products formed from hydrogen abstraction reactions from products P_1. β–H represents products formed through hydrogen abstraction reactions of β radicals. In Table 6.3 the products formed during the cracking of a light naphtha feedstock are classified according to these four specific groups.

$$S \xrightarrow{k_{C-C}} 2\beta$$
$$S + \beta \xrightarrow{k_{ab1}} \mu + H-\beta$$
$$\mu \xrightarrow{k_{\beta1}} P_1 + \beta$$
$$P_1 + \beta \xrightarrow{k_{ad}} \mu' \xrightarrow{k_{\beta2}} P_2 + \beta$$
$$P_1 + \beta \xrightarrow{k_{ab2}} \mu'' + H-\beta$$
$$\mu'' \xrightarrow{k_{\beta3}} P_3 + \beta$$
$$\beta \xrightarrow{k_{\beta4}} H^\bullet + P_1$$
$$\left.\begin{array}{l} 2\beta \\ \beta + \mu \end{array}\right\} \longrightarrow \quad \begin{array}{c} \text{Recombination} \\ \text{products} \end{array}$$
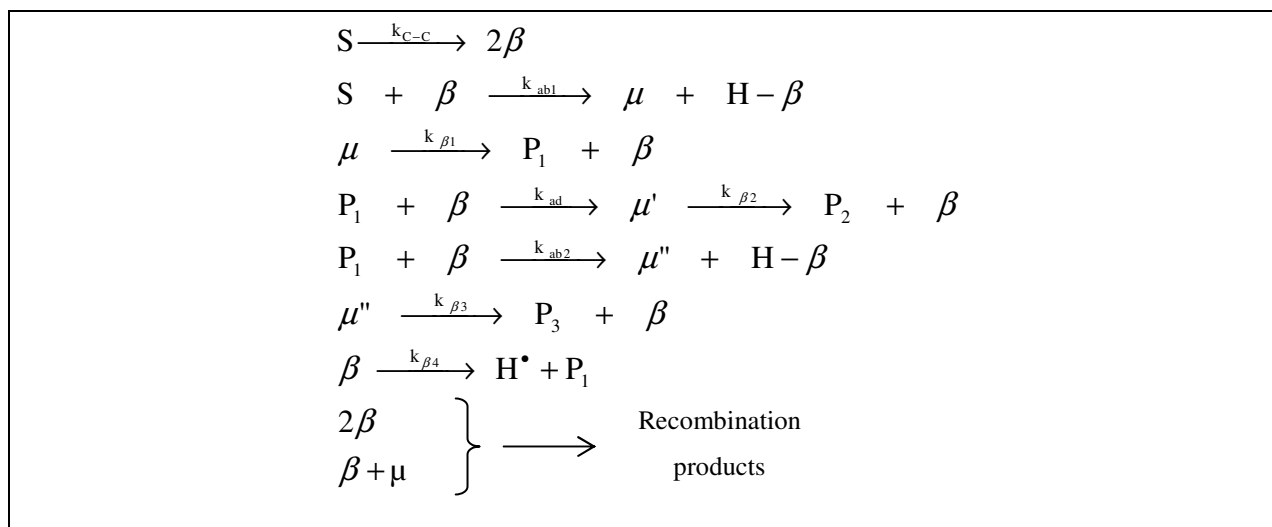
Figure 6.2: Set of elementary steps for the Rice-Herzfeld pyrolysis of a single component S. Reaction network used to identify a severity index that is a reliable measure for the reactants partial pressures. [k_{C-C} is the reaction rate coefficient of a C-C scission reaction, k_{ab1} and k_{ab2} are the reaction rate coefficients of hydrogen abstraction reactions, k_{ad} the reaction rate coefficient of an addition reactions and $k_{\beta1}$, $k_{\beta2}$ and $k_{\beta3}$ the reaction rate coefficients for the β scission reactions.] (Van Geem et al., 2005)

The reaction scheme presented in Figure 6.2 considers all important reaction possibilities. As stated before, cyclization reactions can be considered as internal addition reactions and isomerization reactions as internal hydrogen abstractions. As stated previously some β radicals also have a μ character at high temperatures and hence, the β scission of these β radicals needs to be taken up in the reaction scheme too:

$$\beta \xrightarrow{\ k_{\beta 4}\ } H^{\bullet} + P_1 \qquad\qquad [6.3]$$

with $k_{\beta 4}$ the reaction rate coefficient.

P_1	P_2	P_3	H-β
ethylene	cyclopentadiene	acetylene	hydrogen
propylene	benzene	methyl-acetylene	methane
1-butene		butadiene	ethane
2-butene			propane
isobutene			n-butane

Table 6.3: Classification of the main products into 4 groups according to a simplified reaction scheme. [P_1 are products from the β scission of μ radicals originating from the feed. P_2 are products formed from addition reactions of β radicals and products P_1. P_3 are products formed from hydrogen abstraction reactions from products P_1. H– β are products formed through hydrogen abstraction reactions of β radicals.]

Mathematical expressions for the yields of the products considered in the reaction scheme of Figure 6.2 can be obtained by implementing the rate equations in a reactor model. In this case a 1-dimensional reactor model is used. The set of differential equations for the radicals and products can be formally uncoupled and integrated (Himmelblau et al., 1967). The yields for the different products P_1, P_2, P_3 and H-β are then given by equations [6.4], [6.5], [6.6] and [6.7].

$$Y_{P_1} = \int_0^{\ell} \left(k_{\beta 1}\, p_{\mu} + k_{\beta 4} p_{\beta} - k_{ad}\, p_{\beta}\, p_{P_1} \right) dx \qquad\qquad [6.4]$$

$$Y_{P_2} = \int_0^{\ell} k_{\beta 2}\, p_{\mu'}\, dx \qquad\qquad [6.5]$$

$$Y_{P_3} = \int_0^\ell k_{\beta 3}\, p_{\mu''}\, dx \tag{6.6}$$

$$Y_{H-\beta} = \int_0^\ell k_{ab1}\, p_F p_\beta\, dx \tag{6.7}$$

In these equations p_F is the partial pressure of the feed molecule F, p_1 is the partial pressure of the primary products P_1, p_μ is the partial pressure of μ radicals, $p_{\mu'}$ is the partial pressure of μ' radicals, $p_{\mu''}$ is the partial pressure of μ'' radicals and p_β is the partial pressure of β radicals. Applying the Pseudo Steady State Approximation for the μ' radical

$$k_{ad} p_\beta p_{P1} - k_{\beta 2}\, p_{\mu'} \approx 0 \tag{6.8}$$

allows to transform equations [6.5] and [6.6] in equations [6.9] and [6.10] respectively.

$$Y_{P_2} = \int_0^\ell k_{ad}\, p_\beta p_{P1}\, dx \tag{6.9}$$

$$Y_{P_3} = \int_0^\ell k_{ab2}\, p_\beta p_{P1}\, dx \tag{6.10}$$

The classification of the products into 4 groups is only a first distinction. In several groups a second distinction is possible. Consider for example the group of products P_1. A further differentiation is possible based on the type of the μ radical from which the product P_1 originates, i.e. primary, secondary or tertiary. Primary μ radicals yield mainly ethylene as primary product; while secondary and tertiary radicals lead to longer olefins. The activation energy for the formation of tertiary and secondary radicals by hydrogen abstractions of the feed is significantly lower than for primary radicals, see Table 6.1. This will result in different profiles in the reactor for products P_1 although they are classified in the same group. This is for example the case for the products ethylene and 1-butene.

In the category of products formed by hydrogen abstraction reactions H-β a further differentiation is a direct consequence of the fact that radicals with 2 or more carbon atoms have both a β character and a μ character at high temperatures. Methane and hydrogen are products

originating from pure β radicals. As stated earlier, the yields of methane and hydrogen depend strongly on the temperature profile and increase with increasing temperature. This is however not the case for products such as ethane. At low temperatures ethane is mainly formed via hydrogen abstraction reactions of the ethyl radical but at higher temperatures the ethyl radical can also decompose yielding ethylene at the expense of ethane.

$$C_2H_5^\bullet \longrightarrow \begin{array}{l} \xrightarrow{\text{R-H}} C_2H_6 \qquad\qquad E_a = 50\,\text{kJ mol}^{-1} \\[2em] \longrightarrow C_2H_4 + H^\bullet \qquad E_a = 170\,\text{kJ mol}^{-1} \end{array}$$
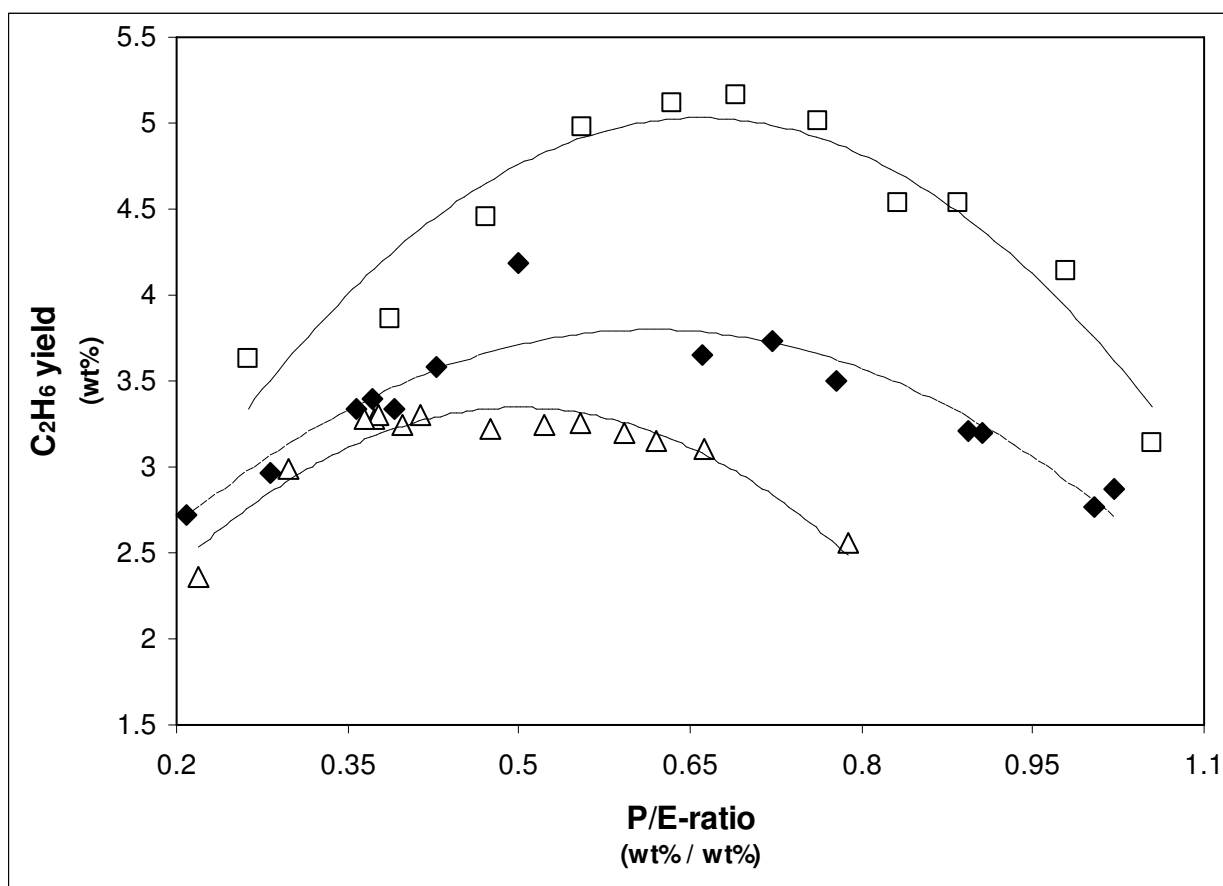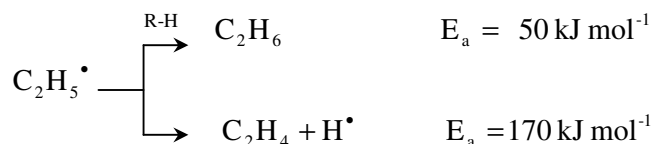
Figure 6.3: Ethane yield versus propylene over ethylene yield ratio for the cracking of a naphtha feedstock in the LPT pilot plant reactor (coil 2) at different dilutions. [□ 0.2 kg steam/ kg HC, COT: 1070 -1130 K; ♦ 0.4 kg steam/ kg HC, COT: 1070 -1130 K; Δ 0.8 kg steam/ kg HC, COT: 1070 -1130 K].

The competition of the unimolecular β scission reactions with the bimolecular hydrogen abstraction for the ethyl radical results in a strong influence of the temperature and the pressure on the ethane yield. This is illustrated in Figure 6.3, where the experimentally observed ethane yield is plotted as a function of the P/E-ratio for the cracking of a light naphtha feedstock. The same reasoning also holds for products such as propane, but the yield of propane is significantly lower. Propane is mainly formed via hydrogen abstraction reactions of n-propyl radicals, but here an additional β scission of the n-propyl radical is possible (second reaction):

$$
n-C_3H_7{}^{\bullet} \longrightarrow
\begin{array}{ll}
C_3H_8 & E_a = 50 \text{ kJ mol}^{-1} \\
C_2H_4 + CH_3{}^{\bullet} & E_a = 120 \text{ kJ mol}^{-1} \\
C_3H_6 + H^{\bullet} & E_a = 170 \text{ kJ mol}^{-1}
\end{array}
$$
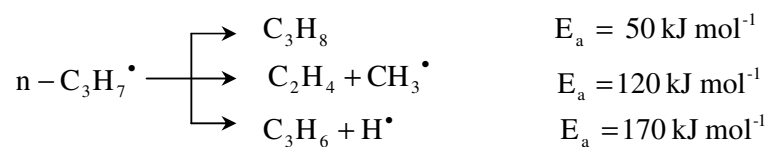
This reaction has a lower activation energy (120 kJ mol^{-1}) than the activation energy of β scission reaction of the ethyl radical (170 kJ mol^{-1}). Hence, the selectivity towards propane from the n-propyl radical is significantly smaller than the selectivity towards ethane from the ethyl radical.

The ethyl radical cannot decompose via a C-C β scission but only via a C-H β scission. This characteristic behavior of the ethyl radical can be used to great advantage. The ratio of the ethylene yield to the ethane yield is indeed an indication of which path is preferred for the ethyl radical; at low partial pressures and high temperatures the route yielding ethylene is favored, at high partial pressures and low temperatures the route yielding ethane. Based on the reaction scheme presented in Figure 6.2 the following mathematical expression for the ethylene to ethane yield ratio (C_2H_4/C_2H_6 ratio) can be obtained if a 1-dimensional reactor model is assumed:

$$
\frac{C_2H_4}{C_2H_6} = \frac{\int_0^1 \left(k_{\beta 1}\, p_\mu + k_{\beta 4} p_\beta - k_{ad}\, p_\beta\, p_{P_1} \right) dx}{\int_0^1 \left(k_{ab1}\, p_F\, p_\beta \right) dx}
\tag{6. 11}
$$

Ethylene is formed via monomolecular β scission reactions and disappears via bimolecular addition reactions. Ethane is formed via bimolecular hydrogen abstractions. Hence, it is obvious that modifying the partial pressure of the reactants has a strong influence on the ethylene to ethane ratio. For instance, increasing the dilution favors monomolecular reactions leading to

ethylene formation over bimolecular reactions producing ethane and consuming ethylene. Consequently the value of the ethylene to ethane ratio increases considerably. This suggests that the ethylene to ethane ratio could function as a severity index that is strongly influenced by the partial pressure of the reactants, providing that its temperature dependence is negligible. However, higher temperatures favor β scission reactions over addition and hydrogen abstraction reactions, leading to higher values of this ratio at higher temperatures. Fortunately, the dependence of the methane yield on the partial pressure of the reactants is weak, and hence a combination of the ethylene to ethane yield ratio with the methane yield could allow determining the product yields in a unique way.

6.2.1.3 *Validation*

Validation of this scale-up approach has been carried out using both simulation and experimental results for a wide range of reactor geometries and scales. Experimental data for a light naphtha feedstock are used to illustrate that the combination of the ethylene to ethane yield ratio and the methane yield characterize the product yields unambiguously under a given set of reactor conditions. Simulations using a 2-dimensional reactor model were performed for n-butane cracking in different reactor geometries, aiming at identical values for the ethylene to ethane yield ratio and the methane yield. The use of a 2-dimensional reactor model is necessary since important radial gradients exist in industrial tubular reactors, not only for the temperature but also for the molecular and in particular for the radical species making the 1-dimensional reactor model insufficient (Van Geem et al., 2004 [a]). The 2-dimensional reactor model equations are specified in Bird et al. (2001), Froment and Bischoff (1990) and Van Geem et al. (2004 [a]). The reactor model is coupled to a radical kinetic model for the cracking of light fractions consisting of 60 molecular and 68 radical species and over 1200 reactions (Clymans and Froment, 1984).

The following reactors were simulated: the LPT pilot plant reactor, a Lummus SRT-I reactor and a 4-2-1 split coil. The characteristics for the reactors used in the simulations and the conditions for realizing identical methane yields and ethylene to ethane yield ratios (C_2H_4/C_2H_6) in the different reactors are specified in Table 6.4. As feedstock n-butane was chosen.

	Lummus SRT-I reactor	LPT Pilot Reactor	4-2-1 Split coil
Reactor length (m)	100.96	12.38	40
Tube diameter (cm)	12.4	0.9	7.6 – 11.4 – 15.2
CIP (MPa)	0.3	0.3	0.3
COP (MPa)	0.15	0.25	0.19
CIT (K)	873	873	873
COT (K)	1130	1139	1139
δ (kg steam/kg HC)	0.77	0.85	0.71
Flow rate (kg/h)	3500	4	5000
Residence time (s)	0.575	0.363	0.273
SEVERITY INDICES			
CH_4 yield (wt %)	20.8	21.0	20.9
$C_3^-/C_3^=$ ratio (wt % / wt %)	4.54	4.54	4.54
P/E-ratio (wt % / wt %)	1.96	1.96	1.96
C_2H_4/C_2H_6 ratio (wt % / wt %)	9.20	9.20	9.21
CONVERSION (wt %)			
C_4H_{10} conversion	92.4	92.6	92.5
PRODUCT YIELDS (wt %)			
H_2	3.1	3.1	3.1
CH_4	20.8	21.0	20.9
C_2H_4	34.5	34.8	34.7
C_2H_6	3.7	3.8	3.8
C_3H_6	17.6	17.8	17.7
C_4H_6	2.7	2.7	2.8
$1-C_4H_8$	1.5	1.5	1.5
C_6H_6	2.7	2.5	2.6

Table 6.4: The characteristics for the different reactors, the conditions used for realizing the same value of both the methane yield and the C_2H_4/C_2H_6 ratio and the simulated conversion and product yields for the cracking of pure n-butane

The results in Table 6.4 are remarkable in view of the huge difference in size of the selected reactors. Not only the reactor length but also the diameter and even the reactor configuration differ significantly for the three reactors. The length of the reaction section of the largest coil, i.e. the Lummus SRT-I ($l = 101.0$ m), is more than eight times the length of the smallest one, i.e. the LPT pilot plant coil 1 ($l = 12.4$ m). Also the residence time in the different reactors varies strongly; from 0.577 s in the Lummus SRT-I reactor, over 0.363 s in the pilot reactor to 0.273 s in the 4-2-1 split coil. Hence, it is obvious that direct experimental scale-up for the steam cracking process does not require identical values for the residence time.
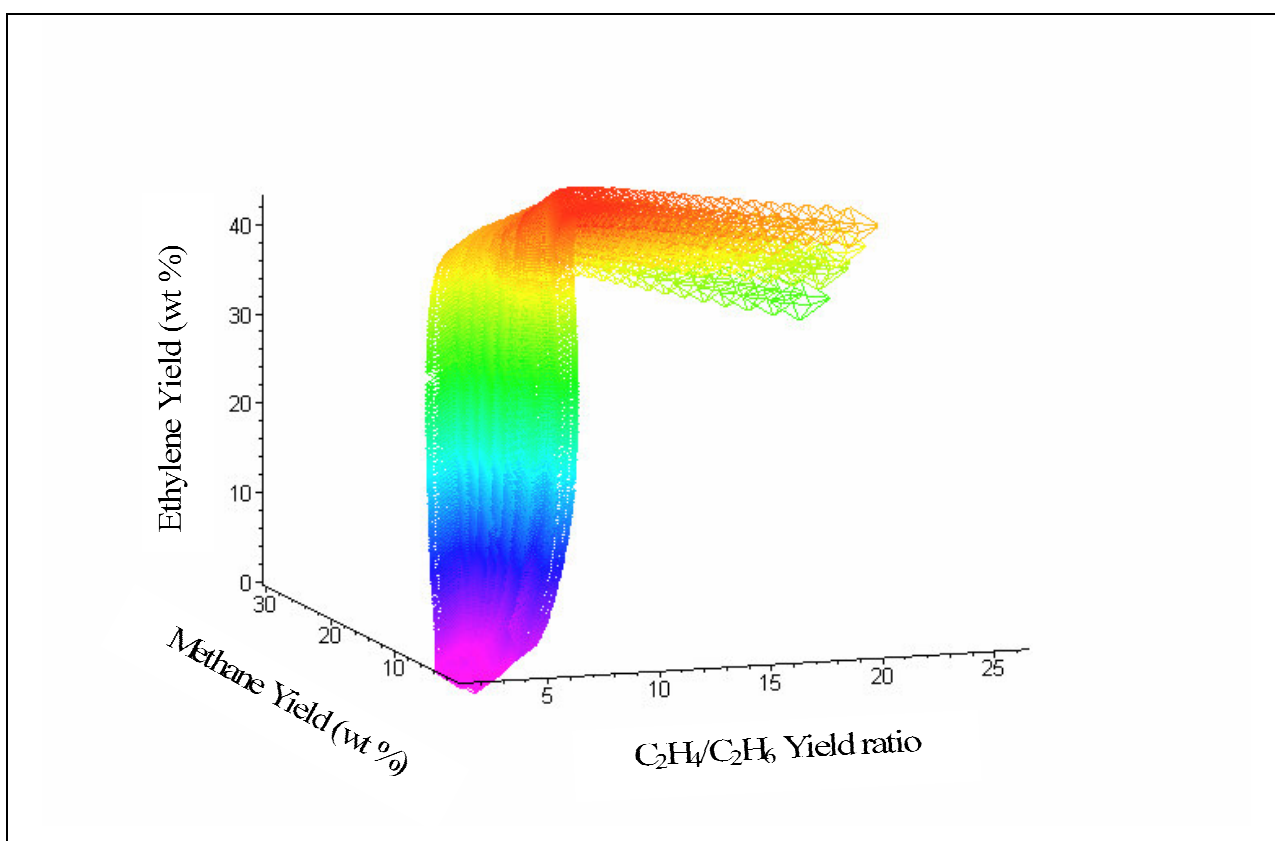
Figure 6.4: Ethylene yield as a function of ethylene to ethane yield ratio and the methane yield. [*Pilot Plant:* Feed flow rate: 3.0-4.3 kg h^{-1}, dilution: 0.2 – 1.0 kg steam/ kg HC, COT: 1000-1150 K, Conversion: 25%-97%; *Lummus SRT-I reactor:* Feed flow rate: 3500 kg h^{-1}, dilution: 0.77 kg steam/ kg HC, COT: 1050-1140 K, Conversion: 25%-90%]

The simulation results for n-butane cracking make it also possible to graphically illustrate the proposed approach. According to the developed theory the yield of a specific product is only function of two parameters independent of the conditions and reactor type/geometry. Hence, there should exist a unique surface in the 3-D space for a product yield as function of the two severity indices, if the feedstock remains unchanged. Consider the results in Figure 6.4 for the ethylene yield. The conditions used to generate these data are obtained from both a pilot and an industrial reactor. Every point corresponds with a set of different experimental conditions. In this specific case results from more than 200 different simulations have been used. The results in Figure 6.4 show that for the ethylene yield such a surface does exist. Hence, it can be concluded that for the ethylene yield there exists a unique relation between the ethylene yield and the 2 proposed severity indices when the feedstock remains unchanged. Similar plots can be constructed for other products such as hydrogen, ethane, propylene or products from the C4-fraction. This implies that also for these products the yield is only dependent on the values of the 2 proposed severity indices.

Specific density, 15/4°	0.676
PIONA-analysis	
Paraffins (wt %)	43.3
Iso-paraffins (wt %)	38.3
Olefines (wt %)	0.66
Naftenes (wt %)	13.19
Aromatics (wt %)	3.88
Average molar H/C ratio	2.26
Average molecular weight (kg kmol^{-1})	85.67

Table 6.5: Characteristics of the naphtha feedstock

The same good agreement is also observed experimentally. Two different reactor geometries have been used to crack the same naphtha feedstock; the LPT pilot plant coil 2 with a length of 23 m and the compact Uno-Quattro coil (Plehiers and Froment, 1991) with a length of 4 m. In

Table 6.5 the characteristics (i.e. specific density, average molecular weight, PIONA weight fractions, H/C-ratio) of the naphtha feedstock are shown. The conditions in the traditional single coil reactor have been varied to realize the same ethylene to ethane yield ratio and the same methane yield as those obtained in the Uno Quattro coil.
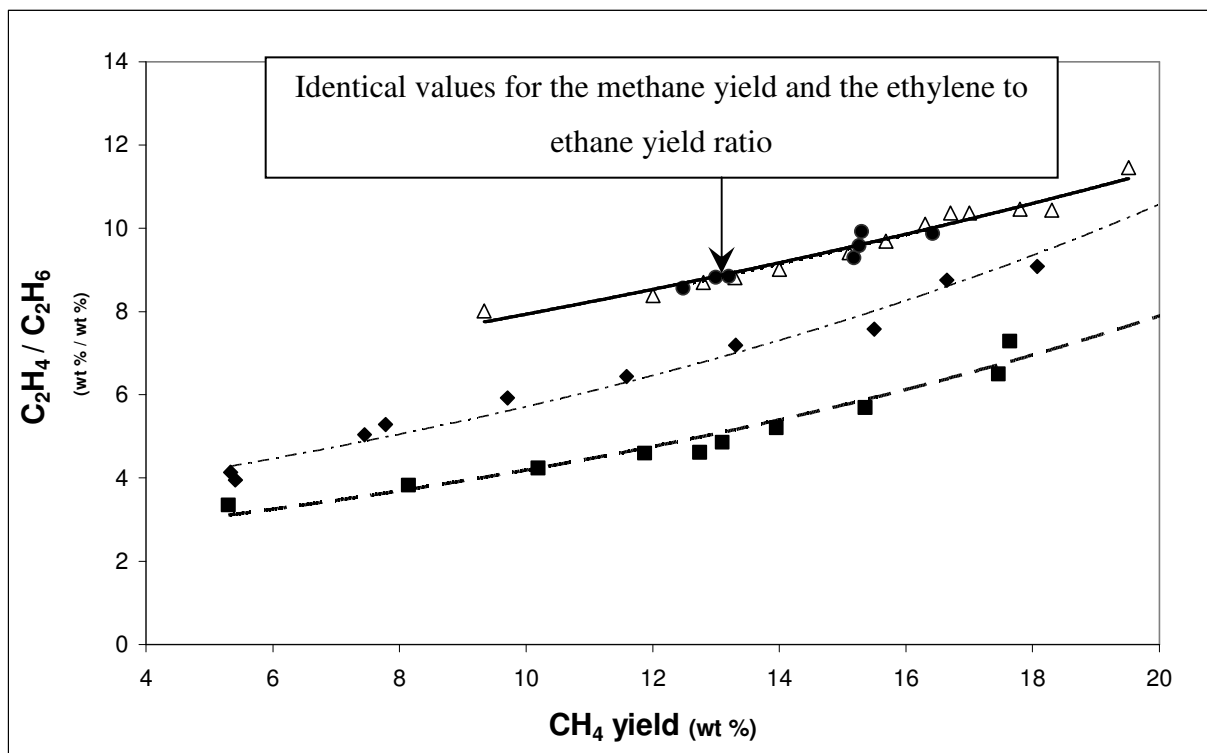
Figure 6.5: The ethylene to ethane yield ratio (C_2H_4/C_2H_6) as a function of the methane yield (CH$_4$ yield) for naphtha cracking experiments carried out in the LPT pilot plant reactor (coil 2) and the Uno-Quattro coil (Plehiers et al., 1991). [■ Single coil reactor. Feed flow rate: 4.3 kg h^{-1}, dilution: 0.2 kg steam/ kg HC, COT: 1070-1130 K; ♦ Single coil reactor. Feed flow rate: 3.2 kg h^{-1}, dilution: 0.4 kg steam/ kg HC, COT: 1070-1130 K ; Δ Single coil reactor. Feed flow rate: 2.1 kg h^{-1}, dilution: 0.8 kg steam/ kg HC, COT: 1070-1130 K; ● Uno-Quattro coil. Feed flow rate: 5.5 kg h^{-1}, dilution: 0.6 kg steam/ kg HC, COT: 1100-1155 K]

In Figure 6.5 the ethylene to ethane yield ratio is plotted versus the methane yield for both reactors. These results clearly indicate that a single severity index cannot uniquely determine the product distribution. A single value of the methane yield corresponds with different values for the ethylene to ethane yield ratio and vice versa. In a specific case, see Figure 6.5, identical values for the ethylene to ethane yield ratio and the methane yield ratio are experimentally

observed for the different reactors. The product yields corresponding to these experiments are specified in Table 6.6. A good agreement is observed between the product yields obtained in the pilot plant and in the Uno-Quattro coil despite the differences in the operating conditions and in the geometry of the reactors. Also in the other cases of Figure 6.5, where identical values for the ethylene to ethane yield ratio and the methane yield ratio are experimentally observed for the different reactors, a good agreement is observed between the product yields.

	Single Coil Reactor	Uno-Quattro coil
CIP (MPa)	0.22	0.22
COP (MPa)	0.18	0.20
CIT (K)	873	873
COT (K)	1103	1133
δ (kg steam/kg HC)	0.8	0.6
Flow rate (kg/h)	2.1	5.5
SEVERITY INDICES		
CH_4 yield (wt %)	13.3	13.2
C_2H_4/C_2H_6 ratio (wt % / wt %)	8.8	8.9
PRODUCT YIELDS (wt %)		
H_2	0.7	0.7
CH_4	13.3	13.2
C_2H_4	28.3	28.5
C_2H_6	3.2	3.2
C_3H_6	16.7	16.7
C_4H_6	4.7	4.8
C_6H_6	5.2	5.1

Table 6.6: Experimentally observed product yields and conditions for the cracking of a light naphtha feedstock in the LPT pilot plant and the Uno-Quattro coil

It can be concluded from the preceding simulations and experimental data that the methane yield and the ethylene over ethane yield ratio are independent indices and that they

unambiguously characterize the observed product yields for a given feedstock: i.e. the use of a third severity index is not necessary.

6.2.2 Industrial applications

6.2.2.1 *Prediction of product yields for different feedstocks*

For a given feedstock the product yields can be characterized by two severity indices, but the question arises: "What if instead of the reactor coil the feedstocks were to be varied?". Indeed in industry the feedstock composition almost continuously changes while the coil stays invariant, hence the sensitivity of this method to the feedstock composition is important. Therefore a set of simulations have been performed using four different naphtha feedstocks. The commercial indices of these four feedstocks, the process conditions for realizing the same methane yield and the same ethylene to ethane yield ratio and the resulting product yields are all given in Table 6.7. The reactor used in the simulations is the LPT pilot coil 1 described in Table 6.4.

Although the feedstocks differ significantly the simulated yields are not that different. The most pronounced differences are observed for the simulated ethylene yield. These results are not unexpected, since it seems obvious that the ethylene yield obtained with a feedstock containing a high content of aromatics such as naphtha 4 differs from the ethylene yield obtained with a feedstock containing no or very little aromatics such as naphtha 1. Cracking of a feedstock containing a high amount of paraffins such as naphtha 3 will lead to more ethylene, while a highly iso-paraffinic feedstock such as naphtha 1 leads to more propylene. Hence, for the prediction of product yields this direct scale-up method should be used with care. Only when similar feedstocks are used, e.g. naphtha 1 and naphtha 2, the product yields are identical if the ethylene to ethane yield ratio and the methane yield are the same. A good rule of thumb is that the highest PIONA weight fraction measured for a feedstock can deviate maximally 5 % (rel.) from the corresponding PIONA weight fraction obtained for the reference feedstock. Stronger deviations in feedstock composition lead to larger differences between the product spectra.

	Naphtha 1	Naphtha 2	Naphtha 3	Naphtha 4
Specific density, 15/4°	0.685	0.680	0.676	0.723
Paraffins (wt %)	7.55	10.31	43.3	1.57
Iso-paraffins (wt %)	78.33	74.19	38.3	76.92
Olefines (wt %)	0.66	0.75	0.66	0.37
Naftenes (wt %)	11.77	12.74	13.19	7.13
Aromatics (wt %)	1.70	2.01	3.88	11.31
Average molar H/C ratio	2.26	2.25	2.26	2.12
Average molecular weight (kg kmol^{-1})	89.48	88.01	85.67	110.77
PROCESS CONDITIONS				
CIP (MPa)	0.22	0.22	0.22	0.22
COP (MPa)	0.18	0.18	0.18	0.18
CIT (K)	873	873	873	873
COT (K)	1103	1100	1117	1139
δ (kg steam/kg HC)	1.1	1.0	0.6	1.0
Flow rate (kg/h)	3.0	3.0	3.0	3.0
SEVERITY INDICES				
CH$_4$ yield (wt %)	13.9	13.9	13.9	13.9
C$_2$H$_4$/C$_2$H$_6$ ratio (wt % / wt %)	9.6	9.6	9.6	9.6
PRODUCT YIELDS (wt %)				
H$_2$	0.7	0.7	0.7	0.7
C$_2$H$_4$	21.6	21.9	27.3	23.8
C$_2$H$_6$	2.2	2.3	2.8	2.5
C$_3$H$_6$	18.6	18.2	17.5	16.0
C$_4$H$_6$	5.3	5.3	5.6	6.3
C$_6$H$_6$	2.9	3.3	3.9	3.6
C$_5^+$-fraction	26.6	27.0	23.1	30.0

Table 6.7: Feedstock characteristics, operating conditions and corresponding simulated product yields of 4 naphtha feedstocks: naphtha 1, naphtha 2, naphtha 3, naphtha 4.

In industry the key day-to-day variable is the changing feedstock composition. The following strategy could be used to define a range of feedstock compositions for which the method based on two severity indices can be applied. To assess feedstock similarity principal component representation of the feedstock can be used. Principal component analyses (PCA) is a multivariate statistical technique whereby the information carried by the original variables is projected onto a smaller number of uncorrelated variables called principal components (PCs) (Wold et al., 1987; Joo et al., 2000). By plotting the PCs, one can detect the interrelationships between different variables and observe and interpret sample patterns, similarities, or differences. Traditionally, 2 PCs are sufficient for feedstock representation. Joo et al. (2000) used two PCs based on the commercial indices of the feedstock to classify a set of naphtha fractions. Hannisdal et al. (2005) used first order-differentiated FT-IR spectra to define two PCs for heavy crude-oils. Only when the values for the PCs are similar, the feedstocks have a similar composition. This strategy implies that an extensive database of reference feedstocks should be compiled for comparison. For example, the database of Joo et al. (2000) consisted of over 200 different naphtha fractions. Moreover, for all these reference feedstocks an extensive set of product yields in a broad range of experimental conditions should be gathered. The experimental conditions should ascertain that a broad range of methane yields and ethylene to ethane yield ratios are covered. Gathering this kind of information is of course very time consuming. However, an important advantage is that experimental data can be obtained in any type of reactor (i.e. industrial installations, pilot plant installations or even bench scale units), because the approach is independent of the scale of the reactor. Combining results from several industrial and small scale units should make it possible to significantly reduce the time for development of the necessary databases.

6.2.2.2 *Process operation and optimization*

The ethylene to ethane yield ratio and the methane yield are not only useful for scale-up and predicting the product distribution if similar feedstocks are used, but they can also be used in process optimization and for controlling the process operation. For process control it is important that a direct relation exists between a process variable and a severity index. As previously stated the ethylene to ethane yield ratio depends strongly on the reactants partial pressure, therefore it is obvious that this index can be controlled by manipulating process conditions such as the dilution

and the coil inlet pressure. The methane yield on the other hand correlates well with the temperature, and hence can be varied easily by changing the heat input. In Figure 6.6 the influence of the dilution and the heat input on the values of the two severity indices is illustrated.
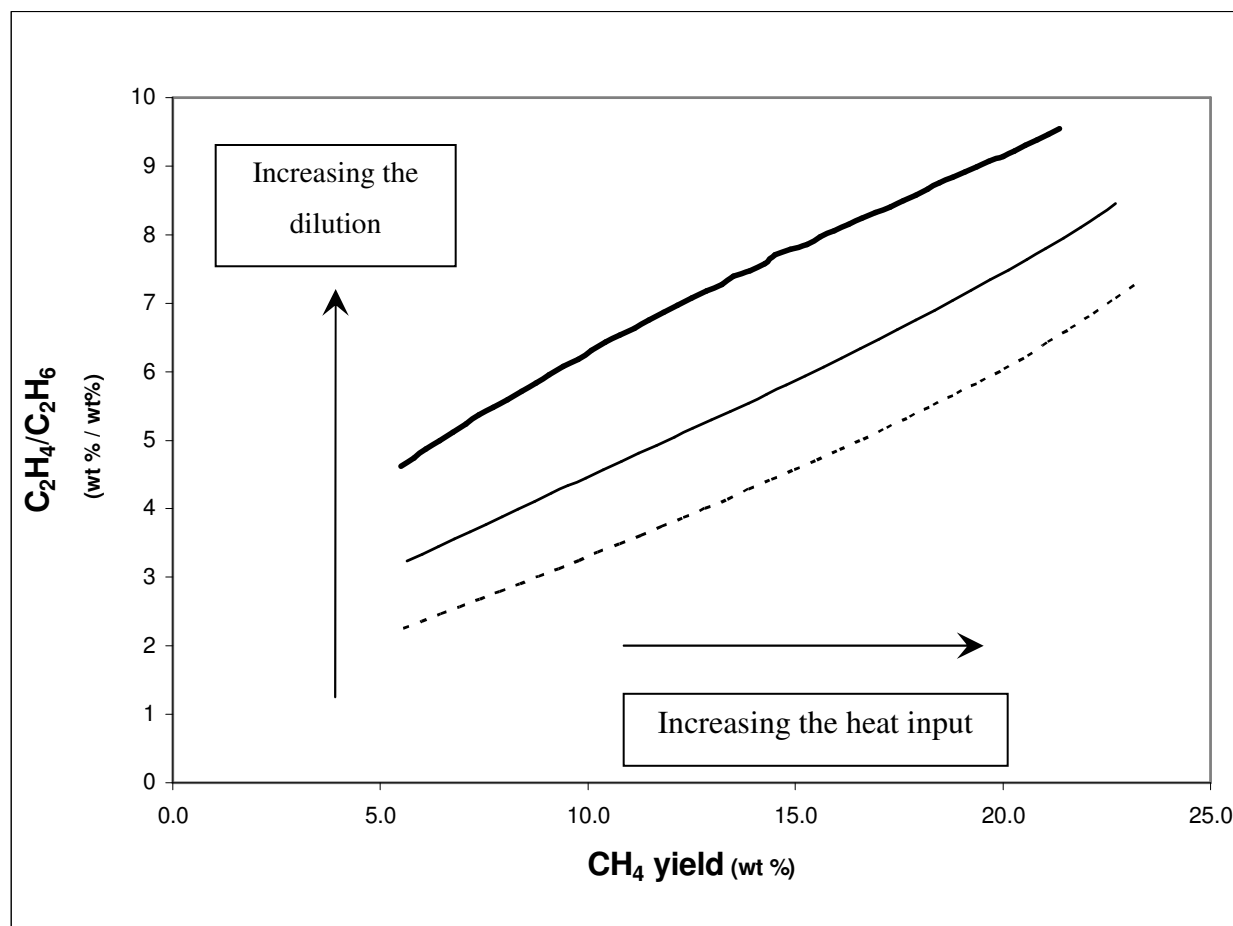
Figure 6.6: Ethylene to ethane yield ratio versus the methane yield in a Lummus SRT-I reactor calculated for the cracking of n-butane at different dilutions and for different COT's. [——— reference profile, Feed flow rate: 3500 kg h^{-1}, dilution: 0.7 kg steam/ kg HC, CIP: 3 MPa, COT: 1070-1130 K; ▬▬ dilution: 0.9 kg steam/ kg HC, CIP: 3 MPa, COT: 1070-1130 K; - - - - - dilution: 0.5 kg steam/ kg HC, CIP: 3 MPa, COT: 1070-1130 K]

Increasing the dilution for a given heat input, increases the ethylene to ethane yield ratio, while increasing the heat input for a given dilution increases the methane yield as the COT increases. Of course the values of the process conditions are restricted to a certain range, e.g. the maximal

external tube wall temperature limits the maximal heat input. Also the steam dilution is restricted to a certain range because adding steam implies that the production decreases.

	Pilot plant reactor	**Lummus SRT-I**	**4-2-1 Split Coil**	**USC-48U reactor**	**Millisecond reactor**
Coil length (m)	12.4	101.0	40.0	20.0	12.1
Tube diameter (cm)	0.9	12.4	7.6–11.4–15.2	7.6	3.6
Wall thickness (mm)	2	8	5	5	8
Flow rate (kg h⁻¹)	4	3500	5000	1000	60 (per tube)
Dilution (kg /kg)	0.5	0.5	0.5	0.5	0.5
CIT (K)	873	873	873	873	873
COT range (K)	1050-1140	1050-1130	1050-1130	1070-1160	1080-1170
CIP (MPa)	0.3	0.3	0.3	0.3	0.3

Table 6.8: The ethylene to ethane yield ratio as performance index. Characteristics and conditions used in the simulations for the different reactors.

It is not straightforward to develop an optimal strategy for the operation of an industrial steam cracker. Several aspects play an important role such as coke formation, furnace and reactor design, the actual market conditions and even maintenance. All these phenomena interact with each other, making accurate profit predictions even more difficult. For example, to increase the profit, high light olefin yields and thus high severities are required, but high severities affect the run length because of the high process temperatures and higher coking rates (Esbesen, 2001). In the ideal case all these effects would be taken into account to continually adjust the operation conditions, maximizing the profit based on the current market conditions. Fortunately it can be safely accepted that the ethylene yield and the ethylene selectivity are the most important parameters influencing the turnover. As stated earlier, the ethylene to ethane yield ratio is an appropriate measure for the ethylene selectivity. Hence the ethylene to ethane yield ratio can be considered as a performance index for the installation and an indicator for the profit made during a run. For similar process conditions and a similar methane yield in different reactors, the most selective reactor will be the one showing a higher value of the ethylene to ethane ratio. This can

be illustrated by a set of simulation results for a set of different reactors with n-butane as feedstock. The selected reactors are: a pilot plant reactor, a Lummus SRT-I reactor, a 4-2-1 split coil, a USC-48U reactor and a Millisecond reactor. The process conditions in the different reactors are summarized in Table 6.8. Some values have been fixed, e.g. the dilution, the coil inlet temperature and the coil inlet pressure. Others such as the flow rate depend on the type of reactor. Typical values for the flow rate have been chosen: 4 kg h^{-1} in the pilot reactor, 3500 kg h^{-1} in the Lummus SRT-I reactor, 5000 kg h^{-1} in the 4-2-1 split coil, 60 kg h^{-1} (per tube) in the Millisecond reactor and 1000 kg h^{-1} (per tube) in the USC-48U tube configuration.
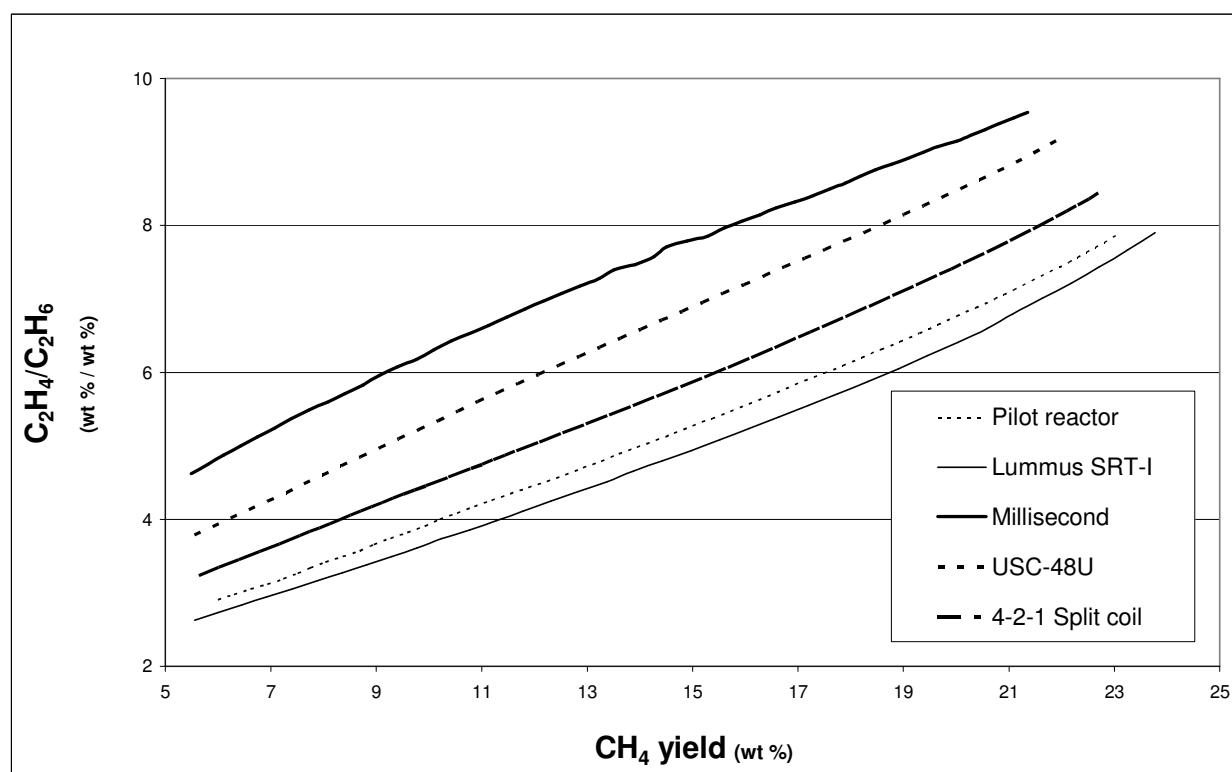
Figure 6.7: The ethylene to ethane yield ratio (C_2H_4/C_2H_6) as a function of the methane yield for 5 different reactor geometries calculated for the cracking n-butane. [Simulation conditions specified in Table 6.8]

The simulation results in Figure 6.7 show that for a given value of the methane yield the ethylene to ethane yield ratio has the highest value in the Millisecond reactor. It is well known that this type of reactor is the most selective reactor towards ethylene (Plehiers and Froment, 1987;

Froment, 1992). Hence, the results in Figure 6.7 illustrate that the ethylene to ethane yield ratio can be used as a measure for the performance of an industrial cracker.

6.2.2.3 *Other severity indices*

The extent to which a feedstock has been cracked is well characterized by the methane yield. It is intuitively clear that if more cracking of hydrocarbons occurs, more molecular chains have been split up, and thus more methane is formed. The methane yield is also known to be a good indicator for coke formation and correlates well with the run length (Golombook et al., 2001). Still industry prefers the propylene over ethylene ratio (P/E-ratio).
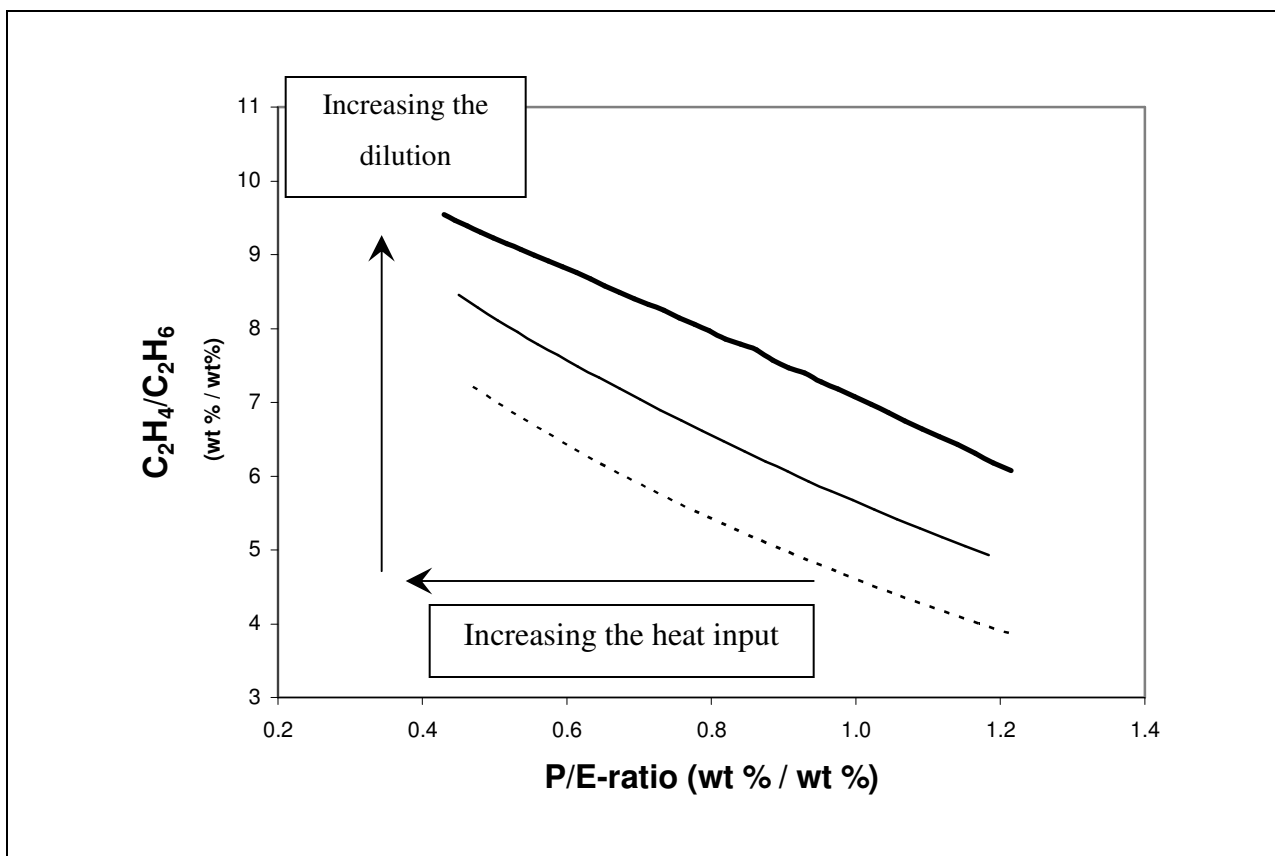
Figure 6.8: Ethylene to ethane yield ratio versus the propylene over ethylene yield ratio in a Lummus SRT-I reactor calculated for the cracking of n-butane at different dilutions and for different COT's. [⎯⎯ reference profile, Feed flow rate: 3500 kg h^{-1}, dilution: 0.7 kg steam/ kg HC, CIP: 3 MPa, COT: 1070-1130 K; ⎯⎯ dilution: 0.9 kg steam/ kg HC, CIP: 3 MPa, COT: 1070-1130 K; - - - - - dilution: 0.5 kg steam/ kg HC, CIP: 3 MPa, COT: 1070-1130 K]
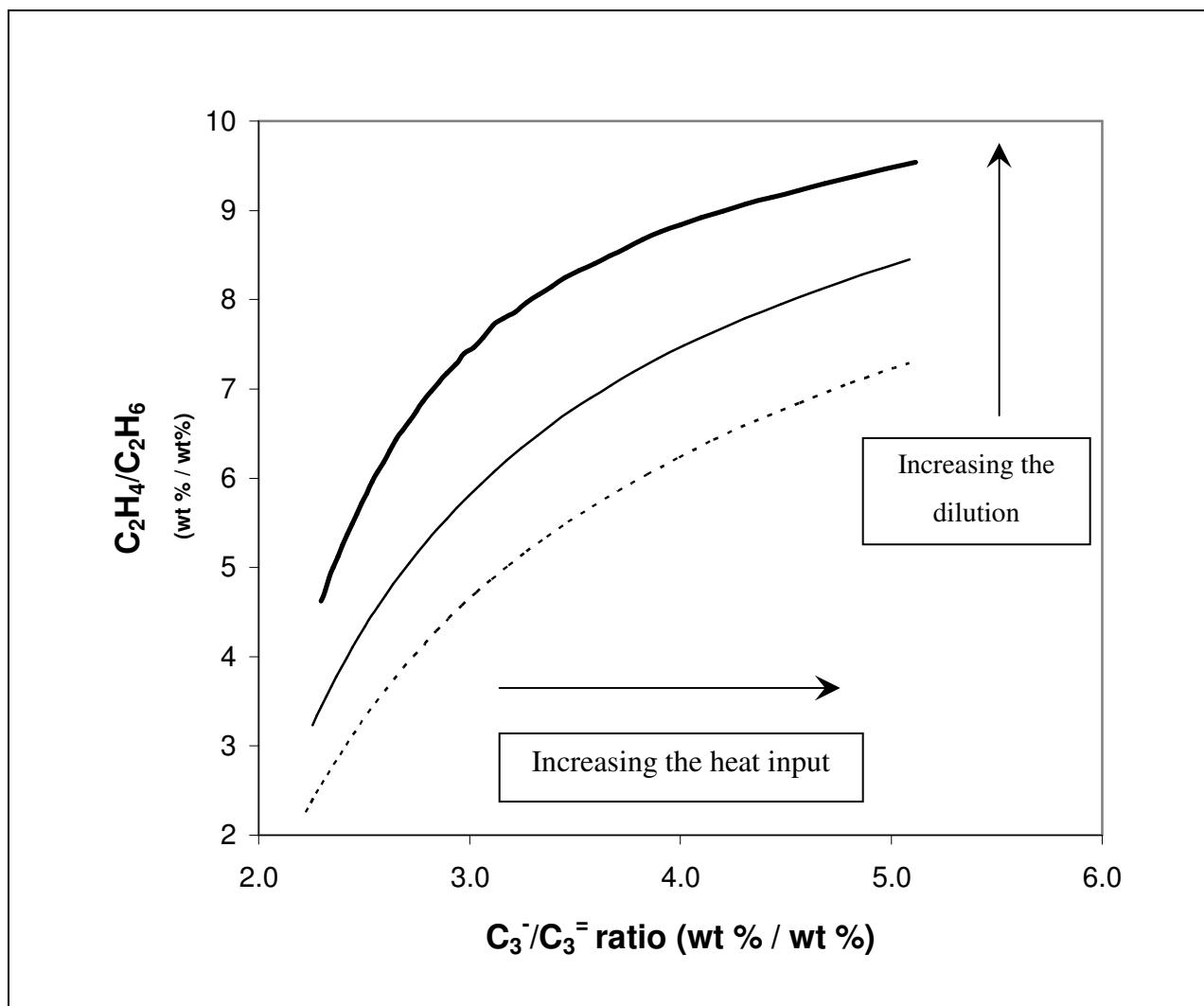
Figure 6.9: Ethylene to ethane yield ratio versus the $C_3^-/C_3^=$ yield ratio in a Lummus SRT-I reactor calculated for the cracking of n-butane at different dilutions and for different COT's. [―― Reference profile, Feed flow rate: 3500 kg h^{-1}, dilution: 0.7 kg steam/ kg HC, CIP: 3 MPa, COT: 1070-1130 K; ▬▬ dilution: 0.9 kg steam/ kg HC, CIP: 3 MPa, COT: 1070-1130 K; - - - - - dilution: 0.5 kg steam/ kg HC, CIP: 3 MPa, COT: 1070-1130 K]

One of the advantages of using the P/E-ratio is that on-line gas chromatographs can easily measure this ratio (Golombook et al., 2001). Indeed, ratio's of yields are more reliable determined than absolute values such as the methane yield (Van Camp et al., 1985). In industry the P/E-ratio is usually fixed at about 0.55. At lower severities, before the propylene yield has reached its maximum, not much cracking has occurred and large amounts of liquid byproducts

are formed. Higher severities, P/E-ratio's ≤ 0.45, lead to higher ethylene yields but also to an increase in coke formation. The question arises from a practical point of view: "What if instead of the methane make the P/E-ratio or another severity index is used?". The results in Table 6.4 show that it is not necessary to use the methane yield as first severity index, the P/E-ratio works just as well. If the P/E-ratio is used instead of the methane yield Figure 6.6 is transformed into Figure 6.8.
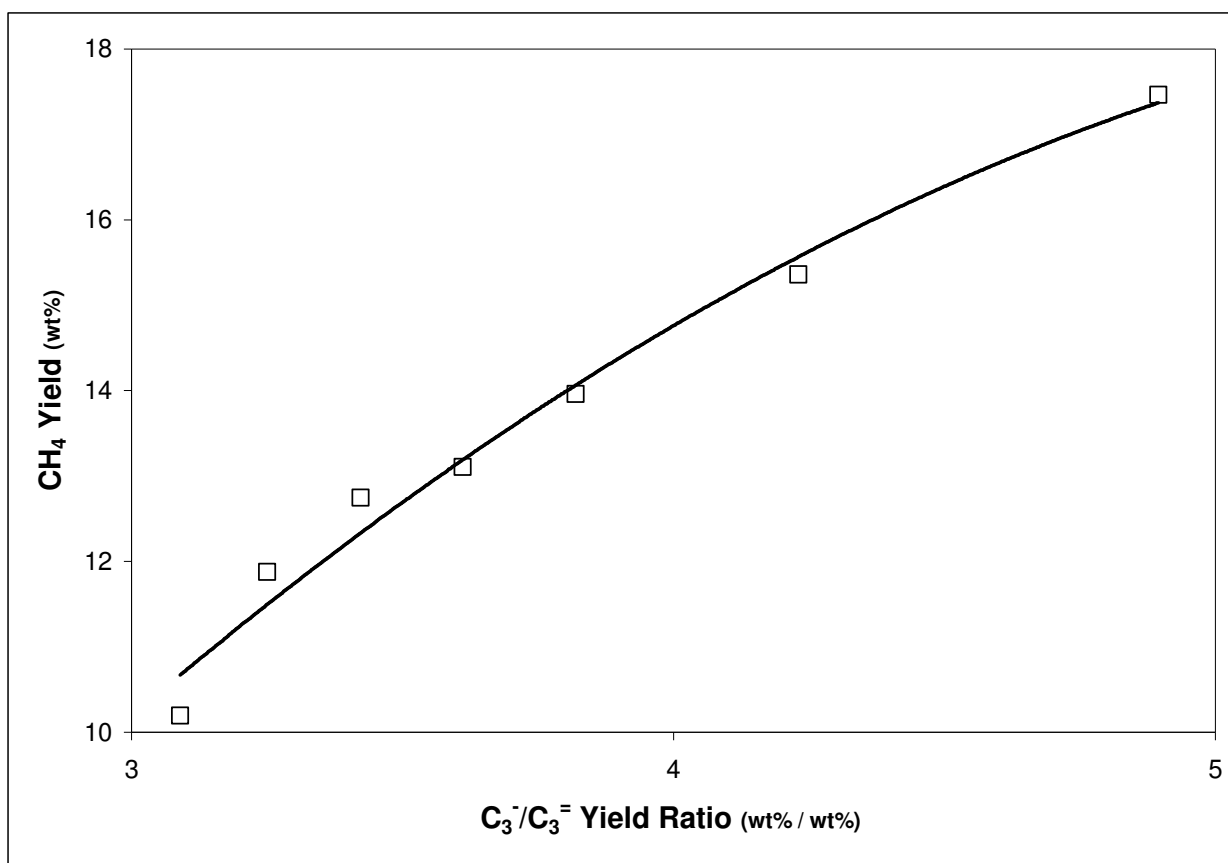
Figure 6.10: The methane yield (CH_4 yield) as a function of the $C_3^-/C_3^=$ Yield Ratio for naphtha cracking experiments carried out in the LPT pilot plant reactor (coil 2). [□ Single coil reactor. Feed flow rate: 4.3 kg h^{-1}, dilution: 0.2 kg steam/ kg HC, COT: 1070-1130 K; ▬▬ trend line for experimental data]

Next to the P/E-ratio as an alternative for the methane make other severity indices can also be used, e.g. the $C_3^-/C_3^=$ yield ratio (Van Camp et al., 1985). The C_3^- fraction contains propylene, propane, propadienes, C_2 components, methane and hydrogen. $C_3^=$ is the yield of propylene.

According to Van Camp et al. (1985) the $C_3^-/C_3^=$ yield ratio can be considered as the best measure of the severity of operation because this index relates to the conversion in a unique way, i.e. without any influence of total pressure and dilution. This behavior suggests that the $C_3^-/C_3^=$ yield ratio is also an appropriate severity index to be used in combination with the ethylene to ethane yield ratio. Indeed, the results in Figure 6.9 show that this ratio in combination with the ethylene to ethane yield ratio functions just as the methane yield in combination with the ethylene to ethane yield ratio. In fact, any combination of the methane yield, the P/E-ratio or the $C_3^-/C_3^=$ yield ratio with the ethylene to ethane yield ratio characterizes the product yields unambiguously. Indeed, it is no surprise that the methane yield can be replaced by the P/E-ratio or the $C_3^-/C_3^=$ yield ratio. All these variables are highly correlated. For example the experimental results in Figure 6.10 show the strong correlation between the methane yield and the $C_3^-/C_3^=$ yield ratio. Other severity indices can also be combined with the ethylene to ethane yield ratio if they are a reliable measure for the conversion and their dependence on the partial pressures of the reactants is not too strongly pronounced.

6.2.3   Conclusions

A new method to relate experimental data obtained for different reactor sizes and geometries is developed for the steam cracking process. This direct scale-up method is based on the "severity" concept. For a given feedstock, scale-up is performed based on experimental data obtained at the same severity. The temperature profile and the partial pressure profiles of the reactants in the reactor are the two independent variables that determine the reaction rates and hence characterize the product yields. Therefore, two carefully chosen severity indices are sufficient to unambiguously characterize the product yields for a given feedstock: one severity index being a measure for the temperature and the other index being a measure for the reactants partial pressure. Reaction path analysis shows that the methane yield is an appropriate measure for the temperature, while the ethylene over ethane yield ratio can be considered as a reliable measure for the reactants partial pressures. Simulations and experiments show that for a given feedstock the methane yield and the ethylene over ethane yield ratio are independent indices and that they unambiguously characterize the observed product yields: i.e. the use of a third severity index is not necessary. Other combinations of severity indices with the ethylene over ethane

yield ratio work just as well. Especially the combination with the P/E-ratio is an interesting alternative for the petrochemical industry because this ratio is easily measured in an industrial installation. Unfortunately, this approach is only valid when similar feedstocks are used. A good rule of thumb is that the highest PIONA weight fraction measured for a feedstock can deviate maximally 5 % (rel.) from the corresponding PIONA weight fraction obtained for the reference feedstock. The applications of this new method are not limited to scale-up. Also in the field of process optimization potential applications exist because the ethylene to ethane yield can be considered as a performance index.

6.3 Dimensional Analysis as a tool for scaling up and down steam cracking coils

Designing a pilot plant reactor for steam cracking based on an industrial installation or vice versa is not straightforward. Steam cracking is an endothermic process and is operated at high temperatures. Next to the intrinsic chemical kinetics, heat and mass transport processes, which are scale dependent, affect the product yields. Product yields on a small and a large scale will only be identical providing that mass and heat transfer processes are similar and the "chemistry" remains the same. The theory of similarity is the ideal tool to help to construct a small scale unit similar to an industrial one. The theory of similarity states that two processes can be defined as similar if they take place in a similar geometrical space, and if all the dimensionless numbers necessary to describe the process, have the same numerical value. In case complete similarity cannot be realized, working under partial similarity can offer an alternative solution. The latter implies that the influences of "non-similarities" are first verified thoroughly using either theoretical calculations or data from experimental tests. Only if a negligible influence on scale-up or scale-down is found, the data can be directly transferred to another scale with reasonable accuracy. Indeed, as the differences in dimensions and typical operating conditions between industrial reactors, pilot plant reactors and laboratory scale reactors are significant, see Table 6.9, some differences between the obtained conversions and product yields are inevitable. Therefore in the next paragraphs conditions are determined that allow accurate transfer of data between steam cracking reactors of different scales. Other interesting aspects such as the effect of the feedstock, the reactor geometry and the role of coke formation on scale-up are also discussed.

	Laboratory scale reactor	**Pilot Plant reactor**	**Industrial reactor**
Reactor length (m)	1 - 2	10 - 25	10 - 100
Tube diameter (m)	$5.10^{-3} - 1.10^{-2}$	$5.10^{-3} - 2.5 \ 10^{-2}$	$3.10^{-2} - 1.5 \ 10^{-1}$
Feed flow rate (kg s^{-1})	$5.10^{-5} - 5.10^{-4}$	$5.10^{-4} - 1.10^{-2}$	$10^{-2} - 1$
Pressure drop (MPa)	< 0.01	0.02 – 0.06	0.07 – 0.15
COT (K)	850 – 1100	900 – 1200	1000 – 1200
Residence time (s)	0.1 – 8	0.1 – 1	0.1 – 1
Re	10^2	$4.10^3 - 1.10^4$	$1.10^5 - 5.10^5$

Table 6.9: Typical dimensions and operating conditions used in steam cracking reactors of different scale

6.3.1   Direct experimental scale-up based on the theory of similarity

All chemical processes involving transfer of mass, heat or momentum can be scale dependent, i.e. they can behave differently in a laboratory, a pilot or in an industrial unit, even in two industrial units of different geometry. It is obvious that in two similar units completely the same behavior can be expected and thus that the difference in scale does not in any way affect the product yields. The theory of similarity enables to determine dimensions and operating conditions for a simulation unit of smaller scale similar to an existing industrial unit (scale-down) or vice versa (scale-up). Complete similarity requires geometrical, material, and process-related similarity (Zlokarnik, 2001). Geometrical similarity implies that the process is mathematically well defined. Material similarity as applied to steam cracking implies that the same feedstock is used, the material of the reactor remains the same, the same diluent is used, etc. Process-related similarity requires that the reactors of different scale are operated under similar conditions, e.g. a similar temperature profile, a similar pressure profile and the same dilution. Only when complete similarity between a small scale and an industrial unit is achieved, the results of the experimental data obtained in the small scale unit can be safely transferred to the industrial scale unit. For more than a century, the theory of similarity has been successfully applied in the field of fluid dynamics and heat transfer. Cars, aircrafts, vessels and heat

exchangers were scaled up according to these principles. The theory has also been used in process engineering, e.g. for dust separators, bubble columns, flotation cells for waste water, centrifugal pumps, etc. (Zlokarnik, 2002; Stichlmair, 2002).

Whether or not two processes are completely similar depends on meeting the criteria of similarity or so-called simplexes of similarity. All corresponding criteria of similarity must have the same value in both systems, e.g. the same Reynolds numbers. These criteria consist entirely of dimensionless numbers and can be found by dimensional analysis. Dimensional analysis is based upon the fact that a mathematical formulation of a chemical or a physical process can only be of general validity if it is dimensionally homogenous, i.e. if it is valid in any system of dimensions (Zlokarnik, 2002). The set of dimensionless numbers resulting from dimensionless analysis is called the Π-set. The applicability of dimensional analysis as a method to determine the criteria for similarity depends on the level of available knowledge on a given process. All the important variables of the process and also the relations between them have to be available (Zlokarnik, 2002, Stichlmair, 2002). An incomplete Π-set can lead to significant inaccuracies in transferring data between units of different scale. A possible method to determine the set of dimensionless numbers is Buckingham's Π-theorem. Buckingham (1914) claimed that the number of dimensionless groups in a complete set is equal to the total number of relevant quantities minus the number of fundamental dimensions in the problem. However this theorem can lead to an incomplete list of necessary criteria, insufficient for successful scale-up (Butterfield, 1999). A safer and more efficient way to gather this information is based on a mathematical description of the process, provided this mathematical description exists (Himmelblau and Bisschhoff, 1968). For the steam cracking process, a mathematical description is available and, if the model equations are made dimensionless, the dimensionless numbers appear in a straightforward way. The list of scale-up criteria is completed with the dimensionless numbers resulting from the boundary conditions of the model equations.

Traditionally a 1-dimensional reactor model is employed in commercial steam cracking software, e.g. SPYRO (Van Goethem et al., 2001; Dente et al. 1979), CRACKER (Joo et al., 2000) and COILSIM (Clymans and Froment, 1984, Van Geem et al., 2004 [b]). However, in some cases the implementation of 2 or 3-dimensional reactor models becomes inevitable, e.g. for cracking coils with internally finned tubes (De Saegher et al., 1996). These high-dimensional models are able to give sufficiently accurate results, also for the simulation of reactors with

extremely high severity (Froment, 1992). The basic continuity equation for a component j in steady state is given by the following equation (Froment and Bischoff, 1990):

$$\nabla(C_j v) - \nabla(D\ \nabla C_j) = \sum_i (v_{i,j}) r_{Vi} \qquad\qquad [6.12]$$

with C_j the concentration of component j, v the velocity, D the effective diffusion coefficient, $v_{i,j}$ the stoechiometric coefficient of the component j in reaction i and r_i the rate of reaction i. The corresponding energy equation is given by (Froment and Bischoff, 1990):

$$\rho c_p \nabla(T\ v) - \nabla(\lambda\ \nabla C_j) = \sum_i (-\Delta_r H_i^0)\ r_{Vi} \qquad\qquad [6.13]$$

with ρ the density, c_p the specific heat capacity, T the temperature, λ the thermal conductivity coefficient and $\Delta_r H^0$ the standard reaction enthalpy.

One of the main reasons to use high dimensional models for simulation is the existence of a significant radial temperature gradient in industrial cracking coils. Elvers et al. (1992), Sundaram and Froment (1980) and Van Geem et al. (2004 [a]) showed that for industrial reactors the radial temperature drop from the wall to the gas core is on the order of 100 K. Furthermore, this radial temperature drop is the origin of small but significant differences between the product yields simulated using a 1- and 2-dimensional reactor model (Van Geem et al., 2004 [a]). Therefore the 1-dimensional reactor model equations are not used, but the complete Π-set is determined based on the 2-dimensional reactor model equations. By transformation of equation [6.12] and [6.13] to cylindrical coordinates a 2-dimensional model, that can be used to simulate of tubes with a circular cross section, is obtained. The 2-dimensional reactor model is based on a 2-dimensional velocity vector. Next to axial and radial convection and reaction, axial and radial dispersion have to be taken into account in the model equations. The mass balance for a component j over an annulus with height dz, internal radius r and external radius r+dr leads to the continuity equation for component j in the process gas mixture (Bird et al., 2001; Froment and Bischoff, 1990):

$$\frac{\partial}{\partial z}(v_a C_j) + \frac{1}{r}\frac{\partial}{\partial r}(r\ v_r C_j) - \frac{\partial}{\partial z}(D_a \frac{\partial C_j}{\partial z}) - \frac{1}{r}\frac{\partial}{\partial r}\left(r\ D_r \frac{\partial C_j}{\partial r}\right) = \sum_i v_{i,j} r_i \qquad [6.14]$$

The corresponding energy equation is given by:

$$\frac{\partial}{\partial z}(v_a T) + \frac{1}{r}\frac{\partial}{\partial r}\left(r\, v_r T\right) - \rho\, c_p \frac{\partial}{\partial z}(\lambda_a \frac{\partial T}{\partial z}) - \frac{1}{r}\frac{\partial}{\partial r}\left(r\lambda_r \frac{\partial T}{\partial r}\right) = \sum_i (-\Delta_r H_i^0)r_i \quad [6.\,15]$$

The first term in equations [6.14] and [6.15] represents convective transport in axial direction and is the most important one in the continuity and energy equations. The second term corresponds to radial convection and is a measure for the macromixing along the cross-section of the coil. In general the contribution of this term is neglected and ideal macro-mixing along the cross-section of the cracking coil is assumed (Sundaram and Froment, 1980; Garg et al., 2005). The third and fourth term represent transport by effective diffusion or conduction in axial and radial direction respectively. Under normal operating conditions back mixing is not important for steam cracking problems and the third term can often be neglected. The fourth term corresponds to radial dispersion and can become very important for steam cracking problems (Sundaram and Froment, 1980; Garg et al., 2005). Terms on the right hand side of equations [6.14] and [6.15] correspond to the reaction chemistry of the process and, obviously, these terms are very important for an accurate steam cracking description.

The momentum equation is obtained by applying Newton's second law on a moving fluid element (Froment and Bischoff, 1990). For steam cracking, only pressure drops and friction forces have to be considered, while radial pressure gradients can be neglected. Hence, the following momentum equation [6.16] is obtained:

$$-\frac{dp_t}{dz} = \alpha\left(\frac{2\,f}{d_t} + \frac{\zeta}{\pi\,r_b}\right)\rho\,v^2 + \alpha\,\rho\,v\,\frac{dv}{dz} \quad\quad [6.\,16]$$

with p_t the total pressure, α a conversion factor, f Fanning's friction factor, d_t the internal diameter of the tube, ζ Nekrasov's factor for bends and r_b the radius of the bend.

The boundary conditions for the 2-dimensional problem are:

- in the center of the tube (r = 0):

$$\frac{\partial T}{\partial r} = 0 \qquad v_r = 0 \qquad\qquad \frac{\partial}{\partial r}\left(\frac{C_j}{\rho}\right) = 0$$

- at the inner reactor wall (r = $d_t/2$) :

$$D_r \, \rho \quad \frac{\partial}{\partial r}\left(\frac{C_j}{\rho}\right) = \frac{r_{c,j}}{M_j}$$

$$\frac{\partial T}{\partial r} = \frac{q}{\lambda_r}$$

- at the inlet (z = 0) :

$$T = T_0 \qquad C_j = C_{j0} \qquad p_t = p_0$$

In the model equations no terms pertaining to coke layer thickness have been added as the calculations are performed for the initial coke formation rate. Coke formation during steam cracking is a slow and complex phenomenon (Froment, 1990). Under typical operating conditions the coke yield is in the order of 0.01 wt%. First, there is a catalytic phase in which the properties of the tube skin material play an important role (Figueiredo, 1989). Once the metal surface is covered with coke, a second heterogeneous, but non-catalytic, mechanism dominates (Bennet and Price, 1981). At the operating conditions prevailing in industrial cracking units, the largest amount of coke formed during the run length results from the heterogeneous, non-catalytic coke formation (Reyniers et al., 1992). It is obvious that to transfer data on coke formation from one reactor to another the conditions at the reactor wall/process gas interface should be similar. The latter implies that the same reactor material is used and that the conditions and the species concentrations near the wall are the same. However, as will be illustrated in the next paragraphs this is impossible for two different steam cracking reactors. Therefore no separate model equation describing coke formation on the wall is included.
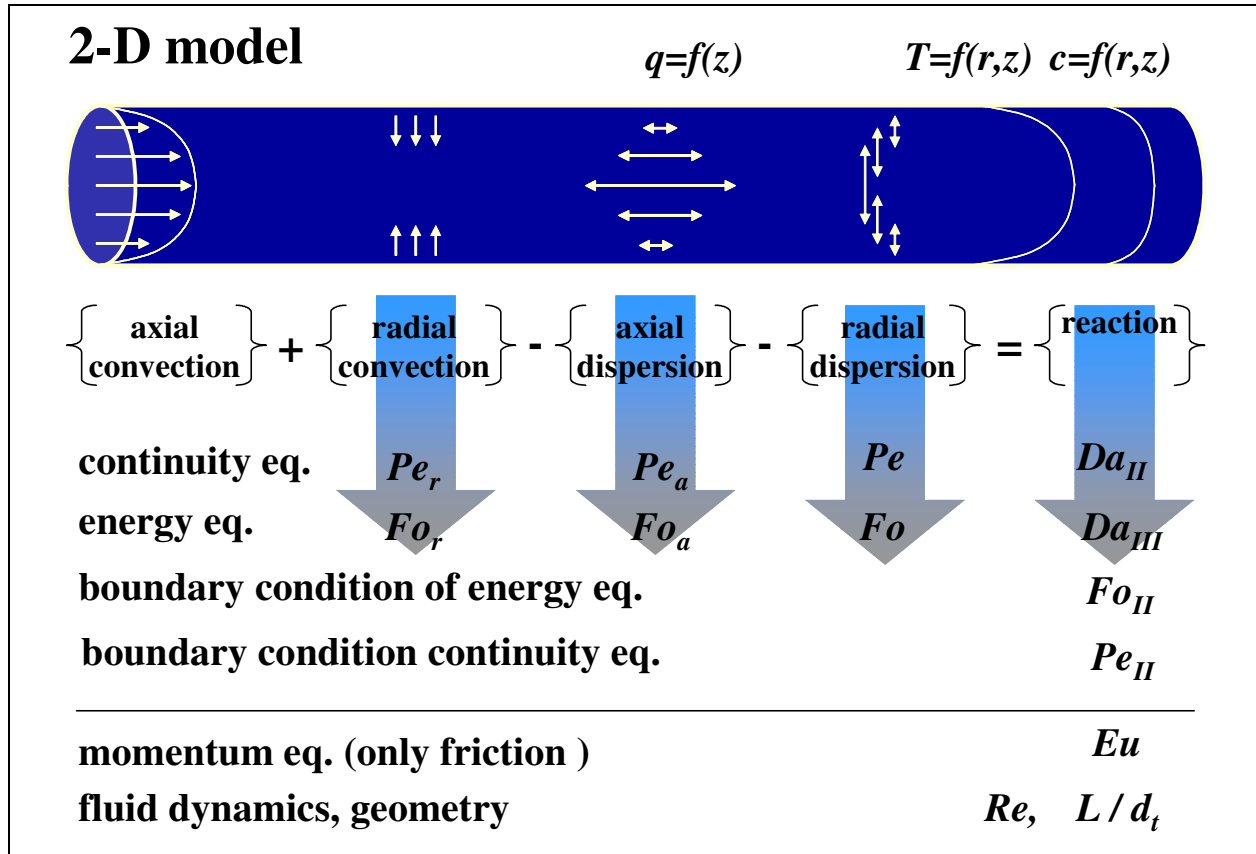
Figure 6.11: Schematical representation of the dimensionless model equations and origin of the dimensionless numbers

As illustrated in Figure 6.11, the model equations [6.14], [6.15] and [6.16] can be easily transformed into a dimensionless form. The dimensionless equations for the continuity equation and the energy equation are obtained by dividing each term in the original equations by the coefficient of the convective term and making variables such as the temperature and concentrations dimensionless. The convective term is chosen because this term is the most important term in the continuity and energy equations. The following dimensionless variables can thus be introduced:

$$z' = \frac{z}{L}, \quad \xi = \frac{2r}{d_t}, \quad y_i = \frac{C_i}{C^0}, \quad r'_i = \frac{r_{Vi}}{r_V^0}, \quad \theta = \frac{T}{T^0}, \quad v'_a = \frac{v_a}{v_a^0}, \quad v'_r = \frac{v_r}{v_r^0},$$

$$D'_r = \frac{D_r}{D_r^0}, \quad \lambda'_r = \frac{\lambda_r}{\lambda_r^0}, \quad -\Delta_r H'_i = \frac{-\Delta_r H_i^0}{\left|\Delta_r H_{ref}^0\right|}$$

with z' the dimensionless axial position, L the length of the reactor, ξ the dimensionless radial position, C^0 the total inlet concentration of the reactants, r'_{vi} the dimensionless reaction rate, r_v^0 the global rate of disappearance of the reactants, θ the dimensionless temperature, v' the dimensionless velocity, D' the dimensionless effective diffusivity, λ' the dimensionless conductivity coefficient, $\Delta_r H^0_{ref}$ a reference reaction enthalpy and $\Delta_r H'_i$ the dimensionless reaction enthalpy.

Figure 6.11 shows that transforming the continuity equation for a specific component into a dimensionless form leads to the introduction of 4 dimensionless numbers: 3 Peclet numbers (Pe, Pe_r and Pe_a) and 1 Damköhler number Da_{II}. The radial Peclet number Pe_r is the ratio between the characteristic time scales for radial diffusion and radial convection and is a measure for macro-mixing along the cross-section. Generally for steam cracking the values for the radial Peclet number Pe_r are very low [$Pe_r \rightarrow 0$] (Sundaram and Froment, 1980; Garg et al., 2005) and ideal macro-mixing along the cross-section of the tube can be assumed. In contrast, the values for the axial Peclet number Pe_a are very high [$Pe_a \rightarrow \infty$] and back mixing can be neglected (Sundaram and Froment, 1980; Garg et al., 2005). If ideal macro mixing in the radial direction is assumed and back mixing is neglected, the dimensionless continuity equation for a component j is given by:

$$\frac{\partial}{\partial z'}(v'_a\, y_j) - \frac{1}{Pe}\frac{1}{\xi}\frac{\partial}{\partial \xi}\left(\xi D'\frac{\partial y_j}{\partial \xi}\right) = Da_{II}\sum_i v_{i,j} r'_i \qquad [6.\,17]$$

Also in the dimensionless energy equation 4 dimensionless numbers are defined: 3 Fourier numbers (Fo, Fo_r and Fo_a) and 1 Damköhler number Da_{III}, see Figure 6.11. As for the continuity equation, the contributions of the terms of axial conduction and radial convection can be neglected, resulting in the following dimensionless energy equation:

$$\frac{\partial}{\partial z'}(v'_a\, \theta) - Fo\frac{1}{\xi}\frac{\partial}{\partial \xi}\left(\xi \lambda'\frac{\partial \theta}{\partial \xi}\right) = Da_{III}\sum_i (-\Delta_r H'_i) r'_i \qquad [6.\,18]$$

If only friction is taken into account, the momentum equation can be transformed into the following dimensionless form:

$$\frac{dp'}{dz'} = \frac{1}{Eu}\left(v'_a\right)^2$$

[6. 19]

with p' the dimensionless pressure and Eu the Euler number.

The boundary conditions for the 2-dimensional problem in dimensionless form are:

- in the center of the tube ($\xi = 0$):

$$\frac{\partial\theta}{\partial\xi} = 0 \qquad v'_r = 0 \qquad\qquad \frac{\partial y_j}{\partial\xi} = 0$$

- at the inner reactor wall ($\xi = 1$) :

$$\frac{\partial y_j}{\partial\xi} = \frac{r_{c,j}}{D_r\, M_j} = Pe_{II}$$

$$\frac{\partial\theta}{\partial\xi} = \frac{2}{d_t}\frac{q}{T^0\,\lambda_r} = Fo_{II}$$

- at the inlet ($z' = 0$) :

$$\theta = 1 \qquad\qquad y_j = 1 \qquad p' = 1$$

The following criteria corresponding to process-related similarity are derived:

- from the continuity equations:

$$Pe = \frac{d_t^2}{4\, D^0}\frac{v_a^0}{L} = \frac{\tau_{Dr}}{\tau}$$

[6. 20]

$$Da_{II} = \frac{L}{v_a^0} \frac{r_v^0}{C^0} = k_{ref}^0 \, \tau \qquad \text{[6. 21]}$$

- from the energy equation:

$$Fo = \frac{4 \, L}{v_a} \frac{\lambda^0}{c_p \, \rho \, d_t^2} = \frac{\tau}{\tau_{\lambda r}} \qquad \text{[6. 22]}$$

$$Da_{III} = \frac{L \, r_v^0}{v_a^0} \frac{\left| \Delta_r H_{global} \right|}{c_P \, \rho \, T^0} \qquad \text{[6. 23]}$$

- from the momentum equation:

$$Eu = \frac{d_t \, p_t^0}{2f \, \rho \, \left(v_a^0\right)^2 \, L} \qquad \text{[6. 24]}$$

- from the boundary conditions:

$$Pe_{II} = \frac{r_{c,j}}{D_r \, M_j} \qquad \text{[6. 25]}$$

$$Fo_{II} = \frac{2}{d_t} \frac{q}{T^0 \, \lambda_r} \qquad \text{[6. 26]}$$

Geometrical similarity requires that the aspect ratio, i.e. the ratio of the length to the diameter of the tube, remains fixed:

$$\frac{L}{d_t} \qquad \text{[6. 27]}$$

Hydrodynamic similarity requires that the Reynolds number has the same value in the different reactors:

$$Re = \frac{v_a \, d_t \, \rho}{\mu} \qquad\qquad [6.\,28]$$

The Π-set defined by equations [6.20]-[6.28] differs from the Π-set derived by Zlokarnik (Zlokarnik, 2002), which was derived for a 1st order reaction occurring in a tubular reactor taking into account the interplay between reaction and mass and heat transfer. However, Zlokarnik (2002) used a 1-dimensional reactor model, and hence radial concentration and temperature gradients and radial convection terms were neglected. The current Π-set also differs from the Π-set derived by Damköhler (Damköhler, 1936). Damköhler started from the 1-dimensional reactor model in his description of an adiabatic catalytic tubular reactor, and hence all radial non-uniformities were neglected.

6.3.2 Complete versus partial similarity

The theory of similarity states that two units of different scale will yield identical results if the complete Π-set describing the different transport phenomena is the same. Hence, if the dimensionless numbers defined by equations [6.20]-[6.28] are the same for two reactors then the temperature profile and the pressure profile are similar and the product distribution is identical. However, Damköhler (1936) and Zlokarnik (2002) have already shown that it is impossible for two different tubular reactors to have identical values for the three dimensionless numbers Da_{II}, Re and L/d_t-ratio, see Figure 6.12. If the internal diameter d_t is increased with a factor n, the axial velocity v_a^0 has to decrease with the same factor to maintain the same value for the Reynolds number. Retaining geometrical similarity implies that the reactor length L should also increase with the same factor, i.e. an identical L/d_t-ratio. Then it is no longer possible to maintain the same Damköhler number. Hence, for tubular reactors scale-up or scale-down under complete similarity is excluded, but working under partial similarity might be an option.

$$\frac{L}{d_t} \qquad \Rightarrow \qquad \frac{L}{d_t} = \frac{n.L*}{n.d_t*}$$

$$Re = \frac{v_a^0 d_t \rho}{\mu} \qquad \Rightarrow \qquad v_a^0 d = \frac{v_a^0 *}{n} n.d_t*$$

$$Da_{II} = \frac{L}{v_a^0} k^0 \qquad \times \qquad Da_{II} = n^2 \frac{L*}{v_a^0 *} k^0$$
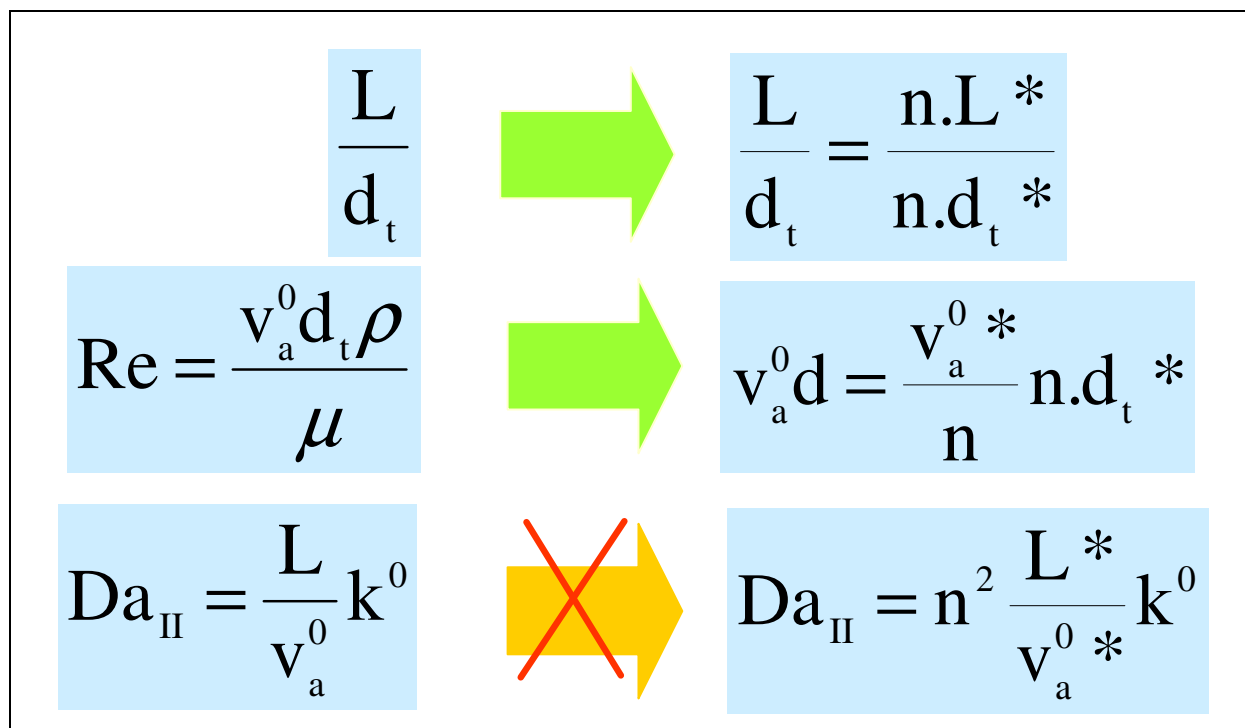
Figure 6.12: Criteria for scale-up under geometrical, hydrodynamic and process related similarity

Scale-up under partial similarity is a challenging task, in particular for tubular reactors. Loss of complete similarity inevitably results in differences when transferring data from one scale to another. A judicious choice of the criterion of similarity to be abandoned is necessary. As the value of the Reynolds number has only a slight influence on the hydrodynamics in the turbulent flow regime, Damköhler (1936) started by abandoning hydrodynamic similarity. In industrial tubular reactors, Reynolds numbers easily reach values of 10^5 while in typical pilot plant reactors the Reynolds number is limited to about 10^4. In a bench scale unit the Reynolds number is even smaller, i.e. on the order of 10^2 (Froment, 1981), resulting in laminar flow through the reactor tube. A change in flow regime can have drastic effects on similarity. Results reported by Van Damme and Froment (1981) showed that the methane yield during naphtha cracking differed significantly (8% rel.) between a bench scale unit operated in laminar regime and a pilot plant unit operated in turbulent regime. Damköhler (1936) further pointed out that abandoning of hydrodynamic similarity only was not sufficient and thus not only abandoned hydrodynamic similarity, but also neglected geometrical similarity in his description of a heterogeneous

catalytic reaction in a tubular packed bed reactor. However, even if hydrodynamic and geometrical similarity are neglected problems remain, in particular in realizing a similar radial temperature and concentration profile. Indeed, consider the dimensionless energy equation and the corresponding dimensionless Fourier number Fo in equation [6.22]. This number is the ratio of the residence time τ to the time scale for radial heat dispersion $\tau_{\lambda r}$. Equation [6.21] shows that to keep the Damköhler number Da_{II} the same the residence time τ should remain fixed upon a change of scale. Hence, to realize a similar radial temperature profile, the time scale for radial heat dispersion $\tau_{\lambda r}$ should also remain unchanged upon a change in scale. However, from equation [6.22], it is a priori clear that $\tau_{\lambda r}$ can only be the same in two reactors if they have the same diameter. Moreover, according to the dimensionless number stemming from the boundary condition of the energy equation, i.e. equation [6.26], not only the diameter of the reactor must remain unchanged, but also the axial heat flux profile must be similar to realize a similar radial temperature profile. However, realizing the same radial temperature and concentration profile is not the only problem. An analysis of the momentum equation shows that problems pertaining to the pressure profile are to be expected too. Van Damme et al. (1981) noticed that it was impossible to obtain similar axial pressure profiles in a bench scale unit and in a pilot plant unit. Nevertheless, it is possible to obtain axial pressure profiles very close to each other by a judicious choice of the tube length, the tube diameter and the inlet flow as can be seen from the momentum equation [6.16]. If identical pressure drops have to be obtained in two different tubular reactors, the Euler number defined in equation [6.24] has to be the same. Next to variables such as tube length, tube diameter and inlet velocity, the Euler number also depends on the Fanning friction factor. The latter is a function of the tube diameter and, different equations have been proposed to calculate its value. According to the Blasius equation for smooth tubes (Perry and Green, 1997) the friction factor can be calculated using the following equation:

$$f = \frac{0.079}{Re^{\frac{1}{4}}} \hspace{4cm} [6.\ 29]$$

The resulting Euler number is then given by:

$$Eu = \frac{d_t^{1.25} \, p_t^0}{0.158 \, \rho_g \, (v_a^0)^2 \, L} = \frac{d_t^{1.25} \, p_t^0 \, \tau^2}{0.158 \, \rho_g \, L^3}$$ [6. 30]

From this equation it is obvious that the same Euler number can be obtained in two different tubular reactors if the length and the diameter are chosen wisely. Using a different expression for the friction factor, such as Prandtl's equation, leads to similar conclusions; a similar pressure profile can be obtained by a carefully chosen combination of the length and the diameter of the reactor. In this case, the Blasius equation is more properly suited as it expresses the Fanning friction factor explicitly as a function of the reactor variables, and hence the relation with the other dimensionless numbers is explicit. However, a decrease of the tube diameter inevitably leads to a decrease of the radial temperature drop. Hence, it is not possible to obtain both the same radial temperature and axial pressure profile in two different steam cracking coils. Two options for scale-up under partial similarity thus remain:

- maintaining a similar axial pressure profile [i.e. the same value of the Euler number, *Eu*] and abandoning similarity of radial transport [i.e. allowing different values of the Peclet number, *Pe,* and the Fanning friction factor, *Fo*]
- maintaining similar radial transport properties [i.e. the same values for *Pe* and *Fo*] and abandoning a similar axial pressure profile [i.e. allowing different values of *Eu*]

In what follows, these two options for scaling up steam cracking coils under partial similarity are discussed in more detail.

6.3.3   Influence of relaxation of criteria of similarity on scale-up

The previous discussion shows that two routes remain available for relaxing the similarity criteria to scale-up or scale-down tubular steam cracking reactors. The influence of relaxation can be investigated either by performing experiments with reactors of different scale or by performing theoretical calculations using a mathematical model. The main disadvantage of the experimental approach is that these experiments can be error-prone, especially when small scale reactors are used as pointed out by Van Damme and Froment (1981). Therefore theoretical

calculations are used to estimate the highest achievable accuracy upon a change of scale for a tubular steam cracking reactor. The differences found for reactant conversions and for the predicted yields of the main products are generally used as measure for the accuracy (Zlokarnik et al., 2002). For very simple systems an analytical solution can be used to estimate the accuracy of scale-up, e.g. the analytical solution for an isothermal plug flow reactor with axial dispersion and a fist order reaction enables to estimate the difference on conversion if axial dispersion is neglected (Nauman and Mallikarjun, 1983). However in this case such an analytical solution is not available and only a detailed mathematical description of the process is appropriate to estimate the differences resulting from a change in scale. Simulation results using a simulation model based on the detailed mathematical description of the steam cracking process then allow estimating the overall accuracy.

A 2-dimensional reactor model is used to simulate the steam cracking process. This enables a straightforward evaluation of both the role of the radial temperature profile and the effect of the axial pressure profile on the conversion and the product yields. For ordinary tubular reactors a 2-dimensional model is sufficient because of axial symmetry, but more complex geometries such as internally finned cracking coils demand a 3-dimensional reactor model (De Saegher et al., 1996). The reactor model equations are given by equations [6.14], [6.15] and [6.16]. For the axial velocity component v_z the von Karman profile (Davies, 1972) is used. After calculating the axial velocity profile, the radial component of the velocity v_r can be deduced from a total mass balance (Van Geem et al., 2004 [a]). The diffusivity and thermal conductivity are calculated based on the correlation of Reichardt, corrected as proposed by Sundaram and Froment (1979). The reactor model is coupled to a radical kinetic model for the cracking of naphtha and ethane. It consists of 60 molecular and 68 radical species and more than 1200 reactions (Clymans, 1984; Van Geem et al., 2004 [a]). This kinetic model has been used and validated for many conditions and feedstocks (Plehiers et al., 1991; Heynderickx and Froment, 1998; Van Geem et al., 2005). The implementation of a kinetic model based on a radical reaction mechanism results in a stiff set of differential equations. Therefore a special solution method is used (Van Geem et al., 2004 [a]). First the differential equations for a specific variable in a radial section are divided in *n* grid points and rewritten in a tridiagonal format. This set of equations is solved simultaneously by the Thomas-algorithm. The two strategies for scaling up or down stream cracking coils can now be evaluated.

6.3.3.1 *Case 1: Similar Axial Pressure Profile*

As mentioned above, a first analysis of the dimensionless numbers shows that the radial temperature profile can be similar in two reactors only if they have the same diameter and if they are operated under a similar axial heat flux profile. Generally this is not the case and the diameter of the small scale reactor is typically an order of magnitude smaller than that of the large scale reactor. Consequently the radial temperature drop is also an order of magnitude smaller in the small scale reactor as compared to the large scale reactor, i.e. of the order of 10 K in the small scale reactor and 100 K in the large scale reactor. The worst case scenario is the situation in which the radial temperature drop is almost non existing $[d_t \rightarrow 0; \text{Pe} \rightarrow 0; \text{Fo} \rightarrow \infty]$ in the small scale reactor, i.e. a 1-dimensional situation, and is strongly pronounced in the large scale reactor. In that case, the effect on the conversion and the product yields is maximal. This maximal difference can thus be estimated by comparing the 2-dimensional simulation results for an industrial reactor, exhibiting an important radial temperature profile, with the results obtained from a 1-dimensional reactor model under the same conditions. In the 1-dimensional simulation, the radial temperature profile is completely ignored. Hence, the 1-dimensional simulation can be considered as a measure for a pilot plant reactor working under completely the same operation conditions as the industrial reactor, i.e. the same residence time, similar axial temperature and pressure profile. The reactor used in the simulations is a traditional Lummus SRT-I reactor with a uniform diameter of 0.12 m and a length of 101 m. As it requires both high heat fluxes and has a large reactor diameter, the radial temperature profile is expected to be pronounced. As feedstock pure ethane is chosen because this feedstock has a strong refractory character and thus requires high temperatures and high heat fluxes to crack. The axial temperature profile used in the 1-dimensional reactor model is the same as the average 2-dimensional temperature profile. To calculate the average 2-dimensional temperature at a certain axial position the cup mixing temperature is applied (Bird et al., 2001):

$$T_{av} = \frac{\int_0^R T(r)\, v(r)\, r\, dr}{\int_0^R v(r)\, r\, dr} \tag{6.31}$$

The results obtained with both reactor models then allow to compare the influence of abandoning the radial dispersion terms in equations [6.17] and [6.18].
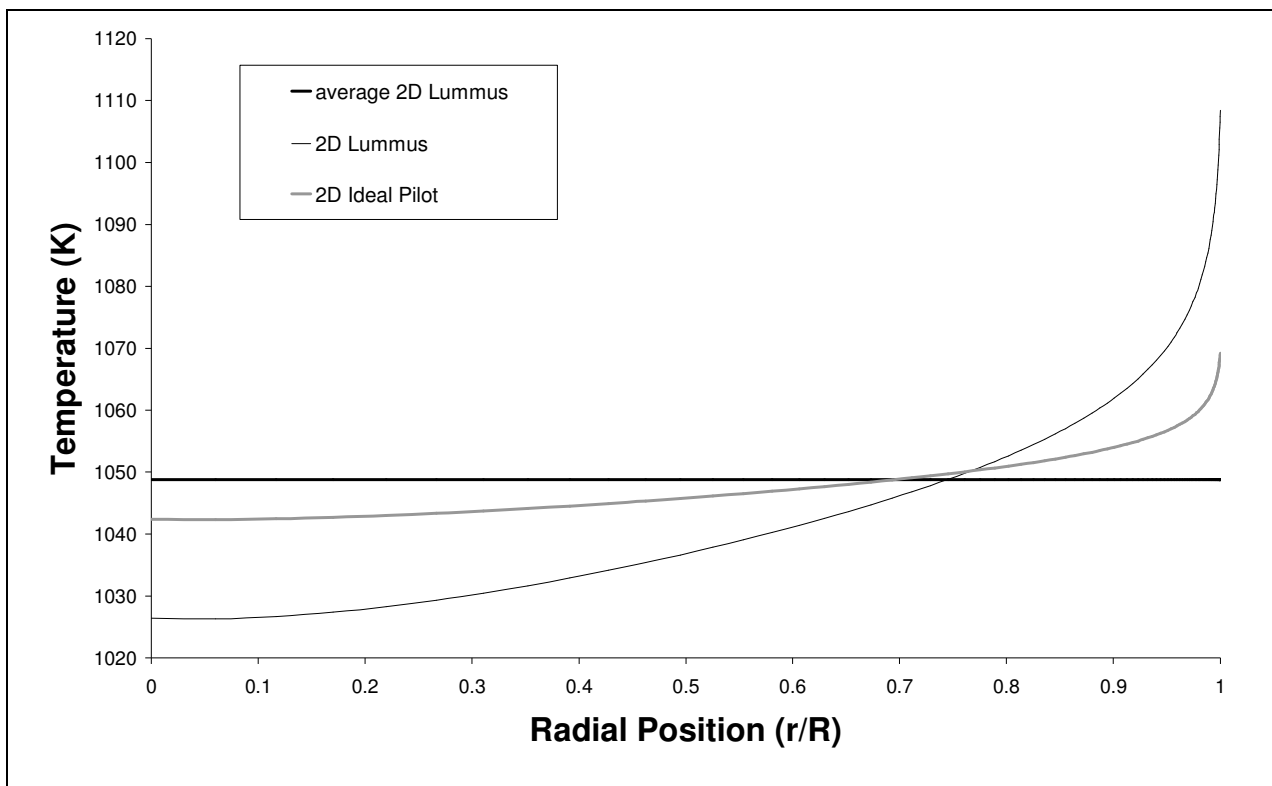
Figure 6.13: Radial temperature profile in the middle of an industrial Lummus SRT-I reactor (101.0 m long and with a diameter of 0.12 m) and in the ideal pilot plant reactor (20.0 m long and with a diameter of $2.5 \ 10^{-2}$ m). [—— 2D simulation of ethane steam cracking in Lummus SRT-I reactor, Feed flow rate: 0.97 kg s^{-1}, dilution: 0.35 kg steam/ kg HC, CIP: 0.34 MPa, COT: 1100 K, Fo = 7; —— 2D simulation of ethane steam cracking in pilot plant reactor, Feed flow rate: $5.1 \ 10^{-3}$ kg s^{-1}, dilution: 0.35 kg steam/ kg HC, CIP: 0.30 MPa, COT: 1100 K, Fo = 170]

In Figure 6.13 the radial temperature profile and the average temperature at the middle of the Lummus SRT-I reactor are shown. The process conditions used in the different simulations and the simulation results are summarized in Table 6.10. Using a similar axial pressure profile but neglecting the radial temperature profile in reactors of different scale can lead to significant differences; 4.0 % (rel.) on the conversion and 1.2 % (rel.) on the ethylene yield.

	Lummus SRT-I reactor				
Reactor length (m)	101.0				
Tube diameter (m)	$1.2 \ 10^{-1}$				
CIT (K)	873				
COT (K)	1100				
Dilution (kg steam/kg HC)	0.35				
Flow rate (kg s⁻¹)	$9.7 \ 10^{-1}$				
Residence time (s)	0.7				
	1 D	**2 D CIP**	**2 D av.**	**2 D COP**	**2 D ref.**
CIP (MPa)	0.34	0.34	0.30	0.26	0.34
COP (MPa)	0.22	0.30	0.26	0.22	0.22
Eu	8.3	25	25	25	8.3
Pe	0	$1.4 \ 10^{-1}$	$1.4 \ 10^{-1}$	$1.4 \ 10^{-1}$	$1.4 \ 10^{-1}$
Fo	∞	7	7	7	7
	Weight Fractions (%)				
H_2	3.0	3.1	3.1	3.1	3.1
CH_4	2.5	2.7	3.0	2.5	2.9
C_2H_2	0.3	0.3	0.3	0.4	0.4
C_2H_4	40.0	40.5	40.7	40.5	40.8
C_3H_6	0.7	1.0	0.8	0.7	0.7
C_4H_6	0.8	1.2	1.1	1.0	1.0
C_4H_{10}	0.9	0.9	0.8	0.8	0.8
C_2H_6**-conversion**	48.7	51.8	50.9	49.7	50.6

Table 6.10: Reactor geometry, operating conditions and simulation results for ethane cracking in an industrial Lummus SRT-I reactor [**1D**: 1-dimensional simulation with same average axial T-profile as 2D ref., **2D CIP**: same T-profile and CIP as 2D ref., **2D av.**: same T-profile and average pressure as 2D ref., **2D COP**: same T-profile and COP as 2D ref., **2D ref.**: 2-dimensional simulation for reference conditions]

The simulation results In Table 6.10 show that using the 2-dimensional reactor model [2D ref.] a higher ethane conversion (1.9 %) is simulated than with the 1-dimensional reactor model [1D]. On the other hand, the difference between the ethylene yield simulated with the 1-dimensional [1D] and the 2-dimensional reactor model [2D ref.] is less pronounced (0.8 %). For the other important products such as hydrogen, methane or propylene the differences remain relatively small (0.1 – 0.4 %). Van Geem et al. (2004 [a]) showed that the radial temperature profile increases the ethane conversion but decreases the ethylene selectivity because light olefins are removed by secondary reactions generating species with higher molecular weight such as propylene and butadiene. Overall the differences are quite important especially for the conversion, and hence, it can be concluded that neglecting the radial temperature profile has a significant influence on the yields of the main products. Hence, when the scale is changed it is important to keep the radial temperature profile as similar as possible; otherwise the product yields will differ significantly although they are operated under similar conditions. Note that in the previous 2-dimensional reactor simulations the heat flux to the process gas is taken uniform around the circumference of the tube. Due to the shadow effects in a furnace there exists a non uniform heat flux along the perimeter of the coils of the cracking furnace. This effect causes a circumferential variation of the internal tube skin temperature of the order of 20 to 30 °C (Heynderickx et al., 1992), resulting in circumferential process gas differences of the order of 10 °C. The latter is quite small compared to the difference of 100 °C in radial direction, and hence, the circumferential non-uniformities will have a negligible influence on the calculated product yields.

6.3.3.2 *Case 2: Similar Radial Temperature Profile*

Estimating the effect of differences in the axial pressure profile on the yields is more difficult than estimating the effect of differences in the radial temperature profile. Generally the pressure drop in the small scale reactor is significantly lower than the pressure drop observed in long industrial reactors such as the Lummus SRT-I reactor used in the previous simulations. For example the pressure drop in the pilot reactor used at the Laboratorium voor Petrochemische Techniek of Ghent University with a length of 12.4 m and a diameter of 0.01 m is typically 0.04 MPa, while in the Lummus SRT-I reactor the pressure drop is over 0.12 MPa under similar operating conditions. By increasing the length of the pilot plant reactor the pressure drop can be

increased but for practical reasons the length of a pilot plant reactor is typically limited to 20 m. To estimate the effect of relaxing the similarity of the axial pressure profile for a given radial temperature profile simulations have to be performed with different axial pressure profiles in the reactor but similar radial temperature profiles. Therefore the simulation results obtained for the base case of the Lummus SRT-I reactor with a pressure drop of 0.12 MPa [2D ref.] are compared with the simulation results obtained for the Lummus SRT-I reactor in which the same radial and axial temperature profile exists but with a pressure drop that matches the one observed in the pilot plant unit, i.e. 0.04 MPa. This last simulation case can be considered as a measure for a pilot plant reactor working under similar operation conditions as the industrial reactor, i.e. the same residence time, similar axial and radial temperature profile, but with a different axial pressure profile. However, different alternatives are available to realize the reduced pressure drop. One alternative is to maintain the same coil inlet pressure (CIP) as in the reference case [2D CIP]. Other alternatives consist in maintaining the same average pressure [2D av.] or in maintaining the same coil outlet pressure (COP) as the reference case [2D COP]. At a first glance, maintaining the same COP seems to be the best option because in the last part of the reactor the temperature is the highest and thus most of the feedstock is converted into light olefins in the final part of the reactor. The conditions and the simulation results for the three different cases are summarized in Table 6.10. The results in Table 6.10 show that scale-up using equal *Pe* and *Fo* numbers but loosing similarity for the axial pressure profile, i.e. different Eu number, can also lead to significant differences. Especially when the same CIP [2D CIP] or the same COP [2D COP] is used the differences can become important. The smallest differences resulting from differences in pressure are found for the reactor that operates under the same average pressure [2D av.] as the reference case [2D ref.]. Table 6.10 shows that although the Eu numbers differ significantly (Eu = 25 in 2D ref.; Eu = 7 in 2D av.) the simulated conversion and the simulated ethylene yield differ less than 0.3 wt%. The differences resulting from relaxing the similarity of the axial pressure profile are then at best 0.6 % (rel.) on the conversion and 0.2 % (rel.) on the ethylene yield. Thus if the scale is changed and the pressure drop is different in the reactors of different scale this should not necessarily lead to difference if the pressure in the small scale unit is chosen appropriately. However, the errors induced by relaxing the similarity of the axial pressure profile can be in the same order as the one from neglecting the radial temperature profile if this rule of thumb is neglected. Summarizing, the previous results suggest,

as more or less expected, that retaining the similarity of the radial temperature profile is more important than retaining a similar axial pressure profile.

6.3.4   The "ideal" pilot plant reactor for direct experimental scale-up

Although application of the theory of similarity to scaling up steam cracking has some shortcomings it clearly is a powerful tool to tackle the problem of scale-up and scale-down. The main objective in what follows is to explore how the previous conclusions can contribute to the design of the ideal pilot plant reactor, i.e. a pilot reactor that, if operated under similar process conditions as the industrial reference unit, results in an almost identical product distribution. The simulation results indicate that it is more important to focus the design of a pilot plant reactor on obtaining a similar radial temperature profile, than on obtaining a similar axial pressure profile. Creating a unit with a similar radial temperature profile requires that the reactors have the same diameter, see equations [6.20] and [6.22], and a similar heat flux profile, see equation [6.26]. The length of the reactor can be chosen freely, as long as the reactor is operated under the same average pressure as the industrial unit. However, practical considerations also affect the design of a pilot plant reactor. The minimum diameter of the pilot reactor tube is limited by the need to measure process variables, such as gas phase temperature. As the available dimensions of the furnace are limited too, the reactor length should not be more than 20 m. Other aspects also affect the design of the reactor. Van Damme et al. (1975) pointed out that the dimensions of the pilot reactor should be chosen so as to achieve turbulent flow conditions in the coil with reasonable flow rates. Therefore the dimensions and the operating conditions should be in the range of those specified in Table 6.9. Taking into account these practical limitations result in a length of 20 m and a diameter of $2.5 \, 10^{-2}$ m for an ideal pilot plant reactor for the Lummus SRT-I reactor. The total flow rate (hydrocarbons + steam) should be about $6.5 \, 10^{-3}$ kg s^{-1} to obtain the same residence time as in the Lummus SRT-I reactor (1 s). These conditions also guarantee a turbulent flow regime (Re > 10000) in the reactor.

It is also important to investigate if these conclusions also apply for feedstocks such as naphtha or gas oil. Therefore simulations have been carried out using n-butane as feedstock. n-Butane is a good model compound for light naphtha feedstocks because the obtained product distribution is close to the product distribution obtained with a naphtha feedstock.

	Lummus SRT-I reactor		
Reactor length (m)	101.0		
Tube diameter (m)	$1.2 \ 10^{-1}$		
CIT (K)	873		
COT (K)	1100		
Dilution (kg steam/kg HC)	0.5		
Flow rate (kg s^{-1})	$9.7 \ 10^{-1}$		
Residence time (s)	0.7		
	1 D	**2 D av.**	**2 D ref.**
CIP (MPa)	0.34	0.34	0.30
COP (MPa)	0.22	0.30	0.26
Eu	8.3	25	8.3
Pe	0	$9.1 \ 10^{-2}$	$9.1 \ 10^{-2}$
Fo	∞	11	11
	Weight Fractions (%)		
H_2	0.8	0.8	0.8
CH_4	22.0	22.9	22.2
C_2H_2	0.7	0.6	0.7
C_2H_4	32.9	34.4	34.1
C_2H_6	4.3	4.6	4.4
C_3H_6	16.7	16.0	16.4
C_4H_6	2.4	2.5	2.5
$1\text{-}C_4H_8$	1.1	1.2	1.1
C_6H_6	3.5	4.3	4.0
C_4H_{10}-**conversion**	91.0	93.3	92.8

Table 6.11: Reactor geometry, process conditions and simulation results for n-butane cracking in an industrial Lummus SRT-I reactor [**1D**: 1-dimensional simulation with same average axial T-profile as 2D ref., **2D CIP**: same T-profile and CIP as 2D ref., **2D COP**: same T-profile and COP as 2D ref., **2D av.**: same T-profile and average pressure as 2D ref., **2D ref.**: 2-dimensional simulation for reference conditions]

	Millisecond reactor		
Reactor length (m)	10.0		
Tube diameter (m)	$3.5 \ 10^{-2}$		
CIT (K)	940		
COT (K)	1130		
Dilution (kg steam/kg HC)	0.35		
Flow rate (kg s^{-1})	$6.4 \ 10^{-2}$		
Residence time (s)	0.1		
	1 D	**2 D av.**	**2 D ref.**
CIP (MPa)	0.25	0.23	0.25
COP (MPa)	0.18	0.19	0.18
Eu	15	45	15
Pe	0	$1.0 \ 10^{-1}$	$1.0 \ 10^{-1}$
Fo	∞	10	10
	Weight Fractions (%)		
H$_2$	3.0	3.1	3.1
CH$_4$	1.6	1.9	1.9
C$_2$H$_2$	0.5	0.6	0.6
C$_2$H$_4$	40.5	41.1	41.0
C$_3$H$_6$	0.5	0.5	0.5
C$_4$H$_6$	0.7	0.8	0.8
C$_4$H$_{10}$	0.6	0.6	0.6
C$_2$H$_6$-conversion	47.8	49.1	49.0

Table 6.12: Reactor geometry, process conditions and simulation results for ethane cracking in an industrial Millisecond reactor [**1D**: 1-dimensional simulation with same average axial T-profile as 2D ref., **2D av.**: same T-profile and average pressure as 2D ref., **2D ref.**: 2-dimensional simulation for reference conditions]

Table 6.11 shows that the same conclusions are found as for ethane cracking. The differences caused by the radial temperature profile and the axial pressure profile are even slightly less

pronounced than for the ethane case. This is because radial non-uniformities are smaller when n-butane is used, see the higher values of the Fourier number *Fo* in Table 6.11. The differences from neglecting the radial temperature profile [Table 6.11, compare 1D and 2D ref.] are 2.0 % (rel.) on the conversion and 3.6 % (rel.) on the ethylene yield, while neglecting the similarity of the axial pressure profile leads to smaller differences [Table 6.11, compare 2D av. and 2D ref.]; 0.8 % (rel.) on the conversion and 1.0 % (rel.) on the ethylene yield. Also for the other important products the differences remain overall relatively small. For the propylene yield the differences caused by neglecting the radial temperature profile are 0.3 %, while for the benzene yield the difference is 0.5 %.

Another important issue is whether the dimensions of the ideal pilot plant reactor will remain valid if instead of a Lummus SRT-1 reactor another reactor is to be scaled down. The dimensionless model equations show that relaxing similarity of the radial temperature profile and the axial pressure profile results in differences in going from one scale to another. Large heat fluxes and large reactor diameters increase the influence of dissimilarity of the radial temperature profile. In fact, the Lummus SRT-I reactor presents the most difficult case as it requires high heat fluxes and also has a large reactor diameter. For other reactors, e.g. the Millisecond reactor requiring high heat fluxes but with a much smaller reactor diameter, the effect of the radial temperature profile on the product yields is less pronounced (Van Geem et al., 2004 [a]). Also, the pressure drop for the Lummus SRT-I reactor is relatively high as compared to other reactors, such as split coils or Millisecond reactors. A Millisecond reactor consists of a large number of tubes [200] of small diameter [$3.5 \ 10^{-2}$ m] and short length [10 m] (Orriss and Yamaguchi, 1987). The total hydrocarbon flow rate of more than 20 ton hr^{-1} results in very high velocities in all of the 200 parallel tubes. Simulation results, see Table 6.12, for one of the parallel tubes of the Millisecond reactor show that also for this type of reactor the effect of neglecting the radial temperature profile remains more important than that of neglecting the axial pressure profile. Neglecting the radial temperature profile [Table 6.12; compare 1D and 2D ref.] leads in this case to a difference of 2.5 % (rel.) on the conversion and 1.2 % (rel.) on the ethylene yield, while the difference for relaxing the pressure similarity [Table 6.12; compare 2D av. and 2D ref.] is 0.2 % (rel.) on the conversion and 0.2 % (rel.) on the ethylene yield. Hence, also the influence of the axial pressure profile is most pronounced for the Lummus SRT-I reactor as compared to other reactor types. In general, it can thus be concluded that in designing a pilot plant reactor priority

should be given to obtain a similar radial temperature profile while dissimilarities of the axial pressure profile can be tolerated to a larger extent. Consequently, the diameter specified previously, i.e. 2.5 10^{-2} m, remains valid for the ideal pilot plant of a Millisecond reactor. However, in this case, it is advised that length of the pilot plant reactor remains below 20 m as this length would require too high flow rates to realize the short residence times used in the Millisecond reactor (0.1 s). Therefore the same length as the Millisecond reactor is chosen, i.e. 10 m. The total flow rate (hydrocarbons + steam) should be higher than 2.0 10^{-2} kg s^{-1} to realize the low residence times and to guarantee a turbulent flow regime in the reactor.

	Lummus SRT-I	Split coil	Millisecond	U tube S&W	Intrinsic kinetics
Diameter (m)	2.5 10^{-2}	2.5 10^{-2}	2.5 10^{-2}	2.5 10^{-2}	5.0 10^{-3}
Length (m)	20	20	10	20	20
Feed flow rate (kg s⁻¹)	6.0 10^{-3}	9.0 10^{-2}	2.0 10^{-2}	1.3 10^{-2}	5.0 10^{-4}
COT (K)	1060 - 1120	1060 - 1140	1150 - 1230	1080 - 1160	950 - 1170
CIP (Mpa)	0.35	0.3	0.25	0.27	0.40 - 0.22
Re	1.0 10^{4}	2.0 10^{4}	5.0 10^{4}	2.0 10^{4}	5.0 10^{3}
Residence time (s)	1	0.4	0.1	0.3	0.5

Table 6.13: Design and typical operation conditions of the ideal pilot plant reactor for scale-down of several industrial reactors (Lummus SRT-I, Split coil, Millisecond, U tube Stone & Webster) and for studying intrinsic kinetics.

The simulation results for n-butane and ethane show that, independent of the feedstock, it is more important to focus the design of a pilot plant reactor on obtaining more or less the same radial temperature profile, than on trying to create a unit with a similar axial pressure profile. In Table 6.13 an overview is given of the dimensions of the ideal pilot reactor and the typical operation conditions if different reactor types are to be scaled down. Irrespective of the type of reactor to be scaled down, the diameter of the ideal pilot plant reactor amounts to 2.5 10^{-2} m. If a split coil [Lummus SRT II–V] or a U-tube in a Stone & Webster furnace is to be scaled down, it is advised that the reactor is as long as possible [20 – 25 m] to retain the similarity of the axial

pressure profile. The residence time in these last two reactors varies between 0.3 s and 0.5 s, therefore the recommended flow rates are higher than in the Lummus SRT-I reactor. For the specified flow rates, a turbulent flow regime in the pilot plant reactor is always guaranteed (Re > 10000). Table 6.13 clearly illustrates that the dimensions of the "ideal" pilot plant reactor do not depend heavily on the type of industrial reactor to be scaled down but that only the flow rate varies significantly if the same residence time as in the industrial reactor is to be obtained.

6.3.5   The "ideal" pilot plant reactor for studying intrinsic kinetics

Although the design of the previous pilot plant is "ideal" for direct experimental scale-up, imperfections still remain. To some extent differences between the observed conversion and product yields in the ideal pilot plant reactor and the industrial reactor are inevitable as the radial temperature drop is still significantly lower in the ideal pilot plant reactor than the one observed in an industrial reactor operated under similar conditions; see Figure 6.12. Therefore, predicting yields based on fundamental simulation models will always yield more accurate results than transferring experimental data from one reactor to another. Moreover, fundamental models, properly describing transport phenomena, have the advantage that they are more user-friendly, significantly faster and less error-prone than a direct experimental scale-up approach. Consequently, the development of fundamental models remains important. As this type of models require intrinsic kinetics, an accurate measurement of the process gas temperature is crucial if the ideal pilot reactor is to be used to gather intrinsic kinetic data. In practice, it is not possible to accurately measure the radial temperature profile at a given axial position. Hence, to study intrinsic kinetics the radial temperature gradient should be kept as small as possible. However, also some practical considerations affect the design of the ideal pilot plant reactor for studying intrinsic kinetics. As stated before, the diameter of the reactor must enable measurement of the process gas temperature and this requires the accommodation of a thermocouple. Taking into account this limitation the diameter of the reactor should be at least $5 \; 10^{-3}$ m. Recommended dimensions for a pilot plant reactor for studying intrinsic kinetics are given in Table 6.13. This design results in a radial temperature gradient in the reactor of only 5 K. Moreover, the latter is almost entirely located in a small zone near the wall, as can be seen in Figure 6.14. Therefore, a pilot plant reactor diameter of $5 \; 10^{-3}$ m is perfectly suited for studying intrinsic kinetics as the

measured gas temperature in the centre of the tube at a given axial position will be almost the same as the gas temperature nearer to the wall. Only near the wall minor differences can be observed in a zone limited to $5 \cdot 10^{-4}$ m. Of course it should be absolutely avoided that wall effects become important because decreasing the diameter results in an increased surface to volume ratio. An increased surface to volume ratio will benefit coke formation and other reactions catalyzed by the reactor wall such as steam reforming. Therefore special materials should be used for constructing the pilot reactor, e.g. with low Ni content. For this reason the reactor is sometimes coated or made in quartz (Golombok et al., 2001).
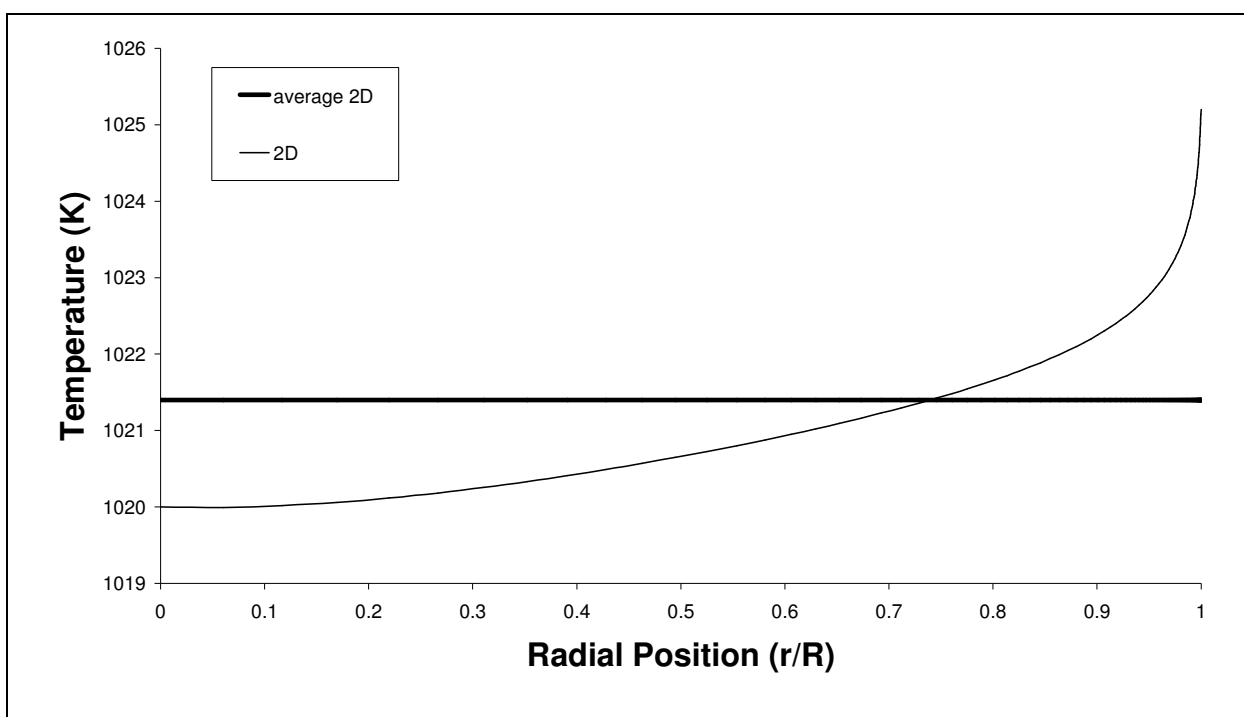
Figure 6.14: Radial temperature profile in the middle of a pilot plant reactor of 20 m long and with a diameter of 5 mm. [—— 2D simulation of ethane steam cracking, Feed flow rate: : $1 \cdot 10^{-3}$ kg s^{-1}, dilution: 0.35 kg steam/ kg HC, CIP: 0.34 MPa, COT: 1100 K, Fo = 5000]

It should be mentioned that until now only operation under initial conditions, i.e. when no coke is formed on the reactor surface, has been considered. To transfer data on coke formation from one reactor to another the conditions at the reactor wall/process gas interface, i.e. pressure, temperature and species concentrations have to be identical. However, analysis of the

dimensionless model equations shows that realizing a similar radial temperature profile and similar axial pressure profile in two tubular reactors for steam cracking is only possible if these reactors are identical. Consequently direct experimental scale-up of results obtained for coke formation data is not possible. The only solution is developing a fundamental coke formation model and predicting the run length based on a simulation model. The role of a pilot plant reactor for studying coke formation is thus limited to developing fundamental coke formation models. Again an accurate measurement of the process gas temperature and the temperature at the reactor wall/process gas interface is crucial. Hence, to study coke formation in a pilot plant reactor the radial temperature drop should be kept as small as possible. The reactor developed for studying intrinsic kinetics is thus also an appropriate reactor for developing a fundamental coke formation model.

6.3.6   Conclusions

The theory of similarity is applied to change the scale of a steam cracking coil. According to the theory of similarity two processes are similar if they take place in a similar geometry, and if all dimensionless numbers necessary to describe the process, have the same numerical value. The dimensionless numbers are found based on the detailed mathematical description of the steam cracking process. These dimensionless model equations show that complete similarity can never be reached for 2 different tubular reactors. The criteria for process-related similarity, geometrical similarity and hydrodynamic similarity cannot be met simultaneously and therefore both geometrical similarity and hydrodynamic similarity need to be abandoned. Scale-up is thus only possible under partial similarity and inevitably this leads to differences. However, if the criteria of similarity are relaxed with care only small differences between units of different scale can be obtained. Further analysis of the dimensionless model equations shows that neglecting hydrodynamic and geometrical similarity is still insufficient. Problems remain, in particular with realizing a similar radial temperature and axial pressure profile. Realizing a similar radial temperature profile and similar axial pressure profile in two tubular reactors for steam cracking is only possible if these reactors are identical. Hence, two different relaxation strategies are applied; the first one aims at realizing a similar axial pressure profile neglecting radial non-uniformities, the second focuses on realizing a similar radial temperature profile. Neglecting the similarity of

the radial temperature profile leads to more important differences compared to the differences resulting from neglecting the similarity of the axial pressure profile. The errors made for ethane cracking in a Lummus SRT-I reactor for neglecting the radial temperature profile are 4.0 % (rel.) for the conversion and 1.2 % (rel.) for the ethylene yield, while for neglecting the axial pressure profile 0.6 % (rel.) for the conversion and 0.2 % (rel.) for the ethylene yield. The preceding rules make it possible to design a so-called ideal pilot plant reactor based on a specific industrial reactor, i.e. a reactor with a similar radial temperature profile as the reference reactor. On the one hand the reactors should have similar diameters. On the other hand the heat flux profile in the two reactors should be as similar as possible. However for practical limitations it is not possible to create pilot reactors with diameters of over $2.5 \ 10^{-2}$ m. The length of the reactor can be chosen freely, as long as the reactor is operated under an average pressure as in the industrial unit. Applying the preceding rules on the Lummus SRT-I reactor leads to a pilot plant reactor with a diameter of $2.5 \ 10^{-2}$ m and a length of 20 m. Clearly, these dimensions are strongly influenced by the practical limitations, but stay unchanged when instead of the Lummus SRT-I coil a split coil or a U-tube [Stone & Webster] should be scaled down. To study the intrinsic kinetics accurately the radial temperature drop should be as small as possible and the effects of transport phenomena should be as small as possible, hence, the diameter of the reactor should be as small as possible. Applying this rule results in a completely different design of the pilot plant reactor. Direct experimental scale-up of results obtained for coke formation is not possible. Only simulations using a fundamental coke formation model are able to provide accurate run lengths of industrial installations.

6.4   References

Bennet M.J., Price J.B. A physical and chemical examination of an ethane steam cracker: coke and of the underlying pyrolysis tube, J. Mater. Sci., 16, 170-188, 1981.

Bird R.B., Lightfood E.N., Stewart W.E. Transport Phenomena, Wiley: New York, 2001.

Broadbelt L.J., Stark S.M., Klein M.T. Termination of Computer Generated Reaction-Mechanisms – Species Rank-Based Convergence Criterion, Ind. & Eng. Chem. Res., 34, 2566-2573, 1995.

Buckingham E. On physically similar systems, illustration of the use of dimensional equations. Phys. Review, 4, 345-376, 1914.

Butterfield R. Dimensional analysis for geotechnical engineers. Géotechnique, 49, 357-366, 1999.

Clymans P.J., Froment G.F. Computer Generation of Reaction Paths and Rate Equations in the Thermal Cracking of Normal and Branched Paraffins, Comp. Chem. Eng., 8, 137, 1984.

Damköhler G.Z. Einflüsse der Strömung, Diffusion und des Wärmeübergenges auf die Leistung von Reactionsöfen, Electrochemie, 42, 846-862, 1936.

Davis H.G., Farell T.J., Relative and absolute rates of decomposition of light paraffins under practical operation conditions, Ind. Eng. Chem. Proc. Des. Dev., 12, 171-181, 1973.

Dente M., Ranzi E. Detailed Prediction of Olefin Yields from Hydrocarbon Pyrolysis through a Fundamental Simulation Program (SPYRO), Comp. & Chem. Eng., 3, 61, 1979.

Dente M., Pierucci S., Ranzi E. New improvements in modeling kinetic schemes for hydrocarbon pyrolysis, Chem. Eng. Sci., 47, 2629-2634, 1992.

De Saegher J.J., De Temmerman T., Froment G.F. Three dimensional simulation of high severity internally finned cracking coils for olefins production. Revue de l'Institut Français du Petrole, 51, 245-260, 1996.

Elvers B., Hawkins S., Schulz G. Tubular reactors, Ullmann's Encyclopedy of Industrial Chemistry. B4, 181-198, 1992.

Esbesen K.H. Multivariate Data Analysis In Practice, 5th ed., CAMO, Aalborg University: Esbjerg, Denmark, 2001.

Figueiredo J.L. Filamentous Carbon. Erdöl und Kohle-Erdgas-Petrochemie, 42, 294-297, 1989.

Froment G.F., Bischoff K.B., Chemical Reactor Design and Analysis, Wiley: New York 1990.

Froment G.F. Thermal Cracking for Olefins Production. Fundamentals and their Application to Industrial Problems, Chem. Eng. Sci., 36, 1271-1282, 1981.

Froment G.F. Coke formation in the thermal cracking of hydrocarbons, Rev. Chem. Eng., 6, 295-328, 1990.

Froment G.F. Kinetics and reactor design in the thermal cracking for olefins production, Chem. Eng. Sci., 47, 2163-2177, 1992.

Garg R.K., Srivastava V.K., Krishnan V.V. Non-isothermal modeling of ethane thermal cracker, AIChE Annual Meeting 2005, Cincinnati, OH, USA, 2005.

Golombok M., Van der Bijl J., Korngoor M. Severity Parameters for Steam Cracking, Ind. & Eng. Chem. Res, 40, 470-472, 2001.

Hannisdal A., Hemmingsen P.V., Sjo1blom J. Group-Type Analysis of Heavy Crude Oils Using Vibrational Spectroscopy in Combination with Multivariate Analysis, Ind. Eng. Chem. Res., 44, 1349-1357, 2005.

Heynderickx G.J., Cornelis G.G., Froment G.F. Circumferential tube skin temperature profiles in thermal cracking coils, AIChE Journal, 38, 1905-1912, 1992.

Heynderickx G.J., Froment G.F. Simulation and Comparison of the Run Length of an Ethane Cracking Furnace with Reactor Tubes of Circular and Elliptical Cross Sections, Ind. & Eng. Chem. Res., 37, 914, 1998.

Hillewaert, P., Dierickx, J.L., Froment, G.F. Computer generation of reaction schemes and rate equations for thermal cracking, AIChE Journal, 34, 17-24, 1988.

Himmelblau D.M., Bishoff K.B. Process analysis and simulation, J. Wiley, New York, 1968.

Himmelblau D.M., Jones C.R., Bischoff K.B. Determination of Rate Constants for Complex Kinetic Models, Ind. & Eng. Chem. Fund., 6, 539-543, 1967.

Joo E., Lee K., Lee M., Park S. CRACKER – a PC Based Simulator for Industrial Cracking Furnaces, Comp. Chem. Eng., 24, 1523-1528, 2000.

Nauman E.B., Mallikarjun R. Optimization in tubular reactors, ACS symposium series, 237, 305-322, 1983.

Nigam A., LaMarca C., Fake D., Klein M.T. Semi-empirical Rate Laws for Rice-Herzfeld Pyrolysis of Mixtures: Capturing Chemistry with Reasonable Computational Burden, Energy & Fuels, 6, 845-853, 1992.

Orriss, R., Yamaguchi, H. Idemitsu's Chiba ethylene plant proves modern technology. Oil & Gas Journal, 9, 27, 1987.

Perry, R.H., Green, D.W. Perry's chemical engineering handbook, McGraw-Hill, New York, 1997.

Pinter A., Tungler A., Nagy L., Vida L., Kovacs I., Kerezsi J. A laboratory steam cracking reactor to characterize raw materials, International Journal of Chemical Reactor Engineering, 2, A15, 2004.

Plehiers P.M., Froment G.F. The Reversed Split Coil improves Ethylene Yield, Oil & Gas Journal, 85, 41-48, 1987.

Plehiers P.M., Froment, G.F. Firebox simulation of olefin units, Chemical Engineering Communications, 80, 81-99, 1989.

Plehiers P.M., Froment G.F. The Uno-quattro Coil - High Severities for Increased Ethylene Selectivity, Ind. & Eng. Chem. Res., 30, 1081-1086, 1991.

Ranzi E., Dente M., Plerucci S., Biardi G. Initial Product Distribution from Pyrolysis of Normal and Branched Paraffins, Ind. & Eng. Chem. Fun., 22, 132-139, 1983.

Reyniers G.C., Froment G.F, Kopinke F.D., Zimmerman G. Coke modeling in the thermal cracking of hydrocarbons. 4. Modeling of coke formation in naphtha cracking, Ind. Eng. Chem. Res., 33, 2584-2590, 1994.

Shu W.R., Ross L.L. Cracking Severity Index in Pyrolysis of Petroleum Fractions, Ind. & Eng. Chem. Res. Proc. Des. Dev., 21 (3), 371-377, 1982.

Stichlmair J.G., Scale-up engineering, Begell house inc., New York, 2002. Sundaram, K.M., Froment G.F., Comparison of simulation models for empty tubular reactors, Chem. Eng. Sci., 34, 117-124, 1979.

Sundaram K.M., Froment G.F. 2 Dimensional model for the simulation of tubular reactors for thermal cracking, Chem. Eng. Sci., 35, 364-371, 1981.

Szepesy L. Feedstock Characterization and Prediction of Product Yields for Industrial Naphtha Crackers on the Basis of Laboratory and Bench-scale Pyrolysis. J. Anal. & Appl. Pyr., 1, 243-268, 1980.

Van Camp C.E., Van Damme P.S., Willems P.A., Clymans P.J., Froment G.F. Severity in the Pyrolysis of Petroleum Fractions: Fundamentals and Industrial Applications, Ind. & Eng. Chem. Res. Proc. Des. Dev., 24 (3), 561-570, 1985.

Van Damme P.S., Froment G.F., Balthasar W.B. Scaling Up of Naphtha Cracking Coils, Ind. & Eng. Chem. Res. Proc. Des. Dev., 20, 366-376, 1981.

Van Damme P.S., Clymans P.J., Froment G.F. Temperature, not time, controls steam cracking, Oil & Gas Journal, 82, 68-72, 1984.

Van Damme P.S., Narayanan S., Froment G.F. Thermal Cracking of Propane and Propane-Propylene Mixtures: Pilot Plant versus Industrial Data, AIChE Journal, 21 (6), 1065-1073, 1975.

Van Geem K.M., Heynderickx G.J., Marin G.B. A Comparison of One and Two-dimensional Reactor Models for Steam Cracking: Effect on Yields and Coking Rate, AIChE Journal, 50, 173 – 183, 2004 [a].

Van Geem K.M., Reyniers M.F., Marin G.B. First principles based reaction network for steam cracking, AIChE Annual Meeting 2004, Austin, TX, USA, 2004 [b].

Van Geem K.M., Reyniers M.F., Marin G.B. Two severity indices for scale-up of steam cracking coils, Ind. Eng. Chem. Res., 44, 3402-3411, 2005.

Van Goethem M.W.M., Kleinendorst F.I., Van Leeuwen C., Van Velzen N. Equation-based SPYRO[®] model and solver for the simulation of the steam cracking process, Comp. & Chem. Eng., 25, 905-911, 2001.

Wold S., Esbensen K., Geladi P. Principal Component Analysis, Chemom. Intell. Lab. Syst., 2, 37, 1987.

Zlokarnik M. Scale-up of processes using material systems with variable physical properties, Chem. Biochem. Eng. Q., 15, 43-47, 2001.

Zlokarnik M. Scale-up in Chemical Engineering, Wiley: Weinheim, 2002.

Chapter 7:

Molecular Reconstruction of Naphtha Fractions

7.1   Introduction

The petrochemical industry is continually striving to improve the performance of their installations. To this end, accurate mathematical simulation models are an indispensable tool. For reactor modeling, only fundamental kinetic models are able to simulate the chemical kinetics over a wide range of process conditions and for a wide range of feedstocks (Froment, 1992). These reactor models account for both the chemical reactions and the physical transport phenomena. Simulation models have the advantage that once the model is developed, results can be easily gathered and computer simulations take only a limited time (Dente et al., 1979). One of the major problems of these models is that a detailed feedstock composition is needed, and obtaining this kind of information is not straightforward. During the past decade, several analytical techniques to obtain a detailed molecular composition, e.g. GC (gas chromatography), GC-MS and HPLC (high performance liquid chromatography) have been developed and improved. However, all these techniques suffer from similar shortcomings; they are error-prone and time-consuming. Nowadays there is an increasing trend to replace these time-consuming analytical techniques by software modules that can be easily implemented in simulation packages. All these modules operate along the same fundamental principle: the reconstruction of the composition of a mixture based on some easily obtainable average properties of the mixture (e.g. the average molecular weight, the specific density, the H/C-ratio, the PIONA weight fractions and a set of ASTM boiling points), i.e. the so-called commercial indices of the mixture.

In literature, a distinction is made between two methods for feedstock reconstruction: methods using a pseudo component representation (lumped components), e.g. SPYRO [Dente et al. (1979, 2001)] and CRACKER [Joo et al. (2001)], and methods that try to obtain a more detailed molecular composition, e.g. Liguras and Allen (1989) [a, b], Quann and Jaffe (1996),

Neurock et al. (1994) and Hudebine and Verstraete (2004). Although methods based on reconstruction via lumped components are significantly faster, they are rather limited in their application range and not easily extendable. Moreover, methods using lumped components have traditionally a rather limited flexibility as they are based on a limited number of well-defined commercial indices. Hence, the method can only be applied if all the required indices are available. Moreover, additional analytical information about the mixture cannot improve the predicted composition because this extra information cannot be taken into account. The stochastic methods such as those developed by Neurock et al. (1994) and Hudebine (2003) do not show these disadvantages but are computationally very demanding (Hudebine et al., 2002). The main reason of the time-consuming character of the stochastic methods is that a new library of possible molecules is generated for each new simulation of the molecular composition. Therefore, stochastic methods are less attractive for implementation in fast commercial packages. The method developed by Liguras and Allen (1989, 1991) is significantly faster than the stochastic reconstruction methods of Neurock et al. (1994) or Hudebine et al. (2002) because these authors worked with a pre-defined molecular library. To determine the mole fractions of the molecules considered in the library, Liguras and Allen (1989, 1991) used information from both NMR spectrometry and GC-MS to specify over 190 constraints for the system of mole fractions. As the number of components exceeds the number of boundary conditions, the authors opted to solve this system by minimizing a weighted objective function P:

$$P = \sum_{i=1}^{N} \omega_i \cdot x_i \qquad [7.\ 1]$$

with ω_i the weight for component i. Allen and Liguras suggested, for example, to minimize the objective function P using the enthalpies of formation as weights for the different molecules. A disadvantage of the approach is that a huge amount of analytical information is needed to generate all these constraints. Still, the method is potentially very useful provided that its flexibility is drastically increased.

Clearly for each type of reconstruction method, several improvements are possible. The main objective in developing a new method for feedstock reconstruction is to retain the strong points and reduce/eliminate the weaknesses as much as possible. The main point in favor of the stochastic methods and those approaches used in SPYRO [Dente et al. (1979, 2001)] and

CRACKER [Joo et al. (2001)] is that the reconstruction of a detailed molecular composition is based on readily available commercial indices of the mixture. Therefore, the novel method developed at IFP (Hudebine et al., 2002; Hudebine, 2003; Wahl et al., 2006) and used in the present work also starts from easily obtainable commercial indices as input for obtaining the detailed feedstock composition. Moreover, similar to the approach followed by Liguras and Allen (1989 [a], 1989 [b]), this method determines the weight fractions of the molecules in the library that minimize an objective function and meet all the boundary conditions imposed by the commercial indices. However, this specific method is based on the optimization of Shannon's entropy criterion (1948), originally applied in the information theory, and results in some important advantages (Hudebine, 2003; Wahl et al., 2006). In what follows the principles of this method for feedstock reconstruction and its build up are discussed and explained. The approach is validated using experimental results obtained from a set of pilot plant experiments and via comparison with analytical results obtained for a number of naphtha feedstocks. Suggestions are made to extend the developed approach for other fractions such as gas oils or even heavier fractions.

7.2   Feedstock Characterization by Maximization of the Entropy

7.2.1   Overview of the Feedstock Characterization method

Shannon's Entropy theory is widely applied in all sorts of engineering fields, ranging from quantum chemistry over civil engineering to hydrodynamics. Shannon's entropy is defined as:

$$S(\pi_i) = -\sum_{i=1}^{N} \pi_i \cdot \ln \pi_i \qquad \text{with} \qquad \sum_{i=1}^{N} \pi_i = 1 \qquad\qquad [7.\,2]$$

in which S represents Shannon's entropy and π_i is the probability of a certain state. Shannon's entropy is a measure of the homogeneity of a probability distribution. The principle of maximum Shannon entropy states that if only partial information concerning the possible outcomes is available, the probabilities are to be chosen so as to maximize the uncertainty on the missing information (Shannon, 1948). A larger entropy corresponds with a more uniform distribution and hence with a larger uncertainty. Although information provides reasons for preferring some

possibilities over others, the best solution to avoid unwarranted conclusions is to assign a probability distribution which is as uniform as possible. This implies that the entropy has to be maximized subject to constraints representing the available information. By applying the principle of maximum entropy, the most random distribution subject to the given constraints can be obtained. Applying this theory to the composition of petroleum fractions implies that the probabilities in equation [7.1] are replaced by the mole fractions x_i of the feedstock components i. The first hypothesis of the method of maximization of the entropy is that in the absence of any information, it is impossible to favor one molecule with regard to another, and thus the distribution of mole fractions is uniform.
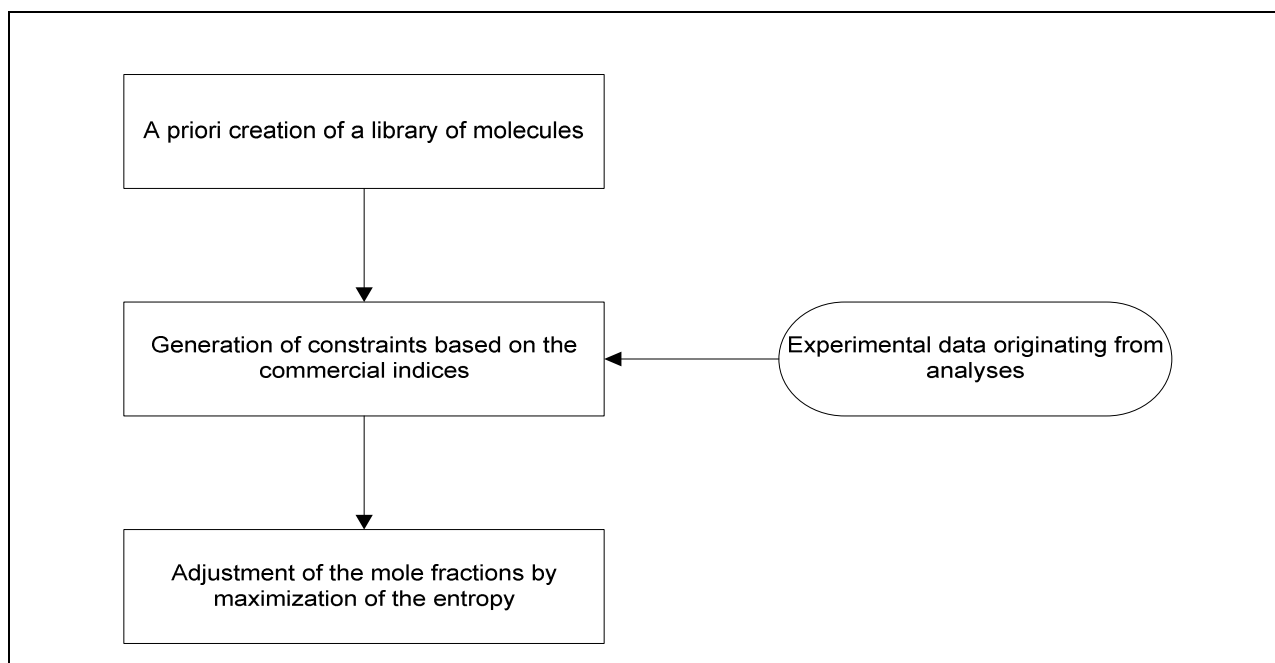
Figure 7.1: General scheme of the method of maximization of the entropy

In Figure 7.1, an overview of the method developed by IFP for feedstock reconstruction based on maximization of the entropy is given (Celie, 2004). First, a molecular library is selected. Next, the mole fractions of the molecules contained in the library are adjusted in order to obtain a mixture with the desired characteristics, i.e. the characteristics imposed by the commercial indices of the feedstock, e.g. the average molecular weight or the specific density. Evidently, the mole fractions should also meet the maximization criterion defined in equation

[7.1]. The computer program maximizes the objective function and delivers a molecular composition that meets the specified boundary conditions. In the following paragraphs, the method's build up is discussed in more detail.

7.2.2 Library Selection

Although the selection of a molecular library might seem trivial for the success of the feedstock characterization method, it is not. Evidently, a library containing components not representative for a feedstock can never result in an accurate characterization. One of the main reasons that a judicial selection of the library is of the utmost importance for the method based on the maximization of the information entropy is that this is a statistical method where no correlations are implemented. This method selects a single composition with maximum Shannon entropy out of a number of compositions that meet the boundary conditions. The molecular library determines the number of possible compositions that satisfy all the boundary conditions, and thus affects the outcome of the maximization method. If an important component is not included in the library, the composition obtained via the method can never be representative for the mixture. There are several possibilities for constructing a molecular library (Hudebine, 2003) ranging from experimental methods (Wahl et al., 2006), over group contribution methods (Hudebine et al., 2002) and even stochastic methods (Hudebine and Verstraete, 2004). As the method in the present work is specifically developed to reconstruct the compositions of naphthas, an experimental method seems most suited because the detailed composition of naphtha fractions can still be determined in a reasonable time. For very heavy feedstocks, such as VGO's, a stochastic method such as those of Neurock et al. (1994) and Verstraete et al. (2004), or a group contribution method as proposed by Quann and Jaffe (1996) is more suited because it becomes more and more difficult to obtain a detailed experimental composition that can serve as a basis for the molecule library.

Table 7.1 contains the list of selected components present in the molecular library for naphtha feedstocks. These components are selected based on the detailed molecular composition of 30 reference naphthas with widely varying characteristics. The range of the naphthas used is specified in Table 7.2. Their average molecular weight varies between 79 and 101g mol^{-1}. Only those components with a weight fraction higher than 1 wt% in at least one of the reference

mixtures are selected. This leads to a total of 34 selected components in the molecular library that cover on average more than 90 wt% of the entire feedstock composition. The library includes 8 n-paraffins, 5 aromatics, 9 naphthenes and 12 iso-paraffins. Including more detail in the feedstock library is useless because of the typical characteristics and limitations of the method as will be explained in the next paragraphs. Furthermore, this library is sufficiently detailed to allow an accurate simulation of the naphtha steam cracking process. Logically, other fractions require the generation of a new molecular library. For example, for gas oils a similar approach can be used. Analyzing of a large amount of gas oil fractions should make it possible to identify the most important components. The latter then constitute the molecular library for this fraction.

C4	iso butane, n-butane	C8	2-methyl heptane, 3-methyl heptane, n-octane, di-methyl cyclo hexane, tri-methyl cyclo pentane, ethylbenzene, xylene
C5	iso pentane, n-pentane, cyclo pentane	C9	2-methyl octane, 3-methyl octane, n-nonane, tri-methyl cyclohexane, tri-methyl benzene
C6	2,3 di-methyl butane, 2-methyl pentane, 3-methyl pentane, n-hexane, methyl cyclo pentane, cyclo hexane, benzene	C10	n-decane
C7	2,3 di-methyl pentane, 2-methyl hexane, 3-methyl hexane, n-heptane, methyl cyclo hexane, di-methyl cyclo pentane, toluene	C11	n-undecane

Table 7.1: Components included in the library of molecules for naphtha feedstock representation

Commercial Index	Range
Specific density, 15/4°	0.66 – 0.73
PIONA-analysis (wt %)	
Paraffins	20 - 48
Iso-paraffins	18 – 44
Olefins	0 - 2
Naphthenes	11 - 33
Aromatics	3 – 14
Average Molecular Weight (g mol^{-1})	79 - 101

Table 7.2: Range of the Commercial Indices used for determining the library of molecules

7.2.3   Determining the State with Maximum Shannon Entropy

Shannon (1948) states that: "To find the most informative state, the change in entropy with regard to the initial state must reach a maximum". This corresponds with maximizing the entropy-equation specified in equation [7.2]. The most obvious method for determining the optima of a function coupled to a set of constraints is the Lagrange multiplier method. The Lagrange multiplier method is used to find the optima of a function f(x) under the constraints $g_j(x)$ that equal zero. A new function which incorporates the function f(x) and all its constraints is introduced:

$$\xi(x) = f(x) + \sum_j \lambda_j \cdot g_j(x) \qquad\qquad [7.3]$$

with λ_j a constant variable called the Lagrange multiplier. The optimization problem is then reduced to finding the optima of $\xi(x)$ in x_i and λ_j. Solving the optimization problem can be drastically simplified when all the constraints are linear in the variables x_i. In this case, the optimization function can be transformed from a non-linear equation in the N mole fractions x_i into a non-linear equation in J parameters λ_j. However, this imposes an important restriction on the commercial indices and affects strongly which commercial indices can and cannot be used. Information such as the Bureau of Mines Correlation Index, the Watson characterization factor

or the vapor pressure cannot be used as commercial indices. The following list of commercial indices can be used in the information entropy maximization method presented in the present work: the average molecular weight, the specific gravity, the H/C-ratio, the PIONA weight fractions, a set of ASTM D2887 or D2892 boiling points, NMR spectra and a detailed distribution of the hydrocarbons per carbon atom via GC-MS. All these commercial indices are obtained via a number of standardized methods (ASTM methods).

The constraints $g_j(x)$ in equation [7.3] correspond with one of the constraints originating from the commercial indices. Each of the commercial indices can be written in the following form:

$$f_j = \sum_{i=1}^{N} f_{i,\,j} \cdot x_i \qquad\qquad [7.\,4]$$

with f_j the value of constraint j, $f_{i,j}$ the coefficient of molecule i for constraint j and N the number of molecules in the library. For instance, for the specific gravity, equation [7.5] is obtained.

$$\frac{1}{d^{\,exp}} = \sum_{i=1}^{N} \frac{x_i \cdot M_i}{d_i} \qquad\qquad [7.\,5]$$

As the constraints $g_j(x)$ have to equal zero, equation [7.5] needs to be rewritten. Under the assumption that the mixture is ideal, equation [7.6] is obtained:

$$\sum_{i=1}^{N} x_i \cdot \left(\frac{1}{d_i} - \frac{1}{d^{\,exp}} \right) \cdot M_i = 0 \qquad\qquad [7.\,6]$$

Table 7.3 gives an overview of the different boundary conditions resulting from the commercial indices that are considered in this method.

As the constraints are based on experimental analyses of petroleum fractions, measurement errors introduce an uncertainty on the value of the constraints. Therefore, it seems appropriate to introduce, next to the exact linear constraints, linear constraints with uncertainties. For every constraint with uncertainty, an extra term has to be added to the optimization function $\xi(x)$. For a linear constraint, this extra term is of the following form:

$$-\frac{1}{2} \cdot \frac{\left(f_k - \sum_{i=1}^{N} x_i \cdot f_{i,k}\right)^2}{\sigma_k^2} \qquad [7.7]$$

with σ_k a measure for the uncertainty of the constraint.

Commercial Indices	$f_{i,j}$	f_j
Molecular Weight	$M^{exp} - M_i$	0
H/C-ratio	$\left(\left(\dfrac{H}{C}\right)^{exp} - \left(\dfrac{H}{C}\right)_i\right) \cdot M_i$	0
Specific Density	$\left(\dfrac{1}{d_i} - \dfrac{1}{d^{exp}}\right) \cdot M_i$	0
PIONA Weight Fraction	If component $i \in$ PIONA class k	
	$\left(\dfrac{\%F_k^{exp}}{100} - 1\right) \cdot M_i$	0
	If component $i \notin$ PIONA class k	
	$\dfrac{\%F_k^{exp}}{100} \cdot M_i$	0
ASTM Boiling Point	If boiling point $i <$ boiling point k	
	$\left(1 - \dfrac{\%G_k^{exp}}{100}\right) \cdot \dfrac{M_i}{d_i}$	0
	If boiling point $i >$ boiling point k	
	$\left(-\dfrac{\%G_k^{exp}}{100}\right) \cdot \dfrac{M_i}{d_i}$	0

Table 7.3: Overview of the constraints resulting from the different boundary conditions

The information entropy maximization method has the tendency to favor the most extreme molecules in comparison to molecules with average properties (Hudebine, 2003). On the other hand, in refining, experimental data show that most compositions approach a Gaussian distribution of the mole fractions, with a large amount of molecules with average properties and only very little extreme molecules. Hence, an extra constraint is necessary that restricts the method to mole fractions with a Gaussian distribution as a function of the carbon number. The only commercial index that is directly related to the number of carbon atoms and is considered in Table 7.3 is the average molecular weight. This means that an extra term and an extra Lagrange multiplier should then be added to the optimization function $\xi(x)$:

$$\nu_1 \cdot \left[\left(\sigma'_m \right)^2 - \sum_{i=1}^{N} x_i \cdot \left(M_i - M_{exp} \right)^2 \right] \tag{7.8}$$

with σ'_m the standard deviation of the molecular weight.

The solution of the optimization problem depends on the specified constraints. In the most general case, the problem includes J exact linear constraints, K linear constraints with uncertainties and a single constraint taking into account the normal distribution for the molecular weight. The criterion that needs to be optimized is of the following form:

$$\xi(x) = \sum_{i=1}^{N} x_i \cdot \ln x_i + \mu \cdot \left(1 - \sum_{i=1}^{N} x_i \right) + \sum_{j=1}^{J} \lambda_j \cdot \left(f_j - \sum_{i=1}^{N} x_i \cdot f_{i,j} \right)$$

$$+ \sum_{k=J+1}^{J+K} -\frac{1}{2} \cdot \frac{\left(f_k - \sum_{i=1}^{N} x_i \cdot f_{i,k} \right)^2}{\sigma_k^2}$$

$$+ \nu_1 \cdot \left[\left(\sigma'_m \right)^2 - \sum_{i=1}^{N} x_i \cdot \left(M_i - M_{exp} \right)^2 \right] \tag{7.9}$$

Setting the derivatives of this equation to the mole fractions x_i equal to 0 results in following expression:

$$\frac{\partial \xi}{\partial x_i} = -1 - \ln x_i - \mu - \sum_{j=1}^{J} \lambda_j \cdot f_{i,j} + \sum_{k=J+1}^{J+K} \frac{f_{i,k}}{\sigma_k} \cdot \varepsilon_k$$

$$- \nu_1 \cdot \left(M_i - M_{exp}\right)^2 \qquad \forall i \in N \qquad [7.\,10]$$

with:

$$\varepsilon_k = \frac{f_k - \sum_{i=1}^{N} x_i \cdot f_{i,k}}{\sigma_k} \qquad \forall k \in K \qquad [7.\,11]$$

Re-ordering the terms in equation [7.10] leads to the following expression:

$$e^{1+\mu} \cdot x_i = \exp\left[-\sum_{j=1}^{J} \lambda_j f_{i,j} + \sum_{k=J+1}^{J+K} \frac{f_{i,k}}{\sigma_k} \varepsilon_k - \nu_1 \left(M_i - M_{exp}\right)^2 \right] \qquad [7.\,12]$$

Summation over all components i makes it possible to eliminate the Lagrange multiplier μ, resulting in an equation for the mole fraction x_i:

$$x_i = \frac{\exp\left[-\sum_{j=1}^{J} \lambda_j f_{i,j} + \sum_{k=J+1}^{J+K} \frac{f_{i,k}}{\sigma_k} \varepsilon_k - \nu_1 \left(M_i - M_{exp}\right)^2 \right]}{Z} \qquad [7.\,13]$$

with:

$$Z = \sum_{i=1}^{N} \exp\left[-\sum_{j=1}^{J} \lambda_j f_{i,j} + \sum_{k=J+1}^{J+K} \frac{f_{i,k}}{\sigma_k} \varepsilon_k - \nu_1 \left(M_i - M_{exp}\right)^2 \right] \qquad [7.\,14]$$

If a normal distribution is imposed on the mole fractions, then the number of parameters becomes larger than the number of commercial indices. To determine the values of the parameters λ_j, ε_k and ν_1 necessary to calculate the mole fractions, the entropy criterion needs be

optimized. Substitution of equation [7.13] in equation [7.9] leads to the following expression for the entropy criterion:

$$E(\lambda,\varepsilon,\nu) = \ln Z + \sum_{j=1}^{J} \lambda_j \cdot f_j + \sum_{k=J+1}^{J+K} \left(\frac{1}{2} \cdot \varepsilon_k^2 - \frac{f_k}{\sigma_k} \cdot \varepsilon_k \right) + \nu_1 \cdot \sigma_1^2 \qquad [7.\,15]$$

The values of λ_j, ε_k and ν_1 at the optimum permit to calculate the most probable mole fractions of the molecules. Finding the optimum of $E(\lambda,\varepsilon,\nu)$ is a task easily performed by any optimization routine.

In the absence of any information about the mixture, the only restriction on the system is that the sum of the mole fractions has to equal 1. Again, the optimum of this function [7.15] can be found by setting the derivatives of the function to the mole fractions x_i equal to zero. The mole fractions of the N library components are then equal to:

$$x_i = \frac{1}{N} \qquad\qquad \forall i \in N \qquad\qquad [7.\,16]$$

This result verifies the first hypothesis of the information entropy maximization method. In the absence of any information, constraint or analysis, it is impossible to favor one molecule with regard to another, and thus the distribution of the mole fractions is uniform. Every commercial index that leads to a constraint specifies some extra information about the mixture, resulting in a loss of the uniform character of the mole fractions.

To use the previously defined method, the physical properties of the molecules in the library have to be known. For some commercial indices like the average molecular weight, the values of the individual components can be easily obtained. For the calculation of the density, this is not so straightforward. The density at 25°C of every individual component considered in the molecular library is calculated by the group contribution method of Fedors (1974). Fedors states that the solubility parameters and the molar volumes of the molecules can be used to estimate the thermodynamic properties of the molecules, such as the density. A general system to determine the molar volume V of a molecule developed by Fedors (1974) is based on the following relation:

$$V = \sum_i n_i \cdot \Delta v_i \qquad\qquad [7. 17]$$

where Δv_i represents the group contributions of the molar volume and n_i the number of times that the atom or group i appears in the molecule. These contributions are applicable at a temperature of 25°C. Based on equation [7.17] and the molecular weight M of the molecule, the density at 25°C is calculated:

$$d = \frac{M}{\sum_i n_i \cdot \Delta v_i} \qquad\qquad [7. 18]$$

Fedors showed that the difference between the estimated and the experimentally measured densities deviates within less than 10%.

To calculate the boiling point of a component, the group interaction contribution (GIC) method from Marrero et al. (1999) is used. This method is specifically developed for hydrocarbons and is known for its high statistical accuracy. A GIC method considers the contribution of the interactions between two bonding groups instead of the contribution of simple groups.

As stated previously, the commercial indices function as boundary conditions for the optimization problem, and hence determine the individual mole fractions of the selected components. On the other hand, they also function as a filter, determining which molecules of the library can and cannot be included in the mixture. Several filters are built in, for example a PIONA filter that eliminates all the components from a specific PIONA fraction if this fraction is not experimentally observed. Another important filter is based on the results of the ASTM boiling point curve and eliminates all the molecules that have a normal boiling point inferior to the initial boiling point or superior to the end boiling point of the distillation.

One of the main advantages of this method over other methods is the limited time necessary to determine a detailed molecular composition. As only linear constraints are considered, the optimization function can be transformed from a non-linear equation in the N mole fractions x_i into a non-linear equation in J+K+1 parameters λ_j, ε_k and v_l. Because N is in the order of 10^2-10^6 and J+K+1 is maximum 13, the gain in the optimization level can be considerable, and the solution of the optimization problem requires only a limited time.

7.3   Results and Discussion

7.3.1   Software Module for Feedstock Reconstruction

The computer program predicting the detailed feedstock composition is part of a complete software package for the simulation of the steam cracking process containing the kinetic module CRACKSIM as its core (Clymans and Froment, 1984). A general overview of the structure of the feedstock module SimCO (Simulated Composition) is given in Figure 7.2.
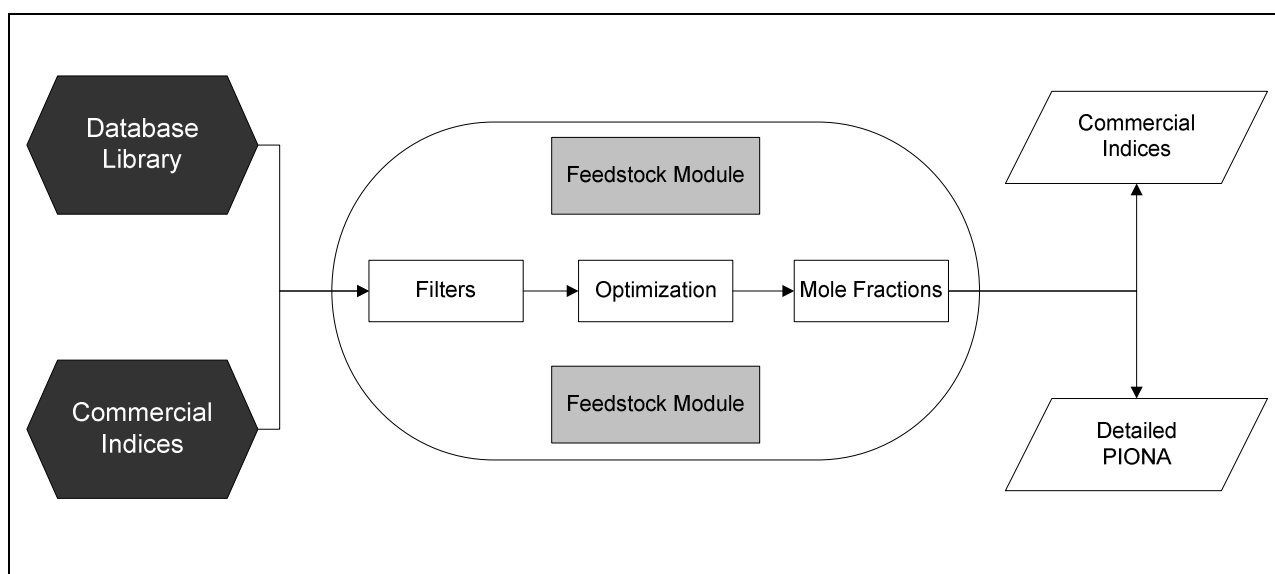
Figure 7.2: Overview of the feedstock module used for the reconstruction of naphtha fractions implemented in the simulation package CRACKSIM

As input, the commercial indices and the database containing the molecules that are included in the library and their properties (molecular weight, density, boiling point) are required. First, the library is reduced by a number of filters based on the actual values of the user-defined commercial indices. Then the entropy criterion is applied. For the optimization of equation [7.15], a robust Rosenbrock optimization routine is implemented. Based on the values obtained for the Lagrange multipliers, the mole fractions of the library components can be calculated using equations [7.13] and [7.14]. Finally, the detailed PIONA weight fractions are determined and the commercial indices of the reconstructed mixture are calculated.

Figure 7.3: The input and results screen of the graphical user interface (GUI) for a mixture with an average molecular weight of 90 and containing only paraffinic components

A graphical user interface (GUI) improves the user friendliness of the software module. The input and results screen of the GUI for a simple demonstration case are shown in Figure 7.3. These results are obtained for a mixture with an average molecular weight of 90 and containing only paraffinic components. The simulation time for obtaining a detailed composition is less than one second on an Intel Pentium IV processor of 3.2 MHz. Also to meet the CAPE-Open standard (Köller and Töbermann, 2002), the GUI is an important asset. Indeed, although designed to work with our simulation package for steam cracking, the module can be used as a stand-alone tool too. As such, SimCO can be implemented in other simulation packages that require a detailed naphtha feedstock composition.

7.3.2   Effect of Introducing Uncertainty and a Gaussian Distribution

One advantage of using the method based on the maximization of the entropy is that next to the boundary conditions originating from the commercial indices other criteria can be used to improve the simulation results. For example, experimental data show that most naphtha fractions have a large amount of molecules with average properties and only very little molecules with extreme properties. Hence, using a Gaussian distribution of the mole fractions as function of the number of carbon atoms could improve the predictions of the feedstock reconstruction module. As shown in equation [7.9], an extra constraint on the system can be introduced to restrict the solution to a normal distribution of the mole fractions as function of the carbon number. Table 7.4 shows the effect of using a Gaussian distribution as extra boundary condition for a mixture containing only n-paraffins.

For very small values of the standard deviation of the Gaussian distribution logically the distribution of mole fractions of the paraffins is also narrow. As the standard deviation [σ'_m] of the Gaussian distribution increases the distribution first becomes more and more uniform. For very high values of the standard deviation σ'_m the distribution of the mole fractions of the paraffins flips. This means that the mole fractions of components with average properties decrease, while the components on the edge of the system, i.e. components with either a very high or a very low molecular weight, become more and more important. This last situation is of course chemically unrealistic as experimental data show that most compositions approach a Gaussian or Gamma distribution of the mole fractions. Practically this means that the values of

the standard deviation σ'_m higher should not be higher than 3 (Van Hecke, 2005). Comparison with experimental data further shows that very low values of the standard deviation σ'_m, i.e. σ'_m lower than 1.5, are unrealistic because then the distribution of the mole fractions becomes too narrow.

Weight fractions (wt%)	$\sigma'_m = 1.5$	$\sigma'_m = 2.5$	$\sigma'_m = 5$	Base Case
n-C_4H_{10}	0.1	2.9	17.9	16.5
n-C_5H_{12}	7.2	15.2	15.6	16.0
n-C_6H_{14}	53.8	33.8	13.7	14.9
n-C_7H_{16}	36.6	32.2	12.2	13.5
n-C_8H_{18}	2.3	13.3	11.0	12.0
n-C_9H_{20}	0	2.4	10.2	10.5
n-$C_{10}H_{22}$	0	0.2	9.8	9.1
n-$C_{11}H_{24}$	0	0	9.6	7.8
Calculated M_m	90	90	90	90

Table 7.4: Distribution of the weight fractions of the paraffinic components as function of the standard deviation [σ'_m] of the Gaussian distribution introduced on the specified average molecular weight. Base Case: $Mm = 90$; $P = 100$; no standard deviation σ'_m.

The simple demonstration case used in the previous paragraph can also be used to illustrate the effect of introducing uncertainty on one of the boundary conditions. In Table 7.5, the effect of using uncertainty on the molecular weight is shown. As the uncertainty on this value increases, the mole fractions become more and more uniformly distributed. Moreover, the deviation of the calculated molecular weight deviates from the specified value of 90. Using an uncertainty on one particular commercial index has the advantage that the importance of that commercial index can be reduced compared to other more accurately known indices. However, this does not imply that the value of this commercial index is completely ignored as can be seen

in Table 7.5. Only for very high values of the uncertainty, i.e. $\sigma_k > 5$, the specified molecular weight is completely ignored.

Weight fractions (wt%)	$\sigma_k = 0.5$	$\sigma_k = 2$	$\sigma_k = 10$	Base Case
n-C_4H_{10}	16.4	14.8	10.9	16.5
n-$C_5 H_{12}$	15.9	14.8	12.0	16.0
n-$C_6 H_{14}$	14.8	14.3	12.7	14.9
n-$C_7 H_{16}$	13.5	13.3	13.0	13.5
n-$C_8 H_{18}$	12.0	12.4	13.2	12.0
n-C_9H_{20}	10.5	11.2	13.0	10.4
n-$C_{10}H_{22}$	9.1	10.1	12.8	9.0
n-$C_{11}H_{24}$	7.8	9.0	12.4	7.7
Calculated M_m	90.2	92.3	98.2	90.0

Table 7.5: Distribution of the weight fractions of the paraffinic components as function of the uncertainty on the molecular weight [σ_k]. Base Case: Mm = 90; P = 100; $\sigma_k = 0$.

7.3.3   Reconstruction of Naphtha Feedstocks

The main objective of the feedstock reconstruction method is to generate in a minimum of time a detailed molecular composition with the desired characteristics as specified by the commercial indices, not to precisely reconstruct the mixture's composition. It is a priori clear that the composition with maximum Shannon entropy will only rarely correspond to the analytically determined one. The composition with maximum Shannon entropy is the statistically favored one, since this composition maximizes the uncertainty on the missing information. The error introduced by the missing information is minimized but nothing more than that. However, it can be expected that this novel method is able to generate a detailed molecular composition that corresponds reasonably well with the analytically determined one. In particular when more and more information about the mixture is known, i.e. more commercial indices are specified,

the agreement should become better and better. In the next paragraph, this will be illustrated in more detail.

Gas chromatography (GC) is considered to be the most appropriate method for determining the detailed molecular composition of naphtha fractions. The calibration factors used for the quantitative analysis are those proposed by Dietz (1967). Calibration factors for components not mentioned here are calculated using the group contribution method of Dierickx et al. (1986). Obviously, the quantitative analysis of the mixture should be preceded by a qualitative analysis. The latter is carried out using GC-MS data, Kovats retention indices and reference data from previously studied naphthas. The molecular composition of the naphtha fraction serves as a basis to determine the detailed PIONA weight fractions used for validation purposes. In Table 7.6, the commercial indices obtained for a specific naphtha fraction, Naphtha 1, are specified. For Naphtha 1, only the specific density, the PIONA weight fractions and three ASTM boiling points are known. Although limited, the available information is sufficient for the software to simulate a possible composition with the desired commercial indices. The commercial indices specified in Table 7.6 are all considered as exact linear constraints for the optimization problem. Neither a Gaussian distribution of the weight fraction, nor error bars on one of the commercial indices is considered. If no error bars are specified on the PIONA weight fractions it is very important that the sum of these weight fractions exactly equals 100%. Otherwise contradicting constraints are specified for the system and no optimum can be found.

In Table 7.7, the simulated detailed PIONA weight fractions are given. The commercial indices of the simulated mixture meet the values specified in Table 7.6 except for the IBP, where a minor difference is observed. The value obtained via simulation was 299 K while a value of 305 K was specified. Figure 7.4 gives an overview of the agreement between the simulated and analytically obtained detailed PIONA weight fractions per carbon number. Because of the low amount of olefins in this feedstock no olefinic fraction as function of the carbon number is shown in Figure 7.4. Overall a good agreement can be observed between the simulated and analytically obtained PIONA weight fractions. Figure 7.4 further shows that if more information is specified about the mixture, such as the molecular weight and some more ASTM-boiling points, a better agreement with the analytically determined PIONA weight fractions is observed. In this case, these last extra values have been calculated from the detailed analytically determined molecular composition. However, they also could have been determined analytically.

COMMERCIAL INDICES	
Specific density, 15/4°	0.71
PIONA-analysis (wt %)	
Paraffins	30.0
Iso-paraffins	35.3
Olefins	0.2
Naphthenes	23.5
Aromatics	11.0
ASTM boiling points (K)	
IBP	305
50 %	365
FBP	434

Table 7.6: Commercial Indices of Naphtha 1

(wt%)	P	I	O	N	A	Sum
C_4	0.2	0.2	-	-	-	0.4
C_5	7.2	0.1	0.0	2.8	-	10.1
C_6	6.7	13.2	0.1	5.1	2.4	27.5
C_7	6.0	11.1	0.1	6.5	2.6	26.2
C_8	5.2	6.0	0.0	6.2	5.5	22.9
C_9	4.5	4.8	-	2.9	0.3	12.5
C_{10}	0.1	0.1	-	-	-	0.2
C_{11}	0.1	-	-	-	-	0.1
Sum	30.1	35.4	0.2	23.6	10.8	100.0

Table 7.7: Simulated detailed PIONA weight fractions (wt%) with the commercial indices specified in Table 7.6
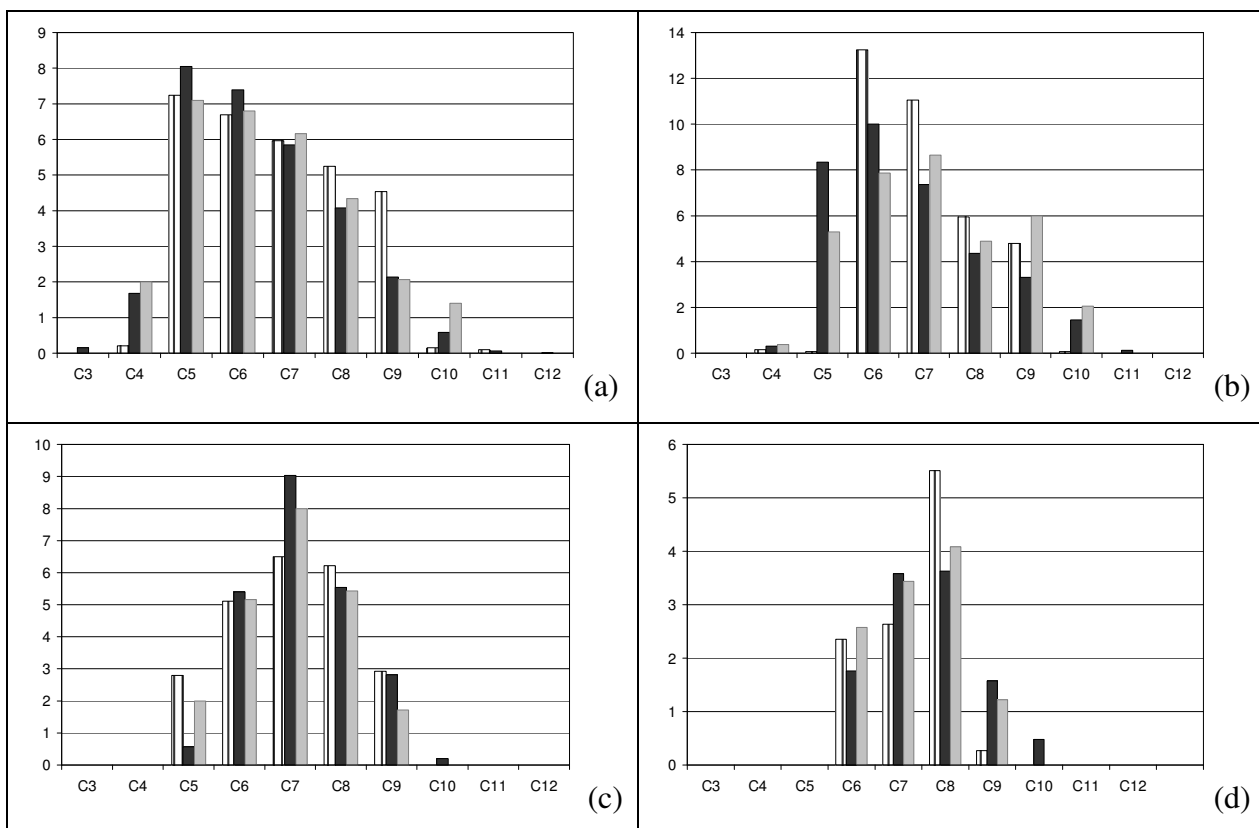
Figure 7.4: Comparison of the detailed PIONA weight fractions. [a] Weight fractions of paraffinic components, [b] Weight fractions of iso-paraffinic components, [c] Weight fractions of naphthenic components, [d] Weight fractions of aromatic components.[‖ Simulated with commercial indices from Table 7.6, ▮ Experimental results, ▯ Simulated with commercial indices from Table 7.6 + M = 92.2 ; 10% Bp = 311 K ; 30% Bp = 334 K; 70% Bp = 383 K; 90% Bp = 414 K]

The differences seen in Figure 7.4 are caused by several reasons. First of all the specified commercial indices in Table 7.6 are rather limited. More information about the mixture seriously improves the agreement as illustrated in Figure 7.4. Secondly, the inaccuracy of certain commercial indices can cause significant deviations. A manually performed sensitivity analysis shows that the method is in particular sensitive to changes of some ASTM-boiling points. This is obvious because the ASTM-boiling point curve is one of the only indices that is directly related with the carbon number distribution of the molecules, and thus strongly influences the distribution of the molecules in a specific PIONA fraction. Finally, as stated previously, this is a statistical method without any correlations. This method selects a single composition with

maximum Shannon entropy out of a number of compositions that meet all the boundary conditions. Hence, it is inherent to the method that some differences exist. The composition with maximum Shannon entropy is not necessary the one obtained experimentally. The same conclusions have been found using other naphtha samples.

A possible solution for the problems encountered with the ASTM boiling points is to impose uncertainties on the constraints linked to the boiling points. If the commercial indices from Table 7.6 are used as input data for the program after addition of an uncertainty of 3 on each of the boiling points, even larger deviations from the actual composition are observed. The method of maximization of the entropy tends to a distribution of the mole fractions that is as uniform as possible. The input of the uncertainties gives the method extra opportunity to make the distribution more uniform. Another option to overcome the shortcomings related to the boiling points is to ignore these commercial indices completely. Only the specific density and the PIONA weight fractions remain as boundary conditions for the optimization of the entropy criterion. As in the situation with imposed uncertainties, less constraints increase the degrees of freedom, resulting in a more uniform distribution of the mole fractions.

7.3.4   Simulation of a Set of Pilot Plant Experiments

The results in the previous paragraph show that the simulation module is able to reconstruct a feedstock composition based on the available commercial indices. However, the most important test for our feedstock reconstruction program SimCO is to compare the simulation results of the complete software package for steam cracking, i.e. feedstock and reactor modeling, with experimental data obtained from the pilot plant installation of the Laboratorium voor Petrochemische Techniek (LPT) in Ghent University [Van Damme et al., 1982; Van Geem et al., 2005]. This experimental setup allows fundamental studies of the kinetics of the cracking reactions [Wauters and Marin, 2002] as well as practical issues such as coke deposition in both the radiant coil [Reyniers and Froment, 1995] and the transfer line exchanger (TLE) [Dhuyvetter et al., 2001]. The pilot plant installation consists of 3 parts: a feed section, the furnace containing the suspended reactor coil and the analysis section. The tubular reactor used in this set of experiments has a length of 23.14 m and has an internal diameter of 10 mm. These dimensions are chosen to achieve turbulent flow conditions in the coil. The temperature and pressure profile

along the reactor can be measured and regulated. As feedstock, 4 different naphtha fractions Naphtha 2-5 are used. In Table 7.8, both the commercial indices of these naphtha fractions as well as the experimental conditions used in the different experiments are specified. In total, 50 pilot plant experiments are simulated for which the experimental conditions vary over a broad range. The flow rate of the hydrocarbon feedstock is varied between 0.6 and 1.2 g s^{-1}, while the coil outlet temperature varies from 953 K to 1170 K. The dilution varies from 0.2 kg $_{steam}$ / kg $_{naphtha}$ to 0.8 kg $_{steam}$ / kg $_{butane}$. The coil outlet pressure varies from 0.15 MPa to 0.18 MPa. These conditions correspond with a P/E-range (propylene to ethylene ratio) from 0.6 to 0.9.

	COMMERCIAL INDICES			
	Naphtha 2	**Naphtha 3**	**Naphtha 4**	**Naphtha 5**
Specific density, 15/4°	0.68	0.69	0.67	0.68
PIONA-analysis (wt %)				
Paraffins	43.4	34.0	40.1	39.9
Iso-paraffins	38.7	38.1	50.5	38.2
Olefins	0.7	0.1	0.4	0.2
Naphthenes	13.5	20.3	5.8	16.4
Aromatics	3.7	7.5	3.2	5.3
Molar H/C ratio	2.23	-	-	-
EXPERIMENTAL CONDITIONS				
CIP (MPa)	2.4 – 2.1			
COP (MPa)	1.8 – 1.5			
CIT (K)	823 - 873			
COT (K)	953 – 1170			
Dilution (kg $_{steam}$/kg $_{Hydrocarbon}$)	0.2 – 0.8			
Hydrocarbon Flow Rate (kg/s)	0.6 10^{-3} – 1.2 10^{-2}			
P/E-ratio (wt % / wt %)	0.9 – 0.6			

Table 7.8: Characteristics of the naphtha feedstocks used for the SimCO simulations and the range of experimental conditions in the LPT pilot plant installation.

(wt%)	P	I	O	N	A	Sum
C_4	9.2	5.9	-	-	-	15.1
C_5	8.2	4.7	0.2	3.7	-	16.8
C_6	6.8	10.7	0.2	8.2	-	26.1
C_7	5.7	8.3	0.2	0.8	0.1	15.1
C_8	4.7	4.4	0.0	0.4	0.8	10.3
C_9	3.8	3.3	-	0.1	2.6	9.9
C_{10}	3.1	1.2	-	-	-	4.3
C_{11}	2.5	-	-	-	-	2.5
Sum	43.9	38.6	0.7	13.3	3.6	100.0

Table 7.9: Simulated detailed PIONA weight fractions (wt%) with the commercial indices specified as in Table 7.8

First, the detailed feedstock composition is simulated using the commercial indices of the different naphthas as input. The simulated detailed PIONA weight fractions of Naphtha 2 are given in Table 7.9. The determined composition exactly meets all the specified boundary conditions specified in Table 7.8. Once the detailed molecular composition of the naphtha feedstock is determined, the reactor simulations can be performed. The experiments carried out in the pilot plant reactor are modeled using a 1-dimensional reactor model. Using a 1-dimensional reactor model for simulating the steam cracking process can lead to small differences compared to using a 2-dimesnional reactor model, e.g. when modeling ethane cracking in a Lummus SRT-I reactor (Van Geem et al., 2004). The source of these errors is that in industrial single coil reactors for ethane cracking important radial temperature gradients (>100 K) exist (d_{reac} = 100 mm) (Van Geem et al., 2004). As the tube diameter in the pilot plant reactor is much smaller (i.e. d_{reac} = 10 mm), the radial temperature gradients are far less pronounced (< 15 K), thereby allowing an accurate simulation using a 1-dimensional reactor model. The reactor model is coupled to a radical kinetic model for the cracking of light fractions consisting of 60 molecular and 68 radical species and over 1200 reactions (Clymans and Froment, 1984). The parity plots for the yields of the main cracking products methane, ethylene, propylene and benzene in Figure 7.5 show that the combination of the feedstock module SimCO with the 1-

dimensional reactor model is able to provide accurate simulation results for naphtha fractions over a wide range of process conditions.
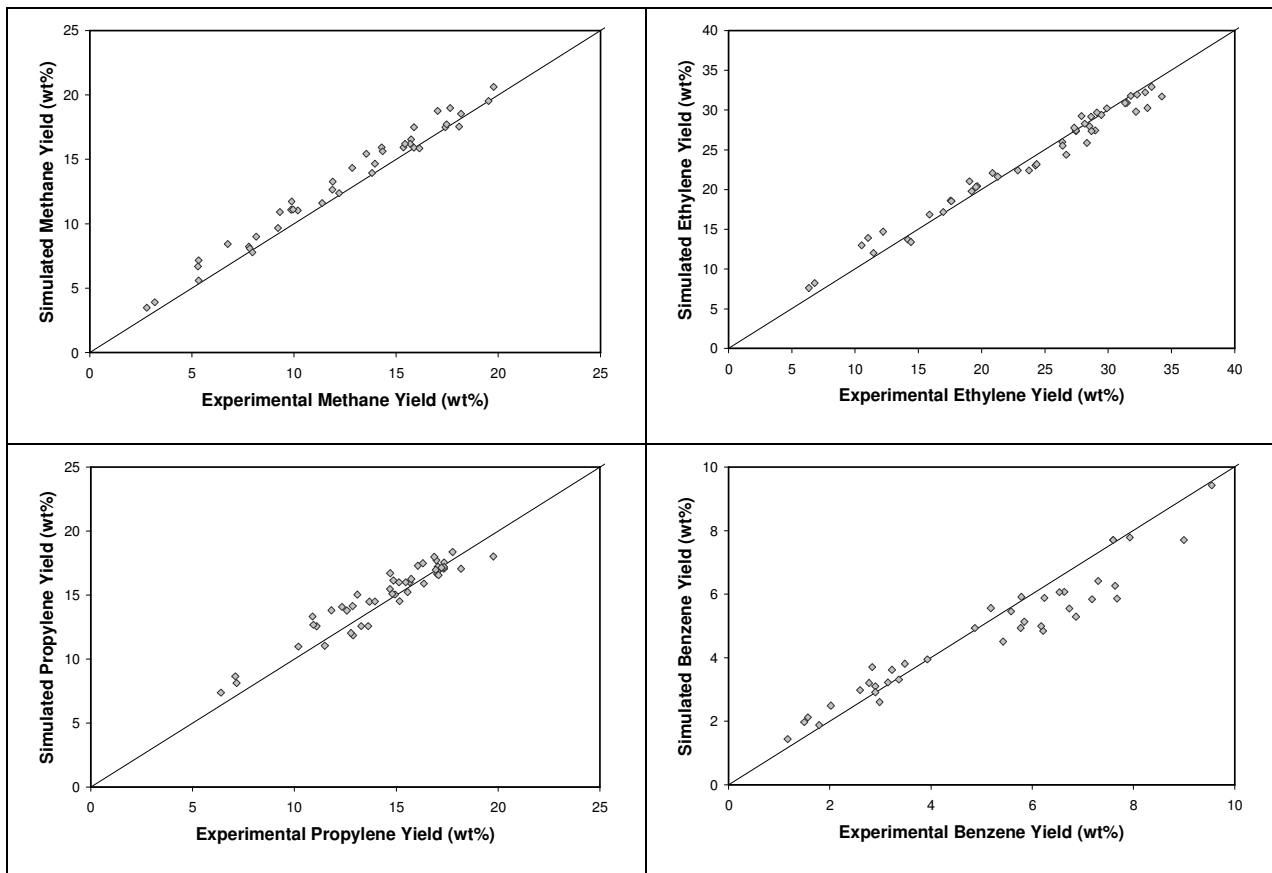
Figure 7.5: Parity plot for the yields of methane, ethylene, propylene and benzene obtained with 4 different naphthas (Naphtha 2-5). Commercial indices of the feedstocks used in the SimCO simulations are specified in Table 7.8. [Simulation Conditions: CIT: 823-873 K; COT: 953 K – 1170 K; CIP: 0.24 – 0.21 MPa; COP: 0.18 MPa -0.15 MPa; F: 0.6 – 1.2 g s^{-1}; δ: 0.2 - 0.8 kg /kg]

As stated earlier a crucial element for the success of the complete simulation package (feedstock reconstruction + reactor modeling) is the judicious selection of candidate feedstock molecules in the molecular library. Using a more extensive library does not necessary lead to better simulation results. On the contrary, the simulation results become worse as can be seen in Table 7.10. Using a more extensive molecular library (Sim1) containing the 173 components

observed during the analysis of the molecular compositions of the 30 reference naphthas leads to worse results than the results obtained with the reduced library containing 34 key molecules (Sim2). This is in particular the case for the two main products ethylene and propylene. Also for other steam cracking experiments this phenomenon is observed.

Product Yields (wt %)	Sim1	Sim2	Sim3	Experimental
H_2	0.6	0.6	0.6	0.6
CH_4	10.1	10.2	10.3	10.4
C_2H_2	0.2	0.2	0.2	0.2
C_2H_4	20.1	21.7	21.5	21.3
C_2H_6	3.0	3.0	3.0	4.1
C_3H_6	18.3	17.3	17.4	17.3
C_4H_6	4.5	5.0	4.9	4.1
$1\text{-}C_4H_8$	3.9	3.7	3.4	2.9
$2\text{-}C_4H_8$	1.0	1.3	1.4	1.5
$iso\text{-}C_4H_8$	3.3	3.2	3.0	3.1
C_6H_6	2.5	2.6	3.0	3.3
P/E-ratio (wt % / wt %)	0.9	0.8	0.8	0.8

Table 7.10: Simulated and experimentally determined product yields obtained for Naphtha 2 in the LPT pilot plant reactor. Sim1: Molecular library of 173 naphtha components; Sim2: Molecular library of 34 key components, Sim3: Simulation with analytically determined composition. [Simulation Conditions: CIT = 823 K; COT = 1073 K; CIP = 0.22 MPa; COP = 0.18 MPa; F= 1.2 10^{-3} kg s^{-1}; δ = 0.2 kg /kg]

The main reason for this behavior is that the entropy method is too insensitive to predict mole fractions of non important components accurately because it tends to a distribution of the mole fractions that is as uniform as possible. If the molecular library contains a lot of components with similar physical properties then it becomes almost impossible to distinguish between these components based on the available commercial indices using the entropy method. This is for example the case for isomers of branched paraffinic and naphthenic components. Although the

physical properties of these isomers are quite similar their cracking behavior can differ significantly, and hence, incorrectly estimating the distribution of the different isomers can affect the simulation results. By carefully constructing the molecular library and by selecting only those components with weight fractions higher than 1 wt% in at least one of the reference mixtures this effect can be minimized. As illustrated in Table 7.10, the simulation results obtained with the molecular library containing 34 key molecules (Sim2) practically coincides with the results obtained with the analytically determined composition (Sim3). These results are confirmed by simulation results obtained for other pilot plant experiments.

7.4   Conclusions

A new method for feedstock reconstruction for naphtha feedstocks is applied using the analytically determined commercial indices as input. This method is based on Shannon's entropy criterion and creates a molecular composition that meets all the boundary conditions set by the available commercial indices. One of the advantages of this method is that not only exact constraints can be used, but also uncertainties can be built in. Indeed, some of the commercial indices are error-prone because they are based on analyses of petroleum fractions with a certain uncertainty. Therefore uncertainties can be specified by the user, resulting in a higher flexibility to adapt the model to one's needs. Furthermore it is also possible to take into account the fact that petroleum fractions possess particular distributions.

One of the key elements for success is a good selection of the library of molecules because no correlations are implemented at any stage of a simulation. Based on the analysis of a large number of reference feedstocks the most important components traditionally present in a naphtha fraction are selected as possible feedstock components. For other feedstocks than naphtha, a new library has to be selected because every type of petroleum fraction has its own molecular characteristics. In this way, the method can be easily extended to other fractions such as gas oils.

One of the main advantages of this method over other methods is the limited time necessary to determine a detailed molecular composition. This is because only linear constraints are considered. With an Intel Pentium IV processor of 3.2 MHz it takes less than one second to obtain a detailed feedstock composition. Comparing the calculated detailed PIONA analysis with the actual analytically determined one shows that there exists a reasonable correspondence

between the two compositions, however these results also bring out some shortcomings. Important is the accuracy of the specified commercial indices because the simulation results can be very sensitive to for example the specified ASTM-boiling points. Furthermore, it is obvious that the number of analytically determined commercial indices also affects the simulation results. If these are accurately determined, more commercial indices lead to better simulation results. It is also important to state that not all the shortcomings are caused by inaccuracies of the indices or by inconsistency between the experimental and the calculated values, also some part is inherent to the method itself. It is obvious that without introducing any correlations it is hard to obtain a completely accurate detailed molecular composition.

The fast reconstruction of a molecular composition makes the feedstock module SimCO very attractive for implementation in the simulation package for steam cracking. The combination of these two simulation tools makes it possible to obtain simulation results even faster than before because no time has to be wasted for determining a detailed molecular composition of the naphtha feedstock. A graphical user interface improves the user-friendliness of the simulation package and minimizes further loss of valuable time. Comparison of the simulation results with pilot plant data obtained from a set of 50 pilot plant experiments performed in the LPT-pilot plant installation shows a good agreement between the simulated and experimentally determined product yields. This result is remarkable considering that only a very limited amount of information is specified for the considered naphtha fractions. One of the key elements for success is a judicious choice of the components included in the molecular library. Simulation results show that the quality of the simulations improves if a library containing only key components of naphtha fractions is used instead of an extensive library. The main reason for this is attributed to the insensitivity of the entropy method. As the entropy method tends to a uniform distribution of the mole fractions it is too insensitive to accurately predict mole fractions of non important components.

7.5   References

Allen D.T., Liguras D. Structural Models of Catalytic Cracking Chemistry: A Case of a Group Contribution Approach to Lumped Kinetic Modeling. Mobil Workshop: Chemical reactions in Complex Mixtures, New York, 1991.

Celie I. Voedingskarakterisatie van Naftakraking aan de hand van Commerciële Indices, Master Thesis, Ghent University, 2004.

Dente M., Ranzi E. Detailed Prediction of Olefin Yields from Hydrocarbon Pyrolysis through a Fundamental Simulation Program SPYRO, Comp. Chem. Eng., 3, 61, 1979.

Dente M., Ranzi E., Bozzano G., Faravelli T., Valkenburg P.J.M. Heavy Component Description in the Kinetic Modeling of Hydrocarbon Pyrolysis, AIChE Spring National Meeting, Houston, TX, USA, 2001.

Dente M., Bozzano G., Sugaya M. McGreavy C. The Characterization of Residual Hydrocarbon Fractions with Model Compounds - Retaining the Essential Information, ACS National Meeting, Boston, 43(3), 653-657, 1998.

Dhuyvetter I. Reyniers M.F., Froment G.F., Marin G.B., The Influence of Dimethyl Disulfide on Naphtha Steam Cracking, Ind. Eng. Chem. Res., 40, 4353-4362, 2001.

Dietz W.A. Response Factors for Gas Chromatographic Analyses. Journal of Gas Chromatography, 5, 68, 1967.

Dierickx J.L., Plehiers P.M. Froment G.F., Online Gas-Chromatographic Analysis of Hydrocarbon Effluents – Calibration Factors and their Correlation. Journal of Chromatography, 362, 155, 1986.

Fedors R. A Method for Estimating Both the Solubility Parameters and Molar Volumes of Liquids, Polymer Engineering and Science, 14, 147, 1974.

Froment G.F. Kinetics and Reactor Design in the Thermal Cracking for Olefin Production, Chem. Eng. Sci., 47, 2163, 1992.

Hudebine D., Vera C., Wahl F. Verstraete J.J., Molecular Representation of Hydrocarbon Mixtures from Overall Petroleum Analyses. AIChE 2002 Spring Meeting, New Orleans, LA, March, 10 – 14, Paper 27a, 2002.

Hudebine D., Verstraete J.J. Molecular Reconstruction of LCO Gasoils from overall Petroleum Analyses. Chem. Eng. Sci., 59, 4755-4763, 2004.

Joo E., Park S., Lee M. Pyrolysis Reaction Mechanism for Industrial Naptha Cracking Funraces, Ind. Eng. Chem. Res.,. 40, 2409-2415, 2001.

Köller J., Töbermann J.C. Global Cape-Open: Migration Cokebook. http://www.colan.org, 2002.

Liguras D.K., Allen D.T. Structural Models for Catalytic Cracking. 2. Reactions of Simulated Oil Mixtures, Ind. Eng. Chem. Res., 28, 665, 1989 [a].

Liguras D.K., Allen D.T. Structural Models for Catalytic Cracking. 1. Model Compound Reactions, Ind. Eng. Chem. Res., 28, 674, 1989 [b].

Marrero M.J., Pardillo F.E. Estimation of Pure Compound Properties Using Group-Interaction Contributions, AIChE Journal, 45(3), 615, 1999.

Neurock M., Nigam A., Trauth D., Klein M.T. Molecular Representation of Complex Hydrocarbon Feedstocks through Efficient Characterization and Stochastic Algorithms, Chem. Eng. Sci., 49, 4153, 1994.

Quann R.J., Jaffe S.B. Building Useful Models for Complex Reaction Systems in Petroleum Refining, Chem. Eng. Sci., 51, 1615, 1996.

Reyniers M.F., Froment G.F. Influence of Metal Surface and Sulfur Addition on Coke Deposition in the Thermal Cracking of Hydrocarbons, Ind. Eng. Chem. Res., 34, 773-785, 1995.

Shannon C.E. A Mathematical Theory of Communications, The Bell System Technical Journal, 27, 379, 1948.

Van Damme P.S., Froment G.F. Putting Computers to Work – Thermal Cracking Computer Control in Pilot Plants, Chem. Eng. Progr., 78 , 77-82, 1982.

Van Geem K.M., Heynderickx G.J., Marin G.B. A Comparison of One and Two-dimensional Reactor Models for Steam Cracking: Effect on Yields and Coking Rate. AIChE Journal, 50, 173–183, 2004.

Van Geem K.M., Reyniers M.F., Marin G.B. Two Severity Indices for Scale-Up of Steam Cracking Coils, Ind. Eng. Chem. Res., 44, 3402-3411, 2005.

Van Hecke K. Feedstock Characterization of Complex Mixtures based on Commercial Indices, Master Thesis, Ghent University, 2004.

Verstraete J.J., Revellin N., Dulot H., Hudebine D. Molecular Reconstruction of Vacuum Gas Oils. Prepr. Pap.-Am. Chem. Soc., Div. Fuel Chem., 49 (1), 20-21, 2004.

Wauters S., Marin G.B. Kinetic Modeling of Coke Formation during Steam Cracking. Ind. Eng. Chem. Res., 41, 2379-2391, 2002.

Wahl F., Hudebine D., Verstraete J.J. Reconstruction of the Molecular Composition of FCC Gasolines from Overall Petroleum Analyses. submitted for publication in Oil & Gas Sci. and Technol. – Rev. IFP, 2006.

Chapter 8:

General Conclusions and Outlook

To accurately simulate steam cracking of a wide variety of feedstocks a new fundamental simulation model was developed. A fundamental simulation model consists of 2 important parts: the reactor model and the single event microkinetic (SEMK) model. Except specified otherwise, a 1-dimensional reactor model is used. The latter is implemented in the FORTRAN code COILSIM1D. In addition, a single event microkinetic model for steam cracking was developed and applied.

Steam cracking of hydrocarbons proceeds through a free radical mechanism and three important reaction families can be distinguished:

- Carbon-carbon and carbon-hydrogen bond scissions of molecules and the reverse radical-radical recombinations:

$$R_1 - R_2 \rightleftarrows R_1^\bullet + R_2^\bullet \qquad [1]$$

- Hydrogen abstraction reactions, both intra- and intermolecular:

$$R_1 - H + R_2^\bullet \rightleftarrows R_1^\bullet + R_2 - H \qquad [2]$$

- Radical addition to olefins and the reverse β scission of radicals, both intra- and intermolecular:

$$R_1^\bullet + R_2 = R_3 \rightleftarrows R_1 - R_2 - R_3^\bullet \qquad [3]$$
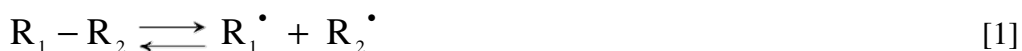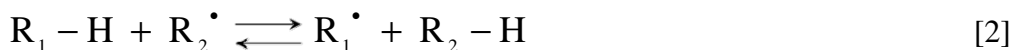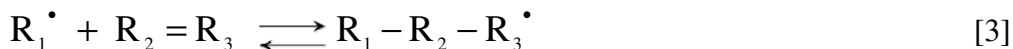
However not all these reactions are equally important. Indeed, the μ radical hypothesis implies that monomolecular reactions dominate for species with more than 5 carbon atoms (μ radicals) apart from some exceptions, e.g. the benzyl radical. Therefore the reaction network is divided in

two sub networks; the monomolecular μ network and the β network. The kinetics for the μ network are described by analytical expressions based on the pseudo steady state assumption for the radical reaction intermediates. Implementation of these kinetics occurs with a code PRIM-SEMK. For β radicals bimolecular reactions cannot be neglected, making it necessary to construct a separate sub network: the β network. The assumptions made for constructing the reaction network are verified using a rate based network generator called RMG. Under the specified conditions the μ radical hypothesis as applied in steam cracking is indeed valid, while the error resulting from assuming the quasi steady state for the group of μ radicals is negligible.

The constructed reaction network is the most extensive reaction network ever generated for steam cracking. The number of reactions considered in the reaction network is drastically extended. For example bimolecular reactions involving radicals with 5 carbon atoms are now also considered. Also the number of molecules considered in the microkinetic model is extended to 478. More aromatic compounds are considered and the maximum carbon number of the molecules is increased to 33. The introduction of more di-, tri-, poly- and naphtheno-aromatic compounds is on the one hand necessary to be able to simulate VGO fractions. On the other hand these molecules form also an important part of the pyrolysis fuel oil (PFO) fraction. The PFO fraction is the heavy fraction (boiling point higher than 473 K) formed during steam cracking of liquid feedstocks. Implementation of the kinetics of the β network occurs with a code β-SEMK, while the β network is coupled to the μ network in the FORTRAN code COILSIM1D.

Although the developed microkinetic model is the most complete microkinetic model ever generated for steam cracking, still several extensions are possible. An important problem encountered when cracking heavy fractions is the presence of significant amounts of hetero-atoms (< 500 ppm sulfur and nitrogen). For example when gas oils or VGO's are cracked the amount of sulfur varies typically in a range between 0.1 and 1.0 wt%. For nitrogen the amounts are slightly lower and are maximally 0.7 wt%. Practically this implies that up to 10 wt% of the molecules are components containing nitrogen or sulfur. Consequently the behavior of these molecules does significantly influence the reactions and the product distribution. Taking into account the reactions of components containing sulfur or nitrogen would be an important extension. This would be also important for better understanding the coke formation phenomenon. Sulfur components can both positively and negatively influence the amount of coke deposited in the reactor and the TLE.

A set of 150 pilot plant experiments obtained from the LPT pilot plant setup is used for validation purposes. Over the years experiments have been carried out on the LPT pilot plant installation using feedstocks with widely varying characteristics, resulting in an extensive experimental database containing over 400 experiments obtained with over 50 different feedstocks. The feedstocks range from light gasses, over naphthas to VGO's and even waxes. Excellent agreement is obtained between the simulated and experimental product yields. In contrast to previous simulation models now even for difficult feedstocks such as VGO, heavy naphthas and ethane/toluene mixtures a good agreement between the simulated and experimentally determined product distribution is obtained. Simulations are performed with COILSIM1D. The use of a stiff solver in COILSIM1D allows accurately integrating the set of differential equations. The single event microkinetic simulation model is also validated using industrial data. Comparison between the industrial and simulated product yields shows that accurate simulation results are obtained in the different cases. The necessity of using more dimensional simulation models is also critically evaluated. This comparison shows that for ethane steam cracking important radial gradients exist, not only for the temperature but also for the molecular and in particular the radical species. These profiles are the origin for small but significant differences between the simulated product yields. Using the 2-dimensional reactor model is even more important for describing coke formation because the 2-dimensional reactor model allows to account for the coke precursor concentrations adequately and, hence, to properly simulate the coking rates in an industrial ethane steam cracker with a fundamental coking model. For other feedstocks a 1-dimensional reactor model allows to obtain accurate product yields. Care should be taken with respect to run length calculations, however. An important improvement is also the development of a graphical user interface. This interface makes it possible to use COILSIM1D on any recent PC running on a Windows operating system. However, it has to be stated that the coupled simulation of reactor and furnace is not straightforward because the furnace simulation programs are not user friendly. It would be an enormous improvement if also for the coupled simulation of reactor and furnace a graphical user interface would be created. This could make this package one of the best in its kind and save petrochemical companies valuable time and money.

A second category of conclusions are related to scale-up issues. Two direct experimental methods are developed to accurately scale-up and down steam cracking coils. The first one is

based on the severity concept. For a given feedstock, scale-up is performed based on experimental data obtained at the same severity, not necessarily under similar conditions. Two carefully chosen severity indices are sufficient to unambiguously characterize the product yields for a given feedstock: one severity index being a measure for the temperature and the other index being a measure for the reactants partial pressure. Simulations and experiments show that for a given feedstock the methane yield and the ethylene over ethane yield ratio are independent indices and that they unambiguously characterize the observed product yields: i.e. the use of a third severity index is not necessary. The second scale-up method is based on dimensional analysis of the reactor model equations and focuses on obtaining identical product distributions under similar process conditions in reactors of different scale. The dimensionless model equations show that complete similarity can never be reached for 2 different tubular reactors. Scale-up is thus only possible under partial similarity and this inevitably leads to differences. However, if the criteria of similarity are relaxed with care only small differences between units of different scale can be obtained. Two different relaxation strategies are distinguished; the first one aims at realizing the same axial pressure profile neglecting radial non-uniformities, the second focuses on realizing the same radial temperature profile. Neglect of similarity of the radial temperature profile leads to larger differences as compared to differences resulting from neglect of the similarity of the axial pressure profile. This insight is used to design a pilot plant reactor ideal to scale down a Lummus SRT-I reactor and a pilot plant reactor for studying intrinsic kinetics.

In the last part of this work a method for feedstock reconstruction for naphtha fractions is discussed using the analytically determined commercial indices as input. Developing a method that is able to predict the detailed molecular composition of any hydrocarbon fraction based on easily available commercial indices is an enormous step forward for possible application of fundamental models in the petrochemical industry. The proposed method is based on Shannon's entropy criterion and creates a molecular composition that meets all the boundary conditions set by the available commercial indices. Implementation occurs with a FORTRAN code feedstock, which is implemented in the Visual Basic.Net program SIMCO. A reasonable correspondence is observed between predicted and experimentally determined naphtha compositions if sufficient commercial indices of the mixture are available. Also in combination with the single event microkinetic model accurate simulation results are obtained without requiring an experimental

determination of the molecular composition. In its current form the method can be easily extended to heavier fractions such as gas oils. The extension to heavier fractions is important because of the increasing trend of using these fractions as feedstock. However, this method possesses also some shortcomings and therefore it seems crucial to evaluate also other methods for predicting detailed molecular compositions. Developing a method that would be able to predict the detailed molecular composition of any hydrocarbon fraction based on easily available commercial indices would be an enormous step forward for possible application of fundamental models in the petrochemical industry. The current method is the first step to realize this objective.

Annex A

Thermodynamic Consistency

For any reversible elementary chemical reaction,

$$A + B \; \underset{k_b}{\overset{k_f}{\rightleftharpoons}} \; C + D \tag{1}$$

there holds a relations between forward reaction kinetics and backward reaction kinetics:

$$K_{c,eq} = \frac{k_f}{k_b} \tag{2}$$

k_f and k_b are given by Arrhenius expressions are:

$$k_f = A_f \exp\left(-\frac{E_{a,f}}{R \, T}\right) \tag{3}$$

$$k_b = A_b \exp\left(-\frac{E_{a,b}}{R \, T}\right) \tag{4}$$

K_{eq} is called the equilibrium coefficient, and it is related to the free energy change of the previous reaction by the equation:

$$K_{c,eq} = \left(R \, T\right)^{-\Delta n} \exp\left(\frac{-\Delta G^0_{rxn}}{R \, T}\right) \tag{5}$$

where T is the reaction temperature, R is the molar gas constant, ΔG°_{rxn} is the reaction free energy, and Δn is the mole change in the reaction. The equilibrium coefficient $K_{c,eq}$ in concentrations is related to the thermodynamic equilibrium coefficient $K_{p,eq}$ in partial pressures by the following equation:

$$K_{c,eq} = \left(\frac{C_{ref}}{p_{ref}} R\ T \right)^{-\Delta n} K_{p,eq} \qquad [6]$$

The reference concentration C_{ref} is set equal to 1000 mol m^{-3}, while the reference pressure is set equal to 100000 Pa. Hence, the following equation is obtained:

$$K_{c,eq} = \left(R'\ T \right)^{-\Delta n} K_{p,eq} \qquad [7]$$

$$\ln\left(K_{c,eq} \right) = -\Delta n\ \left(R'\ T \right) + \frac{\Delta S^\circ}{R} - \frac{\Delta H^\circ}{RT} \qquad [8]$$

with R' equal to R/100. The thermodynamic equilibrium coefficient $K_{p,eq}$ is also given by:

$$\ln\left(K_{p,eq} \right) = -\frac{\Delta H^\circ}{RT} + \frac{\Delta S^\circ}{R} \qquad [9]$$

The derivative of the thermodynamic equilibrium coefficient $K_{p,eq}$ can be rewritten in the following format:

$$\frac{\partial\left(\ln\left(K_{p,eq} \right) \right)}{\partial T} = \frac{\Delta H^\circ}{RT^2} \qquad [10]$$

Equation [10] is the so-called Van't Hoff equation. The derivative of $K_{c,eq}$ can be obtained from equation [6]:

$$\frac{\partial\left(\ln\left(K_{c,eq} \right) \right)}{\partial T} = \frac{\partial\left(\ln\left(K_{p,eq} \right) \right)}{\partial T} - \frac{\Delta n}{T} \qquad [11]$$

$$\frac{\partial\left(\ln\left(K_{c,eq} \right) \right)}{\partial T} = \frac{\Delta H^\circ - \Delta n\ R\ T}{RT^2} \qquad [12]$$

According to equations [2], [3] and [4] the equilibrium coefficient $K_{c,eq}$ is also given by:

$$K_{c,eq} = \frac{A_f}{A_b} \exp\left(-\frac{E_{a,f} - E_{a,b}}{R\,T}\right) \tag{13}$$

$$\ln\left(K_{c,eq}\right) = \ln\left(\frac{A_f}{A_b}\right) - \frac{E_{a,f} - E_{a,b}}{R\,T} \tag{14}$$

The partial derivative of the logarithm of the equilibrium coefficient $K_{c,eq}$ to the temperature is:

$$\frac{\partial\left(\ln\left(K_{c,eq}\right)\right)}{\partial T} = \left(\frac{E_{a,f} - E_{a,b}}{R\,T^2}\right) \tag{15}$$

According to equations [15] and [12] the following equation can be derived for the difference of the activation energies of the forward and backward reaction:

$$E_{a,f} - E_{a,b} = \Delta H^\circ - \Delta n\,R\,T \tag{16}$$

Taking in to account equations [8] and [14] the logarithm of the pre-exponential factors is:

$$\ln\left(\frac{A_f}{A_b}\right) = \frac{\Delta S^\circ}{R} - \Delta n\left(1 + R\ln\left(R'\,T\right)\right) \tag{17}$$

Annex B

LIGHT FEEDSTOCKS

Feed	HC flow		COP	COT	Number of
	[kg/hr]	[kg/kg HC]	[bar]	[°C]	experiments
Ethane	2.1	0.6	1.9	750-880	10
	2.5	0.6	1.9	800	1
	2.8	0.0	1.5	930	1
	2.9	0.7	1.9	800-850	5
	3.0	0.0	1.7	850	1
	3.0	0.4	2.0	800-890	4
	3.8	0.3	1.9	790-860	3
	4.2	0.3	2.4	850	1
	4.2	0.4	1.9	950	1
	4.2	0.4	2.9	870	1
	4.2	0.5	1.9	845	1
n-butane	3.0	0.4	2.0	750-850	16
	3.0	1.0	2.0	770-880	10
i-butane	3.0	0.4	1.7	830	1
	3.0	0.6	1.7	830	1
	3.0	1.0	1.9	750-890	12
n-hexane	3.0	0.4	2.0	800-820	23
n-heptane	3.0	0.0	2.0	860	1
	3.0	0.3	2.0	890	1
	3.0	0.4	2.0	890	1
	3.0	0.7	2.0	775	1
n-decane	3.0	0.7	1.9	700-702	2
C6 mixture	3.8	0.5	1.7	830	1

Feed	HC flow		COP	COT	Number of
	[kg/hr]	[kg/kg HC]	[bar]	[°C]	experiments
Amoco iC6	3.0	0.4	2.0	770-790	3
KTI C6	4.8	0.4	1.7	800-860	14
AMOCO isoC7 mixture	3.0	0.4	2.0	770-825	2
Mix methane - ethane	3.0	0.0	1.7	820-850	4
Mix methane - ethane (2)	3.0	0.0	1.7	850	1
Mix methane - ethane (3)	3.0	0.0	1.7	820	1
Mix methane - ethene - ethane	2.4	0.0	1.4	870-890	2
Mix methane - ethane - propane	3.0	0.0	1.7	850	1
Mix meth-ethane-propane-butane	3.2	0.0	1.7	848	1
Mix meth-ethane-propane-butane (2)	3.1	0.0	1.6	730-840	7
Mix ethane - ethane	4.1	0.3	2.0	860-880	8
Mix ethane - ethene (2)	3.1	0.4	1.3	825-880	6
	3.1	0.4	2.0	840-860	3
Mix ethane - ethene – propane	4.2	0.3	2.0	860-890	12
Mix ethane - ethene - propane (2)	1.2	0.3	2.0	770-870	11
Mix ethane – propane	3.1	0.3	1.7	850	1
	4.2	0.4	2.5	850-870	3
Mix ethane - propane (2)	4.0	0.3	2.9	820	1
	4.0	0.5	2.9	840-860	2
Mix ethane - propane (3)	3.8	0.3	1.9	880	1
	3.8	0.5	1.9	880	1
Mix ethane - propane (4)	4.0	0.3	2.9	860	1
Mix ethane - propane (5)	5.2	0.2	2.0	660-960	23
Mix ethane - propane – butane	3.5	0.0	1.6	820	3
Mix ethane - propane - butane (2)	3.6	0.0	1.6	800-850	3
Mix ethane - propane - butane (3)	2.8	0.0	1.6	790-850	6
Mix ethane - toluene (87-13 wt%)	3.3	0.4	2.0	800-890	4
Mix ethane - toluene (77-23 wt%)	3.6	0.4	2.0	800-890	4

Feed	HC flow		COP	COT	Number of
	[kg/hr]	[kg/kg HC]	[bar]	[°C]	experiments
Mix ethane - toluene (70-30 wt%)	3.8	0.4	2.0	800-890	4
Mix ethane - toluene (60-40 wt%)	4.1	0.4	2.0	800-890	4
Mix propane – propene	3.0	0.4	1.3	825-880	3
	3.0	0.4	2.0	820-880	6
Mix i-butane - n-butane	3.0	0.5	1.8	850	2
	3.0	1.0	1.9	730-870	14
Mix 1 Reyniers	3.0	0.0	1.7	850	1
Mix n-heptane – benzene	3.0	0.6	2.0	875	1

NAPHTHA

Feed	HC flow		COP	COT	Number of
	[kg/hr]	[kg/kg HC]	[bar]	[°C]	experiments
Naphtha HDT	4.8	0.5	1.7	840-865	2
Naphtha ELF '96	4.8	0.5	1.6	845-865	2
Naphtha ELF2 '96	4.8	0.5	1.6	825-865	3
Naphtha IFP	2.1	0.8	1.9	790-900	5
	3.2	0.4	1.9	700-930	27
	4.3	0.2	1.9	710-920	30
Naphtha ELF '84/'85	4.0	0.25	1.7	800-860	6
	5.0	0.19	1.9	740-830	7
Naphtha labofina	3.5	0.6	1.7	870	1
	4.5	0.4	1.7	860-900	4
	5.2	0.4	2.0	860	1
Naphtha Fina research	4.5	0.5	2.2	790-860	9
	4.0	1.0	2.0	780-920	16
	6.5	0.5	2.0	780-940	10
Naphta Shell	4.0	0.6	2.0	810-860	17

Feed	HC flow		COP	COT	Number of
	[kg/hr]	[kg/kg HC]	[bar]	[°C]	experiments
Naphtha Esso	3.3	0.4	2.2	815	1
	4.0	0.48	2.1	810-830	4
Esso Hydrofine	4.0	0.3	1.8	852	1
	5.0	0.0	1.8	820	2
Keroseen	3.0	0.8	2.0	775-825	2
	3.0	0.8	2.5	680-850	3
	3.0	1.5	2.1	760	1
AMOCO light naphtha	3.0	1.0	2.0	750-850	2
AMOCO heavy naphtha	3.0	1.0	2.0	780-830	2

Heavy Feedstocks

Feed	HC flow		COP	COT	Number of
	[kg/hr]	[kg/kg HC]	[bar]	[°C]	experiments
OMV (AGO)	2.7	1.0	1.6	770-830	5
	3.4	0.75	1.6	760-814	4
ATEC (HAGO)	2.0	1.0	1.3	790	1
	2.0	1.0	2.0	790	1
Debutanized Natural GO	3.0	0.4	2.0	810-830	2
AGO ESSO/KOLN	2.4	0.8	2.5	775	1
	2.6	1.2	2.0	810	1
VGO URBK	4.5	0.7	1.6	750-850	7
	4.5	0.7	2.0	750-851	6
VGO fina Raffinaderij Antwerp	4.0	0.9	1.7	750-820	4

Annex C

NAPHTHA 1 Composition

Number	Name	Weight Percent (%)
1	2MC4	0.33
2	n-C5	0.53
3	22diMC4	0.06
4	cyC5	0.28
5	23diMC4	0.21
6	2MC5	1.17
7	3MC5	0.84
8	n-C6	1.89
9	22diMC5	0.12
10	McyC5	2.64
11	24diMC5	0.28
12	223triMC4	0.03
13	Benzene	0.68
14	33diMC5	0.10
15	cyC6	4.37
16	2MC6	1.36
17	23diMC5	0.81
18	11diMcyC5	0.55
19	3MC6	2.00
20	13diMcyC5c	1.10
21	13diMcyC5tr	1.03
22	3EC5	0.20
23	12diMcyC5tr	1.86
24	224triMpentane	0.02
25	n-C7	4.12
26	McyC6	14.28
27	113triMcyC5	0.83
28	EcyC5	0.95
29	25diMC6	0.35
30	24diMC6	0.60
31	124triMcyC5 (trc)	0.83
32	33diMC6	0.16
33	123triMcyC5 (trc)	0.85
34	234triMC5	0.16
35	Toluene	4.90
36	112triMcyC5	0.31

37	23diMC6	0.49
38	2M3EC5	0.15
39	2MC7	1.74
40	4MC7 + 34diMC6	0.95
41	124triMcyC5 (ctr+cc)	0.13
42	13diMcyC6c	3.13
43	3MC7	1.37
44	3EC6 + 14diMcyC6tr	1.75
45	11diMcyC6	0.54
46	1E,3McyC5tr	0.39
47	1E,3McyC5c	0.43
48	1E,2McyC5tr	0.68
49	13diMcyC6tr	0.12
50	12diMcyC6	1.74
51	123triMcyC5	0.02
52	14diMcyC6c	0.98
53	n-C8	3.61
54	isoC3cyC5	0.09
55	1134tetraMcyC5	0.08
56	1134tetraMcyC5	0.01
57	1133tetraMcyC5	0.01
58	1E,2McyC5c	0.07
59	235triMC6	0.18
60	22diMC7	0.14
61	12diMcyC6c	0.32
62	n-C3cyC5+24diMC7	0.47
63	44diMC7	0.05
64	EcyC6 + 135triMcyC5	3.62
65	2M,4EC6	0.05
66	26diMC7	0.56
67	113triMcyC6	1.10
68	xyztriMcyC6	0.19
69	25diMC7	0.53
70	35diMC7 + 33diMC7	0.27
71	1M,2EcyC6	0.20
72	1M,4EcyC6	0.09
73	Ebenzeen	1.32
74	123triMcyC6	0.27
75	xyztriMcyC6	0.63
76	C9-nafteen	0.06
77	135triMcyC6	0.05
78	m-xyleen	3.90
79	p-xyleen	1.14
80	23diMC7	0.84
81	34diMC7	0.52
82	4EC7	0.21

83	4MC8	0.47
84	2MC8	0.53
85	1E,3McyC5	0.19
86	123triMcyC6+3EC7	0.36
87	3MC8	0.63
88	124triMcyC6	0.02
89	o-xyleen	1.69
90	xyztriMcyC6	0.04
91	1135tetraMcyC6	0.25
92	1E4McyC6tr	0.98
93	1E,4McyC6c	0.59
94	1E,2McyC6	0.04
95	1E,3McyC6	0.10
96	hydrindaan	0.12
97	xyztriMcyC6	0.05
98	n-C9	2.01
99	1144tetraMcyC6	0.53
100	1E,1McyC6	0.17
101	isoC3benz	0.22
102	isoC3cyC6	0.51
103	C9-nafteen+235tri	0.29
104	22diMC8	0.08
105	44diMC8	0.25
106	24diMC8	0.05
107	n-C3cyC6	0.07
108	1135tetraMcyC6	0.94
109	n-C4cyC5	0.15
110	27diMC8	0.07
111	1M,4isoC3cyC6tr	0.03
112	36diMC8	0.23
113	33diMC8	0.02
114	n-C3benzeen	0.24
115	1144tetraMcyC6	0.03
116	26diMC8	0.15
117	1123tetraMcyC6	0.03
118	1M,3Ebenzeen	0.46
119	1M,4Ebenzeen	0.21
120	1123tetraMcyC6	0.04
121	135triMbenz	0.25
122	1E23diMcyC6	0.05
123	1E13diMcyC6	0.01
124	5MC9	0.01
125	4MC9	0.05
126	1M,2Ebenzeen	0.14
127	2MC9	0.04

128	C10-nafteen	0.01
129	3EC8	0.02
130	isoC4cyC6	0.02
131	3MC9	0.03
132	1E24diMcyC6	0.01
133	1E24diMcyC6	0.01
134	124triMbenzeen	0.23
135	1M,3C3cyC6	0.03
136	t-C4cyC6	0.03
137	sC4cyC6	0.01
138	1M4iC3cyC6	0.01
139	xE,yzdiMcyC6	0.01
140	1M,4C3cyC6	0.01
141	diEcyC6	0.01
142	sec-C4benzene	0.01
143	n-C10	0.06
144	C10-nafteen	0.01
145	123triMbenzeen	0.03
146	1M,3isoC3benzeen	0.01
147	1M,4isoC3benzeen	0.01
148	P11	0.01
149	26diMC9	0.01
150	nC4cyC6	0.01
151	1M,2isoC3benz	0.01
152	28diMC9	0.01
153	1M,3n-C3benzeen	0.01
154	1E23diMbenzeen	0.01
155	5EC9+trdecaline	0.01
156	4EC9+1M,3n-C3benz	0.01
157	5MC10	0.01
158	4MC10	0.01
159	12diM,2Ebenz	0.01
160	2MC10	0.01
161	12diM,3Ebenz	0.01
162	n-C11	0.01
163	1245tetraMbenzeen	0.02

Annex D

VGO Composition

Number	Name	Weight Percent (%)
1	Benzene	0.39
2	Toluene	0.08
3	n-C10	0.01
4	n-C11	0.01
5	n-C12	0.02
6	1M naphthalene	0.02
7	n-C13	0.05
8	1,2 diM naphthalene	0.04
9	n-C14	0.26
10	3Me C15	0.08
11	n-C15	0.13
12	C16cyc5	0.02
13	C2 biphenyl	0.09
14	n-C16	0.15
15	C3 biphenyl	0.07
16	phenantrene	0.06
17	C5 naphthalene	0.08
18	n-C17	0.19
19	Anthracene	0.07
20	n-C18	0.22
21	diM fluorene	0.04
22	2M phenantrene	0.07
23	n-C19	0.32
24	C6 naphthalene	0.06
25	C3 fluorene	0.13
26	diM phenantrene	0.07
27	n-C20	0.57
28	C4 fluorene	0.10
29	C7 naphthalene	0.14
30	n-C21	1.19
31	C3 phenantrene	0.13
32	C3 anthracene	0.09
33	C3 Ph/An	0.06
34	n-C22	1.48
35	C4 phenantrene	0.18
36	C4 anthracene	0.11

37	Pyrene	0.09
38	n-C23	2.58
39	C5 phenantrene	0.26
40	C5 anthracene	0.17
41	M pyrene	0.30
42	n-C24	4.30
43	C6 phenantrene	0.32
44	C6 anthracene	0.40
45	C2 pyrene	0.55
46	n-C25	6.52
47	C7 phenantrene	0.34
48	C7 anthracene	0.13
49	C3 pyrene	0.18
50	n-C26	7.78
51	C8 phenantrene	0.61
52	C8 anthracene	0.60
53	C4 pyrene	0.30
54	n-C27	9.55
55	C9 phenantrene	1.15
56	C9 anthracene	0.66
57	C5 pyrene	0.45
58	n-C28	9.83
59	C10 phenantrene	1.33
60	C10 anthracene	1.32
61	C6 pyrene	1.35
62	n-C29	10.53
63	C7 pyrene	4.88
64	n-C30	8.69
65	C8 pyrene	1.72
66	n-C31	6.65
67	C9 pyrene	1.02
68	n-C32	4.00
69	C10 pyrene	0.25
70	n-C33	3.35